Human Surfactant Protein D as an Innate Immune Surveillance Molecule

A thesis submitted in fulfilment of the requirement for the

Degree of Doctor of Philosophy

By Valarmathy Murugaiah

January 2021

Division of Biosciences

College of Health, Medicine and Life Sciences

Brunel University London

Dedication

To my beloved Amma: thank you for your unflinching and selfless support

Declaration

I hereby declare that the research presented in this thesis is my own work, except where other specified and has not been submitted for any other degree.

Valarmathy Murugaiah

Acknowledgments

Firstly, I am extremely grateful to my supervisor, Dr Uday Kishore, for accepting me in his research group, and for his continuous supervision during the period of my PhD degree. Without his support and immense knowledge, finishing my PhD research was not possible. Thank you, Dr Kishore, for giving me this opportunity to prove myself academically; I could not have imagined having a better supervisor and mentor!

I would also like to express my sincerest gratitude to Prof. R. B. Sim, for offering profound scientific advices, invaluable reagents, and protocols. I also express my utmost gratitude to Dr Beatrice Nal, for her training and collaborative support for Influenza A Virus research. My thanks are also due to my PhD committee members: Dr Predrag Slijepcevic (my second supervisor), Dr Anthony Tsolaki, Dr Terry Roberts and Prof. Arturo Sala, for their critical comments during PhD review meetings. I am also thankful to Dr Ansar Pathan for his sharing his expertise and knowledge.

Special thanks go to Dr. Roberta Bulla and Dr Chiara Agostinis, for allowing me to work at their laboratory (Medical Faculty of the University of Trieste), and their meticulous training in immunohistochemistry and isolation of primary cells. Additionally, I would like to express my sincere appreciation to Dr Anuvinder Kaur, who has been a source of inspiration when it came to planning and performing experiments. Thank you Anu for the training you offered me.

I would like to acknowledge my colleague and a friend, Praveen Mathews, for his professional and personal support during my PhD study. Thank you for validating my experiments, supporting me when things got tough, and endless stimulating discussions. My warmest thanks to Nazar Beirag, for his laboratory support during the final year of my PhD study.

Finally, I would like to acknowledge with gratitude the support and love of my family and friends.

Table of Contents

List of Tables

List of Figures

List of Abbreviations

ABPA	Allergic Bronchopulmonary Aspergillosis
AEC	3-Amino-9-Ethylcarbazole
AMs	Alveolar macrophages
Bcl-2	B-cell lymphoma 2
BSA	Bovine Serum Albumin
CD	Cluster of Differentiation
CL-43	Collectin-43
CL-46	Collectin-46
CL-K1	Collectin kidney 1
CL-L1	Collectin liver 1
CL-P1	Collectin placenta 1
CLRs	C-type Lectin Receptors
CPE	Cytopathic Effects
CR	Complement receptor
CRD	Carbohydrate Recognition Domain
CRP	C-reactive protein
CT	Chemotherapy
CXCL5	C-X-C motif chemokine 5
DAB	Diaminobenzidine
DAMPs	Damage-Associated Molecular Patterns
DC	Dendritic cell
DC-SIGN	Dendritic Cell-Specific Intercellular Adhesion Molecule-3-Grabbing Non-Integrin
ECL	Enhanced Chemiluminescence
ECM	Extracellular Matrix
EGF	Epidermal Growth factor
EGFR	Epidermal Growth Factor Receptor

EMT	Epithelial–to-Mesenchymal Transition
ER	Endoplasmic Reticulum
ET	Endocrine (hormone) therapy
GAG	Glycosaminoglycan
HA	Hemagglutinin
HAS	Hyaluronan synthase
HB-EGF	Heparin-binding epidermal growth factor-like growth factor
HEK	Human Embryonic Kidney
HER	Human Epidermal Growth Factor Receptor
HIF	Hypoxia-inducible factor
HIV	Human Immunodeficiency Virus
HMGA1	High-Mobility Group A1
HRP	Horseradish Peroxidase
HYA	Hyaluronan
IAV	Influenza A Virus
IFN-γ	Interferon gamma
Ig	Immunoglobulin
IL	Interleukins
INF	Interferon
iNOS	Inducible nitric oxide synthase)
LAL	Limulus Amebocyte Lysate
LAM	Lipoarabinomannan
LCN	Lipocalin
M1	Matrix Protein 1
MAP	Mitogen-Activated Protein
MBP	Maltose Binding Protein
MCP	Monocyte Chemoattractant Protein
MDCK	Madin Darby Canine Kidney

MDSCs	Myeloid-derived suppressor cells
MHC	Major Histocompatibility Complex
MIF	Macrophage migration inhibitory factor
MIP	Macrophage Inflammatory Protein
MMP	Matrix Metalloproteinases
MMTV-PyMT	Mouse mammary tumor virus-polyoma middle Tumor-antigen
mt	Mutant
mTOR	Mammalian Target of Rapamycin
MTT	3-[4,5-Dimethylthiazol-2-yl]-2,5-Diphenyltetrazolium bromide
NA	Neuraminidase
NAb	Naturally occurring antibodies
NK	natural killer
NLRs	NOD-Like Receptors
NP	Influenza Virus Nucleoprotein
PAMPs	Pattern Associated Molecular Patterns
PARP	Poly (ADP-ribose) Polymerase
PBMC	Peripheral Blood Mononuclear Cell
PDAC	Pancreatic Adenocarcinoma
PD-L1	Anti-Programmed Death-Ligand 1
PRRs	Pattern Recognition Receptors
PVHA	Pegvorhyaluronidase
qRT-PCR	Quantitative Real-time Polymerase Chain Reaction
RAPTOR	Regulatory-Associated Protein of mTOR
rfhSP-D	A Recombinant Fragment of Human SP-D
RHAMM	Receptor for HA-Mediated Motility
RICTOR	Rapamycin-Insensitive Companion of mTOR
RLRs	RIG-I-Like Receptors
RNI	Reactive nitrogen intermediates

RNP	Ribonucleoprotein
RT	Radiation therapy
SA	Sialic-acid Receptors
SAP	Serum amyloid P protein
SARS	Severe Acute Respiratory Syndrome
SDS	Sodium Dodecyl Sulfate
SP-A	Lung Surfactant Protein A
SP-D	Lung Surfactant Protein D
STAT3	Signal transducer and activator of transcription 3
TADCs	Tumor-associated dendritic cells
TAMCs	Tumor-associated myeloid cells
TAMs	Tumor-associated macrophages
TANs	Tumor-associated neutrophils
$TCID_{50}$	Tissue Culture Infectious Dose 50%
TEMs	Tie2-expressing monocytes
TGF	Transforming Growth Factor
TLRs	Toll-Like Receptors
TME	Tumour microenvironment
TNBC	Triple-negative breast cancer
TNF	Tumor Necrosis Factor
TPCK	Tosylamide-2-Phenylethyl-Chloromethyl Ketone
uPA	Urokinase-type plasminogen activator
wt	Wild type

Summary of the thesis

Surfactant protein D (SP-D) belongs to the family called Collectins (collagen-containing lectins). It has a primary structure characterised by an N-terminal cysteine-rich region, triple-helical collagen region composed of Gly-X-Y repeats (where X and Y can be any amino acid), an a-helical coiled-coil neck region, and a C-terminal carbohydrate recognition domain (CRD). The primary subunit oligomerizes to form a trimeric structure that can further acquire a cruciform organization and multimers (dodecamers). SP-D is a potent innate immune molecule whose presence in the lungs as well as at a range mucosal surfaces and extrapulmonary tissues allows immune surveillance against pathogens, apoptotic/necrotic cells, allergens, and cancer cells. A recombinant fragment of human SP-D (rfhSP-D) composed of 8 Gly-X-Y repeats, neck and CRD region, expressed in E. coli, is well known to act against a range of pathogen and allergen challenge *in vitro*, *in vivo* and *ex vivo*.

In this thesis, we have examined the interaction between rfhSP-D and two subtypes (pH1N1 and H3N2) of Influenza A Virus (IAV) (Chapter 3). rfhSP-D interacted with haemagglutinin, neuraminidase and matrix protein 1; inhibited their infectivity against lung epithelia cell lines; and suppressed the cytokine storm induced by the viral challenge. The protective role of rfhSP-D against IAV as an entry inhibitor was further validated by the use of pseudotyped lentiviruses containing haemagglutinin and neuraminidase of the two IAV subtypes. Continuing with the theme of innate immune surveillance by SP-D against lung, pancreatic, ovarian, and prostate cancers, we extended on recent studies to breast cancer using HER2 over-expressing (SKBR3), triple-positive (BT474) and triple-negative (BT20) breast cancer cell lines (Chapter 4). rfhSP-D induced apoptosis at 24 h in SKBR3 and BT747 cells (but not in BT20) via intrinsic apoptosis pathway. However, this protective effect of rfhSP-D was fully negated by the presence of hyaluronic acid, a major extracellular matrix component within the tumour microenvironment (Chapter 5). This thesis highlights the therapeutic potential of rfhSP-D in influenza A Virus infection as well as breast cancer and merits pre-clinical trials in murine models.

Chapter 1

Introduction

1.1 Innate Immunity

The innate immunity is the primordial form of the mammalian immune system that represents the first-line defense barrier against invading pathogens. The anti-microbial resistance mechanisms include cellular and physical barriers comprised of skin, mucosal epithelia, and anti-microbial peptides. These epithelial barriers secrete a range of anti-microbial glycoproteins (mucins), protective enzymes (lysozymes), and peptide antibiotics (defensins, cathelicidins and histatins), which inhibit the growth of microbes (Dale and Fredericks, 2005).

1.1.1 Innate immune cellular factors

The innate immune cells such as macrophages and dendritic cells require their pattern recognition receptors (PRRs) to recognize and clear pathogens as well as cellular debris. PRRs are subdivided into membrane bound PRRs, such as Toll like receptors (TLRs), and C-type lectin receptors (CLRs); and cytoplasmic PRRs, including NOD-like receptors (NLRs) and RIG-I-like receptors (RLRs) (Figure 1). PRRs, in turn, detect distinct conserved features on pathogens, commonly termed as Pathogen-Associated Molecular Patterns (PAMPs), or Damage-Associated Molecular Patterns (DAMPs) (Marcus et al., 2014). PAMPs are highly conserved within different microorganisms, and can consist of protein, lipid, carbohydrate moieties or nucleic acids recognized by TLRs:13 TLRs have been discovered so far, and these TLRs are expressed on macrophages, DCs, and NK cells (Hug et al., 2018, Joosten et al., 2016).

Upon recognition of PAMPs on the pathogens, cell surface PRRs induce phagocytic or pro-inflammatory anti-microbial responses by triggering a wide range of intracellular signaling cascades, through activation of adaptor molecules, kinases, and transcription factors (Akira et al. 2004). Thus, PRR-triggered signaling further results in the expression of multiple genes, culminating in secretion of cytokines, chemokines, cell adhesion molecules, as well as immune-receptors (Mogensen, 2009). PAMP-PRR engagement also enhances the expression of major histocompatibility complex (MHC) class II molecules, as well as expression of co-stimulatory molecules such as cluster of differentiation 40 (CD40), CD80 and CD86 (Elgueta et al., 2009) that prepares antigen presenting cells (APCs) such as macrophages and dendritic cells (DCs) for forming immunological synapse with naïve T cells in the lymph nodes.

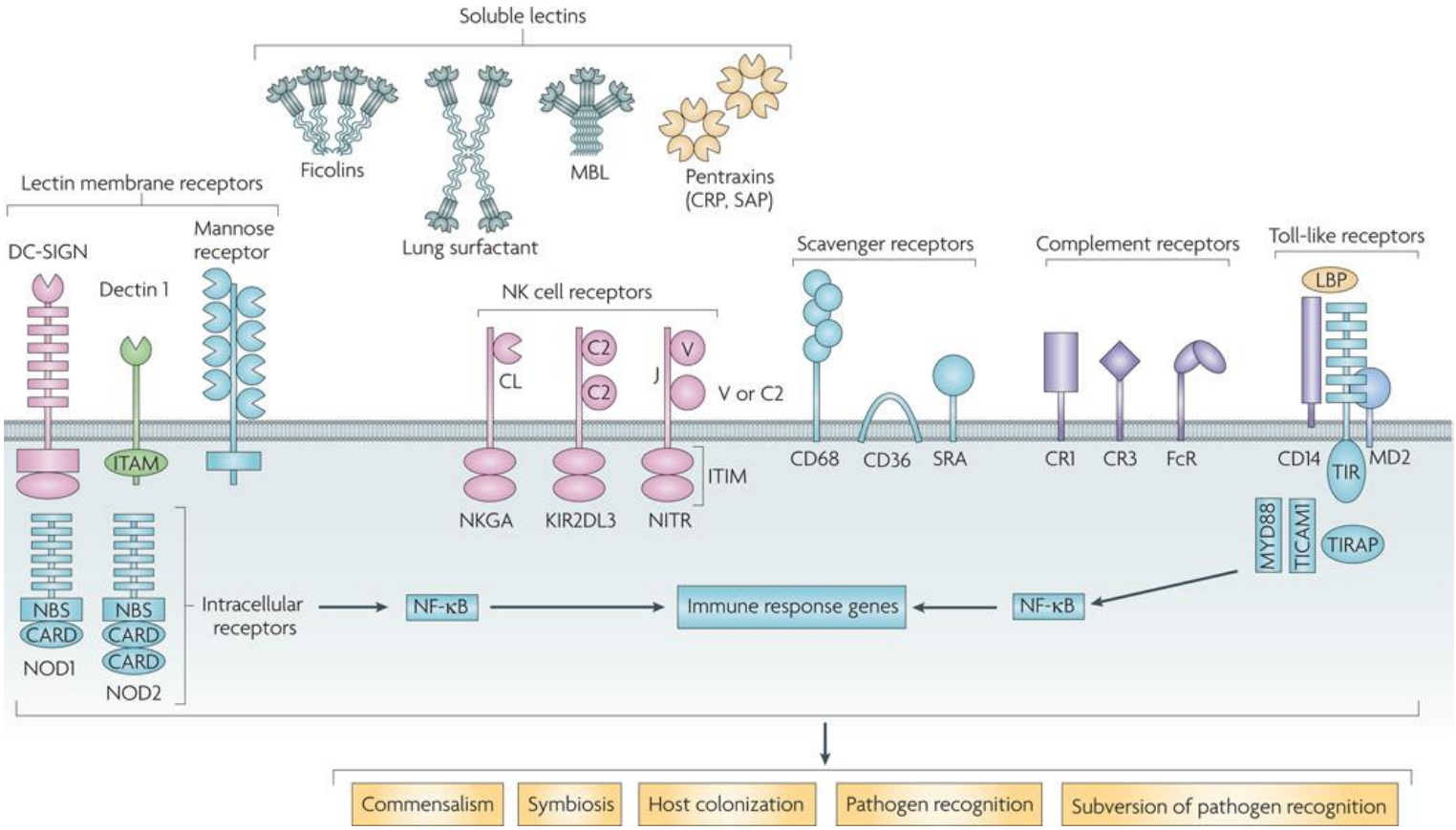

Figure 1: A schematic representation to demonstrate soluble and membrane-bound pattern-recognition receptors (PRRs).

Extracellular PRRs include the soluble C-type lectins, such as collectins (lung surfactant proteins A and D, and MBL), Ficolins and Pentraxins (serum amyloid-P, C-reactive proteins, and long pentraxin 3), and lectin-membrane receptors (DC-SIGN, dectin 1, and mannose receptor). Other membrane bound surface receptors demonstrated are scavenger, TLRs, natural killer (NK) cell, and complement receptors. The intracellular NOD-like receptors (NLRs) and Toll-like receptors (TLRs) are rich in leucine repeats, which trigger immune genes through nuclear factor-□B (NF-□B). These soluble and membrane bound PRRs can regulate the interactions with non-self-cells that could lead to induction of a wide range of immune mechanisms for pathogen clearance and (taken from (Vasta, 2009).

1.1.2 Innate immune humoral response

The innate immune humoral response is comprised of the serine protease-driven cascades of the complement system, as well as naturally occurring antibodies (NAb), collectins and pentraxins (Shishido et al., 2012).

The complement system can be initiated via three distinct pathways, classical (CP), lectin (LP), and alternative (AP), resulting in the formation of C3 convertase. C3 convertase cleaves C3, leading to C3b production and C5 convertase. C5 cleavage by C5 convertase leads to deposition of C5b and result in initiation of the common terminal pathway. The terminal pathway results in the membrane attack complex (MAC), lading to lysis of the pathogenic cell. The formation of C3 and C5 convertase also yields C3a and C5a, two well-known and potent anaphylatoxins. Complement receptor 3 (CR3) found on macrophages and neutrophils enrich the innate immune response via recognizing C3b opsonized pathogens (Carroll, 2004, Kimura et al., 2003). CR2 recognition of iC3b, C3dg and C3d significantly increases antibody production, thus acting as an adjuvant (Dempsey et al., 1996, Molina et al., 1996).

Naturally occurring antibodies (NAb) are produced by subclasses of B lymphocytes (B1), that are involved in innate humoral response. Nab are well-known germline-encoded antibodies, which exhibit restricted epitope specificities, and can also be produced without stimulations of external antigens (Avrameas, 1991). There are different isotypes of Nab, of which IgM is the most common, with IgA and IgG being less abundant (Avrameas, 1991). natural IgM antibodies can mediate the clearance of cellular debris, or apoptotic cells via recruitment of complement components resulting in opsonization (Binder et al., 2005). Pathogen recognition by NAb can also modulate the adaptive immune response via interacting with T, B and DCs (Ochsenbein et al., 1999). Moreover, NAb are also potent initiators of the complement pathways.

Pentraxins are conserved multifunctional acute phase proteins, and well-known PRRs synthesized during tissue damage, infection, and inflammation (Du Clos and Mold, 2004). Each pentraxin is characterised by calcium dependent ligand binding, composed of a common domain in the C-terminal region. The presence and absence of this additional domains subdivide the

family into long or short pentraxins (Du Clos and Mold, 2004).. C-reactive protein (CRP) and serum amyloid P protein (SAP) have been identified as short pentraxins are synthesized by the liver (Du Clos and Mold, 2004). Pentraxin 3 (PTX3) belongs to the long pentraxin subfamily, which was initially identified as an IL-1 or TNF-inducible gene. Pentraxins have similar functions as NAb, such as recognition and binding to a diverse range of pathogens and intrinsic ligands, including extracellular matrix components (ECM) and apoptotic cells (Bassi et al., 2009, Hirschfield et al., 2003, Pepys and Baltz, 1983). CRP, SAP and PTX3 can interact via Fcγ receptors on macrophages and other innate immune cells (Moalli et al., 2010, Mold et al., 2002, Mold et al., 2001). Pentraxins binding to targets can facilitate clearance of cell debris and pathogens through complement activation (Bassi et al., 2009).

1.2 Collectins

Collectins represent an important group of humoural PRRs, which bind to oligosaccharide structures on the surface of microorganisms as well as altered self. Collectins are multimeric proteins, involved in pathogen clearance by aggregation/agglutination, opsonization, enhanced phagocytosis, complement activation, and modulation of inflammation (Murugaiah et al., 2020b, Nayak et al., 2012). Collectins are collagen containing C-type (calcium dependent) lectins, structurally characterised by three polypeptide chains, each containing four domains. The first domain is comprised of NH2-terminal sequences, containing cysteine residues responsible for structural units to form oligomers via disulphide bonds. The collagenous region is the second domain, which consists of Gly-X-Y triplet repeats, where X and Y represent any form of amino acid (Colley and Baenziger, 1987). The triple-helical collagen region also offers rigidity and stability to the molecule. Another key structural feature of the collagenous region is that it can be O-glycosylated (Colley and Baenziger, 1987). The third structural domain contains an alpha-helical coiled-coil neck region, and the fourth domain at the C-terminal end contains a carbohydrate recognition domain (CRD), also known as C-type lectin domain (Figure 2) (Kishore et al., 2006). The interactions of collectins with a range of pathogens are mediated through their CRDs. A broad spectrum of carbohydrate specificity is necessary for collectins to recognize and bind a large repertoire of PAMPs, which is accomplished by an open and flexible trough-like binding pocket presented within the CRDs region. However, recognition and selection of ligands

by this site is mostly depends on the positioning of the vicinal hydroxyl groups of carbohydrates (Ng et al., 1996), which tend to form coordination bonds with the ligated calcium ions, hydrogen bonds and a polar Van der Waals contact (Ng et al., 1996, Murugaiah et al., 2020b).

To date, the collectin family contains nine members, including mannose binding lectin (MBL), lung surfactant protein A (SP-A) and SP-D, conglutinin, Collectin-43 (CL-43) and CL-46, and newly discovered collectin kidney 1 (CL-K1), collectin liver 1 (CL-L1) and collectin placenta 1 (CL-P1) (Figure 2). Various biological functions of collectins have been summarized in Table 1.

1.3 Lung Surfactant Protein D (SP-D)

Human SP-D, a member of the collectin family, is a large hydrophilic and multimeric protein; its single polypeptide chain is 43 kDa, containing cysteine-linked N-terminus region, collagenous region, neck region, and the CRD region (Kishore et al., 2006). Three identical polypeptide chains of 43 kDa form a trimer of 130 kDa subunit. Four such homotrimeric subunits are then connected through their N-terminal regions to form a further tetrameric structure of 520 kDa, assuming an overall cruciform structure (Kishore et al., 2006, Nayak et al., 2012). The trimeric CRD module can interact with pathogens by binding terminal carbohydrate residues, whilst the collagen region of SP-D can bind to its putative receptor, surface-expressed calreticulin-CD91 complexes (Gardai et al., 2003) and brings about effector functions, such as pro-inflammatory cytokine production (Gardai et al., 2003).

Human SP-D is primarily synthesized and secreted into the air space of the lungs by alveolar type II and Clara cells (Crouch et al., 1992, Voorhout et al., 1992). SP-D presence has also been reported at extra-pulmonary sites. Immunohistochemically, SP-D expression has been demonstrated in human brain, heart, kidneys, trachea, salivary gland, testis, pancreas, and small-intestine (Fisher and Mason, 1995, Madsen et al., 2000, Herías et al., 2007). A lower SP-D expression has been reported in uterus, adrenal gland, spleen, and mammary glands (Fisher and Mason, 1995, Madsen et al., 2000, Herías et al., 2007). In addition, SP-D immunoreactivity has also been demonstrated in the epithelial cells of large and small ducts of the parotid gland, sweat and lacrimal glands, epithelial cells of gall bladder and intra-hepatic bile ducts, as well as exocrine pancreatic ducts, esophagus and in the urinary tracts (Madsen et al., 2000).

SP-D interacts with a diverse range of pathogens triggering clearance mechanisms, including agglutination/aggregation, enhanced phagocytosis and superoxidative burst, as well as direct growth microbial inhibition (Nayak et al., 2012, Kishore et al., 2006). Involvement of SP-D has also been reported in the control of pulmonary inflammation (allergy and asthma) (Kishore et al., 2002, Qaseem et al., 2013). Furthermore, SP-D can also link innate immunity with adaptive immunity via modulating dendritic cell (DC) maturation and function, and polarization of helper T-cell (Qaseem et al., 2013, Qaseem et al., 2017).

1.3.1 SP-D interaction with Pathogens

A number of *in vitro* and *in vivo* studies have established a key role of SP-D in the protection against respiratory pathogens (Table 1). SP-D acts as an opsonin, enhancing phagocytic uptake and killing of the target pathogens (Crouch, 2000, Lawson and Reid, 2000, Crouch and Wright, 2001, Shepherd, 2002).

1.3.2 SP-D interaction with Bacteria

Both Gram-negative and Gram-positive bacteria are recognized by SP-D, triggering their phagocytosis by alveolar microphages (AMs) (Pikaar et al., 1995). SP-D binds rough lipopolysaccharide (LPS) via its CRDs, resulting in agglutination of E. *coli* (Kuan et al., 1992). Direct growth inhibition of several Gram-negative bacteria by SP-D has been reported via enhanced the membrane permeability of the bacterial cell wall as well as inhibition of biosynthetic functions in E. *coli*, K. *pneumoniae* and *Enterobacter aerogenes* (Wu et al., 2003).

SP-D can also bind to lipoteichoic acid and peptidoglycan, two Gram-positive bacterial ligands, via its CRD region (de Wetering et al., 2001), and to lipoarabinomannan (LAM) from *Mycobacterium avium* and *M. tuberculosis* (Ferguson et al., 1999, Ferguson et al., 2002, Kudo et al., 2004). SP-D also interacts with cell membrane lipids of *M. pneumoniae (Chiba et al., 2002)*. SP-D binds and agglutinates *M. tuberculosis*, while triggering inhibition of phagocytosis via blocking the LAM interaction with macrophage mannose receptor (Ferguson et al., 1999, Ferguson et al., 2002). SP-D also directly stimulates phagocytosis by enhancing cell surface phagocytic receptors such as mannose receptors present on macrophages, without requiring the need for microbial binding (Kudo et al., 2004).

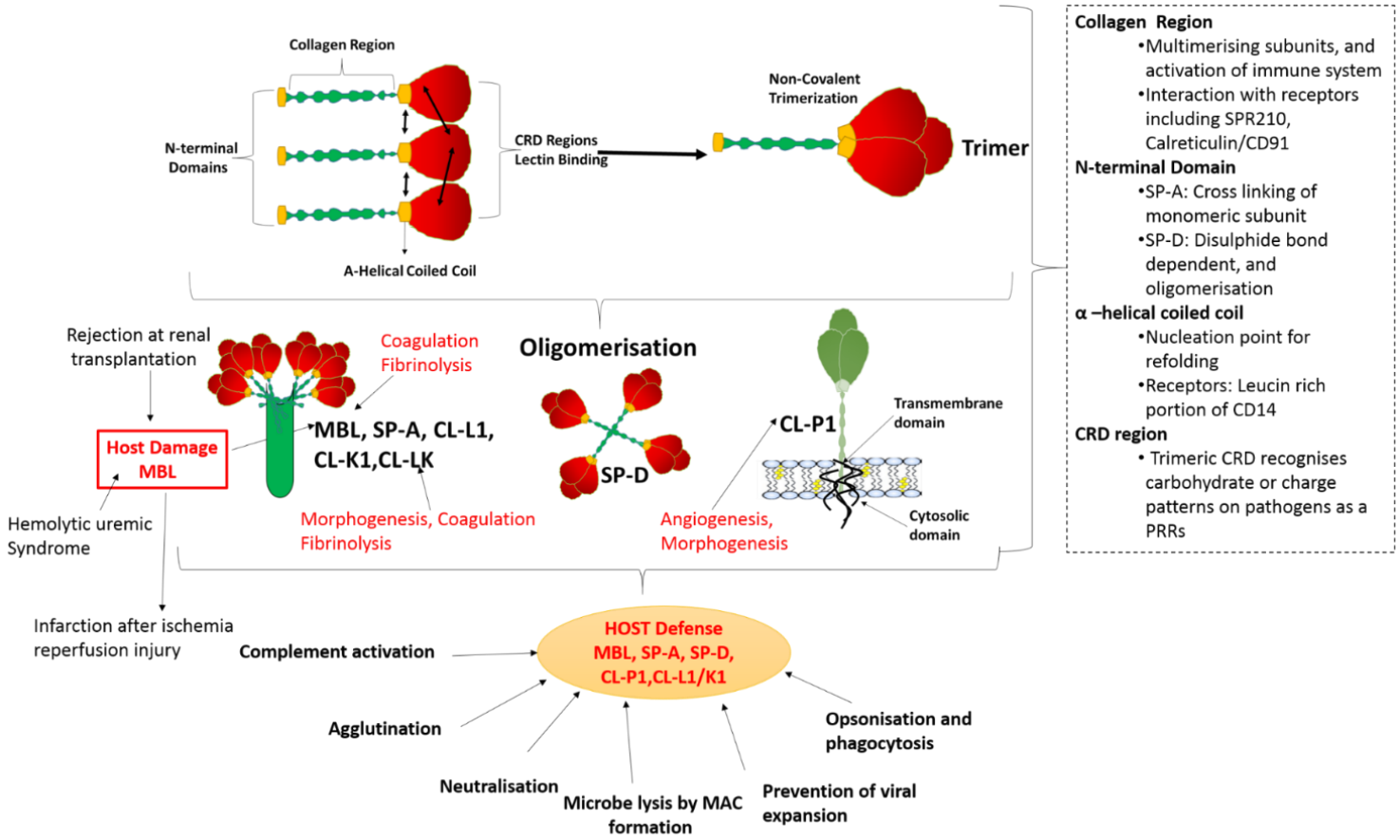

Figure 2: Molecular structural representation and biological functions of human collectins

Collectins are shown as monomeric subunits, followed by trimeric subunits, composed of an N-terminal domain (7-28 amino acid residues), collagen like region (composed of Gly-X-Y triplets repeats), α-helical coiled coil neck region and C-terminal carbohydrate recognition domain (CRD). For most collectins, the subunits are homotrimers, which are composed of three identical polypeptides. However, heterotrimers can be found in the case of SP-A (made up of highly homologous SPA-1 and SPA-2 polypeptides). Heterotrimers can also be found in CL-10 and CL-11. Biological functions of each domain are also briefly described (Murugaiah et al., 2020b).

Table 1: Origin of collectins and their tissue distribution.

Collectins	Tissues of origin	Tissues of presentation	Remarks	References
MBL	Liver and small intestine	Serum	Two variants of MBL (A and C) have been identified in most animals, while only one is found in humans and chimpanzee. MBL is the recognition subcomponent of the complement lectin pathway	(Garred et al., 2006)
Conglutinin, CL-43 and CL-46	Bovine liver	Serum	These bovine collectins plays an important role in the first line of defense against rumen microbes without eliciting general inflammatory response.	(Dec and Wernicki, 2006)
SP-A and SP-D	Clara cells, type II pneumocytes, intestinal mucosa, thymus, prostate gland, Eustachian tube, paranasal sinuses, middle ear, synovium	Alveolar space, mucosal surfaces, semen	Extrapulmonary expression of SP-A is limited to a few tissues, while SP-D expression has been detected in many non-pulmonary tissues.	(Kishore et al., 2006, Nayak et al., 2012).
CL-P1	Placenta, and vascular endothelial cells	Endothelial cells	CL-P1 is the only membrane bound collectin with an intracellular domain. May have a function in bacterial recognition or act as a scavenger receptor for desialylated target.	(Ohtani et al., 2012, Hansen et al., 2016)
CL-K1	---------	Serum	Interacts with negatively charged molecules, including nucleic acid ligands. It is involved in opsonization of apoptotic cells by recognizing a combination of carbohydrate or nucleic ligands.	(Venkatraman Girija et al., 2015, Henriksen et al., 2013)
CL-L1	Liver and hepatocyte	Ubiquitous	May be involved in host defense by recognizing numerous pathogens and interacting with effector proteins, including complement components.	(Hansen et al., 2016)

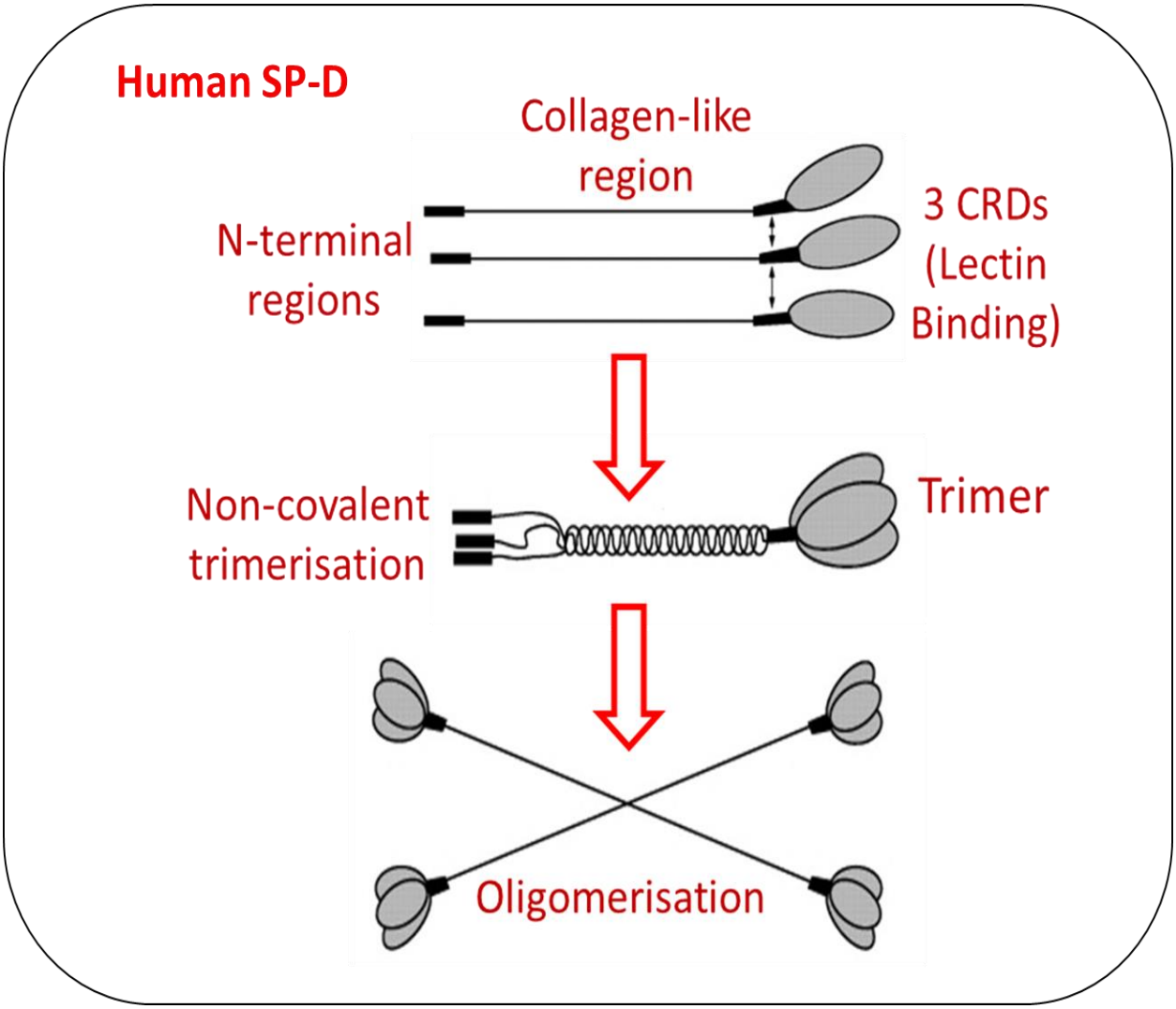

Figure 3: Domain organization of human SP-D

The human SP-D is first shown as monomer, trimer, and oligomer. SP-D is composed of oligomers of a 130 kDa subunit containing three identical polypeptide chains of 43 kDa. The primary structure of SP-D includes an N terminus domain, collagenous region, helical neck, and C terminus CRD region. (Kishore et al., 2002, Kishore et al., 2006).

1.3.3 SP-D interaction with Viruses

Direct interaction of SP-D with a number of viruses, leading to viral neutralization and phagocytosis has been described. SP-D binds to gp120 and inhibits HIV-1 infectivity and replication in a calcium dependent manner (Meschi et al., 2005), whilst a recombinant fragment of human SP-D (rfhSP-D) (containing homotrimeric neck and three CRD region) was also shown to bind gp120 and inhibit infection of U937 monocytic cells, Jurkat T cells and PBMCs, in addition to suppressing HIV-1 triggered cytokine storm (Pandit et al., 2014). A direct interaction between DC-SIGN (dendritic cell-specific intercellular adhesion molecule-3-grabbing non-integrin) and rfhSP-D has been shown to modulate HIV-1 capture and its transfer to $CD4^+$ T cells *in vitro (Dodagatta-Marri et al., 2017).* rfhSP-D can also prevent and restrict HIV-1 transfer across the vaginal epithelial barrier, via modulating the gene expression signature of the vaginal epithelium (Pandit et al., 2014).

Increased levels of serum SP-D have been detected in patients infected with severe acute respiratory syndrome (SARS) coronavirus (Wu et al., 2009). SARS corona virus spike glycoprotein is recognized by SP-D (Leth-Larsen et al., 2007). Interaction between SP-D and HCoV-229E, another coronavirus strain, leads to inhibition of viral infection in human bronchial epithelial (16HBE) cells (Funk et al., 2012). Binding of SP-D to bovine strains of the non-enveloped rotavirus, via the VP7 glycoprotein has been also reported (Reading et al., 1998). However, binding of human as well as porcine SP-D to glycoprotein of Ebola virus can enhance viral infection and dissemination (Favier et al., 2019). Interestingly, bovine SP-D can also bind bovine rotaviruses via the VP7 glycoprotein and neutralise viral infectivity (Reading et al., 1998). SP-D can bind A27 protein of vaccinia virus; SP-D gene-knockout ($^{-/-}$) mice challenged with vaccinia virus show an increased mortality rate, compared to SP-D wild type ($^{+/+}$) mice (Perino et al., 2013). In addition, rfhSP-D has been shown to bind spike glycoprotein (S1) of SARS-CoV-2 and its receptor binding domain (RBD) in a dose dependent manner (Hsieh et al., 2020; Madan et al., 2020). Furthermore, rfhSP-D treatment inhibited interaction of S1 glycoprotein with HEK293T cells overexpressing Angiotensin Converting Enzyme 2 (ACE2) receptor (Hsieh et al., 2020, Madan et al., 2020). Thus, rfhSP-D can act as an entry inhibitor of SARS-CoV-2 as evident from a RLU fold (~0.5) reduction

of luciferase reporter activity using pseudotyped lentiviral particles expressing SARS-CoV-2 S1 protein (Hsieh et al., 2020).

The SP-D binding to Influenza A Virus (IAV) has been extensively studied using SP-$D^{-/-}$ mice. However, the anti-viral effects of SP-D seem to be dependent on the viral subtypes and glycosylation levels of the virulence factors. These include differences of glycosylation found in hemagglutinin (HA) and neuraminidase (NA) glycoproteins (York et al., 2019). SP-D treatment in a murine model of IAV infection showed an enhanced clearance of the virus in the lungs (van Eijk et al., 2019). SP-D neutralizes the IAV and also inhibits the release of IAV virions from infected host cells, via mannose resides of HA or NA (Malhotra et al., 1994). Hemagglutination activity of IAV is also inhibited by SP-D, causing aggregation of IAV viral particles (Hartshorn et al., 1994). NA activity is also restricted by SP-D; this effect can be inhibited in the presence of D-mannose (Reading et al., 1997). Anti-IAV activity by SP-D is suggested to occur via its CRD region binding to carbohydrate pattern (mannosylated, N-linked) on HA and NA of IAV (Hartshorn et al., 1994, Hartshorn et al., 2000). SP-D also restricts the enzymatic activity of HA and NA, neutralizing the ability of pH1N1 IAV subtype to infect human A549 airway epithelial cells line (Job et al., 2010). However, SP-D has been reported to enhance infection in the case of some pandemic pH1N1 strains, which correlates with the differences in N-glycosylation found in the globular head region of HA (Job et al., 2010). Porcine SP-D is very potent in its ability to inhibit seasonal IAV subtypes, several pandemic and avian strains of IAV (van Eijk et al., 2002, Hillaire et al., 2013).

1.3.4 SP-D involvement in lung hypersensitivity and inflammation

SP-D gene knock-out mice, murine models of lung infection and hypersensitivity, structural and functional characterization of cell surface associated receptors have emphasized a key diverse role played by SP-D in the pulmonary immune response and control of lung inflammation. Mice genetically deficient in SP-D showed chronic pulmonary inflammation, ten-fold higher levels of hydrogen peroxide by foamy alveolar macrophages, enhanced activity of matrix metalloproteinases (MMP), emphysema, and formation of fibrosis in the lungs (Wert et al., 2000).

In addition to its protective role against lung pathogens, SP-D may also have actively involved in the initial protective immunity against airway inflammation and asthma. The most well

characterized functional studies of SP-D have been shown using allergy and infection models with reference to opportunistic fungal pathogens. Native full-length SP-D has shown to bind to glycoproteins on A. fumigatus and house dust mite (*Dermatophagoides pteronyssinus*) via its CRD region, and enhancing uptake, phagocytosis, and oxidative burst by neutrophils and alveolar macrophages (Madan et al., 1997a), thus, inhibiting specific immunoglobulin E (IgE) binding to these allergenic extracts, and blocking subsequent allergy-induced histamine release from isolated sensitized basophils (Wang et al., 1996, Madan et al., 1997a, Madan et al., 1997b). An inhibitory effect of SP-D on allergen-induced peripheral blood mononuclear cells (PBMC) proliferation has also been reported in mite-sensitive asthmatic children (Wang et al., 1998). Suppressive effect of SP-D on the secretion of IL-2 by peripheral blood mononuclear cell (PBMC) was also observed (Borron et al., 2000).

The therapeutic effects of exogenous administration of human SP-D and a recombinant fragment of human SP-D, composed of homotrimeric neck and CRD regions (rfhSP-D), was examined in an allergic bronchopulmonary aspergillosis (ABPA) murine model. An extensive infiltration of lymphocytes and eosinophils were seen in the lung sections of the ABPA mice, which were significantly reduced following SP-D/rfhSP-D treatment. Decreased levels of IL-2, IL-4 and IL-5, and an increased level of interferon gamma (INF- γ) in supernatant of the cultured splenocytes were reported, highlighting Th2 to Th1 polarization (Madan et al., 2005). One of the highlights of these studies was that rfhSP-D, representing a small portion (60kDa) of the full-length native human SP-D molecule (540kDa), was also able to protect ABPA mice from allergen provocation. This truncated rfhSP-D was reported to mimic the same therapeutic effect as full-length SP-D; it can therefore bind directly to allergens, prevents interaction between allergens and IgE, block sensitized basophils-mediated histamine release, as well as suppress proliferation of lymphocytes *in vitro* (Madan et al., 1997b, Wang et al., 1998). Similar protective effects of rfhSP-D have also been observed in a murine model of pulmonary hypersensitivity induced by *Derp* allergens (Singh et al., 2003). A significant reduction in *Derp*-specific IgE levels, eosinophilia and pulmonary cellular infiltration were seen with rfhSP-D treatment (Singh et al. 2003). IL-4 and IL-5 levels were decreased, while supernatant of the cultured splenocytes showed an enhanced level of IL-12 and INF-γ, suggesting a Th2-Th1 polarization (Singh et al., 2003).

1.3.5 SP-D interaction with tumour cells

Studies using *in vivo* and *in vitro* cancer models have convincingly demonstrated an involvement of SP-D in the immune surveillance against tumour cells. Anti-leukemic properties by both native and rfhSP-D have been reported using an eosinophilic cell line, AML14.3D10 (Figure 4) (Mahajan et al., 2013, Mahajan et al., 2014). rfhSP-D was observed to bind AML14.3D10 cell line in a dose and calcium-dependent manner. rfhSP-D treatment caused G2/M arrest, with an enhanced p21 level, and Try15 phosphorylation of cdc2 (Figure 4). Activation of pro-apoptotic markers, including cleaved caspase 9 and 3, was also noted following the rfhSP-D treatment, suggesting the involvement of intrinsic apoptotic pathway. rfhSP-D also caused down-regulation of pro-survival HMGA1 (high-mobility group A1) protein, in addition to reducing cell viability of acute lymphoid leukemia cell lines (Jurkat and Raji) and human breast epithelial cell line (MCF-7). However, rfhSP-D treatment did not cause any cell viability reduction in human PBMCs from the healthy controls. Pandit et al. subsequently revealed that rfhSP-D could induce apoptosis in activated PBMCs, but not in non-activated PBMCs by regulating the expression of immunomodulatory receptors and cytokines (Pandit et al., 2016). rfhSP-D treatment significantly downregulated pro-inflammatory receptors, such as CD65, TLR2, TLR4 and CD11c, down-regulated Th1 cytokines, IFN- γ, as well as TNF-α (Tumor necrosis factor alpha) and IL-6 following rfhSP-D. However, Th2 cytokines including IL-4, and anti-inflammatory cytokines, IL-10 as well as TGF- β (Transforming growth factor beta) levels were not significantly affected (Pandit et al., 2016). These studies highlighted the possible immune surveillance role of SP-D against activated cells.

Down-regulation of epidermal growth factor (EGF) signaling by exogenous SP-D treatment has also been reported (Hasegawa et al., 2015). SP-D was able to prevent the interaction between EGF and EGFR (epidermal growth factor receptor), and suppressed cell proliferation, invasion, and migration of A549 cells. SP-D appeared to bind the N-glycans of EGFR via its CRD regions, leading to downregulation of EGF signaling (Hasegawa et al., 2015). Kaur et. subsequently reported anti-tumour role of SP-D against pancreatic cancer, using p53 mutant (mt) and wild-type (wt) pancreatic adenocarcinoma cell lines (Kaur et al., 2018a). rfhSP-D treatment resulted in G1 cell cycle arrest and triggered up-regulation of pro-apoptotic markers including TNF-α. and

NF-κB. NF-κB translocation from the cytoplasm into the nucleus of Panc-1, MiaPaCa-2, and Capan-2 pancreatic cancer cells was also evident. Activation of Fas following rfhSP-D treatment resulted in cleavage of caspase 8 and 3, leading to induction of apoptosis regardless of the p53 status via extrinsic pathway at 48h (Kaur et al., 2018a). In addition, suppression of epithelial–to-mesenchymal transition (EMT) and related gene signatures by rfhSP-D treatment has also been reported (Kaur et al., 2018a). Reduction in the cell invasiveness of Panc-1 and MiaPaCa-2 cells was also observed following rfhSP-D treatment, as evident from downregulation of TGF-β; Vimentin, Zeb1, and Snail expressions when compared to untreated cells were considerably reduced (Kaur et al., 2018b) . Another study using an ovarian cell line, SKOV3, reported apoptosis induction by rfhSP-D via Fas-mediated pathway (Kumar et al., 2019). Activation of caspase 3 cleavage and expression of Fas and TNF-α were observed in rfhSP-D treated SKOV3 cells. rfhSP-D treatment also triggered downregulation of mTOR (mammalian target of rapamycin) pathway in both pancreatic and ovarian cell lines as evident by decreased mRNA levels of Rictor (rapamycin-insensitive companion of mTOR) and Raptor (regulatory-associated protein of mTOR) in treated cells, explaining the possible inhibitory mechanisms of cell growth and proliferation (Kumar et al., 2019, Kaur et al., 2018a).

Anti-cancer effects of rfhSP-D has also been reported in androgen-resistant and androgen-responsive prostate cancer cells involving p53 and pAkt pathways (Figure 5) (Thakur et al., 2019). Upregulation of BAX, Bcl2, cytochrome C and cleaved caspase 7 expression was seen with rfhSP-D treatment, suggesting the apoptotic trigger via intrinsic pathway. In a bioinformatics study, elevated SP-D mRNA expression in ovarian and lung cancers appeared to correlate with a favorable prognosis (Mangogna et al., 2018). Recently, Murugaiah et al. reported protective effects of rfhSP-D against breast cancer cell lines (Murugaiah et al., 2020a). rfhSP-D induced apoptosis in triple-positive ($ER^+/PR^+/HER2^+$) and $HER2^+$-over-expressing breast cancer cell lines (BT474 and SKBR3) via intrinsic pathway, while no effect in triple-negative breast cancer cell line (BT20). Hyaluronic acid (HYA), an abundant component of the extracellular matrix (ECM), was found to interact with rfhSP-D; this interaction negated the anti-tumour properties of rfhSP-D against BT474 and SKBR3 breast cancer cell lines (Murugaiah et al., 2020a). rfhSP-D treated cells in the presence of HYA were unable to induce apoptosis in both BT474 and SKBR3 cell lines. These

studies therefore suggest the potential immune surveillance role of SP-D against a wide range of tumour cells and modulation of downstream signaling pathways.

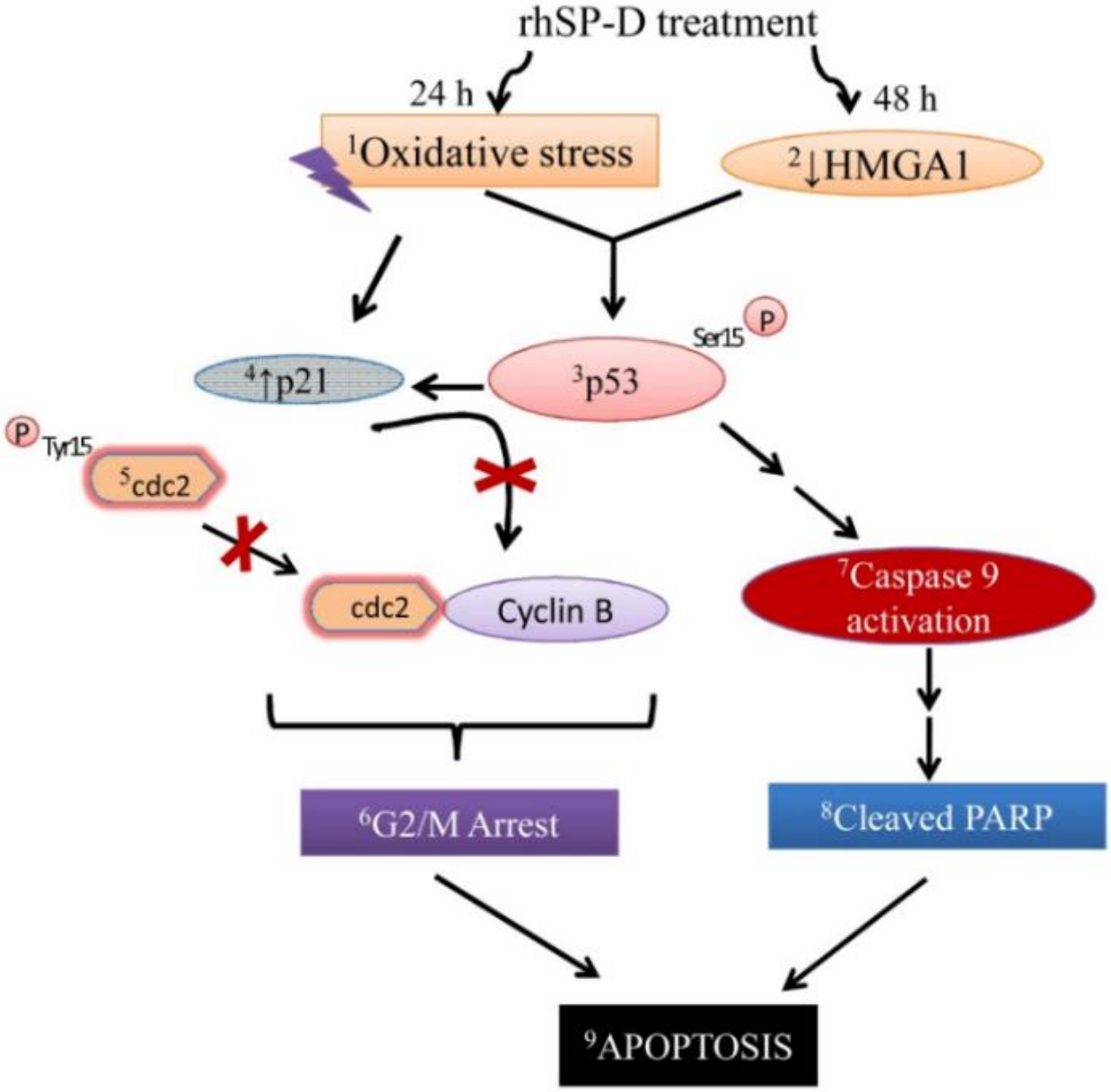

Figure 4: Proposed mechanism for apoptosis induction by rfhSP-D in AML14.3D10 leukemic cell line.

Increased oxidative stress and HMGA1 downregulation was observed in rfhSP-D treated AML14.3D10 cells. P21 levels were upregulated following rfhSP-D treatment, which resulted in cell cycle arrest at G2/M phase. Phosphorylation of P53 and activation of cleaved caspase 9 further triggered cleavage of Poly (ADP-ribose) polymerase (PARP), and subsequent apoptosis induction by rfhSP-D treatment (Mahajan et al., 2013).

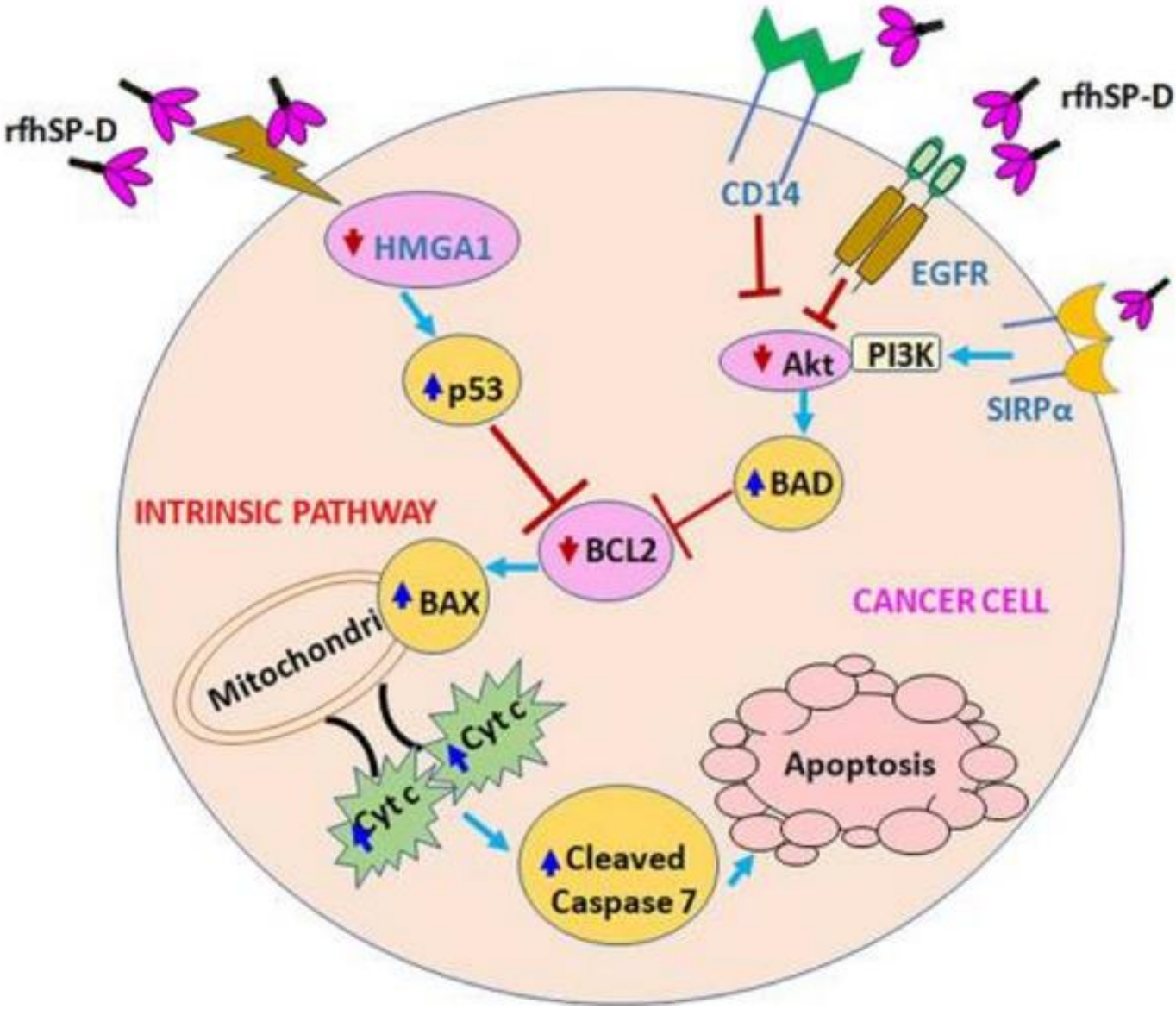

Figure 5: Proposed mechanisms for rfhSP-D mediated apoptosis in prostate cancer cells.

rfhSP-D treatment induces upregulation of p53 and downregulation of pAkt pathway, leading in increased expression levels of Bad, Bax, and release of cytochrome c, thus, result in cleavage of caspase 7. Interaction of SP-D with HMGA1, SIRPα, CD14, and EGFR has been reported in previous studies and may be important as part of the proposed mechanisms of p53 and Akt (Thakur et al., 2019).

1.4 Influenza A Virus (IAV)

Influenza A virus (IAV) is an enveloped RNA virus and a member of Orthomyxoviridae family that possess eight single-stranded RNA segments in negative orientation (Le et al., 2005), which encode up to thirteen viral proteins, including two surface glycoproteins, an ion Chanel protein, nucleocapsid protein, structural scaffolding protein, a tripartite polymerase complex, two non-structural proteins, and three non-essential proteins (Le et al., 2005). Influenza viruses are classified into five different genera, such as influenza A, influenza B, influenza C, Thogotovirus, and Isavirus (Shao et al., 2017). Among all the five genera of influenza viruses, IAV infection is most common and it causes severe respiratory infection in humans, swine and avian species. Being diverse in host specificity, it is also well known to cause pandemic. IAV was shown as a major human respiratory pathogen during 1918 pH1N1 influenza pandemic (Taubenberger and Kash, 2010), which is believed to have resulted from zoonotic transmission of an avian virus (Taubenberger and Kash, 2010). However, the pathogenicity of the 2009 H1N1 pandemic virus (H1N1) is reported to be more severe compared to seasonal IAV in humans.

1.4.1 Structure of IAV

The IAV genome is composed of eight single stranded viral RNA segments (Table 2), encoding for the eleven viral genes; hemagglutinin (HA), neuraminidase (NA), matrix protein 1 (M1), matrix protein 2 (M2), nucleoprotein (NP), non-structural protein 1 (NSP1), nuclear export protein (NEP), polymerase acidic protein (PA), RNA-polymerase subunit 1 (PB1), RNA-polymerase subunit 2 (PB2), and RNA-polymerase subunit 1-frame 2 (PB1-F2) (Samji, 2009, Nayak et al., 2009, Scheiffele et al., 1999, Palese et al., 1974).

The IAV is organized within a lipid bilayer that is comprised of three transmembrane proteins: HA, NA and M2 (Figure 6) (Scheiffele et al., 1999) (Zhang et al., 2000). HA is a viral envelope glycoprotein (80 kDa monomer), a spike-shaped trimer extending outward from the envelope or lipid layer (Scheiffele et al., 1999). HA protein initiates the life cycle of IAV by binding to sialic acid receptors on host cell surface. It also plays a crucial role in mediating fusion between the endocytic vesicle and viral membrane during penetration, thereby, facilitating the release of the viral genome into the cytoplasm (Zhang et al., 2000). Proteolytic cleavage of HA from HA0 generates two domains; HA1 and HA2, which, performs essential functions for viral entry into

infection-susceptible cells and the form globular head structure by HA1 at the end of the HA protein, which is responsible for the virus attachment to sialic acid residues of host cell glycoproteins (Samji, 2009).

NA is an exo-sialidase (60 kDa monomer), which cleaves α-ketosidic linkage between the sialic acid (also referred as to N-acetylneuraminic acid) and an adjacent sugar residue (Shtyrya et al., 2009). The well-established nine subtypes of NA are divided into two phylogenic groups: the first group containing N1, N4, N5 and N8 subtypes, and the second one with N2, N3, N6, N7 and N9 subtypes (Shtyrya et al., 2009). The NA molecule comprises 470 amino acid residues and oligomerizes to form a homotetramer that has cytoplasmic, transmembrane, head and stem domains. In addition, the N-terminus of NA anchors to the viral membrane and the head domain consists of enzymatic activity which is required for the cleavage of sialic acid (McAuley et al., 2019). NA protein is also critical for the budding of newly synthesized viral particles, as well as for preventing viral aggregation (Palese et al., 1974). While coming across the respiratory tract mucins, NA cleaves neuraminic acid residues, which facilitates movements of viral particles to the target cell (McAuley et al., 2019).

M2 is a type-III integral membrane protein which has important roles in virus entry, assembly and budding. M2 consists of a short ectodomain, a transmembrane domain, and a cytoplasmic tail (Park et al., 1998, Iwatsuki-Horimoto et al., 2006). Like HA and NA, it is translated in the ER membrane and delivered to the apical plasma membrane, but it does not associate with lipid rafts. M2 can stabilize the site of budding, and enables polymerisation of the matrix protein, as well as formation of filamentous virions (Rossman and Lamb, 2011). In addition, it is also crucial for altering membrane curvature at the neck of the budding virus, resulting in membrane scission and causing the release of the progeny virion (Rossman and Lamb, 2011). M2 has also been shown to form a tetrameric proton ion channel that enables acidification of the interior of the virion, resulting in conformational changes and uncoating of the ribonucleoprotein complexes (RNP) viral complex (Pielak and Chou, 2011).

M1 protein, the most abundant protein, lies beneath the lipid layer, and it is, essential for viral stability and integrity. M1 can bind to cytoplasmic tails of HA and NA molecules (Enami et al.

1996), therefore, it can polymerise and form the emerging viral interior structure. Additionally, the cytoplasmic tail-bound M1 serves as a docking site for the recruitment of the viral RNPs through its C-terminal domain (Zhang et al., 2017). M1 localizes at the apical plasma membrane (Kerviel et al., 2016) through its interaction with lipids and cytoplasmic-exposed portions of HA, NA and M2 (Kerviel et al., 2016). Once at the plasma membrane, subunits of M1 proteins interact with each other to form a scaffolding matrix for the assembly of newly synthesized viral particles (Pohl et al., 2016).

Other IAV proteins that make up viral RNPs, including NP, PA, PB1 and PB2, have nuclear localization signals, which can interact with cellular nuclear import machinery. For the influenza genome to be transcribed, the negative sense RNA is converted into positive sense RNA, which can serve as a template for viral RNA production. The synthesis of viral RNA is then triggered by viral RNA-dependent RNA polymerase (RdRp) (Pohl et al., 2016). Once the viral RNPs are exported from the nucleus, the enveloped virions use the plasma membrane of the host cells to form new viral particles that can infect other cells. One of the crucial steps that occurs before newly made virions leave the plasma membrane is the cleavage of sialic acid residues by NA, which is essential for the export of the viral particles from the plasma membrane (Palese et al., 1974).

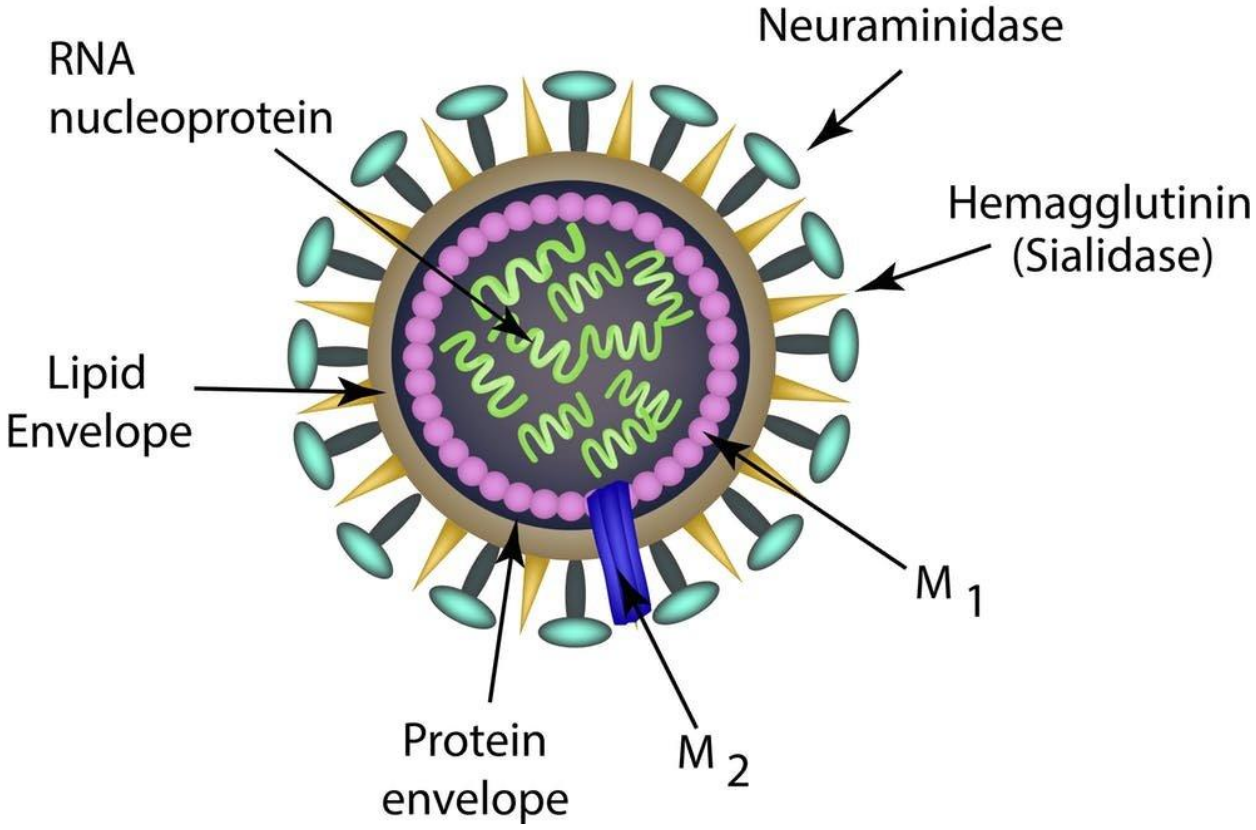

Figure 6: Life Cycle of Influenza A Virus (IAV).

The surface of the virus is covered with the glycoproteins- hemagglutinin (HA) that looks like a spike, and mushroom-shaped neuraminidase (NA) frequently intersperesed with matrix 2 (M2) proteins. The interior of the virus contains the ribonucleoprotein (RNP) complex, which is a complex formed with the binding of the vRNA, RNA polymerase complex and influenza virus nucleoprotein (NP). HA and NA occur in a 4:1 ratio (Bouvier and Palese, 2008).

1.4.2 Replication of IAV

Infection and multiplication of IAV involves receptor binding and cell entry, membrane fusion and uncoating of the viral core, RNA replication and translation, assembly and budding of progeny virions (Figure 7). Binding of the viral HA to sialic acid residues on glycoproteins on the host cell surface. The HA binding specificity depends on the nature of the terminal glycosidic linkage between the sialic acid and the penultimate galactose residues on the glycan receptors on the host cell (Byrd-Leotis et al., 2017). Following receptor binding, the uptake of the virus occurs through receptor mediated endocytosis, where viral particles are engulfed by the plasma membrane of the host cell. As a result, the virus is transported to the endosomal lumen (Byrd-Leotis et al., 2017). The uptake of substances by endocytosis generally ends up in lysosomes and degraded by hydrolytic enzymes. However, the IAV genome escapes degradation through viral fusion with the endosomal membrane and enters the cell.

The acidic pH present in the endosomal vesicles triggers fusion of the viral membrane with the host, by inducing conformational changes in HA, exposing the fusion peptide, the HA2 domain of HA (Samji, 2009). The acidic environment of the endosome also opens the matrix 2 (M2) protein ion channel. Opening M2 channel facilitate acidification of interior of the viral core. This leads to the release of the viral RNP (vRNP) complex, which is free to enter the host cell's cytoplasm (Samji, 2009). The vRNP complex consists of viral proteins such as NP, PA, PB1 and PB2, and these proteins are known to have nuclear localization signals (NLSs). The released vRNP complex is delivered to the nucleus, where trimeric viral polymerase complex (PB1, PB2 and PA) transcribes viral RNAs to positive sense mRNAs. The mRNAs are then delivered back to the cell cytosol and translated to viral proteins. Subsequently, M1 protein initiates its interaction with C-terminal domain of HA and NA found on plasma membrane, leading to formation of high -density patches of HA and NA (Das et al., 2010). Following the attachment of newly formed vRNPs to M1 on the cell plasma membrane, new virus particles are assembled. NA protein is also involved in the cleavage of sialic acid, either from host cells or virion glycoprotein, resulting in the release of virion, thus prevents their aggregation (Matsuoka et al., 2013). NS1 is also known to play a critical

role in the regulation of influenza virus replication, although it is not incorporated into the virion (Matsuoka et al., 2013).

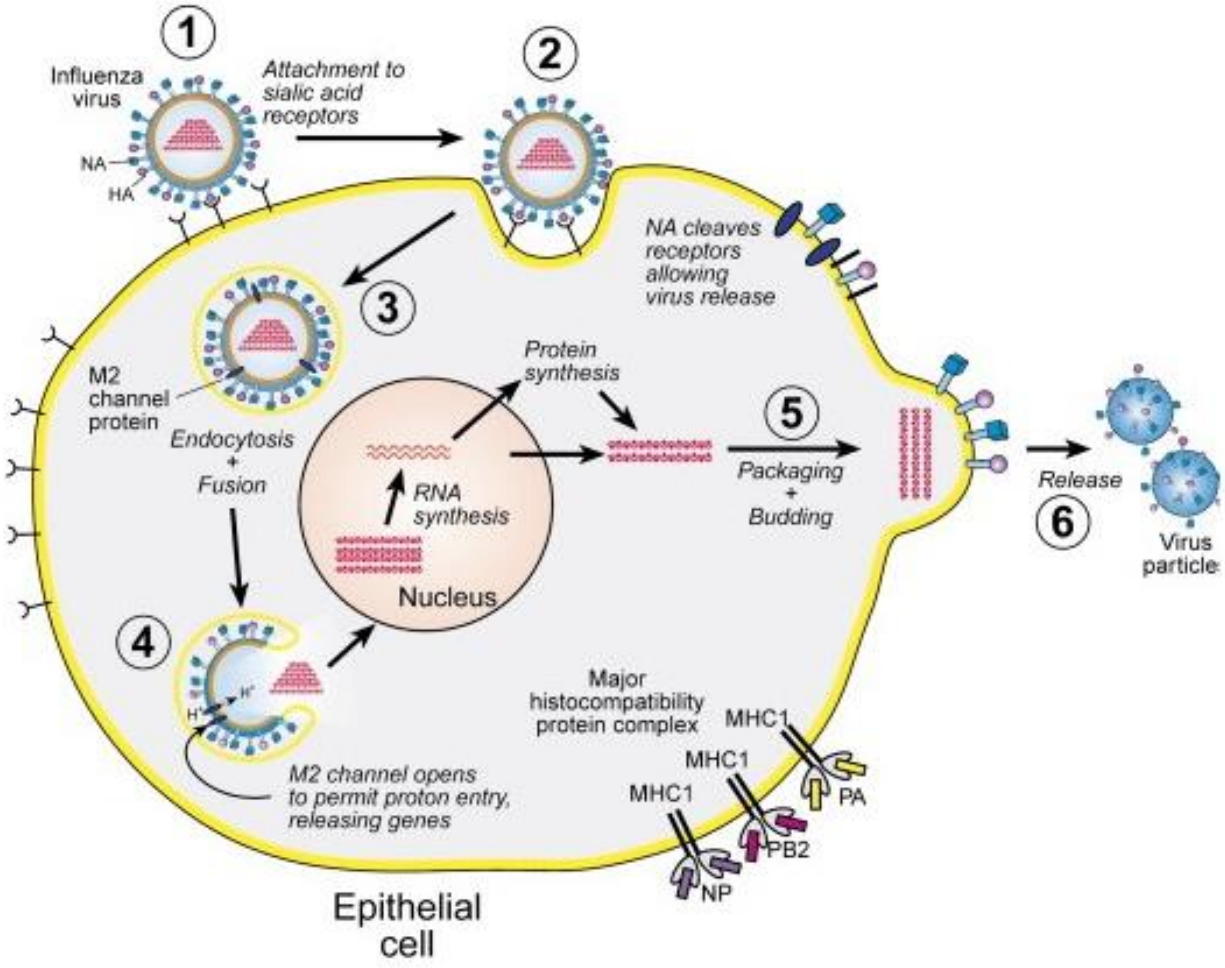

Figure 7: Life Cycle of Influenza A Virus (IAV).

1,2: Hemagglutinin (HA) protein binding to sialic acid attaches virus to cell. 3: Virion is internalized by endocytosis and fusion. 4: M2 channel opening allows proton flow across the viral membrane. This leads to fusion of viral and endosomal membranes which releases the viral genes which is transported to the nucleus. 5: Proteins and genes assemble and bud as virions from the cytoplasm. 6: Viral neuraminidase (NA) cleaves sialic acid receptors from the cell membrane releasing virions (Subbarao et al., 2006).

1.4.3 Host innate defense mechanisms against IAV

Both innate and adaptive responses are stimulated when IAV infects the cells of the respiratory tract. The innate immunity is critical in the early stage of infection and induces the production of cytokines and chemokines, either by infected epithelial cells or monocytes/macrophages (Figure 8). Several soluble innate inhibitors provide an initial infection barrier. Dendritic cells (DCs), phagocytes and natural killer (NK) cells, attracted to the site of infection, also mediate viral clearance, and promote innate and adaptive responses. Activation of these responses requires Toll-like receptors 3/7 (Figure 8) and cytoplasmic RNA sensors (Paulson et al., 2012). Following influenza virus infection, NK cells enhance responses of both DCs and adaptive T cells (Elton et al., 1999). Macrophages infected with IAV produce chemokines such as monocyte chemoattractant protein-1 (MCP-1), RANTES (CCL5), monocytes, and macrophage inflammatory protein 1 alpha (MIP-1α). This leads to recruitment of mononuclear cells to the lungs, to facilitate viral clearance (Kaufmann et al., 2007). NKT cells, $CD8^+$ T cells, and macrophages prevented IAV infected mice from severe influenza induced diseases (Tessmer et al., 2009). Type I interferon is also essential for NK cell responses of both IFN-γ and granzyme B in response to influenza infection (Madera et al., 2016). DC can be also infected by influenza viruses; however, the infection is abortive and does not produce progeny virus (Taubenberger and Kash, 2010). Some studies have demonstrated that highly pathogenic H5N1 viruses can replicate in both human and mouse DCs, leading to cytopathic effects (Peiris et al., 2009).

1.4.4 Role of cytokines and chemokines in IAV infection

Cytokines and chemokine play a pivotal role in establishing virus-specific immunity. However, uncontrolled activation of immune cells may result in dysregulated homeostasis, leading to pathological manifestations. In vitro experiments have revealed conflicting evidence of influenza virus mediated cytokine responses. IAV infection was shown to induce up-regulation of pro-inflammatory IL-1β, IL-6, TNF-α, CCL-2 (MCP-1), CCL3 (RANTES), CCL3 (MIP1-α) and CXCL10 (IP-10) (Perrone et al., 2008). IL-17, involved in the activation and migration of neutrophils, has pathological effects following infection (Lamichhane and Samarasinghe, 2019). A bronchial epithelial cell line (NCI-H292), infected with IAV (H3N2), produces significant amount of IL-6, IL-8 and RANTES (Matsukura et al., 1996). In addition, interferons are produced at the site of viral

infection, which are classified in two subtypes; type I (IFN-ß and IFN-α) and type II (IFN-γ) (Figure 8) (Matsukura et al., 1996). In addition, potent antiviral properties are possessed by type-I IFN, which is pivotal in controlling infection with IAV.

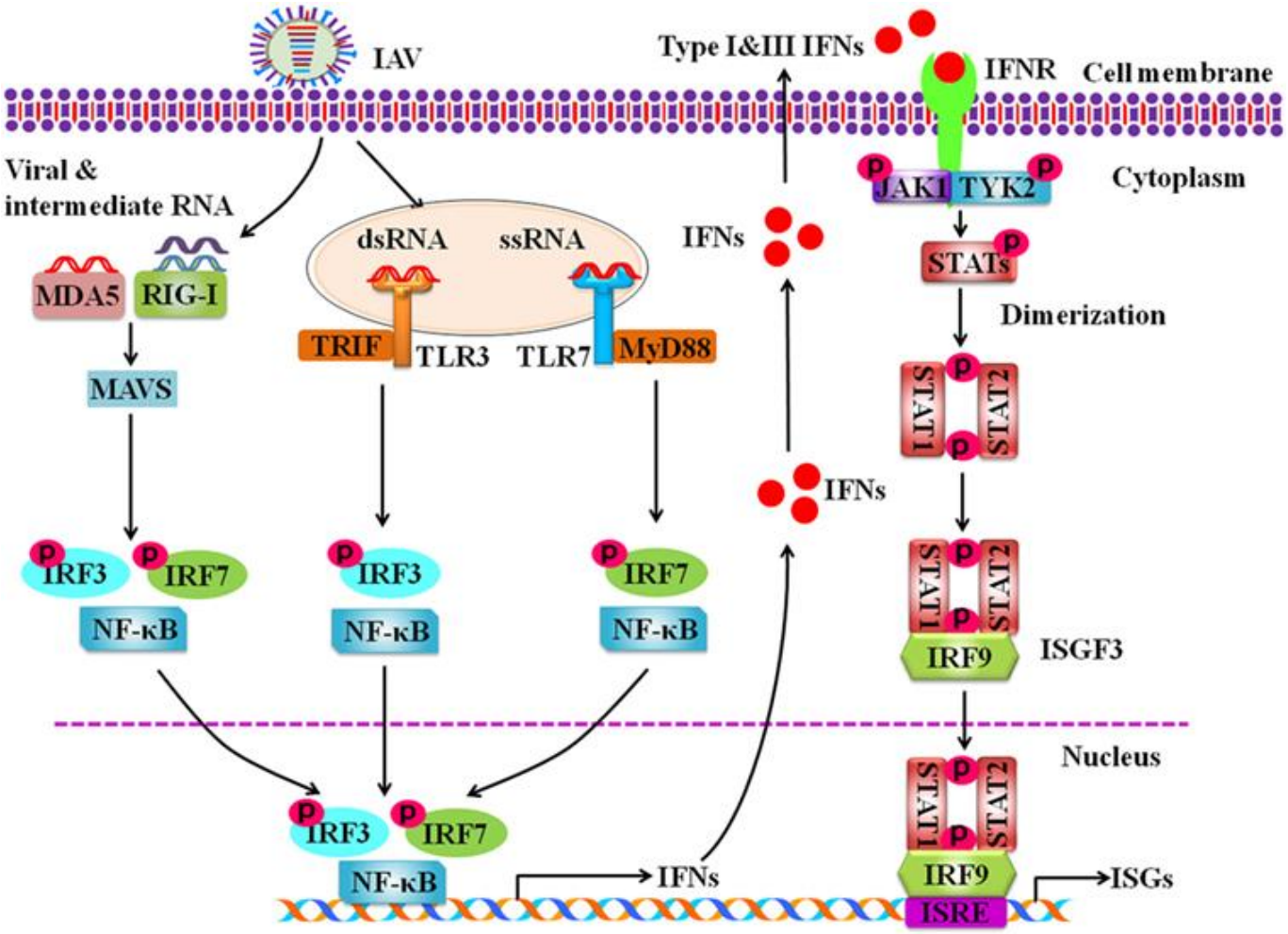

Figure 8: Innate Immune Response against Influenza A Virus (IAV) Infection.

Recognition of intracellular IAV infection by the host pathogen recognition receptors (PRRs) triggers NF-κB, interferon regulatory factor 3 (IRF3), and IRF7. Retinoic acid-inducible gene-I protein (RIG-I), melanoma differentiation-associated gene 5 (MDA5), and toll-like receptors (TLRs) are well known PRRs. Activated transcription factors, in turn, activate type I and type II interferons (IFNs), which are secreted by the infected cells. Interaction of IFNs with their receptors leads to activation of Janus kinase (JAK)-signal transducer, further triggering the transcription signaling pathways that induces the expression of other IFN-stimulated genes (Chen et al., 2018b).

Table 2: Influenza A Virus (IAV) genome structure and function.

Genome Segment	Protein	Location in virion	Functions
1	RNA-polymerase subunit 2 (PB2)	Internal	Trascription/capping/ replication
2	RNA-polymerase subunit 1 (PB1) PB1-Frame 2 (PB1-F2)	Internal Non-strcutural cellular	Trascription/replication Apoptosis
3	RNA-polymerase subunit (PA)	Internal	Trascription/replication
4	Hemagglutinin (HA)	Transmembrane	Receptor/uncoating
5	Nucleoprotein (NP)	Internal	RNA-synthesis
6	Neuraminidase (NA)	Transmembrane	Viral release
7	Matrix Protein 1 (M1) Matrix Protein 2 (M2)	Internal Trasnsmembrane	Assembly/regulation Uncoating
8	Non-structrual protein 1 (NS1) Nuclear-export protein (NEP)	Non-stractural Internal	IFN-antagonist Nuclear export

1.5 Innate immune surveillance in cancer

The ability of innate immune system to recognise and eliminate cancer cells has been studied for many years using *in vitro*, *in vivo* and *ex vivo* models. Thus, immune cells, effector molecules, and signalling pathways work together as extrinsic tumour suppressor mechanisms. Carciogensis is associated with accumulation of genetic and epigentic events. Such events rapidly change the phenotye of the cells via the modification in the morphology, structure, and membrane components of the cell (including abnomal glycosylation and orgin tumour-drived antigens (Hakomori, 2002). The major roles of the innate immune system against carcinogenesis include eliminating or inhibiting viral infections; tumour elimination based on the expression of tumour-specific antigens induced by cellular stress, and tumour immune surveillance (Gonzalez et al., 2018). However, the formation of tumours can also be caused in the presence of functioning immune system, and whereby tumour immunoediting (Figure 9) (Swann and Smyth, 2007). has been discovered to explain the complete role of immune system during tumour development.

The tumour immunoediting concept is subdivided into three main phases; elimination, equilibrium and escape (Figure 9) (Swann and Smyth, 2007). The elimination phase includes both innate and adaptive responses, where the immune system detects and eliminates tumour cells as a result of failed intrinsic tumour suppressor mechanisms. For example, innate effectors NK, NKT and Gamma delta (γδ) T cells are activated as a result of pro-inflammatory cytokines, which are released by macrophages, stromal and tumour cells. The cytokines in turn, recruit additional immune cells, where they produce interlukins 12 (IL-12) and interferon gamma (IFN-γ) to eliminate the invading tumour cells. In addition, Perforin-, FasL- and TRAIL-mediated killing of tumour cells result in the release of tumour antigens, which further leads to adaptive immune responses (Kim et al., 2007). As a result of cross-interaction between NK and dendritic cells (DCs), maturation of DCs is promoted by NK cells; thus, resulting in tumour antigen presentation to naïve T cells.

During the equilibrium process, the newly produced tumour variants that have overcome the elimination phase enter into the dynamic equilibrium, whereby tumour cells with reduced immunogenicity undergo immune selection (Mittal et al., 2014). During this process, both lymphocytes and IFN-γ plays a crucial role in exerting immune selection pressure tumour cells.

Thus, original tumour variants are killed, while new variants with mutations increase their resistance to immune attack, thus, proceed to the escape phase. In the escape phase, tumour cells continue to grow and proliferate progressively amidst an immunosuppressive tumour microenvironment (Rabinovich et al., 2007).

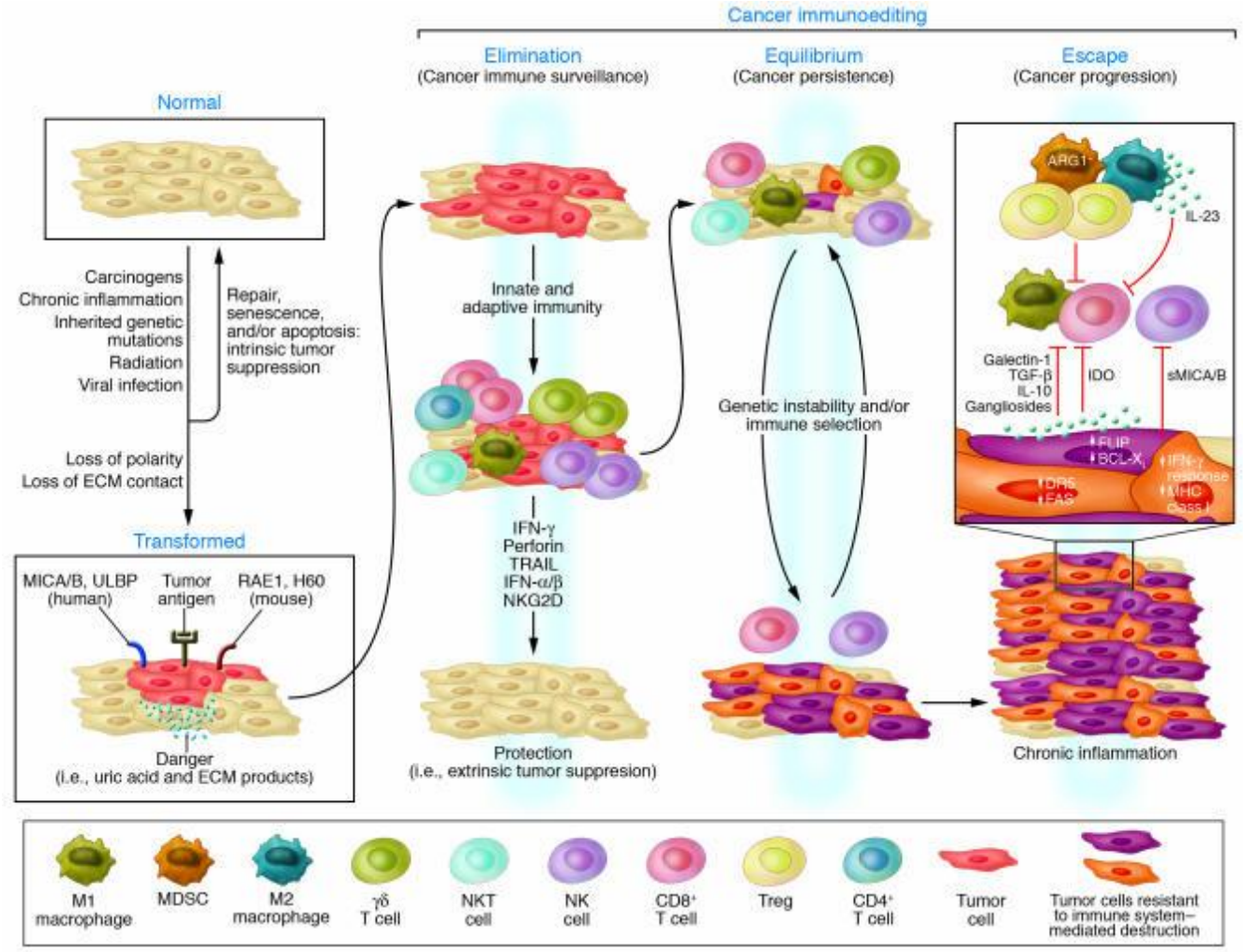

Figure 9: Extrinsic tumour suppressor mechanisms by the immune system.

Cancer immunoediting is subdivided into three main phases: elimination, equilibrium, and escape. Normal healthy cells undergo aberrant transformation in response to oncogenic stimuli. During the initial stage of tumour development, tumour specific antigens and markers is expressed by these transformed cells, thus, may secrete danger signals. This initiates immunoediting process, which begins with elimination phase, whereby transformed cells are subjected to elimination by the innate and adaptive immune system. As a result of incomplete event of elimination, the cancer cells enter the equilibrium phase, whereby, they alter the immune responses and causes production of new tumour variants. During the escape phage, the newly produced tumour variants become resistant over the immune responses (Swann and Smyth, 2007).

1.5.1 Breast cancer

Breast cancer is the foremost regularly diagnosed cancer among women around the world (Ferlay et a. 2008), causing approximately 60% mortality in lower-income countries (Coleman et al. 2018). There is an estimated 5-year survival rate of ~80% in developed nations, and below ~40% in low-income nations (Coleman et al., 2018).

Breast cancer is characterised by an irregular development of abnormal cells within the mammary glands. The physiological conditions that lead to breast tumorigenesis incorporate acquired hereditary transformation and epigenetic alterations, which can lead to premalignant change in mammary cells. The transformed cells then undergo elimination by intrinsic or extrinsic tumour mechanisms (Figure 9). Thus, development of advanced breast tumour is a consequence of immune selection and immune evasion. Breast cancer is subdivided into five different molecular subtypes; luminal A, luminal B, triple negative, human epidermal growth factor receptor (HER) 2 enriched, and normal-like breast cancer (Table 3). The progression and metastasis of breast tumours appear to be affected by intrinsic innate immune surveillance molecules and inflammatory mediators within the tumour microenvironment (described in section 1.4) (Goldberg and Schwertfeger, 2010).

1.5.2 Conventional Modalities of Treating Breast cancer

There are several conventional treatment options available for breast cancer patients, including surgery, radiation therapy (RT), chemotherapy (CT), endocrine (hormone) therapy (ET), and targeted therapy (Dhankhar et al., 2010). Breast conservation surgery is performed for localized breast tumours (Matsen and Neumayer, 2013), thus, the surgery is preceded by adjuvant therapy to shrink the tumour mass and prevent metastasis (Dhankhar et al. 2010). Tumour cells that may not be detected during surgery can be eliminated by RT to minimize the risk of local cancer recurrence (Dhankhar et al., 2010). Combination of RT and CT after surgery can also shrinks the tumour (Akram and Siddiqui, 2012), with some side effects, including reduced sensation in the breast tissues, and other skin-related problems. ET is administered to either balance or block the respective hormones (Dhankhar et al., 2010). Tamoxifen is used as an ER antagonist in premenopausal women, which is also associated with an increased risk of endometrial

hyperplasia, endometrial cancer, and other thromboembolic complications (Hirsimaki et al., 2002). Fulvestrant is prescribed to postmenopausal women diagnosed with hormone receptor-positive and HER2-negative metastatic breast cancer (Rocca et al., 2018, Nathan and Schmid, 2017).

Trastuzumab has been developed to treat early-stage or advanced-stage/metastatic $HER2^{+}$ positive breast cancer patients (Boekhout et al., 2011). Pertuzumab is also used as an adjuvant therapy to treat patients with HER2-positive early-stage breast cancer (Swain et al., 2015). These anti-HER2 therapies have shown promising results via inhibiting HER2/HER3 dimerization, and ligand-dependent signaling, as well as antibody-dependent cell-mediated cytotoxicity (Baselga and Swain, 2009, Scheuer et al., 2009). The use of anti-HER2 blockade therapies associated with CT (trastuzumab/lapatinib, or trastuzumab/pertuzumab) has shown improved outcome when compared to CT associated with using one anti-HER2 agent (Tsang and Finn, 2012). Dysregulation of mammalian target of rapamycin (mTOR) and phosphatidylinositol 3-kinase (PI3K) pathways has been reported in breast cancer (Vinayak and Carlson, 2013). mTOR inhibitor (everolimus) has shown promising anti-tumour activity in numerous cancers, including hormone receptor positive breast cancer (Yardley, 2013). Additionally, targeting cyclin -dependent kinases (CDKs) for cancer treatment has emerged as an effective option for treating hormone positive breast cancer patients (Mayer, 2015). Palbociclib-letrozole combination as an endocrine-based therapy has been used in post-menopausal women with $HER2^{-}/ER^{+}$ advanced breast cancer (Mayer, 2015). Furthermore, a potent inhibitor of CDK4/6 (abemaciclib) is under investigation (Gelbert et al., 2014).

Table 3: Summary of molecular subtypes of breast cancer, correlation with KI-67 staining by immunohistochemistry (IHC).

Molecular Subtype of Breast Cancer	Grade	IHC Status	Prevalence (%)	Reference
Luminal A	1|2	[ER+|PR+] $HER2^-$ $KI67^-$	23.7	(Cheang et al., 2009)
Luminal B	2|3	[ER^+|PR^+] $HER2^-$ $KI67^+$ [ER^+|PR^+] $HER2^+$ KI67+	38.8 14	(Cheang et al., 2009)
$HER2^+$ over-expression	2|3	[ER^-|PR^-] $HER2^+$	11.2	(Cheang et al., 2009)
Basal, Triple negative	3	[ER^-|PR^-] $HER2^-$, basal marker+	12.3	(Cheang et al., 2009)
Normal-like	1|2|3	[ER^+|PR^+] $HER2^-$ $KI67^-$	7.8	(Smid et al., 2008)

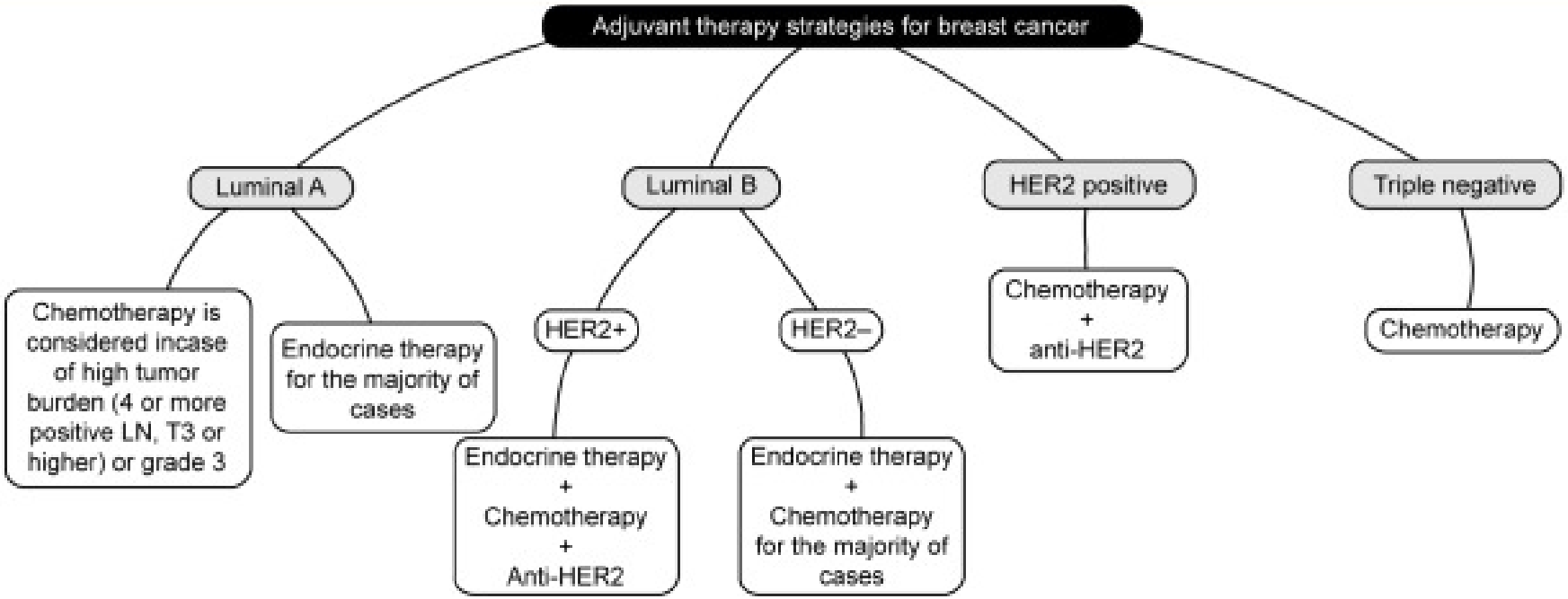

Figure 10: Illustration of the adjuvant therapy options used in breast cancer patients according to the molecular subtypes (Senkus et al., 2013).

1.5.3 Role of TAMs and MDSCs in breast cancer TME

TAMs in the breast cancer TME are involved in initiation of breast cancer progression and metastasis. Breast cancer epidemiological study has reported TAMs correlation with a poor clinical prognosis (Obeid et al., 2013). Anti-tumour T cell response suppression by TAM-derived anti-inflammatory cytokines is one of the known mechanisms of tumour evasion (Figure 11). Previous *in vivo* studies using animal models of breast cancer have suggested that IL-10 secreted by TAMs suppress the activation of $CD8^+$ T cell (Ruffell et al., 2014, DeNardo et al., 2011). Other studies have also suggested that decreased tumoricidal TAM activity is associated with tumour immune evasion. Down-regulation of IL-12 and iNOS (inducible nitric oxide synthase) is evident in macrophages isolated from the mouse breast cancer tissue (Handel-Fernandez et al., 1997, Dinapoli et al., 1996). Increased TAM infiltration is associated with enhanced angiogenesis (Leek et al., 1996, Ch'ng et al., 2011) in human breast cancer. As evident by a gene expression profiling study, TAMs (isolated from late-stage breast cancer) secreted 2-fold levels of angiogenesis-related mediators when compared to control cells (Ojalvo et al., 2009). Furthermore, human breast ductal carcinoma in situ (DCIS) and invasive ductal carcinoma (IDC) showed increased expression levels of urokinase receptor (uPAR) in TAMs found in the peritumoral region (Rabbani and Xing, 1998). In addition, cancer stem cells (CSCs) are triggered by various TAMs-derived cytokines, which affects the prognosis of breast cancer (Sainz et al., 2016). TAMs-derived IL-6 can promote prolongation of CSC-like features of cancer cells in both the premalignant and metastatic stages (Sainz et al., 2016). Furthermore, a proteomics study has reported the interaction of TAMs with breast CSCs in mediating ephrin type-A receptor 4 (EphA4) responses, thus, promoting tumorigenesis, as well as facilitating maintenance of CSCs (von Boehmer et al., 1989). In addition, TAMs are correlated with distant metastasis in triple-negative breast cancer (TNBC) tissues (Yuan et al., 2014). Enhanced number of TAMs-derived $CD68^+$/ VEGF-C^+ has been detected in human breast cancer tissues with lymph node metastasis (Yang et al., 2015, Ding et al., 2012). TAMs-derived CXCL1 [chemokine (C-X-C motif) ligand 1] has been suggested to increase metastasis in mouse and human breast cancer cell lines via nuclear factor (NF)-κB signaling (Wang et al., 2018).

In breast cancer, MDSCs play an important role in cancer development and progression (Figure 12). Recruitment of MDSCs to the tumour site is directed by various chemokines (Kumar et al. 2016, 26858199), such as CXCL5 (C-X-C motif chemokine 5) (Yang et al., 2008), CXCL12 (Ouyang et al., 2016), and C-C Motif Chemokine Ligand 2 (CCL2) (Huang et al., 2007). Higher levels of MDSCs is evident in breast cancer patients and is significantly associated with metastasis (Almand et al., 2000, Diaz-Montero et al., 2009). Furthermore, breast cancer patients undergoing chemotherapy show reduced levels of granulocytic MDSCs; lower levels of baseline MDSCs are also reported in chemo-responsive patients (Montero et al., 2012). Most tumour, including breast tumour, show an abundant level of granulocytic MDSCs in peripheral blood (Messmer et al., 2015); however, prostate cancer displays an increased level of monocytic MDSCs compared to granulocytic MDSCs (Solito et al., 2014).

In breast cancer, granulocytic MDSCs are triggered by IL-17 from tumor-infiltrating γδ T-cells, causing $CD8^+$ T-cell inhibition and promoting lymph node and lung metastasis (Coffelt et al., 2015). A study using murine model of breast cancer has reported the MDSC interaction with NK cells enhanced cancer metastasis by lowering the cytotoxicity of NK cells (Sceneay et al., 2012). The AKT signaling pathway is triggered by MDSCs in a mouse model (treated with human breast cancer cell line), which causes upregulation of matrix metallopeptidase (MMPs), thus, promoteing invasion and metastasis of cancer cells (Liu et al., 2012).MDSCs are also recruited by CCL3 derived from breast cancer cells, which triggers the PI3K-AKT-mTOR cascade, causing EMT induction, migration, and invasion of tumour cells (Luo et al., 2020).

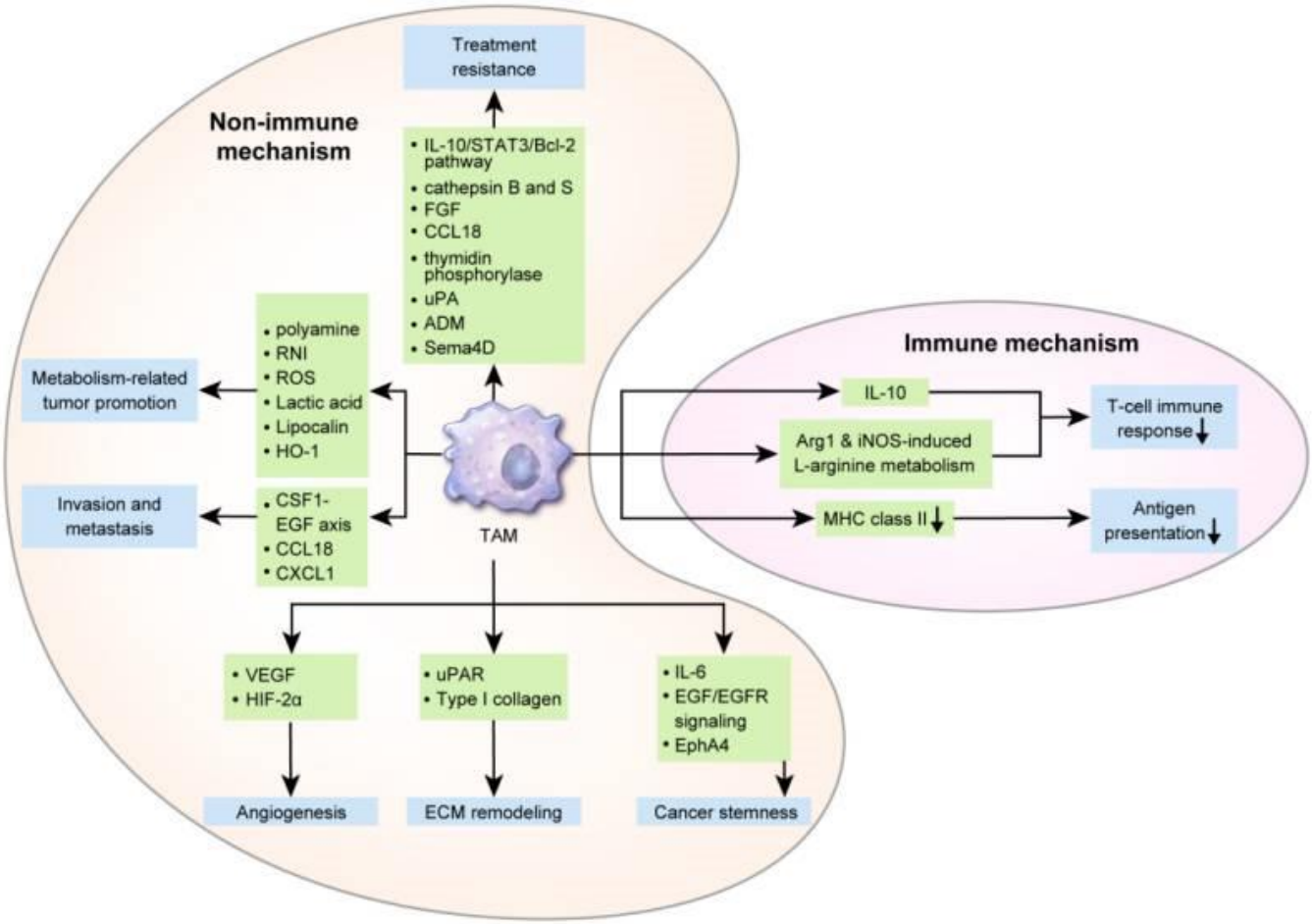

Figure 11: The role of tumor-associated macrophages (TAMs) in breast carcinogenesis.

The diagram underlines the key immunogenic mechanisms of TAM-derived IL-10 in breast cancer, which inhibits the T-cell response, and antigen presentation by downregulating the levels of major histocompatibility complex (MHC) class II. Non-immunological events include angiogenesis via VEGF and hypoxia-inducible factor (HIF)-2α production; extracellular matrix (ECM) remodeling via urokinase receptor (uPAR) and type I collagen release; cancer stemness evoking through secretion of IL-6, epidermal growth factor (EGF) and EGF receptor (EGFR) signaling. Cancer invasion and metastasis is contributed by TAMs via CCL18 (Chemokine ligand 18), and CXCL1 (C-X-C Motif Chemokine Ligand 1). Breast cancer progression is also promoted by TAM metabolites, including ROS (reactive oxygen species), lactic acid, lipocalin (LCN), and reactive nitrogen intermediates (RNI). TAMs-induced treatment resistance is supported by IL-10/STAT3/Bcl-2 signaling pathways and other immune factors [CCL18, thymidine phosphorylase, fibroblast growth factor, and urokinase-type plasminogen activator (uPA)] (Chanmee et al., 2014).

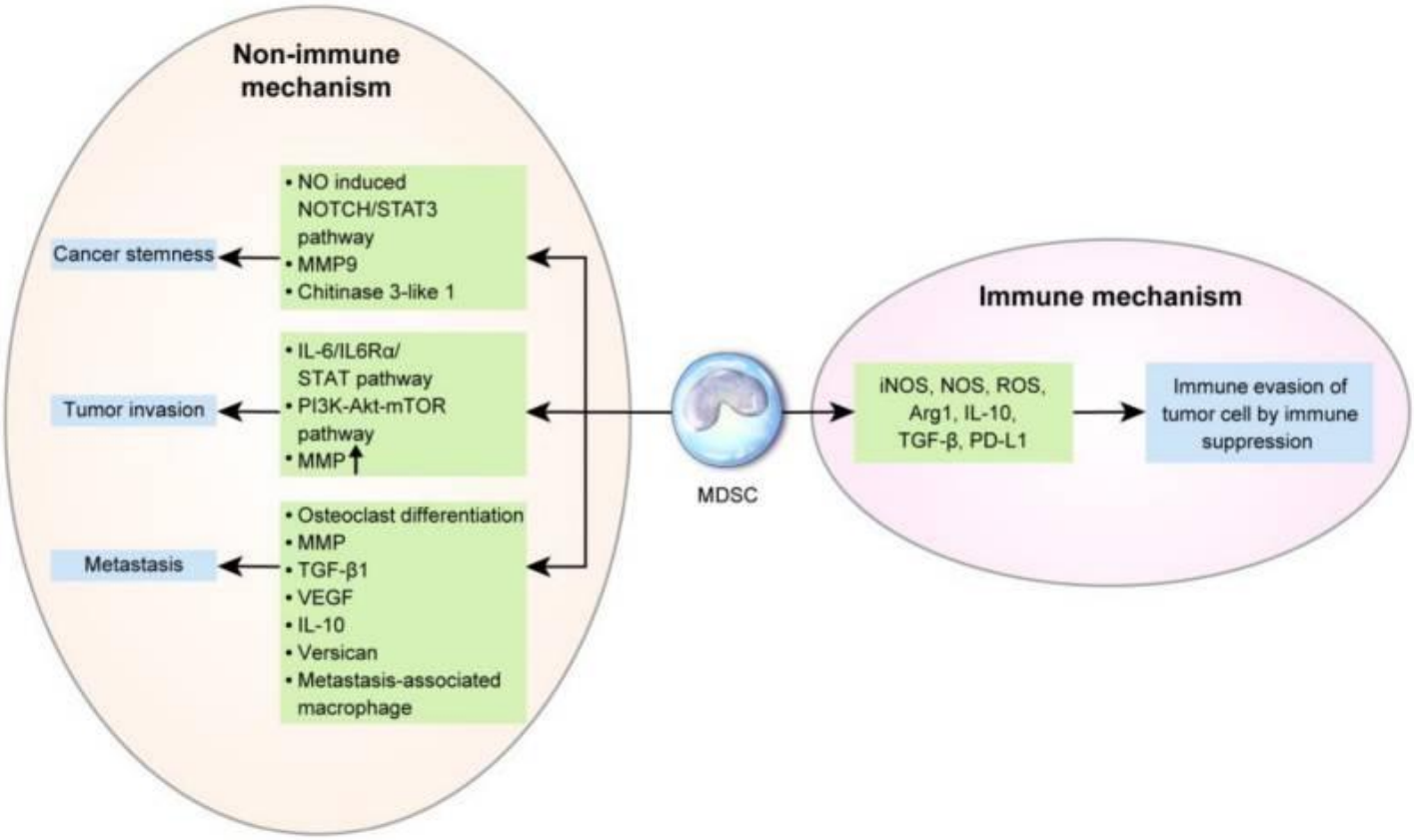

Figure 12: The role of myeloid-derived suppressor cells (MDSCs) in breast carcinogenesis.

The key immunogenic pathways activated by MDSCs during the progression of breast cancer are the immunosuppression induction by NOS, iNOS, ROS, IL-10, PD-L1 and TGF-β, causing immune evasion of cancer cells. Non-immunogenic events such as enrichment of tumour stemness by activator of transcription 3 (STAT3) cascade, matrix metallopeptidase (MMP) 9 and the nitric oxide (NO)-induced Notch/ signal transducer, as well as facilitation of cancer invasiveness by the phosphoinositide 3-kinase (PI3K)-Akt-mammalian target of rapamycin (mTOR), and IL-6/IL6Rα/STAT pathway. During metastasis process, MDSCs can polarize into osteoclasts, causing osteolytic bone metastasis, thus, promotes TGF-β1, VEGF, MMP, and IL-10 production (Cha and Koo, 2020).

1.5.4 TAMs and MDSCs as therapeutic target in breast cancer

TAMs and breast cancer cells within the TME respond to cancer treatment differently, whereby polarization of TAMs influences the impact of treatment responses and outcome to chemotherapy (Chanmee et al., 2014, Whiteside, 2008). IL-10 secreted by TAM shows an increased bcl-2 (B-cell lymphoma 2) and STAT3 (Signal transducer and activator of transcription 3) expression, leading to TAM-mediated treatment resistance in human breast cancer cell lines (T47D, BT549) (Yang et al., 2015). TAMs are shown to be correlated with tamoxifen resistance in breast cancer patients (Xuan et al., 2014). Recruitment of $CD8^+$ cytotoxic T-cells are suppressed by TAMs, leading to drug resistance in MMTV-PyMT (mouse mammary tumor virus-polyoma middle tumor-antigen) breast cancer model (DeNardo et al., 2009). Moreover, suppression of TAM-derived angiogenesis-inducing factors has revealed promising improvement in the chemotherapy efficacy (Bolat et al., 2006, Tsutsui et al., 2005). IL-6 inhibitor (curcumin) has been developed to inhibit secretion of IL-6 in breast tumour cells, which lowers the number of MDSCs (Singh et al., 2013). R84 is a well-known VEGF inhibitor has been designed to inhibit VEGF binding to VEGFR2, which is promising in controlling the growth of tumour cells and preventing infiltration of MDSCs, Treg and macrophages (Roland et al., 2009). R84 inhibitor downregulates the expression of IL-6, IL-1β and CXCL1 (Roland et al., 2009). SB-265610 and Sulforaphane are potent inhibitors of CXCR2 and macrophage migration inhibitory factor (MIF), which can prevent migration of MDSCs (Liu et al., 2012, Simpson et al., 2012). Furthermore, Silibinin plays an important role in breast cancer cells by suppressing the expression of CCR2 in MDSCs, thus, preventing recruitment of MDSCs at the tumour sites (Forghani et al., 2014). Additionally, the use of anti-CCL5 antibody has shown reduced MDSC activity, thus, evoked T cell proliferation, which is suggested to be a promising therapeutic measure for triple-negative breast cancer (Zhang et al., 2013b).

1.6 Hyaluronic acid (HYA) and tumour microenvironment

Tumour microenvironment, which primes survival, growth and tumour invasion, plays a crucial role in the development of tumorigenesis. Hyaluronic acid (HYA) (also known as hyaluronan), an abundant component of extracellular network and TME, plays an imperative part in

inflammation, angiogenesis, fibrosis, and cancer progression (Ghatak et al., 2015, Petrey and de la Motte, 2014).

1.6.1 Structure of HYA

HYA is an anionic molecule, and a member of the glycosaminoglycan (GAG) family, composed of repeating polymeric disaccharide, where both glucuronic acid and N-acetylglucosamine are linked together via alternating β-1, 3 and β-1, 4 linkages (Figure 13) (Itano and Kimata, 2002). The total number of disaccharides in each HYA molecule is reported to be 2000-25000, thus, is a linear chain GAG with molecular weight of 105-107 Da (Toole, 2002). Specific stable tertiary structures of HYA have been reported in aqueous solutions (Scott and Heatley, 1999). Polymers of HYA exist in numerous configurations, depending on their size, pH, salt concentration and associated cations (Scott and Heatley, 1999). HYA encompasses a higher biocompatibility, viscoelasticity, moisture retention capacity, as well as hygroscopic properties, even at lower concentrations (Turino and Cantor, 2003, Jiang et al., 2011).

1.6.2 Biosynthesis and distribution of HYA

HYA is synthesized by membrane-bound internal protein, known as hyaluronan synthase (HAS) (Prehm, 1984). There are three isoforms of HAS reported in vertebrates, including HAS-1, HAS-2, and HAS-3; each isoform exhibits distinct enzymatic properties varying in different sizes (Weigel et al., 1997, Itano et al., 1999, Itano and Kimata, 2002). Furthermore, different size of HYA is also synthesized by these HAS isozymes, which are also differentially regulated at transcriptional, translational as well as post-translational levels, including sub-cellular localization, alternative splicing and epigenic processes. EHA is detected in the lymphatic system and blood stream, thus, can interact with specific receptors present on cell surfaces (George and Stern, 2004). HYA is also found in the skin structure, joints, ligaments, skeleton as well as distributed between other organs, including brain, lung, muscle, kidney, and liver (Fraser et al., 1997).

During initiation and progression of tumorigenesis, a transcriptional switch in HAS- derived isoforms has been reported in transformed malignant cells (Itano and Kimata, 2002, Itano et al., 1999). Overexpression of HAS 2 in mammary glands of a transgenic mouse resulted in an

aggressive growth of mammary tumour, thus, accelerating tumour angiogenesis through stromal cell recruitment (Koyama et al., 2007).

However, overexpression of HAS 2 has also been suggested to suppress the tumorigenesis of glioma cells (Enegd et al., 2002). Clinical samples have revealed an increased deposition of HYA in TME, which is associated with malignant tumour progression in several cancers, including breast, pancreatic, ovarian, and colorectal cancer (McCarthy et al., 2018, Sato et al., 2016).

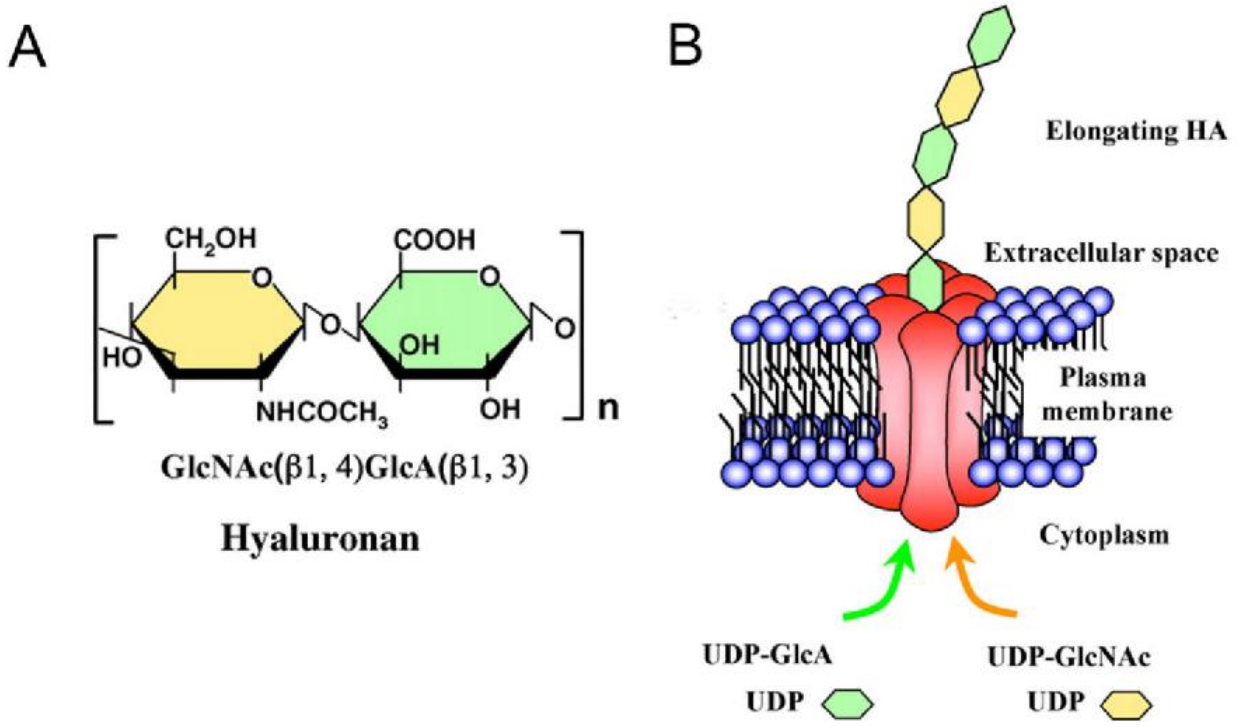

Figure 13: A schematic representation showing the chemical structure (A) and biosynthesis of Hyaluronan, also known as Hyaluronic acid (HYA).

HYA is composed of chemical properties of repeating polymeric disaccharide, linking β-1,4-D-glucuronic acid, and β-1,3-N-acetylglucosamines units. HYA is produced by membrane-bound internal hyaluronan synthase (HAS), of which vertebrates have three isoforms; HAS-1, HAS-2, and HAS-3, each having two separate binding domains for UDP-sugars. HYA polymerization seems to take place at the inner side of the plasma membrane, where HAS can add UDP-GlcA and UDP-GlcNAc monomers to the reducing end of HYA polymer. Thus, non-reducing end of sugar is then translocated into the extracellular space in the HAS structure (Zhang et al., 2014).

1.6.3 Biological roles of HYA and its receptors

In the TME, HYA provides a molecular 3D-framework for cells and mediates modulation of stromal as well as tumour cells (Itano and Kimata, 2002, Itano et al., 1999). Functions of HYA are well- established in transmitting cell signaling, and regulating cell adhesion, motility, growth, and differentiation (Turley, 1992). Exposure of HYA to tumour cells triggers several intracellular signaling cascades, including c-Src, Ras, and mitogen-activated protein (MAP) kinases through interaction with cell-surface receptors. It results in genomic transcription relating to the cell growth and survival, cell induction of cytoskeletal rearrangement, and membrane ruffling, leading to migration. Increased HYA synthesis has been reported during wound healing and tissue injury (Weigel et al., 1986, Slevin et al., 2002). Thus, HYA regulates tissue repair by activating inflammatory cells to increase immune response (McKee et al., 1996, Teriete et al., 2004). HYA is also involved in providing framework for formation of blood vessels (Slevin et al., 2002), and migration of fibroblasts (Li et al., 2006, Turley, 1989) that may be involved in progression of tumour cells (Knudson, 1996). Furthermore, HYA found on the surface of cancer cells is significantly associated with metastatic behavior (Zhang et al., 1995).

The interaction of extracellular HYA with cell surface receptors, such as cluster of differentiation 44 (CD44), HYA-mediated motility (RHAMM) (Figure 14), and intercellular adhesion molecule 1 (ICAM-1) has been reported (Savani et al., 2001). CD44 is a well-established receptor for HYA, with diverse roles in cell-to-cell, and cell-to-matrix interactions (Misra et al., 2015). Interaction of CD44 with a wide range of ligands, including collagens, osteopontin, and MMPs (Goodison et al., 1999) has also been described. CD44 exists in several isoforms generated through splicing of messenger RNA (Warzecha et al., 2009). A CD44 variant (CD44v) isoform comprising v3 or v6 (sequence encoded by variant exon 3 or 6) has been suggested to undergo modification. CD44v3 has been reported to interact with growth factors, such as fibroblast growth factor and heparin-binding epidermal growth factor-like growth factor (HB-EGF) (Bennett et al., 1995). CD44v6 can act as a co-receptor for the receptor tyrosine kinase c-Met (Orian-Rousseau et al., 2002). CD44v6 has been shown to promote tumour progression, and metastatic invasion in lung, breast, and colon cancer (Chen et al., 2018a, Ma et al., 2019). Engagement of HYA-CD44 in breast cancer cells leads to overexpression of P-glycoprotein (multidrug resistance gene) and Bcl, which further

promotes proliferation and survival of tumour cells (Bourguignon et al., 2009). HYA oligosaccharides from tumour cells enhances cleavage of intracellular CD44, thus, tumour cell motility (Sugahara et al., 2006). Furthermore, HAS-1 modulates growth, invasion, and angiogenesis of bladder cancer cells through downregulation of CD44 isoforms: CD44 variant exon 3 (CD44v3), CD44v6, and CD44s (Golshani et al., 2008).

RHAMM is another key receptor for HA and various isoforms of RHAMM have been established (Hardwick et al., 1992, Turley, 1992, Yang et al., 1993). HYA- RHAMM interaction has been suggested to control the cell growth and migration by several signal transduction events, as well as interactions with cytoskeleton (Mohapatra et al., 1996). HYA has also shown to directly promote cell locomotion through HYA- RHAMM interaction (Samuel et al. 1993, 7693717). RHAMM is also important for CD44 localization to the cell surface, thus, leading to the formation of CD44-ERK1/2 complexes, suggesting that RHAMM is a crucial regulator of ERK1/2 signaling cascade (Tolg et al., 2006). T-cell responses directed against RHAMM in patients with acute myeloid leukemia is correlated with improved clinical outcome (Spranger et al., 2012). Immunotherapies including adoptive transfer of RHAMM-T cells or peptide vaccination has been suggested to improve the immune response of AML patients (Casalegno-Garduno et al., 2012).

1.7 Main Aims of this Study

1. Expression of a recombinant fragment of human SP-D (rfhSP-D) under bacteriophage T7 promoter in E. coli and purification to homogeneity, free from LPS.
2. Demonstration of rfhSP-D as an entry inhibitor of IAV and modulator of cytokine storm.
3. Demonstration of the ability of rfhSP-D to induce apoptosis in breast cancer cell lines, and dissection of the mechanisms of apoptosis induction.
4. Assessment of the modulation of protective properties of rfhSP-D in the presence of HYA.

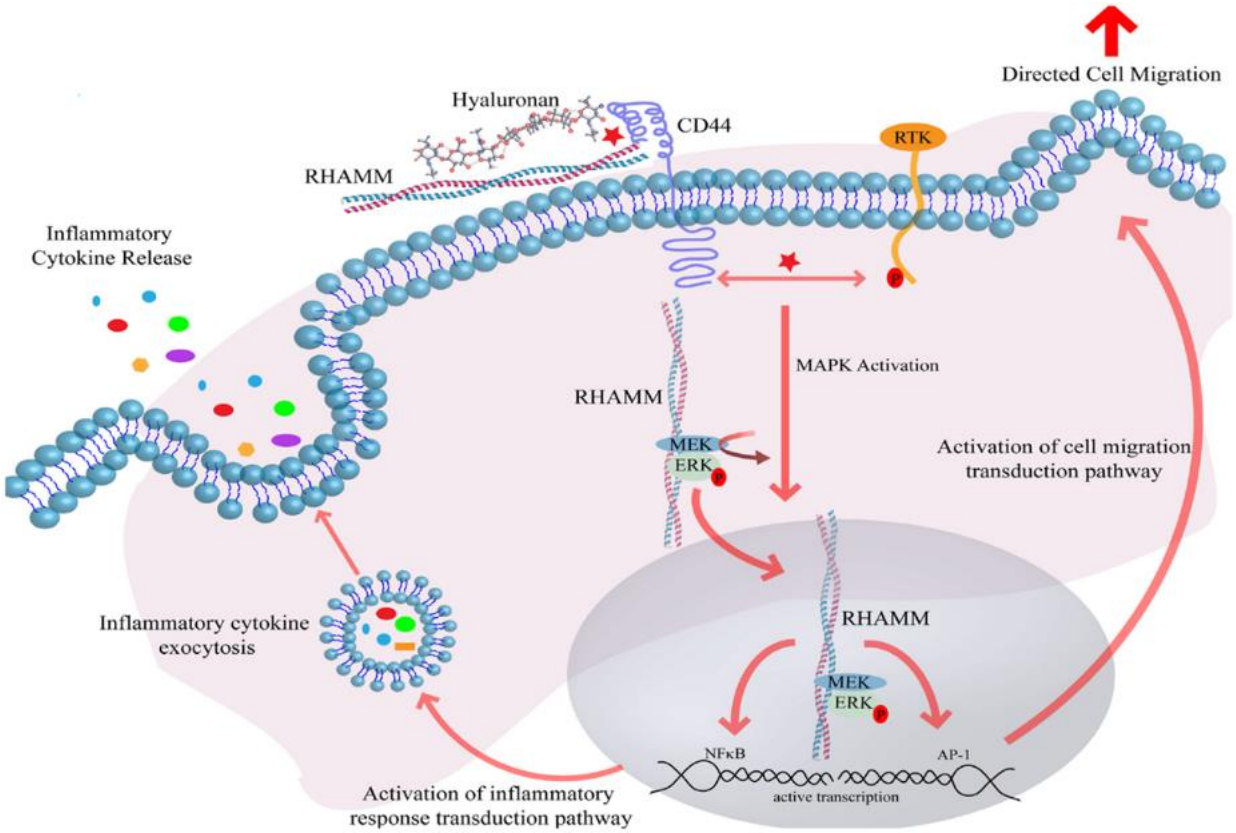

Figure 14: A schematic diagram demonstrating receptor-mediated signaling by Hyaluronic acid (HYA), also known as hyaluronan, through binding interaction with cell-surface HYA binding receptors.

HA interaction with its receptors CD44 and RHAMM induces clustering of CD44 receptor and triggers intracellular RHAMM-regulated MAPK cascade, resulting in phosphorylation of extracellular signal-regulated kinase (ERK), and downstream activation of NFκB and activator protein 1 (AP-1). Trigger of NFκB and AP-1 result in cell migration, thus, release of inflammatory cytokines (Golshani et al., 2008).

Chapter 2

Methods and Materials

2.1 Expression and Purification of rfhSP-D

Expression and purification of rfhSP-D (composed of the 8 Gly-X-Y repeats, neck, and CRD region) involves steps including preparation of competent cells, transformation, pilot-scale expression, large-scale production, bacterial lysis, sonication and preparation of inclusion bodies, denaturation/renaturation procedure, rfhSP-D purification by affinity chromatography, and endotoxin removal.

2.1.1 Competent Cells

A single colony of *Escherichia coli* BL21 (λDE3) pLysS (Invitrogen) was inoculated in Luria Broth (LB) medium (10 ml) containing chloramphenicol (34 µg/ml) (Sigma-Aldrich) (Sigma-Aldrich) and grown at 37°C overnight on a shaker. The next day, a primary inoculum of 500 µl bacterial culture was inoculated into fresh 10 ml of LB medium containing chloramphenicol (34 µg/ml) and grown to A_{600} of 0.3-0.4. The bacterial culture was subjected to centrifugation for 10 mins at 2000 × g, followed by resuspension the bacterial pellet in 1 ml of 0.1M $CaCl_2$ (Fisher-Scientific), and then adjusting to a final volume of 12.5 ml of 0.1M $CaCl_2$. The $CaCl_2$ resuspended bacterial pellet was incubated on ice for 1 h, then centrifuged for 10 mins at 2000 ×g, followed by resuspension in 2ml of $CaCl_2$ (0.1M) and kept on ice until further use.

2.1.2 Transformation

Plasmid pUK-D1 (2 µl) (Mahajan et al., 2013), containing cDNA sequences for the 8 Gly-X-Y repeats, neck and CRD regions of human SP-D was added to Escherichia coli BL21 (λDE3) pLysS competent cells (200 µl).and incubated on ice for 1 h, followed by heat shock at 42°C for 90 sec. Next, 800 µl of LB medium was added to the cells and incubated for 45 mins at 37°C with gentle shaking at regular intervals. Post incubation transformed bacterial cells were spread on an agar plate containing ampicillin (100 µg/ml) (Thermo-Scientific) and chloramphenicol (34 µg/ml). The agar plates were then incubated at 37°C incubator overnight to allow growth of transformed bacterial colonies. The grown colonies were then used to carry out pilot and large-scale expression analysis.

2.1.3 Pilot-Scale Expression

For pilot-scale expression, a single colony was inoculated in 5 ml of LB medium, containing ampicillin (100 µg/ml) and chloramphenicol (34 µg/ml) and grown at 37°C overnight in a shaker. Next day, 500 µl of primary inoculum was added to fresh 10 ml of LB medium containing antibiotics and incubated for 3h at 37°C on a shaker until A_{600} of 0.6-0.8 was reached. An uninduced sample (1 ml) was collected as a control and the remaining bacterial culture was induced with 0.5mM Isopropyl β-D-1- thiogalactopyranoside (IPTG) (Sigma-Aldrich) for 3h at 37°C on a shaker; the bacterial cells were centrifuged at 13,800 ×g for 10 minutes. The cell pellet from uninduced and induced samples were resuspended in 2 × treatment buffer (50 mM Tris pH 6.8, 2% β-mercaptoethanol, 2% SDS, 0.1% bromophenol blue, and 10% glycerol) (Sigma-Aldrich), and heated for 10 minutes at 100°C. 20 µl of each sample was subjected to 15% (v/v) SDS-PAGE for 90 minutes at 120V for assessing the expression of rfhSP-D.

2.1.4 Large-Scale Expression

For large-scale expression analysis, a single colony was inoculated in 25 ml of LB medium with chloramphenicol (34 µg/ml) and ampicillin (100 µg/ml) and grown overnight at 37°C on a shaker. The next day, a primary inoculum (12.5 ml) was mixed with fresh LB medium (500 ml) with both antibiotics and grown to A_{600} of 0.6-0.8. 1ml of uninduced sample was collected from the grown bacterial culture and the remaining culture was induced with 0.5mM IPTG, followed by incubation at 37°C for 3h on a shaker. After 3h of incubation, 1ml of bacterial cells was collected from uninduced and induced samples and subjected to centrifugation at 13,800 ×g for 10 mins. The bacterial cell pellet was treated with 2× treatment buffer and heated for 10 mins at 100°C. The heated samples (20 µl) were then subjected to 15% (v/v) SDS-PAGE for 90 minutes at 120V for assessing the expression of rfhSP-D protein. Additionally, the remaining induced bacterial culture was centrifuged at 15,000 ×g for 30 minutes at 4°C, and the bacterial cell pellet was stored at −20°C to process for the rfhSP-D purification later.

2.1.5 Lysis and Sonication

The bacterial cell pellet, stored at −20°C, was resuspended in lysis buffer (50ml) (50mM Tris-HCl, 200mM NaCl, 5mM EDTA, 0.1% v/v Triton X-100, 0.1mM PMSF, pH 7.5 and 50 µg/ml lysozyme) (Sigma-Aldrich), and incubated at 4°C for 1 h on a rotary shaker. The lysed bacterial cell

suspension was sonicated (equipment details here) for 30 sec at 60Hz with 2 mins interval and repeated it for 12 cycles. The sonicated bacterial cell suspension was centrifuged at 15,000 ×g for 20 mins at 4°C.

2.1.6 Denaturation and Renaturation cycle

The inclusion bodies containing rfhSP-D was suspended in 25 ml of solubilization buffer (50mM Tris-HCl pH 7.5, 100mM NaCl, 10mM 2-Mercaptoethanol and 8M urea) for 1 h at 4°C and then centrifuged at 15,000 × g for 20 mins at 4°C. The supernatant was then dialysed for 2h at 4°C stepwise against 4 M, 2 M, 1 M and no urea buffer containing (50mM Tris-HCl pH 7.5, 100mM NaCl, and 10mM 2-Mercaptoethanol). The final dialysis was carried out against solubilization buffer containing 5 mM $CaCl_2$ for 3 h at 4°C; the dialysate was then centrifuged at 15,000 ×g for 20 minutes to remove aggregates and stored at 4°C.

2.1.7 rfhSP-D Purification by Affinity Chromatography

A maltose agarose column (5ml) (Sigma-Aldrich) was equilibrated with 50 ml of high salt buffer (50 mM Tris-HCL, pH 7.5, 1 M NaCl) and followed by 50 ml of affinity buffer (50 mM Tris-HCL, pH 7.5, 0.1 M NaCl,5 mM $CaCl_2$). The dialysate was loaded onto the maltose agarose column, and the bound rfhSP-D was eluted using elution buffer (50 mM Tris–HCl pH 7.5 and 100 mM NaCl containing 10 mM EDTA). The OD_{280} was measured to determine the concentration of eluted rfhSP-D fractions. To assess the purity, the purified rfhSP-D protein (5 µg/well) was resuspended in 2× treatment buffer and denatured by heating at 100°C for 10 mins and run on 15% (v/v) SDS-PAGE and subjected to western blotting to analyze and confirm the purity of the purified rfhSP-D protein.

2.2 Sodium Dodecyl Sulphate-Polyacrylamide Gel Electrophoresis (SDS-PAGE)

The resolving (10 ml) and stacking (5 ml) layers were prepared by mixing a varied volume of components (Table 3). The glass plates (tall and short glass plates) were clamped into the casting stands ensuring there was no leakage. The resolving polyacrylamide solution was first pipetted to fill the space between the two glass plates using a plastic transfer pipette until the resolving gel solution reached above the green clamps. After loading the resolving solution, deionized water was added gently on top of the resolving layer so smoothen the surface during

polymerization. After 10 mins, water was poured off and the stacking gel solution was loaded over the polymerized resolving gel; a 10-well comb was inserted. After the polymerization of the stacking gel, the comb was carefully removed, and the glass plates were put in the buffer dam and the tank using 1 liter of 1 × running buffer (25 mM Tris, 192 mM glycine and 0.1% SDS). The samples were treated with 2 × treatment buffer (50 mM Tris pH 6.8, 2% β-mercaptoethanol, 2% SDS, 0.1% bromophenol blue, and 10% glycerol) and heated for 10 mins at 100°C; samples were loaded into the wells along with a standard protein marker (Thermo Fisher). The samples were run for 90 mins at 120V until the blue dye front reached the end of the gel. The gel was stained for 2 h in the staining solution (0.1% w/v Coomassie, 10% v/v acetic acid, 40% v/v methanol and 50% H_2O); destaining was carried out in de-staining solution made with (10% acetic acid, 40% methanol and 50% H_2O).

Table 4: The required volume of resolving and stacking components for 12 and 15 % of SDS-PAGE.

Resolving Gel	12%	15%	Stacking Gel	12%	15%
dH_2O	3.3 ml	2.3 ml	dH_2O	3.4 ml	3.4ml
30% Bis-Acrylamide mix	4 ml	5 ml	30% Bis-Acrylamide mix	0.83 ml	0.83 ml
1.5M Tris-HCl, pH8.8	2.5 ml	2.5 ml	1.0M Tris-HCl, pH6.8	0.63 ml	0.63 ml
10% SDS (Sodium dodecyl sulphate)	0.1 ml	0.1 ml	10% SDS (Sodium dodecyl sulphate)	0.05 ml	0.05 ml
10% APS (Ammonium Persulfate)	0.1 ml	0.1 ml	10% APS (Ammonium Persulfate)	0.05 ml	0.05 ml
TEMED (Tetramethylethylenediamine)	0.015 ml	0.015 ml	TEMED (Tetramethylethylenediamine)	0.015 ml	0.015 ml

2.3 Endotoxin Removal from the rfhSP-D preparation and Limulus Amebocyte Lysate Assay

The eluted fractions of purified rfhSP-D were subjected to removal of lipopolysaccharide (LPS) using Pierce™ High-Capacity Endotoxin Removal Resin (Qiagen). The endotoxin removal resin was

packed in a 5ml bed volume column and washed with sterilized H_2O (50 ml), followed by 1% sodium deoxycholate (50 ml) (Sigma-Aldrich) and 50 ml of sterilized H_2O. Purified rfhSP-D fractions showing higher concentration were loaded onto the column and OD_{280} in the flow-through was determined using Nanodrop (Thermo-Scientific). The endotoxin levels in the rfhSP-D flow-through fractions were measured via QCL-1000 Limulus amebocyte lysate (LAL) kit (Lonza). The LAL proenzyme is activated by the catalytic activity of Gram-negative bacterial endotoxin. The activated enzyme further catalyses the release of p- nitroanilides (NA) from the substrate. The released pNA is measured at an absorbance of 405-410 nm (Young et al., 1972). Briefly, rfhSP-D (5 µg/ml) was mixed with the LAL (50 µl) and incubated for 10 mins at 37°C. A chromogenic substrate solution (100 µl) was then added and incubated at 37°C for 6 mins. The reaction was stopped using a stop reagent (100 µl), and the presence of endotoxin in the sample was concomitant with a yellow colour read at 405-410 nm. The concentration of the endotoxin was calculated using a standard curve, where 1 EU/ml was equivalent to 0.1ng endotoxin/ml.

2.4 Extraction of full-length native SP-D from human bronchoalveolar lavage fluid

Human full-length native SP-D (hFL-SP-D) was purified as published earlier (Strong et al., 1998). Bronchoalveolar lavage fluid (BAL) collected from pulmonary alveolar proteinosis patients was made up with buffer I, containing 20 mM Tris−HCl and 10 mM EDTA (helps solubilize any aggregated SP-D), pH 7.4, and stirred for an hour at room temperature. The turbid solution was then centrifuged at 10,000 × g at 4°C for 40 mins to separate pellet rich in SP-A from supernatant which contains most of the SP-D. Prior to loading on to a maltose-agarose column, the SP-D containing supernatant was made 20 mM with respect to $CaCl_2$, followed by adjusting the pH to 7.4. The column was washed with buffer II (20 mM Tris–HCl, pH 7.4, 10 mM $CaCl_2$, 0.02% (w/v) sodium azide), followed by washing again with buffer II containing 1 M NaCl to remove any non-specifically bound albumin or a 9 kDa fragment of histone H4 that has been identified in BAL. The maltose-bound SP-D was eluted 50 mM $MnCl_2$, 20 mM Tris–HCl, 0.02% (w/v) sodium azide (Sigma-Aldrich), pH 7.4. The pooled SP-D fractions were then dialysed against 20 mM Tris–HCl, 100 mM NaCl, 5 mM EDTA pH 7.4.

2.5 Purification of full-length SP-D from cancer cells

A maltose agarose column (5ml) (Sigma-Aldrich) was equilibrated with 50 ml of high salt buffer (50 mM Tris-HCL, pH 7.5, 1 M NaCl) and followed by 50 ml of affinity buffer (50 mM Tris-HCL, pH 7.5, 0.1 M NaCl,5 mM $CaCl_2$). The culture supernatant (200 ml) from the cancer cell lines, BT20, BT474 and SKBR3 was collected and centrifuged at 5,000 ×g for 30 mins at 4°C. The centrifuged supernatant was then loaded onto the maltose-agarose column, and the bound full-length SP-D (FL-SP-D) was eluted using elution buffer (50 mM Tris–HCl pH 7.5 and 100 mM NaCl containing 10 mM EDTA). The OD_{280} was measured to determine the concentration of eluted FL-SP-D fractions. To assess the purity, the purified FL-SP-D protein (5 µg/well) was resuspended in 2× treatment buffer and subjected to western blotting to analyze and confirm the purity of the purified FL-SP-D protein.

2.6 Western Blotting

2.6.1 Determination of rfhSP-D or full-length SP-D immunoreactivity

Purified rfhSP-D (10 µg/well) or full-length SP-D (FL-SP-D) (5 µg/well) isolated from BT474 cell line was resuspended in 2 × treatment buffer and heated for 10 mins at 100°C. BSA was used as a negative control protein. The heated samples were subjected to 15% (v/v) SDS-PAGE and then electrophoretically transferred onto a nitrocellulose membrane (320mA for 2h) (Sigma-Aldrich) in 1 × transfer buffer containing 25mM Tris–HCl pH 7.5, 190 mM glycine, and 20% v/v methanol. The membrane was incubated in 1× PBS containing 5% v/v dried milk powder (Sigma-Aldrich) for 2h at 4°C to block non-specific binding. After blocking, the membrane was washed with PBS three times (5 mins each wash). The membrane was incubated with polyclonal rabbit anti-human SP-D primary antibody. The unbound primary antibodies were removed by washing the membrane with PBS+ 0.05% Tween 20 (PBST) (3 times, 10 min each wash). The membrane was then probed with secondary Goat anti-rabbit IgG horseradish peroxidase (HRP)-conjugate (1:1000; Fisher Scientific) at RT for 1 h. Following washes, the membrane-bound proteins were visualized by developing the membrane using 3'-diaminobenzidine (DAB) substrate kit (Thermo Fisher).

2.6.2 Determination of Caspase Activation

BT20, BT474 and SKBR3 cells (0.4×10^6) were seeded in 6-well plates and incubated with rfhSP-D (20µg/ml) in serum-free RPMI medium, along with untreated controls for 12h and 24h. Next, the

medium was discarded, and the cells were washed gently with PBS. The washed cells were then lysed within the wells using lysis buffer (50 mM Tris-HCl pH 6.8, 2% v/v SDS, 2% v/v β-mercaptoethanol, 10% v/v glycerol and 0.1% w/v bromophenol blue). The cell lysate was then sonicated for 15s, followed by heating for 10 mins at 100°C and were subjected to 12% (v/v) SDS-PAGE. Western blotting was performed as mentioned in section 2.6.1, with respective antibodies-rabbit anti-human caspase (anti- cleaved caspase 9 and anti-cleaved caspase 3; Cell Signaling) primary antibodies (1:1000 in PBS) and Protein-A HRP-conjugate (1:1000) at room temperature (RT) for 1 h. The membrane was developed with DAB.

2.7 Viruses and Reagents

IAV subtypes used in this study, including A/England/2009 (pH1N1) and the A/HK/99 (H3N2), were provided by Dr Wendy Barclay (Imperial College London) and Dr Leo Poon (University of Hong Kong). The plasmids used to generate the lentiviral particles pseudo-typed by H1+N1 were obtained from Addgene. The pHIV-Luciferase backbone plasmid was obtained from Dr Bryan Welm (Addgene plasmid # 21375); the packaging plasmid, psPAX2 was offered by Dr Didier Trono (Addgene plasmid # 12260); Vesicular Stomatitis Virus (VSV-G) was a gift from of Dr Bob Weinberg (Addgene plasmid #8454). Monoclonal Anti-Influenza Virus H1 HA, A/California/04/2009 (pH1N1) pdm09, Clone 5C12, NR-42019 and Polyclonal Anti-Influenza Virus H3 HA, A/Hong Kong/1/1968 (H3N2) (antiserum, Goat), NR-3118 were acquired from BEI Resources, NIAID, NIH, USA.

2.8 Cell Culture and Treatments for IAV

Madin Darby Canine Kidney (MDCK), human embryonic kidney (HEK) 293T, and Adenocarcinomic human alveolar basal epithelial cells (A549) cell lines were cultured in complete Dulbecco's Modified Eagle's Medium (DMEM) (Sigma-Aldrich) [100 U/ml penicillin (Sigma-Aldrich), 100 µg/ml streptomycin (Sigma-Aldrich), 1 mM sodium pyruvate (Sigma-Aldrich), 2 mM l-glutamine, and 10% v/v fetal bovine serum (FBS) (Sigma-Aldrich)]. The cells were left to grow at 37°C under 5% (v/v) CO_2 for approximately 3 days until the desired confluency was achieved. Since these cells were adherent, they were subjected to trypsinization using 2× Trypsin-EDTA (0.5%) (Fisher Scientific) for 10 min at 37°C. The detached cells were then diluted in complete DMEM, followed by centrifugation for 5 min at 1,200 rpm and re-suspension of the cell pellet in

complete DMEM. The cell count and viability were determined by mixing an equal volume of cell suspension and Trypan Blue dye (0.4% w/v) (Fisher Scientific). The cells were counted using a hemocytometer with Neubauer rulings (Sigma-Aldrich). Required number of cells were re-suspended in complete DMEM for further use.

2.9 Purification of IAV Subtypes

MDCK cells at 80% confluency were incubated with pH1N1 (2×10^4) or H3N2 (3.3×10^4) (600 µl/flask) at 37°C for 1 h. Unbound viral particles were washed off three times using sterile PBSs. The virus bound MDCK cells were incubated at 37°C for 3 days in 25 ml of infection medium [DMEM containing 1% penicillin/streptomycin, 0.3% bovine serum albumin (BSA), and 1 µg/ml of l-1-Tosylamide-2-phenylethyl-chloromethyl ketone (TPCK)—Trypsin] (Sigma-Aldrich). The culture supernatant containing the IAV particles was centrifuged twice at 3,000 × g at 4°C for 15 min. Viral supernatants (25ml) was slowly added to ultra-clear tubes containing 30% w/v sucrose (8 ml/tube) (Sigma-Aldrich), and centrifuged at 25,000 × g for 90 min at 4°C. Both upper phase of the supernatant and the sucrose phase were carefully removed. The IAV particles, which remained at the bottom of ultra-clear tubes, were suspended in sterile PBS (100 µl/ tube). The purified IAV suspension (10 µl) was analysed by 12% v/v SDS-PAGE and ELISA.

2.10 Production of H1+N1 Pseudotyped Lentiviral Particles

HEK293T cells (0.4×10^6) were co-transfected with pcDNA3.1-swineH1-flag (H1 from swine pH1N1 A/California/04/09) (20 µg) (Invitrogen), pcDNA3.1-swine N1-flag (N1 from swine pH1N1 A/California/04/09) (20 µg) (Invitrogen), pHIV-Luciferase backbone (20 µg) (Addgene). The pHIV-Luciferase backbone carries modified proviral HIV-1 genome with env deleted and is designed to express the firefly luciferase reporter, and psPAX2 (Addgene). psPAX2 is a well-known lentiviral packaging plasmid (second-generation) and can be used with second or third generation lentiviral vectors and envelope expressing plasmid. VSV-G lentivirus as a control was generated in a similar way as described above, without H1+N1 pcDNAs. The released H1+N1 pseudotyped and VSV-G lentiviral particles were harvested in the supernatant at 24 and 48 h. The harvested virus particles were then centrifuged at 5,000 ×g for 10 min to remove any cell debris, and clear supernatant was concentrated via ultra-centrifugation at 25,000 ×g for 90 min. The ultra-centrifuged lentiviral

particles were resuspended in sterilized 1 × PBS and analyzed via $TCID_{50}$ assay, western blotting, and luciferase activity assay.

2.11 Tissue Culture Infectious Dose 50% ($TCID_{50}$) Assay

Tissue Culture Infectious Dose 50% ($TCID_{50}$) Assay was performed to determine the titer of viral particles and their cytopathic effects (CPE) on infected cells (Hollý et al. 2017). Purified stocks of pH1N1 and H3N2 viruses or pseudotyped lentiviral particles were prepared with an initial dilution of 10^{-2} in DMEM using a Maxisorp 96-well microtiter plate and 146 µl of the diluted virus was added to all wells. Uninfected MDCK cells were used as a control. 46 µl of pH1N1, H3N2 or lentiviral particles were serially diluted ($1/2_{log10}$ to 10^{-7}) and incubated in a microtiter plate at 37°C for 1 h. MDCK cells (1×10^5), suspended in 2 × infection medium, were added to each well and incubated at 37°C under 5% v/v CO_2 for 3-5 days, and examined under microscope to record positive and negative dilutions for CPE.

2.12 Far western Blotting

rfhSP-D (5µg) or 10 µl of concentrated H1N1/H3N2 (1.36×10^6 pfu/ml) were ran separately on a 12% (w/v) SDS-PAGE and then transferred onto a nitrocellulose membrane and membrane was blocked and washed as described above. The membrane was incubated with 5µg/ml rfhSP-D for 1 h at RT and 1 hour at 4°C. Following PBST wash, the membrane was probed with monoclonal anti-influenza virus H1 (BEI-Resources), polyclonal anti-infuenza virus H3 (BEI-Resources) or polyclonal rabbit anti-human SP-D (1:1000) in PBS for 1 h at RT. The membrane was again washed three times with PBST, 10 minutes each before probing with secondary antibodies, Protein-A HRP-conjugate, or anti-mouse IgG HRP-conjugate (1:1000) (Fisher Scientific) in PBS (100µl/well) for 1 h at RT. For detecting M1 expression, untreated (A549 cells + virus) and treated samples (A549 cells + virus + 10 µg/ml rfhSP-D) were collected following 6 h post treatment. The collected cells were lysed, sonicated and the cell lysates were run on a 12% (w/v) SDS-PAGE, and transferred onto a nitrocellulose membrane, as described above. The M1 expression was detected using anti-M1 monoclonal antibody (BEI-Resources) (1:1000) diluted in PBS. After washing with PBST, the blot was developed either using DAB or Enhanced Chemiluminescence (ECL) (Thermo-Fisher).

2.13 rfhSP-D-IAV interaction via enzyme-linked immunosorbent assay (ELISA)

A decreasing concentration of rfhSP-D (5, 2.5, 1.25, and 0.625 µg/well) was coated in a Maxisorp 96-well microtiter plate (Thermo-Scientific) in carbonate/bicarbonate (CBC), pH 9.6 buffer overnight at 4°C, followed by blocking with 2% w/v BSA in PBS at 37°C for 2h. The microtiter wells were washed with PBST three times. 20 µl of concentrated pH1N1, H3N2 (1.36×10^6 pfu/ml), or purified recombinant HA (2.5 µg/ml) were diluted in 200 µl of PBS; 10 µl of diluted virus was added to each well and incubated for 2h at RT in buffer containing 50 mM Tris-HCL, pH 7.5, 100 mM NaCl and 5 mM $CaCl_2$. VSV-G pseudotyped lentivirus was used as a negative control. The wells were washed with PBST three times. The binding between rfhSP-D and IAV subtypes were determined by probing with primary antibodies, polyclonal anti-influenza virus H3 (BEI-Resources), and monoclonal anti-influenza virus H1 (BEI-Resources) antibody (1:5,000 dilution in PBS) for 1 h at 37°C. after washing the wells with PBST three times, the corresponding wells were incubated with secondary antibody: Protein A-HRP-conjugate (Fisher Scientific), and anti-mouse IgG-Horseradish peroxidase (HRP)-conjugate (1:5,000) (Fisher Scientific) in PBS (100 µl/well) for 1 h at 37°C. The colour was developed using 3,3',5,5'-Tetramethylbenzidine (TMB) substrate (100 µl/well) (Sigma-Aldrich), and stopped using 2 N H_2SO_4 (100 µl/well). The absorbance was read at 450 nm using iMark™ microplate absorbance reader (Bio-Rad).

2.14 Cell-rfhSP-D-IAV Binding Assay

A549 cells (1×10^5/well) were seeded in a 96-microtiter well plate in complete DMEM containing 10% FBS and grown overnight. The complete medium was gently removed, and the cells were washed gently with PBS three times. A varied concentration of purified rfhSP-D (10, 5, 2.5, and 1.25 µg/ml) was pre-incubated with pH1N1 or H3N2 virus (1.36×10^6 pfu/ml) diluted in 200 µl of PBS + 5 mM $CaCl_2$. 10 µl of diluted virus was added to the corresponding wells and incubated for 2h at RT. In a parallel experiment, maltose-binding protein (MBP) (10, 5, 2.5, and 1.25 µg/ml), pre-incubated with pH1N1 or H3N2 virus (1.36×10^6 pfu/ml), was used as a negative control. After removing unbound proteins, the microtiter wells were then washed with PBS three times, followed by fixation with 4% PFA for 10 min at RT. After PBS washes, the wells were blocked with 2% w/v BSA diluted in PBS for 2 h at 37°C. The wells were washed again using PBST three times and then incubated with monoclonal anti-influenza virus H1 (BEI-Resources) or polyclonal anti-

influenza virus H3 (BEI-Resources) in PBS (1:5,000) (100 µl/well) for 1 h at 37°C. After PBST washing step, goat anti-mouse IgG-HRP-conjugate (Thermo-Fisher), or Protein A-HRP conjugate (1:5,000) in PBS was added to the corresponding wells and incubated for 1 h at 37°C. The wells were washed again with PBST three times and the colour was developed using TMB substrate (100 µl/well); the reaction was stopped using 2 M H_2SO_4, followed by absorbance reading at 450 nm.

2.15 Titration Assay

Maxisorb 96-well plates were incubated with 0.01% w/v collagen (100 µl/well) (Sigma-Aldrich) at RT for 3 h. The excess unbound collagen was removed, the wells were washed twice with PBS. A549 cells (1×10^5) were seeded and grown at 37°C overnight under 5% (v/v) CO_2, until 80% confluency. After washing the cells with PBS twice, pH1N1 or H3N2 virus (MOI of 1), diluted in DMEM with 10 µg/ml rfhSP-D, was added to cells, respectively. The plates were covered with an aluminium foil and incubated for 1 h at 37°C. The unbound virus/rfhSP-D mix was removed, and the wells were washed twice with PBS, followed by addition of infection medium (200 µl) to the cells, and incubation at 37°C for 24 h with 5% (v/v) CO_2. The medium of the infected cells with and without rfhSP-D was collected and viral titer was estimated by $TCID_{50}$ for treated and untreated samples.

2.16 Quantitative Real-time (qRT) Polymerase Chain Reaction (PCR) Analysis

A549 cells (0.5×10^7) were grown in DMEM medium containing 10% v/v FBS until 85% cell confluency was reached. The following day, the medium was removed, and the dead cells were washed off using PBS. A549 cells were incubated with rfhSP-D (10 µg/well) in DMEM containing 5 mM $CaCl_2$ with MOI 1 of pH1N1 or H3N2 virus, and incubated first for 1h at RT, and then for 1h at 4°C. The unbound rfhSP-D protein and virus (pH1N1/H3N2) were removed carefully, cells were washed with sterilized PBS twice, followed by addition of infection medium, and incubation for 2 and 6 h at 37°C. The treated A549 cells were detached using a sterile cell scrapper (Sigma-Aldrich), centrifuged at 1,500 × g for 3 min, and the cell pellet was frozen at −80°C for RNA extraction later.

2.16.1 Total RNA Extraction

The infected A549 cell pellets were subjected to RNA extraction using the GenElute Mammalian Total RNA Purification Kit. The cell pellets were lysed using lysis solution (250 µl/ 0.3 x 10^7 cells) containing 2-mercaptoethanol (2.5 µl) and vortexed until the clumps disappeared. The cell lysates were then mixed with 70% ethanol (250 µl), vortexed gently and added to the RNA binding columns. The columns containing the lysates (mixed with 70% ethanol) were centrifuged at 13, 000 × g for 15 sec. The columns were then washed twice with washing buffer I, and second washes with buffer II (provided in the RNA extraction kit). The columns were transferred to fresh 2 ml Eppendorf tube, and RNA was extracted using elution solution (50 µl/tube) by centrifuging for 1 min at 13, 000 ×g.

2.16.2 DNase Treatment and cDNA Synthesis

Contaminating DNA was removed by DNase treatment with DNase 1 (SLBC 3g35 DMPD kit) (Sigma-Aldrich). DNase I enzyme (5 µl) and 10 x buffer (5 µl), provided in the kit, were added to total RNA (50 µl) and mixed gently by tilting the Eppendorf. DNase 1 treated samples were then incubated at RT for 15 mins, followed by addition of stop solution (5µl/tube). The samples were heat-inactivated at 70°C. The concentration of total RNA was measured at A_{260} nm using NanoDrop 2000/2000c (Sigma-Aldrich); RNA purity was assessed using A_{260}/A_{280} ratio between 1.8 and 2.1, respectively.

cDNA synthesis was performed by converting the total RNA (2 µg) into cDNA using SuperScript II Reverse Transcriptase (Thermo-Fisher Scientific). Mater mix was prepared by mixing 2 × RT buffer (10 µl) and 20 × enzyme mix (1 µl), and the mix was added to RNA samples (2 µg), followed by the addition of Oligo-dT primers to initiate cDNA synthesis, and to prevent labeling of the rRNA and tRNA.

2.16.3 Primers

Both forward and reverse primer sequences used in this thesis were designed for specificity using the Primer-BLAST software (Basic Local Alignment Search Tool) (http://blast.ncbi.nlm.nih.gov/Blast.cgi). The primers used in this thesis are listed below (Table 4).

Table 5: Target genes, forward primers, and reverse primers used for qPCR analysis.

Target	Forward Primer	Reverse Primer
18S	5′-ATGGCCGTTCTTAGTTGGTG-3′	5′-CGCTGAGCCAGTCAGTGTAG-3′
IL-6	5′-GAAAGCAGCAAAGAGGCACT-3′	5′-TTTCACCAGGCAAGTCTCCT-3′
IL-12	5′-AACTTGCAGCTGAAGCCATT-3′	5′-GACCTGAACGCAGAATGTCA-3′
TNF-α	5′-AGCCCATGTTGTAGCAAACC-3′	5′-TGAGGTACAGGCCCTCTGAT-3′
M1	5′AAACATATGTCTGATAACGAAGGAGAACAG TTCTT-3′	5′GCTGAATTCTACCTCATGGTCTTCT TGA-3′
RANTES	5'-GCGGGTACCATGAAGATCTCTG-3'	5'-GGGTCAGAATCAAGAAACCCTC-3'
IFN-α	5′-TTT CTC CTG CCT GAA GGA CAG-3′	5′-GCT CAT GAT TTCTGC TCT GAC A-3′
IFN-β	5′-AAA GAA GCA GCA ATT TTC AGC-3′	5′-CCT TGG CCT TCAGGT AAT GCA-3′
p21	5′-TGGAGACTCTCAGGGTCGAAA-3′	5′-CGGCGTTTGGAGTGGTAGAA-3′
p27	5′-CCGGTGGACCACGAAGAGT-3′	5′-GCTCGCCTCTTCCATGTCTC-3′

2.16.4 Gene Expression Analysis

The qRT-PCR was performed using the Light Cycler System (Applied Biosciences) to measure the mRNA expression levels of various targeted genes (Table 4). Each qRT-PCR reaction was conducted in triplicates, containing Power SYBR Green MasterMix (5 µl) (Applied Biosciences), forward and reverse primers (75 nM) and cDNA (500 ng), making up to total volume of 10 µl/well. The samples were incubated at 50°C and 95°C for 2 and 10 min, respectively, followed by amplification of the template for 40 cycles (15 seconds each cycle at 95°C and 1 min at 60°C). The specificity of the qRT-PCR was determined by melting-curve analysis. The gene expression of each target genes was normalized using the expression of human 18s rRNA (endogenous control). The cycle threshold (Ct) mean value for each target gene was used to calculate the relative expression of each reaction using the Relative Quantification (RQ) value and formula: RQ = 2–ΔΔCt, which was compared with 18s relative expression.

2.17 Luciferase Reporter Activity Assay

MDCK cells (0.4×10^6) were cultured in complete DMEM supplemented with 10% FBS until about 70–80% confluency. H1+N1 pseudotyped particles, harvested at 24 and 48 h, were used to carry out luciferase reporter activity using luciferase one-step assay kit (Thermo Scientific). Purified

rfhSP-D (5 and 10 μg/ml) was used to examine its effect on the luciferase reporter activity; cells + H1+N1, and cells only acted as controls. Luciferase readings were measured using a GloMax 96 Microplate Luminometer (Promega).

2.18 Multiplex Cytokine Array Analysis

A549 cells (0.5×10^7) were incubated with IAV subtypes with or without rfhSP-D (20 μg/ml) in serum-free DMEM medium for 24h at 37°C under 5% (v/v) CO_2. After incubation, the supernatant was collected in separate Eppendorf tubes for measuring the levels of secreted cytokines (TNF-α, IL-6, IL-10, IL-1α, IFN-α, and IL-12p40), chemokine (eotaxin), and growth factors (GM-CSF and VEGF). The levels of secreted cytokines in the supernatants were measured using MagPixMilliplex kit (EMD Millipore). The assay buffer (25 μl), provided in the kit, was added to each well of a 96-well plate, followed by addition of standard (25 μl), control (25 μl), or culture supernatant (25 μl) with IAV subtypes (in the presence or absence of rfhSP-D). Magnetic beads (25 μl) coupled to analytes were added to each corresponding well and incubated at 4°C for 18h. The wells were then washed with the assay buffer (25 μl) three times, and detection antibodies (25 μl) were incubated with the beads at RT for 1h. After washes with the assay buffer again (25 μl), Streptavidin–Phycoerythrin (25 μl) was added to the wells, followed by incubation at RT for 30 mins. Following washes, sheath fluid (150 μl) was added to each well, and the readout was measured using the Luminex Magpix instrument. Assays were performed in triplicates.

2.19 Cell Culture and Treatments for Breast Cancer Study

Human breast cancer cell lines used in this study were selected based on their phenotypes, including triple-negative BT20 ($ER^-/PR^-/HER2^-$) (ATCC-HTB19), triple-positive BT474 ($ER^+/PR^+/HER2^+$) (ATCC-HTB20) and HER2-postive SKBR3 ($ER^-/PR^-/HER2^+$) (ATCC-HTB30). Each cell line was grown in complete RPMI medium (Sigma-Aldrich), supplemented with 10% v/v Fetal Bovine Serum (FBS), 100U/ml penicillin (Sigma-Aldrich), 2mM L-glutamine, 100μg/ml streptomycin (Sigma-Aldrich) and 1mM sodium pyruvate (Sigma-Aldrich) under 5% (v/v) CO_2 at 37°C until 85% confluency was achieved. Since all three cell lines were adherent, a required number of cells were detached using 2 × Trypsin-EDTA (0.5%) (Fisher Scientific) as described

above. Cell number and viability were determined using Trypan Blue (0.4% w/v) and haematocytometer, as described above.

2.20 rfhSP-D-HYA interaction

For HYA (1500 kDa)-rfhSP-D interaction analysis, ELISA was performed as mentioned in section 2.13. Briefly, a fixed concentration of HYA (1500 kDa; 20µg/ml) (provided by Prof. Ivan Donati, Department of Life Sciences, University of Trieste) diluted in CBC, pH 9.6 buffer was incubated overnight at 4°C. After blocking and washing, different amounts of rfhSP-D (20,10,5,2.5 or 1.25 ug/ml) were added to corresponding wells and incubated at 37°C for 2h. In a parallel experiment, maltose-binding protein (MBP) (20,10,5,2.5 or 1.25 ug/ml) was used as a negative control. The unbound proteins were washed off using PBST three times. The binding between HYA-rfhSP-D/MBP was probed using polyclonal anti-rabbit human SP-D antibody (1:5000) (MRC Immunochemistry Unit, Oxford) or rabbit anti-MBP polyclonal antibody (1:5000) (Thermo Fisher), and protein A-HRP secondary conjugate (1:5000) (Sigma-Aldrich).

2.21 Fluorescence Microscopy

BT20, BT474 and SKBR3 ($0.5x10^5$) breast cancer cell lines were grown on round coverslips (Sigma-Aldrich) overnight under standard cell culture conditions in complete RPMI medium. The next day, the complete medium was removed, and the cells were washed gently with sterilized PBS twice, and incubated with rfhSP-D (10 or 20 µg/ml) in serum-free RPMI medium for different timepoints.

2.21.1 rfhSP-D Binding to breast cancer cell lines

After 1 h incubation of cells treated with rfhSP-D (10 µg/ml), unbound rfhSP-D was removed by washing the cells twice with PBS gently. The cells were then probed with primary antibodies- mouse anti-human SP-D or rabbit anti-human SP-D (MRC Immunochemistry Unit, Oxford) (1:200) for 1 h at RT. The cells were then washed twice with PBS ensuring the removal of excess antibody, and then incubated with secondary antibodies- anti-rabbit Alexa 488 conjugated with FITC (Thermo-Fisher) or anti-mouse conjugated with CY5 (Biogen) (1:500) and Hoechst (Thermo-Fisher) (1:10,000) for 1 h at RT. After washing, cells were fixed with 4 % paraformaldehyde (PFA) (Fisher-Scientific) for 1 min at RT. After fixation, 5 µl of antifade (Citiflour) was added on top of

the coverslips and the slides were viewed under the HF14 Leica DM4000 microscope for immunofluorescence analysis.

2.21.2 Apoptosis Microscopy

After treating the BT20, BT474 and SKBR3 ($0.5x10^5$) cells with rfhSP-D (20 µg/ml) for 24h, the coverslips were washed twice with 1× PBS carefully, and then incubated with FITC-Annexin V binding buffer containing FITC annexin (1:200) and PI (1:200) (Biolegend) for 15 min in dark at RT. After PBS wash three times, the coverslips were fixed with 4% PFA, followed by addition of antifade (5 µl) on top of the coverslips. The coverslips were then mounted on slides to view under a HF14 Leica DM4000 microscope.

2.22 MTT Assay

MTT [3-(4,5-dimethylthiazol-2-yl)-2,5-diphenyltetrazolium bromide] (Sigma-Aldrich) assay was performed to measure the cell metabolic activity among un-treated and treated cells. In this assay, MTT dye enters the mitochondria, where it is reduced into an insoluble formazan product. The cells are then solubilized with an organic solvent, and the released solubilized formazan is measured spectrophotometrically. BT20, BT474 and SKBR3 cells ($0.1x10^5$) were seeded in 96 well plates in RPMI complete medium. Once 80% of cell confluency was obtained, the cells were incubated with a range of rfhSP-D concentration (5, 10, and 20 µg/ml) in serum free RPMI medium for 24h and 48h. Following washes, different concentrations of rfhSP-D (5, 10, and 20 µg/ml) were added and incubated at 4°C for 6 hours. After removing the excess unbound rfhSP-D, 10,000 breast cancer cells were added and incubated at 37°C for 24h. r Post treatment, the cells were incubated with 50 µg/µl MTT (5 mg/ml stock) per well for 4 h at 37°C. After 4 h of incubation, 75 µl of media was removed, leaving behind 25 µl per well, which was then mixed thoroughly with 50 µl of dimethyl sulfoxide (DMSO) and incubated for another 10 min at 37°C. The absorbance was read at 570 nm using an ELISA plate reader.

2.23 Flow Cytometry

BT20, BT474 and SKBR3 cells (0.4×10^6) were seeded in culture petri dishes (Nunc) using RPMI medium containing 10% FCS. Next day, the cells were washed twice with sterilized PBS and incubated with a varied concentration of rfhSP-D (5, 10, and 20 µg/ml), along with an untreated

control in serum-free RPMI medium for 24h and 48h for apoptosis analysis. The cells were detached using 2 × Trypsin-EDTA (0.5%). Staurosporine (1μM/ml) was used as a positive control for apoptosis induction. Apoptosis induction was also examined using the FL-SP-D (20 μg/ml) purified from BT474 cell culture medium. After gentle washes with PBS, the cells were incubated with Alexa Fluor® 488 (1:200) (Sigma-Aldrich) and Hoechst (1:10,000) (Sigma-Aldrich) for 15 mins at RT in dark. Following washes with 1×PBS three times, apoptosis induction by rfhSP-D/FL-SP-D/Staurosporine was measured using Novocyte Flow Cytometer. Compensation parameters were acquired using unstained, untreated FITC stained, and untreated PI-stained samples for all three cell lines.

For solid phase studies, constant concentration of HYA (1500 kDa) (20 μg/ml) was coated in a 6 well plates overnight at 4°C with and without rfhSP-D (20 μg/ml). After removing unbound HYA and rfhSP-D, the wells were washed with PBS, followed by addition of 0.4×10^6 cells to the HYA/rfhSP-D-coated wells and incubation at 37°C for 24h. For cell proliferation studies, the cells (0.4×10^6) were washed with PBS, probed with anti-mouse Ki-67 (Bio-Legend) diluted in permeabilization reagent of the FIX&PERM kit (Fisher Scientific), and incubated at RT for 30 minutes. After PBS washes, the cells were incubated with goat anti-mouse-FITC conjugate (1:200) (Fisher Scientific) at RT in dark for 30 minutes. Cells (12,000) were acquired for each experiment and compensated before plotting the acquired data.

2.24 Immunohistochemical analysis

Breast cancer tissues and adjacent peritumoral mammary parenchymas used in this experiment were selected following ethical approval by the University Hospital of Palermo, Italy. The written consent for the use of subsequent tissue and blood specimens were signed and approved by the participants legally. The immunohistochemical experiments (Immunohistochemistry and Alcian blue staining) were performed by Dr Beatrice Belmonte (Tumor Immunology Unit, Human Pathology Section, Department of Health Sciences, University of Palermo, Palermo, Italy).

2.24.1 Immunohistochemistry (IHC)

Luminal A, Luminal B, $HER2^+$ and triple-negative breast cancer (TNBC) tissues were used, along with normal breast tissue as a control. Immunohistochemistry (IHC) technique was carried out

using a polymer detection method. The selected breast cancer tissues were fixed using 10% (v/v) buffered formalin and 4 µm-thick tissue sections were deparaffinised and rehydrated. The antigen unmasking procedure was performed using Novocastra Epitope Retrieval Solutions, pH 6 (EDTA-based) (Leica Biosystems) in a water bath for 30 min at 98°C. The tissue sections were then brought to RT, followed by gentle washes with PBS twice. The endogenous peroxidase was neutralized using 3% (v/v) H_2O_2, followed by Fc blocking (Novocastra, Leica Biosystems); the samples were then incubated at 4°C overnight with mouse anti-human SP-D monoclonal antibody (1:800) (Abcam). The staining was assessed via polymer detection kit (Novocastra, Leica Biosystems) and AEC (3-amino-9-ethylcarbazole) (Dako, Denmark) substrate chromogen. The slides were counterstained with Harris Hematoxylin (Novocastra, Leica Biosystems), and the prepared tissue sections were viewed under the Axio Scope A1 optical microscope (Zeiss). Axiocam 503 color digital camera (Zeiss) was used to collect microphotographs and analysed using the Zen2 software.

2.24.2 Alcian Blue Staining

The presence of HYA in the breast cancer tissue sections were detected using alcian blue staining. Deparaffinised and rehydrated tissue sections were incubated in 1 % Alcian blue (Dako) (diluted in 3 % v/v acetic acid, pH 2.5) at RT for 30 min. After incubation, the tissue sections were gently washed under running water for 10 mins and the sections were dehydrated in progressively increasing percentages of ethanol (80, 90 and 100 %). The mounted slides were then viewed under a Leica DM 3000 optical microscope; and images were collected using a Leica DFC320 digital camera (Leica Microsystems, Wetzlar, Germany).

2.25 Adhesion Assay

BT20, BT474 and SKBR3 cells (0.5×10^5) were seeded in T75 culture flask and grown in complete RPMI medium overnight at 37°C under 5% (v/v) CO_2. The following day, the complete medium was removed, the cells were gently washed with PBS, and labelled with FAST DiI fluorescent dye (Molecular Probes, Invitrogen). The stained cells (resuspended in serum free RPMI medium) were then allowed to adhere to 96 microtiter wells pre-coated with 20 µg/ml of HYA, rfhSP-D and BSA (negative control). The cell adhesion was measured after 35 mins of incubation at 37°C under standard cell culture conditions. The wells were washed with PBS twice to remove the non-

adhered cells, and the remaining cells were lysed using lysis buffer containing 10 mM Tris–HCl, pH 7.4 + 0.1% (v/v) SDS. The plate was read at 544nm using Infinite200 (TECAN), and the data were expressed as percentage adhesion with reference to a standard curve established using an increasing number of FAST DiI stained cells.

2.26 mRNA Transcript Analysis of Cell Cycle Inhibitors

BT20, BT474, or SKBR3 cells (0.5 x 10^7) were grown in RPMI containing 10% FCS until 85% cell confluency was reached. Cells (0.3 x 10^7) were added on to pre-coated 6-well plate with HYA (20 µg/ml), HYA+rfhSP-D (20 µg/ml), and rfhSP-D (20 µg/ml) and incubated at 37°C for 24h. The treated cell pellet was frozen at −80°C for RNA extraction later. The, RNA and cDNAs were prepared as mentioned in section 2.16. p21/p27 mRNA levels were performed via qRT-PCR (as described in section 2.16.4) using the primers listed in table 5.

2.27 Intracellular Signaling Analysis

Signaling pathways in rfhSP-D treated breast cancer cells in the presence of HA were analysed using the 'PathScan Intracellular Signaling Array Kit (Cell Signaling Technology). BT20, BT474 and SKBR3 cells (0.5 × 10^6) were seeded in a 6-well plate in serum-free RPMI medium. Following washes with PBS, cells (resuspended in serum free RPMI medium), cells were left to adhere to pre-coated plates with HYA and rfhSP-D (20 µg/ml) for 25 min at 37°C under 5% (v/v) CO_2. The medium was discarded, and the unbound cells were washed with cold PBS, followed by cell lysis using ice-cold lysis buffer containing a cocktail of protease inhibitors (Roche Diagnostics). The wells were then incubated with array diluent blocking buffer (100 µ/well) at RT for 15 mins on the multi-well gasket. After incubation, the array blocking buffer was decanted, and the cell lysate (75 µl) (0.8 mg/ml) was added to each corresponding well, followed by incubation at RT for 2h on an orbital shaker. The contents in the wells were then discarded and washed with 1x Array Wash Buffer (100 µl) three times (5 mins each wash). Biotinylated detection cocktail antibody (100 µl/well) was added to the wells, and incubated at RT for 1 h, followed by probing with Streptavidin-conjugated DyLight 680 (100 µl/well) for 30 mins. The fluorescence readout was measured using the LI-COR Biosciences Infrared Odyssey imaging system (Millennium science) and collected data was processed by the software Image studio 5.0.

2.28 Statistical Analysis

The graphs included in this thesis were generated using the GraphPad Prism 6.0 software, a one-way ANOVA test was carried out for statistical significance analysis. Significant values were considered based on *$p < 0.05$, **$p < 0.01$, and ***$p < 0.001$, between untreated and treated samples. Error bars represents the SD or SEM (n=3), as indicated in the figure legends.

Chapter 3

Interaction between rfhSP-D and Influenza A Virus

3.1 Abstract

Human surfactant protein D (SP-D) can modulate host response against pathogens via a diverse range of mechanisms. The direct interaction between influenza A virus (IAV) and SP-D has been shown to result in virus neutralization and enhanced phagocytosis. Anti-viral role of SP-D during IAV infection is well-documented; SP-D binds via its CRD region to carbohydrate pattern on hemagglutinin (HA) and neuraminidase (NA) of the IAV. SP-D- HA binding leads to direct inhibition of cellular infection via restriction of HA-sialic acid (SA) interaction. In this study, anti-IAV role of a recombinant fragment of human SP-D (rfhSP-D), composed of homotrimeric neck and CRD regions, has been examined. rfhSP-D bound both IAV subtypes (H1N1 and H3N2) in a dose- and calcium-dependent manner. Far-western blotting analysis revealed that rfhSP-D binds to HA (~70 kDa), NA (~60 kDa), and M1 (~25 kDa). rfhSP-D can modulate IAV entry, as evident from down-regulation of matrix protein 1 (M1) in A549 cells infected with IAV subtypes, pH1N1 and H3N2 at 2h rfhSP-D treatment. In addition, IAV-induced mRNA levels of IFN-α, IFN-β, TNF-α, IL-6, and RANTES were reduced following rfhSP-D treatment for both pH1N1 and H3N2, particularly at 2h post-infection of A549 cell line. rfhSP-D was also found to interfere with IAV infection of MDCK cells through HA binding and reduce luciferase reported activity in MDCK cells transfected with H1+N1 pseudotyped lentiviral particles. ~30% reduction in luciferase activity was seen with rfhSP-D (10 μg/ml) treatment, suggestive of an entry inhibitory role of rfhSP-D against IAV infectivity. Furthermore, rfhSP-D treatment also led to suppression of crucial pro-inflammatory cytokines and chemokines levels, as revealed by the multiplex cytokine array analysis. In the case of pH1N1 subtype, rfhSP-D treatment resulted in suppressed levels of IFN-α, TNF-α, IL-12 (p40), IL-10, GM-CSF, eotaxin and VEGF at 24h post-treatment. However, down-regulation of IL-12 (p40), IL-10, eotaxin and VEGF was not so evident in the case of H3N2 infected A549 cells, with the exception IFN-α, TNF-α, and GM-CSF. These data demonstrate that the anti-IAV effect of rfhSP-D and its immunomodulatory effect on host cells can depend on an IAV-subtype-specific manner.

3.2 Introduction

The immune system is composed of innate and adaptive immunity, consisting of effector mechanisms that contribute to host defense against a variety of pathogens. The initial primary response to an infection in a host is the trigger of its innate immune system. To distinguish self from non-self, the innate immune cells recognize pathogen associated molecular patterns (PAMS) via its pattern recognition receptors (PRRs) such as C-type lectin receptors (CLRs) and toll-like receptors (TLRs). Collectins are soluble multimeric lectins, representing an important group of Ca^{2+}-dependent soluble PRRs detected in the pulmonary surfactant and several mucosal surfaces (Nayak et al., 2012). Collectins are involved in the first line of defense against several pathogens via binding and interacting with specific glycoconjugates and lipid moieties found on the surface of microorganisms (Van Iwaarden et al., 1994, Murugaiah et al., 2020b).

In vivo and *in vitro* studies have demonstrated the immunomodulatory roles of human SP-D against pathogens. SP-D is composed of a cysteine-linked N-terminal region, a triple-helical collagen region, an α-helical neck region, and the C-terminal carbohydrate recognition domains (CRDs) or C-type lectin domain (Kishore et al., 2006). SP-D is present in pulmonary, as well as non-pulmonary, epithelia, but primarily synthesized by Clara cells and alveolar type II (Kishore et al., 2006). SP-D can induce numerous protective functions against including agglutination, opsonization, neutralization and enhanced phagocytosis (Kishore et al., 2006). SP-D is also involved in controlling pulmonary inflammation, and thus, linking innate immunity with adaptive via modulation of maturation of dendritic cell and helper T cells polarization (Madan et al., 1997b, Nayak et al., 2012).

Direct interaction between SP-D and various viruses often results in viral neutralization and phagocytosis induction *in vitro* (Hartshorn et al., 1994, Hartshorn et al., 2000). Anti-viral activity of human SP-D during Influenza A Virus (IAV) infection have been reported, where SP-D can bind HA and NA, and inhibit hemagglutination at initial stages of the infection (Hillaire et al., 2013). IAV is an enveloped RNA virus, it encodes two surface glycoproteins, nucleocapsid protein, an ion channel protein, structural scaffolding protein, two non-structural proteins, a tripartite polymerase complex, and three non-essential proteins (Roberts et al., 2015). IAV is subtyped based on HA and NA glycoproteins, and both glycoproteins are involved in viral replication and

pathogenicity (Mitnaul et al., 2000). IAV binding to target host cells is mediated by the globular head region of HA to SA receptors found on the surface of a host cell (Skehel and Wiley, 2000, Wilson and Cox, 1990). Subtypes of IAV have been suggested to bind α (2–6) linkage of SA receptors in humans (Glaser et al., 2005). It is reported that SA and its linkage are important for the initiation of IAV infection of both epithelial and immune cells. Thus, SA receptor binding inhibition or enzymatic switching of SA-mediated linkages can result in cell resistant or alter susceptibility to IAV infection. Subsequently, SA present on cell surfaces is considered as an imperative essential receptor and determinant of IAV tropism, contributing to immune response trigger as well as to viral pathogenesis.

It is crucial to study the molecular mechanisms of host defense against viruses, including IAV to produce novel anti-IAV therapies. SP-D-HA binding interaction results in direct inhibition of cellular viral infection by preventing HA-SA receptor binding (Hartshorn et al., 2008). Interaction of SP-D with HA-mediated glycosylation sites has been reported, and SP-D has been identified as a β-type inhibitor of IAV. This interaction is Ca^{2+}-dependent, thus, SP-D binding to NA can also inhibits the release of progeny viral particles from infected host cells (Tecle et al., 2007, Hartshorn et al., 2000). Furthermore, recombinant full-length porcine SP-D is involved in anti-viral activity against different subtypes of IAV by similar mechanisms, more than human SP-D due to differences in their structural domains, such as additional loop in its CRD region, an additional cysteine in the collagen domain and, an additional glycosylation site (Hillaire et al., 2014).

In this study, a well-characterized recombinant homotrimeric fragment of human SP-D comprising neck and CRD region (rfhSP-D) was used to examine its ability to act as an entry inhibitor of IAV using pseudotyped viral particles, and modulation of subsequent immunological response *in vitro*.

3.3 Results

3.3.1 Expression and Purification of a Recombinant Fragment of Human SP-D (rfhSP-D)

Recombinant expression of human SP-D and has been previously reported in *E.coli* BL21 (λDE3) pLysS under bacteriophage T7 promoter (Singh et al., 2003), containing the pUK-D1 construct (compromising eight Gly-X-Y repeats, the neck and CRD regions). The transformants expressed a ~20 kDa protein following IPTG induction, compared to the un-induced cells (Figure 15). The over-expressed insoluble rfhSP-D from inclusion bodies was refolded by the method of denaturation and renaturation. The soluble rfhSP-D fractions were purified using maltose-agarose column and appeared as a single band on 15% SDS-PAGE (v/v) under reducing condition (Figure 15). The purified peak fractions of rfhSP-D were loaded onto to the Pierce™ High-Capacity Endotoxin Removal Resin (Qiagen) column to remove LPS and the endotoxin levels were found to be 0.5 pg/μg of rfhSP-D (Figure 16). The immunoreactivity of affinity purified rfhSP-D was analysed and confirmed via western blotting, using anti- SP-D polyclonal antibody that was raised against native human SP-D (Figure 17).

3.3.2 Affinity Purified rfhSP-D Binds to IAV Subtypes

The ability of microtiter-coated rfhSP-D to bind pH1N1 and H3N2 IAV subtypes was determined using direct binding ELISA (Figure 17). rfhSP-D bound both pH1N1 andH3N2 in a calcium and dose-dependent manner. VSV-G pseudotyped lentivirus was used as a negative control RNA virus, which did not show any binding with all rfhSP-D concentrations tested. The ability of rfhSP-D to interfere with IAV binding *in vitro* was then assessed via cell binding assay using A549 cells (Figure 18). A549 cells were challenged with purified pH1N1 or H3N2, pre-incubated with a varied concentration of rfhSP-D. Increased IAV binding in the presence of rfhSP-D was observed at the concentration of 10 μg/ml for both IAV subtypes, and the binding was found to occur in a dose-calcium dependent manner. MBP was used as a negative control; no significant binding was observed.

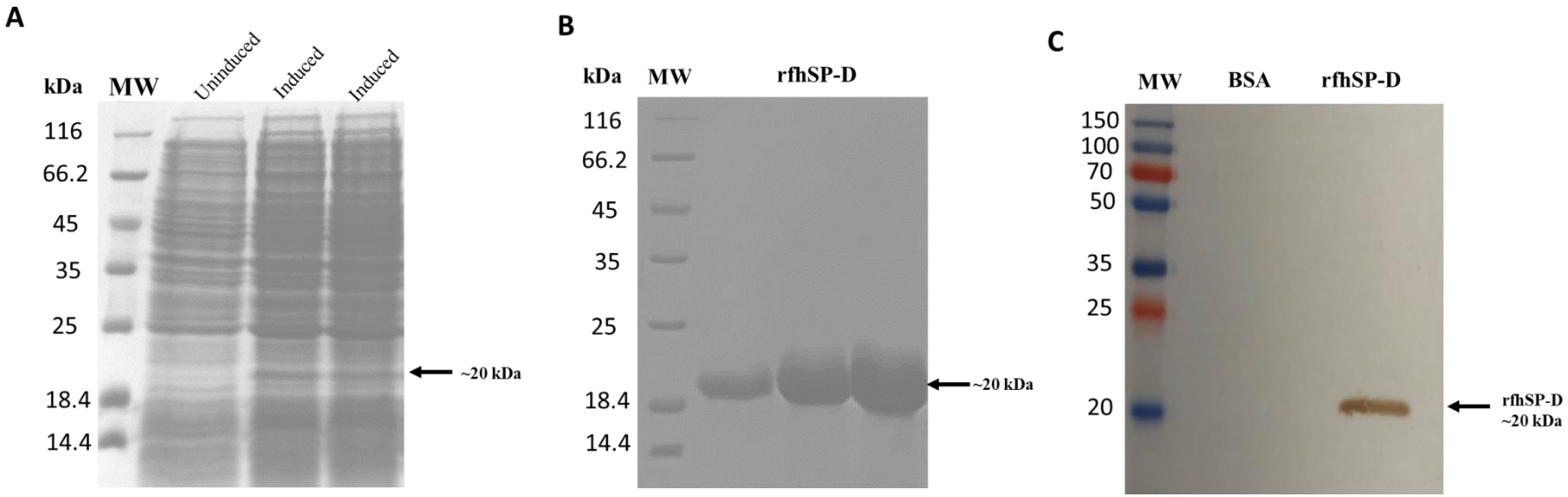

Figure 15: Expression and Purification of a Recombinant form of Human Surfactant Protein D (rfhSP-D).

(A) Expression of rhSP-D under bacteriophage T7 promoter, expressed as ~20kDa insoluble protein. Different colonies that were tested for rfhSP-D expression following IPTG induction (Lanes 2-3). (B) Eluted fractions (lanes 1-3) were passed through a maltose agarose column appeared as a single band at ~20kDa. (C) Immunoreactivity of affinity purified rfhSP-D was examined via wester blotting; lane 1: BSA as negative control and lane 2: purified rfhSP-D.

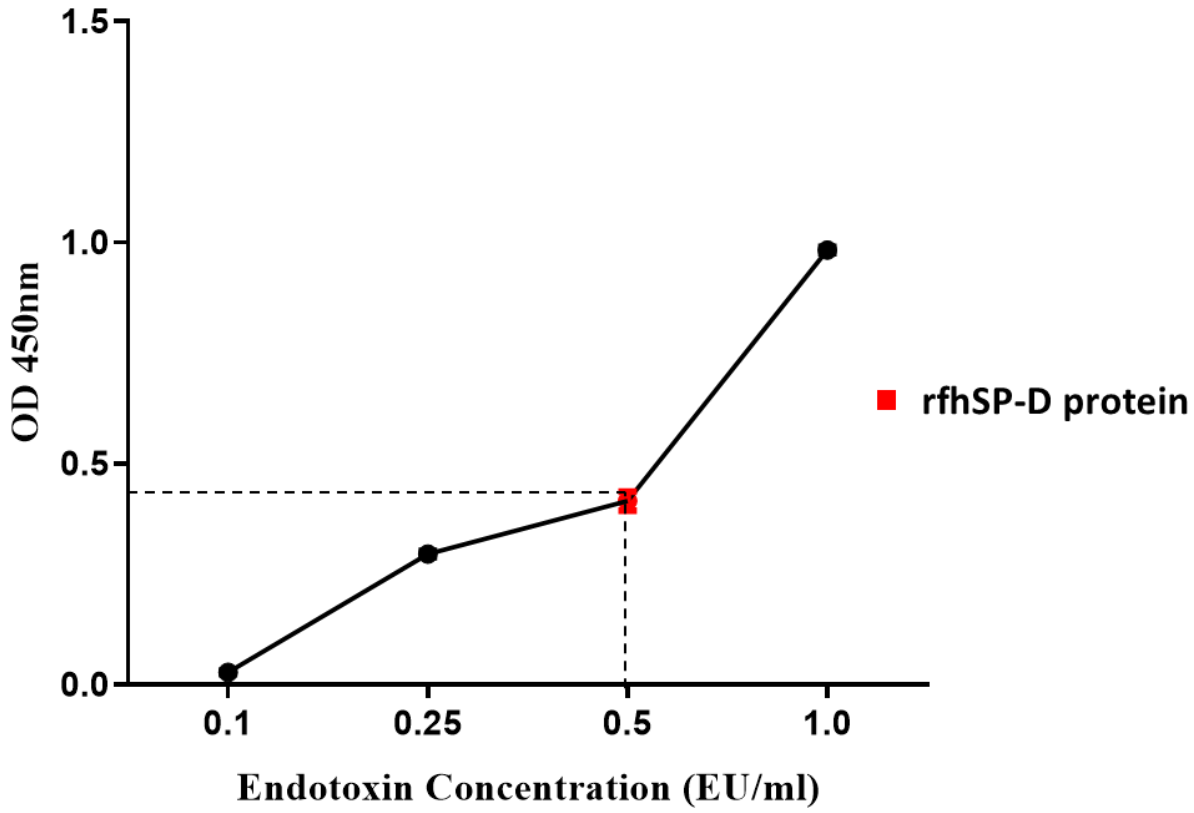

Figure 16: Expression and Purification of a Recombinant form of Human Surfactant Protein D (rfhSP-D).

The endotoxins trigger Factor C proteolytic activity found in limulus amebocyte lysate (LAL), which is photometrically measured using chromogenic substrate 405 nm. A standard curve is generated using 4 E. coli endotoxin standards, which were plated in parallel to the test (rfhSP-D) sample. Using standard curve, where 1 EU/ml is equivalent to 0.1ng endotoxin/ml, the endotoxin levels of purified rfhSP-D were found to be ~0.5 pg/µg.

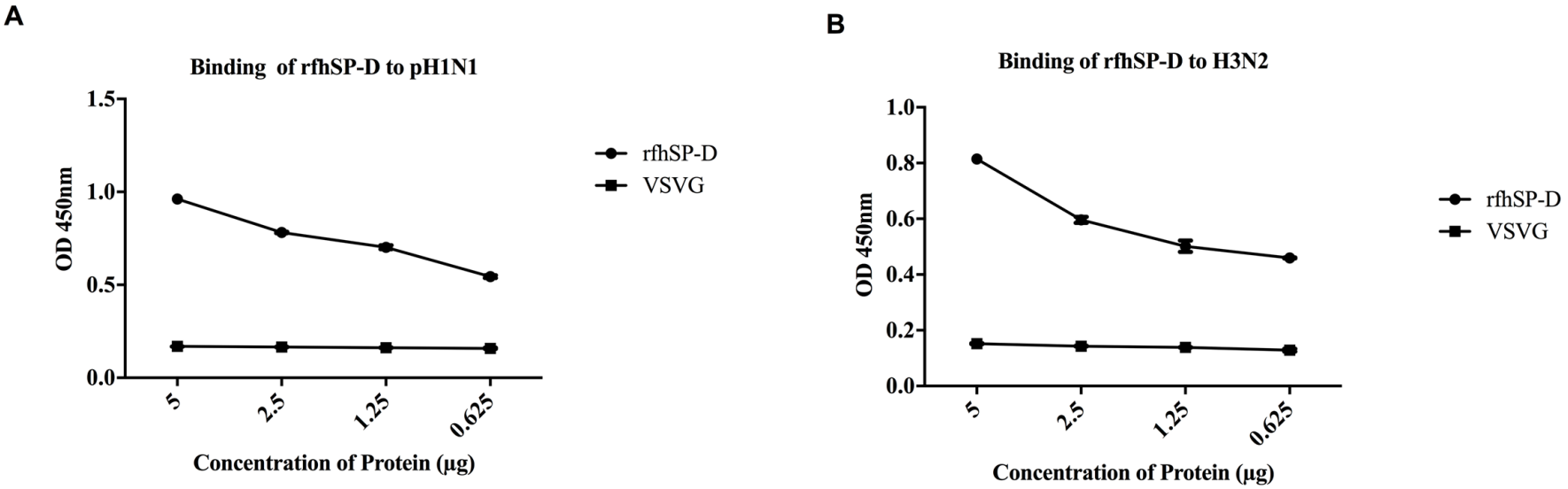

Figure 17: ELISA to show rfhSP-D binding to (A) pH1N1 and (B) H3N2 IAV subtypes.

96-microtiter wells were coated with varied concentrations of rfhSP-D (5, 2.5, 1.25, and 0.625 µg/ml). 20 µl of concentrated pH1N1 or H3N2 virus (1.36×10^6 pfu/ml) was diluted in PBS (200 µl) + 5 mM CaCl2 and 10 µl of diluted virus was added to all the wells and incubated at 37°C for 2h. The wells were then probed with either monoclonal anti-influenza virus H1 or polyclonal anti-influenza virus H3 antibody (1:5000). VSV-G pseudotyped lentivirus was used as a negative RNA virus control. The data were plotted as mean of three independent experiments done in triplicates ± SEM.

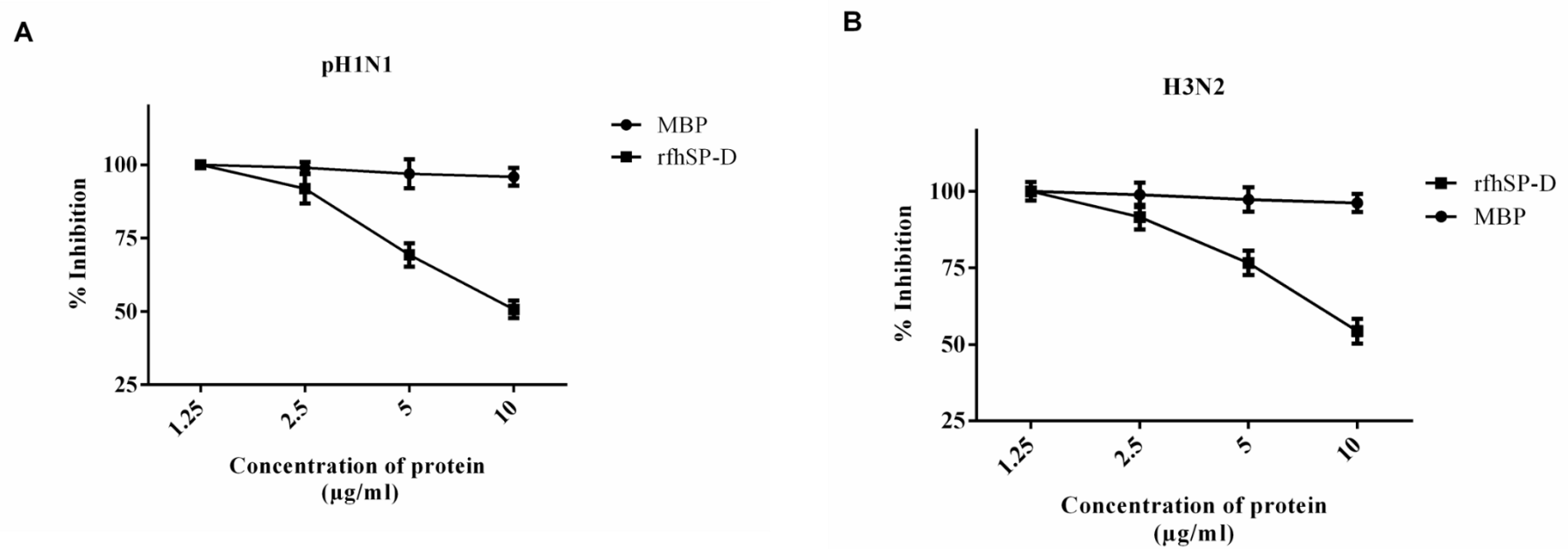

Figure 18: Cell-binding assay to show binding of (A) pH1N1 and (B) H3N2 IAV subtypes pre-incubated with rfhSP-D to A549 cells.

96-microtiter wells were coated with A549 cells (1×10^5 cells/ml) and incubated overnight at 37°C under standard cell culture conditions. Different concentrations of pre-incubated rfhSP-D (10, 5, 2.5, or 1.25 µg/ml) with pH1N1 and H3N2 virus were added to the corresponding wells and incubated for 2h at room temperature. Following fixation with 4% paraformaldehyde solution, monoclonal anti-influenza virus H1, or polyclonal anti-influenza virus H3 were added to corresponding well. Pre-incubated maltose-binding protein (MBP) (10, 5, 2.5, or 1.25 µg/ml) with pH1N1 and H3N2 virus was used as a negative control protein. The data were expressed as mean of three independent experiments done in triplicates ± SEM.

3.3.3 rfhSP-D Interacts with HA and Restricts IAV Replication in A549 Cells

Human SP-D binding to the glycosylation site of HA1 domain on IAV is well documented (Hartshorn et al., 2000). Binding of rfhSP-D (10 μg/ml) to HA (~70 kDa) and M1 (~27 kDa) of pH1N1 and H3N2 IAV subtypes was established using far western-blotting (Figure 19). A direct binding ELISA was also performed to examine the ability of rfhSP-D (5, 10 and 20 μg/ml) to bind purified recombinant HA protein of IAV (Figure 19). rfhSP-D interacted with HA dose- and –calcium dependently; no significant binding was seen with VSV-G pseudotyped particles.

In view of rfhSP-D binding to key IAV proteins, an infection assay was carried out to assess the impact of this interaction on IAV viral infectivity and replication. rfhSP-D interaction with key proteins of IAV may suppress cellular viral infection, i.e. by inhibiting HA interaction with SA containing receptors, and HA-induced fusion to endosomes. rfhSP-D-HA interaction may appear to be another dimension at which rfhSP-D may inhibit target cell infection, thus, intracellular replication. The mechanism of direct inhibition of IAV infectivity by purified rfhSP-D (10 μg/ml) protein was thus investigated via infection assay (Figure 20). An up-regulation of M1 mRNA expression at 2 and 6h was seen in A549 cells infected with pH1N1 or H3N2 (Figure 20). However, A549 cells infected with IAV subtypes pre-incubated with rfhSP-D showed down regulation of M1 expression compared to A549 cells challenged with pH1N1 or H3N2 virus alone. M1 downregulation due to rfhSP-D preincubation was found to be more effective in the case of pH1N1 when compared to H3N2 subtype; a -8 $\log_{10}$ fold downregulation was seen at 2 h rfhSP-D preincubation. This suppressive effect by rfhSP-D was validated using western-blotting (19); a lower level of M1 expression was detected in rfhSP-D treated sample following post 6h incubation, compared to untreated samples (A549 cells + virus). In addition, titration assay was also performed to establish the anti-IAV effect of rfhSP-D (Figure 21). Nearly 40% virus titer reduction was observed with rfhSP-D (10 μg/ml) treated cells compared to untreated samples, suggestive of rfhSP-D's ability to act as an entry inhibitory of IAV infection. However, differential inhibitory effects of rfhSP-D on IAV subtypes may reflect on the glycosylation of IAV glycoproteins, including HA or NA, implying a significant correlation between HA-glycan binding and susceptibility of IAV subtypes to inhibition by rfhSP-D that involve specific binding sites on IAV glycoproteins.

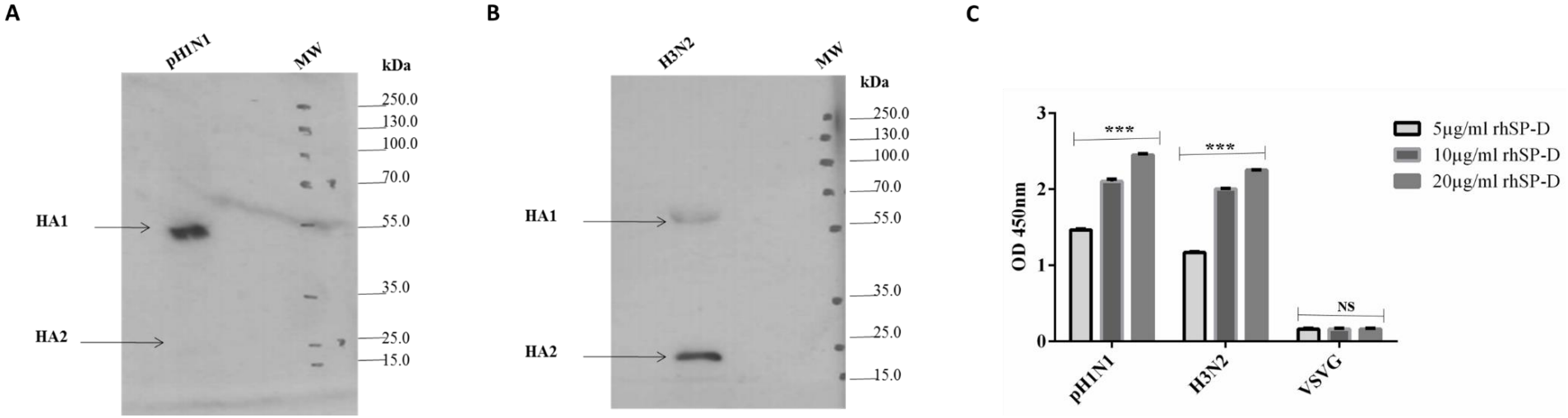

Figure 19: Far-western blot analysis to show binding of rfhSP-D to purified (A) pH1N1 and (B) H3N2 subtypes of IAV.

Concentrated virus (10 µl) (1.36×10^6 pfu/ml) was first run on the 12% (v/v) SDS-PAGE, and then transferred onto a nitrocellulose membrane, followed by incubation with rfhSP-D (5 µg). The membrane was probed with anti-rabbit SP-D polyclonal antibodies in PBS (1:1000). (A&B) rfhSP-D bound to hemagglutinin (HA) (~70 kDa) and matrix protein 1 (~M1) (27 kDa) in the case of both pH1N1 and H3N2 IAV subtypes. (C) ELISA to show the rfhSP-D binding to purified recombinant HA (5, 10, and 20 µg/ml). VSV-G was used as a negative control protein. The data were plotted as mean of three independent experiments carried out in triplicates ± SEM. Significance was determined using the unpaired one-way ANOVA test (***$p < 0.0001$) ($n = 3$).

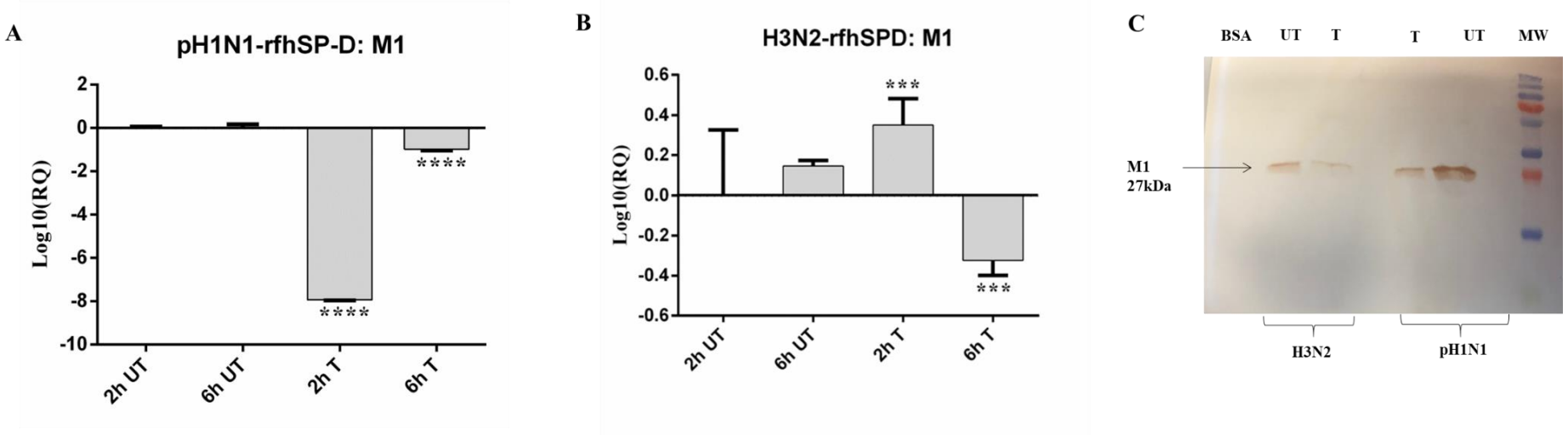

Figure 20: rfhSP-D suppress replication of (A) pH1N1 and (B) H3N2 in target human A549 cells.

(A&B) Expression of M1 in pH1N1 and H3N2 subtypes of IAV after infection of A549 cells at 2 and 6 h. A549 cells (0.4×10^6 cells/ml) were incubated either with pre-incubated pH1N1 and H3N2 with or without purified rfhSP-D (10 µg). Cell pellets harvested at 2 and 6 h were subjected to qRT-PCR to analyze the M1 expression of IAV. Infection was measured via qRT-PCR using M1 primers and 18S (an endogenous control). Data shown are normalized to M1 levels at 2 h untreated control (cells + virus). Significance was determined using the unpaired one-way ANOVA test (**$p < 0.01$, ***$p < 0.001$, and ****$p < 0.0001$) ($n = 3$). (C) Western blotting to shown expression of M1 in untreated (cells + virus) and treated (cells + virus + 10 µg/ml rfhSP-D) following 6 h incubation. A549 cells (1×10^5 cells/ml) were incubated either with pre-incubated pH1N1 and H3N2 with or without purified rfhSP-D (10 µg). Cell pellets were harvested, sonicated, and the proteins separated on 12% (v/v) transferred on to nitrocellulose membrane, blocked with 5% milk and probed with anti-mouse M1 antibody for 1 h followed by anti-rabbit conjugated with HRP for 1 h before developing colour with DAB.

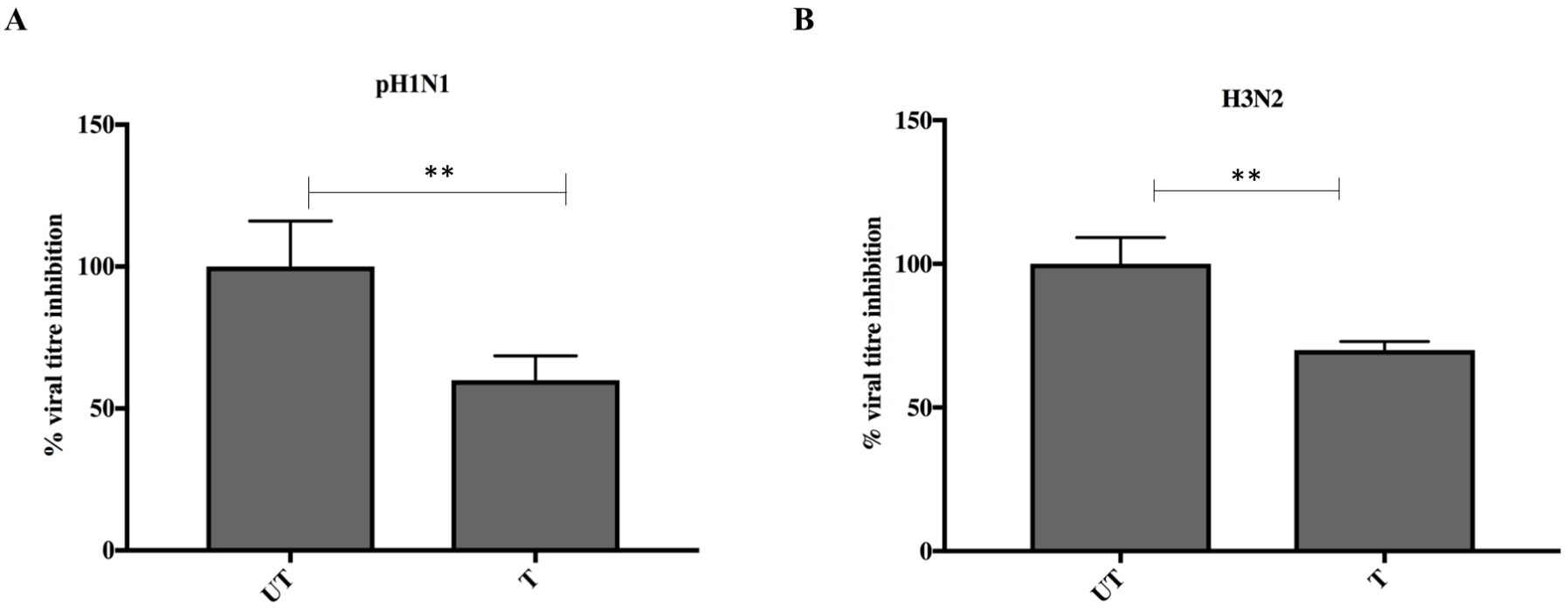

Figure 21: Titration assay to show the anti-IAV activity of rfhSP-D (10 µg/ml), using both pH1N1 (A) and H3N2 (A) IAV subtypes.

A549 cells (0.4×10^6 cells/ml) were infected with pH1N1/H3N2 (MOI 1) for 24 h. Then, the supernatants were harvested, and viral titer measured using a $TCID_{50}$ assay. rfhSP-D (10 µg/ml) treatment reduced viral titer by approximately 40%, suggesting that rfhSP-D acts as an entry inhibitor of IAV subtypes tested.

3.3.4 rfhSP-D Triggers an Anti-inflammatory Response in A549 cells Following Viral Challenge

The mRNA expression of pro-inflammatory cytokines and chemokines following rfhSP-D (10 μg/ml) treatment was determined via qRT-PCR analysis. The relative mRNA expression levels of pro-inflammatory cytokines, TNF-α and IL-6, by H3N2 strain were upregulated at 6 h post treatment, which were brought down slightly by rfhSP-D treatment at 2 h (Figure 22 & 23). However, TNF-α and IL-6 mRNA levels were found to be downregulated in pH1N1-infected A549 cells considerably by rfhSP-D at 2 h, which gradually recovered by 6 h (Figure 21 & 22). By contrast, reduced mRNA level of IL-12 was observed in both pH1N1/H3N2 challenged A549 cells incubated with rfhSP-D, suggesting a likely Th1 response reduction and suppression of IFN-γ production by $CD4^+$ T cells. RANTES (1 $\log_{10}$ fold) levels were also suppressed by rfhSP-D at 2 h treatment in the case of pH1N1. However, in the case of H3N2 infected cells, RANTES levels were also downregulated by 0.5-fold ($\log_{10}$) at 2 h following rfhSP-D treatment when compared to untreated sample (cells + virus). Furthermore, rfhSP-D treatment also led to suppression of type 1 interferons, IFN-α and IFN-β, at 2 and 6h post-treatment (Figure 23). Suppressive effects by rfhSP-D on type 1 INF levels is an indication of rfhSP-D ability to reduce the rate of viral replication and infectivity, thereby, downregulating the levels of INF produced by the innate immune cells as a first line of defense.

3.3.5 Differential Ability of rfhSP-D to Downregulate Pro-inflammatory Cytokines and Chemokines

A multiplex cytokine array was performed to assess secretion of cytokines, chemokines, and growth factors using supernatants of the IAV challenged and rfhSP-D treated A549 cells 24 h post rfhSP-D treatment. A dramatic suppression of some of the key pro-inflammatory cytokines and chemokines were seen with rfhSP-D (10 μg/ml) treatment when compared to virus infected A549 cells. In the case of pH1N1, rfhSP-D treatment led to downregulation of IFN-α, TNF-α, IL-10, IL-12 (p40), GM-CSF, VEGF, and eotaxin at 24 h (figure 25 & 26). However, these suppressive effects on IL-10, eotaxin, VEGF, and IL-12 (p40) were not observed in H3N2 subtype, with the exception of IFN-α, TNF-α, and GM-CSF. These data seem to suggest that the anti-IAV effect of SP-D and its immunomodulatory effect on host cells can depend on an IAV-subtype-specific manner.

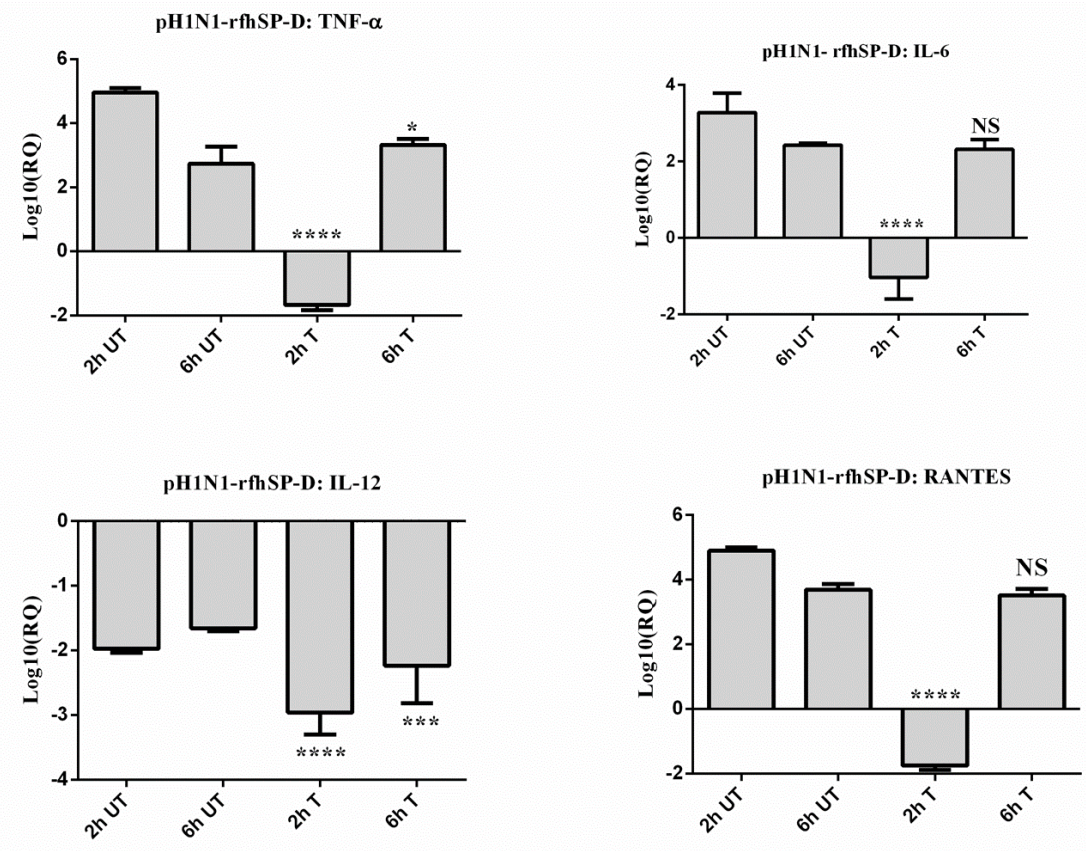

Figure 22: mRNA expression profile of A549 cells challenged with pre-incubated pH1N1 with rfhSP-D (10 µg/ml) in both untreated (cells + virus) and treated samples (cells + virus + rfhSP-D).

mRNA transcript expression levels of cytokines and chemokine were measured using qRT-PCR and the data were normalized using 18S rRNA expression as a control. The relative expression (RQ) was calculated by using cells only time point as the calibrator. RQ = $2^{-\Delta\Delta Ct}$ was used to calculate the RQ value. Assays were conducted in triplicates and error bars represents ± SEM. Significance was determined using the unpaired one-way ANOVA test (*$p < 0.05$, **$p < 0.01$, ***$p < 0.001$, and ****$p < 0.0001$) (n = 3).

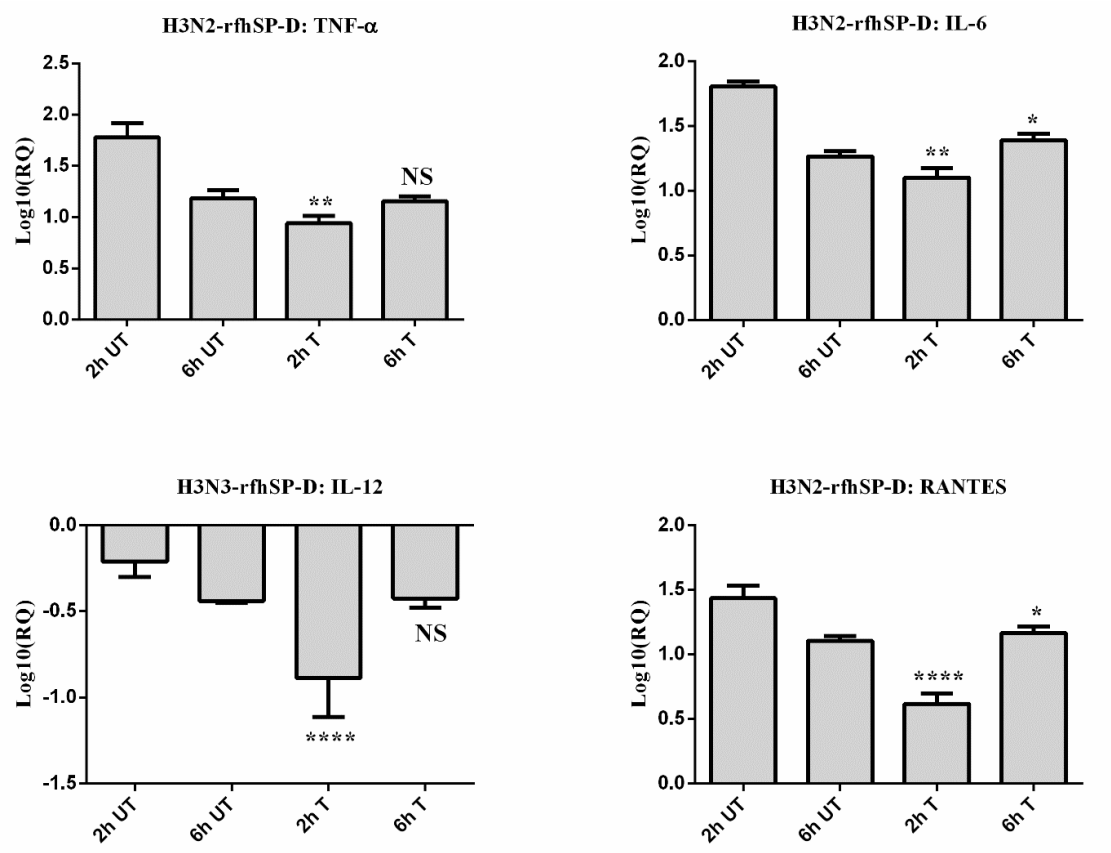

Figure 23: mRNA expression profile of A549 cells challenged with pre-incubated H3N2 with rfhSP-D (10 µg/ml) in both untreated (cells + virus) and treated samples (cells + virus + rfhSP-D).

mRNA transcript expression levels of cytokines and chemokine were measured using qRT-PCR and the data were normalized using 18S rRNA expression as a control. The relative expression (RQ) was calculated by using cells only time point as the calibrator. RQ = 2−ΔΔCt was used to calculate the RQ value. Assays were conducted in triplicates and error bars represents ± SEM. Significance was determined using the unpaired one-way ANOVA test (*$p < 0.05$, **$p < 0.01$, ***$p < 0.001$, and ****$p < 0.0001$) (n = 3).

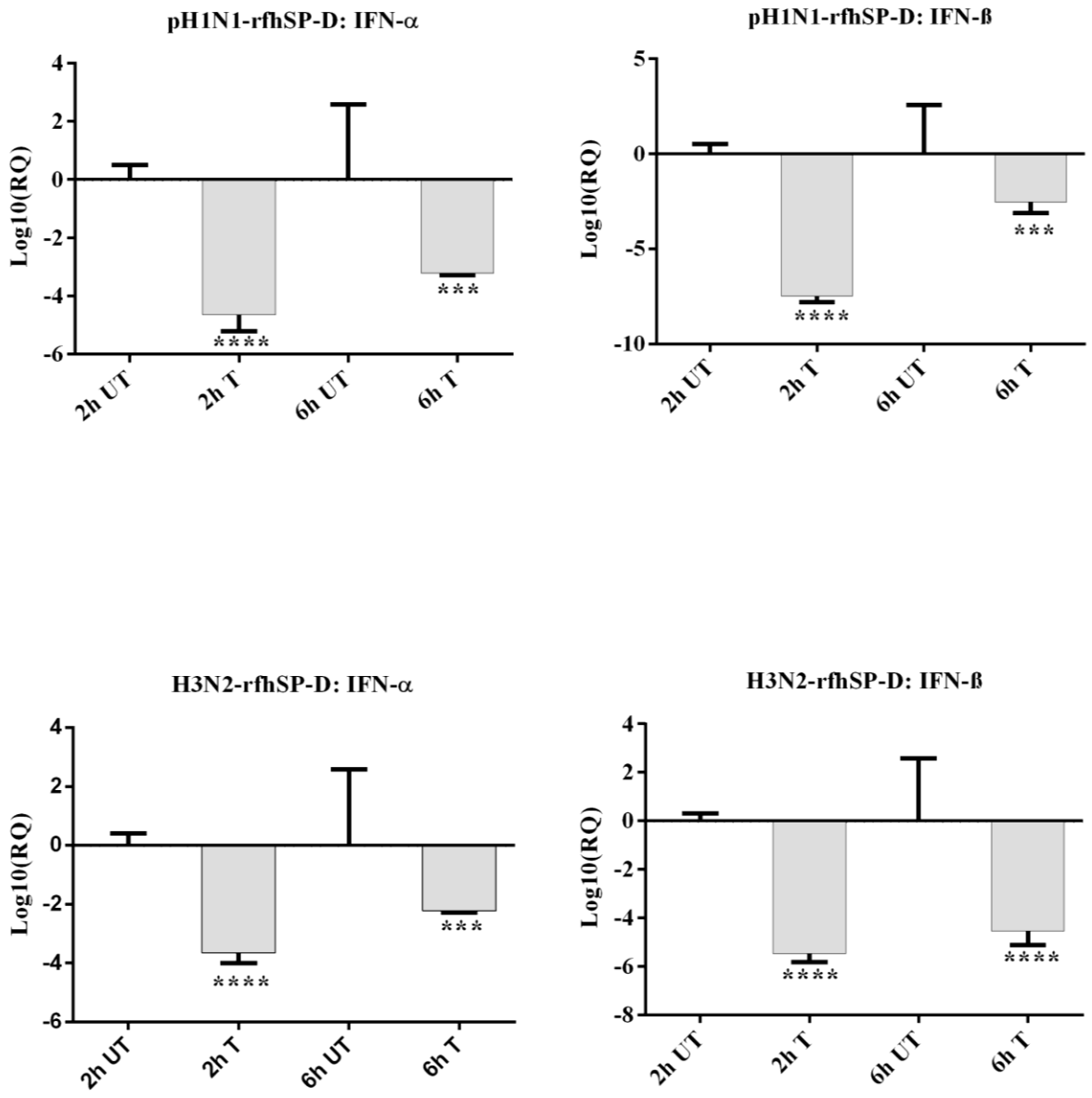

Figure 24: mRNA expression profile of A549 cells challenged with pre-incubated H3N2 with rfhSP-D (10 µg/ml) in both untreated (cells + virus) and treated samples (cells + virus + rfhSP-D).

mRNA transcript expression levels of type I interferon (IFN) subtypes were measured using qRT-PCR and the data were normalized using 18S rRNA expression as a control. The relative expression (RQ) was calculated by using cells only time point as the calibrator. RQ = 2−ΔΔCt was used to calculate the RQ value. Assays were conducted in triplicates and error bars represents ± SEM. Significance was determined using the unpaired one-way ANOVA test (*$p < 0.05$, **$p < 0.01$, ***$p < 0.001$, and ****$p < 0.0001$) (n = 3).

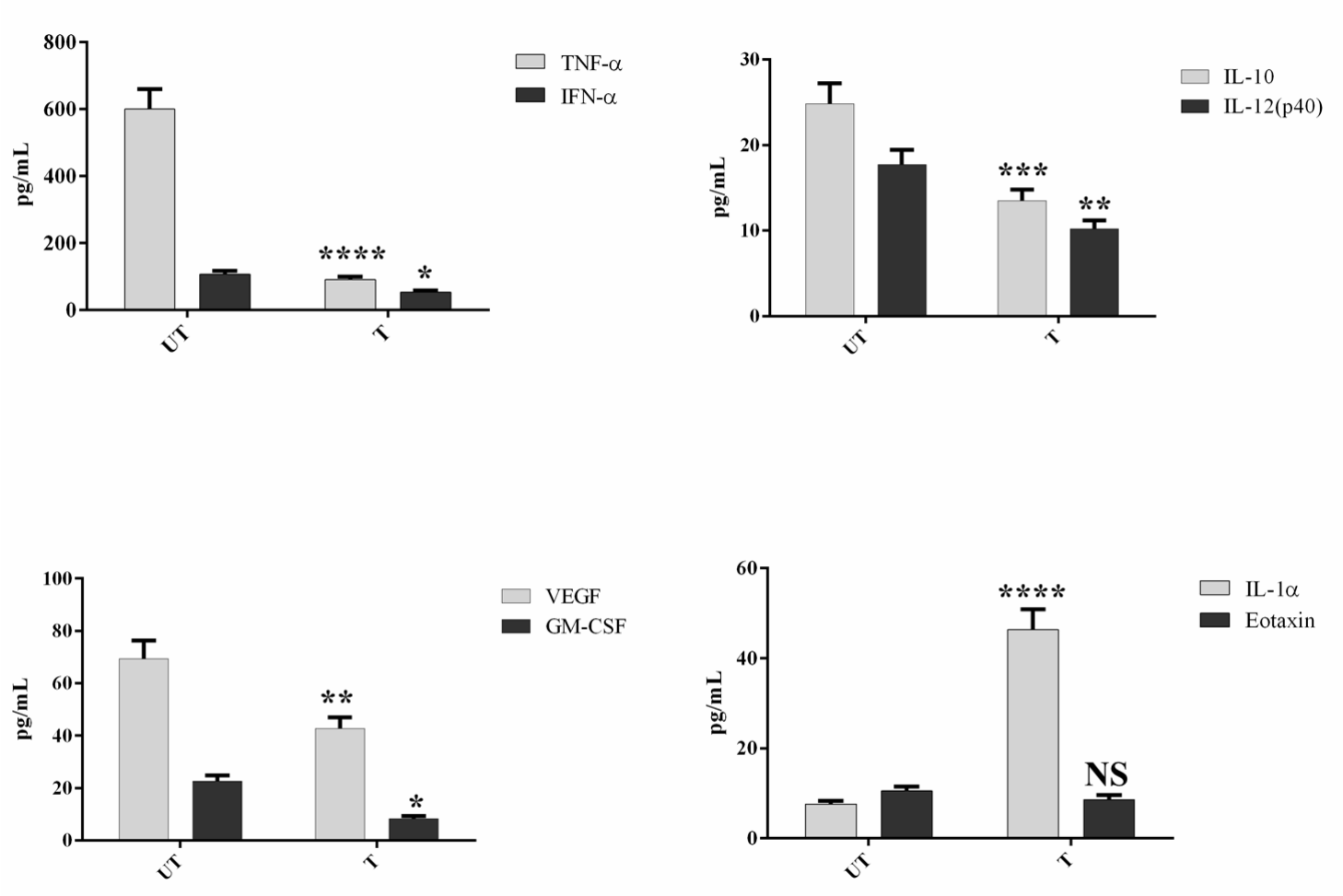

Figure 25: Multiplex cytokine array analysis of culture supernatants that were collected at 24 h time point.

A549 (1×10^6) cells were infected with pH1N1 IAV subtype, followed by rfhSP-D (10 µg/ml). The levels of cytokines levels (TNF-α, IL-6, IL-10, IL-1α, IFN-α, and IL-12p40), chemokine (eotaxin), and growth factors (GM-CSF and VEGF) were measured using a commercially available MagPix Milliplex kit (EMD Millipore). Experimental assays were performed in triplicates and error bars represent ± SEM (n = 3); significance was determined using unpaired one-way ANOVA test (*$p < 0.05$, **$p < 0.01$, ***$p < 0.001$ and ****$p < 0.0001$).

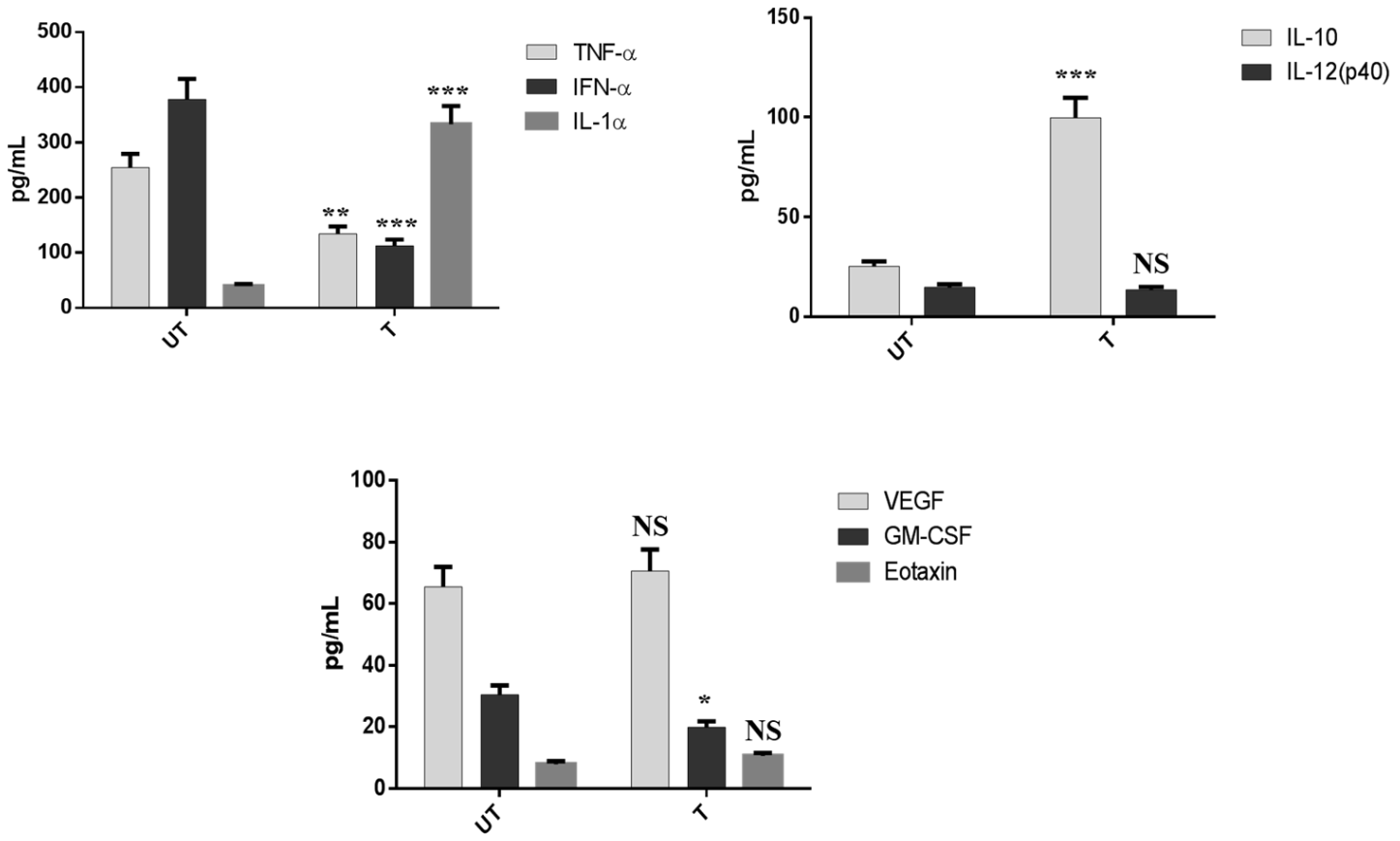

Figure 26: Multiplex cytokine array analysis of culture supernatants that were collected at 24 h time point.

A549 (1×10^6) cells were infected with H3N2 IAV subtype, followed by rfhSP-D (10 µg/ml). The levels of cytokines levels (TNF-α, IL-6, IL-10, IL-1α, IFN-α, and IL-12p40), chemokine (eotaxin), and growth factors (GM-CSF and VEGF) were measured using a commercially available MagPix Milliplex kit (EMD Millipore). Experimental assays were performed in triplicates and error bars represent ± SEM (n = 3); significance was determined using unpaired one-way ANOVA test (*$p < 0.05$, **$p < 0.01$, ***$p < 0.001$ and ****$p < 0.0001$.

3.3.6 rfhSP-D Acts as an Entry Inhibitor of IAV Infection

In this study, H1+N1 pseudotyped lentiviral particles were generated as a safe strategy to determine the involvement of IAV glycoproteins in the recognition and neutralization of IAV by rfhSP-D. Generation of H1+N1 pseudotypes was carried out by co-transfecting HEK293T cells with plasmid composed of the coding sequence of the indicated H1+N1, psPAX2, and pHIV-Luciferase backbone via calcium phosphate transfection method. Post-transfection, H1+N1 pseudotyped particles and cell lysates were harvested from the culture supernatant at 24 and 48h, and analysed via western blotting; the HA expression was determined using anti-H1 monoclonal antibody (Figure 27). HA expression was evident ~70 kDa, confirming the success of pseudotyped production. Furthermore, rfhSP-D bound to HA at ~70 kDa, as evident from far western-blotting analysis (Figure 27), suggesting the rfhSP-D-HA binding is crucial for suppression of infectivity of IAV. In addition, purified H1+N1 pseudotyped particles were used to transfect MDCK cells to determine the luciferase reporter assay with and without rfhSP-D (5 and 10 µg/ml). Increased levels of luciferase reporter activity were measured at 24h post transfection compared to 48h (Figure 28). Approximately, rfhSP-D (10 µg/ml) treatment led to approximately 30% reduction in the luciferase reporter activity when compared to cells only challenged with H1+N1 pseudotyped particles. These data suggest the entry inhibitory effect of rfhSP-D against IAV.

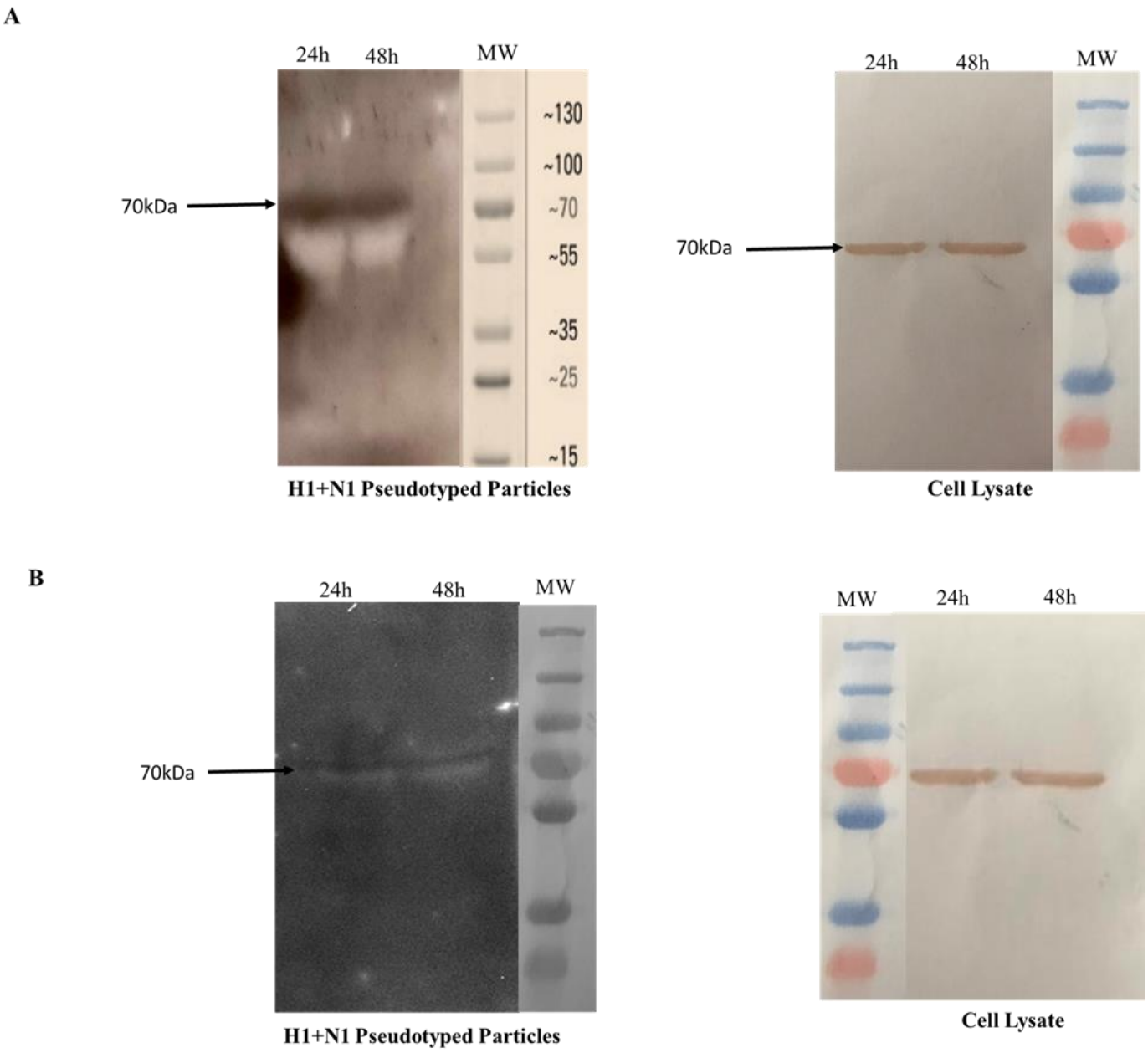

Figure 27: Analysis of purified H1+N1 pseudotyped lentiviral particles.

(A) Western blotting to show the expression of hemagglutinin (HA) glycoprotein of IAV in purified H1+N1 pseudotyped lentiviral particles and cell lysate harvested at 24 and 48 h post-transfection. The presence of HA was identified at ~70 kDa. (B) Far western blotting to show binding of rfhSP-D to purified H1+N1 pseudotyped lentiviral particles and cell lysate at 24 and 48 h. HA was evident at ~70 kDa when probed with rfhSP-D antibody.

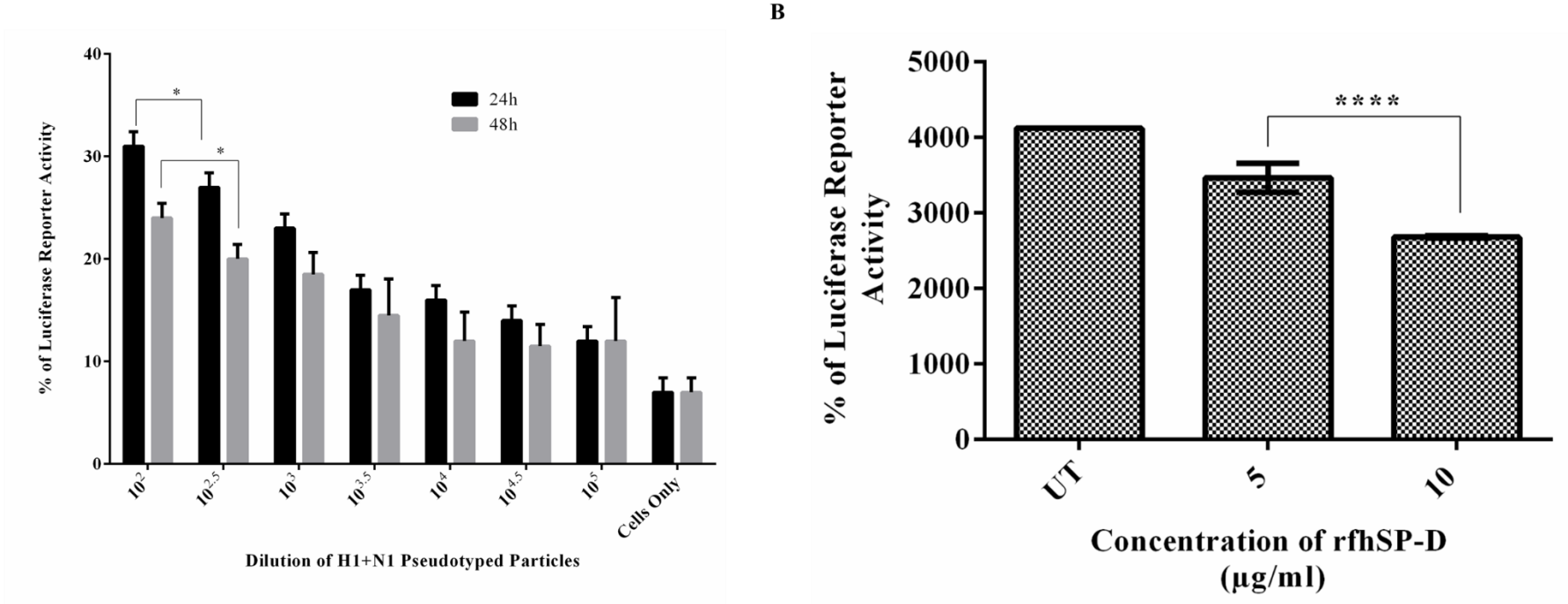

Figure 28: rfhSP-D Binds to H1+N1 Pseudotyped Lentivirus and Reduces Luciferase Reporter Activity.

(A) Luciferase reporter activity of purified H1+N1 pseudotyped lentiviral particles harvested at 24 and 48 h, and (B) Luciferase reporter activity of rfhSP-D treated MDCK cells transfected with these lentiviral particles. Significance was determined using the unpaired one-way ANOVA test (*$p < 0.05$ and ****$p < 0.0001$) (n = 3).

3.4 Discussion

The immune system has evolved several defense mechanisms to overcome IAV-mediated respiratory tract infections for suppressing their replication and infectivity. IAV infection is responsible for up to half a million mortality rates worldwide, and higher morbidity outcome (five million cases per year) (Clayville, 2011). It is fundamentally crucial to study the molecular mechanisms of host's first line of defense in order to develop effective anti-IAV therapies. The primary targets for IAV are airway and alveolar epithelial cells, which bind to sialic acid receptor, and result in alveolar epithelial damage (Shin et al., 2020, Denney and Ho, 2018). Human SP-D is primarily detected in the alveolar space of the lungs and synthesized by Clara cells (Crouch et al., 2009) and alveolar type-II cells (Kishore et al., 2006). SP-D has been reported have a wide range of anti-viral role against IAV (Ng et al., 2012), including neutralization, agglutination, opsonization and clearance of virions. Interaction of SP-D with HA or NA glycoproteins of IAV has been shown to result in suppression of viral attachment and entry into the host cells (Yang et al., 2013). However, inhibition of IAV infection by SP-D and its subsequent immune response is not fully studied. Therefore, this study was aimed at investigating the ability of rfhSP-D to act as an entry inhibitor of IAV infection and modulate immunological responses *in vitro*.

Using pH1N1 and H3N2 IAV subtypes, this study demonstrates that viral entry inhibition by rfhSP-D is not limited to specific IAV subtypes. rfhSP-D interaction with IAV viral proteins was established via protein-to-protein studies using ELISA, cell-binding assay, and far western blotting. As evident from the ELISA, the maximum binding of rfhSP-D to pH1N1 and H3N2 subtypes was observed at the concentration of 5 µg/ml. rfhSP-D also bound to purified recombinant HA in a concentration- and calcium- dependent manner. Furthermore, far-western blotting analysis revealed that rfhSP-D bound pH1N1 or H3N2 via HA (~70 kDa) in addition to recognizing M1 (~25 kDa). It is well known that N-linked oligosaccharides found on IAV glycoproteins (HA or NA) can be recognised by the CRD of SP-D. Therefore, rfhSP-D is likely to suppress IAV infection by inhibiting HA-SA containing receptor interactions. A reverse genetic method has been developed to analyze the role of the N-glycosylation site on the H1 head in regulating SP-D sensitivity *in vivo* and *in vitro* (Tate et al., 2011b). Asn_{144} is a crucial determinant of sensitivity to mouse bronchoalveolar lavage (BAL), a rich source of SP-D (Tate et al., 2011a),

and hence, virulence in mice. However, Asn_{144} deletion from HA of Brazil-H1N1 (A/Brazil/11/78) strain can reduce sensitivity to mouse BAL and can lead to enhanced virulence in mice (Tate et al., 2011b) . Furthermore, simultaneous deletion of addition of Asn_{144} or Asn_{104} from Brazil HA led to significant changes in sensitivity to mouse BAL as well as virulence compared to loss of either residue/site alone (Tate et al., 2011b). These studies indicate that simultaneous SP-D binding to multiple glycans on HA of IAV strains is likely to enhance the overall binding affinity and thereby antiviral activity.

The immune response of A549 lung epithelial cells following IAV challenge with and without rfhSP-D was examined using qRT-PCR. Using qPCR and multiple cytokine arrays, the ability of rfhSP-D to modulate viral replication and inflammatory immune response after IAV challenge was examined. We measured M1 mRNA expression levels between rfhSP-D treated and untreated A549 cells challenged with IAV subtypes. In the case of pH1N1, rfhSP-D suppressed M1 mRNA expression at 2h, while showed reduced viral M1 expression at 6h in the case of H3N2. Suppression of M1 expression levels were also evident using western blotting; rfhSP-D treated cells showed lowered M1 expression when compared to untreated cells at 6h incubation. Thus, rfhSP-D treatment also caused reduced viral replication as evident from titration assay, suggesting that rfhSP-D acted as an entry inhibitor against IAV subtypes tested. HA is suggested to undergo N-linked glycosylation, leading to modulation of antigenicity, fusion, receptor binding specificity, and IAV-mediated immune responses. Therefore, SP-D could play anti-IAV role via binding to glycans found on viral HA. Studies have reported that mutations flanking the CRD region of human SP-D can confer anti-viral effects for pandemic IAV (Nikolaidis et al., 2014).

Many studies have shown that there is a direct and indirect relationship between cytokine levels and viral replication (Mogensen and Paludan, 2001). The primary targets for IAV is the lung epithelial cells, and after the initial exposure, progeny virus particles can proliferate and infect surrounding cells, including alveolar macrophages (Chen et al., 2018b). Therefore, the acute inflammatory response is induced by the activation of pro-inflammatory cytokines and chemokines (Betakova et al., 2017, Oslund and Baumgarth, 2011, Tisoncik et al., 2012), where increased levels can cause a dramatic cytokine storm. Altered levels of IFNs, TNFs, interleukins and chemokines have been reported in patients infected with IAV (Liu et al., 2019, Ramos and

Fernandez-Sesma, 2015). Higher IFN levels in the early stages of IAV infection can cause irreversible lung damage in mice infected with H5N1 (Tisoncik et al., 2012, Hu et al., 2012). However, IFN signaling may also be crucial in preventing the spread of H5N1 (Zeng et al., 2007, Alibek and Liu, 2006). TNFs are crucial soluble factors in the cytokine storm during IAV infection. The survival rate of H5N1-infected mice lacking TNF receptors and H5N1-infected mice treated with anti-TNF-α antibody was unchanged compared with healthy controls (Peiris et al., 2009). In addition, IL-1 and IL-6 are the crucial pro-inflammatory cytokines produced by the host cells following IAV infection. IL-1 expression is observed in the early stage of IAV infection, followed by an upregulation of IL-6 levels (Tisoncik et al., 2012). H5N1 infected mice lacking IL-6 receptors have shown poor survival, indicating the protective effect of IL-6 pathway in the cytokine storm (Tisoncik et al., 2012). These data suggest that cytokine storm could also lead to the destruction of the vascular barrier, causing tissue edema, capillary leakage, and multiple organ failure (Tisoncik et al., 2012). However, there is no report of a specific singular mechanism when it comes to inducing a cytokine storm caused by influenza virus strains.

In this study, altered levels of pro-inflammatory cytokines were observed in pH1N1 and H3N2 challenged A549 cells with and without rfhSP-D. Up-regulation of TNF-α and IL-6 was observed in H3N2 infected cells, compared to pH1N1 challenged cells. However, rfhSP-D treatment caused suppression of TNF-α and IL-6 levels at 2 h. IL-12 mRNA levels were also considerably reduced by rfhSP-D treatment in the case of both IAV subtypes, suggesting the likely suppression of Th1 immune response. RANTES mRNA transcript levels were downregulated ($\log_{10}1$ fold) following rfhSP-D treatment at 2 h when compared to pH1N1-infected cells only. Conversely, H3N2 infected cells treated with rfhSP-D seemed to have reduced RANTES levels ($\log_{10}1$ fold). Furthermore, rfhSP-D treatment also caused suppression of IFN-α and IFN-β levels at 2 and 6 h. Enriched mRNA levels of IFN-α and IFN-β were observed in untreated sample (cells + virus), which was three-fold (log10 fold) suppressed following rfhSP-D treatment at 6 h. This indicates that when the cells are infected with IAV subtypes, A549 cells will produce higher levels of IFN-α and IFN-β to eliminate viral particles. Since the addition of rfhSP-D can inhibit viral replication, lower levels of INF are detected. In addition, the expression of certain key pro-inflammatory cytokines, chemokines and other soluble factors was significantly down-regulated following rfhSP-D

treatment, as evident from cytokine array analysis. Through rfhSP-D treatment, the downregulation of various humoral factors can also promote the prevention of life-threatening secondary bacterial infections caused by virus-mediated abnormal immune regulation.

Targeting entry of viruses into host cells is an emerging method for developing antiviral treatments, because in the early stages of the virus cycle, virus reproduction can be restricted or prevented, thereby minimizing the drug resistance of the released viral particles. In this study, lentiviral pseudotyped particles were generated as a safe alternative model that mimics the structure and surface of IAV to determine whether rfhSP-D can act as an entry inhibitor in cells transduced with pseudotyped IAV particles (limited to one replicative cycle). H1+N1 pseudotyped particles were analysed and validated via SDS-PAGE and western botting. HA expression in H1+N1 pseudotyped particles was assessed by western blotting using monoclonal anti-H1 antibody. Incubation of H1+N1 pseudotyped lentiviral particles with rfhSP-D was found to facilitate its binding to HA that evident at 70 kDA in the far western blot. Luciferase reporter activity assay was performed to validate the entry inhibitory role of rfhSP-D. rfhSP-D treatment caused 30% reduction in luciferase reporter activity in MDCK cells transduced with H1+N1 pseudotyped particles. Therefore, this indicates the ability of rfhSP-D to inhibit viral infection by binding to the HA found on the infected MDCK cells.

In conclusion, M1 suppression, downregulation of pro-inflammatory cytokines/chemokines, and reduced levels of luciferase reporter activity following rfhSP-D treatment highlight the potential of rfhSP-D as cell entry inhibitor against IAV subtypes tested in this study.

Chapter 4

rfhSP-D Induces Apoptosis in Breast Cancer Cell Lines

4.1 Abstract

Breast cancer is a heterogeneous disease; its four molecular subtypes exhibit distinct molecular and immunological signatures. Breast tumours vary according to the circulating levels of oestrogen, progesterone receptors and HER2 over-expression. Protective effects of SP-D (as well as rfhSP-D) has been reported against lung adenocarcinoma, pancreatic and prostate cancer cell lines, and primary explants. Here, the effects of the recombinant form of human SP-D (rfhSP-D) on a range of breast cancer lines in terms of cell viability reduction, apoptosis induction, and signaling pathways were investigated. rfhSP-D (5 μg/ml) was able to bind to BT20, BT474 and SKBR3 breast cancer cell lines regardless of their phenotypes. The cell viability of HER2 over-expressing and triple-positive breast cancer cell lines (SKBR3: ~68%; BT474: ~61%), were reduced following culture in the presence of immobilized rfhSP-D (20 μg/ml) at 24h; no significant effect was seen in triple-negative cell line (BT20). Cleaved caspase 3 (~17kDa) and 9 (~37kDa) were also detected in rfhSP-D treated BT474 and SKBR3 cells, suggesting involvement of intrinsic apoptosis pathway. Furthermore, rfhSP-D treatment upregulated p53 phosphorylation at Ser15, and p21 and p27 expression levels, indicating the possibility of cdc2-cyclin B1 reduction leading to G2/M cell cycle arrest and p53-dependent apoptosis induction.

4.2 Introduction

The immune surveillance of transformed cells remains one of the targeted areas of research for designing and developing therapeutic approaches (Swann et al. 2007; Kim et al. 2007). Studies using *in vivo* and *in vitro* tumour models have reported the involvement of effector immune cells, soluble factors, and signaling cascades in anti-cancer immune responses. However, both innate and adaptive immunity can also help in the progression of transformed cells by inducing immunosuppression, promoting angiogenesis and metastasis of cancer cells (Palucka and Coussens, 2016, Vesely et al., 2011).

Lung surfactants (SP-A, SP-B, and SP-D) has been used as a biomarker for cancer studies. Expression levels of SP-A in cancer cells has been shown to be associated with patient prognosis (Mitsuhashi et al., 2013), especially in carcinoma originating from type II pneumocytes. Deletion of SP-A gene (*SFTPA1*) in non-small cell lung cancer cells has also been shown to be significantly correlated with tumour progression (Mitsuhashi et al., 2013, Jiang et al., 2005).

Recently, studies have reported interaction of SP-D with a range of cancer cells (leukemia, lung, pancreatic and prostate). rfhSP-D treatment resulted in the suppression of tumour progression, invasion, EMT and induction of enhanced apoptosis, suggesting inhibition of cell proliferation (Kaur et al., 2018a, Kaur et al., 2018b, Kumar et al., 2019, Thakur et al., 2019, Mahajan et al., 2014, Hasegawa et al., 2015). These studies therefore suggest that SP-D has an immune surveillance role against cancer cells. In this context, the current study was aimed at examining the role of rfhSP-D in breast cancer, which contributes to nearly 60% mortality rate in lower-income nations (Sun et al., 2017, Ferlay et al., 2010). In this study, the possible protective effects of rfhSP-D in triple-negative ($ER^-/PR^-/HER2^-$), triple-positive ($ER^+/PR^+/HER2^+$), and $HER2^+$-overexpressing breast cancer cell lines have been investigated.

4.3 Results

4.3.1 rfhSP-D Binds Breast Cancer Cell lines and Reduces Cell Viability

Breast cancer cell lines, BT20, BT474 and SKBR3, bound rfhSP-D (10 µg/ml) following 1h incubation at 4°C and revealed membrane localization (Figure 29). The nucleus of the cell was stained with Hoechst dye, while localization of the bound rfhSP-D on the cell membrane was detected using green FITC fluorescence. All rfhSP-D treated breast cancer cell lines showed a similar 'cluster' like binding pattern on the cell membrane. No FITC was detected in the untreated controls, when probed with both primary and secondary antibodies for each cell line, suggesting that the rfhSP-D binding observed in the treated sample was protein-specific.

The quantitative analysis of cell viability in rfhSP-D treated and untreated cells was carried out using MTT assay at 24h and 48h time point (Figure 30). The cells were incubated with a varied concentration of rfhSP-D (5, 10, and 20 µg/ml) in serum free RPMI medium, along with an untreated control, where no protein was added. The cell viability of HER2 over-expressing and triple positive breast cancer cell lines (SKBR3: ~40%; BT474: ~30%) were reduced following solution phase rfhSP-D (20 µg/ml) treatment at 24h in a dose dependent manner, whereas no significant effect was seen in triple negative cell line (BT20) (Figure 30). In the case of FL-SP-D, the reduction on cell viability was concentration dependent, where maximum reduction was seen with 20 µg/ml for both SKBR3 and BT474 cell lines, while BT20 had no effect as seen. However, no significant difference was seen at all concentration of rfhSP-D treatment for 48h in all the cell lines investigated in this study (Data not shown).

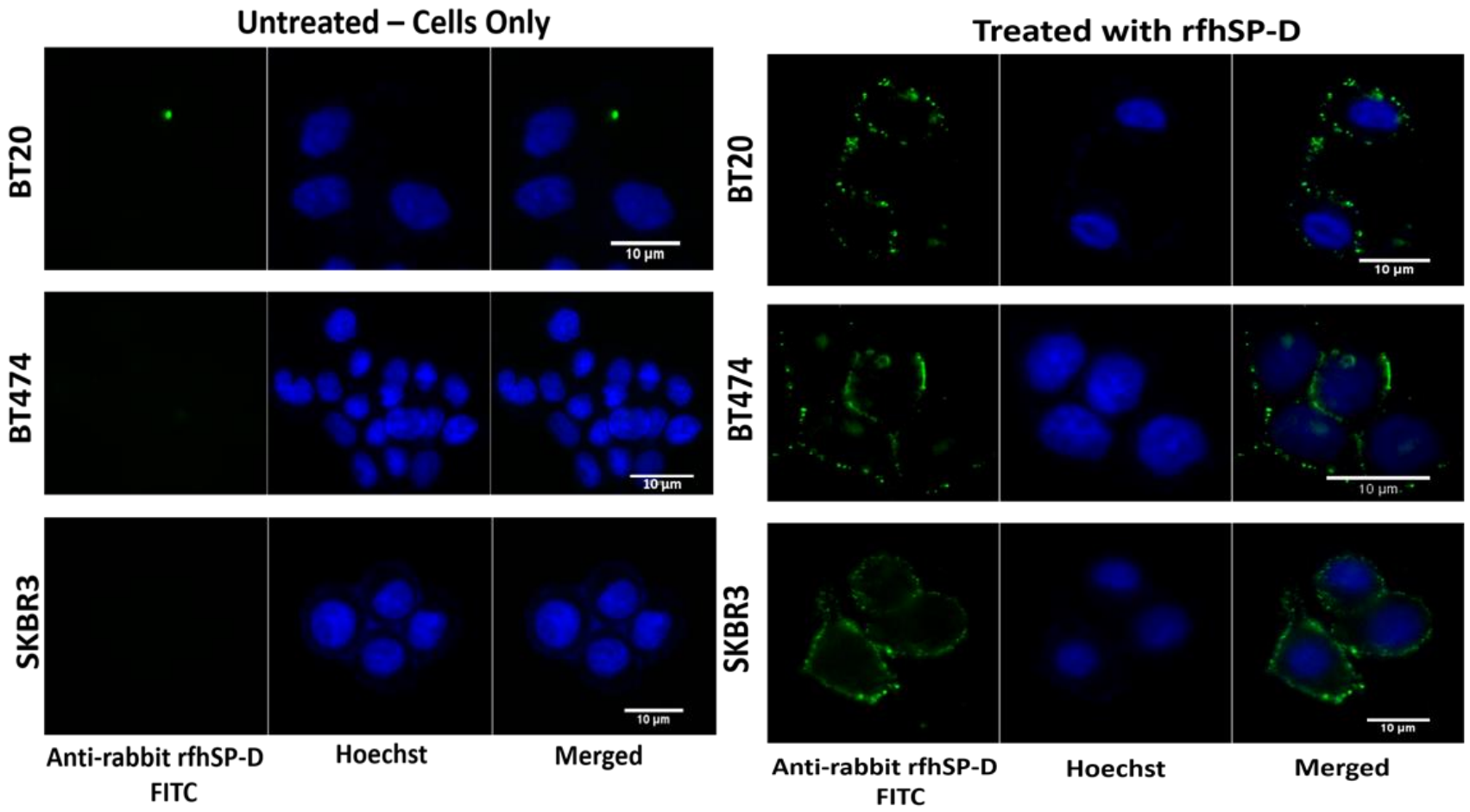

Figure 29: rfhSP-D (10 µg/ml) binding to triple negative (BT20), triple positive (BT474) and HER2+-overexpressing (SKBR3) breast cancer cell lines using fluorescence microscopy.

The cell nucleus was stained with Hoechst (1:10,000), and both untreated (cells only) and rfhSP-D-treated cells were probed with polyclonal anti-human SP-D/FITC antibody (1:200). Membrane localization of the bound proteins was only detected in the rfhSP-D-treated cells, while no FITC was detected in the untreated control (cells only).

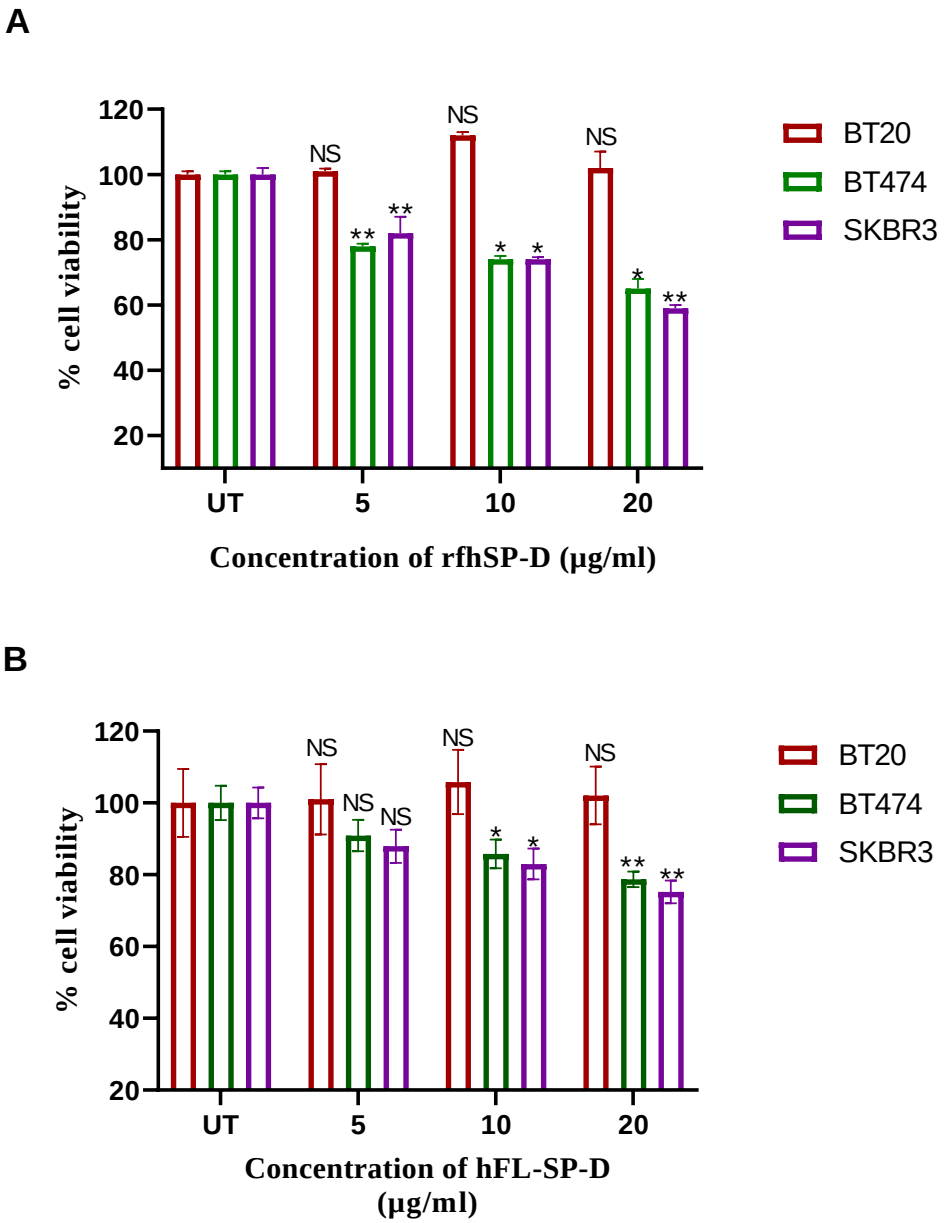

Figure 30: Cell viability reduction by rfhSP-D in breast cancer cell lines via MTT assay.

Cells ($0.1x10^5$) were treated with varied concentration of rfhSP-D (5, 10, 20 µg/ml) (A) and human full-length SP-D (hFL-SP-D) (B), followed by incubation for 24h at 37°C under standard cell culture conditions. Assays were done in triplicates ± SEM and the significance were established using the unpaired one-way ANOVA test (*$p < 0.05$ and **$p < 0.01$) ($n = 3$). The statistical analysis was performed between cells only and rfhSP-D-treated breast cancer cells.

4.3.2 Apoptosis Induction by rfhSP-D in Breast cancer cell lines

The quantitative and qualitative analysis of apoptosis induction by rfhSP-D was performed using flow cytometry and immunofluorescence microscopy, respectively. A significant proportion of breast cancer cells treated with rfhSP-D induced apoptosis at 24h of post treatment as revealed by FACS analysis (Figure 31 & 32). rfhSP-D (20 µg/ml) in solution was effective in inducing the maximum apoptosis at 24h; SKBR3 (~34%), BT474 (~27%), while the treatment had no significant effect on BT20 cell line in terms of cell death at all the protein concentrations tested. However, both BT474 and SKBR3 cell lines became more susceptible to apoptosis induction following immobilized rfhSP-D (20 µg/ml) compared to rfhSP-D in solution (Figure 31 & 32). An increased apoptosis was seen in SKBR3 (~68%), and BT474 (~61%), while immobilized rfhSP-D had no effect on BT20 cell line. These data suggest that immobilized rfhSP-D is more effective apoptosis inducer than solution-phase, probably due to the way rfhSP-D protein molecules are presented in an array platform, exposing their CRD regions to interact with putative cell receptors. However, solution-phase protein molecules are free floating molecules which may possibly have competitive binding with their receptors.

For both BT47 and SKBR3 cell lines, approximately around 56% cells were both stained with FITC and PI positive, suggesting that annexin V/FITC was able to bind to phosphatidylserine (PS) found on the surface of cells undergoing apoptosis. However, the higher percentage of cells stained for PI alone was found in BT474 cell line when compared to SKBR3 cell line, suggesting that these cells were either at the late stage of apoptosis or undergoing necrosis. The percentage of viable cells in the untreated (cells only) sample was significantly higher as compared to rfhSP-D treated sample: BT474 (~92%), and SKBR3 (~96%). This suggested that apoptosis induction was a protein (rfhSP-D)-specific effect, where the integrity of the cell membrane was intact in untreated cells, and hence, the cells were still viable, blocking the translocation of PS from inner cell membrane to outer plasma membrane, and preventing the PS - Annexin V interaction. Staurosporine (1 µM/ml) was used as a potent apoptosis inducer; Staurosporine-treated BT20, BT474, and SKBR3 showed ~70% of apoptosis induction at 24 h (Figure 31 & 32).

Fluorescence microscopic analysis of apoptosis induction by rfhSP-D in BT474 and SKBR3 cell lines revealed a positive staining for cell membrane integrity marker, Annexin V (conjugated to FITC), and disoriented cell membrane morphology (Figure 33). PI positive staining was seen only in rfhSP-D treated BT474 and SKBR3 cells compared to untreated controls. However, no positive staining of Annexin V or PI was detected in BT20 treated cells as well as untreated control.

4.3.3 Apoptosis induction in BT474 and SKBR3 by rfhSP-D via Intrinsic Pathway

Since rfhSP-D induced apoptosis in BT474 and SKBR3 breast cancer cell lines, further studies were performed to examine the likely apoptotic pathways that may be activated due to rfhSP-D treatment. Since apoptosis can be initiated via intrinsic or extrinsic pathways, expression of caspases was examined in breast cancer cell lines treated with rfhSP-D (20 µg/ml) via western blotting (Figure 34). Cleavage of caspase 9 (~37 kDa) and 3 (~17 kDa) (Figure 34) was observed in rfhSP-D-treated BT474 and SKBR3 cells at 12h, suggestive of a possible involvement of intrinsic apoptotic pathway. However, cleavage of caspase 3 and 9 was not detected in untreated controls (cells only) and in BT20 cells. Additionally, cleaved caspase 8 was also tested to determine the trigger of extrinsic pathway, but there was no difference observed between untreated controls and rfhSP-D treated cells (data not shown).

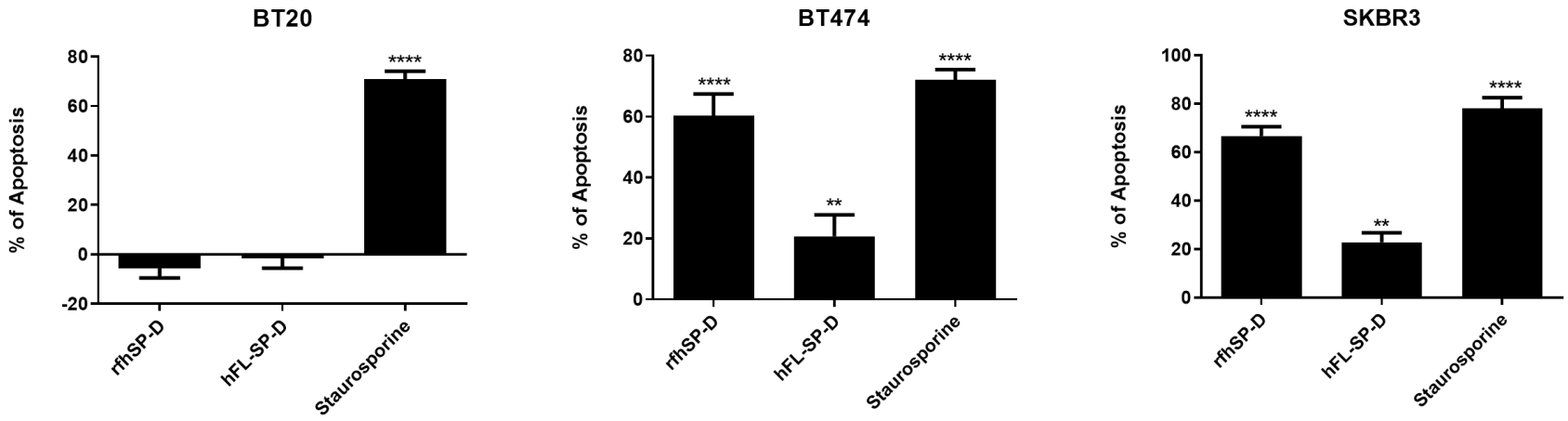

Figure 31: Flow cytometric analysis of apoptosis induction in triple negative (BT20), triple positive (BT474) and HER2+-overexpressing (SKBR3) breast cancer cell lines treated with immobilized rfhSP-D and human full-length SP-D (hFL-SP-D) (20 µg/ml) for 24 h.

For both Annexin V/FITC and DNA/PI staining, 12,000 cells were acquired and plotted. A significant difference was detected among rfhSP-D/hFL-SP-D-treated and untreated (cells only) samples, as evident by the shift in the fluorescence intensity. The data were expressed as the mean of three independent experiments (n = 3) done in triplicates ± SEM. Statistical significance was performed using the unpaired one-way ANOVA test (**p < 0.01 and ****p < 0.0001). The percentage of apoptosis induction was calculated by normalizing the rfhSP-D/hFL-SP-D-treated cells with their untreated (cells only) counterparts.

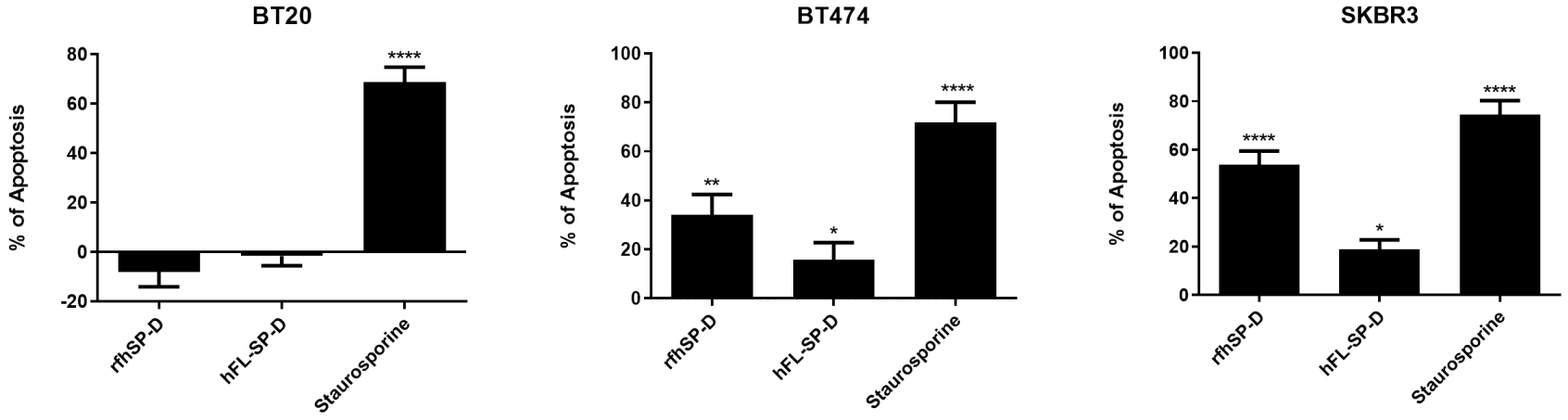

Figure 32: Flow cytometric analysis of apoptosis induction in triple negative (BT20), triple positive (BT474) and HER2+-overexpressing (SKBR3) breast cancer cell lines treated with solution-phase rfhSP-D and human full-length SP-D (hFL-SP-D) (20 µg/ml) for 24 h.

For both Annexin V/FITC and DNA/PI staining, 12,000 cells were acquired and plotted. A significant difference was detected among rfhSP-D/hFL-SP-D-treated and untreated (cells only) samples, as evident by the shift in the fluorescence intensity. The data were expressed as the mean of three independent experiments (n = 3) done in triplicates ± SEM. Statistical significance was performed using the unpaired one-way ANOVA test (**p < 0.01 and ****p < 0.0001). The percentage of apoptosis induction was calculated by normalizing the rfhSP-D/hFL-SP-D-treated cells with their untreated (cells only) counterparts.

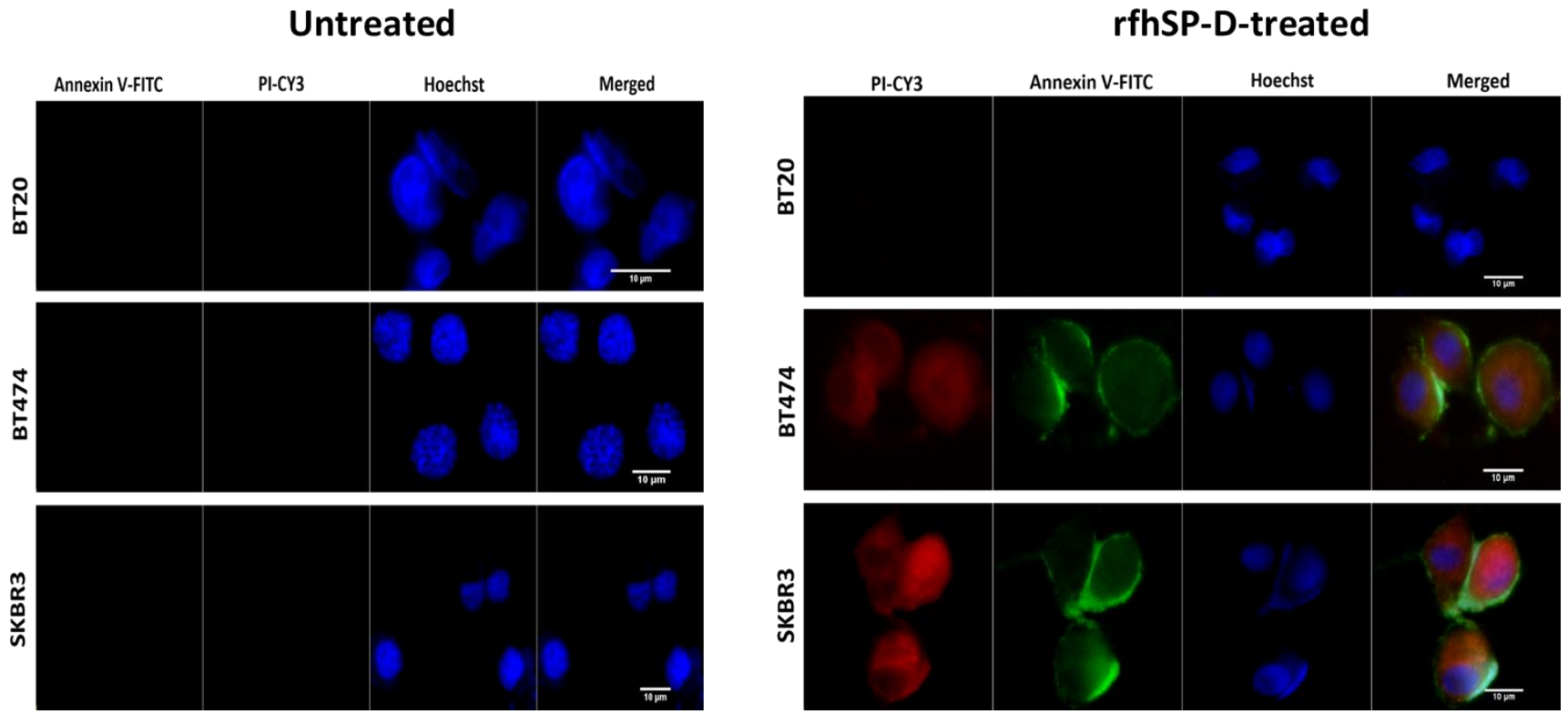

Figure 33: Fluorescence microscopy analysis of rfhSP-D-mediated apoptosis induction in breast cancer cells for 24 h, using an Annexin V with a propidium iodide (PI) staining kit.

The nucleus of the cells was stained with Hoechst (1:10,000), and the cell membrane was stained positively with Annexin V and PI (1:200) in rfhSP-D-treated cell lines, suggesting that cells treated triggered apoptosis at 24 h, where PS translocated to the outer plasma membrane was able to bind Annexin V due to loss of membrane integrity and PI stain was taken, which stained the DNA of apoptotic cells. No Annexin V/PI staining was detected in untreated (cells only) control.

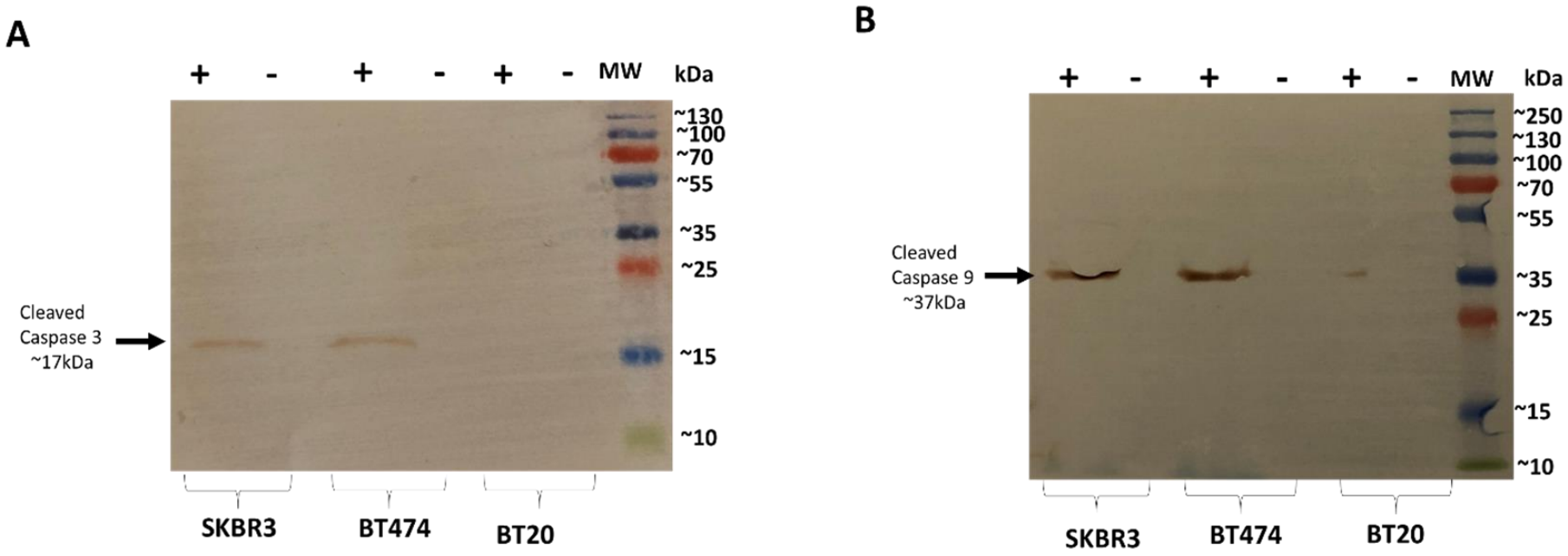

Figure 34: Activation of caspases in triple positive (BT474) and HER2+-overexpressing (SKBR3) breast cancer cell lines following rfhSP-D treatment at 12 h.

Western blot analysis showed cleaved caspase 3 at 17kDa (A) and cleaved caspase 9 at 37kDa (B) in the rfhSP-D-treated cells for 24 h, suggesting induction of the intrinsic pathway.

4.3.4 rfhSP-D Induced Up-regulation of Cell Cycle Inhibitors and p53-dependent Apoptosis mechanism.

p53 is a transcription factor, known to be involved in the regulation of oncogenic responses including DNA damage, cell cycle arrest, and apoptosis induction. Thus, the levels of activated p53 in rfhSP-D-treated breast cancer cells were determined using the PathScan Intracellular Signaling Array Kit (Figure 36). rfhSP-D (20 μg/ml) treated SKBR3 cells showed increased levels of p53 phosphorylation at Ser15 (Figure 36). However, downregulation was observed in BT20 cells following rfhSP-D treatment, suggesting up-regulation of p53 may also have contributed to p53-dependent apoptosis induction by rfhSP-D in SKBR3 cells. In addition, rfhSP-D treatment also caused upregulation of p21 and p27 transcript levels in BT474 and SKBR3 cell lines (Figure 35) at 12h. This may indicate the possibility of cdc2-cyclin B1 reduction, leading to G2/M cell cycle arrest. In contrast, no significance differences were observed in terms of p21 and p27 mRNA levels in rfhSP-D treated BT20 cells.

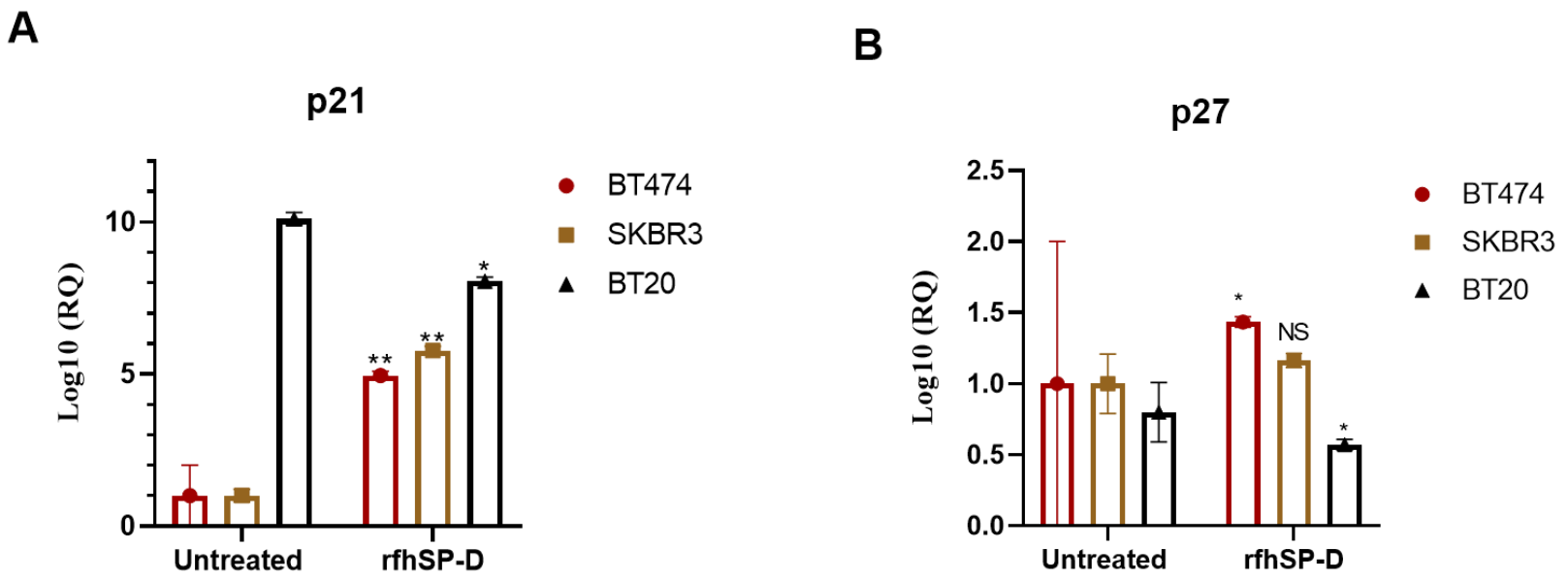

Figure 35: rfhSP-D treatment caused upregulation of p21 (A) and p27 (B) cell cycle inhibitors in triple positive (BT474) and HER2+-overexpressing (SKBR3) breast cancer cell lines.

BT20, BT474, and SKBR3 (0.4×10^6) cells were seeded in a pre-coated plate with rfhSP-D (20 µg/ml). The treated cancer cells were lysed and pelleted down. The pelleted cells were subjected to RNA extraction, followed by cDNA synthesis and qPCR. The comparative quantification method was carried out to calculate the efficiencies of each targeted gene for each individual PCR. The takeoff results obtained with p21/p27 primers were normalized with TBP (housekeeping gene) primers. Assays was conducted in triplicates, and error bars represent ± SEM. Unpaired one-way ANOVA test was performed to measure the significance; *$p < 0.05$ and **$p < 0.01$ ($n = 3$). The statistical analysis was performed between untreated (cells only) and rfhSP-D-treated breast cancer cells.

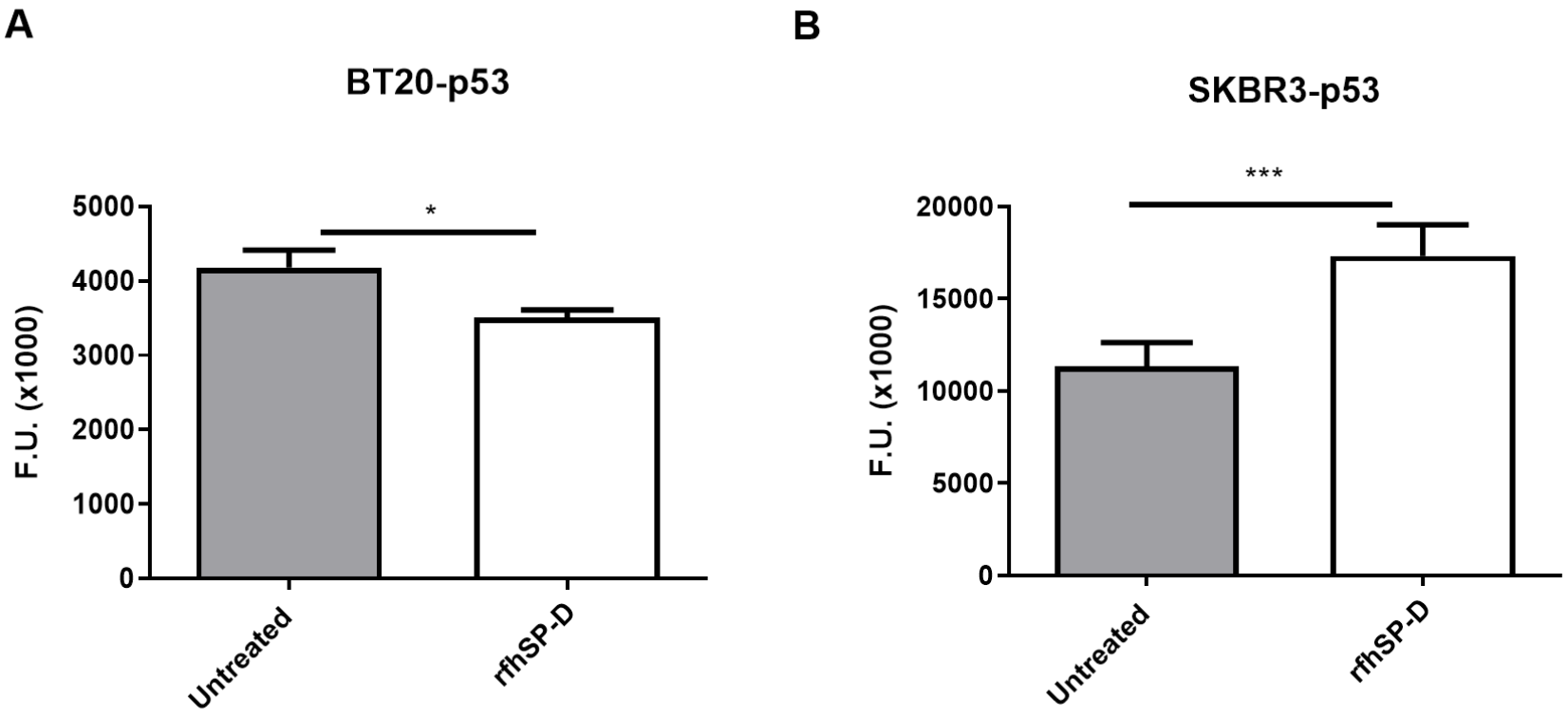

Figure 36: Intracellular signaling to show p53 phosphorylation (at Ser15) in rfhSP-D-treated triple negative (BT20) (A) and HER2+-overexpressing (SKBR3) (B) breast cancer cell lines.

The phosphorylation status of p53 was evaluated using total cell lysates with a PathScan Antibody Array Kit (Cell Signaling). Data were generated from at least three independent experiments and presented as mean ± SD. Unpaired one-way ANOVA test was performed to measure the significance: *$p < 0.05$, and ***$p < 0.001$ ($n = 3$). The statistical analysis was performed between untreated (cells only) and rfhSP-D-treated breast cancer cells.

4.4 Discussion

In this study, it was found that rfhSP-D binds to all breast cancer cell lines tested regardless of their phenotypes: BT20 ($ER^-/PR^-/HER2^-$), BT474 ($ER^+/PR^+/HER2^+$), and SKBR3 ($ER^-/PR^-/HER2^+$). However, the putative receptor or the ligand rfhSP-D is binding to on the breast cancer cell surface, is not yet known. Recently, the interaction between the CRD region of human SP-D and the N-glycan of EGFR has been reported, which leads to down-regulation of EGF signal transduction in human lung adenocarcinoma cells (Hasegawa et al., 2015). In addition, SP-D's ability to trigger TNF-α produced in human $CCR2^+$ monocytes by interacting with the receptor OSCAR has been reported (Barrow et al., 2015). rfhSP-D treatment reduced cell viability of BT474 and SKBR3 cell lines and induced apoptosis at 24 h. Cell viability assay was carried out using varied concentrations of rfhSP-D (5, 10, and 20 μg/ml) and different time points (12, 24, and 48 h); rfhSP-D was only effective in inducing the optimal cell viability reduction and apoptosis at the concentration of 20 μg/ml at 24 h. A significant percentage reduction in viable cells was observed in rfhSP-D-treated BT474 and SKBR3 cells compared to untreated control (cells only) sample, as evident from the MTT assay. However, in terms of cell viability, rfhSP-D has had no effect on triple negative (BT20) cell line.

The significant increase in the number of Annexin V-/PI-positive breast cancer cells observed by flow cytometry and fluorescence microscopy demonstrated the ability of rfhSP-D to induce apoptosis in SKBR3 and BT474 cell lines within 24 hours. The cell surface of healthy cells is composed of lipids distributed asymmetrically on the inner and outer surfaces of the plasma membrane. PS is one of these lipids, which is confined to the inner surface of the plasma membrane and therefore only exposed to the cytoplasm of the cell. However, when stress factors trigger cell apoptosis, the lipid asymmetry disappears, and PS shifts to the outer leaflet of the plasma membrane (Porter and Janicke, 1999). Annexin V (36kDa) is a calcium-binding intracellular protein that binds to PS, and Annexin V can also stain cells that undergo necrosis due to membrane rupture, which allows Annexin V to enter the entire plasma membrane. Immobilised rfhSP-D induced apoptosis in SKBR3 (~68%) and BT474 (~61%), while no effect was observed on BT20 cell line. In the two cell lines, approximately 56% cells were stained with FITC as well as PI, suggesting that annexin V/FITC was able to bind to PS found on the surface of cells

undergoing apoptosis. However, the BT474 showed higher percentage of PI alone stained cells when compared to SKBR3 cell line, indicating that these cells were at the late stage of apoptosis. However, no significant difference in terms of cell viability reduction and apoptosis induction was observed at all concentration of rfhSP-D treatment for 48h in all the cell lines investigated in this study. Lack of apoptosis induction at 48h seems to imply that the rest of viable cells (~30%) which are not affected by rfhSP-D treatment at 24h are probably recovering.

Western blot analysis of BT474 and SKBR3 breast cancer cells treated with rfhSP-D showed that caspase 9 and 3 were cleaved after 12 h of rfhSP-D treatment. Caspase is a well-known cysteine aspartic protease, which plays a vital role in apoptosis. Caspase 9 is triggered by cellular stress (such as DNA damage) by binding to the apoptotic protease activator 1 (Apaf-1). Apaf-1/procaspase 9 triggers executor cysteine proteases 3 and 7 in turn (Julien and Wells, 2017). Caspase 3 is an essential apoptotic executor, triggered by the proteolytic enzyme cleavage at Asp175, which leads to inactivation of Poly (ADP-ribose) polymerase (PARP) (Walsh et al., 2008, Porter and Janicke, 1999). Our findings indicate that the apoptosis induction in SKBR3 and BT474 cell lines by rfhSP-D may occur through the intrinsic apoptotic pathway (Elmore, 2007). Recently, the indispensable role of rfhSP-D in innate immune surveillance against prostate cancer has been reported. It has been shown that rfhSP-D-mediated apoptosis occurs through two different mitochondrial pathways (Thakur et al., 2019).

To further understand the mechanism of apoptosis induced by rfhSP-D treatment, the signal pathways that may be related to tumor proliferation and cell death were analyzed. rfhSP-D treatment leads to increased phosphorylation of p53 (at Ser15) in BT474 and SKBR3 cell lines, which may be mediated by oxidative stress caused by rfhSP-D (Kaur et al., 2018a, Janssen et al., 2008). The up-regulation of p53 in BT474 and SKBR3 cell lines treated with rfhSP-D leads to down-regulation of the pAkt pathway, leading to increased levels of Bad and Bax, which triggers the release of cytochrome c, caspase 9 cleavage and apoptosis induction. Furthermore, elevated expression levels of phosphorylated p53 and p21/p27 cause inactivation of the cyclin B–cdc2 complex, which is essential for regulating the transition of G2/M cell cycle, leading to DNA repair or induction of apoptosis (Kaur et al., 2018a). The apoptosis mediated by rfhSP-D may be due to

the expression of HER2 on BT474 and SKBR3 cells. The absence of HER2 expression seems to be the likely cause of BT20 cell being resistant to rfhSP-D-induced apoptosis. Whether HER2 is involved in mediating rfhSP-D-induced apoptosis is under investigation. In addition, previous studies have reported the interaction of SP-D with HMGA1, CD14, CD91-calreticulin complex, SIRPα and EGFR (Janssen et al., 2008, Thakur et al., 2019, Mahajan et al., 2013, Hasegawa et al., 2015). The SP-D interaction with these key molecules appear to be part of the possible mechanism/receptor that rfhSP-D may mediate its apoptotic effects on breast cancer cells. As demonstrated in previous studies, the CRD region of SP-D can interact with pattern recognition receptors TLR-2, TLR-4 (Ohya et al., 2006), and CD14 (Augusto et al., 2003), which may inactivate and suppress the pro-inflammatory and pro-survival downstream signaling on breast cancer cells. However, further research is essential to understand the involvement of CRD region of SP-D and its possible interaction partners involved in inducing the downstream mechanisms leading to induction of apoptosis.

In conclusion, rfhSP-D treatment can induce apoptosis in BT474 and SKBR3 cell lines involving intrinsic apoptotic pathways, but it has no effect on the triple-negative BT20 cell line. Most conventional anti-cancer therapies only target actively proliferating tumour cells. New strategies involving immune surveillance molecules like rfhSP-D can potentially target signaling cascades to reduce cell growth.

Chapter 5

Hyaluronic Acid Modulates the Pro-apoptotic Effects of rfhSP-D on Breast Cancer Cell Lines

5.1 Abstract

The oncogenesis and progression of tumour including metastasis is profoundly dictate by tumour microenvironment including a range of extracellular matrix components (e.g., hyaluronic acid; HYA) and infiltrating immune cells (e.g., tumour-associated macrophages; TAMs). Having established a likely role of SP-D in innate immune surveillance against breast cancer, we sought to investigate if SP-D itself is present in the breast cancer tissues and if yes, what are the likely sources for its production. In addition, we wanted to know if the TME factors especially HYA can modulate the pro-apoptotic effects of rfhSP-D. In this study, the effect of a recombinant fragment of human SP-D (rfhSP-D) on a range of breast cancer lines was examined in the presence of HYA. Breast cancer is classified into four molecular subtypes characterized by varied expressions of estrogen (ER), progesterone (PR), and epidermal growth factor (EGF) receptors (HER2). As established in the previous chapter, rfhSP-D treatment triggered apoptosis induction in HER2-overexpressing (SKBR3) and triple-positive (BT474) breast cancer cell lines [but not in the triple-negative cell line (BT20)] at 24 h. Upregulation of p21/p27 cell cycle inhibitors and p53 phosphorylation (Ser15) was also evident in rfhSP-D-treated BT474 and SKBR3 cell lines, suggestive of G2/M cell cycle arrest. rfhSP-D-treated BT474 and SKBR3 cells also showed cleaved caspases 9 and 3, indicating an involvement of the intrinsic apoptosis pathway. However, rfhSP-D-induced apoptosis was nullified in the presence of hyaluronic acid (HYA). rfhSP-D bound to solid-phase HYA and promoted cell proliferation of BT474 and SKBR3 cell lines. Decreased transcriptional levels of p53 was observed in rfhSP-D-treated SKBR3 cells in the presence of HYA compared to cells treated with rfhSP-D only. Thus, HYA seems to negate the anti-tumorigenic effects of rfhSP-D against BT474 and SKBR3 breast cancer cells.

5.2 Introduction

Breast cancer is correlated with an increased mortality rate due to angiogenesis, metastasis, and resistance to conventional chemotherapy (Al-Mahmood et al., 2018). Furthermore, the development, progression and metastasis of breast cancer appears to be impacted by innate immune molecules and associated inflammatory mediators in the tumour microenvironment (Al-Mahmood et al., 2018, Qu et al., 2018).

While acting as a bridge between innate and adaptive immunity, human SP-Dis known for its activity in immune surveillance and immunomodulation in infection, allergy, and cancer (Kishore et al., 2006, Hasegawa et al., 2015, Kaur et al., 2018a, Kaur et al., 2018b, Kumar et al., 2019, Thakur et al., 2019, Mahajan et al., 2013). A recombinant fragment of SP-D (rfhSP-D) composed of homotrimeric neck region and CRD was reported to induce apoptosis several cancers in p53-dependent manner (Mahajan et al., 2013, Thakur et al., 2019, Kaur et al., 2018a). Furthermore, rfhSP-D treatment was also effective in inducing apoptosis in primary tumour cells isolated from patients with metastatic prostate cancer (Thakur et al., 2019).These studies therefore suggest that rfhSP-D has an immune surveillance role against cancer cells.

During the breast tumorigenesis, the tumor cells appear to interact with surrounding stroma to create a tumor microenvironment, supporting the growth, survival, and invasion of tumour cells. The extracellular matrix (ECM) is an important constituent of the niche, composed of several proteoglycans and glycosaminoglycans, which offer structural basis for tissue organization. This contributes to progression of malignant tumour formation, cell survival, proliferation and invasion via angiogenesis and metastasis (Heldin et al., 2013, Bernert et al., 2011). Hyaluronic acid (HYA), a polymeric non-sulfated glycosaminoglycan, and the most abundant component of the ECM plays an essential role in inflammation, angiogenesis, and cancer progression (Bernert et al., 2011). Several studies have reported that HYA participates in the regulation of breast tumor cell migration and invasion *in vitro* and tumor progression *in vivo* (Tolg et al., 2006, Bourguignon et al., 2009). Abnormal levels of HYA in the initial and late stage of ductal breast carcinoma *in situ* (DCIS) microenvironment appears to correlate with tumour stage progression and migration (Corte et al., 2010).

Pro-tumorigenic effects of HYA and its altered expression levels in breast tumors and possible mechanisms through which HYA might induce proliferation of tumour cells are areas of great interest. As HYA and SP-D are overexpressed in several carcinomas, targeting both HYA and SP-D is clinically relevant to inhibit HYA-mediated intracellular signaling that promotes tumour cell progression and invasion. Therefore, this study was aimed at examining the interaction between HYA and rfhSP-D and its implication on the cell adhesion and proliferation of triple-negative, triple-positive, and HER2-overexpressing breast cancer cells.

5.3 Results

5.3.1 Expression of Human SP-D in Breast cancer tissues

The expression of human SP-D was analyzed in eight cases of invasive ductal carcinoma using immunohistochemistry (IHC) technique (Figure 37). The study involved two cases for each molecular phenotypes of breast cancer (luminal A, luminal B, triple negative and Her2-Neu), which are based on the expression of the ER, PR, and the Her2-Neu status. The molecular phenotypes reflect the neoplastic heterogeneity of breast cancer, and can also vary in gene expressions, clinical and morphological features, treatment responses and outcome (Turashvili and Brogi, 2017). This study was aimed to analyze the presence of human SP-D distribution in all molecular phenotypes of breast cancer and to dissect its relevant biological role in neoplastic progression, thus, determine potential prognostic markers of mammary carcinoma. IHC analysis revealed heterogeneous inter-tumor and intra-tumor expressions of SP-D within the molecular subtypes mentioned above. IHC staining for SP-D expression showed a cytoplasmic expression in both the healthy peritumoral mammary parenchyma and neoplastic tissues, as previously demonstrated (Mangogna et al., 2018). Furthermore, SP-D distribution was also evident in cytoplasmic labelling and highlighted enriched SP-D expression in the neoplastic subclones of luminal A type and the ductal epithelium of peritumoral mammary parenchyma. However, a lower SP-D expression was evident in triple-negative breast cancer (TBNC) (Figure 37). A heterogeneous SP-D expression was also observed in luminal B and HER2 groups.

5.3.2 Expression of HYA in Breast Cancer Tissues

Serial sections for the HYA localization within the tumor microenvironment was examined following histochemical analysis of breast cancer and normal healthy tissue specimens. Presence of acid mucins was revealed by Alcian blue staining, containing sialic acid and HYA (Zugibe, 1970, Pearse, 1968, Conn, 1953) in the tumour stroma. Alcian blue staining highlighted a very faint HYA and sialic acid distribution in the peritumoral mammary parenchyma in all the molecular classes of breast cancer tested. In the luminal B and HER2 groups, a higher heterogeneous expression of HYA was also evident (Figure 38). Thus, a stronger staining for Alcian blue staining was evident

where a lower SP-D expression was detected, indicating that a modification of ECM might be correlated with a variable SP-D distribution.

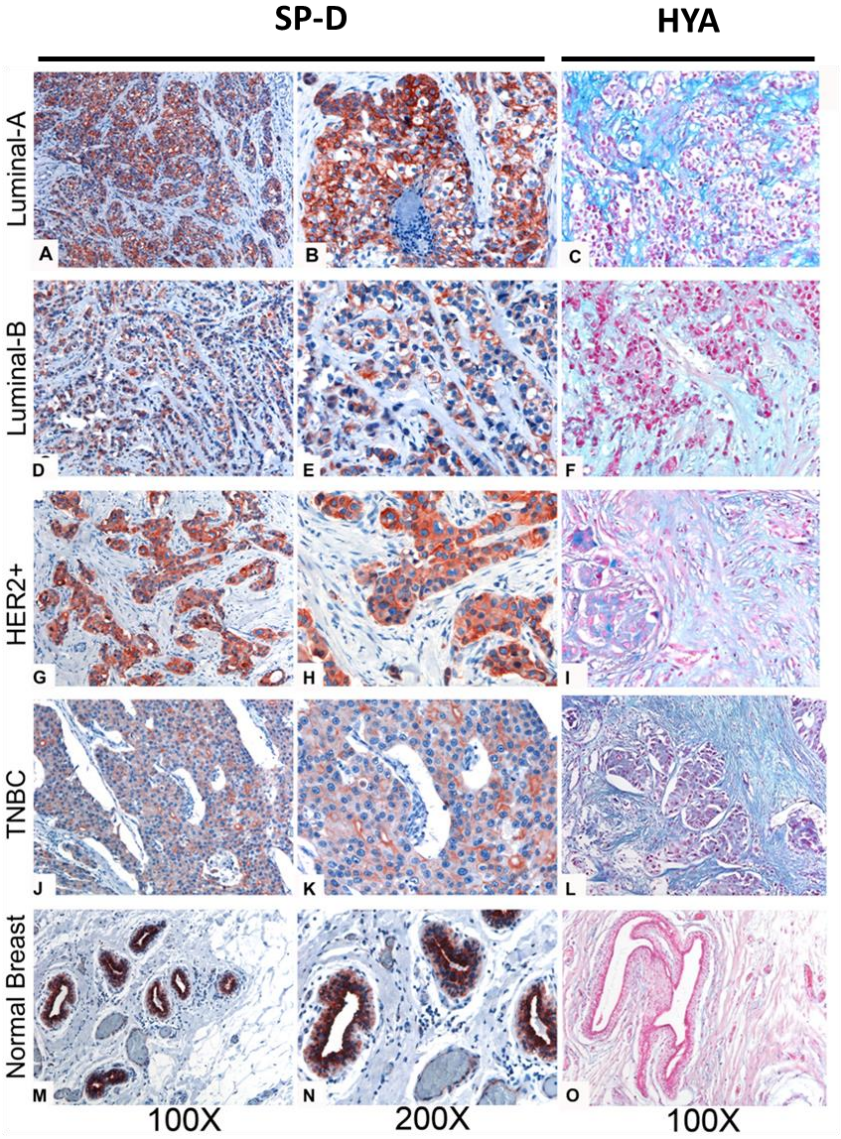

Figure 37: Presence of human SP-D and hyaluronic acid (HYA) in different histotypes of neoplastic breast and normal ductal mammary epithelium.

Detection of SP-D and HYA expression was detected by immunohistochemical (IHC) staining. SP-D was highly expressed by the ductal epithelium of peritumoral mammary parenchyma and the neoplastic sub-clones of luminal A type. Reduced SP-D expression was evident in triple-negative breast cancer (TBNC). AEC (red) chromogen was used to visualize the binding of anti-human SP-D antibodies. Histochemical staining with Alcian Blue underlined distribution of HYA in normal and breast cancer tissue sections; in particular, the staining was greatly visible in tumor-associated stroma.

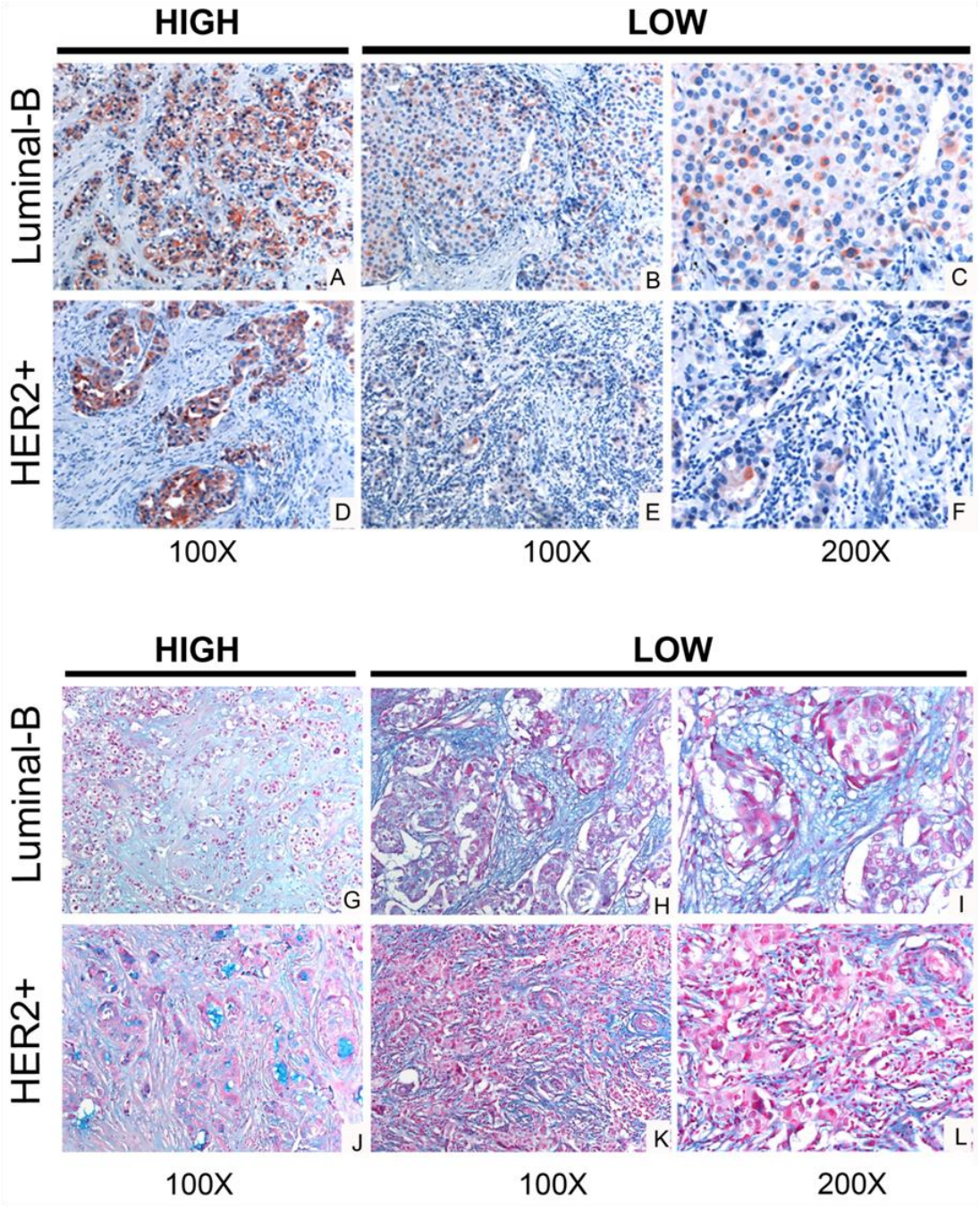

Figure 38: Immunohistochemical and histochemical analysis of SP-D (A–F) and HYA (G–L) expression in Luminal-B and Her2+/ER-/PR- breast carcinoma.

A higher variability of SP-D and HYA distribution was seen within the same isotype. There is a slight inverse correlation between expression of SP-D and HYA. AEC (red) chromogen was used to visualize the binding of anti-human SP-D antibodies, whereas histochemical staining with Alcian Blue highlighted HYA presence.

5.3.3 rfhSP-D Binds to High Molecular Weight HYA (1500 kDa) and Promotes Breast Cancer Cell Adhesion

The confirmation of HYA and SP-D distribution in breast cancer tissues prompted to examine whether rfhSP-D binds to HYA and can modulate the nature of the interaction between rfhSP-D and breast cancer cells. rfhSP-D bound to solid-phase HYA (1,500 kDa) in a dose-dependent manner (Figure 39). Furthermore, interaction of breast cancer cells with immobilized rfhSP-D (20 µg/ml) or HYA (20 µg/ml)-bound rfhSP-D was established using cell adhesion assay (Figure 40). All three breast cancer cell lines, including BT20, BT474, and SKBR3 were able to adhere to immobilized rfhSP-D, HYA, and to HYA-bound rfhSP-D. Immobilised rfhSP-D alone showed a higher cell adhesion in BT20 cell line when compared to immobilized HYA alone or HYA-bound rfhSP-D. However, there was no significant cell adhesion observed with immobilised rfhSP-D, HYA or HYA-bound rfhSP-D in BT474 or SKBR3 cell lines (Figure 40).

5.3.4 HYA Modulates Pro-apoptotic Effects of rfhSP-D in Breast Cancer Cell Lines

The interaction between rfhSP-D and HYA, and its implication on breast cancer cells were investigated via flow cytometry (Figure 41). Pre-coated HYA, HYA + rfhSP-D, and rfhSP-D-only wells were incubated with breast cancer cells, along with untreated control (cells only with no HYA +/-rfhSP-D), and the cells were subjected to Annexin V/FITC staining after 24h incubation. Flow cytometry analysis for the quantification of apoptosis revealed that HYA addition to rfhSP-D treated cells reduced apoptosis by ~45%. Additionally, proliferation assay was also performed to determine whether rfhSP-D together with HYA induced a proliferative response in the breast cancer cell lines. Therefore, the HYA + rfhSP-D treated breast cancer cells, along with untreated control, were stained with mouse anti-Ki-67 antibody to measure the percentage of proliferation. rfhSP-D (20 µg/ml)-treated SKBR3 cells incubated with HYA (20 µg/ml) resulted in ~30% cell proliferation (Figure 42), suggesting that addition of HYA negated pro-apoptotic effects of rfhSP-D against breast cancer cell lines. In the case of BT474 cell line, approximately ~47% of proliferative cells were seen following rfhSP-D treatment, while HYA + rfhSP-D-treated BT474 cells showed ~95% of proliferative cells stained with Ki-67 antibody. BT474 cells treated with HYA only showed ~88% of Ki-67-positive cells, while ~66% of proliferative cells were quantified in HYA-

treated SKBR3 cells. However, in the case of BT20 cell line, the cell proliferation was not significantly affected by either HYA or rfhSP-D treatment, suggesting that these cells continue to proliferate and grow unhindered. The % of cell proliferation were compared to untreated controls (cells only).

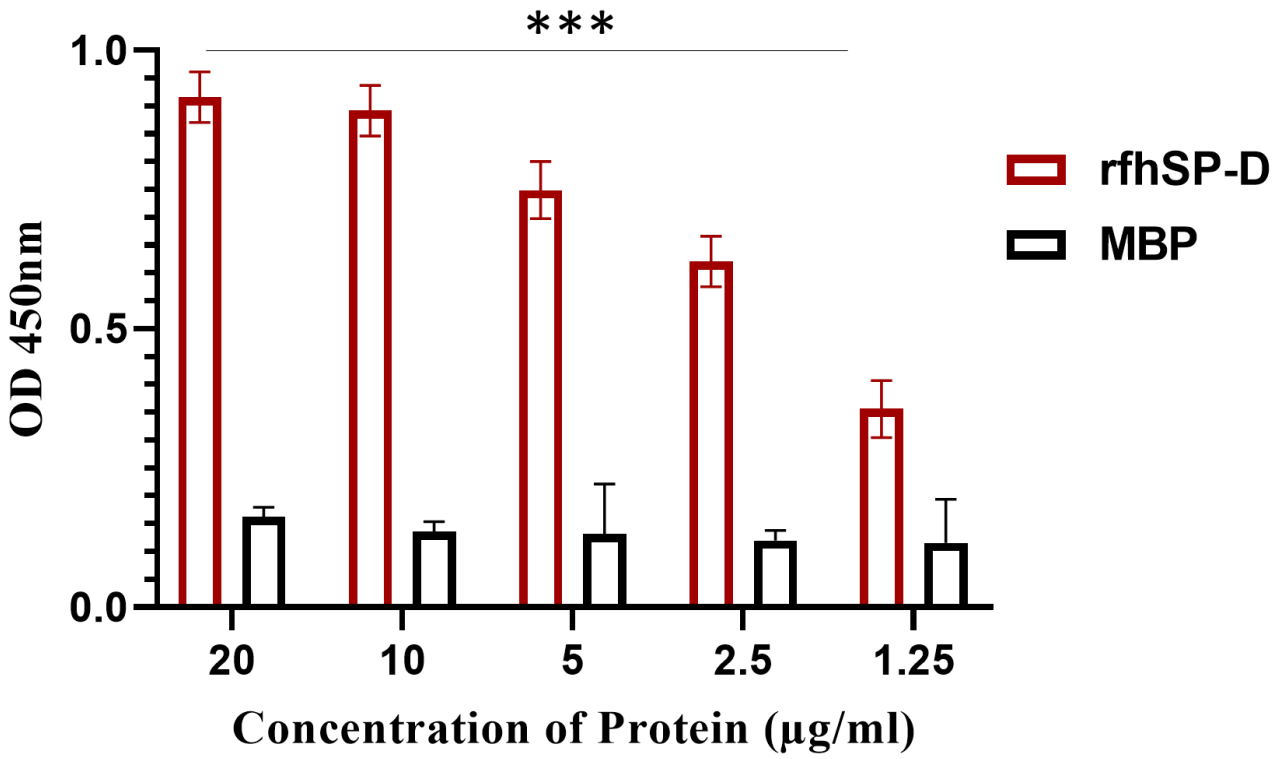

Figure 39: Interaction of rfhSP-D with hyaluronic acid (HYA).

Constant concentration of 1500kDa HYA (20ug/ml) coated in ELISA plates and incubated with decreasing concentration of rfhSP-D (20,10,5,2.5 or 1.25 ug/ml) at 37°C. In a parallel experiment, maltose-binding protein (MBP) (20,10,5,2.5 or 1.25 ug/ml) was used as a negative control protein. Following washes, the bound HYA-rfhSP-D/MBP interaction was detected using anti-rabbit SP-D polyclonal antibody (1:5000) or rabbit anti-MBP polyclonal antibody (1:5000) (Thermo Fisher). The reaction was developed using TMB substrate and the reading was read at 450 nm and the data were expressed as mean of three independent experiments done in triplicates ± SEM. Significance was determined using unpaired one-way ANOVA test (***$p < 0.001$).

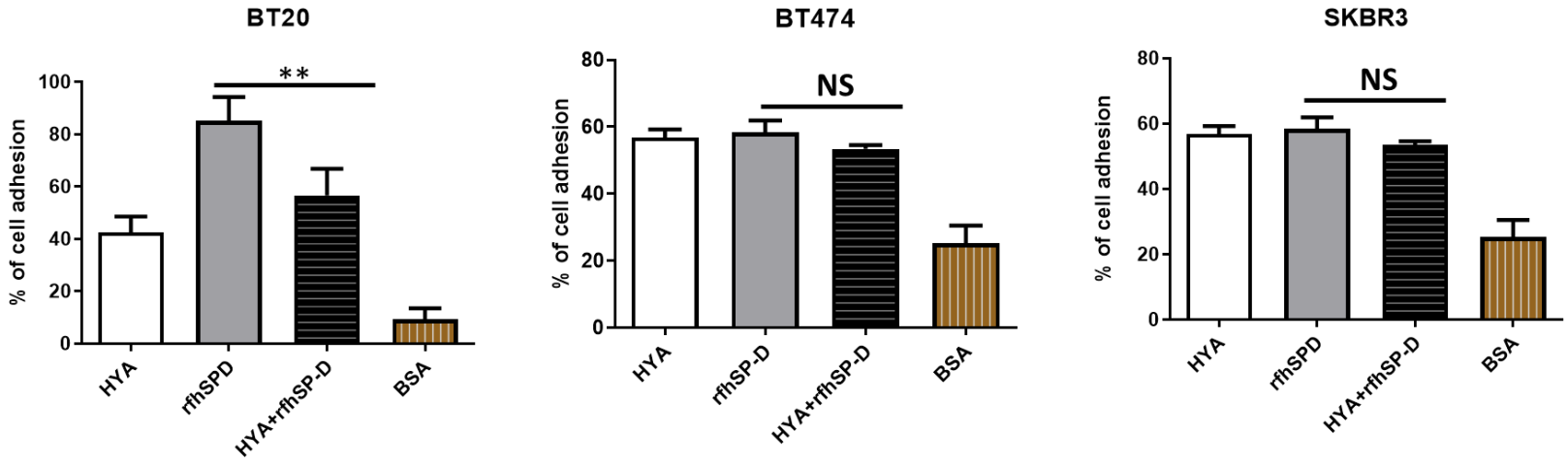

Figure 40: The effects of rfhSP-D on triple negative (BT20), triple positive (BT474) and HER2+-overexpressing (SKBR3) breast cancer lines adhesion.

FAST DiI fluorescent dye-labelled cells allowed to adhere to wells pre-coated with HYA, rfhSP-D, HYA+ rfhSP-D, and BSA (negative control). The cell adhesion was measured after 35 minutes of incubation at 37°C under 5% CO_2. The data is expressed as adhesion percentage with reference to a standard curve established using an increasing number of FAST DiI -labeled cells. The data is expressed as the mean of three independent experiments (n = 3) done in triplicates ± SEM. Statistical significance was determined using the unpaired one-way ANOVA test (**$p < 0.01$). The statistical analysis was carried out between rfhSP-D and HYA + rfhSP-D -treated breast cancer cells.

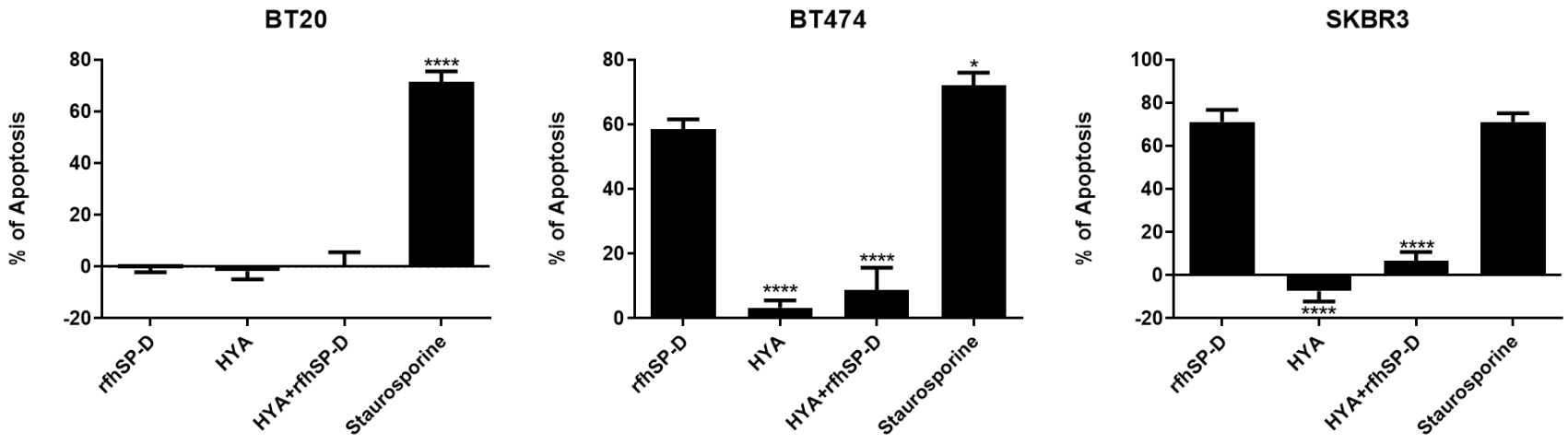

Figure 41: Induction of apoptosis induction in triple negative (BT20), triple positive (BT474) and HER2+-overexpressing (SKBR3) breast cancer lines following HYA (20 µg/ml) challenge in the presence and absence of rfhSP-D (20 µg/ml).

The data were expressed as the mean of three independent experiments (n = 3). A significant difference was seen among rfhSP-D treated and untreated samples, as made evident by the shift in the fluorescence intensity. Staurosporine (1 µM/ml) was used as a positive control, a known inducer of apoptosis. The data were generated from three independent experiments (n = 3) and expressed as mean ± SD (*p < 0.1, **p < 0.01, and ****p < 0.0001). Untreated sample (cells only) was used as a negative control and data shown are normalized to untreated sample. The statistical analysis was carried out between rfhSP-D and HYA + rfhSP-D-treated breast cancer cells.

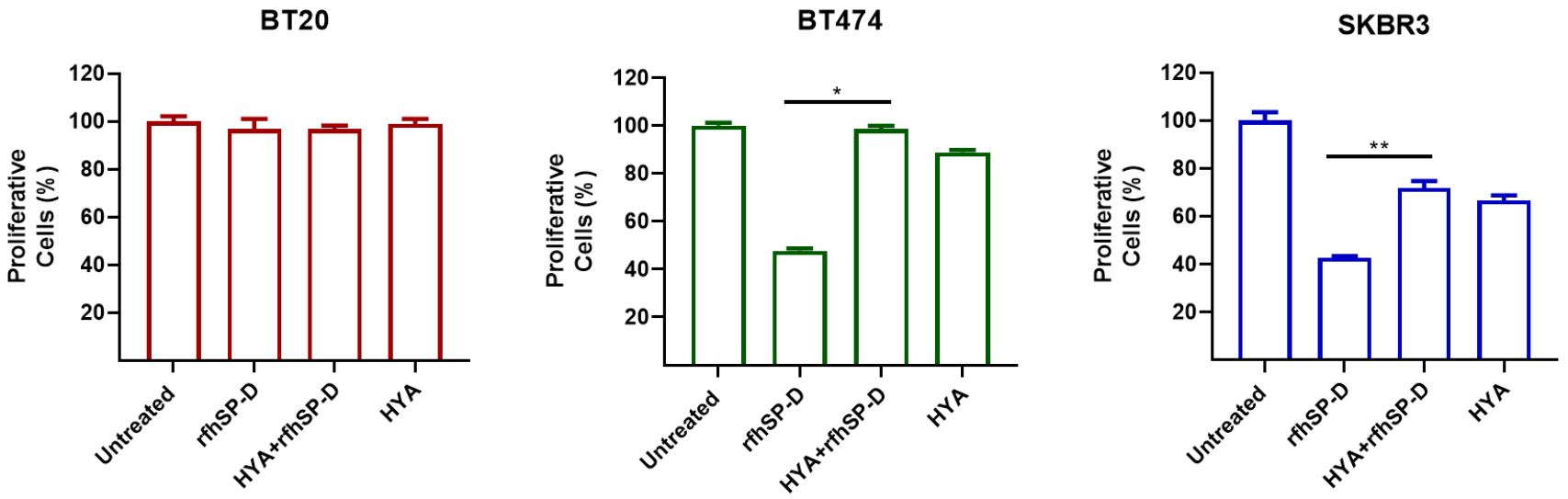

Figure 42: Proliferative effects of rfhSP-D treatment on triple negative (BT20), triple positive (BT474) and HER2+-overexpressing (SKBR3) breast cancer lines.

BT20, BT474 and SKBR3 cells were seeded in wells pre-coated with rfhSP-D, HYA + rfhSP-D, and HYA. Proliferative cell percentage was assessed by staining the cells with mouse anti-human KI-67 antibody, and KI-67-stained cells were measured via flow cytometry. The data were generated from three independent experiments (n = 3) and expressed as mean ± SD (*$p < 0.1$, **$p < 0.01$, and ****$p < 0.0001$). The statistical analysis was carried out between rfhSP-D and HYA + rfhSP-D-treated breast cancer cells.

5.3.5 Secretion of SP-D by Breast Cancer Cell Lines

Given the distribution of SP-D in the breast cancer tissues, further studies were carried out to purify SP-D from the culture supernatants of the breast cancer cells on the assumption that breast cancer cells may also be a possible source of SP-D distribution in the tumor microenvironment. The presence of SP-D in culture medium from the breast cancer cell lines was confirmed and analyzed via western blotting (Figure 43). Culture medium collected from BT20, BT474, and SKBR3 cell lines were passed through a maltose Sepharose column, and the EDTA-eluted fractions (5 μg/ml) were validated via western blotting; full-length SP-D (FL-SP-D) was detected at ~43kDa only for BT474 supernatant. Both BT20 and SKBR3 cell lines did not secrete any FL-SP-D. Furthermore, secreted FL-SP-D by BT474 was tested for its ability to induce apoptosis in these cell lines (Figure 43). However, the culture supernatant-purified FL-SP-D (20 μg/ml) was not able to trigger apoptosis in BT474, as well as in BT20 and SKBR3 cell lines (Figure 43).

5.3.6 Down-regulation of p53 by HYA addition in rfhSP-D-treated Breast Cancer Cell Lines

To further understand the mechanism of apoptosis inhibition mediated by HYA addition in rfhSP-D-treated breast cancer cell lines, the status of p53 and cell cycle inhibitors was analyzed. Down-regulation of phosphorylated p53, p21, p27 as well as caspase 3 was detected in HYA + rfhSP-D-treated BT474 and SKBR3 cells (Figure 44 & 46). There were no significant differences found in terms of p21 and p27 mRNA expression levels in the case of BT20 between HYA + rfhSP-D and rfhSP-D-treated BT20 cells. Down-regulation of these key mediators may possibly suggest the resistance of the breast cancer cells to apoptosis in the presence of HYA.

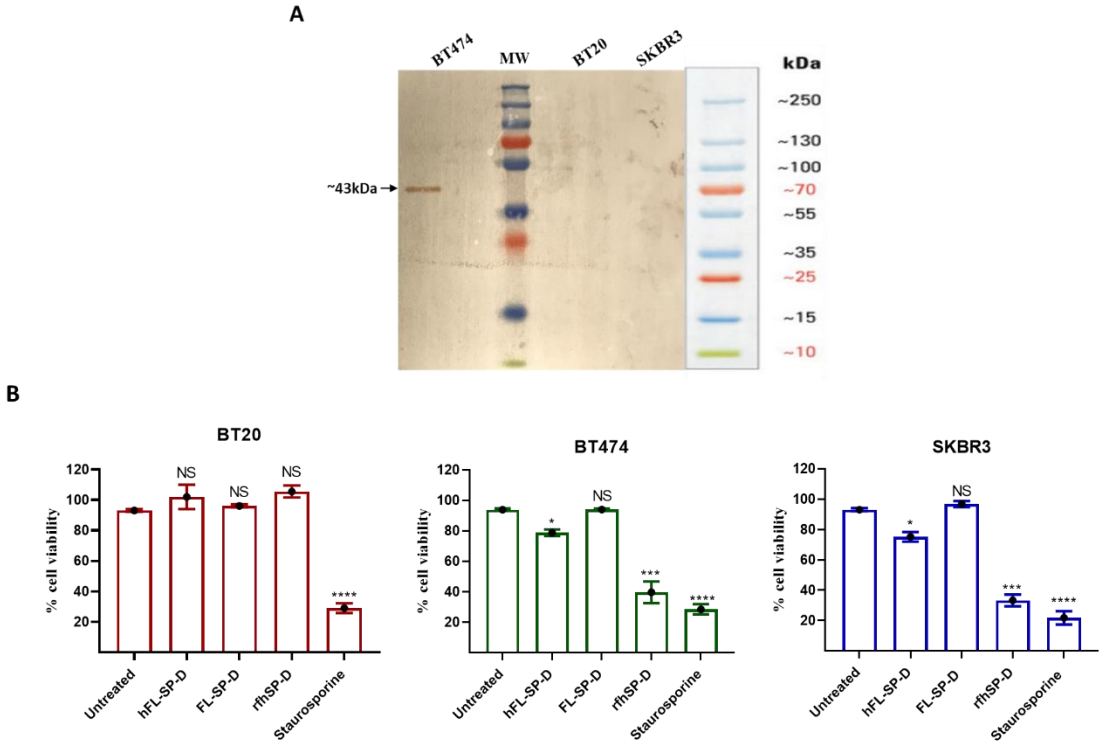

Figure 43: Secretion of full-length human SP-D were detected in culture medium from triple positive (BT474) breast cancer cell line.

The levels were confirmed and analyzed via western blotting (A). The collected culture medium from BT20, BT474, and SKBR3 cell lines was passed through a maltose Agarose column, and the eluted fractions (5 µg/well) were validated via western blotting; full-length SP-D (FL-SP-D) was detected at ~43 kDa only from BT474 culture medium. Secreted FL-SP-D by BT474 was examined for its ability to induce apoptosis (B). No effect of secreted full-length SP-D (20 µg/ml) was observed in terms of cell viability and induction of apoptosis. FL-SP-D purified from human lung lavage (hFL-SP-D) (20 µg/ml) and rfhSP-D (20 µg/ml) was also used in the sample experiment, along with Staurosporine (1µM/ml) as a positive control of apoptosis induction. Unpaired one-way ANOVA test was performed to measure the significance: *$p < 0.05$, and ***$p < 0.001$ ($n = 3$). The statistical analysis was performed between untreated (cells only) and protein-treated breast cancer cells.

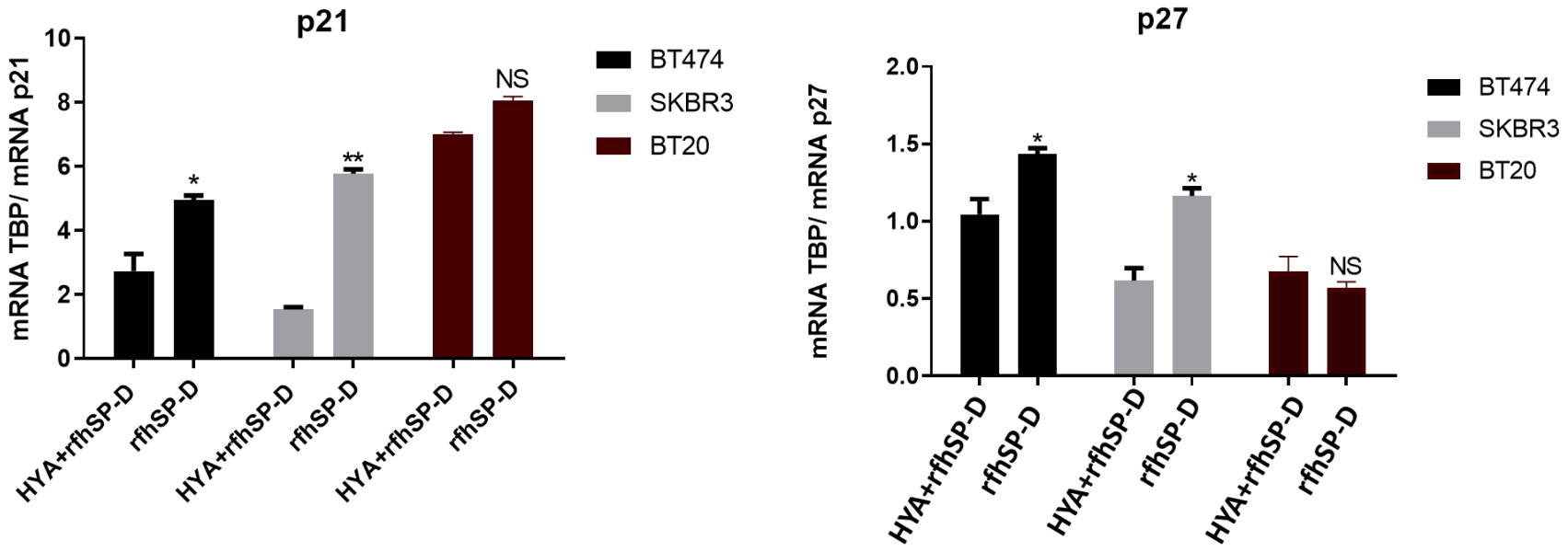

Figure 44: rfhSP-D treatment caused upregulation of p21 and p27 cell cycle inhibitors in triple positive (BT474) and HER2+-overexpressing (SKBR3) breast cancer cell lines.

BT20, BT474, and SKBR3 (0.4 × 106) cells were seeded in a pre-coated plate with HYA + rfhSP-D or rfhSP-D alone. The treated cancer cells were lysed and pelleted down. The pelleted cells were subjected to RNA extraction, followed by cDNA synthesis and qPCR. The comparative quantification method was carried out to calculate the efficiencies of each targeted gene for each individual PCR. The takeoff results obtained with p21/p27 primers were normalized with TBP (housekeeping gene) primers. Assays was conducted in triplicates, and error bars represent ± SEM. Unpaired one-way ANOVA test was performed to measure the significance; *$p < 0.05$ and **$p < 0.01$ ($n = 3$). The statistical analysis was performed between rfhSP-D and HYA+ rfhSP-D-treated breast cancer cells.

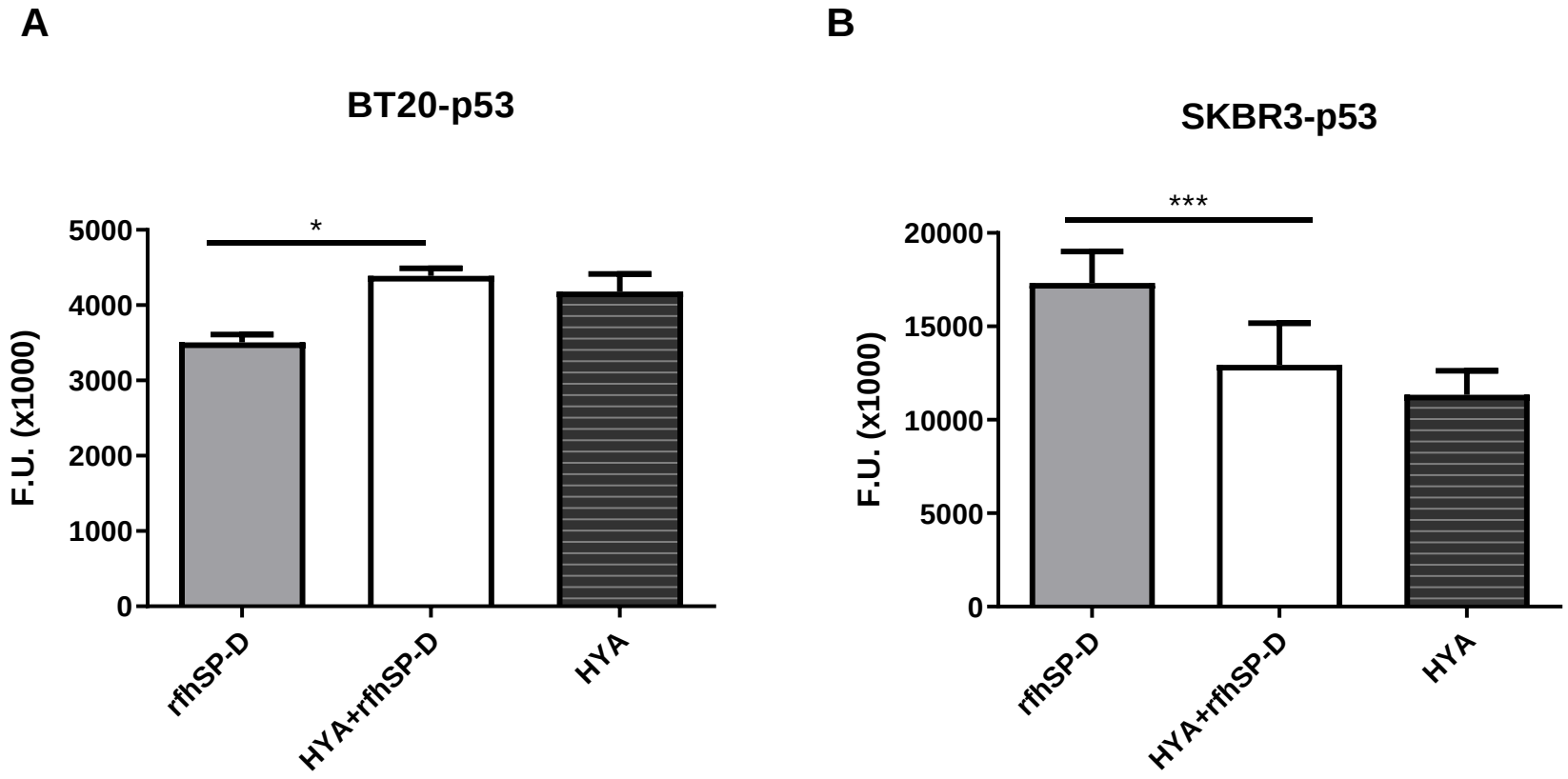

Figure 45: Intracellular signaling to show p53 phosphorylation (at Ser15) in rfhSP-D-treated triple negative (BT20) (A) and HER2+-overexpressing (SKBR3) (B) breast cancer cell lines.

The phosphorylation status of p53 was evaluated using total cell lysates with a PathScan Antibody Array Kit (Cell Signaling). Data were generated from at least three independent experiments and presented as mean ± SD. Unpaired one-way ANOVA test was performed to measure the significance: *$p < 0.05$ and ***$p < 0.001$ ($n = 3$). The statistical analysis was performed between rfhSP-D and HYA+ rfhSP-D-treated breast cancer cells.

5.4 Discussion

During the development of breast tumors, tumor cells interact with the surrounding matrix to form a tumor microenvironment (TME), thereby supporting the growth, survival, and invasion of cancer cells. ECM is an important constituent of the TME, leading to the progression of the formation and spread of malignant tumors. ECM is composed of a variety of proteoglycans and glycosaminoglycans, helping cell survival, proliferation, invasion, angiogenesis, and immune cell infiltration (Heldin et al., 2013, Bernert et al., 2011). HYA, an abundant component of ECM, is synthesized as a large linear anionic polymer on the cell surface. The role of HYA in inflammation-mediated breast cancer has been established (Soria and Ben-Baruch, 2008, Ponting et al., 1992) as well as its ability to modify tumor cell migration and invasion (Li et al., 2007). Compared with normal breast epithelial tissue, HYA synthesis and accumulation have been detected in aggressive breast cancer cells (Li et al., 2007). Furthermore, cancer cells overexpressing HYA synthase 2 have been reported to enhance angiogenesis and stromal cell recruitment, indicating that enhanced HYA levels in the tumor stroma support breast carcinoma (Bernert et al., 2011). To understand the inherent mechanisms of the pro-tumor effect of an increased HYA expression in breast tumors and its consequence on tumor proliferation via its receptors, including CD44, are likely to influence future therapeutic strategies. This study involved studying rfhSP-D-HYA interaction and its effect on the adhesion and proliferation of BT20, BT474 and SKBR3 breast cancer cells.

Direct binding ELISA showed that rfhSP-D bound HYA in a dose-dependent manner. The ability of breast cancer cells to interact with HYA-bound rfhSP-D was examined by cell adhesion assay. Compared with rfhSP-D combined with HYA or HYA alone, a clear cell adhesion binding pattern was observed with rfhSP-D alone. This may be due to the interaction of rfhSP-D-treated breast cancer cells with apoptotis-related receptors. Apoptosis and proliferation experiments were also performed to study the effect of HYA-bound rfhSP-D. Compared with rfhSP-D alone, SKBR3 cells seeded on HYA-bound rfhSP-D showed increased cell proliferation (1.7-fold). For BT474 cells treated with rfhSP-D, the addition of HYA resulted in a two-fold increase in proliferating cells. However, in the presence of rfhSP-D combined with HYA, the percentage of proliferating cells was not significantly different from the percentage of HYA alone or untreated SKBR3 and BT474 cells. Therefore, these findings indicate that the pro-apoptotic effect of rfhSP-D is negated by the

addition of HYA. However, no significant difference in the proliferation of BT20 cells was seen among all the conditions, indicating that these cells continued to grow and were not affected by rfhSP-D treatment alone or in combination with HYA. The addition of HYA may also regulate the interaction between rfhSP-D-treated cells and pro-apoptotic signaling pathways, thereby limiting the possibility of apoptosis induction. Therefore, the addition of HYA can promote cell proliferation by interacting with the proliferation signal cascades (e.g. PI3K-Akt and Ras-ERK) (Misra et al., 2015). Even though breast cancer tissues express SP-D, the distribution of HYA in the breast tumor microenvironment seems to provide a self-protective layer, thereby negating the anti-tumor effects of SP-D since rfhSP-D treated BT474 and SKBR3 cells undergo apoptosis, and the addition of HYA to rfhSP-D can enhance cell proliferation. Thus, breast cancer cells are likely to use HYA in their tumor microenvironment as an escape mechanism from SP-D (rfhSP-D) mediated apoptosis induction.

To further understand the mechanism of rfhSP-D mediated apoptosis, the possible signal pathways related to tumor adhesion and proliferation were analyzed. Decreased levels of caspase 3 and p53 were detected in HYA + rfhSP-D-treated BT474 and SKBR3 cells, which may indicate that cells became resistant to rfhSP-D-mediated apoptosis by the addition of HYA. Additionally, down-regulation of p21 and p27 was detected in HYA + rfhSP-D-treated BT474 and SKBR3 cells. Although p21 triggering is p53-dependent in certain events (such as DNA damage), in some cases the expression of p21 is independent of the state of p53, for example in normal tissue development and differentiation (Shamloo and Usluer, 2019, Zilfou and Lowe, 2009). p21 can lead to tumor evolution for tumor growth by slowing the accumulation of DNA damage. It has been suggested that the induction of p21 expression is required to promote tumor cell motility and tumorigenesis (Kreis et al., 2019, Shamloo and Usluer, 2019). Due to the controversy over the role of p21, because of its cytoplasmic location, it can be considered as an oncoprotein and/or tumor suppressor gene. The dual role of p21 as an oncogenic or tumor suppressor protein makes it difficult to understand the mechanism of p53–p21-triggered apoptosis induction or development of cancer progression (Shamloo and Usluer, 2019, Abbas and Dutta, 2009).

In conclusion, the participation of rfhSP-D and its related pro-apoptotic properties in cancer models may be a new type of therapeutic agent targeting multiple cells signaling pathways,

including tumor cell survival factors, transcription factors, protein kinases and pro-apoptotic gene markers. The mechanism by which rfhSP-D induces apoptosis and inhibits tumor cell proliferation is tumor-specific, due to its different effects on cell types and the expression of possible putative receptors. The interaction between HYA + rfhSP-D and cell receptors on a wide range of cancer, including breast cancer is currently under investigation. Furthermore, it is significant to note that full-length SP-D purified from BT474 culture medium was not able to trigger apoptosis in any of the three breast cancer cell lines tested in this study. The possible reasons could be that the cancer cells could produce a dysfunctional protein owing to protein misfolding, altered oligomerization and or mutations. The roles of SP-D in the cancer biology is complex and is strongly dependent on the TME composition. SP-D and HYA are overexpressed in breast and other cancers. Targeting HYA and SP-D is clinically relevant for the inhibition of HYA-mediated intracellular signal transmission, which counteracts the pro-apoptotic effect of rfhSP-D.

Chapter 6

General Discussion and Future Perspectives

This thesis provides the evidence that human SP-D has an immune surveillance role against IAV infection and breast cancer. Having generated biologically active rfhSP-D, this study considered it imperative to examine some of the protective effects of rfhSP-D against different subtypes of IAV (pH1N1 and H3N2) (Chapter 3) and phenotypes of breast cancer (BT20, BT474 and SKBR3) (Chapter 4 and 5). Previous studies have reported that the direct interaction of IAV with human SP-D resulted in virus neutralization and enhanced phagocytosis (Hartshorn et al., 1994, Hartshorn et al., 1993). In this study, it was clear the that the ability of rfhSP-D to act as an entry inhibitor against IAV infection was not limited to a specific IAV-subtype. The important aspect of host–pathogen interaction arising out of chapter 3 is the ability of rfhSP-D to bind HA and M1 IAV proteins, thus, suppressing replication in both pH1N1 and H3N2 subtypes. In addition, rfhSP-D-treated A549 cells infected with pH1N1 and H3N2 subtypes showed downregulation of mRNA transcript levels of TNF-α, IFN-α, IFN-β, IL-6, and RANTES, particularly during the initial stage of IAV infection. Furthermore, rfhSP-D treatment was found to reduce luciferase reporter activity of MDCK cells transfected with H1+N1 pseudotyped lentiviral particles, indicative of an entry inhibitory role of rfhSP-D against infectivity of IAV. Following rfhSP-D treatment, a dramatic suppression of key pro-inflammatory cytokines and chemokines levels was also evident in IAV challenged A549 cells. These data appear to highlight that the extent of immunomodulatory effects of SP-D on host cells can differ depending on IAV subtype. Since full-length human SP-D as well as rfhSP-D clearly interact with the IAV glycoproteins, thus acting as an entry inhibitor, it would be worth examining the possible amino acid residues involved in rfhSP-D- HA/NA binding. This can be performed by *in silico* docking analysis and confirmed using site-directed mutagenesis.

Chapter 4 reveals that rfhSP-D can interfere with breast cancer cell lines with the exception of the triple-negative ($ER^-/PR^-/HER2^-$); triple-positive ($ER+/PR^+/HER2^+$) and $HER2^+$ overexpressing breast cancer cell lines are susceptible to rfhSP-D induced apoptosis although rfhSP-D bound triple negative- BT20, triple-positive BT474 and $HER2^+$-positive SKBR3 breast cancer cell lines equally well. Upregulation of cell cycle inhibitors (p21/p27) and p53 phosphorylation (Ser15) was also evident in rfhSP-D-treated BT474 and SKBR3 cell lines, which signified cell cycle arrest at G2/M checkpoints. Exogenous rfhSP-D treatment also caused cleavage of caspase 9 and 3 in triple

positive and HER2^{+}-overexpressing breast cancer cell lines, highlighting the involvement of intrinsic apoptosis pathway. Additionally, interaction between SP-D and HYA, abundant component of the ECM, which plays a crucial role in inflammation, angiogenesis, and cancer progression has been reported (Chapter 5). Interaction of breast cancer cells with HYA can sustain growth and promote malignant progression of tumour cells. rfhSP-D bound to HYA in a calcium and dose-dependent manner and a greater cell adhesion binding pattern was seen with rfhSP-D alone compared to HYA alone or HYA-bound-rfhSP-D treated breast cancer cells. HYA-bound-rfhSP-D-treated SKBR3 and BT474 cells showed an increased cell proliferation, when compared to rfhSP-D alone treated SKBR3/BT474 cells. Therefore, these findings indicate that pro-apoptotic activity of rfhSP-D are modulated by HYA -in rfhSP-D treated triple positive and HER2^{+}-overexpressing breast cancer cell lines. However, following rfhSP-D treatment, the cell proliferation was not affected in triple negative cell line among all the conditions, suggestive of continuous growth of these cells. Expression of human SP-D was also evident in breast cancer tissues with varying phenotypes and HYA distribution within the breast tumour microenvironment appears to provide a self-protective coat, thus, modulating the anti-tumorigenic effects of SP-D.

Since triple positive and HER2^{+}-overexpressing breast cancer cell lines, treated with rfhSP-D undergo apoptosis, and HYA addition to rfhSP-D enhances cell proliferation, this suggest that breast cancer cells can use HYA as an escape mechanism from rfhSP-D-triggered apoptosis induction. Transfecting BT2O cell line with WT HER2^{+} plasmid to examine if HER2^{+} WT transfected BT20 cell line undergo apoptosis induction by rfhSP-D will be one way to prove that rfhSP-D susceptibility is due to HER2 expression on BT474 and SKBR3 cells; a lack of it seems to increase BT20 cells resistant to rfhSP-D effect. If HER2 is implicated in mediating rfhSP-D induced apoptosis, examining the molecular mechanism of downstream signaling pathways including MAPK and/or PI3K/AKT/mTOR pathways will be crucial to validate the hypothesis. Furthermore, RNA-sequencing will be an ideal method to investigate other pathways implicated in the treatment of breast cancer with rfhSP-D. The data generated from RNA-sequencing should be validated by qRT-PCR and western blotting, and generation of cellular knockout models for the implicated pathways. Furthermore, using rfhSP-D combined with commercially available anti-

breast cancer drug such as trastuzumab (Herceptin™) would also be a logical way to study if rfhSP-D can act as an adjuvant therapy in murine models.

Although, these *in vitro* studies in this thesis provided the first evidence of anti-tumour properties of rfhSP-D against breast cancer cell lines, respectively, further validation *in vivo* (i.e. using animal models) will be the next logical step. Studies have involved several animal models of breast cancer to study the molecular mechanisms involved in the development of breast tumorigenesis in vivo. Given the genetic complexity that is associated with the progression of each breast cancer subtypes, mouse models have become a potent tool for cancer research, and those can be subclassified into xenograft models, chemically, virally, or ionizing radiation (IR)-triggered models and genetically engineered mice (GEMs) including transgenics and knockouts (Hanahan et al., 2007, Wagner, 2004). The use of xenograft models is primarily based on the transplantation of human breast cancer cell lines into immunocompromised mice. Cancer cells in the xenograft models show the development of tumor growth, but do not metastasize (Zhang et al., 2013a) as is the case for luminal B (BT474) and triple negative (MDA-MB-231/ MDA-MB-435) (Goetz et al., 2017, Dai et al., 2017) cell lines. Furthermore, luminal A (MCF7 and T47D) and triple negative (MDA-MB-231, MDA-MB-435, and SUM1315) cell lines have been used to create breast cancer models of spontaneous metastasis through orthotopic injection (Iorns et al., 2012, Holliday and Speirs, 2011). Thus, the use of metastatic cell-derived xenografts (CDX) transplantation models in which breast cancer cells (MDA-MB-231 and SUM149) are injected into the tail vein of mouse are suitable for observing experimental metastasis and invasion (Gomez-Cuadrado et al., 2017). Experiments to examine the effect of rfhSP-D in xenografts models would initially require estimation of the lethal dose (LD_{50}), effective dose (ED_{50}) and the half-life of rfhSP-D. These results would help determine the means of administration for rfhSP-D in murine models. Taken together, the use of xenografts models will be useful for studying tumor development, as well as validating the tumor markers, and signaling pathways involved. This can aid in the evaluation of anti-cancer drug development involving rfhSP-D for breast cancer.

Therapeutic approaches targeting HYA synthesis, or HYA-receptor interaction would be a crucial measure for cancer treatment. Inhibition of HYA synthesis in breast cancer cells by 4-MU suppresses proliferation and migration *in vitro* and metastatic lesions of bone *in vivo* (Nagy et al.,

2015, Bohrer et al., 2014, Saito et al., 2013, Urakawa et al., 2012). Furthermore, the use of 4-MU treatment has also been shown to inhibit intracellular and cell surface HYA (Urakawa et al., 2012) and suppress Akt phosphorylation (Urakawa et al., 2012). In addition, bacteriophage hyaluronidase can prevent growth, migration, and invasion of breast cancer cells (Lee et al., 2010). The use of recombinant human hyaluronidase (rHUPH20) has been reported to improve the outcome of drug delivery of antibody-based trastuzumab targeted therapy in $HER2^{+}$ overexpressing breast cancer (Shpilberg and Jackisch, 2013). Other studies also suggest that degradation of HYA using by pegvor-hyaluronidase (PVHA) can remodel the TME in a murine model of breast cancer, thus, increasing the uptake of anti-Programmed Death-Ligand 1 (PD-L1) therapeutic antibody (Clift et al., 2019). PVHA treatment demonstrated a dramatic effectiveness of anti-PD-L1 antibody in reducing the breast tumor growth (Clift et al., 2019). Such pre-treatments against HYA can enhance the follow-up treatment with rfhSP-D in murine models.

Time is ripe for taking the knowledge about the involvement of rfhSP-D and its associated anti-viral or anti-tumour effects forward to the development as a novel therapeutic approach to target multiple cellular signaling pathways. The mechanisms which enable rfhSP-D to trigger anti-viral effect or apoptosis induction/inhibition of tumor cell proliferation are viral/tumor specific due to the differential effects and variation on the cell types and presence of putative receptors. Our preliminary data shows that rfhSP-D binds CD44 as well; CD44 is identified as a receptor for HYA, and CD44 signaling plays a critical role in breast cancer cell survival and proliferation. Investigating how rfhSP-D and HYA interaction affects the CD44 downstream signaling pathways will be the next logical step. There is a clear therapeutic potential of rfhSP-D against IAV strains/cancer where increased glycosylation leads to evasion of antibody susceptibility but increased susceptibility against soluble pattern recognition receptors (PRRs) such as SP-D. As a HA and NA-based inhibitor against IAV infection, rfhSP-D may be a viable therapeutic agent that may be administered as an inhalation formulation to control IAV infection. Having established the specific nature of interactions between rfhSP-D and IAV/breast cancer, we can hope to examine in future host response in the murine models of infection/cancer using wild type, and SP-D knock-out mice.

References

Abbas T and Dutta A, *P21 in cancer: Intricate networks and multiple activities.* Nat Rev Cancer, 2009. **9**(6): p. 400-14 DOI: 10.1038/nrc2657.

Akram M and Siddiqui SA, *Breast cancer management: Past, present and evolving.* Indian J Cancer, 2012. **49**(3): p. 277-82 DOI: 10.4103/0019-509X.104486.

Al-Mahmood S, Sapiezynski J, Garbuzenko OB, and Minko T, *Metastatic and triple-negative breast cancer: Challenges and treatment options.* Drug Deliv Transl Res, 2018. **8**(5): p. 1483-1507 DOI: 10.1007/s13346-018-0551-3.

Alibek K and Liu G, *Biodefense shield and avian influenza.* Emerg Infect Dis, 2006. **12**(5): p. 873-5 DOI: 10.3201/eid1205.051480.

Almand B, Resser JR, Lindman B, Nadaf S, Clark JI, Kwon ED, Carbone DP, and Gabrilovich DI, *Clinical significance of defective dendritic cell differentiation in cancer.* Clin Cancer Res, 2000. **6**(5): p. 1755-66.

Augusto LA, Synguelakis M, Johansson J, Pedron T, Girard R, and Chaby R, *Interaction of pulmonary surfactant protein c with cd14 and lipopolysaccharide.* Infect Immun, 2003. **71**(1): p. 61-7 DOI: 10.1128/iai.71.1.61-67.2003.

Avrameas S, *Natural autoantibodies: From 'horror autotoxicus' to 'gnothi seauton'.* Immunology today, 1991. **12**(5): p. 154-159.

Barrow AD, Palarasah Y, Bugatti M, Holehouse AS, Byers DE, Holtzman MJ, Vermi W, Skjodt K, Crouch E, and Colonna M, *Oscar is a receptor for surfactant protein d that activates tnf-alpha release from human ccr2+ inflammatory monocytes.* J Immunol, 2015. **194**(7): p. 3317-26 DOI: 10.4049/jimmunol.1402289.

Baselga J and Swain SM, *Novel anticancer targets: Revisiting erbb2 and discovering erbb3.* Nat Rev Cancer, 2009. **9**(7): p. 463-75 DOI: 10.1038/nrc2656.

Bassi N, Zampieri S, Ghirardello A, Tonon M, Zen M, Cozzi F, and Doria A, *Pentraxins, anti-pentraxin antibodies, and atherosclerosis.* Clinical reviews in allergy & immunology, 2009. **37**(1): p. 36 DOI: 10.1007/s12016-008-8098-6.

Bennett KL, Jackson DG, Simon JC, Tanczos E, Peach R, Modrell B, Stamenkovic I, Plowman G, and Aruffo A, *Cd44 isoforms containing exon v3 are responsible for the presentation of heparin-binding growth factor.* J Cell Biol, 1995. **128**(4): p. 687-98 DOI: 10.1083/jcb.128.4.687.

Bernert B, Porsch H, and Heldin P, *Hyaluronan synthase 2 (has2) promotes breast cancer cell invasion by suppression of tissue metalloproteinase inhibitor 1 (timp-1).* J Biol Chem, 2011. **286**(49): p. 42349-59 DOI: 10.1074/jbc.M111.278598.

Betakova T, Kostrabova A, Lachova V, and Turianova L, *Cytokines induced during influenza virus infection.* Curr Pharm Des, 2017. **23**(18): p. 2616-2622 DOI: 10.2174/1381612823666170316123736.

Binder CJ, Shaw PX, Chang M-K, Boullier A, Hartvigsen K, Hörkkö S, Miller YI, Woelkers DA, Corr M, and Witztum JL, *Thematic review series: The immune system and atherogenesis. The role of natural antibodies in atherogenesis.* Journal of lipid research, 2005. **46**(7): p. 1353-1363.

Boekhout AH, Beijnen JH, and Schellens JH, *Trastuzumab.* Oncologist, 2011. **16**(6): p. 800-10 DOI: 10.1634/theoncologist.2010-0035.

Bohrer LR, Chuntova P, Bade LK, Beadnell TC, Leon RP, Brady NJ, Ryu Y, Goldberg JE, Schmechel SC, Koopmeiners JS, McCarthy JB, and Schwertfeger KL, *Activation of the fgfr-stat3 pathway in breast cancer cells induces a hyaluronan-rich microenvironment that licenses tumor formation.* Cancer Res, 2014. **74**(1): p. 374-86 DOI: 10.1158/0008-5472.CAN-13-2469.

Bolat F, Kayaselcuk F, Nursal TZ, Yagmurdur MC, Bal N, and Demirhan B, *Microvessel density, vegf expression, and tumor-associated macrophages in breast tumors: Correlations with prognostic parameters.* J Exp Clin Cancer Res, 2006. **25**(3): p. 365-72.

Borron P, McIntosh JC, Korfhagen TR, Whitsett JA, Taylor J, and Wright JR, *Surfactant-associated protein a inhibits lps-induced cytokine and nitric oxide production in vivo.* Am J Physiol Lung Cell Mol Physiol, 2000. **278**(4): p. L840-7 DOI: 10.1152/ajplung.2000.278.4.L840.

Bourguignon LY, Xia W, and Wong G, *Hyaluronan-mediated cd44 interaction with p300 and sirt1 regulates beta-catenin signaling and nfkappab-specific transcription activity leading to mdr1 and bcl-xl gene expression and chemoresistance in breast tumor cells.* J Biol Chem, 2009. **284**(5): p. 2657-71 DOI: 10.1074/jbc.M806708200.

Bouvier NM and Palese P, *The biology of influenza viruses.* Vaccine, 2008. **26 Suppl 4**: p. D49-53 DOI: 10.1016/j.vaccine.2008.07.039.

Byrd-Leotis L, Cummings RD, and Steinhauer DA, *The interplay between the host receptor and influenza virus hemagglutinin and neuraminidase.* Int J Mol Sci, 2017. **18**(7) DOI: 10.3390/ijms18071541.

Carroll MC, *The complement system in regulation of adaptive immunity.* Nature immunology, 2004. **5**(10): p. 981-986 DOI: 10.1038/ni1113.

Casalegno-Garduno R, Meier C, Schmitt A, Spitschak A, Hilgendorf I, Rohde S, Hirt C, Freund M, Putzer BM, and Schmitt M, *Immune responses to rhamm in patients with acute myeloid leukemia after chemotherapy and allogeneic stem cell transplantation.* Clin Dev Immunol, 2012. **2012**: p. 146463 DOI: 10.1155/2012/146463.

Ch'ng ES, Jaafar H, and Tuan Sharif SE, *Breast tumor angiogenesis and tumor-associated macrophages: Histopathologist's perspective.* Patholog Res Int, 2011. **2011**: p. 572706 DOI: 10.4061/2011/572706.

Cha YJ and Koo JS, *Role of tumor-associated myeloid cells in breast cancer.* Cells, 2020. **9**(8) DOI: 10.3390/cells9081785.

Chanmee T, Ontong P, Konno K, and Itano N, *Tumor-associated macrophages as major players in the tumor microenvironment.* Cancers (Basel), 2014. **6**(3): p. 1670-90 DOI: 10.3390/cancers6031670.

Cheang MC, Chia SK, Voduc D, Gao D, Leung S, Snider J, Watson M, Davies S, Bernard PS, Parker JS, Perou CM, Ellis MJ, and Nielsen TO, *Ki67 index, her2 status, and prognosis of patients with luminal b breast cancer.* J Natl Cancer Inst, 2009. **101**(10): p. 736-50 DOI: 10.1093/jnci/djp082.

Chen C, Zhao S, Karnad A, and Freeman JW, *The biology and role of cd44 in cancer progression: Therapeutic implications.* J Hematol Oncol, 2018a. **11**(1): p. 64 DOI: 10.1186/s13045-018-0605-5.

Chen X, Liu S, Goraya MU, Maarouf M, Huang S, and Chen JL, *Host immune response to influenza a virus infection.* Front Immunol, 2018b. **9**: p. 320 DOI: 10.3389/fimmu.2018.00320.

Chiba H, Pattanajitvilai S, Evans AJ, Harbeck RJ, and Voelker DR, *Human surfactant protein d (sp-d) binds mycoplasma pneumoniae by high affinity interactions with lipids.* Journal of Biological Chemistry, 2002. **277**(23): p. 20379-20385 DOI: 10.1074/jbc.M201089200.

Clayville LR, *Influenza update: A review of currently available vaccines.* P T, 2011. **36**(10): p. 659-84.

Clift R, Souratha J, Garrovillo SA, Zimmerman S, and Blouw B, *Remodeling the tumor microenvironment sensitizes breast tumors to anti-programmed death-ligand 1 immunotherapy.* Cancer Res, 2019. **79**(16): p. 4149-4159 DOI: 10.1158/0008-5472.CAN-18-3060.

Coffelt SB, Kersten K, Doornebal CW, Weiden J, Vrijland K, Hau CS, Verstegen NJM, Ciampricotti M, Hawinkels L, Jonkers J, and de Visser KE, *Il-17-producing gammadelta t cells and neutrophils conspire to promote breast cancer metastasis.* Nature, 2015. **522**(7556): p. 345-348 DOI: 10.1038/nature14282.

Coleman RE, Collinson M, Gregory W, Marshall H, Bell R, Dodwell D, Keane M, Gil M, Barrett-Lee P, Ritchie D, Bowman A, Liversedge V, De Boer RH, Passos-Coelho JL, O'Reilly S, Bertelli G, Joffe J, Brown JE, Wilson C, Tercero JC, Jean-Mairet J, Gomis R, and Cameron D, *Benefits and risks of adjuvant treatment with zoledronic acid in stage ii/iii breast cancer. 10 years follow-up of the azure randomized clinical trial (big 01/04).* J Bone Oncol, 2018. **13**: p. 123-135 DOI: 10.1016/j.jbo.2018.09.008.

Colley K and Baenziger J, *Identification of the post-translational modifications of the core-specific lectin. The core-specific lectin contains hydroxyproline, hydroxylysine, and glucosylgalactosylhydroxylysine residues.* Journal of Biological Chemistry, 1987. **262**(21): p. 10290-10295.

Conn HJ, *Biological stains. A handbook on the nature and uses of the dyes employed in the biological laboratory.* Biological stains. A handbook on the nature and uses of the dyes employed in the biological laboratory., 1953(Edn 6).

Corte MD, Gonzalez LO, Junquera S, Bongera M, Allende MT, and Vizoso FJ, *Analysis of the expression of hyaluronan in intraductal and invasive carcinomas of the breast.* J Cancer Res Clin Oncol, 2010. **136**(5): p. 745-50 DOI: 10.1007/s00432-009-0713-2.

Crouch E, Hartshorn K, Horlacher T, McDonald B, Smith K, Cafarella T, Seaton B, Seeberger PH, and Head J, *Recognition of mannosylated ligands and influenza a virus by human surfactant protein d: Contributions of an extended site and residue 343.* Biochemistry, 2009. **48**(15): p. 3335-45 DOI: 10.1021/bi8022703.

Crouch E, Parghi D, Kuan S, and Persson A, *Surfactant protein d: Subcellular localization in nonciliated bronchiolar epithelial cells.* American Journal of Physiology-Lung Cellular and Molecular Physiology, 1992. **263**(1): p. L60-L66 DOI: 10.1152/ajplung.1992.263.1.L60.

Crouch E and Wright JR, *Surfactant proteins a and d and pulmonary host defense.* Annual review of physiology, 2001. **63**(1): p. 521-554 DOI: 10.1146/annurev.physiol.63.1.521.

Crouch EC, *Surfactant protein-d and pulmonary host defense.* Respiratory research, 2000. **1**(2): p. 6 DOI: 10.1186/rr19.

Dai X, Cheng H, Bai Z, and Li J, *Breast cancer cell line classification and its relevance with breast tumor subtyping.* J Cancer, 2017. **8**(16): p. 3131-3141 DOI: 10.7150/jca.18457.

Dale BA and Fredericks LP, *Antimicrobial peptides in the oral environment: Expression and function in health and disease.* Current issues in molecular biology, 2005. **7**(2): p. 119.

Das K, Aramini JM, Ma LC, Krug RM, and Arnold E, *Structures of influenza a proteins and insights into antiviral drug targets.* Nat Struct Mol Biol, 2010. **17**(5): p. 530-8 DOI: 10.1038/nsmb.1779.

de Wetering JKv, Van Eijk M, Van Golde LM, Hartung T, Van Strijp JA, and Batenburg JJ, *Characteristics of surfactant protein a and d binding to lipoteichoic acid and peptidoglycan, 2 major cell wall components of gram-positive bacteria.* The Journal of infectious diseases, 2001. **184**(9): p. 1143-1151.

Dec M and Wernicki A, *Conglutinin, cl-43 and cl-46--three bovine collectins.* Pol J Vet Sci, 2006. **9**(4): p. 265-75.

Dempsey PW, Allison ME, Akkaraju S, Goodnow CC, and Fearon DT, *C3d of complement as a molecular adjuvant: Bridging innate and acquired immunity.* Science, 1996. **271**(5247): p. 348-350.

DeNardo DG, Barreto JB, Andreu P, Vasquez L, Tawfik D, Kolhatkar N, and Coussens LM, *Cd4(+) t cells regulate pulmonary metastasis of mammary carcinomas by enhancing protumor properties of macrophages.* Cancer Cell, 2009. **16**(2): p. 91-102 DOI: 10.1016/j.ccr.2009.06.018.

DeNardo DG, Brennan DJ, Rexhepaj E, Ruffell B, Shiao SL, Madden SF, Gallagher WM, Wadhwani N, Keil SD, Junaid SA, Rugo HS, Hwang ES, Jirstrom K, West BL, and Coussens LM, *Leukocyte complexity predicts breast cancer survival and functionally regulates response to chemotherapy.* Cancer Discov, 2011. **1**(1): p. 54-67 DOI: 10.1158/2159-8274.CD-10-0028.

Denney L and Ho LP, *The role of respiratory epithelium in host defence against influenza virus infection.* Biomed J, 2018. **41**(4): p. 218-233 DOI: 10.1016/j.bj.2018.08.004.

Dhankhar R, Vyas SP, Jain AK, Arora S, Rath G, and Goyal AK, *Advances in novel drug delivery strategies for breast cancer therapy.* Artif Cells Blood Substit Immobil Biotechnol, 2010. **38**(5): p. 230-49 DOI: 10.3109/10731199.2010.494578.

Diaz-Montero CM, Salem ML, Nishimura MI, Garrett-Mayer E, Cole DJ, and Montero AJ, *Increased circulating myeloid-derived suppressor cells correlate with clinical cancer stage, metastatic tumor burden, and doxorubicin-cyclophosphamide chemotherapy.* Cancer Immunol Immunother, 2009. **58**(1): p. 49-59 DOI: 10.1007/s00262-008-0523-4.

Dinapoli MR, Calderon CL, and Lopez DM, *The altered tumoricidal capacity of macrophages isolated from tumor-bearing mice is related to reduce expression of the inducible nitric oxide synthase gene.* J Exp Med, 1996. **183**(4): p. 1323-9 DOI: 10.1084/jem.183.4.1323.

Ding M, Fu X, Tan H, Wang R, Chen Z, and Ding S, *The effect of vascular endothelial growth factor c expression in tumor-associated macrophages on lymphangiogenesis and lymphatic metastasis in breast cancer.* Mol Med Rep, 2012. **6**(5): p. 1023-9 DOI: 10.3892/mmr.2012.1043.

Dodagatta-Marri E, Mitchell DA, Pandit H, Sonawani A, Murugaiah V, Idicula-Thomas S, Nal B, Al-Mozaini MM, Kaur A, and Madan T, *Protein–protein interaction between surfactant protein d and dc-sign via c-type lectin domain can suppress hiv-1 transfer.* Frontiers in immunology, 2017. **8**: p. 834.

Du Clos TW and Mold C, *C-reactive protein.* Immunologic research, 2004. **30**(3): p. 261-277 DOI: 10.1385/IR:30:3:261.

Elgueta R, Benson MJ, de Vries VC, Wasiuk A, Guo Y, and Noelle RJ, *Molecular mechanism and function of cd40/cd40l engagement in the immune system.* Immunol Rev, 2009. **229**(1): p. 152-72 DOI: 10.1111/j.1600-065X.2009.00782.x.

Elmore S, *Apoptosis: A review of programmed cell death.* Toxicol Pathol, 2007. **35**(4): p. 495-516 DOI: 10.1080/01926230701320337.

Elton D, Medcalf E, Bishop K, and Digard P, *Oligomerization of the influenza virus nucleoprotein: Identification of positive and negative sequence elements.* Virology, 1999. **260**(1): p. 190-200 DOI: 10.1006/viro.1999.9818.

Enegd B, King JA, Stylli S, Paradiso L, Kaye AH, and Novak U, *Overexpression of hyaluronan synthase-2 reduces the tumorigenic potential of glioma cells lacking hyaluronidase activity.* Neurosurgery, 2002. **50**(6): p. 1311-8 DOI: 10.1097/00006123-200206000-00023.

Favier A-L, Reynard O, Gout E, Van Eijk M, Haagsman HP, Crouch E, Volchkov V, Peyrefitte C, and Thielens NM, *Involvement of surfactant protein d in ebola virus infection enhancement via glycoprotein interaction.* Viruses, 2019. **11**(1): p. 15.

Ferguson JS, Voelker DR, McCormack FX, and Schlesinger LS, *Surfactant protein d binds to mycobacterium tuberculosis bacilli and lipoarabinomannan via carbohydrate-lectin interactions resulting in reduced phagocytosis of the bacteria by macrophages1.* The Journal of immunology, 1999. **163**(1): p. 312-321.

Ferguson JS, Voelker DR, Ufnar JA, Dawson AJ, and Schlesinger LS, *Surfactant protein d inhibition of human macrophage uptake of mycobacterium tuberculosis is independent of bacterial agglutination.* The Journal of Immunology, 2002. **168**(3): p. 1309-1314.

Ferlay J, Shin HR, Bray F, Forman D, Mathers C, and Parkin DM, *Estimates of worldwide burden of cancer in 2008: Globocan 2008.* Int J Cancer, 2010. **127**(12): p. 2893-917 DOI: 10.1002/ijc.25516.

Fisher JH and Mason R, *Expression of pulmonary surfactant protein d in rat gastric mucosa.* American journal of respiratory cell and molecular biology, 1995. **12**(1): p. 13-18 DOI: 10.1165/ajrcmb.12.1.7811466.

Forghani P, Khorramizadeh MR, and Waller EK, *Silibinin inhibits accumulation of myeloid-derived suppressor cells and tumor growth of murine breast cancer.* Cancer Med, 2014. **3**(2): p. 215-24 DOI: 10.1002/cam4.186.

Fraser JR, Laurent TC, and Laurent UB, *Hyaluronan: Its nature, distribution, functions and turnover.* J Intern Med, 1997. **242**(1): p. 27-33 DOI: 10.1046/j.1365-2796.1997.00170.x.

Funk CJ, Wang J, Ito Y, Travanty EA, Voelker DR, Holmes KV, and Mason RJ, *Infection of human alveolar macrophages by human coronavirus strain 229e.* The Journal of general virology, 2012. **93**(Pt 3): p. 494 DOI: 10.1099/vir.0.038414-0.

Gardai SJ, Xiao Y-Q, Dickinson M, Nick JA, Voelker DR, Greene KE, and Henson PM, *By binding sirpα or calreticulin/cd91, lung collectins act as dual function surveillance molecules to suppress or enhance inflammation.* Cell, 2003. **115**(1): p. 13-23.

Garred P, Larsen F, Seyfarth J, Fujita R, and Madsen HO, *Mannose-binding lectin and its genetic variants.* Genes Immun, 2006. **7**(2): p. 85-94 DOI: 10.1038/sj.gene.6364283.

Gelbert LM, Cai S, Lin X, Sanchez-Martinez C, Del Prado M, Lallena MJ, Torres R, Ajamie RT, Wishart GN, Flack RS, Neubauer BL, Young J, Chan EM, Iversen P, Cronier D, Kreklau E, and de Dios A, *Preclinical characterization of the cdk4/6 inhibitor ly2835219: In-vivo cell cycle-*

dependent/independent anti-tumor activities alone/in combination with gemcitabine. Invest New Drugs, 2014. **32**(5): p. 825-37 DOI: 10.1007/s10637-014-0120-7.

George J and Stern R, *Serum hyaluronan and hyaluronidase: Very early markers of toxic liver injury.* Clin Chim Acta, 2004. **348**(1-2): p. 189-97 DOI: 10.1016/j.cccn.2004.05.018.

Ghatak S, Maytin EV, Mack JA, Hascall VC, Atanelishvili I, Moreno Rodriguez R, Markwald RR, and Misra S, *Roles of proteoglycans and glycosaminoglycans in wound healing and fibrosis.* Int J Cell Biol, 2015. **2015**: p. 834893 DOI: 10.1155/2015/834893.

Glaser L, Stevens J, Zamarin D, Wilson IA, Garcia-Sastre A, Tumpey TM, Basler CF, Taubenberger JK, and Palese P, *A single amino acid substitution in 1918 influenza virus hemagglutinin changes receptor binding specificity.* J Virol, 2005. **79**(17): p. 11533-6 DOI: 10.1128/JVI.79.17.11533-11536.2005.

Goetz MP, Kalari KR, Suman VJ, Moyer AM, Yu J, Visscher DW, Dockter TJ, Vedell PT, Sinnwell JP, Tang X, Thompson KJ, McLaughlin SA, Moreno-Aspitia A, Copland JA, Northfelt DW, Gray RJ, Hunt K, Conners A, Sicotte H, Eckel-Passow JE, Kocher JP, Ingle JN, Ellingson MS, McDonough M, Wieben ED, Weinshilboum R, Wang L, and Boughey JC, *Tumor sequencing and patient-derived xenografts in the neoadjuvant treatment of breast cancer.* J Natl Cancer Inst, 2017. **109**(7) DOI: 10.1093/jnci/djw306.

Goldberg JE and Schwertfeger KL, *Proinflammatory cytokines in breast cancer: Mechanisms of action and potential targets for therapeutics.* Curr Drug Targets, 2010. **11**(9): p. 1133-46 DOI: 10.2174/138945010792006799.

Golshani R, Lopez L, Estrella V, Kramer M, Iida N, and Lokeshwar VB, *Hyaluronic acid synthase-1 expression regulates bladder cancer growth, invasion, and angiogenesis through cd44.* Cancer Res, 2008. **68**(2): p. 483-91 DOI: 10.1158/0008-5472.CAN-07-2140.

Gomez-Cuadrado L, Tracey N, Ma R, Qian B, and Brunton VG, *Mouse models of metastasis: Progress and prospects.* Dis Model Mech, 2017. **10**(9): p. 1061-1074 DOI: 10.1242/dmm.030403.

Gonzalez H, Hagerling C, and Werb Z, *Roles of the immune system in cancer: From tumor initiation to metastatic progression.* Genes Dev, 2018. **32**(19-20): p. 1267-1284 DOI: 10.1101/gad.314617.118.

Goodison S, Urquidi V, and Tarin D, *Cd44 cell adhesion molecules.* Mol Pathol, 1999. **52**(4): p. 189-96 DOI: 10.1136/mp.52.4.189.

Hakomori S, *Glycosylation defining cancer malignancy: New wine in an old bottle.* Proc Natl Acad Sci U S A, 2002. **99**(16): p. 10231-3 DOI: 10.1073/pnas.172380699.

Hanahan D, Wagner EF, and Palmiter RD, *The origins of oncomice: A history of the first transgenic mice genetically engineered to develop cancer.* Genes Dev, 2007. **21**(18): p. 2258-70 DOI: 10.1101/gad.1583307.

Handel-Fernandez ME, Cheng X, Herbert LM, and Lopez DM, *Down-regulation of il-12, not a shift from a t helper-1 to a t helper-2 phenotype, is responsible for impaired ifn-gamma production in mammary tumor-bearing mice.* J Immunol, 1997. **158**(1): p. 280-6.

Hansen SW, Ohtani K, Roy N, and Wakamiya N, *The collectins cl-l1, cl-k1 and cl-p1, and their roles in complement and innate immunity.* Immunobiology, 2016. **221**(10): p. 1058-67 DOI: 10.1016/j.imbio.2016.05.012.

Hardwick C, Hoare K, Owens R, Hohn HP, Hook M, Moore D, Cripps V, Austen L, Nance DM, and Turley EA, *Molecular cloning of a novel hyaluronan receptor that mediates tumor cell motility.* J Cell Biol, 1992. **117**(6): p. 1343-50 DOI: 10.1083/jcb.117.6.1343.

Hartshorn KL, Crouch EC, White MR, Eggleton P, Tauber AI, Chang D, and Sastry K, *Evidence for a protective role of pulmonary surfactant protein d (sp-d) against influenza a viruses.* J Clin Invest, 1994. **94**(1): p. 311-9 DOI: 10.1172/JCI117323.

Hartshorn KL, Sastry K, White MR, Anders EM, Super M, Ezekowitz RA, and Tauber AI, *Human mannose-binding protein functions as an opsonin for influenza a viruses.* J Clin Invest, 1993. **91**(4): p. 1414-20 DOI: 10.1172/JCI116345.

Hartshorn KL, Webby R, White MR, Tecle T, Pan C, Boucher S, Moreland RJ, Crouch EC, and Scheule RK, *Role of viral hemagglutinin glycosylation in anti-influenza activities of recombinant surfactant protein d.* Respir Res, 2008. **9**: p. 65 DOI: 10.1186/1465-9921-9-65.

Hartshorn KL, White MR, Voelker DR, Coburn J, Zaner K, and Crouch EC, *Mechanism of binding of surfactant protein d to influenza a viruses: Importance of binding to haemagglutinin to antiviral activity.* Biochem J, 2000. **351 Pt 2**: p. 449-58.

Hasegawa Y, Takahashi M, Ariki S, Asakawa D, Tajiri M, Wada Y, Yamaguchi Y, Nishitani C, Takamiya R, and Saito A, *Surfactant protein d suppresses lung cancer progression by downregulation of epidermal growth factor signaling.* Oncogene, 2015. **34**(7): p. 838-845.

Heldin P, Basu K, Olofsson B, Porsch H, Kozlova I, and Kahata K, *Deregulation of hyaluronan synthesis, degradation and binding promotes breast cancer.* J Biochem, 2013. **154**(5): p. 395-408 DOI: 10.1093/jb/mvt085.

Henriksen ML, Brandt J, Iyer SS, Thielens NM, and Hansen S, *Characterization of the interaction between collectin 11 (cl-11, cl-k1) and nucleic acids.* Mol Immunol, 2013. **56**(4): p. 757-67 DOI: 10.1016/j.molimm.2013.07.011.

Herías MV, Hogenkamp A, van Asten AJ, Tersteeg MH, van Eijk M, and Haagsman HP, *Expression sites of the collectin sp-d suggest its importance in first line host defence: Power of combining in situ hybridisation, rt-pcr and immunohistochemistry.* Molecular immunology, 2007. **44**(13): p. 3324-3332 DOI: 10.1016/j.molimm.2007.02.025.

Hillaire ML, Haagsman HP, Osterhaus AD, Rimmelzwaan GF, and van Eijk M, *Pulmonary surfactant protein d in first-line innate defence against influenza a virus infections.* J Innate Immun, 2013. **5**(3): p. 197-208 DOI: 10.1159/000346374.

Hillaire ML, van Eijk M, Vogelzang-van Trierum SE, Fouchier RA, Osterhaus AD, Haagsman HP, and Rimmelzwaan GF, *Recombinant porcine surfactant protein d inhibits influenza a virus replication ex vivo.* Virus Res, 2014. **181**: p. 22-6 DOI: 10.1016/j.virusres.2013.12.032.

Hirschfield GM, Herbert J, Kahan MC, and Pepys MB, *Human c-reactive protein does not protect against acute lipopolysaccharide challenge in mice.* The Journal of Immunology, 2003. **171**(11): p. 6046-6051.

Hirsimaki P, Aaltonen A, and Mantyla E, *Toxicity of antiestrogens.* Breast J, 2002. **8**(2): p. 92-6 DOI: 10.1046/j.1524-4741.2002.08204.x.

Holliday DL and Speirs V, *Choosing the right cell line for breast cancer research.* Breast Cancer Res, 2011. **13**(4): p. 215 DOI: 10.1186/bcr2889.

Hsieh M-H, beirag N, Murugaiah V, Chou Y-C, Kuo W-S, Kao H-F, Madan T, Kishore U, and Wang J-Y, *Human surfactant protein d binds s1 and receptor binding domain of spike protein and*

acts as an entry inhibitor of sars-cov-2 pseudotyped viral particles <em>in vitro</em&gt. bioRxiv, 2020: p. 2020.12.18.423418 DOI: 10.1101/2020.12.18.423418.

Hu Y, Jin Y, Han D, Zhang G, Cao S, Xie J, Xue J, Li Y, Meng D, Fan X, Sun LQ, and Wang M, *Mast cell-induced lung injury in mice infected with h5n1 influenza virus.* J Virol, 2012. **86**(6): p. 3347-56 DOI: 10.1128/JVI.06053-11.

Huang B, Lei Z, Zhao J, Gong W, Liu J, Chen Z, Liu Y, Li D, Yuan Y, Zhang GM, and Feng ZH, *Ccl2/ccr2 pathway mediates recruitment of myeloid suppressor cells to cancers.* Cancer Lett, 2007. **252**(1): p. 86-92 DOI: 10.1016/j.canlet.2006.12.012.

Hug H, Mohajeri MH, and La Fata G, *Toll-like receptors: Regulators of the immune response in the human gut.* Nutrients, 2018. **10**(2): p. 203 DOI: 10.3390/nu10020203.

Iorns E, Drews-Elger K, Ward TM, Dean S, Clarke J, Berry D, El Ashry D, and Lippman M, *A new mouse model for the study of human breast cancer metastasis.* PLoS One, 2012. **7**(10): p. e47995 DOI: 10.1371/journal.pone.0047995.

Itano N and Kimata K, *Mammalian hyaluronan synthases.* IUBMB Life, 2002. **54**(4): p. 195-9 DOI: 10.1080/15216540214929.

Itano N, Sawai T, Yoshida M, Lenas P, Yamada Y, Imagawa M, Shinomura T, Hamaguchi M, Yoshida Y, Ohnuki Y, Miyauchi S, Spicer AP, McDonald JA, and Kimata K, *Three isoforms of mammalian hyaluronan synthases have distinct enzymatic properties.* J Biol Chem, 1999. **274**(35): p. 25085-92 DOI: 10.1074/jbc.274.35.25085.

Iwatsuki-Horimoto K, Horimoto T, Noda T, Kiso M, Maeda J, Watanabe S, Muramoto Y, Fujii K, and Kawaoka Y, *The cytoplasmic tail of the influenza a virus m2 protein plays a role in viral assembly.* J Virol, 2006. **80**(11): p. 5233-40 DOI: 10.1128/JVI.00049-06.

Janssen WJ, McPhillips KA, Dickinson MG, Linderman DJ, Morimoto K, Xiao YQ, Oldham KM, Vandivier RW, Henson PM, and Gardai SJ, *Surfactant proteins a and d suppress alveolar macrophage phagocytosis via interaction with sirp alpha.* Am J Respir Crit Care Med, 2008. **178**(2): p. 158-67 DOI: 10.1164/rccm.200711-1661OC.

Jiang D, Liang J, and Noble PW, *Hyaluronan as an immune regulator in human diseases.* Physiol Rev, 2011. **91**(1): p. 221-64 DOI: 10.1152/physrev.00052.2009.

Jiang F, Caraway NP, Nebiyou Bekele B, Zhang HZ, Khanna A, Wang H, Li R, Fernandez RL, Zaidi TM, Johnston DA, and Katz RL, *Surfactant protein a gene deletion and prognostics for patients with stage i non-small cell lung cancer.* Clin Cancer Res, 2005. **11**(15): p. 5417-24 DOI: 10.1158/1078-0432.CCR-04-2087.

Job ER, Deng YM, Tate MD, Bottazzi B, Crouch EC, Dean MM, Mantovani A, Brooks AG, and Reading PC, *Pandemic h1n1 influenza a viruses are resistant to the antiviral activities of innate immune proteins of the collectin and pentraxin superfamilies.* J Immunol, 2010. **185**(7): p. 4284-91 DOI: 10.4049/jimmunol.1001613.

Joosten LA, Abdollahi-Roodsaz S, Dinarello CA, O'Neill L, and Netea MG, *Toll-like receptors and chronic inflammation in rheumatic diseases: New developments.* Nat Rev Rheumatol, 2016. **12**(6): p. 344-57 DOI: 10.1038/nrrheum.2016.61.

Julien O and Wells JA, *Caspases and their substrates.* Cell Death Differ, 2017. **24**(8): p. 1380-1389 DOI: 10.1038/cdd.2017.44.

Kaufmann DE, Kavanagh DG, Pereyra F, Zaunders JJ, Mackey EW, Miura T, Palmer S, Brockman M, Rathod A, Piechocka-Trocha A, Baker B, Zhu B, Le Gall S, Waring MT, Ahern R, Moss K, Kelleher AD, Coffin JM, Freeman GJ, Rosenberg ES, and Walker BD, *Upregulation of ctla-*

4 by hiv-specific cd4+ t cells correlates with disease progression and defines a reversible immune dysfunction. Nat Immunol, 2007. **8**(11): p. 1246-54 DOI: 10.1038/ni1515.

Kaur A, Riaz MS, Murugaiah V, Varghese PM, Singh SK, and Kishore U, *A recombinant fragment of human surfactant protein d induces apoptosis in pancreatic cancer cell lines via fas-mediated pathway.* Frontiers in immunology, 2018a. **9**: p. 1126 DOI: 10.3389/fimmu.2018.01126.

Kaur A, Riaz MS, Singh SK, and Kishore U, *Human surfactant protein d suppresses epithelial-to-mesenchymal transition in pancreatic cancer cells by downregulating tgf-β.* Frontiers in immunology, 2018b. **9**: p. 1844 DOI: 10.3389/fimmu.2018.01844.

Kerviel A, Dash S, Moncorge O, Panthu B, Prchal J, Decimo D, Ohlmann T, Lina B, Favard C, Decroly E, Ottmann M, Roingeard P, and Muriaux D, *Involvement of an arginine triplet in m1 matrix protein interaction with membranes and in m1 recruitment into virus-like particles of the influenza a(h1n1)pdm09 virus.* PLoS One, 2016. **11**(11): p. e0165421 DOI: 10.1371/journal.pone.0165421.

Kim R, Emi M, and Tanabe K, *Cancer immunoediting from immune surveillance to immune escape.* Immunology, 2007. **121**(1): p. 1-14 DOI: 10.1111/j.1365-2567.2007.02587.x.

Kimura Y, Madhavan M, Call MK, Santiago W, Tsonis PA, Lambris JD, and Del Rio-Tsonis K, *Expression of complement 3 and complement 5 in newt limb and lens regeneration.* The Journal of Immunology, 2003. **170**(5): p. 2331-2339 DOI: 10.4049/jimmunol.170.5.2331.

Kishore U, Greenhough TJ, Waters P, Shrive AK, Ghai R, Kamran MF, Bernal AL, Reid KB, Madan T, and Chakraborty T, *Surfactant proteins sp-a and sp-d: Structure, function and receptors.* Molecular immunology, 2006. **43**(9): p. 1293-1315 DOI: 10.1016/j.molimm.2005.08.004.

Kishore U, Madan T, Sarma PU, Singh M, Urban BC, and Reid KB, *Protective roles of pulmonary surfactant proteins, sp-a and sp-d, against lung allergy and infection caused by aspergillus fumigatus.* Immunobiology, 2002. **205**(4-5): p. 610-618.

Knudson W, *Tumor-associated hyaluronan. Providing an extracellular matrix that facilitates invasion.* Am J Pathol, 1996. **148**(6): p. 1721-6.

Koyama H, Hibi T, Isogai Z, Yoneda M, Fujimori M, Amano J, Kawakubo M, Kannagi R, Kimata K, Taniguchi S, and Itano N, *Hyperproduction of hyaluronan in neu-induced mammary tumor accelerates angiogenesis through stromal cell recruitment: Possible involvement of versican/pg-m.* Am J Pathol, 2007. **170**(3): p. 1086-99 DOI: 10.2353/ajpath.2007.060793.

Kreis NN, Louwen F, and Yuan J, *The multifaceted p21 (cip1/waf1/cdkn1a) in cell differentiation, migration and cancer therapy.* Cancers (Basel), 2019. **11**(9) DOI: 10.3390/cancers11091220.

Kuan S-F, Rust K, and Crouch E, *Interactions of surfactant protein d with bacterial lipopolysaccharides. Surfactant protein d is an escherichia coli-binding protein in bronchoalveolar lavage.* The Journal of clinical investigation, 1992. **90**(1): p. 97-106.

Kudo K, Sano H, Takahashi H, Kuronuma K, Yokota S-i, Fujii N, Shimada K-i, Yano I, Kumazawa Y, and Voelker DR, *Pulmonary collectins enhance phagocytosis of mycobacterium avium through increased activity of mannose receptor.* The Journal of Immunology, 2004. **172**(12): p. 7592-7602.

Kumar J, Murugaiah V, Sotiriadis G, Kaur A, Jeyaneethi J, Sturniolo I, Alhamlan F, Chatterjee J, Hall M, and Kishore U, *Surfactant protein d as a potential biomarker and therapeutic target in ovarian cancer.* Frontiers in oncology, 2019. **9**: p. 542.

Lamichhane PP and Samarasinghe AE, *The role of innate leukocytes during influenza virus infection.* J Immunol Res, 2019. **2019**: p. 8028725 DOI: 10.1155/2019/8028725.

Lawson PR and Reid KB, *The roles of surfactant proteins a and d in innate immunity.* Immunological reviews, 2000. **173**(1): p. 66-78 DOI: 10.1034/j.1600-065x.2000.917308.x.

Le QM, Kiso M, Someya K, Sakai YT, Nguyen TH, Nguyen KH, Pham ND, Ngyen HH, Yamada S, Muramoto Y, Horimoto T, Takada A, Goto H, Suzuki T, Suzuki Y, and Kawaoka Y, *Avian flu: Isolation of drug-resistant h5n1 virus.* Nature, 2005. **437**(7062): p. 1108 DOI: 10.1038/4371108a.

Lee JH, Moore LD, Kumar S, Pritchard DG, Ponnazhagan S, and Deivanayagam C, *Bacteriophage hyaluronidase effectively inhibits growth, migration and invasion by disrupting hyaluronan-mediated erk1/2 activation and rhoa expression in human breast carcinoma cells.* Cancer Lett, 2010. **298**(2): p. 238-49 DOI: 10.1016/j.canlet.2010.07.011.

Leek RD, Lewis CE, Whitehouse R, Greenall M, Clarke J, and Harris AL, *Association of macrophage infiltration with angiogenesis and prognosis in invasive breast carcinoma.* Cancer Res, 1996. **56**(20): p. 4625-9.

Leth-Larsen R, Zhong F, Chow VT, Holmskov U, and Lu J, *The sars coronavirus spike glycoprotein is selectively recognized by lung surfactant protein d and activates macrophages.* Immunobiology, 2007. **212**(3): p. 201-11 DOI: 10.1016/j.imbio.2006.12.001.

Li L, Heldin CH, and Heldin P, *Inhibition of platelet-derived growth factor-bb-induced receptor activation and fibroblast migration by hyaluronan activation of cd44.* J Biol Chem, 2006. **281**(36): p. 26512-9 DOI: 10.1074/jbc.M605607200.

Li R, Todd NW, Qiu Q, Fan T, Zhao RY, Rodgers WH, Fang HB, Katz RL, Stass SA, and Jiang F, *Genetic deletions in sputum as diagnostic markers for early detection of stage i non-small cell lung cancer.* Clin Cancer Res, 2007. **13**(2 Pt 1): p. 482-7 DOI: 10.1158/1078-0432.CCR-06-1593.

Liu G, Chen S, Hu A, Zhang L, Sun W, Chen J, Tang W, Zhang H, Liu C, Ke C, and Chen X, *The establishment and validation of the human u937 cell line as a cellular model to screen immunomodulatory agents regulating cytokine release induced by influenza virus infection.* Virol Sin, 2019. **34**(6): p. 648-661 DOI: 10.1007/s12250-019-00145-w.

Liu Y, Lai L, Chen Q, Song Y, Xu S, Ma F, Wang X, Wang J, Yu H, Cao X, and Wang Q, *Microrna-494 is required for the accumulation and functions of tumor-expanded myeloid-derived suppressor cells via targeting of pten.* J Immunol, 2012. **188**(11): p. 5500-10 DOI: 10.4049/jimmunol.1103505.

Luo A, Meng M, Wang G, Han R, Zhang Y, Jing X, Zhao L, Gu S, and Zhao X, *Myeloid-derived suppressor cells recruited by chemokine (c-c motif) ligand 3 promote the progression of breast cancer via phosphoinositide 3-kinase-protein kinase b-mammalian target of rapamycin signaling.* J Breast Cancer, 2020. **23**(2): p. 141-161 DOI: 10.4048/jbc.2020.23.e26.

Ma L, Dong L, and Chang P, *Cd44v6 engages in colorectal cancer progression.* Cell Death Dis, 2019. **10**(1): p. 30 DOI: 10.1038/s41419-018-1265-7.

Madan T, Biswas B, Varghese PM, Subedi R, Pandit H, Idicula-Thomas S, Kundu I, Rooge S, Agarwal R, Tripathi DM, Kaur S, Gupta E, Gupta SK, and Kishore U, *A recombinant fragment of human surfactant protein d binds spike protein and inhibits infectivity and replication of sars-cov-2 in clinical samples.* bioRxiv, 2020: p. 2020.12.18.423415 DOI: 10.1101/2020.12.18.423415.

Madan T, Eggleton P, Kishore U, Strong P, Aggrawal SS, Sarma PU, and Reid KB, *Binding of pulmonary surfactant proteins a and d to aspergillus fumigatus conidia enhances phagocytosis and killing by human neutrophils and alveolar macrophages.* Infect Immun, 1997a. **65**(8): p. 3171-9 DOI: 10.1128/IAI.65.8.3171-3179.1997.

Madan T, Kishore U, Shah A, Eggleton P, Strong P, Wang JY, Aggrawal SS, Sarma PU, and Reid KB, *Lung surfactant proteins a and d can inhibit specific ige binding to the allergens of aspergillus fumigatus and block allergen-induced histamine release from human basophils.* Clin Exp Immunol, 1997b. **110**(2): p. 241-9 DOI: 10.1111/j.1365-2249.1997.tb08323.x.

Madan T, Reid KB, Singh M, Sarma PU, and Kishore U, *Susceptibility of mice genetically deficient in the surfactant protein (sp)-a or sp-d gene to pulmonary hypersensitivity induced by antigens and allergens of aspergillus fumigatus.* J Immunol, 2005. **174**(11): p. 6943-54 DOI: 10.4049/jimmunol.174.11.6943.

Madera S, Rapp M, Firth MA, Beilke JN, Lanier LL, and Sun JC, *Type i ifn promotes nk cell expansion during viral infection by protecting nk cells against fratricide.* J Exp Med, 2016. **213**(2): p. 225-33 DOI: 10.1084/jem.20150712.

Madsen J, Kliem A, Tornøe I, Skjødt K, Koch C, and Holmskov U, *Localization of lung surfactant protein d on mucosal surfaces in human tissues.* The Journal of Immunology, 2000. **164**(11): p. 5866-5870 DOI: 10.4049/jimmunol.164.11.5866.

Mahajan L, Gautam P, Dodagatta-Marri E, Madan T, and Kishore U, *Surfactant protein sp-d modulates activity of immune cells: Proteomic profiling of its interaction with eosinophilic cells.* Expert Rev Proteomics, 2014. **11**(3): p. 355-69 DOI: 10.1586/14789450.2014.897612.

Mahajan L, Pandit H, Madan T, Gautam P, Yadav AK, Warke H, Sundaram CS, Sirdeshmukh R, Sarma PU, Kishore U, and Surolia A, *Human surfactant protein d alters oxidative stress and hmga1 expression to induce p53 apoptotic pathway in eosinophil leukemic cell line.* PLoS One, 2013. **8**(12): p. e85046 DOI: 10.1371/journal.pone.0085046.

Malhotra R, Haurum JS, Thiel S, and Sim RB, *Binding of human collectins (sp-a and mbp) to influenza virus.* Biochem J, 1994. **304 (Pt 2)**: p. 455-61 DOI: 10.1042/bj3040455.

Mangogna A, Belmonte B, Agostinis C, Ricci G, Gulino A, Ferrara I, Zanconati F, Tripodo C, Romano F, and Kishore U, *Pathological significance and prognostic value of surfactant protein d in cancer.* Frontiers in immunology, 2018. **9**: p. 1748 DOI: 10.3389/fimmu.2018.01748.

Marcus A, Gowen BG, Thompson TW, Iannello A, Ardolino M, Deng W, Wang L, Shifrin N, and Raulet DH, *Recognition of tumors by the innate immune system and natural killer cells*, in *Advances in immunology*ed. 2014, Elsevier. p. 91-128.

Matsen CB and Neumayer LA, *Breast cancer: A review for the general surgeon.* JAMA Surg, 2013. **148**(10): p. 971-9 DOI: 10.1001/jamasurg.2013.3393.

Matsukura S, Kokubu F, Noda H, Tokunaga H, and Adachi M, *Expression of il-6, il-8, and rantes on human bronchial epithelial cells, nci-h292, induced by influenza virus a.* J Allergy Clin Immunol, 1996. **98**(6 Pt 1): p. 1080-7 DOI: 10.1016/s0091-6749(96)80195-3.

Matsuoka Y, Matsumae H, Katoh M, Eisfeld AJ, Neumann G, Hase T, Ghosh S, Shoemaker JE, Lopes TJ, Watanabe T, Watanabe S, Fukuyama S, Kitano H, and Kawaoka Y, *A comprehensive map of the influenza a virus replication cycle.* BMC Syst Biol, 2013. **7**: p. 97 DOI: 10.1186/1752-0509-7-97.

Mayer EL, *Targeting breast cancer with cdk inhibitors.* Curr Oncol Rep, 2015. **17**(5): p. 443 DOI: 10.1007/s11912-015-0443-3.

McAuley JL, Gilbertson BP, Trifkovic S, Brown LE, and McKimm-Breschkin JL, *Influenza virus neuraminidase structure and functions.* Front Microbiol, 2019. **10**: p. 39 DOI: 10.3389/fmicb.2019.00039.

McCarthy JB, El-Ashry D, and Turley EA, *Hyaluronan, cancer-associated fibroblasts and the tumor microenvironment in malignant progression.* Front Cell Dev Biol, 2018. **6**: p. 48 DOI: 10.3389/fcell.2018.00048.

McKee CM, Penno MB, Cowman M, Burdick MD, Strieter RM, Bao C, and Noble PW, *Hyaluronan (ha) fragments induce chemokine gene expression in alveolar macrophages. The role of ha size and cd44.* J Clin Invest, 1996. **98**(10): p. 2403-13 DOI: 10.1172/JCI119054.

Meschi J, Crouch EC, Skolnik P, Yahya K, Holmskov U, Leth-Larsen R, Tornoe I, Tecle T, White MR, and Hartshorn KL, *Surfactant protein d binds to human immunodeficiency virus (hiv) envelope protein gp120 and inhibits hiv replication.* Journal of general virology, 2005. **86**(11): p. 3097-3107 DOI: 10.1099/vir.0.80764-0.

Messmer MN, Netherby CS, Banik D, and Abrams SI, *Tumor-induced myeloid dysfunction and its implications for cancer immunotherapy.* Cancer Immunol Immunother, 2015. **64**(1): p. 1-13 DOI: 10.1007/s00262-014-1639-3.

Misra S, Hascall VC, Markwald RR, and Ghatak S, *Interactions between hyaluronan and its receptors (cd44, rhamm) regulate the activities of inflammation and cancer.* Front Immunol, 2015. **6**: p. 201 DOI: 10.3389/fimmu.2015.00201.

Mitnaul LJ, Matrosovich MN, Castrucci MR, Tuzikov AB, Bovin NV, Kobasa D, and Kawaoka Y, *Balanced hemagglutinin and neuraminidase activities are critical for efficient replication of influenza a virus.* J Virol, 2000. **74**(13): p. 6015-20 DOI: 10.1128/jvi.74.13.6015-6020.2000.

Mitsuhashi A, Goto H, Kuramoto T, Tabata S, Yukishige S, Abe S, Hanibuchi M, Kakiuchi S, Saijo A, Aono Y, Uehara H, Yano S, Ledford JG, Sone S, and Nishioka Y, *Surfactant protein a suppresses lung cancer progression by regulating the polarization of tumor-associated macrophages.* Am J Pathol, 2013. **182**(5): p. 1843-53 DOI: 10.1016/j.ajpath.2013.01.030.

Mittal D, Gubin MM, Schreiber RD, and Smyth MJ, *New insights into cancer immunoediting and its three component phases--elimination, equilibrium and escape.* Curr Opin Immunol, 2014. **27**: p. 16-25 DOI: 10.1016/j.coi.2014.01.004.

Moalli F, Doni A, Deban L, Zelante T, Zagarella S, Bottazzi B, Romani L, Mantovani A, and Garlanda C, *Role of complement and fcγ receptors in the protective activity of the long pentraxin ptx3 against aspergillus fumigatus.* Blood, The Journal of the American Society of Hematology, 2010. **116**(24): p. 5170-5180.

Mogensen TH, *Pathogen recognition and inflammatory signaling in innate immune defenses.* Clinical microbiology reviews, 2009. **22**(2): p. 240-273 DOI: 10.1128/CMR.00046-08.

Mogensen TH and Paludan SR, *Molecular pathways in virus-induced cytokine production.* Microbiol Mol Biol Rev, 2001. **65**(1): p. 131-50 DOI: 10.1128/MMBR.65.1.131-150.2001.

Mohapatra S, Yang X, Wright JA, Turley EA, and Greenberg AH, *Soluble hyaluronan receptor rhamm induces mitotic arrest by suppressing cdc2 and cyclin b1 expression.* J Exp Med, 1996. **183**(4): p. 1663-8 DOI: 10.1084/jem.183.4.1663.

Mold C, Baca R, and Du Clos TW, *Serum amyloid p component and c-reactive protein opsonize apoptotic cells for phagocytosis through fcγ receptors.* Journal of autoimmunity, 2002. **19**(3): p. 147-154.

Mold C, Gresham HD, and Du Clos TW, *Serum amyloid p component and c-reactive protein mediate phagocytosis through murine fcγrs.* The journal of Immunology, 2001. **166**(2): p. 1200-1205.

Molina H, Holers VM, Li B, Fung Y, Mariathasan S, Goellner J, Strauss-Schoenberger J, Karr RW, and Chaplin DD, *Markedly impaired humoral immune response in mice deficient in complement receptors 1 and 2.* Proceedings of the national academy of sciences, 1996. **93**(8): p. 3357-3361 DOI: 10.1073/pnas.93.8.3357.

Montero AJ, Diaz-Montero CM, Deutsch YE, Hurley J, Koniaris LG, Rumboldt T, Yasir S, Jorda M, Garret-Mayer E, Avisar E, Slingerland J, Silva O, Welsh C, Schuhwerk K, Seo P, Pegram MD, and Gluck S, *Phase 2 study of neoadjuvant treatment with nov-002 in combination with doxorubicin and cyclophosphamide followed by docetaxel in patients with her-2 negative clinical stage ii-iiic breast cancer.* Breast Cancer Res Treat, 2012. **132**(1): p. 215-23 DOI: 10.1007/s10549-011-1889-0.

Murugaiah V, Agostinis C, Varghese PM, Belmonte B, Vieni S, Alaql FA, Alrokayan SH, Khan HA, Kaur A, Roberts T, Madan T, Bulla R, and Kishore U, *Hyaluronic acid present in the tumor microenvironment can negate the pro-apototic effect of a recombinant fragment of human surfactant protein d on breast cancer cells.* Frontiers in Immunology, 2020a. **11**(1171): p. 1171 DOI: 10.3389/fimmu.2020.01171.

Murugaiah V, Tsolaki AG, and Kishore U, *Collectins: Innate immune pattern recognition molecules*, in *Lectin in host defense against microbial infections*ed. 2020b, Springer. p. 75-127.

Nagy N, Kuipers HF, Frymoyer AR, Ishak HD, Bollyky JB, Wight TN, and Bollyky PL, *4-methylumbelliferone treatment and hyaluronan inhibition as a therapeutic strategy in inflammation, autoimmunity, and cancer.* Front Immunol, 2015. **6**: p. 123 DOI: 10.3389/fimmu.2015.00123.

Nathan MR and Schmid P, *A review of fulvestrant in breast cancer.* Oncol Ther, 2017. **5**(1): p. 17-29 DOI: 10.1007/s40487-017-0046-2.

Nayak A, Dodagatta-Marri E, Tsolaki AG, and Kishore U, *An insight into the diverse roles of surfactant proteins, sp-a and sp-d in innate and adaptive immunity.* Frontiers in immunology, 2012. **3**: p. 131.

Nayak DP, Balogun RA, Yamada H, Zhou ZH, and Barman S, *Influenza virus morphogenesis and budding.* Virus Res, 2009. **143**(2): p. 147-61 DOI: 10.1016/j.virusres.2009.05.010.

Ng KK-S, Drickamer K, and Weis WI, *Structural analysis of monosaccharide recognition by rat liver mannose-binding protein.* Journal of Biological Chemistry, 1996. **271**(2): p. 663-674 DOI: 10.1074/jbc.271.2.663.

Ng WC, Tate MD, Brooks AG, and Reading PC, *Soluble host defense lectins in innate immunity to influenza virus.* J Biomed Biotechnol, 2012. **2012**: p. 732191 DOI: 10.1155/2012/732191.

Nikolaidis NM, White MR, Allen K, Tripathi S, Qi L, McDonald B, Taubenberger J, Seaton BA, McCormack FX, Crouch EC, and Hartshorn KL, *Mutations flanking the carbohydrate binding site of surfactant protein d confer antiviral activity for pandemic influenza a viruses.* Am J Physiol Lung Cell Mol Physiol, 2014. **306**(11): p. L1036-44 DOI: 10.1152/ajplung.00035.2014.

Obeid E, Nanda R, Fu YX, and Olopade OI, *The role of tumor-associated macrophages in breast cancer progression (review).* Int J Oncol, 2013. **43**(1): p. 5-12 DOI: 10.3892/ijo.2013.1938.

Ochsenbein AF, Fehr T, Lutz C, Suter M, Brombacher F, Hengartner H, and Zinkernagel RM, *Control of early viral and bacterial distribution and disease by natural antibodies.* Science, 1999. **286**(5447): p. 2156-2159 DOI: 10.1126/science.286.5447.2156.

Ohtani K, Suzuki Y, and Wakamiya N, *Biological functions of the novel collectins cl-l1, cl-k1, and cl-p1.* J Biomed Biotechnol, 2012. **2012**: p. 493945 DOI: 10.1155/2012/493945.

Ohya M, Nishitani C, Sano H, Yamada C, Mitsuzawa H, Shimizu T, Saito T, Smith K, Crouch E, and Kuroki Y, *Human pulmonary surfactant protein d binds the extracellular domains of toll-like receptors 2 and 4 through the carbohydrate recognition domain by a mechanism different from its binding to phosphatidylinositol and lipopolysaccharide.* Biochemistry, 2006. **45**(28): p. 8657-64 DOI: 10.1021/bi060176z.

Ojalvo LS, King W, Cox D, and Pollard JW, *High-density gene expression analysis of tumor-associated macrophages from mouse mammary tumors.* Am J Pathol, 2009. **174**(3): p. 1048-64 DOI: 10.2353/ajpath.2009.080676.

Orian-Rousseau V, Chen L, Sleeman JP, Herrlich P, and Ponta H, *Cd44 is required for two consecutive steps in hgf/c-met signaling.* Genes Dev, 2002. **16**(23): p. 3074-86 DOI: 10.1101/gad.242602.

Oslund KL and Baumgarth N, *Influenza-induced innate immunity: Regulators of viral replication, respiratory tract pathology & adaptive immunity.* Future Virol, 2011. **6**(8): p. 951-962 DOI: 10.2217/fvl.11.63.

Ouyang L, Chang W, Fang B, Qin J, Qu X, and Cheng F, *Estrogen-induced sdf-1alpha production promotes the progression of er-negative breast cancer via the accumulation of mdscs in the tumor microenvironment.* Sci Rep, 2016. **6**: p. 39541 DOI: 10.1038/srep39541.

Palese P, Tobita K, Ueda M, and Compans RW, *Characterization of temperature sensitive influenza virus mutants defective in neuraminidase.* Virology, 1974. **61**(2): p. 397-410 DOI: 10.1016/0042-6822(74)90276-1.

Palucka AK and Coussens LM, *The basis of oncoimmunology.* Cell, 2016. **164**(6): p. 1233-1247 DOI: 10.1016/j.cell.2016.01.049.

Pandit H, Gopal S, Sonawani A, Yadav AK, Qaseem AS, Warke H, Patil A, Gajbhiye R, Kulkarni V, and Al-Mozaini MA, *Surfactant protein d inhibits hiv-1 infection of target cells via interference with gp120-cd4 interaction and modulates pro-inflammatory cytokine production.* PloS one, 2014. **9**(7): p. e102395 DOI: 10.1371/journal.pone.0102395.

Pandit H, Thakur G, Koippallil Gopalakrishnan AR, Dodagatta-Marri E, Patil A, Kishore U, and Madan T, *Surfactant protein d induces immune quiescence and apoptosis of mitogen-activated peripheral blood mononuclear cells.* Immunobiology, 2016. **221**(2): p. 310-22 DOI: 10.1016/j.imbio.2015.10.004.

Park EK, Castrucci MR, Portner A, and Kawaoka Y, *The m2 ectodomain is important for its incorporation into influenza a virions.* J Virol, 1998. **72**(3): p. 2449-55 DOI: 10.1128/JVI.72.3.2449-2455.1998.

Paulson JC, Macauley MS, and Kawasaki N, *Siglecs as sensors of self in innate and adaptive immune responses.* Ann N Y Acad Sci, 2012. **1253**: p. 37-48 DOI: 10.1111/j.1749-6632.2011.06362.x.

Pearse AG, *Histochemistry, theoretical and applied.* 1968.

Peiris JS, Cheung CY, Leung CY, and Nicholls JM, *Innate immune responses to influenza a h5n1: Friend or foe?* Trends Immunol, 2009. **30**(12): p. 574-84 DOI: 10.1016/j.it.2009.09.004.

Pepys MB and Baltz ML, *Acute phase proteins with special reference to c-reactive protein and related proteins (pentaxins) and serum amyloid a protein*, in *Advances in immunology*ed. 1983, Elsevier. p. 141-212.

Perino J, Thielens NM, Crouch E, Spehner D, Crance J-M, and Favier A-L, *Protective effect of surfactant protein d in pulmonary vaccinia virus infection: Implication of a27 viral protein.* Viruses, 2013. **5**(3): p. 928-953 DOI: 10.3390/v5030928.

Perrone LA, Plowden JK, Garcia-Sastre A, Katz JM, and Tumpey TM, *H5n1 and 1918 pandemic influenza virus infection results in early and excessive infiltration of macrophages and neutrophils in the lungs of mice.* PLoS Pathog, 2008. **4**(8): p. e1000115 DOI: 10.1371/journal.ppat.1000115.

Petrey AC and de la Motte CA, *Hyaluronan, a crucial regulator of inflammation.* Front Immunol, 2014. **5**: p. 101 DOI: 10.3389/fimmu.2014.00101.

Pielak RM and Chou JJ, *Influenza m2 proton channels.* Biochim Biophys Acta, 2011. **1808**(2): p. 522-9 DOI: 10.1016/j.bbamem.2010.04.015.

Pikaar JC, Voorhout WF, van Golde LM, Verhoef J, Van Strijp JA, and van Iwaarden JF, *Opsonic activities of surfactant proteins a and d in phagocytosis of gram-negative bacteria by alveolar macrophages.* Journal of Infectious Diseases, 1995. **172**(2): p. 481-489 DOI: 10.1093/infdis/172.2.481.

Pohl MO, Lanz C, and Stertz S, *Late stages of the influenza a virus replication cycle-a tight interplay between virus and host.* Journal of General Virology, 2016. **97**(9): p. 2058-2072 DOI: 10.1099/jgv.0.000562.

Ponting J, Howell A, Pye D, and Kumar S, *Prognostic relevance of serum hyaluronan levels in patients with breast cancer.* Int J Cancer, 1992. **52**(6): p. 873-6 DOI: 10.1002/ijc.2910520607.

Porter AG and Janicke RU, *Emerging roles of caspase-3 in apoptosis.* Cell Death Differ, 1999. **6**(2): p. 99-104 DOI: 10.1038/sj.cdd.4400476.

Prehm P, *Hyaluronate is synthesized at plasma membranes.* Biochem J, 1984. **220**(2): p. 597-600 DOI: 10.1042/bj2200597.

Qaseem AS, Singh I, Pathan AA, Layhadi JA, Parkin R, Alexandra F, Durham SR, Kishore U, and Shamji MH, *A recombinant fragment of human surfactant protein d suppresses basophil activation and t-helper type 2 and b-cell responses in grass pollen–induced allergic inflammation.* American journal of respiratory and critical care medicine, 2017. **196**(12): p. 1526-1534 DOI: 10.1164/rccm.201701-0225OC.

Qaseem AS, Sonar S, Mahajan L, Madan T, Sorensen GL, Shamji MH, and Kishore U, *Linking surfactant protein sp-d and il-13: Implications in asthma and allergy.* Molecular immunology, 2013. **54**(1): p. 98-107 DOI: 10.1016/j.molimm.2012.10.039.

Qu X, Tang Y, and Hua S, *Immunological approaches towards cancer and inflammation: A cross talk.* Front Immunol, 2018. **9**: p. 563 DOI: 10.3389/fimmu.2018.00563.

Rabbani SA and Xing RH, *Role of urokinase (upa) and its receptor (upar) in invasion and metastasis of hormone-dependent malignancies.* Int J Oncol, 1998. **12**(4): p. 911-20 DOI: 10.3892/ijo.12.4.911.

Rabinovich GA, Gabrilovich D, and Sotomayor EM, *Immunosuppressive strategies that are mediated by tumor cells.* Annu Rev Immunol, 2007. **25**: p. 267-96 DOI: 10.1146/annurev.immunol.25.022106.141609.

Ramos I and Fernandez-Sesma A, *Modulating the innate immune response to influenza a virus: Potential therapeutic use of anti-inflammatory drugs.* Front Immunol, 2015. **6**: p. 361 DOI: 10.3389/fimmu.2015.00361.

Reading PC, Holmskov U, and Anders EM, *Antiviral activity of bovine collectins against rotaviruses.* Journal of General Virology, 1998. **79**(9): p. 2255-2263 DOI: 10.1099/0022-1317-79-9-2255.

Reading PC, Morey LS, Crouch EC, and Anders EM, *Collectin-mediated antiviral host defense of the lung: Evidence from influenza virus infection of mice.* J Virol, 1997. **71**(11): p. 8204-12 DOI: 10.1128/JVI.71.11.8204-8212.1997.

Roberts KL, Manicassamy B, and Lamb RA, *Influenza a virus uses intercellular connections to spread to neighboring cells.* J Virol, 2015. **89**(3): p. 1537-49 DOI: 10.1128/JVI.03306-14.

Rocca A, Maltoni R, Bravaccini S, Donati C, and Andreis D, *Clinical utility of fulvestrant in the treatment of breast cancer: A report on the emerging clinical evidence.* Cancer Manag Res, 2018. **10**: p. 3083-3099 DOI: 10.2147/CMAR.S137772.

Roland CL, Lynn KD, Toombs JE, Dineen SP, Udugamasooriya DG, and Brekken RA, *Cytokine levels correlate with immune cell infiltration after anti-vegf therapy in preclinical mouse models of breast cancer.* PLoS One, 2009. **4**(11): p. e7669 DOI: 10.1371/journal.pone.0007669.

Rossman JS and Lamb RA, *Influenza virus assembly and budding.* Virology, 2011. **411**(2): p. 229-36 DOI: 10.1016/j.virol.2010.12.003.

Ruffell B, Chang-Strachan D, Chan V, Rosenbusch A, Ho CM, Pryer N, Daniel D, Hwang ES, Rugo HS, and Coussens LM, *Macrophage il-10 blocks cd8+ t cell-dependent responses to chemotherapy by suppressing il-12 expression in intratumoral dendritic cells.* Cancer Cell, 2014. **26**(5): p. 623-37 DOI: 10.1016/j.ccell.2014.09.006.

Sainz B, Jr., Carron E, Vallespinos M, and Machado HL, *Cancer stem cells and macrophages: Implications in tumor biology and therapeutic strategies.* Mediators Inflamm, 2016. **2016**: p. 9012369 DOI: 10.1155/2016/9012369.

Saito T, Tamura D, Nakamura T, Makita Y, Ariyama H, Komiyama K, Yoshihara T, and Asano R, *4-methylumbelliferone leads to growth arrest and apoptosis in canine mammary tumor cells.* Oncol Rep, 2013. **29**(1): p. 335-42 DOI: 10.3892/or.2012.2100.

Samji T, *Influenza a: Understanding the viral life cycle.* Yale J Biol Med, 2009. **82**(4): p. 153-9.

Sato N, Kohi S, Hirata K, and Goggins M, *Role of hyaluronan in pancreatic cancer biology and therapy: Once again in the spotlight.* Cancer Sci, 2016. **107**(5): p. 569-75 DOI: 10.1111/cas.12913.

Savani RC, Cao G, Pooler PM, Zaman A, Zhou Z, and DeLisser HM, *Differential involvement of the hyaluronan (ha) receptors cd44 and receptor for ha-mediated motility in endothelial cell function and angiogenesis.* J Biol Chem, 2001. **276**(39): p. 36770-8 DOI: 10.1074/jbc.M102273200.

Sceneay J, Chow MT, Chen A, Halse HM, Wong CS, Andrews DM, Sloan EK, Parker BS, Bowtell DD, Smyth MJ, and Moller A, *Primary tumor hypoxia recruits cd11b+/ly6cmed/ly6g+ immune suppressor cells and compromises nk cell cytotoxicity in the premetastatic niche.* Cancer Res, 2012. **72**(16): p. 3906-11 DOI: 10.1158/0008-5472.CAN-11-3873.

Scheiffele P, Rietveld A, Wilk T, and Simons K, *Influenza viruses select ordered lipid domains during budding from the plasma membrane.* J Biol Chem, 1999. **274**(4): p. 2038-44 DOI: 10.1074/jbc.274.4.2038.

Scheuer W, Friess T, Burtscher H, Bossenmaier B, Endl J, and Hasmann M, *Strongly enhanced antitumor activity of trastuzumab and pertuzumab combination treatment on her2-positive human xenograft tumor models.* Cancer Res, 2009. **69**(24): p. 9330-6 DOI: 10.1158/0008-5472.CAN-08-4597.

Scott JE and Heatley F, *Hyaluronan forms specific stable tertiary structures in aqueous solution: A 13c nmr study.* Proc Natl Acad Sci U S A, 1999. **96**(9): p. 4850-5 DOI: 10.1073/pnas.96.9.4850.

Shamloo B and Usluer S, *P21 in cancer research.* Cancers (Basel), 2019. **11**(8) DOI: 10.3390/cancers11081178.

Shao W, Li X, Goraya MU, Wang S, and Chen JL, *Evolution of influenza a virus by mutation and re-assortment.* Int J Mol Sci, 2017. **18**(8) DOI: 10.3390/ijms18081650.

Shepherd VL, *Pulmonary surfactant protein d: A novel link between innate and adaptive immunity.* American Journal of Physiology-Lung Cellular and Molecular Physiology, 2002. **282**(3): p. L516-L517.

Shin DL, Yang W, Peng JY, Sawatsky B, von Messling V, Herrler G, and Wu NH, *Avian influenza a virus infects swine airway epithelial cells without prior adaptation.* Viruses, 2020. **12**(6) DOI: 10.3390/v12060589.

Shishido SN, Varahan S, Yuan K, Li X, and Fleming SD, *Humoral innate immune response and disease.* Clinical immunology, 2012. **144**(2): p. 142-158 DOI: 10.1016/j.clim.2012.06.002.

Shpilberg O and Jackisch C, *Subcutaneous administration of rituximab (mabthera) and trastuzumab (herceptin) using hyaluronidase.* Br J Cancer, 2013. **109**(6): p. 1556-61 DOI: 10.1038/bjc.2013.371.

Shtyrya YA, Mochalova LV, and Bovin NV, *Influenza virus neuraminidase: Structure and function.* Acta Naturae, 2009. **1**(2): p. 26-32.

Simpson KD, Templeton DJ, and Cross JV, *Macrophage migration inhibitory factor promotes tumor growth and metastasis by inducing myeloid-derived suppressor cells in the tumor microenvironment.* J Immunol, 2012. **189**(12): p. 5533-40 DOI: 10.4049/jimmunol.1201161.

Singh M, Madan T, Waters P, Parida SK, Sarma PU, and Kishore U, *Protective effects of a recombinant fragment of human surfactant protein d in a murine model of pulmonary hypersensitivity induced by dust mite allergens.* Immunol Lett, 2003. **86**(3): p. 299-307 DOI: 10.1016/s0165-2478(03)00033-6.

Singh M, Ramos I, Asafu-Adjei D, Quispe-Tintaya W, Chandra D, Jahangir A, Zang X, Aggarwal BB, and Gravekamp C, *Curcumin improves the therapeutic efficacy of listeria(at)-mage-b vaccine in correlation with improved t-cell responses in blood of a triple-negative breast cancer model 4t1.* Cancer Med, 2013. **2**(4): p. 571-82 DOI: 10.1002/cam4.94.

Skehel JJ and Wiley DC, *Receptor binding and membrane fusion in virus entry: The influenza hemagglutinin.* Annu Rev Biochem, 2000. **69**: p. 531-69 DOI: 10.1146/annurev.biochem.69.1.531.

Slevin M, Kumar S, and Gaffney J, *Angiogenic oligosaccharides of hyaluronan induce multiple signaling pathways affecting vascular endothelial cell mitogenic and wound healing responses.* J Biol Chem, 2002. **277**(43): p. 41046-59 DOI: 10.1074/jbc.M109443200.

Smid M, Wang Y, Zhang Y, Sieuwerts AM, Yu J, Klijn JG, Foekens JA, and Martens JW, *Subtypes of breast cancer show preferential site of relapse.* Cancer Res, 2008. **68**(9): p. 3108-14 DOI: 10.1158/0008-5472.CAN-07-5644.

Solito S, Marigo I, Pinton L, Damuzzo V, Mandruzzato S, and Bronte V, *Myeloid-derived suppressor cell heterogeneity in human cancers.* Ann N Y Acad Sci, 2014. **1319**: p. 47-65 DOI: 10.1111/nyas.12469.

Soria G and Ben-Baruch A, *The inflammatory chemokines ccl2 and ccl5 in breast cancer.* Cancer Lett, 2008. **267**(2): p. 271-85 DOI: 10.1016/j.canlet.2008.03.018.

Spranger S, Jeremias I, Wilde S, Leisegang M, Starck L, Mosetter B, Uckert W, Heemskerk MH, Schendel DJ, and Frankenberger B, *Tcr-transgenic lymphocytes specific for hmmr/rhamm limit tumor outgrowth in vivo.* Blood, 2012. **119**(15): p. 3440-9 DOI: 10.1182/blood-2011-06-357939.

Strong P, Kishore U, Morgan C, Lopez Bernal A, Singh M, and Reid KB, *A novel method of purifying lung surfactant proteins a and d from the lung lavage of alveolar proteinosis patients and from pooled amniotic fluid.* J Immunol Methods, 1998. **220**(1-2): p. 139-49 DOI: 10.1016/s0022-1759(98)00160-4.

Subbarao K, Murphy BR, and Fauci AS, *Development of effective vaccines against pandemic influenza.* Immunity, 2006. **24**(1): p. 5-9 DOI: 10.1016/j.immuni.2005.12.005.

Sugahara KN, Hirata T, Hayasaka H, Stern R, Murai T, and Miyasaka M, *Tumor cells enhance their own cd44 cleavage and motility by generating hyaluronan fragments.* J Biol Chem, 2006. **281**(9): p. 5861-8 DOI: 10.1074/jbc.M506740200.

Sun YS, Zhao Z, Yang ZN, Xu F, Lu HJ, Zhu ZY, Shi W, Jiang J, Yao PP, and Zhu HP, *Risk factors and preventions of breast cancer.* Int J Biol Sci, 2017. **13**(11): p. 1387-1397 DOI: 10.7150/ijbs.21635.

Swain SM, Baselga J, Kim SB, Ro J, Semiglazov V, Campone M, Ciruelos E, Ferrero JM, Schneeweiss A, Heeson S, Clark E, Ross G, Benyunes MC, Cortes J, and Group CS, *Pertuzumab, trastuzumab, and docetaxel in her2-positive metastatic breast cancer.* N Engl J Med, 2015. **372**(8): p. 724-34 DOI: 10.1056/NEJMoa1413513.

Swann JB and Smyth MJ, *Immune surveillance of tumors.* J Clin Invest, 2007. **117**(5): p. 1137-46 DOI: 10.1172/JCI31405.

Tate MD, Brooks AG, and Reading PC, *Inhibition of lectin-mediated innate host defences in vivo modulates disease severity during influenza virus infection.* Immunol Cell Biol, 2011a. **89**(3): p. 482-91 DOI: 10.1038/icb.2010.113.

Tate MD, Brooks AG, and Reading PC, *Specific sites of n-linked glycosylation on the hemagglutinin of h1n1 subtype influenza a virus determine sensitivity to inhibitors of the innate immune system and virulence in mice.* J Immunol, 2011b. **187**(4): p. 1884-94 DOI: 10.4049/jimmunol.1100295.

Taubenberger JK and Kash JC, *Influenza virus evolution, host adaptation, and pandemic formation.* Cell Host Microbe, 2010. **7**(6): p. 440-51 DOI: 10.1016/j.chom.2010.05.009.

Tecle T, White MR, Crouch EC, and Hartshorn KL, *Inhibition of influenza viral neuraminidase activity by collectins.* Arch Virol, 2007. **152**(9): p. 1731-42 DOI: 10.1007/s00705-007-0983-4.

Teriete P, Banerji S, Noble M, Blundell CD, Wright AJ, Pickford AR, Lowe E, Mahoney DJ, Tammi MI, Kahmann JD, Campbell ID, Day AJ, and Jackson DG, *Structure of the regulatory hyaluronan binding domain in the inflammatory leukocyte homing receptor cd44.* Mol Cell, 2004. **13**(4): p. 483-96 DOI: 10.1016/s1097-2765(04)00080-2.

Tessmer MS, Fatima A, Paget C, Trottein F, and Brossay L, *Nkt cell immune responses to viral infection.* Expert Opin Ther Targets, 2009. **13**(2): p. 153-62 DOI: 10.1517/14712590802653601.

Thakur G, Prakash G, Murthy V, Sable N, Menon S, ALROKAYAN S, Khan HA, Murugaiah V, Bakshi G, and Kishore U, *Human sp-d acts as an innate immune surveillance molecule against androgen-responsive and androgen-resistant prostate cancer cells.* Frontiers in Oncology, 2019. **9**: p. 565.

Tisoncik JR, Korth MJ, Simmons CP, Farrar J, Martin TR, and Katze MG, *Into the eye of the cytokine storm.* Microbiol Mol Biol Rev, 2012. **76**(1): p. 16-32 DOI: 10.1128/MMBR.05015-11.

Tolg C, Hamilton SR, Nakrieko KA, Kooshesh F, Walton P, McCarthy JB, Bissell MJ, and Turley EA, *Rhamm-/- fibroblasts are defective in cd44-mediated erk1,2 motogenic signaling, leading to defective skin wound repair.* J Cell Biol, 2006. **175**(6): p. 1017-28 DOI: 10.1083/jcb.200511027.

Toole BP, *Hyaluronan promotes the malignant phenotype.* Glycobiology, 2002. **12**(3): p. 37R-42R DOI: 10.1093/glycob/12.3.37r.

Tsang RY and Finn RS, *Beyond trastuzumab: Novel therapeutic strategies in her2-positive metastatic breast cancer.* Br J Cancer, 2012. **106**(1): p. 6-13 DOI: 10.1038/bjc.2011.516.

Tsutsui S, Yasuda K, Suzuki K, Tahara K, Higashi H, and Era S, *Macrophage infiltration and its prognostic implications in breast cancer: The relationship with vegf expression and microvessel density.* Oncol Rep, 2005. **14**(2): p. 425-31.

Turashvili G and Brogi E, *Tumor heterogeneity in breast cancer.* Front Med (Lausanne), 2017. **4**: p. 227 DOI: 10.3389/fmed.2017.00227.

Turino GM and Cantor JO, *Hyaluronan in respiratory injury and repair.* Am J Respir Crit Care Med, 2003. **167**(9): p. 1169-75 DOI: 10.1164/rccm.200205-449PP.

Turley EA, *The role of a cell-associated hyaluronan-binding protein in fibroblast behaviour.* Ciba Found Symp, 1989. **143**: p. 121-33; discussion 133-7, 281-5 DOI: 10.1002/9780470513774.ch8.

Turley EA, *Hyaluronan and cell locomotion.* Cancer Metastasis Rev, 1992. **11**(1): p. 21-30 DOI: 10.1007/BF00047600.

Urakawa H, Nishida Y, Wasa J, Arai E, Zhuo L, Kimata K, Kozawa E, Futamura N, and Ishiguro N, *Inhibition of hyaluronan synthesis in breast cancer cells by 4-methylumbelliferone suppresses tumorigenicity in vitro and metastatic lesions of bone in vivo.* Int J Cancer, 2012. **130**(2): p. 454-66 DOI: 10.1002/ijc.26014.

van Eijk M, Hillaire MLB, Rimmelzwaan GF, Rynkiewicz MJ, White MR, Hartshorn KL, Hessing M, Koolmees PA, Tersteeg MH, van Es MH, Meijerhof T, Huckriede A, and Haagsman HP, *Enhanced antiviral activity of human surfactant protein d by site-specific engineering of*

the carbohydrate recognition domain. Front Immunol, 2019. **10**: p. 2476 DOI: 10.3389/fimmu.2019.02476.

van Eijk M, van de Lest CH, Batenburg JJ, Vaandrager AB, Meschi J, Hartshorn KL, van Golde LM, and Haagsman HP, *Porcine surfactant protein d is n-glycosylated in its carbohydrate recognition domain and is assembled into differently charged oligomers.* Am J Respir Cell Mol Biol, 2002. **26**(6): p. 739-47 DOI: 10.1165/ajrcmb.26.6.4520.

Van Iwaarden JF, Pikaar JC, Storm J, Brouwer E, Verhoef J, Oosting RS, van Golde LM, and van Strijp JA, *Binding of surfactant protein a to the lipid a moiety of bacterial lipopolysaccharides.* Biochem J, 1994. **303 (Pt 2)**: p. 407-11 DOI: 10.1042/bj3030407.

Vasta GR, *Roles of galectins in infection.* Nature Reviews Microbiology, 2009. **7**(6): p. 424-438 DOI: 10.1038/nrmicro2146.

Venkatraman Girija U, Furze CM, Gingras AR, Yoshizaki T, Ohtani K, Marshall JE, Wallis AK, Schwaeble WJ, El-Mezgueldi M, Mitchell DA, Moody PC, Wakamiya N, and Wallis R, *Molecular basis of sugar recognition by collectin-k1 and the effects of mutations associated with 3mc syndrome.* BMC Biol, 2015. **13**: p. 27 DOI: 10.1186/s12915-015-0136-2.

Vesely MD, Kershaw MH, Schreiber RD, and Smyth MJ, *Natural innate and adaptive immunity to cancer.* Annu Rev Immunol, 2011. **29**: p. 235-71 DOI: 10.1146/annurev-immunol-031210-101324.

Vinayak S and Carlson RW, *Mtor inhibitors in the treatment of breast cancer.* Oncology (Williston Park), 2013. **27**(1): p. 38-44, 46, 48 passim.

von Boehmer H, Teh HS, and Kisielow P, *The thymus selects the useful, neglects the useless and destroys the harmful.* Immunol Today, 1989. **10**(2): p. 57-61 DOI: 10.1016/0167-5699(89)90307-1.

Voorhout W, Veenendaal T, Kuroki Y, Ogasawara Y, Van Golde L, and Geuze H, *Immunocytochemical localization of surfactant protein d (sp-d) in type ii cells, clara cells, and alveolar macrophages of rat lung.* Journal of Histochemistry & Cytochemistry, 1992. **40**(10): p. 1589-1597 DOI: 10.1177/40.10.1527377.

Wagner KU, *Models of breast cancer: Quo vadis, animal modeling?* Breast Cancer Res, 2004. **6**(1): p. 31-8 DOI: 10.1186/bcr723.

Walsh JG, Cullen SP, Sheridan C, Luthi AU, Gerner C, and Martin SJ, *Executioner caspase-3 and caspase-7 are functionally distinct proteases.* Proc Natl Acad Sci U S A, 2008. **105**(35): p. 12815-9 DOI: 10.1073/pnas.0707715105.

Wang JY, Kishore U, Lim BL, Strong P, and Reid KB, *Interaction of human lung surfactant proteins a and d with mite (dermatophagoides pteronyssinus) allergens.* Clin Exp Immunol, 1996. **106**(2): p. 367-73 DOI: 10.1046/j.1365-2249.1996.d01-838.x.

Wang JY, Shieh CC, You PF, Lei HY, and Reid KB, *Inhibitory effect of pulmonary surfactant proteins a and d on allergen-induced lymphocyte proliferation and histamine release in children with asthma.* Am J Respir Crit Care Med, 1998. **158**(2): p. 510-8 DOI: 10.1164/ajrccm.158.2.9709111.

Wang N, Liu W, Zheng Y, Wang S, Yang B, Li M, Song J, Zhang F, Zhang X, Wang Q, and Wang Z, *Cxcl1 derived from tumor-associated macrophages promotes breast cancer metastasis via activating nf-kappab/sox4 signaling.* Cell Death Dis, 2018. **9**(9): p. 880 DOI: 10.1038/s41419-018-0876-3.

Warzecha CC, Sato TK, Nabet B, Hogenesch JB, and Carstens RP, *Esrp1 and esrp2 are epithelial cell-type-specific regulators of fgfr2 splicing.* Mol Cell, 2009. **33**(5): p. 591-601 DOI: 10.1016/j.molcel.2009.01.025.

Weigel PH, Fuller GM, and LeBoeuf RD, *A model for the role of hyaluronic acid and fibrin in the early events during the inflammatory response and wound healing.* J Theor Biol, 1986. **119**(2): p. 219-34 DOI: 10.1016/s0022-5193(86)80076-5.

Weigel PH, Hascall VC, and Tammi M, *Hyaluronan synthases.* J Biol Chem, 1997. **272**(22): p. 13997-4000 DOI: 10.1074/jbc.272.22.13997.

Wert SE, Yoshida M, LeVine AM, Ikegami M, Jones T, Ross GF, Fisher JH, Korfhagen TR, and Whitsett JA, *Increased metalloproteinase activity, oxidant production, and emphysema in surfactant protein d gene-inactivated mice.* Proc Natl Acad Sci U S A, 2000. **97**(11): p. 5972-7 DOI: 10.1073/pnas.100448997.

Whiteside TL, *The tumor microenvironment and its role in promoting tumor growth.* Oncogene, 2008. **27**(45): p. 5904-12 DOI: 10.1038/onc.2008.271.

Wilson IA and Cox NJ, *Structural basis of immune recognition of influenza virus hemagglutinin.* Annu Rev Immunol, 1990. **8**: p. 737-71 DOI: 10.1146/annurev.iy.08.040190.003513.

Wu H, Kuzmenko A, Wan S, Schaffer L, Weiss A, Fisher JH, Kim KS, and McCormack FX, *Surfactant proteins a and d inhibit the growth of gram-negative bacteria by increasing membrane permeability.* The Journal of clinical investigation, 2003. **111**(10): p. 1589-1602 DOI: 10.1172/JCI16889.

Wu Y, Liu Z, Wei R, Pan S, Mao N, Chen B, Han J, Zhang F, Holmskov U, and Xia Z, *Elevated plasma surfactant protein d (sp-d) levels and a direct correlation with anti-severe acute respiratory syndrome coronavirus-specific igg antibody in sars patients.* Scandinavian journal of immunology, 2009. **69**(6): p. 508-515 DOI: 10.1111/j.1365-3083.2009.02245.x.

Xuan QJ, Wang JX, Nanding A, Wang ZP, Liu H, Lian X, and Zhang QY, *Tumor-associated macrophages are correlated with tamoxifen resistance in the postmenopausal breast cancer patients.* Pathol Oncol Res, 2014. **20**(3): p. 619-24 DOI: 10.1007/s12253-013-9740-z.

Yang B, Zhang L, and Turley EA, *Identification of two hyaluronan-binding domains in the hyaluronan receptor rhamm.* J Biol Chem, 1993. **268**(12): p. 8617-23.

Yang J, Li M, Shen X, and Liu S, *Influenza a virus entry inhibitors targeting the hemagglutinin.* Viruses, 2013. **5**(1): p. 352-73 DOI: 10.3390/v5010352.

Yang J, Li X, Liu X, and Liu Y, *The role of tumor-associated macrophages in breast carcinoma invasion and metastasis.* Int J Clin Exp Pathol, 2015. **8**(6): p. 6656-64.

Yang L, Huang J, Ren X, Gorska AE, Chytil A, Aakre M, Carbone DP, Matrisian LM, Richmond A, Lin PC, and Moses HL, *Abrogation of tgf beta signaling in mammary carcinomas recruits gr-1+cd11b+ myeloid cells that promote metastasis.* Cancer Cell, 2008. **13**(1): p. 23-35 DOI: 10.1016/j.ccr.2007.12.004.

Yardley DA, *Combining mtor inhibitors with chemotherapy and other targeted therapies in advanced breast cancer: Rationale, clinical experience, and future directions.* Breast Cancer (Auckl), 2013. **7**: p. 7-22 DOI: 10.4137/BCBCR.S10071.

York IA, Stevens J, and Alymova IV, *Influenza virus n-linked glycosylation and innate immunity.* Biosci Rep, 2019. **39**(1) DOI: 10.1042/BSR20171505.

Young NS, Levin J, and Prendergast RA, *An invertebrate coagulation system activated by endotoxin: Evidence for enzymatic mediation.* J Clin Invest, 1972. **51**(7): p. 1790-7 DOI: 10.1172/JCI106980.

Yuan ZY, Luo RZ, Peng RJ, Wang SS, and Xue C, *High infiltration of tumor-associated macrophages in triple-negative breast cancer is associated with a higher risk of distant metastasis.* Onco Targets Ther, 2014. **7**: p. 1475-80 DOI: 10.2147/OTT.S61838.

Zeng H, Goldsmith C, Thawatsupha P, Chittaganpitch M, Waicharoen S, Zaki S, Tumpey TM, and Katz JM, *Highly pathogenic avian influenza h5n1 viruses elicit an attenuated type i interferon response in polarized human bronchial epithelial cells.* J Virol, 2007. **81**(22): p. 12439-49 DOI: 10.1128/JVI.01134-07.

Zhang H, Dicker KT, Xu X, Jia X, and Fox JM, *Interfacial bioorthogonal cross-linking.* ACS Macro Lett, 2014. **3**(8): p. 727-731 DOI: 10.1021/mz5002993.

Zhang J, Pekosz A, and Lamb RA, *Influenza virus assembly and lipid raft microdomains: A role for the cytoplasmic tails of the spike glycoproteins.* J Virol, 2000. **74**(10): p. 4634-44 DOI: 10.1128/jvi.74.10.4634-4644.2000.

Zhang L, Underhill CB, and Chen L, *Hyaluronan on the surface of tumor cells is correlated with metastatic behavior.* Cancer Res, 1995. **55**(2): p. 428-33.

Zhang W, Zheng W, Toh Y, Betancourt-Solis MA, Tu J, Fan Y, Vakharia VN, Liu J, McNew JA, Jin M, and Tao YJ, *Crystal structure of an orthomyxovirus matrix protein reveals mechanisms for self-polymerization and membrane association.* Proc Natl Acad Sci U S A, 2017. **114**(32): p. 8550-8555 DOI: 10.1073/pnas.1701747114.

Zhang X, Claerhout S, Prat A, Dobrolecki LE, Petrovic I, Lai Q, Landis MD, Wiechmann L, Schiff R, Giuliano M, Wong H, Fuqua SW, Contreras A, Gutierrez C, Huang J, Mao S, Pavlick AC, Froehlich AM, Wu MF, Tsimelzon A, Hilsenbeck SG, Chen ES, Zuloaga P, Shaw CA, Rimawi MF, Perou CM, Mills GB, Chang JC, and Lewis MT, *A renewable tissue resource of phenotypically stable, biologically and ethnically diverse, patient-derived human breast cancer xenograft models.* Cancer Res, 2013a. **73**(15): p. 4885-97 DOI: 10.1158/0008-5472.CAN-12-4081.

Zhang Y, Lv D, Kim HJ, Kurt RA, Bu W, Li Y, and Ma X, *A novel role of hematopoietic ccl5 in promoting triple-negative mammary tumor progression by regulating generation of myeloid-derived suppressor cells.* Cell Res, 2013b. **23**(3): p. 394-408 DOI: 10.1038/cr.2012.178.

Zilfou JT and Lowe SW, *Tumor suppressive functions of p53.* Cold Spring Harb Perspect Biol, 2009. **1**(5): p. a001883 DOI: 10.1101/cshperspect.a001883.

Zugibe FT, *Diagnostic histochemistry.* 1970.

Appendix

Papers Published During PhD

1. Kaur A, Sultan SH, **Murugaiah V**, Pathan AA, Alhamlan FS, Karteris E, Kishore U. Human C1q Induces Apoptosis in an Ovarian Cancer Cell Line via Tumor Necrosis Factor Pathway. Front Immunol. 2016 Dec 21;7:599. doi: 10.3389/fimmu.2016.00599. PMID: 28066412; PMCID: PMC5174108.

2. Ferluga J, Kouser L, **Murugaiah V**, Sim RB, Kishore U. Potential influences of complement factor H in autoimmune inflammatory and thrombotic disorders. Mol Immunol. 2017 Apr;84:84-106. doi: 10.1016/j.molimm.2017.01.015. Epub 2017 Feb 16. PMID: 28216098.

3. Dodagatta-Marri E, Mitchell DA, Pandit H, Sonawani A, **Murugaiah V**, Idicula-Thomas S, Nal B, Al-Mozaini MM, Kaur A, Madan T, Kishore U. Protein-Protein Interaction between Surfactant Protein D and DC-SIGN via C-Type Lectin Domain Can Suppress HIV-1 Transfer. Front Immunol. 2017 Jul 31;8:834. doi: 10.3389/fimmu.2017.00834. PMID: 28824609; PMCID: PMC5534670.

4. Al-Mozaini MA, Tsolaki AG, Abdul-Aziz M, Abozaid SM, Al-Ahdal MN, Pathan AA, **Murugaiah V**, Makarov EM, Kaur A, Sim RB, Kishore U, Kouser L. Human Properdin Modulates Macrophage: Mycobacterium bovis BCG Interaction via Thrombospondin Repeats 4 and 5. Front Immunol. 2018 May 8;9:533. doi: 10.3389/fimmu.2018.00533. PMID: 29867915; PMCID: PMC5951972.

5. Kaur A, Riaz MS, **Murugaiah V**, Varghese PM, Singh SK, Kishore U. A Recombinant Fragment of Human Surfactant Protein D induces Apoptosis in Pancreatic Cancer Cell Lines via Fas-Mediated Pathway. Front Immunol. 2018 Jun 4;9:1126. doi: 10.3389/fimmu.2018.01126. PMID: 29915574; PMCID: PMC5994421.

6. Al-Ahdal MN, **Murugaiah V**, Varghese PM, Abozaid SM, Saba I, Al-Qahtani AA, Pathan AA, Kouser L, Nal B, Kishore U. Entry Inhibition and Modulation of Pro-Inflammatory Immune Response Against Influenza A Virus by a Recombinant Truncated Surfactant Protein D. Front Immunol. 2018 Jul 30;9:1586. doi: 10.3389/fimmu.2018.01586. PMID: 30105014; PMCID: PMC6077238.

7. Al-Qahtani AA, **Murugaiah V**, Bashir HA, Pathan AA, Abozaid SM, Makarov E, Nal-Rogier B, Kishore U, Al-Ahdal MN. Full-length human surfactant protein A inhibits influenza A virus infection of A549 lung epithelial cells: A recombinant form containing neck and lectin domains promotes infectivity. Immunobiology. 2019 May;224(3):408-418. doi: 10.1016/j.imbio.2019.02.006. Epub 2019 Feb 11. PMID: 30954271.

8. Kumar J, **Murugaiah V**, Sotiriadis G, Kaur A, Jeyaneethi J, Sturniolo I, Alhamlan FS, Chatterjee J, Hall M, Kishore U, Karteris E. Surfactant Protein D as a Potential Biomarker and Therapeutic Target in Ovarian Cancer. Front Oncol. 2019 Jul 9;9:542. doi: 10.3389/fonc.2019.00542. PMID: 31338320; PMCID: PMC6629871.

9. Thakur G, Prakash G, Murthy V, Sable N, Menon S, Alrokayan SH, Khan HA, **Murugaiah V**, Bakshi G, Kishore U, Madan T. Human SP-D Acts as an Innate Immune Surveillance Molecule Against Androgen-Responsive and Androgen-Resistant Prostate Cancer Cells. Front Oncol. 2019 Jul 11;9:565. doi: 10.3389/fonc.2019.00565. PMID: 31355132; PMCID: PMC6637921.

10. **Murugaiah V**, Tsolaki AG, Kishore U. Collectins: Innate Immune Pattern Recognition Molecules. Adv Exp Med Biol. 2020;1204:75-127. doi: 10.1007/978-981-15-1580-4_4. PMID: 32152944; PMCID: PMC7120701.

11. DeCordova S, Abdelgany A, **Murugaiah V**, Pathan AA, Nayak A, Walker T, Shastri A, Alrokayan SH, Khan HA, Singh SK, De Pennington N, Sim RB, Kishore U. Secretion of functionally active complement factor H related protein 5 (FHR5) by primary tumour cells derived from Glioblastoma Multiforme patients. Immunobiology. 2019 Sep;224(5):625-631. doi: 10.1016/j.imbio.2019.07.006. Epub 2019 Aug 5. PMID: 31519376.

12. **Murugaiah V**, Varghese PM, Saleh SM, Tsolaki AG, Alrokayan SH, Khan HA, Collison KS, Sim RB, Nal B, Al-Mohanna FA, Kishore U. Complement-Independent Modulation of Influenza A Virus Infection by Factor H. Front Immunol. 2020 Mar 25;11:355. doi: 10.3389/fimmu.2020.00355. PMID: 32269562; PMCID: PMC7109256.

13. **Murugaiah V**, Agostinis C, Varghese PM, Belmonte B, Vieni S, Alaql FA, Alrokayan SH, Khan HA, Kaur A, Roberts T, Madan T, Bulla R, Kishore U. Hyaluronic Acid Present in the Tumor Microenvironment Can Negate the Pro-apototic Effect of a Recombinant Fragment of Human Surfactant Protein D on Breast Cancer Cells. Front Immunol. 2020 Jul 8;11:1171. doi: 10.3389/fimmu.2020.01171. PMID: 32733438; PMCID: PMC7360846.

14. **Murugaiah V**, Yasmin H, Pandit H, Ganguly K, Sulebi R, Al-Mozaini MA, Madan T, Kishore U. Innate immune response against HIV-1. Microbial Pathogenesis: Infection and Immunity. Springer Nature. 2020.

15. Varghese PM, **Murugaiah V**, Beirag N, Temperton N, Khan HA, Alrokayan SH, Al-Ahdal MN, Nal B, Al-Mohanna FA, Sim RB, Kishore U. C4b Binding Protein Acts as an Innate Immune Effector Against Influenza A Virus. Front Immunol. 2021 Jan 8;11:585361. doi: 10.3389/fimmu.2020.585361. PMID: 33488586; PMCID: PMC7820937.

16. Hsieh M-H, beirag N, **Murugaiah V**, Chou Y-C, Kuo W-S, Kao H-F, Madan T, Kishore U, and Wang J-Y. Human surfactant protein d binds s1 and receptor binding domain of spike protein and acts as an entry inhibitor of sars-cov-2 pseudotyped viral particles. Front Immunol. 2021 (*in-revision*)

frontiers in Immunology

ORIGINAL RESEARCH
published: 21 December 2016
doi: 10.3389/fimmu.2016.00599

Human C1q Induces Apoptosis in an Ovarian Cancer Cell Line *via* Tumor Necrosis Factor Pathway

*Anuvinder Kaur[1], Sami H. A. Sultan[1], Valarmathy Murugaiah[1], Ansar A. Pathan[1], Fatimah S. Alhamlan[2], Emmanouil Karteris[1,3] and Uday Kishore[1]**

[1] Biosciences, College of Health and Life Sciences, Brunel University London, Uxbridge, UK, [2] Department of infection and Immunity, King Faisal Specialist Hospital and Research Centre, Riyadh, Saudi Arabia, [3] Institute of Environment, Heath and Societies, Brunel University London, Uxbridge, UK

Complement protein C1q is the first recognition subcomponent of the complement classical pathway that plays a vital role in the clearance of immune complexes, pathogens, and apoptotic cells. C1q also has a homeostatic role involving immune and non-immune cells; these functions not necessarily involve complement activation. Recently, C1q has been shown to be expressed locally in the microenvironment of a range of human malignant tumors, where it can promote cancer cell adhesion, migration, and proliferation, without involving complement activation. C1q has been shown to be present in the ascitic fluid formed during ovarian cancers. In this study, we have examined the effects of human C1q and its globular domain on an ovarian cancer cell line, SKOV3. We show that C1q and the recombinant globular head modules induce apoptosis in SKOV3 cells in a time-dependent manner. C1q expression was not detectable in the SKOV3 cells. Exogenous treatment with C1q and globular head modules at the concentration of 10 μg/ml induced apoptosis in approximately 55% cells, as revealed by immunofluorescence microscopy and FACS. The qPCR and caspase analysis suggested that C1q and globular head modules activated tumor necrosis factor (TNF)-α and upregulated Fas. The genes of mammalian target of rapamycin (mTOR), RICTOR, and RAPTOR survival pathways, which are often overexpressed in majority of the cancers, were significantly downregulated within few hours of the treatment of SKOV3 cells with C1q and globular head modules. In conclusion, C1q, *via* its globular domain, induced apoptosis in an ovarian cancer cell line SKOV3 *via* TNF-α induced apoptosis pathway involving upregulation of Bax and Fas. This study highlights a potentially protective role of C1q in certain cancers.

Keywords: complement, C1q, ovarian cancer, apoptosis, TNF, mTOR

OPEN ACCESS

Edited by:
Francesco Tedesco, Istituto Auxologico Italiano, Italy

Reviewed by:
Michael Kirschfink, Heidelberg University, Germany
Cordula M. Stover, University of Leicester, UK

****Correspondence:***
Uday Kishore
uday.kishore@brunel.ac.uk, ukishore@hotmail.com

Specialty section:
This article was submitted to Molecular Innate Immunity, a section of the journal Frontiers in Immunology

Received: *27 September 2016*
Accepted: *30 November 2016*
Published: *21 December 2016*

Citation:
Kaur A, Sultan SHA, Murugaiah V, Pathan AA, Alhamlan FS, Karteris E and Kishore U (2016) Human C1q Induces Apoptosis in an Ovarian Cancer Cell Line via Tumor Necrosis Factor Pathway. Front. Immunol. 7:599. doi: 10.3389/fimmu.2016.00599

INTRODUCTION

C1q is the first subcomponent of the C1 complex that recognizes the IgG- or IgM-containing immune complexes and initiates the complement classical pathway. It can bind to various self- and non-self ligands and bring about a range of homeostatic functions including clearance of pathogens and apoptotic cells (1). Human C1q molecule is composed of 18 polypeptide chains (6A, 6B, and 6C).

Each C1q chain has a short N-terminal region, a triple-helical collagen region, and a C-terminal globular (gC1q) domain (1, 2). Recently, a wide range of immunomodulatory functions of C1q have become evident that are independent of its involvement in the complement activation (3, 4); these include modulation of dendritic cell functions (5), cancer progression (6), and neuronal synapse pruning (7).

Ovarian cancer is the sixth most frequently diagnosed cancer among women worldwide and has the highest mortality rate than any other female reproductive system-associated cancer. Approximately 70% of the ovarian cancers are diagnosed at an advanced stage III or IV, with nearly 85% expected mortality (8). The intraperitoneally ascitic fluid (AF) formed during ovarian cancer has been shown to have high levels of complement components such as C3a and soluble C5b–9, which form the membrane attack complex, suggesting potential for the activation of complement *in vivo*. However, complement activation appears to be dampened due to the expression of membrane regulators such as CD46, CD55, and CD59 on the ovarian cancer cells, rendering complement system as an inefficient immune surveillance mechanism. The malignant ovarian tumor cells isolated from AF have been shown to have C1q and C2 deposited on the surface, which were rendered susceptible to complement-mediated killing by AF in the presence of anti-CD59-neutralizing antibody (9). In a recent study, the presence of C1q has been shown in the stroma and vascular endothelium of a number of human malignant tumors, including lung adenocarcinoma, melanoma, colon adenocarcinoma, breast adenocarcinoma, and pancreatic carcinoma (6). This has raised a tumor growth-fostering role for locally synthesized C1q *via* promotion of adhesion, migration, and proliferation.

The importance of complement in cancer immunotherapy has acquired great interest recently. A broad array of cell surface tumor-associated antigens that are overexpressed, mutated, or partially expressed, as compared to normal tissues, have offered various antibody targets in different cancers (10). A number of these anti-cancer antibodies work *via* receptor or checkpoint blockade or as an agonist, apoptosis induction, immune-mediated cytotoxicity either *via* complement or antibody, and T cell function regulation. In addition, therapeutic antibodies targeting growth factors and their receptors such as epidermal growth factor receptor, insulin-like growth factor 1 receptor, tumor necrosis factor (TNF)-related apoptosis-inducing ligand receptors, and receptor activator nuclear factor-κB ligand (RANKL) have also been exploited for cancer treatment (11).

In this study, we sought to investigate the complement-independent effects of exogenous C1q and recombinant forms of globular head modules on an ovarian cancer cell line, SKOV3.

MATERIALS AND METHODS

Cell Culture and Treatments

A human ovarian clear cell adenocarcinoma cell line, SKOV3 (ATCC, Rockville, MD, USA) was used as an *in vitro* model for epithelial ovarian cancer. Cells were cultured in DMEM-F12 media containing 10% v/v fetal calf serum, 2mM L-glutamine, and penicillin (100 U/ml)/streptomycin (100 μg/ml) (Thermo Fisher). Cells were grown at 37°C under 5% v/v CO_2 until 80–90% confluency was reached.

Purification of Human C1q

Human C1q was purified as published earlier (12). Briefly, freshly thawed human plasma was made 5 mM EDTA, centrifuged at 5,000 × *g* for 10 min, and any aggregated lipids were removed using Whatmann filter paper (GE Healthcare, UK). The plasma was then incubated with non-immune IgG-Sepharose (GE Healthcare, UK) for 2 h at room temperature. C1q bound IgG-Sepharose was washed extensively with 10 mM HEPES, 140 mM NaCl, 0.5 mM EDTA, and pH 7.0 before eluting C1q with CAPS (*N*-cyclohexyl-3-aminopropanesulfonic acid) buffer (100 mM CAPS, 1 M NaCl, 0.5 mM EDTA, pH 11). The eluted C1q fractions were then passed through a HiTrap Protein G column (GE Healthcare, UK) to remove IgG contaminants, followed by dialysis against 0.1 M HEPES buffer, pH 7.5.

Recombinant Expression and Purification of ghA, ghB, and ghC Modules of Human C1q

The recombinant forms of the globular head regions of human C1q A (ghA), B (ghB), and C (ghC) chains were expressed as fusions to *Escherichia coli* maltose-binding protein (MBP) and purified, as reported previously (13). Expression constructs pKBM-A, pKBM-B, and pKBM-C were transformed into *E. coli* BL21 (Invitrogen) cells in the presence of ampicillin (100 μg/ml). The primary bacterial culture was grown overnight by inoculating a single colony in 25 ml of Luria-Bertani medium containing ampicillin. The bacterial culture was then grown in a 1 L batch until OD_{600} 0.6 and then induced with 0.4 mM isopropyl β-D-thiogalactoside (IPTG) (Sigma-Aldrich, UK) for 3 h at 37°C on a shaker and centrifuged (5,000 × *g*, 4°C, 15 min). Subsequently, the cell pellet for each fusion protein was lysed in 50 ml lysis buffer (20 mM Tris–HCl, pH 8.0, 0.5 M NaCl, 0.2% v/v Tween 20, 1 mM EGTA pH 7.5, 1 mM EDTA pH 7.5, and 5% v/v glycerol) containing lysozyme (100 μg/ml, Sigma-Aldrich, UK) and 0.1 mM phenylmethylsulfonyl fluoride (PMSF; Sigma-Aldrich, UK) at 4°C for 30 min. The resultant cell suspension was sonicated at 60 Hz for 30 s with an interval of 2 min each (12 cycles) and centrifuged (16,000 × *g* for 30 min). The supernatant was diluted 5-fold with buffer I (20 mM Tris–HCl, pH 8.0, 100 mM NaCl, 0.2% v/v Tween 20, 1 mM EDTA pH 7.5, and 5% v/v glycerol) and passed through an amylose resin column (50 ml; New England Biolabs). The column was then washed extensively with buffer I (150 ml), followed by buffer II (250 ml of buffer I without Tween 20) before eluting 1 ml fractions of fusion proteins with 100 ml buffer II containing 10 mM maltose. The peak fractions were then passed through Pierce™ High Capacity Endotoxin Removal Resin (Qiagen) to remove lipopolysaccharide. Endotoxin levels in the purified protein samples were analyzed using the QCL-1000 Limulus amebocyte lysate system (Lonza). The assay was linear over a range of 0.1–1.0 EU/ml (10 EU = 1 ng of endotoxin), and the amount of endotoxin levels was <4 pg/μg of the recombinant proteins.

Fluorescence Microscopy

SKOV3 cells (0.5×10^5) were grown on coverslips and incubated with human C1q, ghA, ghB, or ghC (10 μg/ml) in a serum-free DMEM-F12 medium for 1 h for analyzing cell binding, 24 h for apoptosis induction, and 15 h for mammalian target of rapamycin (mTOR) activation analysis. For binding analysis, the coverslips were washed three times with PBS and then incubated with rabbit anti-human C1q polyclonal antibody (MRC Immunochemistry Unit, Oxford, 1:200) for C1q and rabbit anti-MBP polyclonal antibody (Thermo Fisher) for MBP fusions of the globular head modules. Coverslips were washed three times with PBS, and then incubated with Alexa Fluor® 488 (1:500, Thermo Fisher) and Hoechst (1:10,000, Thermo Fisher) for immunofluorescence analysis. Apoptosis was analyzed *via* immunofluorescence using a FITC-Annexin V apoptosis detection kit with propidium iodide (PI) (Biolegend). After 24 h incubation with proteins, the coverslips were then incubated with Annexin V-binding buffer containing FITC Annexin V (1:200) and PI (1:200) for 15 min and washed twice with PBS before mounting on the slides to visualize under a HF14 Leica DM4000 microscope. For mTOR analysis, following the 15-h incubation with proteins, the coverslips were washed three times with PBS. The cells were fixed and permeabilized using ice-cold 100% methanol at −20°C for 10 min, followed by 1 h incubation with rabbit anti-human mTOR (1:500, Sigma), and then 1 h incubation with Alexa Fluor® 488 (rabbit anti-human 1:500, Thermo Fisher) and Hoechst (1:10,000, Thermo Fisher) for immunofluorescence analysis. In order to detect caspase 3 activation, the protein-treated SKOV3 cells were fixed and permeabilized using ice-cold 100% methanol at −20°C for 10 min, followed by 1 h incubation with rabbit anti-human cleaved caspase 3 (1:500, Cell Signaling), and then 1 h incubation with secondary antibody (anti-rabbit) probed with CY3 (1:500, Thermo Fisher) and Hoechst (1:10,000, Thermo Fisher) for immunofluorescence analysis.

Dye Exclusion Assay

SKOV3 cells (0.1×10^6) were grown in a 12-well plate and incubated with C1q, ghA, ghB, ghC, or MBP (10 μg/ml) along with an untreated control in serum-free DMEM-F12 for 24 h. Cells were detached using 5 mM EDTA, pH 8.0 and centrifuged at $1,200 \times g$ for 5 min. The cell pellet was re-suspended in 1 ml DMEM-F12, and 10 μl of cell suspension was stained with 10 μl of Trypan blue (60%; Sigma-Aldrich, UK) for cell counting using hemocytometer. The viable cells, i.e., unstained cells, were counted in 5 different optical fields with a threshold value of 200 cells per field.

MTT Assay

MTT [3-(4,5-dimethylthiazol-2-yl)-2,5-diphenyltetrazolium bromide] (Thermo Fisher) assay was performed by incubating SKOV3 cells (0.1×10^5) in a 96-well microtiter plate with C1q, ghA, ghB, ghC, or MBP (10 μg/ml each) and an untreated control in serum-free DMEM-F12 medium for 24 h, followed by incubation with 50 μg/μl MTT (5 mg/ml stock) per well for 4 h at 37°C. Majority of the media was removed leaving behind 25 μl per well, which was mixed thoroughly with 50 μl of dimethyl sulfoxide (DMSO) and incubated for another 10 min at 37°C. The absorbance was read at 570 nm using a plate reader.

Flow Cytometry

SKOV3 cells (0.1×10^7) were incubated with C1q, ghA, ghB, or ghC (10 μg/ml), along with an untreated control, in a six-well plate for 24 h, followed by cell detachment using 5 mM EDTA and centrifugation at $1,200 \times g$ for 5 min. FITC Annexin V apoptosis detection kit with PI (Biolegend) was used, as per the manufacturer's instructions. Compensation parameters were acquired using unstained, untreated FITC stained, and untreated PI stained SKOV3 cells. SKOV3 cells (0.1×10^4) were acquired for each experiment and compensated before plotting the acquired data. For protein-binding analysis, SKOV3 cells (0.5×10^6) were incubated with C1q, ghA, ghB, and ghC (10 μg/ml) and BSA-treated cells as a negative control. Cells were incubated at 4°C for 1 h, followed by 1 h incubation with rabbit anti-human C1q polyclonal antibody (1:200) for C1q and rabbit anti-MBP (Thermo Fisher, 1:200) for globular head modules treated cells as well as their respective BSA-treated controls. The cells were then incubated with Alexa Fluor® 488 (1:1,000, Thermo Fisher) for 1 h and cells were washed with PBS three times between each step. Compensation parameters were acquired using unstained, untreated Alexa Fluor® 488-stained SKOV3 cells. SKOV3 cells (0.1×10^4) were acquired using Novocyte Flow Cytometer for each experiment and compensated before plotting the acquired data.

Western Blot

SKOV3 cells (0.1×10^7) were plated in a six-well plate (Nunc) and incubated with C1q, ghA, ghB, or ghC (10 μg/ml), along with an untreated control in serum-free DMEM-F12 medium for 12 and 24 h. The cells were lysed within the wells using lysis buffer (50 mM Tris–HCL, pH 7.5, 10% v/v glycerol, and 150 mM NaCl) over ice for 10 min, before being gently transferred to a pre-cooled microcentrifuge tube, and centrifuged for 15 min at $13,000 \times g$ at 4°C. The cell lysate was mixed with the treatment buffer (50 mM Tris pH 6.8, 2% β-merceptoethanol, 2% SDS, 0.1% bromophenol blue, and 10% glycerol) in order to run on SDS-PAGE (12% w/v) for 90 min at 120 V. The SDS-PAGE separated proteins were then electrophoretically transferred onto a nitrocellulose membrane (Sigma) using transfer buffer (25 mM Tris, 190 mM glycine, and 20% methanol, pH 8.3) for 2 h at 320 mA, followed by blocking with 5% w/v dried milk powder (Sigma) in 100-ml PBS at room temperature for 2 h on a rotatory shaker. The membrane was washed with PBST (PBS + 0.05% Tween 20) three times, 10 min each, and incubated with primary anti-human C1q (polyclonal antibody), anti-caspase 9, anti-caspase 3, or anti-cleaved caspase 3 antibodies (1:1000 Cell Signaling Technology) at 4°C overnight. The membrane was washed with PBST (three times, 10 min each) before incubating with secondary anti-rabbit IgG HRP-conjugate (1:1,000; Promega) for 1 h at room temperature. The bands were visualized using enhanced chemiluminescence (Thermo Fisher) in the Biorad ChemiDoc MP imaging system, or using 3,3-diaminobenzidine (DAB) substrate kit (Thermo Fisher).

Quantitative RT-PCR

SKOV3 cells (0.5×10^6) were incubated with C1q, ghA, ghB, or ghC (10 μg/ml) for various time points, and the centrifuged cell pellets were stored at −80°C. GenElute Mammalian Total RNA Purification Kit (Sigma-Aldrich, UK) was used, as per

the manufacturer's instructions, to extract total RNA, followed by treatment with DNase I (Sigma-Aldrich, UK) to remove any DNA contaminants. The concentration and purity of total RNA were determined by measuring the absorbance at 260 nm and 260:280 nm ratio, respectively, using NanoDrop 2000/2000c (Thermo Fisher Scientific). Total RNA (2 μg) was used to synthesize cDNA using High Capacity RNA to cDNA Kit (Applied Biosystems).

Forward and reverse primer sequences (**Table 1**) were designed using the web-based Basic Local Alignment Search Tool and Primer-BLAST (http://blast.ncbi.nlm.nih.gov/Blast.cgi). The qPCR reactions were performed to measure the mRNA expression level of various target genes. Each reaction was conducted in triplicates and consisted of 5 μl Power SYBR Green MasterMix (Applied Biosystems), 75 nM of forward and reverse primers, and 500 ng cDNA, making up to a 10 μl final volume per well. Relative mRNA expression was determined by qPCR using the 7900HT Fast Real-Time PCR System (Applied Biosystems). Samples were initially incubated at 50°C and 95°C for 2 and 10 min, respectively, followed by amplification of the template for 40 cycles (each cycle involved 15 s at 95°C and 1 min at 60°C). The gene expression was normalized using the expression of human 18S rRNA as an endogenous control. The cycle threshold (Ct) mean value for each target gene was used to calculate the relative expression using the relative quantification (RQ) value and formula: $RQ = 2^{-\Delta\Delta Ct}$, which was compared with the relative expression of 18S.

Statistical Analysis

GraphPad Prism 6.0 was used to make graphs, and the statistical analysis was carried out using an unpaired one-way ANOVA test. Significant values were considered based on $^{*}p < 0.05$, $^{*}p < 0.01$, and $^{***}p < 0.001$ between treated and untreated conditions. Error bars show the SD or SEM, as indicated in the figure legends.

RESULTS

Human C1q and Recombinant Globular Head Modules Bind SKOV3

The qualitative binding analysis of C1q and recombinant form of individual globular head (ghA, ghB, and ghC) modules (10 μg/ml) to SKOV3 cells using immunofluorescence microscopy revealed the membrane localization of these proteins following 1 h incubation at 4°C (**Figure 1A**). The nucleus, stained with Hoechst, showed a blue fluorescence (**Figure 1A**, panel A). The bound proteins localized on the cell membrane *via* green fluorescence; all the four proteins showed similar binding pattern (**Figure 1A**, panels B and D). FACS analysis revealed similar binding pattern, consistent with the observations made under the immunofluorescence microscopy. SKOV3 cells, treated with C1q and globular head modules, were over 90% positive in the FITC positive quadrant, as compared to the control protein, BSA (**Figure 1B**).

C1q and Recombinant Globular Head Modules Reduce Cellular Viability *via* Induction of Apoptosis in SKOV3 Cells

C1q and globular head modules (at 10 μg/ml concentration) were incubated with SKOV3 cells for 24 h. Trypan blue dye exclusion (**Figure 2A**) revealed a significant decrease in the cell viability following incubation with C1q (~50%), ghA (~50%), ghB (~40%), and ghC (~55%). MTT assay also confirmed the above mentioned observations (**Figure 2B**). Furthermore, the qualitative apoptosis analysis was performed using immunofluorescence microscopy. A significant proportion of SKOV3 cells, when treated with C1q proteins (10 μg/ml) for 24 h, stained positive for cell membrane integrity marker, Annexin V (conjugated to FITC), which binds to phosphatidylserine (PS) of the membrane of cells undergoing apoptosis (**Figure 3**, panel B). The nucleus was stained using Hoechst, which showed blue fluorescence (**Figure 3**, panel A). No FITC fluorescence was detected in the untreated cells, suggesting that the integrity of the cell membrane was intact, and hence, the cells were still viable (**Figure 3**).

FACS analysis revealed that the treatment of SKOV3 cells with C1q (10 μg/ml) for 24 h yielded approximately 58% (C1q, quadrant Q2-2; **Figure 4**) cells positive for both FITC (Annexin V marker) and PI (stains DNA) quadrant, significantly higher than 1.42% untreated control cells (UT, quadrant Q2-2; **Figure 4**), which represented a cell population undergoing late apoptosis. In addition, 16% of cells stained positive for FITC only (C1q, quadrant Q2-4; **Figure 4**), which represented an early apoptotic cell population.

Similar trends were also observed when SKOV3 cells were treated with ghA, ghB, and ghC; approximately 50% (ghA and ghC) and 40% (ghB) of cells had undergone apoptosis after 24 h treatment as seen in quadrant Q2-2 (ghA, ghB, and ghC in **Figure 4**). Approximately, 15–20% of early apoptotic cells stained positive for FITC alone (quadrant Q2-4; **Figure 4**) following treatment with each globular head module. In the untreated cells, approximately 90% of the cell population was both FITC and PI negative (UT, quadrant Q2-3; **Figure 4**). A shift in the florescence

TABLE 1 | Target genes and terminal primers used in the qPCR analysis.

Target gene	Forward primer	Reverse primer
18S	5′-ATGGCCGTTCTTAGTTGGTG-3′	5′-CGCTGAGCCAGTCAGTGTAG-3′
Bax	5′-TGCTTCAGGGTTTCATCCAGG-3′	5′-GGAAAAAGACCTCTCGGGGG-3′
Fas	5′-ACACTCACCAGCAACACCAA-3′	5′-TGCCACTGTTTCAGGATTTAA-3′
Mammalian target of rapamycin (mTOR)	5′-TGCCAACTATCTTCGGAACC-3′	5′-GCTCGCTTCACCTCAAATTC-3′
RICTOR	5′-GGAAGCCTGTTGATGGTGAT-3′	5′-GGCAGCCTGTTTTATGGTGT-3′
RAPTOR	5′-ACTGATGGAGTCCGAAATGC-3′	5′-TCATCCGATCCTTCATCCTC-3′
Tumor necrosis factor (TNF)-α	5′-GTATCGCCAGGAATTGTTGC-3′	5′-AGCCCATGTTGTAGCAAACC-3′
NF-κB	5′-TGAGGTACAGGCCCTCTGAT-3′	5′-GTATTTCAACCACAGATGGCACT-3′

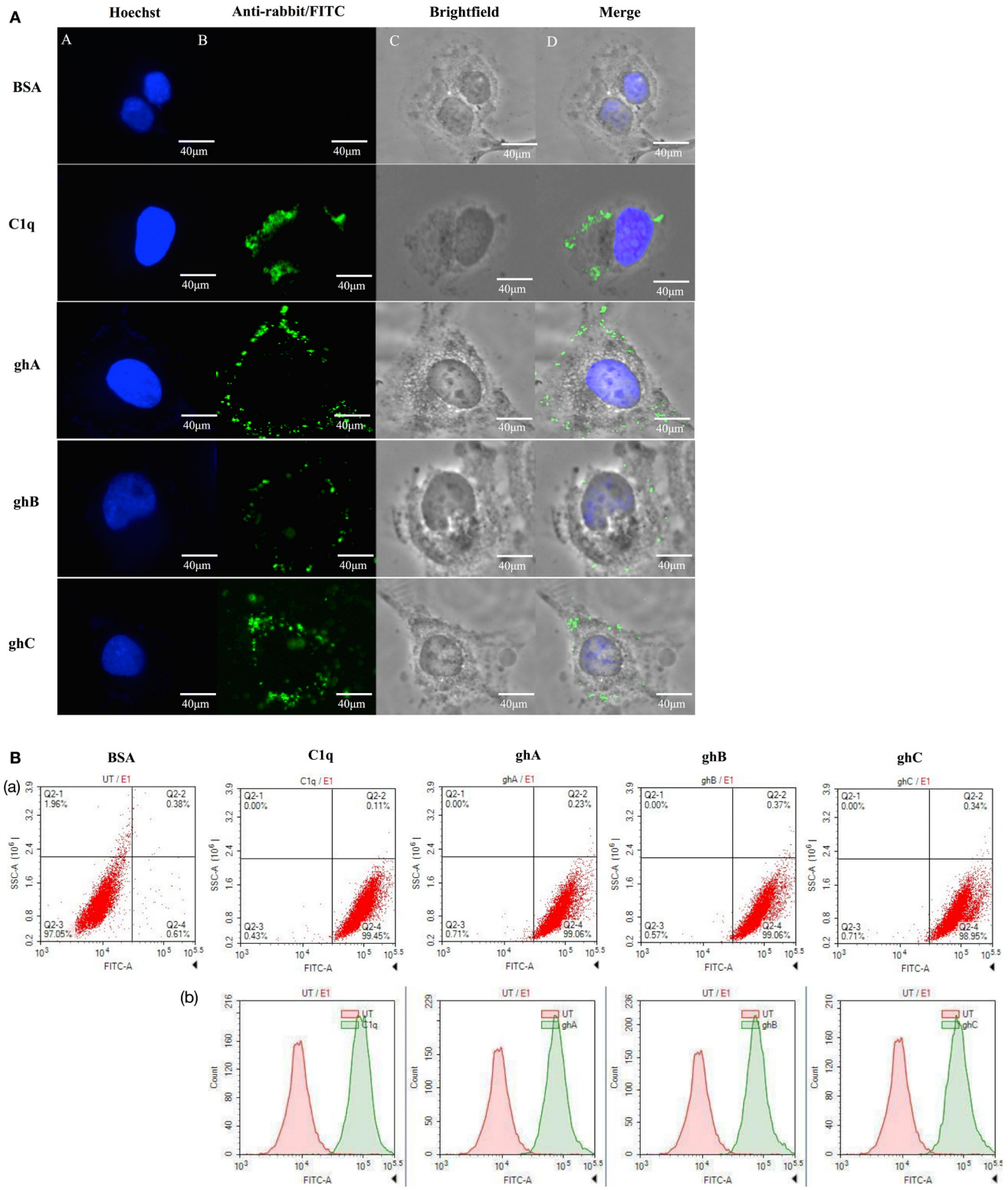

FIGURE 1 | **(A)** Binding of human C1q and recombinant globular head modules, ghA, ghB, and ghC (10 μg/ml; 1 h incubation) to SKOV3 cells using immunofluorescence microscopy. Panel A shows the nucleus of the cells stained with Hoechst. Panel B shows the cells probed with anti-C1q (C1q) and anti-maltose-binding protein (MBP) (globular heads) polyclonal antibodies, followed by anti-rabbit IgG labeled with FITC; the bound proteins are visible on the cell membrane (panels C and D). **(B)** Flow cytometric analysis to show binding of human C1q and ghA, ghB, and ghC (10 μg/ml) to SKOV3 cells after 1 h incubation. Panel a shows the number of cells probed with anti-C1q (C1q) and anti-MBP (globular heads) antibodies followed by anti-rabbit IgG labeled with FITC, as compared to the untreated cells. Panel b shows the shift in the fluorescent intensity from untreated to treated cells.

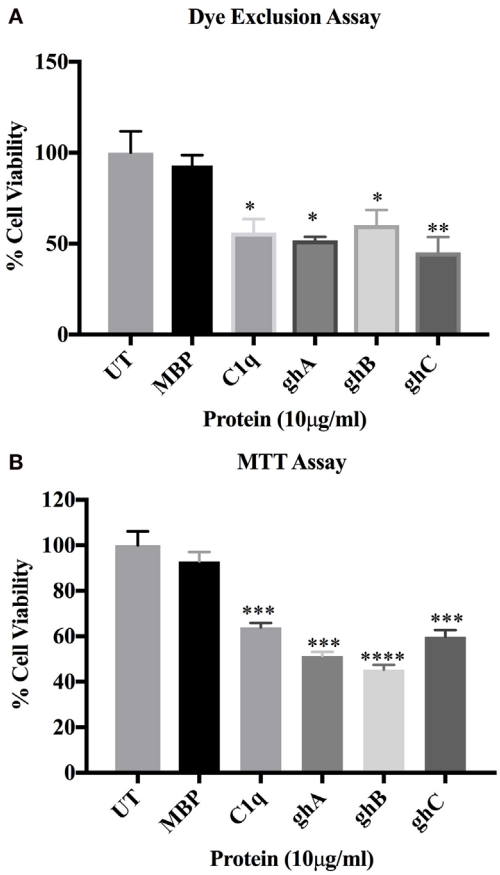

FIGURE 2 | SKOV3 cell viability assay *via* Trypan blue exclusion (A) and MTT (B) following treatment with human C1q, ghA, ghB, ghC, and maltose-binding protein (MBP) (10 μg/ml)and untreated control for 24 h (±SEM, of three independent experiments). Cell numbers were reduced by approximately 50% in the treated as compared to untreated and MBP controls. Significance was established using the unpaired one-way ANOVA test (*$p < 0.05$, *$p < 0.01$, and ***$p < 0.001$) ($n = 6$).

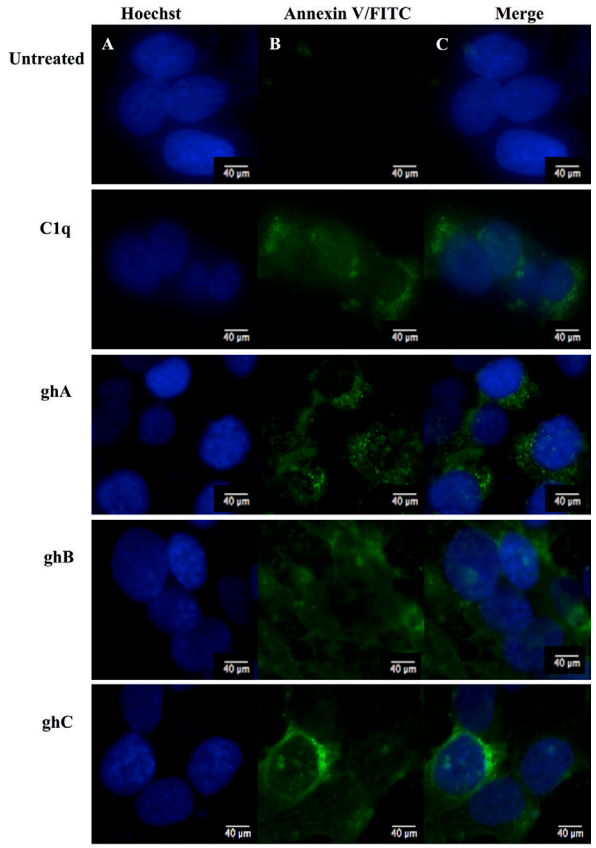

FIGURE 3 | Analysis of apoptosis using immunofluorescence microscopy in SKOV3 cells treated with human C1q, ghA, ghB, and ghC (10 μg/ml) and an untreated control after 24 h. Panel A shows the nucleus stained with Hoechst. Panel B shows the cell membrane integrity marker FITC Annexin V, which binds to PS of the cell membrane of cells undergoing apoptosis. No FITC was detected in the untreated SKOV3 cells.

intensity in the treated SKOV3 cells, as compared to the untreated cells, further confirmed these observations (**Figure 4**).

C1q and Individual Globular Head Modules Upregulate TNF-α Transcripts by SKOV3 Cells with Concomitant Upregulation of NF-κB

The mRNA expression level of pro-inflammatory cytokine, TNF-α, was significantly upregulated at 12 h following C1q ($\log_{10}$ 1.2-fold) and globular head modules; ghA ($\log_{10}$ 0.4-fold), ghB ($\log_{10}$ 1-fold), and ghC ($\log_{10}$ 0.7-fold) treatment in comparison to an untreated control, as determined by qPCR (**Figure 5A**). NF-κB was also significantly upregulated ($\log_{10}$ 0.7-fold) at 12 h, as anticipated, consistent with TNF-α upregulation (**Figure 5B**). Both TNF-α (not shown) and NF-κB mRNA expressions were downregulated by 24 h (**Figure 5C**), which could be attributed to the late apoptosis stage. In addition, TNF-α transcriptional upregulation occurred at an earlier time point for ghA, i.e., at 6 h as compared to the other treated samples (data not shown). These results prompted us to further investigate the mRNA expression of pro-apoptotic makers of intrinsic (Bax) and extrinsic (Fas) apoptosis pathways.

C1q Upregulates Expression of Pro-apoptotic Bax and Fas in SKOV3 Cells

C1q- and globular head module-mediated apoptosis was further investigated by analyzing the expression of pro-apoptotic genes, Bax and Fas, *via* qPCR. Fas was transcriptionally upregulated in the C1q ($\log_{10}$ 0.4-fold) treated SKOV3 cells, most significantly at 12 and 24 h relative to the untreated control cells (**Figure 6A**). The globular head module-treated cells showed minimal mRNA expression levels at 12 h (data not shown) and significant upregulation of Fas at 24 h ($\log_{10}$ 0.4-fold) (**Figure 6B**). Similar trend of minimal mRNA expression at 12 h (data not shown) and significant upregulation at 24 h (**Figure 6C**) were observed for Bax mRNA expression in case of ghA, ghB, or ghC. The activation of apoptotic pathway causes the loss of cell membrane integrity, which was previously observed in the immunofluorescence

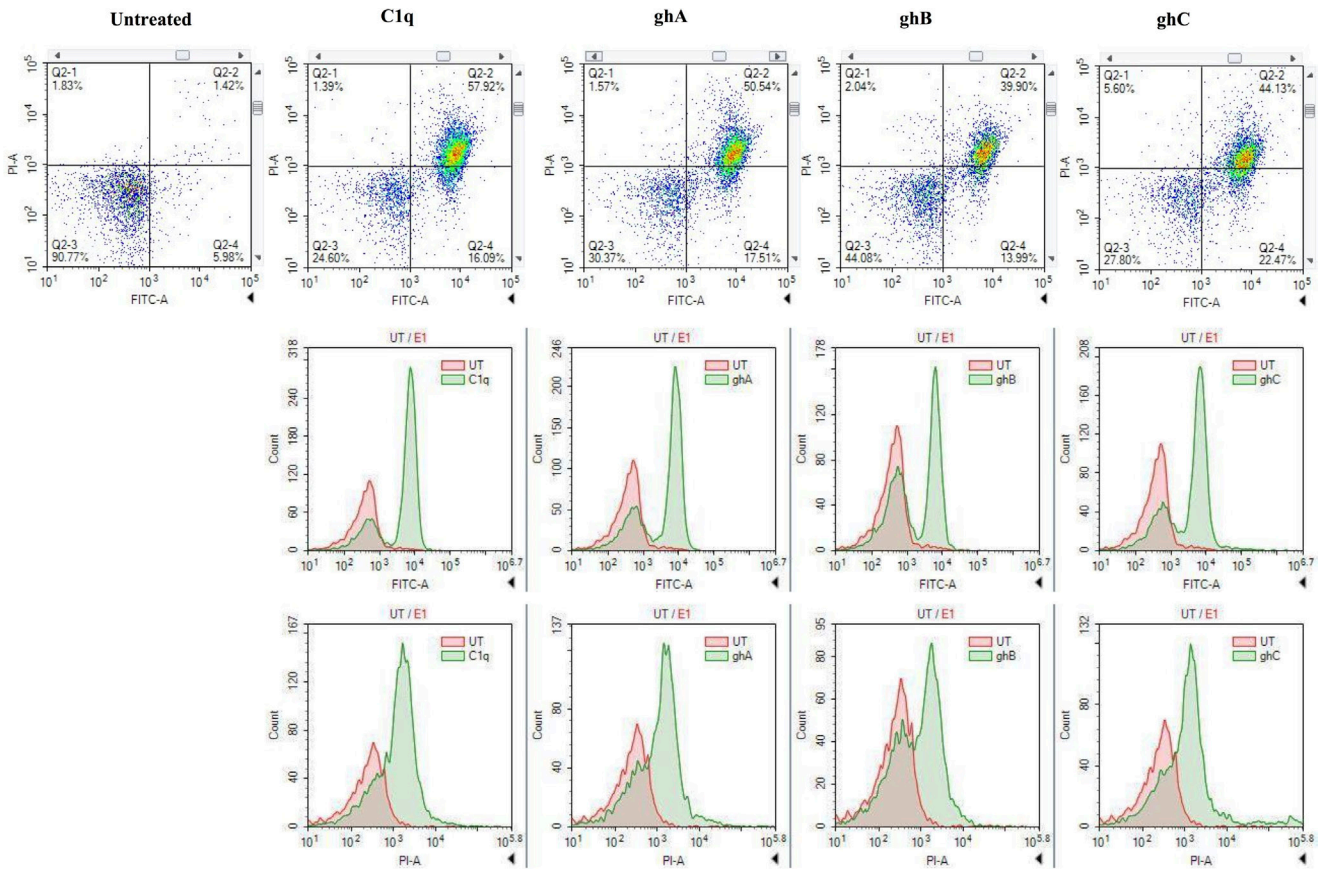

FIGURE 4 | **The quantitative analysis of apoptosis using FACS**. SKOV3 cells, treated with C1q and globular head modules for 24 h, yielded approximately 50% (C1q, ghA, ghB, and ghC quadrant Q2-2) cells positive for both FITC and PI, significantly higher than 1.42% untreated control cells (untreated, quadrant Q2-2). Approximately 20% cells stained positive for FITC only (C1q, ghA, ghB, and ghC quadrant Q2-4).

microscopy at 24 h, consistent with the upregulation of mRNA expression of these genes. To further validate these results, the activation of Caspase 3 was investigated *via* western blot.

C1q and the Globular Head Modules Activate Caspase 3 in SKOV3 Cells

Apoptotic markers, caspase 3 and cleaved caspase 3, were detected in the SKOV3 cells, treated with C1q and globular head modules, in comparison with the untreated cells. The cleaved caspase 3 was detected at 17 kDa after 24 h of C1q, ghA, and ghB treatment in the western blot (**Figure 7B**). A reduction in the abundance of the full length at 32 kDa was seen after 24 h in comparison to 12 h (**Figure 7A**) β-actin (45 kDa) was used as a loading control for 12 h and 24 h (**Figure 7C**). In addition, the activation of caspase 3 was also seen by immunofluorescence in parallel to apoptosis staining for Annexin V-FITC at 24 h following treatment with C1q or globular head modules. Activated caspase 3 was clearly visible in the cytoplasm probed with Cy3, suggesting that the SKOV3 cells were in the early stages of apoptosis as the membrane was stained positively for Annexin V-FITC, in comparison to the control where no staining was detected (**Figure 7D**). The cleaved caspase 3 in the ghC treatment sample could not be detected *via* western blot; however, activated caspase 3 was detected *via* immunofluorescence.

C1q, ghA, ghB, and ghC Downregulate Prosurvival Factors Such as RICTOR, mTOR, and RAPTOR

In addition to the apoptosis markers, we also investigated the expression of mTOR signaling pathways since it is frequently detected in ovarian cancers (14). The mRNA expressions of mTOR, RICTOR, and RAPTOR (**Figure 8A**) were significantly downregulated (~$\log_{10}$ 0.5-fold) at 6 h, thereby suggesting that the effects of C1q and globular head modules can compromise mTOR signaling within the first few hours of the treatment. Additionally, the presence of mTOR was detected abundantly in the cytoplasm (green) of the untreated cells, compared to SKOV3 cells treated with C1q and globular heads at 15 h time point *via* immunofluorescence microscopy (**Figure 8B**).

DISCUSSION

We report here, for the first time, that exogenous treatment with human C1q and recombinant globular head modules ghA, ghB,

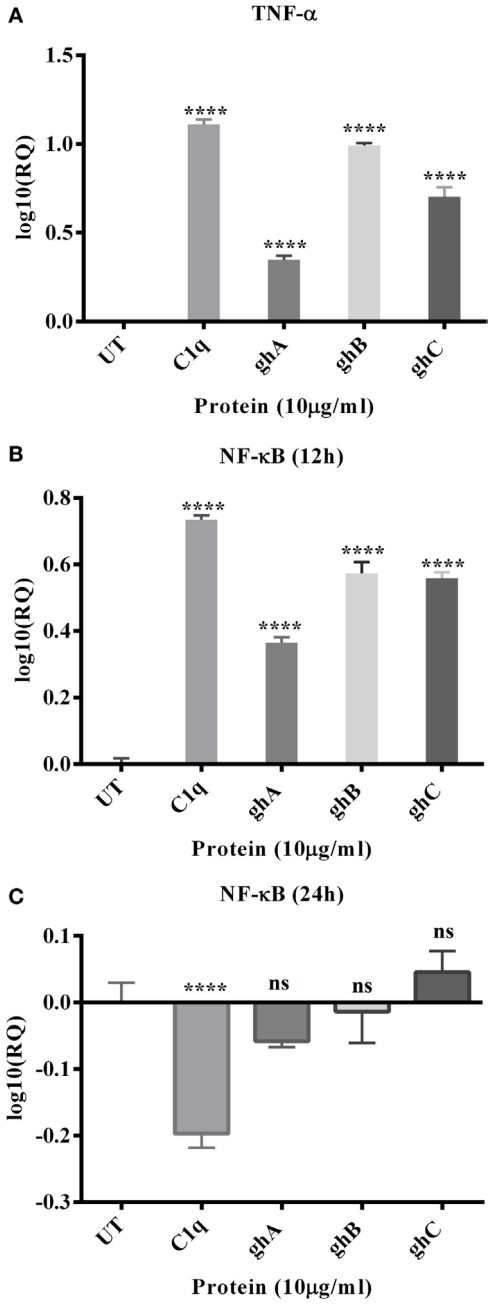

FIGURE 5 | Relative quantification comparisons of TNF-α (A) and NF-κB (B,C) mRNA expression in SKOV3 cells treated with C1q, ghA, ghB, and ghC. The transcriptional expressions of both TNF-α and NF-κB were upregulated (log_{10} 0.5- to 1-fold) after 12 h treatment and NF-κB at 24 h was downregulated. Significance was ascertained using the unpaired one-way ANOVA test (*$p < 0.05$, *$p < 0.01$, and ***$p < 0.001$) ($n = 3$).

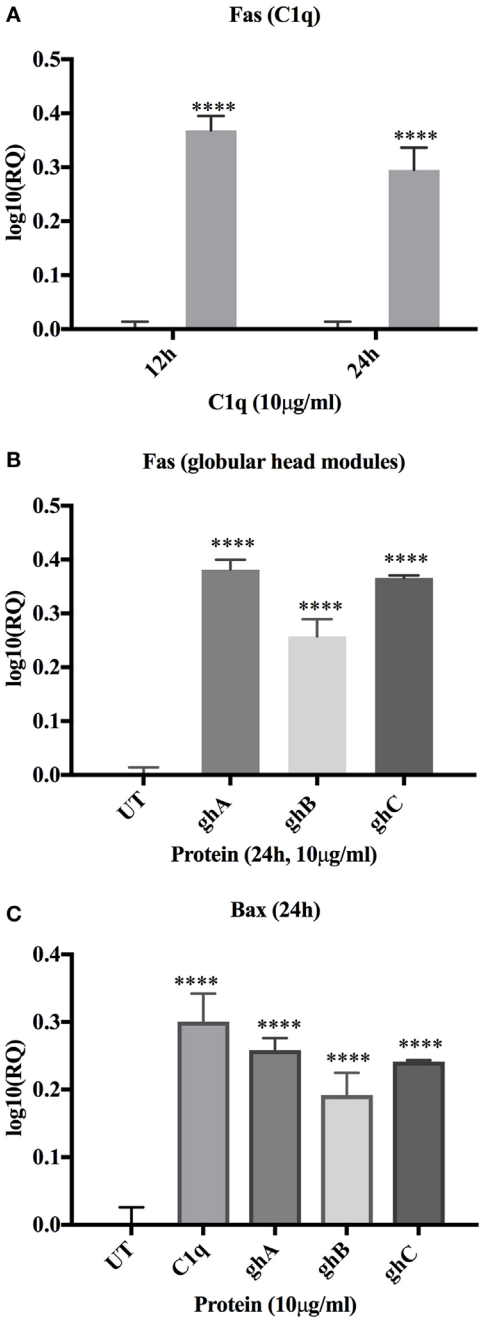

FIGURE 6 | Relative quantification comparisons of Fas (A) and Bax (B,C) mRNA expression in SKOV3 cells treated with C1q, ghA, ghB, and ghC (10 μg/ml). Fas expression was upregulated (~log_{10} 0.5-fold) at 12 h (C1q only) and 24 h (both for C1q and globular head modules). Bax expression was upregulated (~log_{10} 0.5-fold) at 24 h. Significance was determined using the unpaired one-way ANOVA test (*$p < 0.05$, *$p < 0.01$, and ***$p < 0.001$) ($n = 3$).

and ghC caused apoptosis in an ovarian cancer cell line, SKOV3. This was evident from a significant increase in the number of Annexin V-positive cells that were examined *via* immunofluorescence microscopy and FACS, presence of cleaved caspase 9 (data not shown) and 3 *via* western blot, and transcriptional upregulation of pro-apoptotic markers, such as TNF-α, Bax, and Fas as illustrated in **Figure 9**. Based on these observations, it appears likely that C1q and individual globular head modules can induce apoptosis in SKOV3 cells *via* TNF-α-induced apoptosis pathway. However, other pathways could potentially be involved.

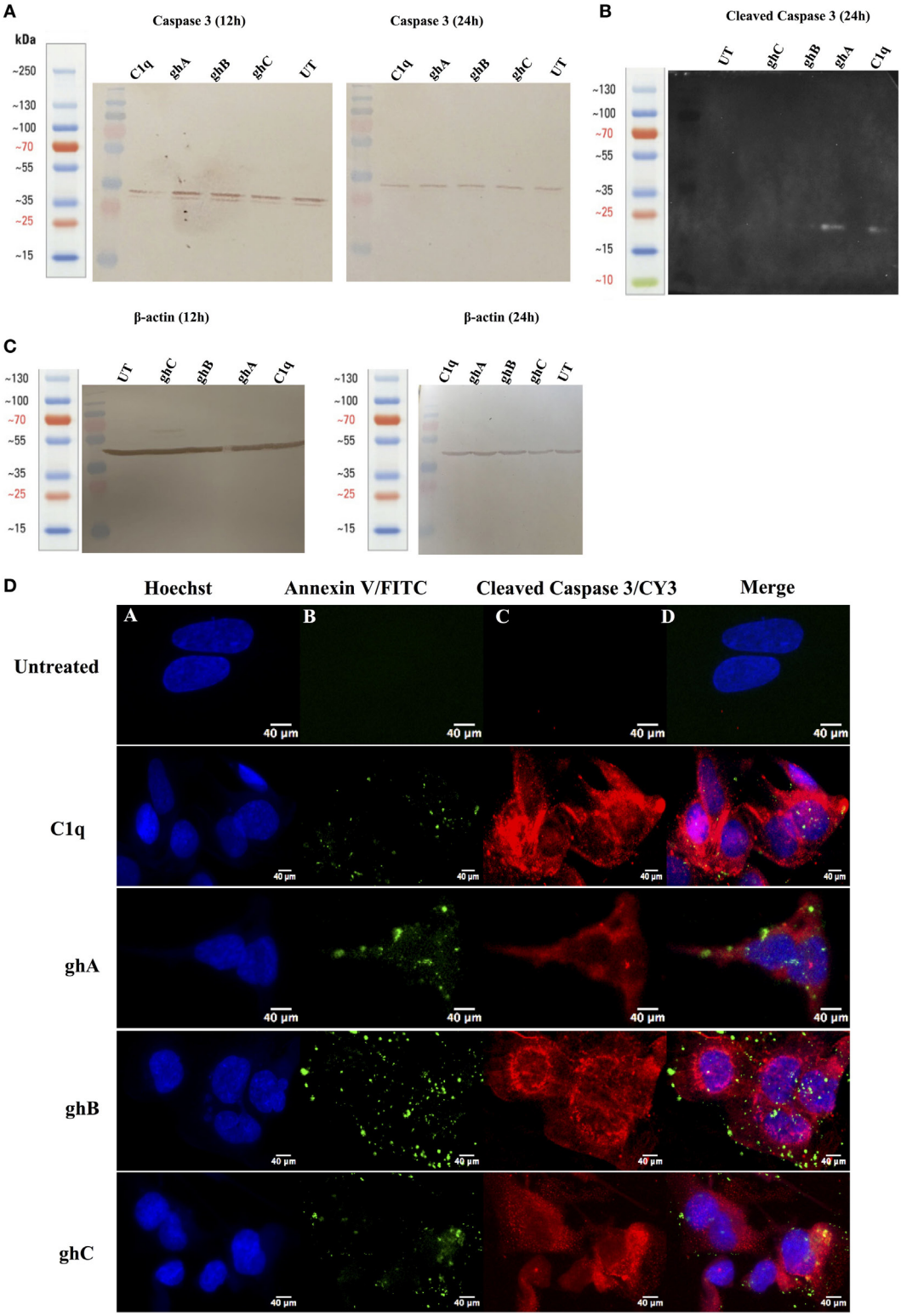

FIGURE 7 | **Caspase activation in SKOV3 cells following treatment with C1q and globular head modules**. **(A)** Western blot analysis of full-length/total caspase 3 at 32 kDa after 12 and 24 h of the treatment with C1q, ghA, ghB, ghC, and untreated. **(B)** The cleaved caspase 3 was observed at 17 kDa after 24 h of treatment with C1q, ghA, ghB, ghC, and untreated **(C)** Western blot analysis for β-actin as a loading control for 12 h and 24 h at 45 kDa. **(D)** The activation of caspase 3 was also shown by immunofluorescence microscopy at 24 h in parallel with apoptosis staining for Annexin V-FITC, where activated caspase 3 was clearly visible in the cytoplasm probed with CY3 at 24 h.

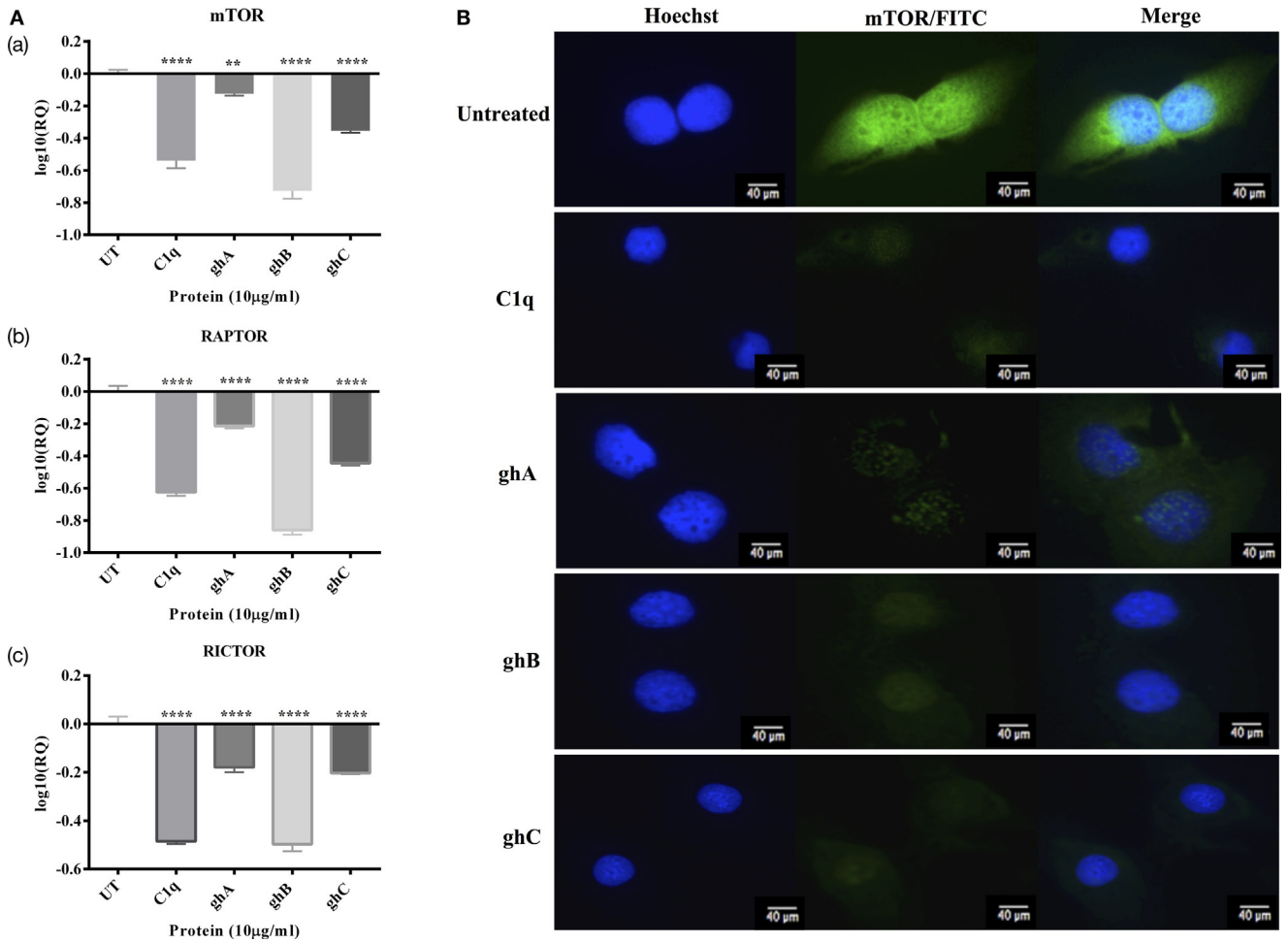

FIGURE 8 | (A) Relative quantification comparisons of mammalian target of rapamycin (mTOR) (a), RAPTOR (b), and RICTOR (c) mRNA expression in SKOV3 cells treated with C1q, ghA, ghB, and ghC (10 µg/ml) at 6 h. Significance was obtained using the unpaired one-way ANOVA test (*$p < 0.05$, *$p < 0.01$, and ***$p < 0.001$) ($n = 3$). **(B)** Immunofluorescence microscopy to show the presence of mTOR detected abundantly in the cytoplasm (green) of the untreated cells, compared to SKOV3 cells treated with C1q and globular heads at 15 h time point.

During early apoptosis, the integrity of the cell membrane is lost and phosphatidylserine (PS) is exposed for Annexin V binding (21). A significant number of SKOV3 cells were stained positive for Annexin V, when examined under immunofluorescence microscope, suggesting that the cell membrane integrity was no longer intact as Annexin V labeled with FITC was able to bind to PS, which is usually present on the intracellular leaflet of the healthy cells. However, it is translocated to the outer leaflet during apoptosis. Hence, it provided the first evidence that SKOV3 cells were undergoing apoptosis following the treatment with C1q or globular heads for 24 h (**Figure 3**). Trypan blue exclusion (**Figure 2A**) and MTT assays (**Figure 2B**), as well as FACS analysis (**Figure 4**) of treated SKOV3 cells, validated C1q-induced apoptosis of SKOV3 cells. Thus, we investigated if the levels of pro-apoptosis factors such as Fas and Bax were altered following C1q treatment of SKOV3 cells. This subsequently led us to examine the TNF-induced apoptosis pathway.

Tumor necrosis factor-α is a prototypical member of pro-inflammatory cytokine family that performs various roles in inflammation and cell death (22). Members of the TNF family are associated with a wide range of immune processes and play an important role in cancer immune surveillance For example, TNF-α can mediate apoptosis selectively in tumor cells *via* death receptors involving TRAIL/FasL ligands (23). Following treatment of SKOV3 cells with C1q or globular head modules, the gene expression of TNF-α was upregulated at 6 h (C1q) and 12 h (C1q, ghA, ghB, and ghC; **Figure 5A**), which underwent apoptosis by 24 h. Interaction of TNF-α with its receptor TNFR1 can cause upregulation of NF-κB, as was the case in our study (**Figure 5B**). Fas mRNA upregulation is observed, as expected (**Figure 6A**), suggesting that Fas, a receptor for FasL and a member of TNF receptor family, mediated apoptosis crosstalk. Intriguingly, Bax, a marker of dysfunctional mitochondria, was also seen to be transcriptionally upregulated (**Figure 6B**). Bax

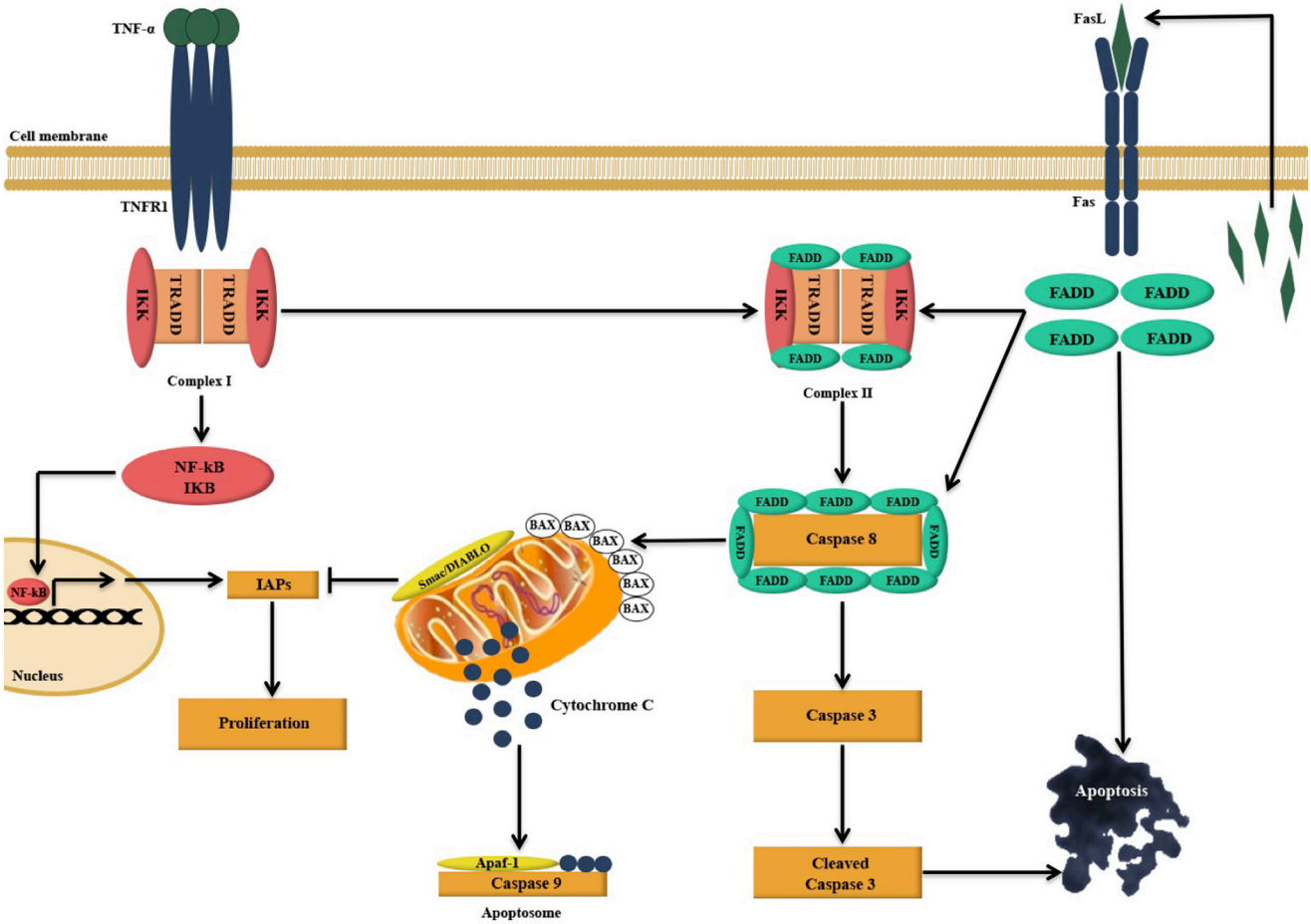

FIGURE 9 | Illustration of the likely apoptosis pathway in action following C1q binding to SKOV3 cells. Exogenous treatment of SKOV3 cells with C1q and individual globular head modules can induce upregulation of TNF-α and Fas. TNF-α stimulation triggers two parallel, but contrasting, pathways: the pro-apoptotic caspase (15) and the anti-apoptotic NFκB-IκB inhibitor of apoptosis proteins (IAP) pathway (16). The cell survival or death, however, depends upon interactions among the components of these two pathways as well as other factors such as mitochondrial dysfunction (15, 16). TNF-α can bind to TNF type I receptor (TNFR1), which is then internalized to first form a complex with TNFR1-associated DEATH domain, receptor-interacting protein 1 (RIP1), TNF receptor-associated factor 2 (TRAF2), and cellular inhibitor of apoptosis protein-1 (c-IAP1) (complex I), triggering the upregulation of nuclear factor-κB (NF-κB). A second complex (complex II) is later formed when complex I bind to Fas-associated protein with death domain (FADD), which is recruited upon activation of Fas (15, 17). Complex II subsequently causes downstream activation of apoptosis signal by activating caspase cascade, resulting in the cleavage of initiator caspase 8 and effector caspase 3 leading to apoptosis (15, 17–19). However, NF-κB upregulation may intersect apoptotic pathway as it can promote the induction of various cellular apoptosis inhibitors such as TRAF1, TRAF2, cIAP-1, c-IAP-2, and X-linked inhibitor of apoptosis protein (XIAP) (15, 20).

acts as a signal for the release of apoptogenic factors such as cytochrome *c*, Smac (second mitochondria-derived activator of caspase)/DIABLO (direct inhibitor of apoptosis protein-binding protein), apoptosis-inducing factor, Omi/HtrA2, or endonuclease G from the mitochondria. Release of Smac/DIABLO and Omi/HtrA2 into cytosol has been shown to promote caspase activation by antagonizing the IAPs, which are formed following the NF-κB upregulation (16). This suggests that Bax upregulation in our study may have negated the effects of NF-κB signaling pathway to cause inhibition of apoptosis. In addition, Bax can also trigger caspase activation by forming a cytochrome *c*/apoptotic protease activating factor 1/caspase 9-complex, which can further cause cleavage of caspase 3, or by proceeding via caspase-independent death effectors (16, 24–26).

SKOV3 cell line has previously been reported to have a dysfunctional apoptosome, which causes the activation of caspase 9, to some extent, to further cleave caspase 3 (27). This is supported by our results since activation of caspase 9 was observed (data not shown), which was unable to activate caspase 3, suggesting that cleaved caspase 3 (**Figure 7B**) could not have arisen exclusively due to mitochondrial pathway and validated a crosstalk between intrinsic and extrinsic pathways. This observation appears to suggest that C1q-induced apoptosis in SKOV3 cells had taken place, primarily *via* the extrinsic pathway.

Ovarian cancer cells, including SKOV3 cancer cell line, exhibit constitutive activation of Akt/mTOR survival pathway, thus protecting the cancer cells from apoptosis (28). mTOR, a serine–threonine kinase, upon activation by Akt, forms

two distinct multi-protein complexes, mTOR complex 1 (mTORC1) and mTOR complex 2 (mTORC2). mTORC1 then phosphorylates p70S6K, an essential protein required for cell proliferation and G1 cell cycle progression (14, 29). Hence, we investigated if treatment of SKOV3 cells with C1q and globular heads modulated the gene expression of mTOR as well as components of mTORC1 [regulatory-associated protein of mTOR (RAPTOR)] (30) and mTORC2 [rapamycin-insensitive companion of mTOR (RICTOR)] (31). Following the treatment with C1q and globular head modules, the mRNA levels of mTOR, RICTOR, and RAPTOR were significantly downregulated at 6 h (**Figure 8A**). We also used immunofluorescence microscopy to show that there was a dramatic downregulation of mTOR at the protein level following treatment with C1q, ghA, ghB, or ghC (**Figure 8B**). These observations further supported that C1q and globular head modules not only induced apoptosis signaling pathway but also downregulated the cell survival regulators.

In conclusion, exogenous treatment of SKOV3 cells with C1q and recombinant globular head modules (ghA, ghB, and ghC) induce upregulation of TNF-α and Fas and induce apoptosis either independently, or *via* caspase cascade, in addition to downregulating the mTOR cell survival pathways. C1q has been shown to promote proliferation in the tumor microenvironment without involvement of complement activation C1q can act as an extracellular matrix protein, thus facilitating tumor growth and invasion. Experiments using C1q gene-deficient mice have also suggested that the frequency of proliferating tumor cells is considerably reduced *in vivo* (6). In another study, an opposite complement-independent function of C1q has been reported. C1q can induce apoptosis in DU145 prostate cancer cells *via* activation of WOX1, a tumor suppressor and a pro-apoptotic protein, and destabilize the cell adhesion (32). We report here that SKOV3 ovarian cancer cells are susceptible to apoptosis induction by C1q *via* TNF pathway.

C1q has a number of diverse functions including clearance of immune complexes, pathogens, and apoptotic and necrotic cells. Being the key molecule of the classical pathway of the complement system, it is a potent link between innate and adaptive immunity. However, C1q is a primordial innate immune molecule. The identification of C1q family (33, 34), based on the presence of gC1q domain, has given rise to the notion that C1q has several complement-independent functions (3). Indeed, C1q is involved in cellular differentiation, immunologic tolerance, pathology of pregnancy, developmental synaptic pruning, and extensive dialog with extracellular matrix proteins (4). Based on the jellyroll topology of the gC1q domain (33), it has also become evident that C1q is potentially a prototypical (ancestral) molecule of TNF family members, hence, existence of a C1q–TNF superfamily (1). Thus, of several overlaps of functions between C1q and TNF family members, the current study adds an additional layer of criss-cross mechanism, establishing the ability of C1q to regulate TNF-α in cancer, leading to apoptosis of the target cells. In this context, a cytokine-like property of C1q has been proposed recently (35). It is perhaps no co-incidence that the recombinant fragments of the gC1q domain of human C1q (ghA, ghB, and ghC) are able to induce apoptosis in SKOV3 cells.

It will be interesting to correlate the levels of C1q in serum and AF with the diagnosis and classification of the severity of the ovarian cancer. Due to the lack of a genuine mouse model of ovarian cancer, it will be pertinent to further establish the susceptibility and/or resistance of primary ovarian cancer cells to C1q-mediated induction of apoptosis.

AUTHOR CONTRIBUTIONS

AK carried out key experiments with technical help from SS and VM; FA and EK provided important reagents; AP provided technical and scientific supervision to the project; and UK led the work and, together with AK, wrote the manuscript.

REFERENCES

1. Kishore U, Gaboriaud C, Waters P, Shrive AK, Greenhough TJ, Reid KB, et al. C1q and tumor necrosis factor superfamily: modularity and versatility. *Trends Immunol* (2004) 25(10):551–61. doi:10.1016/j.it.2004.08.006
2. Kishore U, Reid KB. C1q: structure, function, and receptors. *Immunopharmacology* (2000) 49(1–2):159–70. doi:10.1016/S0162-3109(00)80301-X
3. Kouser L, Madhukaran SP, Shastri A, Saraon A, Ferluga J, Al-Mozaini M, et al. Emerging and novel functions of complement protein C1q. *Front Immunol* (2015) 6:317. doi:10.3389/fimmu.2015.00317
4. Kishore U, Thielens NM, Gaboriaud C. Editorial: state-of-the-art research on C1q and the classical complement pathway. *Front Immunol* (2016) 7:398. doi:10.3389/fimmu.2016.00398
5. van Kooten C, Fiore N, Trouw LA, Csomor E, Xu W, Castellano G, et al. Complement production and regulation by dendritic cells: molecular switches between tolerance and immunity. *Mol Immunol* (2008) 45(16):4064–72. doi:10.1016/j.molimm.2008.07.015
6. Bulla R, Tripodo C, Rami D, Ling GS, Agostinis C, Guarnotta C, et al. C1q acts in the tumour microenvironment as a cancer-promoting factor independently of complement activation. *Nat Commun* (2016) 7:10346. doi:10.1038/ncomms10346
7. Stevens B, Allen NJ, Vazquez LE, Howell GR, Christopherson KS, Nouri N, et al. The classical complement cascade mediates CNS synapse elimination. *Cell* (2007) 131(6):1164–78. doi:10.1016/j.cell.2007.10.036
8. Permuth-Wey J, Sellers TA. Epidemiology of ovarian cancer. *Methods Mol Biol* (2009) 472:413–37. doi:10.1007/978-1-60327-492-0_20
9. Bjørge L, Hakulinen J, Vintermyr O, Jarva H, Jensen TS, Iversen OE, et al. Ascitic complement system in ovarian cancer. *Br J Cancer* (2005) 92(5):895–905. doi:10.1038/sj.bjc.6602334
10. Ramsland PA, Hutchinson AT, Carter PJ. Therapeutic antibodies: discovery, design and deployment. *Mol Immunol* (2015) 67(2 Pt A):1–3. doi:10.1016/j.molimm.2015.05.004
11. Scott AM, Wolchok JD, Old LJ. Antibody therapy of cancer. *Nat Rev Cancer* (2012) 12(4):278–87. doi:10.1038/nrc3236
12. Tan LA, Yu B, Sim FCJ, Kishore U, Sim RB. Complement activation by phospholipids: the interplay of factor H and C1q. *Protein Cell* (2010) 1(11):1033–49. doi:10.1007/s13238-010-0125-8
13. Kishore U, Gupta SK, Perdikoulis MV, Kojouharova MS, Urban BC, Reid KB. Modular organization of the carboxyl-terminal, globular head region of

human C1q A, B, and C chains. *J Immunol* (2003) 171(2):812–20. doi:10.4049/jimmunol.171.2.812
14. Altomare DA, Wang HQ, Skele KL, De Rienzo A, Klein-Szanto AJ, Godwin AK, et al. AKT and mTOR phosphorylation is frequently detected in ovarian cancer and can be targeted to disrupt ovarian tumor cell growth. *Oncogene* (2004) 23(34):5853–7. doi:10.1038/sj.onc.1207721
15. Micheau O, Tschopp J. Induction of TNF receptor I-mediated apoptosis via two sequential signaling complexes. *Cell* (2003) 114(2):181–90. doi:10.1016/S0092-8674(03)00521-X
16. Saelens X, Festjens N, Walle LV, Van Gurp M, van Loo G, Vandenabeele P. Toxic proteins released from mitochondria in cell death. *Oncogene* (2004) 23(16):2861–74. doi:10.1038/sj.onc.1207523
17. Hsu H, Shu HB, Pan MG, Goeddel DV. TRADD-TRAF2 and TRADD-FADD interactions define two distinct TNF receptor 1 signal transduction pathways. *Cell* (1996) 84(2):299–308. doi:10.1016/S0092-8674(00)80984-8
18. Zhang SQ, Kovalenko A, Cantarella G, Wallach D. Recruitment of the IKK signalosome to the p55 TNF receptor: RIP and A20 bind to NEMO (IKKγ) upon receptor stimulation. *Immunity* (2000) 12(3):301–11. doi:10.1016/S1074-7613(00)80183-1
19. Fulda S, Debatin KM. Extrinsic versus intrinsic apoptosis pathways in anticancer chemotherapy. *Oncogene* (2006) 25(34):4798–811. doi:10.1038/sj.onc.1209608
20. Park YC, Ye H, Hsia C, Segal D, Rich RL, Liou H, et al. A novel mechanism of TRAF signaling revealed by structural and functional analyses of the TRADD–TRAF2 interaction. *Cell* (2000) 101(7):777–87. doi:10.1016/S0092-8674(00)80889-2
21. Lee SH, Meng XW, Flatten KS, Loegering DA, Kaufmann SH. Phosphatidylserine exposure during apoptosis reflects bidirectional trafficking between plasma membrane and cytoplasm. *Cell Death Differ* (2013) 20(1):64–76. doi:10.1038/cdd.2012.93
22. Ashkenazi A, Dixit VM. Death receptors: signaling and modulation. *Science* (1998) 281(5381):1305–8. doi:10.1126/science.281.5381.1305
23. Chan FK, Siegel RM, Lenardo MJ. Signaling by the TNF receptor superfamily and T cell homeostasis. *Immunity* (2000) 13(4):419–22. doi:10.1016/S1074-7613(00)00041-8
24. Yuan S, Yu X, Asara JM, Heuser JE, Ludtke SJ, Akey CW. The holo-apoptosome: activation of procaspase-9 and interactions with caspase-3. *Structure* (2011) 19(8):1084–96. doi:10.1016/j.str.2011.07.001
25. Würstle ML, Laussmann MA, Rehm M. The central role of initiator caspase-9 in apoptosis signal transduction and the regulation of its activation and activity on the apoptosome. *Exp Cell Res* (2012) 318(11):1213–20. doi:10.1016/j.yexcr.2012.02.013
26. Janicke RU, Sprengart ML, Wati MR, Porter AG. Caspase-3 is required for DNA fragmentation and morphological changes associated with apoptosis. *J Biol Chem* (1998) 273(16):9357–60. doi:10.1074/jbc.273.16.9357
27. Liu JR, Opipari AW, Tan L, Jiang Y, Zhang Y, Tang H, et al. Dysfunctional apoptosome activation in ovarian cancer: implications for chemoresistance. *Cancer Res* (2002) 62(3):924–31.
28. Peng D, Wang J, Zhou J, Wu GS. Role of the Akt/mTOR survival pathway in cisplatin resistance in ovarian cancer cells. *Biochem Biophys Res Commun* (2010) 394(3):600–5. doi:10.1016/j.bbrc.2010.03.029
29. Laplante M, Sabatini DM. mTOR signaling at a glance. *J Cell Sci* (2009) 122(Pt 20):3589–94. doi:10.1242/jcs.051011
30. Hara K, Maruki Y, Long X, Yoshino K, Oshiro N, Hidayat S, et al. Raptor, a binding partner of target of rapamycin (TOR), mediates TOR action. *Cell* (2002) 110(2):177–89. doi:10.1016/S0092-8674(02)00833-4
31. Sarbassov DD, Ali SM, Kim D, Guertin DA, Latek RR, Erdjument-Bromage H, et al. Rictor, a novel binding partner of mTOR, defines a rapamycin-insensitive and raptor-independent pathway that regulates the cytoskeleton. *Curr Biol* (2004) 14(14):1296–302. doi:10.1016/j.cub.2004.06.054
32. Hong Q, Sze C, Lin S, Lee M, He R, Schultz L, et al. Complement C1q activates tumor suppressor WWOX to induce apoptosis in prostate cancer cells. *PLoS One* (2009) 4(6):e5755. doi:10.1371/journal.pone.0005755
33. Shapiro L, Scherer PE. The crystal structure of a complement-1q family protein suggests an evolutionary link to tumor necrosis factor. *Curr Biol* (1998) 8(6):335–8. doi:10.1016/S0960-9822(98)70133-2
34. Ghai R, Waters P, Roumenina LT, Gadjeva M, Kojouharova MS, Reid KB, et al. C1q and its growing family. *Immunobiology* (2007) 212(4–5):253–66. doi:10.1016/j.imbio.2006.11.001
35. Ghebrehiwet B, Hosszu KK, Valentino A, Peerschke EI. The C1q family of proteins: insights into the emerging non-traditional functions. *Front Immunol* (2012) 3:52. doi:10.3389/fimmu.2012.00052

Conflict of Interest Statement: The authors declare that the research was conducted in the absence of any commercial or financial relationships that could be construed as a potential conflict of interest.

frontiers in Immunology

ORIGINAL RESEARCH
published: 31 July 2017
doi: 10.3389/fimmu.2017.00834

Protein–Protein Interaction between Surfactant Protein D and DC-SIGN *via* C-Type Lectin Domain Can Suppress HIV-1 Transfer

*Eswari Dodagatta-Marri[1], Daniel A. Mitchell[2], Hrishikesh Pandit[3], Archana Sonawani[3], Valarmathy Murugaiah[1], Susan Idicula-Thomas[3], Béatrice Nal[1,4], Maha M. Al-Mozaini[5], Anuvinder Kaur[1], Taruna Madan[3] and Uday Kishore[1]**

[1] Department of Life Sciences, College of Health and Life Sciences, Brunel University London, Uxbridge, United Kingdom, [2] Clinical Sciences Research Laboratories, Warwick Medical School, University Hospital Coventry and Warwickshire Campus, Coventry, United Kingdom, [3] Department of Innate Immunity, National Institute for Research in Reproductive Health, Indian Council of Medical Research, Mumbai, India, [4] Institute of Environment, Health and Societies, Brunel University London, Uxbridge, United Kingdom, [5] Department of Infection and Immunity, King Faisal Specialist Hospital and Research Centre, Riyadh, Saudi Arabia

Surfactant protein D (SP-D) is a soluble C-type lectin, belonging to the collectin (collagen-containing calcium-dependent lectin) family, which acts as an innate immune pattern recognition molecule in the lungs at other mucosal surfaces. Immune regulation and surfactant homeostasis are salient functions of SP-D. SP-D can bind to a range of viral, bacterial, and fungal pathogens and trigger clearance mechanisms. SP-D binds to gp120, the envelope protein expressed on HIV-1, through its C-type lectin or carbohydrate recognition domain. This is of importance since SP-D is secreted by human mucosal epithelial cells and is present in the female reproductive tract, including vagina. Another C-type lectin, dendritic cell (DC)-specific intercellular adhesion molecule-3-grabbing non-integrin (DC-SIGN), present on the surface of the DCs, also binds to HIV-1 gp120 and facilitates viral transfer to the lymphoid tissues. DCs are also present at the site of HIV-1 entry, embedded in vaginal or rectal mucosa. In the present study, we report a direct protein–protein interaction between recombinant forms of SP-D (rfhSP-D) and DC-SIGN *via* their C-type lectin domains. Both SP-D and DC-SIGN competed for binding to immobilized HIV-1 gp120. Pre-incubation of human embryonic kidney cells expressing surface DC-SIGN with rfhSP-D significantly inhibited the HIV-1 transfer to activated peripheral blood mononuclear cells. *In silico* analysis revealed that SP-D and gp120 may occupy same sites on DC-SIGN, which may explain the reduced transfer of HIV-1. In summary, we demonstrate, for the first time, that DC-SIGN is a novel binding partner of SP-D, and this interaction can modulate HIV-1 capture and transfer to $CD4^+$ T cells. In addition, the present study also reveals a novel and distinct mechanism of host defense by SP-D against HIV-1.

Keywords: surfactant protein D, DC-SIGN, HIV-1 infection, protein–protein interactions, gp120

OPEN ACCESS

Edited by:
Jagadeesh Bayry, Institut national de la santé et de la recherche médicale, France

Reviewed by:
Kenneth Reid, Green Templeton College University of Oxford, United Kingdom
Jiu-Yao Wang, National Cheng Kung University, Taiwan
Kevan Hartshorn, Boston University School of Medicine, United States

****Correspondence:***
Uday Kishore
uday.kishore@brunel.ac.uk, ukishore@hotmail.com

Specialty section:
This article was submitted to Molecular Innate Immunity, a section of the journal Frontiers in Immunology

Received: *22 December 2016*
Accepted: *03 July 2017*
Published: *31 July 2017*

Citation:
Dodagatta-Marri E, Mitchell DA, Pandit H, Sonawani A, Murugaiah V, Idicula-Thomas S, Nal B, Al-Mozaini MM, Kaur A, Madan T and Kishore U (2017) Protein–Protein Interaction between Surfactant Protein D and DC-SIGN via C-Type Lectin Domain Can Suppress HIV-1 Transfer. Front. Immunol. 8:834. doi: 10.3389/fimmu.2017.00834

INTRODUCTION

Surfactant protein D (SP-D) is a collagen-containing C-type lectin, belonging to the collectin family (1). The primary structure of human SP-D is composed of three subunits of polypeptide chains; each subunit consists of a short N-terminal region, a triple-helical collagen-like region, an α-helical coiled-coil neck region, and a calcium-dependent highly conserved C-type lectin or carbohydrate recognition domain (CRD) at the C-terminus (2, 3). The primary structure can get cross-linked *via* the cysteine-containing N-terminal region to give rise to a cruciform structure, which can undergo further multimerization to yield a fuzzy ball, where the CRD regions are facing toward the exterior. SP-D, *via* its homotrimeric CRD region, is known to interact with a wide range of viral, bacterial, and fungal pathogens and bring about clearance mechanisms that involve aggregation or agglutination, opsonization, enhanced phagocytosis, and super-oxidative burst (3, 4). Primarily found in the lungs as a part of pulmonary surfactant, SP-D has been localized at a range of extrapulmonary sites as a part of mucosal defense system (5).

SP-D is present throughout the female genital tract, with likely involvement in the prevention of uterine infections (6). Epithelial linings of vagina, cervix, uterus, fallopian tubes, and ovaries are positively immunostained for SP-D (7). SP-D has been shown to bind to different strains of HIV-1 (BaL and IIIB) at pH 7.4 (physiological) and 5.0 similar to the pH found in the female urogenital tract (8). Glycoprotein gp120, a highly conserved mannosylated oligosaccharide present on the envelope of HIV-1 virion, plays an important role in the viral entry and facilitates viral replication by activating the NF-κB pathway. SP-D has been shown to bind gp120 of various strains of HIV-1 and prevent HIV-1 interaction with CD4 receptor on T cells, thereby inhibiting viral entry and replication (9, 10).

Another pattern recognition immune regulatory molecule, DC-SIGN/CD209, a type-II transmembrane protein of 44 kDa present on dendritic cell (DC) surface (11), plays a major role in mediating DC adhesion, migration, inflammation, and activation of T cell. DC-SIGN can serve as a route of immune escape for pathogens and tumors (12) and is a known receptor for many viruses, including HIV-1 and HIV-2. DC-SIGN is expressed by both mature and immature DCs in lymphoid tissues (11, 13), but not on follicular DCs, plasmacytoid DCs or $CD1a^+$ Langerhans cells (14), monocytes, T cells, B cells, thymocytes, and $CD34^+$ bone marrow cells. It is also expressed by polarized (M2) macrophages that infiltrate tumors (15), and on antigen-presenting cells such as macrophages, and in chorionic villi of placenta (16). Cells expressing DC-SIGN are located in T cell area of lymph nodes, tonsils, and spleen and dermal DCs in skin ($CD14^+$ macrophages) (17). DC-SIGN expressing cells are seen in mucosal tissue of rectum (18) (with high antigen-presenting capacities), cervix, and uterus, in hepatic sinusoid and lymphatic sinus (19, 20).

HIV-1 virus, when exposed to genital and anal mucosal tissues, binds to DC-SIGN on tissue embedded DCs (21, 22) and gets transmitted to $CD4^+$ T cells, activating adaptive immune response (23, 24). DC-SIGN facilitates HIV-1 transmission in both *cis* and *trans* fashion (25). Expression of DC-SIGN is regulated by IL-4 during monocyte–DC differentiation pathway, along with GM-CSF (26). TGF-β and IFNs are known to be inhibitors of DC-SIGN expression, and, thus, indirectly regulate HIV-1 transmission (26).

The interaction between HIV-1 and DC-SIGN takes place in the mucosal tract where SP-D is present. Since both SP-D and DC-SIGN can bind gp120, we set out to examine if interplay between these proteins can modulate DC-SIGN-mediated viral transfer of HIV-1. This view was further substantiated by observations that SP-D levels are increased in the broncho-alveolar fluid of HIV-1 patients (27); and recombinant forms of SP-D (rfhSP-D) can bind to gp120 of HIV-1, acting as a potent inhibitor of viral infection *in vitro via* inhibition of the interaction between CD4 and gp120 (10). In this study, we show, using recombinant forms of tetrameric and monomeric forms of DC-SIGN and its homolog, DC-SIGNR, that there is a protein–protein interaction between the two C-type lectins *via* CRD regions. They compete for binding to HIV-1 gp120, and thus, SP-D suppresses DC-SIGN mediated transfer of HIV-1 to $CD4^+$ cells.

MATERIALS AND METHODS

Recombinant Expression and Purification of Soluble Forms of Tetrameric and Monomeric DC-SIGN and DC-SIGNR

E. coli strain BL21 (λDE3) (Invitrogen, UK) was transformed with pT5T plasmid encoding DC-SIGN and DC-SIGNR sequences (inserted at the BamHI restriction site into plasmid construct) with and without multimerizing neck region. In the presence of neck region, the bacterial cells expressed tetrameric DC-SIGN and DC-SIGNR; without the neck region, the corresponding constructs produced monomeric forms of DC-SIGN and DC-SIGNR (28). *E. coli* strain BL21 (λDE3) cells containing ampicillin (50 μg/ml) (Sigma-Aldrich) resistant plasmids [except in the case of DC-SIGNR monomer expressing construct that was kanamycin (50 μg/ml) (Sigma-Aldrich) resistant] were subcultured overnight at 37°C. One liter LB medium containing ampicillin or kanamycin was inoculated with 10 ml of overnight bacterial culture and grown at 37°C until the OD_{600} reached 0.7, and then induced with 0.5 mM isopropyl β-D-1-thiogalactopyranoside (IPTG). After 3 h, the bacterial cells were centrifuged at 13,800 × *g* for 15 min to collect the bacterial pellet. Protein expression was analyzed *via* 12% SDS-PAGE.

The cell pellet was treated with 22 ml of lysis buffer, containing 100 mM Tris, pH 7.5, 0.5 M NaCl, lysozyme (50 μg/ml), 2.5 mM EDTA, pH 8.0, and 0.5 mM phenylmethylsulfonyl fluoride (PMSF), and left to stir for 1 h at 4°C. Cells were then sonicated for 10 cycles, each cycle of 30 sec with 2 min interval. The sonicated cell suspension was spun at 10,000 × *g* for 15 min at 4°C. The inclusion bodies, present in the pellet, were solubilized in 20 ml of 6 M urea, 10 mM Tris–HCl, pH 7.0, and 0.01% β-mercaptoethanol (β-ME) by rotating on a shaker for 1 h at 4°C. The mixture was then centrifuged at 13,000 × *g* for 30 min at 4°C and the supernatant was drop-wise diluted fivefold with loading buffer containing 25 mM Tris–HCl, pH 7.8, 1 M NaCl, and 2.5 mM $CaCl_2$ with gentle stirring. This was then dialyzed against 2 l of loading buffer with three buffer changes every 3 h. Following further centrifugation

at 13,000 × *g* for 15 min at 4°C, the supernatant was loaded onto a Mannan agarose column (5 ml; Sigma) pre-equilibrated with the loading buffer. The column was washed with five bed volumes of the loading buffer and the bound protein was eluted in 1 ml fractions using the elution buffer containing 25 mM Tris–HCl, pH 7.8, 1 M NaCl, and 2.5 mM EDTA. The absorbance was read at 280 nm and the peak fractions were frozen at −20. Purity of protein was analyzed by 15% w/v SDS-PAGE.

Expression and Purification of rfhSP-D

E. coli BL21 (λDE3) pLysS containing plasmid pUK-D1 (containing cDNA sequences for 8 Gly–X–Y repeats, neck, and CRD region of human SP-D) was cultured in ampicillin (100 μg/ml) (Sigma-Aldrich) and chloramphenicol (50 μg/ml) (Sigma-Aldrich) at 37°C overnight. Expression and purification was carried out as described earlier (29, 30). Bacterial cells were grown until the OD_{600} reached 0.6 to 0.8, then induced with 0.4 mM IPTG and allowed to grow for an additional three hours. Cells were then pelleted *via* centrifugation and was re-suspended in 50 ml of lysis buffer (50 mM Tris–HCl, pH 7.5, 200 mM NaCl, 5 mM EDTA with freshly added 0.1 mM PMSF, and 100 μg/ml lysozyme) at 4°C for 1 h. The cell lysate was then sonicated at 4 kHz for 30 s with 2 min interval for 15 cycles. The sonicate was centrifuged at 13,800 × *g* for 15 min at 4°C to collect the rfhSP-D-rich pellet containing inclusion bodies. 25 ml of solubilization buffer (50 mM Tris–HCl, pH 7.5, 100 mM NaCl, 5 mM EDTA, 6 M urea) was used to re-suspend the pellet, and incubated at 4°C for 1 h. The dialysate was then centrifuged at 13,800 × *g*, at 4°C for 15 min, and the supernatant was dialyzed against solubilization buffer containing 4 M urea and 10 mM β-ME for 2 h at 4°C. The dialysis buffer was serially changed to solubilization buffer containing 2, 1, and 0 M urea at 4°C, 2 h each. Final dialysis was done in solubilization buffer containing 5 mM $CaCl_2$ for 3 h to completely remove any traces of urea. The dialysate was centrifuged at 13,800 × g, 4°C for 15 min and the clear supernatant containing rfhSP-D was affinity-purified using maltosyl-agarose column (Sigma-Aldrich). The bound protein was eluted with solubilization buffer containing 10 mM EDTA, pH 7.5. Endotoxin levels were removed by passing the purified protein fractions through Polymyxin B column (Detoxi-Gel, Peirce & Warriner, UK) and the levels were measured using the Limulus Amebocyte Lysate Assay (BioWhitaker, UK). The endotoxin level was found to be <5 pg/μg rfhSP-D.

SDS-PAGE and Far Western Blot Analysis

DC-SIGN and DC-SIGNR proteins were separated on a 12% (w/v) SDS-PAGE under reducing conditions. After electrophoresis, the polyacrylamide gels were stained with Coomassie Brilliant Blue. For the far western blotting, proteins were electrotransferred onto polyvinylidene difluoride (PVDF) membrane (Sigma) and blocked with 5% w/v milk in PBS. The membrane bound proteins were probed with rfhSP-D (5 μg/ml) for 2 h, followed by addition of anti-SP-D (1:1,000) (Medical Research Council Immunochemistry Unit, Oxford) polyclonal antibodies. The blot was then probed with Protein A-HRP Conjugate (1:1,000) (Sigma), followed by color development with diaminobenzidine as a substrate (Sigma-Aldrich, UK).

ELISA

Microtitre wells were coated with DC-SIGN and DC-SIGNR proteins in carbonate/bicarbonate buffer, pH 9.6 in decreasing double dilutions (5–0.625 μg/well) in duplicates and left overnight at 4°C. The microtiter wells were blocked with 2% w/v BSA in PBS for 2 h at 37°C. The wells were then washed three times with PBS + 0.05% v/v Tween 20 and incubated with a constant concentration (2.5 μg) of rfhSP-D in 20 mM Tris–HCl, pH 7.5, 100 mM NaCl, 5 mM $CaCl_2$ or 5 mM EDTA at 37°C for 1 h, followed by 1 h at 4°C. Following PBS + Tween 20 wash, the bound rfhSP-D was detected using anti-SP-D (1:5,000) polyclonal antibody and Protein A-HRP conjugate (1:5,000). Color was developed using *o*-Phenylenediamine (OPD) as a substrate and absorbance was measured at 490 nm.

Competitive ELISA

The ability of rfhSP-D to compete with and DC-SIGN for binding to HIV-1 gp120 (Abcam; ab167715) gp120 was analyzed by competitive ELISA. Gp120 was coated at 250 ng/well in duplicates and left overnight at 4°C. Wells were blocked with 2% BSA in PBS for 2 h at 37°C. The wells were washed three times with PBS + 0.05% v/v Tween 20. A constant concentration of DC-SIGN tetramer (5 μg/ml) and decreasing concentrations of rfhSP-D (5 − 0.625 μg/well) in calcium buffer were added to the wells, which were subsequently probed with anti-DC-SIGN (1:5000) polyclonal antibodies. Following washes, the wells were incubated with Protein HRP conjugate (1:1,000). Color was developed using OPD as a substrate.

Fluorescence Microscopy

Human embryonic kidney cells 293 (HEK 293), transfected with DC-SIGN construct (DC–HEK) (31), were grown and maintained in DMEM (Life technologies, UK) containing 10% v/v fetal calf serum, 2 mM L-glutamine, penicillin (100 U/ml)/streptomycin (100 μg/ml) (Thermo Fisher), and blasticidin (5 μg/ml) (Gibco). HEK 293 cells were grown and maintained in DMEM (Life technologies) containing 10% FBS. Both cell lines were grown under standard conditions (37°C, 5% v/v CO_2) until 80–90% confluency was reached. HEK 293 and DC–HEK cells (0.5×10^5) were grown on the coverslips in a 24-well plate (Nunc) overnight to perform three different sets of immunofluorescence experiments; DC-SIGN expression (primary antibody: rabbit anti-DC-SIGN, 1:500 and secondary antibody: anti-rabbit/CY3, 1:500, Thermo Fisher), rfhSP-D (10 μg/ml) binding to DC-SIGN (primary antibody: monoclonal anti-SP-D, 1:500 and secondary antibody: anti-mouse conjugated/CY5, 1:500, Abcam) and co-localization of DC-SIGN and rfhSP-D (primary antibodies: anti-DC-SIGN polyclonal and anti-SP-D monoclonal, 1:500 and secondary antibodies: anti-rabbit/CY3 and anti-mouse/FITC, 1:500) on the cell surface of DC–HEK cells. HEK 293 cells were used as a control for all experiments and DC–HEK cells were incubated with secondary antibody alone as an additional control. Hoechst (1:10,000, Thermo Fisher) was used to stain the nucleus for all the staining experiments. The cells were incubated for 1 h with primary antibody followed by 1 h incubation with secondary antibodies as described earlier with three times

phosphate-buffered saline (PBS, Thermo Fisher) washes between each step. For rfhSP-D binding with DC-SIGN analysis, the rfhSP-D was incubated with the cells for 1 h at 4°C. The cells were fixed with 4% paraformaldehyde (Sigma) before mounting on the coverslips to visualize under a HF14 Leica DM4000 microscope.

Viral Transfer Assay

Pooled human peripheral blood mononuclear cells (PBMCs) (HiMedia Laboratories, India) were stimulated in RPMI 1640 medium (Sigma-Aldrich) containing 10% v/v FBS, 1% Penicillin–Streptomycin and 5 µg/ml phytohemaglutinin (PHA) and 10 U/ml of rhIL-2 (Gibco) for 24 h. PHA/IL-2 was washed off and activated PBMCs were cultured further in complete RPMI medium. For the experiment, DC–HEK cells were grown in a 12-well tissue culture plate until 80% confluence in complete DMEM/F12 (Sigma-Aldrich, USA) containing 10% FBS (Gibco) and blasticidin. Indicated concentrations of rfhSP-D containing 5 mM $CaCl_2$ was added to each well and incubated for 2 h to allow binding to DC-SIGN. The wells without rfhSP-D were used as controls. Excess protein was removed, and cells were challenged for 1 h with 5 ng/ml p24 of HIV-1 SF-162 strain (kindly provided by Dr. Jay Levy, AIDS Program, National Institutes of Health, USA). 5 mM EDTA was added along with the virus in EDTA controls. Unbound virus was washed off and DC–HEK cells were cocultured with PHA/IL-2 activated PBMCs for 24 h to facilitate transfer. PBMCs along with the medium were then

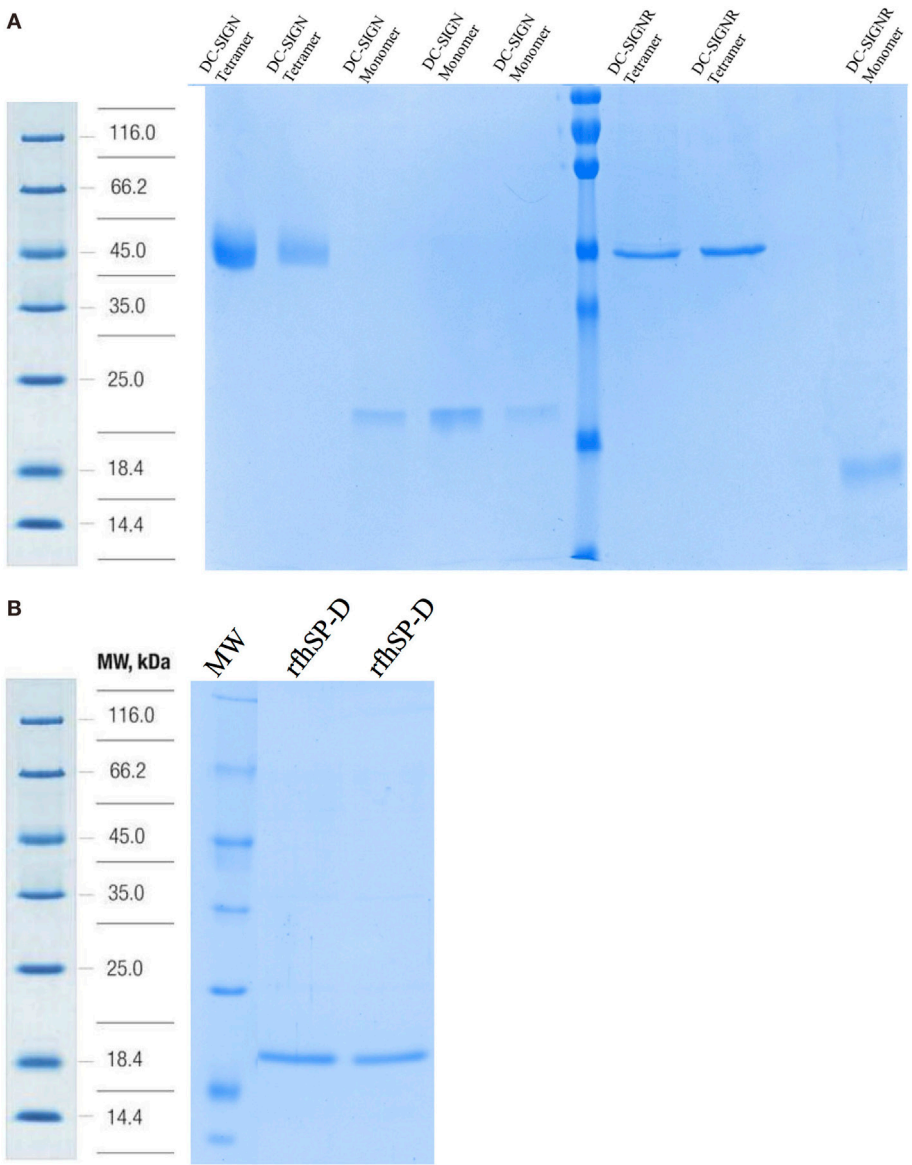

FIGURE 1 | SDS-PAGE analysis of purified recombinant forms of DC-SIGN, DC-SIGNR, and recombinant forms of SP-D (rfhSP-D). **(A)** 12% SDS-PAGE of affinity-purified tetrameric and monomeric forms of DC-SIGN and DC-SIGNR under reduced conditions. **(B)** 12% v/v SDS-PAGE of affinity-purified rfhSP-D.

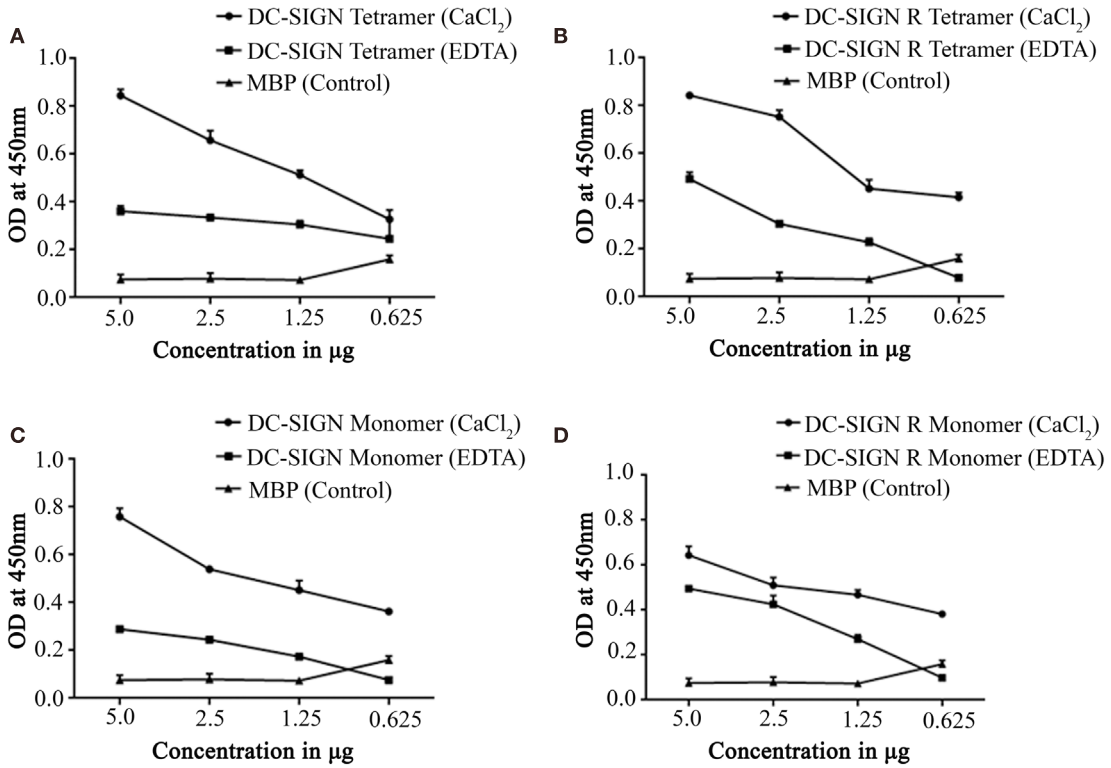

FIGURE 2 | Direct binding ELISA showing interaction between recombinant forms of SP-D (rfhSP-D) and DC-SIGN/DC-SIGNR. DC-SIGN tetramer **(A)**, DC-SIGNR tetramer **(B)**, DC-SIGN monomer **(C)**, and DC-SIGNR monomer **(D)** were coated at decreasing double dilutions from 5 to 0.625 µg/well and then probed with 2.5 µg of rfhSP-D in either in calcium or EDTA buffer. The binding was detected using anti-human surfactant protein D polyclonal antibodies (1:5,000 dilutions). The data represent mean and SD values of at least five experiments.

separated (siphoned off) from the DC–HEK monolayer and were transferred to fresh plates. They were cultured further in RPMI 1640 medium containing 10% FBS for 7 days, and viral titers were determined in supernatants on day 4 and 7 using HIV-1 p24 antigen ELISA kit (XpressBio Life Science Products, Frederick, MD, USA).

Molecular Modeling and Bioinformatics

The crystal structures of trimeric human lung SP-D (PDB ID: 1PW9), CD4 bound to HIV-1 envelope glycoprotein gp120 (PDB ID:1GC1) and homo 10-mer DC-SIGN complexed with sugars (PDB ID:1K9I) were retrieved from Protein Data Bank. The tetrameric form of non-glycosylated DC-SIGN was used for docking studies as this structure was found to bind to rfhSP-D *in vitro* experiments. DC-SIGN tetramer was docked to CD4 already bound to HIV-1 envelope glycoprotein gp120 (PDB ID: 1GC1) using Patch Dock server with default parameters.

The CRD-mediated protein–protein interaction between trimeric SP-D and tetrameric DC-SIGN, as observed in this study was further examined by docking these two molecules using ZDOCK algorithm of Discovery Studio (Accelrys Inc.). The best pose of these two molecules was subsequently docked into gp120 using Patch Dock server. The shortlisted poses from PatchDock and ZDOCK were further refined using Fire Dock and RDOCK, respectively.

RESULTS

rfhSP-D and DC-SIGN Can Interact with Each Other *via* Their C-Type Lectin Domains

Structurally, DC-SIGN is composed of an extracellular domain (ECD) which exists as a tetramer, stabilized by an N-terminal α-helical neck region, followed by a CRD. DC-SIGN and DC-SIGNR comprising of the entire ECD (tetramer) (**Figure 1A**) and the CRD region alone (monomer) (**Figure 1A**) were expressed in *E. coli* and affinity-purified on Mannose-agarose (28). The CRD regions of DC-SIGN and SIGNR bound mannose weakly as majority of the proteins appeared in the flow through. The ECD domains of both DC-SIGN and DC-SIGNR bound to mannose with much greater affinity in the presence of Ca^{2+} and eluted with EDTA. A recombinant form of human SP-D, containing 8 Gly–X–Y repeats of the collagen, neck, and CRD regions were expressed and purified as homotrimeric molecules, as described earlier (29, 30) (**Figure 1B**). Tetrameric and monomeric forms of DC-SIGN and DC-SIGNR were checked for their respective interactions with rfhSP-D *via* ELISA (**Figure 2**), which showed a calcium- and dose-dependent interaction between the two lectins; tetrameric forms bound rfhSP-D better than the monomers. This was confirmed by a far western blot (**Figure 3A**), which revealed that rfhSP-D was able to bind to DC-SIGN and DC-SIGNR

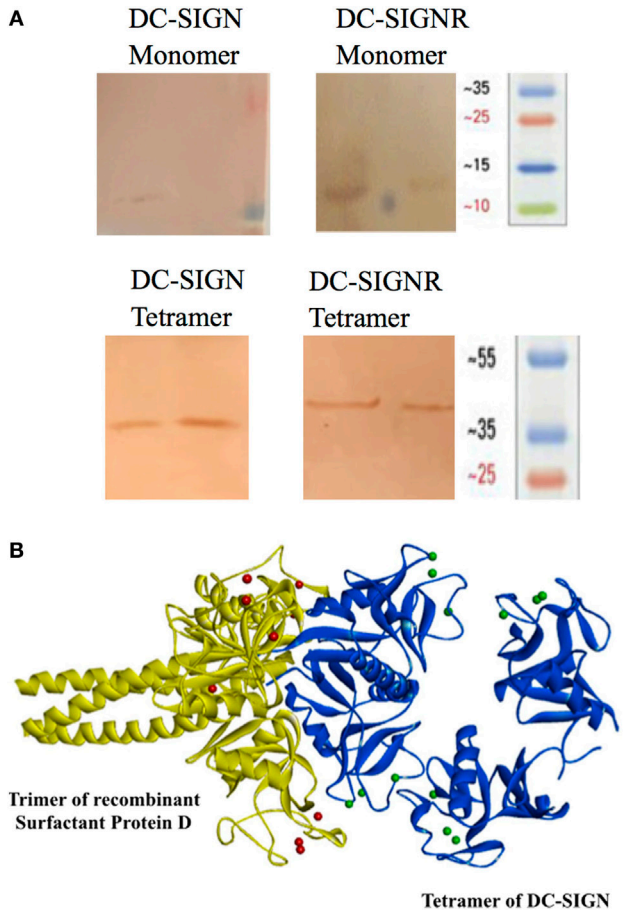

FIGURE 3 | Far western blot to detect binding of recombinant forms of SP-D (rfhSP-D) to PVDF bound DC-SIGN and DC-SIGNR. **(A)** Tetrameric and monomeric variants of DC-SIGN and DC-SIGNR were run on a SDS-PAGE and were transferred to a PVDF membrane followed by incubation with 5 μg/ml rfhSP-D and then probed with anti-SP-D polyclonal antibody. **(B)** Docked structure of trimeric surfactant protein D (SP-D) (yellow cartoon) and tetrameric DC-SIGN (blue cartoon). The two molecules interact *via* their carbohydrate recognition domains.

proteins immobilized on PVDF membrane. The CRD-mediated protein–protein interaction between trimeric SP-D and tetrameric DC-SIGN was further studied by docking these two molecules. The docked pose showed that the two molecules likely interact *via* their CRD regions (**Figure 3B**).

rfhSP-D:DC-SIGN Interaction Leads to Competition for Binding to HIV-1 gp120

To examine if rfhSP-D can inhibit the binding of DC-SIGN to gp120, we carried out a competitive ELISA. As expected, both rfhSP-D and DC-SIGN tetramer bound gp120 in a dose- and calcium-dependent manner (data not shown) (32). In order to assess a likely interference by rfhSP-D in DC-SIGN: gp120 interaction, a constant concentration of DC-SIGN tetramer was used against different concentrations of rfhSP-D and added to solid-phase gp120 (**Figure 4**). With increasing concentration, rfhSP-D was able to inhibit DC-SIGN-gp120 interaction, suggesting that

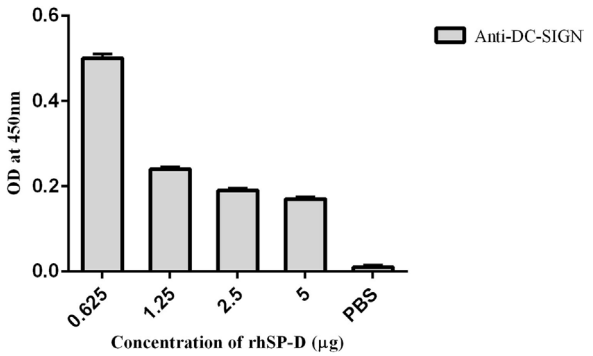

FIGURE 4 | Competitive inhibition ELISA to show that recombinant form of SP-D (rfhSP-D) inhibits DC-SIGN binding to immobilized HIV-1 gp120. HIV-1 gp120 trimer (250 ng per well) was first coated to which 5–0.625 μg/well of rfhSP-D and a constant concentration (5 μg/well) of DC-SIGN tetramer were added. Bound DC-SIGN tetramer was detected by anti-DC-SIGN polyclonal antibodies. Protein A-HRP conjugate (1:1,000) was used to detect the antibodies bound and color was developed using *o*-Phenylenediamine. 0 in the graph represents the control where only PBS was used instead of gp120, and the experiments were repeated three times.

the binding sites on these two C-type lectins for gp120 may be overlapping.

rfhSP-D Co-Localizes with DC-SIGN on the Surface of Transfected HEK 293 Cells

Human embryonic kidney cells transfected with DC-SIGN construct (DC–HEK cells) were shown to express DC-SIGN *via* immunofluorescence microscopy. The DC-SIGN expression seen on the cell surface on DC–HEK cells was evenly distributed, as compared to HEK 293 cells, which were used as a control, using anti-DC-SIGN polyclonal antibody (**Figure 5A**). DC–HEK cells, incubated with secondary antibody alone, did not show any expression (**Figure 5A**). rfhSP-D binding was visible on the cell surface of DC–HEK cells, whereas rfhSP-D binding could not be detected in either HEK 293 cells or DC–HEK cells incubated with secondary antibody alone as controls (**Figure 5B**). rfhSP-D and DC-SIGN co-localized on the HEK cell surface transfected with DC-SIGN construct (**Figure 5C**).

rfhSP-D Inhibits DC-SIGN-Mediated Viral Transfer to PBMCs in a Dose-Dependent Manner

To understand whether interaction between rfhSP-D and DC-SIGN impacted upon DC-SIGN-mediated HIV-1 transfer to T cells, we performed a coculture assay using DC–HEK cells and mitogen-activated PBMCs. Presence of rfhSP-D led to a significantly ($p < 0.005$) reduced HIV-1 p24 levels in day 4 and day 7 PBMC culture supernatants in a dose-dependent manner (**Figure 6**). This suggested that, in presence of rfhSP-D, the viral uptake by DC–HEK was significantly inhibited resulting in reduced transfer and replication of HIV-1 in PBMC cultures. It is likely that rfhSP-D may have occupied sites on both DC-SIGN as well as HIV-1 gp120 that resulted in reduced

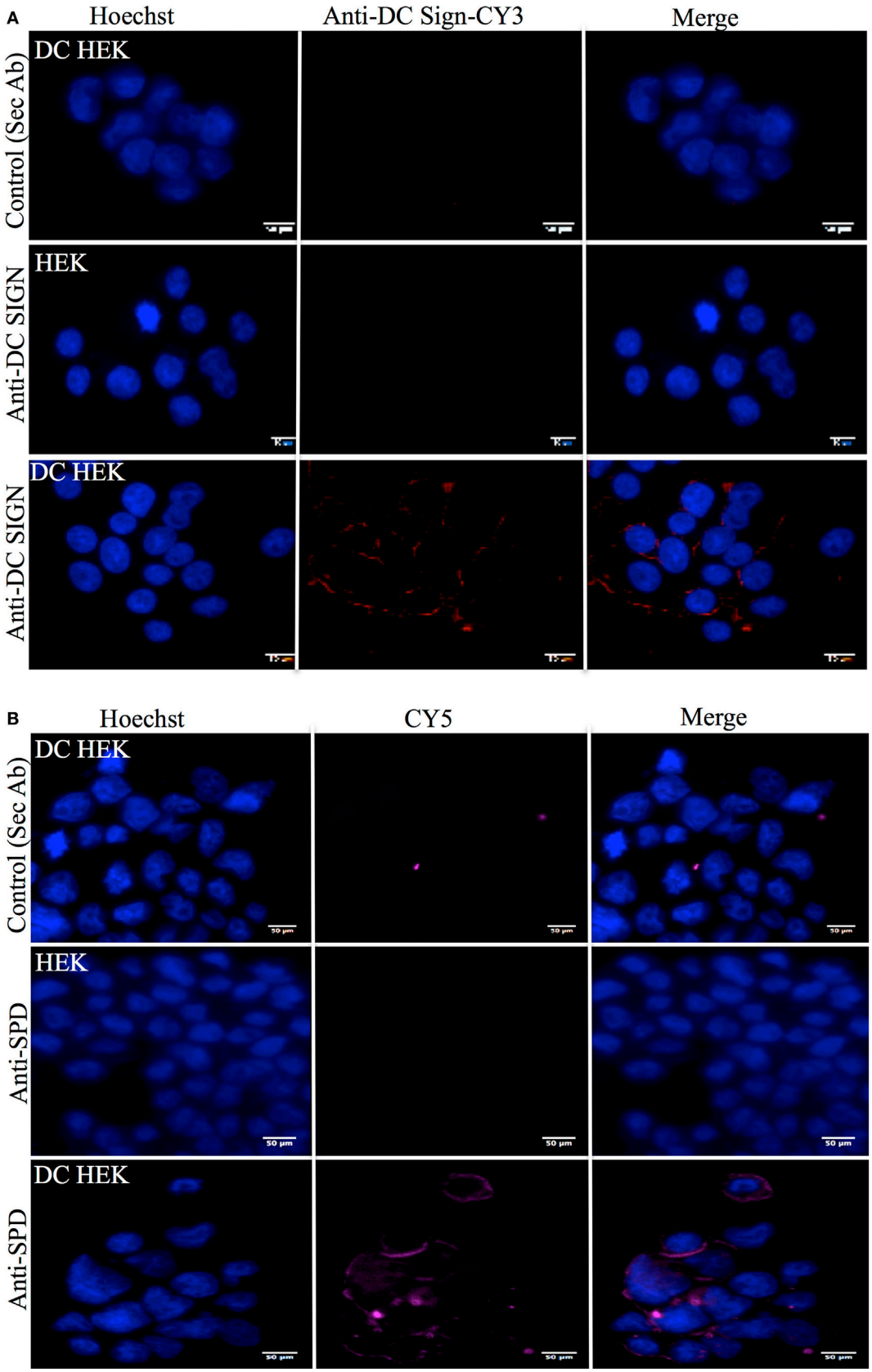

FIGURE 5 | Continued

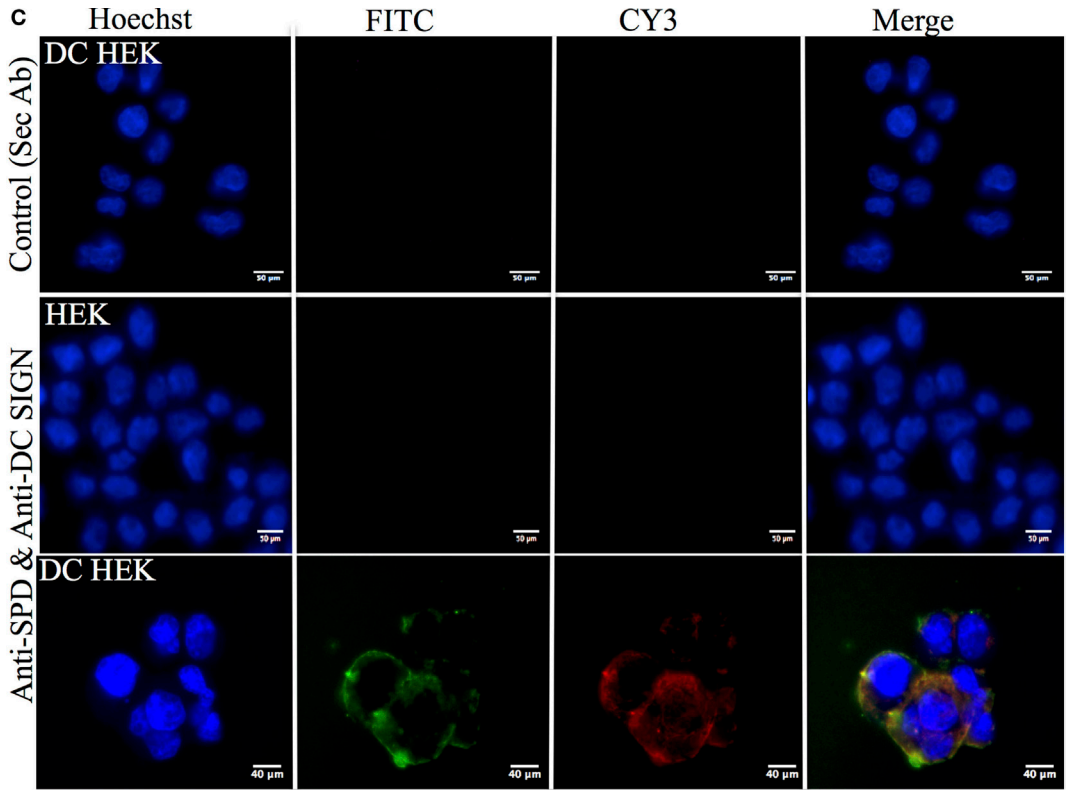

FIGURE 5 | Immunofluorescence microscopy to show recombinant forms of SP-D (rfhSP-D) binding to DC-SIGN on the surface of the human embryonic kidney (HEK) cells transfected with DC-SIGN construct (DC–HEK cells). **(A)** DC–HEK cells incubated with anti-rabbit/CY3 did not show DC-SIGN expression (control). DC–HEK and HEK cells incubated with anti-DC-SIGN followed by anti-rabbit conjugated with CY3 showed the DC-SIGN expression in DC–HEK cells only and not HEK cells. Hoechst was used to stain the nucleus. **(B)** Analysis of rfhSP-D binding to DC-SIGN on the DC–HEK cells *via* immunofluorescence. DC–HEK cells incubated with anti-SP-D for 1 h and then probed with anti-mouse/CY5 did not show binding. DC–HEK cells incubated with rfhSP-D (5 µg/ml) for 1 h, followed by anti-SP-D for 1 h and then anti-mouse/CY5 showed the binding on the cell surface. **(C)** DC-SIGN expression and rfhSP-D binding co-localization analysis *via* immunofluorescence microscopy. DC–HEK cells incubated with secondary antibodies only (anti-mouse/FITC and anti-rabbit/FITC) for 1 h did not show immunofluorescence. DC–HEK and HEK cells incubated with rfhSP-D for 1 h prior to incubation anti-SP-D monoclonal and anti-DC-SIGN polyclonal for 1 h followed by anti-mouse/FITC and anti-rabbit/CY3 for 1 h showed co-localization for rfhSP-D binding and DC–HEK expression.

DC-SIGN interaction with HIV-1 gp120. EDTA significantly inhibited DC–HEK-mediated viral transfer, as reported previously (33).

Bioinformatics Analysis Revealed That HIV-1 gp120 and rfhSP-D May Occupy the Same Site on the CRDs of DC-SIGN

To support our hypothesis that DC-SIGN once bound to rfhSP-D may not interact with gp120, we performed *in silico* analyses. The best-docked pose of rfhSP-D and DC-SIGN was subsequently docked to gp120 using Patch Dock server. The shortlisted poses from Patch Dock and ZDOCK were further refined using Fire Dock and RDOCK, respectively. Two poses appear to suggest that HIV-1 gp120 and rfhSP-D possibly occupy the same site on the CRD of DC-SIGN (**Figure 7**). Thus, in the presence of rfhSP-D, it is likely that interaction of DC-SIGN with gp120 could be inhibited. To validate our bioinformatics strategy, we evaluated the known interaction of gp120 with DC-SIGN followed by docking with CD4. DC-SIGN binds to gp120 at a site distant from its CD4 binding site, and hence, DC-SIGN-bound HIV-1 possibly interacts with CD4 for viral transmission (**Figure 8**). The global energy of these docked complexes has also been presented (**Table 1**).

DISCUSSION

In this study, we report, for the first time, an interaction of DC-SIGN and SP-D, two C-type lectins and pattern recognition receptors; both proteins are known to bind to HIV-1 gp120. We demonstrate that this interaction involves their CRD domains, which is relevant in inhibiting DC-SIGN-mediated HIV-1 trans-infection of $CD4^+$ T cells. Interaction of HIV-1 gp120 with DC-SIGN not only increases the affinity of gp120 for CD4 (34) but also leads to a productive infection *via* reactivation of provirus involving NF-κB pathway (35, 36). This interaction also results in downregulation of Nef-induced release of IL-6 (37) and leads to Ask-1-dependent activation leading to induction of apoptosis of human DCs (38). Simultaneous binding of rfhSP-D to both

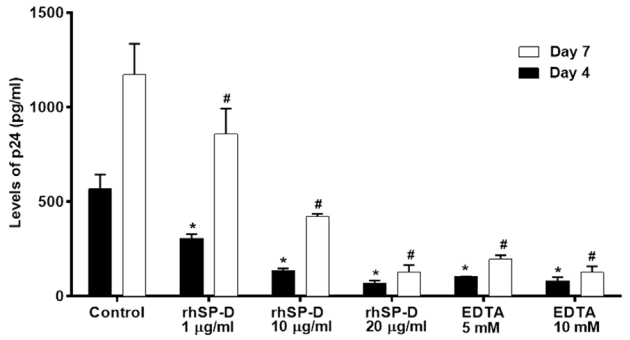

FIGURE 6 | DC-SIGN-mediated HIV-1 transfer assay. DC–HEK cells were grown in a 12-well plate until 80% confluence. 20, 10, and 1 μg/ml of recombinant forms of SP-D (rfhSP-D) concentrations were added to the cells and incubated for 2 h for binding. Unbound protein was removed and cells were challenged with 2.5 ng/ml p24 of HIV-1 (SF-162 strain) for 1 h (to bind to DC-SIGN). After 1 h, unbound virus was washed off and cells were cocultured with phytohemaglutinin-activated peripheral blood mononuclear cells (PBMCs) for 24 h. This allows the DC-SIGN captured virus to be transferred to $CD4^+$ cells, where virus will multiply. PBMCs were separated from the monolayer and cultured separately for 4 days to determine viral titer.

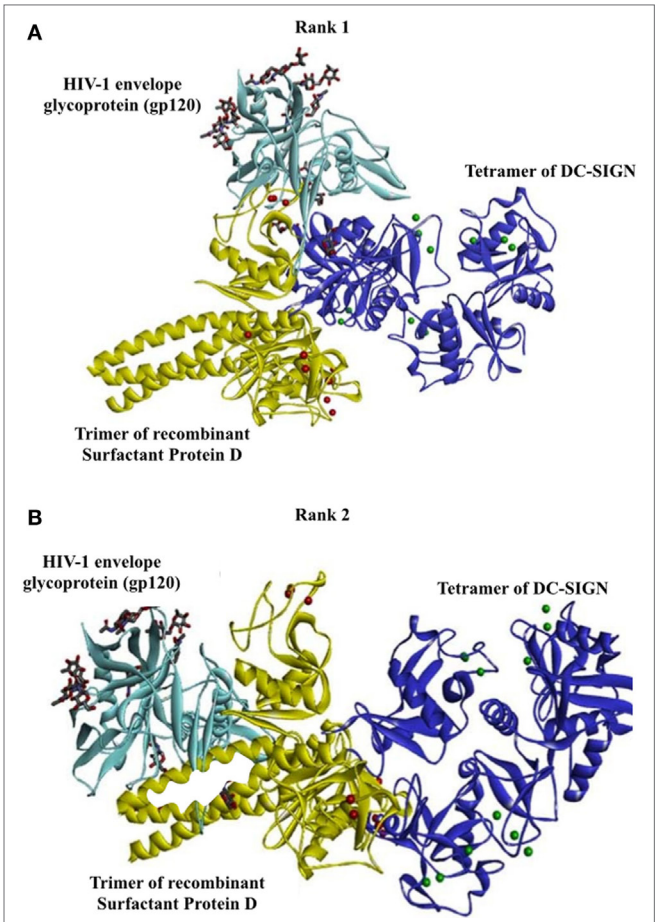

FIGURE 7 | Two poses suggesting that HIV-1 gp120 and recombinant forms of SP-D possibly occupy the same site on carbohydrate recognition domain of DC-SIGN. Docked structures of surfactant protein D trimer (yellow cartoon and calcium ions as red spheres) complexed with DC-SIGN tetramer (blue cartoon and calcium ions as green spheres) and HIV-1 envelope glycoprotein, gp120 (cyan cartoon). The sugars present in gp120 are shown as sticks. The calcium ions of DC-SIGN are represented as green spheres. **(A)** Rank no. 1. **(B)** Rank no. 2.

gp120 and DC-SIGN, thus, may result in blockade of DC-SIGN-mediated viral transmission and inhibition of replication.

Structure–function studies have revealed that the CRD region of DC-SIGN is the specific ligand-binding site that is reliant on the neck region within the extracellular domain (ECD) (39). This notion was validated in our binding ELISA type assays when we used the tetrameric forms of DC-SIGN and DC-SIGNR (comprising of the ECD and CRD region) as well as the monomeric forms, which only consist of the CRD region. The binding studies involving rfhSP-D highlighted that multimeric forms of DC-SIGN and DC-SIGNR bind better, not surprisingly, due to multivalent nature of interactions. Since DC-SIGN promotes HIV-1 infection, we examined if rfhSP-D by virtue to its ability to bind gp120 as well as DC-SIGN can potentially interfere with HIV-1 (40–42). We also included DC-SIGNR (DC-SIGN-Related), a homolog of DC-SIGN, in our study. DC-SIGNR, expressed on endothelium including liver sinusoidal, lymph node sinuses, and placental capillary, can also bind gp120 to facilitate HIV-1 viral infection (43).

The current study provides the first evidence that DC-SIGN is a novel immune receptor or adaptor for the CRD region of SP-D, modulating the HIV-1 infection. Interaction of gp120 and rfhSP-D is calcium dependent as reported earlier (8–10). Tetrameric DC-SIGN also efficiently binds gp120 in a dose-dependent manner, which is not significantly inhibited in presence of sugars similar to previous reports (28, 44). The recombinant rfhSP-D has been shown to inhibit the gp120-CD4 interaction (10) while, DC-SIGN-bound trimeric gp140 interacts with CD4 more avidly (34). *In vitro* competitive assays and the bioinformatics analysis confirmed that rfhSP-D and DC-SIGN compete for gp120. The reduced p24 levels confirmed that rfhSP-D significantly inhibits the DC-SIGN mediated viral transfer.

The rfhSP-D molecule (a recombinant fragment of human SP-D comprising homotrimeric C-type lectins), with part of collagen region, α-helical coiled-coil neck, and CRD region, has been extensively studied *via in vitro*, *in vivo*, and *ex vivo* experiments. In a number of studies, rfhSP-D has worked at par with full-length SP-D, as evident from its ability to be therapeutic in murine models of allergic bronchopulmonary aspergillosis (45, 46), invasive pulmonary aspergillosis (45), and dust mite allergy (47). It can also induce apoptosis in activated eosinophils (29, 48) and PBMCs (49). Thus, rfhSP-D is an excellent well-tested therapeutically active molecule.

Mannose-binding lectin, another serum collectin, is also known to inhibit DC-SIGN-mediated trans-infection of HIV-1 T cells (50) whereas SP-A and SP-D facilitate this transfer (8, 51). Madsen et al. incubated SP-D-HIV-1 complexes with immature monocyte-derived DCs and demonstrated increased viral uptake and transfer from DCs to PM-1 cells. However, the assay system employed in the two studies (Madsen and ours) significantly differed, thus the observed variation in the results. Further studies in appropriate animal models will

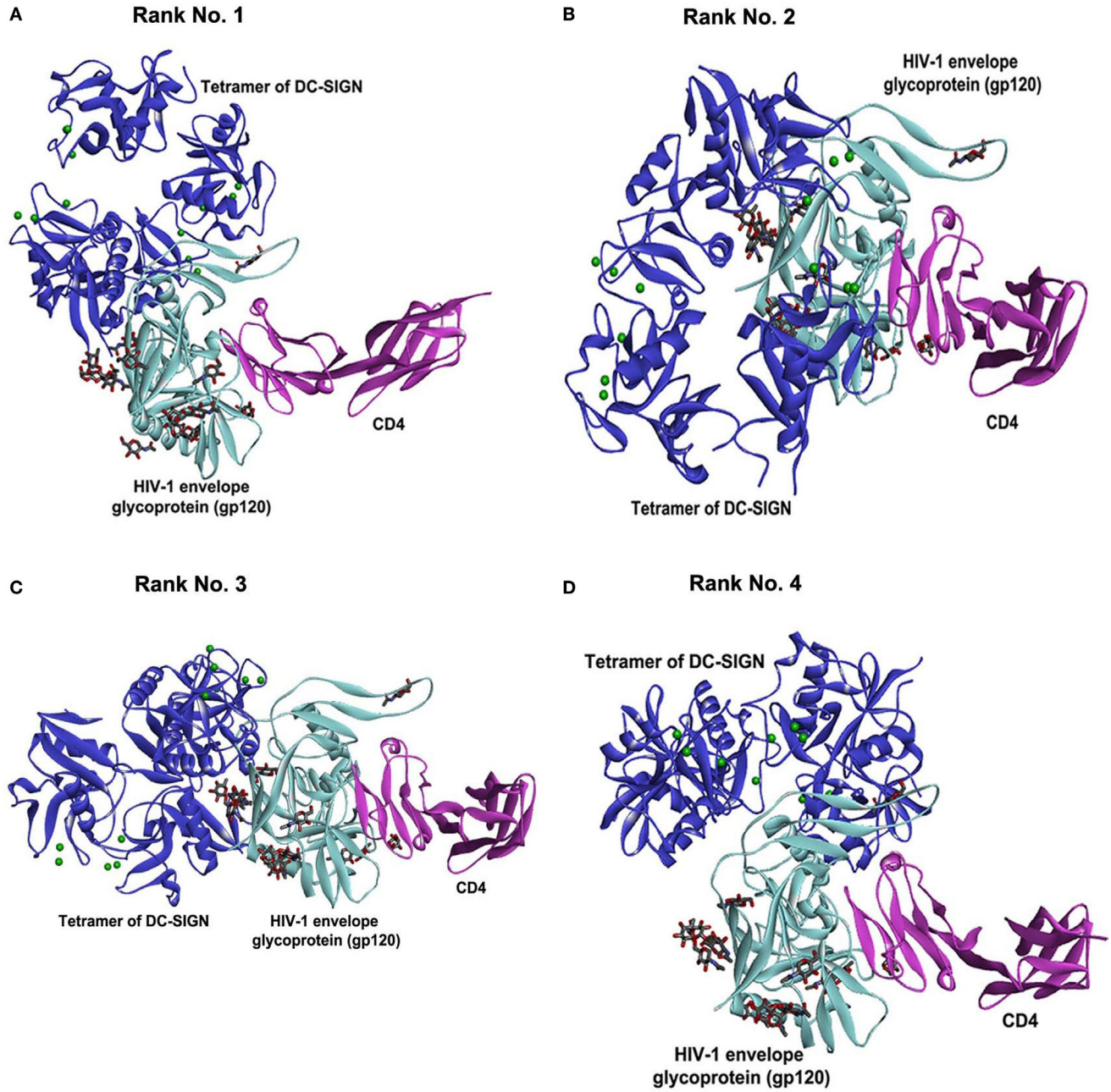

FIGURE 8 | Known interaction of gp120 with DC-SIGN followed by docking with CD4. Selected docked poses of tetrameric DC-SIGN (blue cartoon) and HIV-1 envelope glycoprotein gp120 (cyan cartoon) bound to CD4 (pink cartoon). The sugars present in gp120 are shown as sticks. **(A)** Rank no. 1. **(B)** Rank no. 2. **(C)** Rank no. 3. **(D)** Rank no. 4.

TABLE 1 | Energy for docked complexes of DC-SIGN and gp120 bound to CD4 refined using FireDock.

Rank no.	Global energy (kcal/mol)
1	−27.01
2	−21.83
3	−11.99
4	−10.94

help to determine the overall effects of SP-D and DC-SIGN binding during virus infections. Our findings have revealed a new phenomenon in SP-D-mediated viral transfer through DCs as rfhSP-D occupies similar sites as gp120 on DC-SIGN. Hence, pre-incubation of rfhSP-D may have occupied gp120-binding site on DC-SIGN (displacement of gp120 *via* ELISA and *in silico* analysis), resulting in poor uptake. This must

have resulted in reduced transfer of viral particles to activated PBMCs, adding another aspect to rfhSP-D-mediated anti-HIV activity.

To summarize, rfhSP-D has the ability to directly inhibit the viral entry by interacting with gp120 and to significantly inhibit the DC-SIGN-mediated viral transfer. Importantly, these molecular interactions inhibit the immunomodulation mediated by gp120 and DC-SIGN further disfavoring the HIV-1 pathogenesis. DC-SIGN binding to SP-D could be one of the ligand–receptor interactions that in turn could play a major role in the inhibition of viral entry. Further, *in vivo* assays and clinical trials can elucidate the physiological conditions for therapeutic purposes against the infection.

ACKNOWLEDGMENTS

We are extremely grateful to Dr. Peter Kwong and Marie Pancerea, Structural Biology Section, NIAIDS, NIH for providing PDB coordinates of HIV-1 gp120 modelled with glycans.

AUTHOR CONTRIBUTIONS

ED-M, DM, HP, and AK carried out crucial set of experiments; supporting experiments were done by AS, VM, ST, BN, and MA-M; TM supervised critical infection assays; UK led the project and wrote the manuscript with due help from ED-M, HP, and TM.

REFERENCES

1. Holmskov U, Thiel S, Jensenius JC. Collections and ficolins: humoral lectins of the innate immune defense. *Annu Rev Immunol* (2003) 21:547–78. doi:10.1146/annurev.immunol.21.120601.140954
2. Kishore U, Reid KB. Structures and functions of mammalian collectins. *Results Probl Cell Differ* (2001) 33:225–48. doi:10.1007/978-3-540-46410-5_12
3. Kishore U, Greenhough TJ, Waters P, Shrive AK, Ghai R, Kamran MF, et al. Surfactant proteins SP-A and SP-D: structure, function and receptors. *Mol Immunol* (2006) 43:1293–315. doi:10.1016/j.molimm.2005.08.004
4. Tino MJ, Wright JR. Surfactant protein A stimulates phagocytosis of specific pulmonary pathogens by alveolar macrophages. *Am J Physiol* (1996) 270:L677–88.
5. Nayak A, Dodagatta-Marri E, Tsolaki AG, Kishore U. An insight into the diverse roles of surfactant proteins, SP-A and SP-D in innate and adaptive immunity. *Front Immunol* (2012) 3:131. doi:10.3389/fimmu.2012.00131
6. Madhukaran SP, Alhamlan FS, Kale K, Vatish M, Madan T, Kishore U. Role of collectins and complement protein C1q in pregnancy and parturition. *Immunobiology* (2016) 221:1273–88. doi:10.1016/j.imbio.2016.06.002
7. Leth-Larsen R, Floridon C, Nielsen O, Holmskov U. Surfactant protein D in the female genital tract. *Mol Hum Reprod* (2004) 10:149–54. doi:10.1093/molehr/gah022
8. Madsen J, Gaiha GD, Palaniyar N, Dong T, Mitchell DA, Clark HW. Surfactant Protein D modulates HIV infection of both T-cells and dendritic cells. *PLoS One* (2013) 8:e59047. doi:10.1371/journal.pone.0059047
9. Meschi J, Crouch EC, Skolnik P, Yahya K, Holmskov U, Leth-Larsen R, et al. Surfactant protein D binds to human immunodeficiency virus (HIV) envelope protein gp120 and inhibits HIV replication. *J Gen Virol* (2005) 86:3097–107. doi:10.1099/vir.0.80764-0
10. Pandit H, Gopal S, Sonawani A, Yadav AK, Qaseem AS, Warke H, et al. Surfactant protein D inhibits HIV-1 infection of target cells via interference with gp120-CD4 interaction and modulates pro-inflammatory cytokine production. *PLoS One* (2014) 9:e102395. doi:10.1371/journal.pone.0102395
11. Geijtenbeek TB, Krooshoop DJ, Bleijs DA, van Vliet SJ, van Duijnhoven GC, Grabovsky V, et al. DC-SIGN-ICAM-2 interaction mediates dendritic cell trafficking. *Nat Immunol* (2000) 1:353–7. doi:10.1038/79815
12. van Kooyk Y, Geijtenbeek TB. DC-SIGN: escape mechanism for pathogens. *Nat Rev Immunol* (2003) 3:697–709. doi:10.1038/nri1182
13. Bleijs DA, Geijtenbeek TB, Figdor CG, van Kooyk Y. DC-SIGN and LFA-1: a battle for ligand. *Trends Immunol* (2001) 22:457–63. doi:10.1016/S1471-4906(01)01974-3
14. Engering A, Geijtenbeek TB, van Vliet SJ, Wijers M, van Liempt E, Demaurex N, et al. The dendritic cell-specific adhesion receptor DC-SIGN internalizes antigen for presentation to T cells. *J Immunol* (2002) 168:2118–26. doi:10.4049/jimmunol.168.5.2118
15. Dominguez-Soto A, Sierra-Filardi E, Puig-Kroger A, Perez-Maceda B, Gomez-Aguado F, Corcuera MT, et al. Dendritic cell-specific ICAM-3-grabbing non-integrin expression on M2-polarized and tumor-associated macrophages is macrophage-CSF dependent and enhanced by tumor-derived IL-6 and IL-10. *J Immunol* (2011) 186:2192–200. doi:10.4049/jimmunol.1000475
16. Soilleux EJ, Morris LS, Lee B, Pohlmann S, Trowsdale J, Doms RW, et al. Placental expression of DC-SIGN may mediate intrauterine vertical transmission of HIV. *J Pathol* (2001) 195:586–92. doi:10.1002/path.1026
17. Ochoa MT, Loncaric A, Krutzik SR, Becker TC, Modlin RL. "Dermal dendritic cells" comprise two distinct populations: CD1+ dendritic cells and CD209+ macrophages. *J Invest Dermatol* (2008) 128:2225–31. doi:10.1038/jid.2008.56
18. Kamada N, Hisamatsu T, Honda H, Kobayashi T, Chinen H, Kitazume MT, et al. Human CD14+ macrophages in intestinal lamina propria exhibit potent antigen-presenting ability. *J Immunol* (2009) 183:1724–31. doi:10.4049/jimmunol.0804369
19. Jameson B, Baribaud F, Pohlmann S, Ghavimi D, Mortari F, Doms RW, et al. Expression of DC-SIGN by dendritic cells of intestinal and genital mucosae in humans and rhesus macaques. *J Virol* (2002) 76:1866–75. doi:10.1128/JVI.76.4.1866-1875.2002
20. Zhou T, Chen Y, Hao L, Zhang Y. DC-SIGN and immunoregulation. *Cell Mol Immunol* (2006) 3:279–83.
21. Royce RA, Sena A, Cates W Jr, Cohen MS. Sexual transmission of HIV. *N Engl J Med* (1997) 336:1072–8. doi:10.1056/NEJM199704103361507
22. Masurier C, Salomon B, Guettari N, Pioche C, Lachapelle F, Guigon M, et al. Dendritic cells route human immunodeficiency virus to lymph nodes after vaginal or intravenous administration to mice. *J Virol* (1998) 72:7822–9.
23. Banchereau J, Briere F, Caux C, Davoust J, Lebecque S, Liu YJ, et al. Immunobiology of dendritic cells. *Annu Rev Immunol* (2000) 18:767–811. doi:10.1146/annurev.immunol.18.1.767
24. Banchereau J, Steinman RM. Dendritic cells and the control of immunity. *Nature* (1998) 392:245–52. doi:10.1038/32588
25. Soilleux EJ, Coleman N. Expression of DC-SIGN in human foreskin may facilitate sexual transmission of HIV. *J Clin Pathol* (2004) 57:77–8. doi:10.1136/jcp.57.1.77
26. Relloso M, Puig-Kroger A, Pello OM, Rodriguez-Fernandez JL, de la Rosa G, Longo N, et al. DC-SIGN (CD209) expression is IL-4 dependent and is negatively regulated by IFN, TGF-beta, and anti-inflammatory agents. *J Immunol* (2002) 168:2634–43. doi:10.4049/jimmunol.168.6.2634
27. Jambo KC, French N, Zijlstra E, Gordon SB. AIDS patients have increased surfactant protein D but normal mannose binding lectin levels in lung fluid. *Respir Res* (2007) 8:42. doi:10.1186/1465-9921-8-42
28. Mitchell DA, Fadden AJ, Drickamer K. A novel mechanism of carbohydrate recognition by the C-type lectins DC-SIGN and DC-SIGNR. Subunit organization and binding to multivalent ligands. *J Biol Chem* (2001) 276:28939–45. doi:10.1074/jbc.M104565200
29. Mahajan L, Madan T, Kamal N, Singh VK, Sim RB, Telang SD, et al. Recombinant surfactant protein-D selectively increases apoptosis in eosinophils of allergic asthmatics and enhances uptake of apoptotic eosinophils by macrophages. *Int Immunol* (2008) 20:993–1007. doi:10.1093/intimm/dxn058

30. Dodagatta-Marri E, Qaseem AS, Karbani N, Tsolaki AG, Waters P, Madan T, et al. Purification of surfactant protein D (SP-D) from pooled amniotic fluid and bronchoalveolar lavage. *Methods Mol Biol* (2014) 1100:273–90. doi:10.1007/978-1-62703-724-2_22
31. Lang SM, Bynoe MO, Karki R, Tartell MA, Means RE. Kaposi's sarcoma-associated herpesvirus K3 and K5 proteins down regulate both DC-SIGN and DC-SIGNR. *PLoS One* (2013) 8:e58056. doi:10.1371/journal.pone.0058056
32. Hong PW, Nguyen S, Young S, Su SV, Lee B. Identification of the optimal DC-SIGN binding site on human immunodeficiency virus type 1 gp120. *J Virol* (2007) 81:8325–36. doi:10.1128/JVI.01765-06
33. Pohlmann S, Leslie GJ, Edwards TG, Macfarlan T, Reeves JD, Hiebenthal-Millow K, et al. DC-SIGN interactions with human immunodeficiency virus: virus binding and transfer are dissociable functions. *J Virol* (2001) 75:10523–6. doi:10.1128/JVI.75.21.10523-10526.2001
34. Hijazi K, Wang Y, Scala C, Jeffs S, Longstaff C, Stieh D, et al. DC-SIGN increases the affinity of HIV-1 envelope glycoprotein interaction with CD4. *PLoS One* (2011) 6:e28307. doi:10.1371/journal.pone.0028307
35. Gringhuis SI, Geijtenbeek TB. Carbohydrate signaling by C-type lectin DC-SIGN affects NF-kappaB activity. *Methods Enzymol* (2010) 480:151–64. doi:10.1016/S0076-6879(10)80008-4
36. van der Sluis RM, Jeeninga RE, Berkhout B. Establishment and molecular mechanisms of HIV-1 latency in T cells. *Curr Opin Virol* (2013) 3:700–6. doi:10.1016/j.coviro.2013.07.006
37. Sarkar R, Mitra D, Chakrabarti S. HIV-1 gp120 protein downregulates Nef induced IL-6 release in immature dendritic cells through interplay of DC-SIGN. *PLoS One* (2013) 8:e59073. doi:10.1371/journal.pone.0059073
38. Chen Y, Hwang SL, Chan VS, Chung NP, Wang SR, Li Z, et al. Binding of HIV-1 gp120 to DC-SIGN promotes ASK-1-dependent activation-induced apoptosis of human dendritic cells. *PLoS Pathog* (2013) 9:e1003100. doi:10.1371/journal.ppat.1003100
39. Lozach PY, Lortat-Jacob H, de Lacroix de Lavalette A, Staropoli I, Foung S, Amara A, et al. DC-SIGN and L-SIGN are high affinity binding receptors for hepatitis C virus glycoprotein E2. *J Biol Chem* (2003) 278:20358–66. doi:10.1074/jbc.M301284200
40. Balzarini J, Van Damme L. Microbicide drug candidates to prevent HIV infection. *Lancet* (2007) 369:787–97. doi:10.1016/S0140-6736(07)60202-5
41. Balzarini J, Van Laethem K, Daelemans D, Hatse S, Bugatti A, Rusnati M, et al. Pradimicin A, a carbohydrate-binding nonpeptidic lead compound for treatment of infections with viruses with highly glycosylated envelopes, such as human immunodeficiency virus. *J Virol* (2007) 81:362–73. doi:10.1128/JVI.01404-06
42. Hoorelbeke B, Xue J, LiWang PJ, Balzarini J. Role of the carbohydrate-binding sites of griffithsin in the prevention of DC-SIGN-mediated capture and transmission of HIV-1. *PLoS One* (2013) 8:e64132. doi:10.1371/journal.pone.0064132
43. Bashirova AA, Geijtenbeek TB, van Duijnhoven GC, van Vliet SJ, Eilering JB, Martin MP, et al. A dendritic cell-specific intercellular adhesion molecule 3-grabbing nonintegrin (DC-SIGN)-related protein is highly expressed on human liver sinusoidal endothelial cells and promotes HIV-1 infection. *J Exp Med* (2001) 193:671–8. doi:10.1084/jem.193.6.671
44. Geijtenbeek TB, van Kooyk Y. DC-SIGN: a novel HIV receptor on DCs that mediates HIV-1 transmission. *Curr Top Microbiol Immunol* (2003) 276:31–54.
45. Madan T, Kishore U, Singh M, Strong P, Clark H, Hussain EM, et al. Surfactant proteins A and D protect mice against pulmonary hypersensitivity induced by *Aspergillus fumigatus* antigens and allergens. *J Clin Invest* (2001) 107:467–75. doi:10.1172/JCI10124
46. Madan T, Kaur S, Saxena S, Singh M, Kishore U, Thiel S, et al. Role of collectins in innate immunity against aspergillosis. *Med Mycol* (2005) 43(Suppl 1): S155–63. doi:10.1080/13693780500088408
47. Singh M, Madan T, Waters P, Parida SK, Sarma PU, Kishore U. Protective effects of a recombinant fragment of human surfactant protein D in a murine model of pulmonary hypersensitivity induced by dust mite allergens. *Immunol Lett* (2003) 86:299–307. doi:10.1016/S0165-2478(03)00033-6
48. Mahajan L, Gautam P, Dodagatta-Marri E, Madan T, Kishore U. Surfactant protein SP-D modulates activity of immune cells: proteomic profiling of its interaction with eosinophilic cells. *Expert Rev Proteomics* (2014) 11:355–69. doi:10.1586/14789450.2014.897612
49. Pandit H, Thakur G, Koippallil Gopalakrishnan AR, Dodagatta-Marri E, Patil A, Kishore U, et al. Surfactant protein D induces immune quiescence and apoptosis of mitogen-activated peripheral blood mononuclear cells. *Immunobiology* (2016) 221:310–22. doi:10.1016/j.imbio.2015.10.004
50. Spear GT, Zariffard MR, Xin J, Saifuddin M. Inhibition of DC-SIGN-mediated trans infection of T cells by mannose-binding lectin. *Immunology* (2003) 110:80–5. doi:10.1046/j.1365-2567.2003.01707.x
51. Gaiha GD, Dong T, Palaniyar N, Mitchell DA, Reid KB, Clark HW. Surfactant protein A binds to HIV and inhibits direct infection of CD4+ cells, but enhances dendritic cell-mediated viral transfer. *J Immunol* (2008) 181:601–9. doi:10.4049/jimmunol.181.1.601

Conflict of Interest Statement: The authors declare that the research was conducted in the absence of any commercial or financial relationships that could be construed as a potential conflict of interest.

frontiers in Immunology

ORIGINAL RESEARCH
published: 08 May 2018
doi: 10.3389/fimmu.2018.00533

Human Properdin Modulates Macrophage: *Mycobacterium bovis* BCG Interaction *via* Thrombospondin Repeats 4 and 5

Maha Ahmed Al-Mozaini[1,2], Anthony G. Tsolaki[1], Munirah Abdul-Aziz[1,3], Suhair M. Abozaid[1,2], Mohammed N. Al-Ahdal[2], Ansar A. Pathan[1], Valarmathy Murugaiah[1], Evgeny M. Makarov[1], Anuvinder Kaur[1], Robert B. Sim[3], Uday Kishore[1] and Lubna Kouser[1]**

[1] College of Health and Life Sciences, Brunel University London, London, United Kingdom, [2] Department of Infection and Immunity, King Faisal Specialist Hospital and Research Centre, Riyadh, Saudi Arabia, [3] Department of Biochemistry, Oxford University, Oxford, United Kingdom

Mycobacterium tuberculosis can proficiently enter macrophages and diminish complement activation on its cell surface. Within macrophages, the mycobacterium can suppress macrophage apoptosis and survive within the intracellular environment. Previously, we have shown that complement regulatory proteins such as factor H may interfere with pathogen–macrophage interactions during tuberculosis infection. In this study, we show that *Mycobacterium bovis* BCG binds properdin, an upregulator of the complement alternative pathway. TSR4+5, a recombinant form of thrombospondin repeats 4 and 5 of human properdin expressed in tandem, which is an inhibitor of the alternative pathway, was also able to bind to *M. bovis* BCG. Properdin and TSR4+5 were found to inhibit uptake of *M. bovis* BCG by THP-1 macrophage cells in a dose-dependent manner. Quantitative real-time PCR revealed elevated pro-inflammatory responses (TNF-α, IL-1β, and IL-6) in the presence of properdin or TSR4+5, which gradually decreased over 6 h. Correspondingly, anti-inflammatory responses (IL-10 and TGF-β) showed suppressed levels of expression in the presence of properdin, which gradually increased over 6 h. Multiplex cytokine array analysis also revealed that properdin and TSR4+5 significantly enhanced the pro-inflammatory response (TNF-α, IL-1β, and IL-1α) at 24 h, which declined at 48 h, whereas the anti-inflammatory response (IL-10) was suppressed. Our results suggest that properdin may interfere with mycobacterial entry into macrophages via TSR4 and TSR5, particularly during the initial stages of infection, thus affecting the extracellular survival of the pathogen. This study offers novel insights into the non-complement related functions of properdin during host–pathogen interactions in tuberculosis.

Keywords: complement, cytokine, properdin, macrophage, *Mycobacterium tuberculosis*, *Mycobacterium bovis* BCG, phagocytosis, thrombospondin repeats

OPEN ACCESS

Edited by:
Cees Van Kooten,
Leiden University, Netherlands

Reviewed by:
Michael Kirschfink,
Universität Heidelberg, Germany
Lubka T. Roumenina,
INSERM UMRS 1138, France

***Correspondence:**
Uday Kishore
uday.kishore@brunel.ac.uk,
ukishore@hotmail.com;
Lubna Kouser
lubna_k@hotmail.co.uk

Specialty section:
This article was submitted to Molecular Innate Immunity, a section of the journal Frontiers in Immunology

Received: *03 July 2017*
Accepted: *01 March 2018*
Published: *08 May 2018*

Citation:
Al-Mozaini MA, Tsolaki AG, Abdul-Aziz M, Abozaid SM, Al-Ahdal MN, Pathan AA, Murugaiah V, Makarov EM, Kaur A, Sim RB, Kishore U and Kouser L (2018) Human Properdin Modulates Macrophage: Mycobacterium bovis BCG Interaction via Thrombospondin Repeats 4 and 5. Front. Immunol. 9:533. doi: 10.3389/fimmu.2018.00533

INTRODUCTION

Properdin is an upregulator of the alternative pathway of complement activation. In one of the three pathways of the complement system, the alternative pathway, the activation of the major complement opsonin, C3, is driven by a complex serine protease, C3bBb, also called the C3 convertase, which is bound to the surface of the complement-activating target. To form C3bBb, factor B associates

with C3b in the presence of Mg^{2+} and factor D, a serine protease, which cleaves factor B into Bb and Ba fragments producing a C3 convertase C3bBb (1). This complex, which has a half-life of 90 s, is stabilized by the binding of properdin, which increases the half-life by 5- to 10-fold (2). Furthermore, C3b molecules are generated by C3bBb and deposited near to the surface-bound convertase leading to the opsonization of the target and formation of C5 convertase, producing C5a and C5b, leading on to the lytic pathway and cell lysis (3).

The monomer of human properdin (53 kDa) has a flexible rod-like structure with a length of 26 nm and a diameter of 2.5 nm, composed of seven thrombospondin type I repeats (TSR). Each TSR is of about 60 amino acids, typically containing six conserved cysteine residues: these occur in TSR1–TSR6 (4–6), but the N-terminal domain, TSR0, is truncated. TSR4 is crucial for binding to C3bBb and TSR5 for binding to C3bBb, suggesting that both TSRs may be important for stabilizing the C3 convertase complex (5). Recently, TSR4+5, expressed as a double domain, has been shown to bind to properdin ligands such as C3b and inhibit the alternative complement pathway (7). These studies demonstrate the important role that these TSRs may play in the alternative pathway and in their interaction with pathogens.

Properdin circulates in plasma at a concentration of about 4–25 μg/ml existing as cyclic oligomers, dimer, trimer, and tetramer in a ratio of 26:54:20 (4). The dissociation and reassociation of properdin upon denaturation–renaturation cycles stimulated by guanidine or low pH indicates properdin ratio stability in solution (8). The interaction between properdin monomers involves the N-terminal end of one monomer and the C-terminal end of another (9). Properdin can also bind to microbial surfaces of several pathogens, including *Neisseria gonorrhoeae* (10), *Salmonella typhimurium* lipopolysaccharide (LPS), *Neisseria meningitidis* lipooligosaccharide (11), and *Chlamydia pneumoniae* (12). Binding of properdin to microbial surfaces results in the recruitment of fluid phase C3b, inducing assembly of C3 convertase C3bBb and causing further deposition of C3b on the pathogen surface (13–15), subsequently generating a C5 convertase, MAC formation, and cell lysis. At 10 μg/ml, recombinant properdin enhanced complement deposition on *N. meningitidis* and *S. pneumoniae* and dramatically enhanced serum lysis of these bacteria, and in the mouse model, significantly reduced bacteremia and increased survival rates (16).

Although *Mycobacterium tuberculosis* and its close-relative *Mycobacterium bovis* have significant interaction with components of the innate immune system, e.g., toll-like receptors, complement, surfactant proteins SP-A and SP-D (17), the initial stages of tuberculosis pathogenesis remain poorly understood. Many bacteria have evolved mechanisms to evade immune responses: by inhibiting complement activation by proteolytic cleavage of complement proteins, having their own complement inhibitors (18), or binding complement regulatory proteins like factor H (15, 19).

Mycobacterium tuberculosis is a highly specialized intracellular pathogen and may exploit complement proteins to enhance its uptake by macrophages. Although it has been shown that *M. tuberculosis* can activate all three pathways of the complement system (20, 21), it is unclear how the pathogen uses complement proteins in tuberculosis pathogenesis. *M. tuberculosis* has been shown to bind to complement receptors (CR) CR1, CR3, and CR4 and gain entry into macrophages (22–24). There is also evidence that enhanced phagocytosis of *M. tuberculosis* by human alveolar and monocyte-derived macrophages results from C3 opsonization (24). The ability of *M. tuberculosis* to bind to CR3 non-opsonically has also been shown which may be important for bacterial invasion when complement is sparse, for example, in the lung (25). Properdin has recently been considered as a pattern recognition receptor (PRR) on its own, i.e., binding to recognition patterns without need for prior deposition of C3b or C3bBb (26–28). Therefore, we investigated the role of properdin in tuberculosis pathogenesis, by using the model organism *M. bovis* BCG.

Here, we show, for the first time, that properdin and recombinant form of TSR4+5 expressed as a two-module protein binds to *M. bovis* BCG, demonstrating its role as a soluble PRR. Properdin and TSR4+5 were found to inhibit the uptake of *M. bovis* BCG by macrophages during phagocytosis, altering the pro- and anti-inflammatory cytokine response, and thus, possibly shaping the adaptive immune response in tuberculosis pathogenesis.

MATERIALS AND METHODS

Purification of Native Properdin

The affinity columns, IgG Sepharose and anti-properdin monoclonal antibody Sepharose, were prepared as described previously (7). The IgG-Sepharose column was prepared from human non-immune IgG (~26 mg IgG/ml of Sepharose) coupled to CNBr-activated Sepharose (GE Healthcare, UK). For preparation of the anti-human properdin column, CNBr-activated Sepharose (GE Healthcare Life Sciences, UK) was used to couple to anti-properdin mouse monoclonal antibody (2 mg/ml). One liter of human plasma (TCS Biosciences) containing 5 mM EDTA was filtered through Whatman filter paper before applying to IgG Sepharose to deplete C1q (which would otherwise have bound to the IgG on the anti-properdin Sepharose). The column was washed with three bed volume of HEPES buffer (10 mM HEPES, 140 mM NaCl, 0.5 mM EDTA, and pH 7.4). Plasma was then applied to the monoclonal anti-properdin column and washed with the same HEPES buffer. Bound properdin was eluted with 3 M $MgCl_2$ and the peak fractions were dialyzed against HEPES buffer overnight at 4°C. Contaminants were further removed by applying the pooled protein fractions to a HiTrap Q FF-Sepharose (GE Healthcare) ion-exchange column, followed by washing the column with three bed volumes of 50 mM Tris–HCl, pH 7.5, 50 mM NaCl, and 5 mM EDTA. Properdin did not bind to the Q Sepharose column and appeared in the flow-through free from contaminants as demonstrated by SDS-PAGE.

For the size exclusion chromatography analysis, 50 μl of the proteins at the concentrations varying from 0.3 mg/mL to 1.0 mg/mL were applied to a TSKgel G2000SWXL, 5 μm, 7.8 × 300 mm column (Tosoh Bioscience). The column was equilibrated with buffer containing 50 mM sodium phosphate, pH7.0 and 300 mM NaCl at the flow rate 0.3 ml/min using SCL-10Avp HPLC system

(Shimadzu). The absorbance was detected at 230 and 280 nm. The Bio-Rad Gel Filtration Standard (Cat # 151-1901) were used for the protein molecular weight calibration of the column.

Expression and Purification of TSR4+5

The recombinant maltose-binding protein (MBP) fusion proteins MBP-TSR4+5, MBP-TSR4, or MBP-TSR5 were expressed in *Escherichia coli* as described previously (7, 29). The *E. coli* BL21 bacterial cells (Life Technologies) were grown in 1 L of Luria–Bertani medium with 100 μg/ml ampicillin, shaking at 37°C until an optical density at 600 nm (OD_{600}) of between 0.6 and 0.8 was reached. Protein expression was then induced in the bacterial cell culture with 0.4 mM isopropyl β-D-1-thiogalactopyranoside (IPTG) (Sigma-Aldrich) for 3 h shaking at 37°C. The cells were then pelleted at 4,500 rpm, 4°C for 10 min, lysed using 50 ml lysis buffer [20 mM Tris–HCl, pH 8.0, 0.5 M NaCl, 1 mM EDTA, 0.25% v/v Tween 20, 5% v/v glycerol, 100 μg/ml lysozyme (Sigma-Aldrich), and 0.1 mM phenylmethanesulfonyl fluoride (Sigma-Aldrich)], and incubated for 1 h at 4°C on a rotary shaker. The cell lysate was then sonicated using a Soniprep 150 (MSE, London, UK) at 60 Hz for 30 s with an interval of 2 min (12 cycles) and then centrifuged at 13,000 rpm for 15 min at 4°C. The supernatant was diluted five-fold with buffer A (20 mM Tris–HCl, pH 8.0, 100 mM NaCl, 1 mM EDTA, and 0.25% v/v Tween 20) and passed through an amylose resin column (25 ml bed) (New England Biolabs) that was equilibrated in buffer A. The affinity column was washed with buffer A without Tween 20 and with 1 M NaCl, 20 mM Tris–HCl, pH 8.0, 1 mM EDTA, followed by buffer B (20 mM Tris–HCl, pH 8.0, 100 mM NaCl, 1 mM EDTA). The MBP-TSR4+5 fusion protein was eluted with 100 ml of buffer B containing 10 mM maltose (Sigma-Aldrich) (affinity elution buffer). Trace contaminants were further removed by applying the fusion protein to a DEAE Sepharose column. Thus, the affinity purified fusion protein in affinity elution buffer was applied to the ion-exchange (5 ml bed) column and washed with three column volumes of low salt buffer containing 50 mM Tris–HCl, pH 7.5, 100 mM NaCl, 5 mM EDTA, at pH 7.5. After extensive washing with low salt buffer, the fusion protein eluted at 0.2 M NaCl using a NaCl gradient (50 mM to 1 M). The peak elutions were then passed through Pierce™ High Capacity Endotoxin Removal Resin (Qiagen) to remove LPS. Endotoxin levels were determined using the QCL-1000 Limulus amebocyte lysate system (Lonza), and the assay was linear over a range of 0.1–1.0 EU/ml (10 EU = 1 ng of endotoxin). The endotoxin levels were less than 4 pg/μg of the MBP-TSR4+5.

Mycobacterial Cell Culture

Mycobacterium bovis BCG (Pasteur strain) were grown in liquid culture using Middlebrook 7H9 media (Sigma-Aldrich), supplemented with 0.2% (v/v) glycerol, 0.05% (v/v) Tween-80, and 10% (v/v) albumin dextrose catalase (ADC) (BD BBL, Becton Dickinson). Green fluorescent protein (GFP)-expressing *M. bovis BCG* (Danish Strain 1331) containing the pGFPHYG2 plasmid was a kind gift from B. Robertson, Imperial College, London, UK. GFP-*M. bovis* BCG was grown in the above conditions/media but with the addition of 50 μg/ml of hygromycin to maintain the plasmid. Cultures were incubated at 37°C with agitation (~120 rpm) for 7–10 days until the bacteria had reached the exponential growth phase at $OD_{600nm} = 0.60–1.00$.

Assay of Human Properdin and TSR4+5 Binding to Mycobacteria

Mycobacterium bovis BCG, harvested and washed in PBS, was adjusted to a concentration of 1.25×10^9 cells/ml in PBS ($OD_{600} = 1$ equates to approximately 1×10^9 cell/ml). Then 200 μl of bacterial suspension was dispensed into individual microtiter wells of a 96-well plate (Maxisorp™, NUNC). Plates were incubated at 4°C overnight and washed with buffer 1 [10 mM HEPES pH 7.5, 140 mM NaCl, 0.5 mM EDTA, and 100 μg/ml hen ovalbumin (Sigma-Aldrich)]. Wells were blocked for 2 h at 37°C with buffer 1 + 10% (w/v) Marvel Dried Milk powder.

Human properdin (up to 50 μg/ml) or TSR4+5 (up to 30 μg/ml) were added, in two-fold serial dilutions (100 μl/well) in buffer 1 and incubated for 2 h at 37°C. Individual TSR4 and TSR5 proteins, MBP and BSA were used as negative controls. Microtiter wells were washed three times with buffer 1. Mouse anti-properdin monoclonal antibody (1.19 mg/ml) diluted 1/2,500 in buffer 1 (29) was added to the wells containing properdin. Mouse anti-MBP monoclonal antibody (Sigma-Aldrich) was added to wells containing TSR4+5, TSR4 and TSR5, diluted 1/5,000 in buffer 1, and incubated for 1 h at 37°C. For the BSA negative control, mouse anti-BSA monoclonal antibody (Sigma-Aldrich) was used (1/5,000 dilution). Plates were washed an additional three times in buffer 1 and then incubated with goat anti-mouse IgG-horseradish peroxidase conjugate (Sigma-Aldrich), diluted 1/5,000 in buffer 1. The substrate *p*-nitrophenol phosphate (Sigma-Aldrich) was then added to each well, and the plates read at 405 nm.

Fluorescence Microscopy for TSR4+5 Binding to Mycobacteria

Mycobacterium bovis BCG bacteria (approximately 10^6 cells) were spotted on poly-L-lysine coated microscope slides (Sigma-Aldrich) and incubated at 37°C for cells to adhere. After washing three times with PBS, bacterial cells were then fixed with 4% paraformaldehyde for 5 min. Slides were washed three times with PBS and then incubated at 37°C for 1 h with 0, 1, or 10 μg/ml of TSR4+5, or 10 μg/ml of BSA (negative control) in buffer 1. Slides were washed three times with PBS, and then the primary monoclonal antibody (mouse anti-MBP) added at 1/500 dilution and incubated for 1 h at room temperature. After washing three times with PBS, goat anti-mouse conjugated with AlexaFluor488 (1/500 dilution) was added as the secondary antibody and incubated for 1 h at room temperature. Slides were then washed three times with PBS and mounted with antifade (Citifluor AF3) PBS solution and viewed using a LeicaDM4000 Fluorescence microscope. Images were processed using Image J.[1]

[1] http://imagej.nih.gov/ij.

Phagocytosis Assay

THP-1 macrophage cells were cultured in RPMI-1640 (Gibco) (RPMI) containing 10% (v/v) fetal bovine serum (FBS) (Sigma-Aldrich), 2 mM L-glutamine (Sigma-Aldrich), 100 U/ml penicillin (Sigma-Aldrich), 100 μg/ml streptomycin (Sigma-Aldrich), and 1 mM sodium pyruvate (Sigma-Aldrich) and left to grow in 5% CO_2 at 37°C for approximately 3 days before passaging. Cells were resuspended in RPMI and adjusted to 1×10^6 cells/well (in 1.8 ml) in a 24-well plate. To induce adherence onto the wells, THP-1 cells were treated with 50 ng/ml of phorbol 12-myristate 13-acetate (PMA) (Sigma-Aldrich) into RPMI-1640 without FBS, penicillin or streptomycin and left to settle for at least 30 min before adding 200 μl of bacterial culture (1×10^9 bacteria/ml).

M. bovis BCG bacteria were pelleted at mid-exponential phase, at an $OD_{600nm} = 0.6–1.0$ by centrifugation at $1{,}000 \times g$ for 10 min at 4°C. The mycobacterial pellet was resuspended in the buffer 1. This mycobacterial culture was then separated into different microfuge tubes and treated with varying concentrations of properdin (2 or 20 μg/ml) or MBP-TSR4+5 (1 or 5 μg/ml). Control samples were left untreated, and all were incubated for 2 h at 37°C for binding to occur. The mycobacterial suspension was washed once in growth medium before resuspending in RPMI medium without FBS, penicillin, or streptomycin. 200 μl of the mycobacterial suspension was added to each well of THP-1 cells. Mycobacterial concentration was adjusted to give approximate multiplicity of infection (MOI) ratio of 10:1.

Plates were gently swirled and incubated at 37°C, 5% CO_2 for up to 48 h to allow mycobacterial uptake. THP-1 cells were sampled at 15, 30, and 45 min and 1, 2, and 6 h. Supernatants were collected after 24 and 48 h of incubation for multiplex analysis. Plates were washed three times with PBS to remove extracellular bacteria. THP-1 cells were then lifted by adding 1 ml of 0.25% trypsin to the wells and incubated for 10 min at 37°C, 5% CO_2. THP-1 cells were collected by centrifugation at $1{,}000 \times g$ for 10 min at 4°C.

To recover and count the ingested mycobacteria, THP-1 cells were lysed by resuspending the cell pellets in 1 ml of sterile water, followed by a series of vortex mixing for 10 min at room temperature. 24-well plates containing 2 ml Middlebrook 7H10 agar with 10% Oleic Acid+ADC (OADC) (BD, BBL, Becton Dickinson) were prepared. Four serial 1/10 dilutions were made, and 10 μl of the concentrated mycobacterial suspension and diluted suspension from each time point was spotted onto the 7H10 agar wells. The 24-well plates were secured with parafilm and wrapped in aluminum foil, inverted and incubated at 37°C for 10–14 days. Wells were photographed, and the colony-forming unit (CFU) count determined. The same procedure was used to quantify the initial input number of bacteria incubated with THP-1 cells.

Fluorescence Microscopy for Phagocytosis Assay

THP-1 cells were cultured as described above and seeded at 1×10^5 cells per 13 mm coverslip and differentiated with PMA as described above. GFP-expressing *M. bovis* BCG was incubated with 0, 1, 10 μg/ml of TSR4+5 for 2 h at 37°C in buffer 1. Cells were also incubated with 10 μg/ml of BSA as a negative control.

TABLE 1 | Primers used for quantitative real-time PCR.

	Forward primer	Reverse primer
18S	5′-ATGGCCGTTCTTAGTTGGTG-3′	5′-CGCTGAGCCAGTCAGTGTAG-3′
IL-1β	5′-GGACAAGCTGAGGAAGATGC-3′	5′-TCGTTATCCCATGTGTCGAA-3′
IL-6	5′-GAAAGCAGCAAAGAGGCACT-3′	5′-TTTCACCAGGCAAGTCTCCT-3′
IL-10	5′-TTACCTGGAGGAGGTGATGC-3′	5′-GGCCTTGCTCTTGTTTTCAC-3′
IL-12	5′-AACTTGCAGCTGAAGCCATT-3′	5′-GACCTGAACGCAGAATGTCA-3′
TGF-β	5′-GTACCTGAACCCGTGTTGCT-3′	5′-GTATCGCCAGGAATTGTTGC-3′
TNF-α	5′-AGCCCATGTTGTAGCAAACC-3′	5′-TGAGGTACAGGCCCTCTGAT-3′

Cells were washed twice in PBS and then resuspended in plain RPMI media. 1×10^6 GFP-*M. bovis* BCG was added to the THP-1 cells (MOI of 10:1) and incubated for phagocytosis for 2 h at 37°C. THP-1 cells were then washed three times in PBS to remove extracellular bacteria and then fixed in 4% paraformaldehyde for 5 min. After washing three times in PBS, THP-1 cells were incubated with 2 μg/ml of AlexaFluor546-conjugated wheat germ agglutinin (Invitrogen) to reveal the plasma membrane. Cells were then washed three times and mounted using Vectashield antifade with DAPI (Vector Labs) to reveal nucleus. Slides were observed under a Leica DM4000 fluorescence microscope at 40× magnification. Images were processed using Image J (see text footnote 1).

Quantitative Real-Time PCR (qPCR) Analysis of mRNA Expression of Cytokines

THP-1 cell pellets were collected from each time point as described above. RNA extraction was performed using the GenElute Mammalian Total RNA Purification Kit (Sigma-Aldrich) according to the manufacturer's protocol. Samples were then treated with DNase I (Sigma-Aldrich) to remove any contaminating DNA according to the manufacturer's protocol. The amount of RNA was measured using the NanoDrop 2000/2000c spectrophotometer (Thermo Fisher Scientific) at 260 nm, and the ratio of absorbance at 260 and 280 nm was used to assess the purity of the RNA. Complementary DNA (cDNA) was synthesized using High Capacity RNA to cDNA Kit (Applied Biosystems, UK) according to the manufacturer's protocol. Primer sequences (**Table 1**) were designed and analyzed for specificity using the nucleotide Basic Local Alignment Search Tool and Primer-BLAST.[2]

PCR was performed on all cDNA samples to assess the quality of the cDNA. The qPCR assays were performed for the expression of pro- and anti-inflammatory cytokines. The qPCR reaction consisted of 5 μl Power SYBR Green MasterMix (Applied Biosystems), 75 nM of forward and reverse primer, 500 ng template cDNA in a 10 μl final reaction volume. qPCR was performed in a 7900HT Fast Real-Time PCR System (Applied Biosystems). The initial steps were 2 min incubation at 50°C followed by 10 min incubation at 95°C, the template was then amplified for 40 cycles under these conditions: 15 s incubation at 95°C and 1 min incubation at 60°C. Samples were normalized using the expression of human 18S rRNA. Data were analyzed using the relative quantification (RQ) Manager Version 1.2.1 (Applied Biosystems). Cycle threshold (Ct) values for each cytokine target

[2]http://blast.ncbi.nlm.nih.gov/Blast.cgi.

gene were calculated, and the relative expression of each cytokine target gene was calculated using the RQ value, using the formula: $RQ = 2^{-\Delta\Delta Ct}$ for each cytokine target gene, and comparing relative expression with that of the 18S rRNA constitutive gene product. Assays were conducted twice in triplicate.

Multiplex Analysis

Supernatants were collected from the phagocytosis assay at 24 and 48 h to determine the levels of secreted cytokines (IL-6, IL-10, IL-12p40, IL-12p70, IL-1α, IL-1β, TNF-α, IL-13, IL-15, IL-17A, IL-9, and TNF-β), chemokines (MCP-3, MDC, Eotaxin, Fractalkine, GRO, IL-8, IP-10, MCP-1, and MIP-1α), growth factors (IL-2, EGF, FGF-2, G-CSF, GM-CSF, IL-3, IL-4, IL-5, IL-7, and VEGF), and other related ligands and receptors (IFN-α2, IFN-ϒ, FLT-3L, IL-1RA, and sCD40L). MagPix Milliplex kit (EMD Millipore) was used to measure immune response following the manufacturer's protocol. 25 µl of assay buffer was added to each well of a 96-well plate, followed by the addition of 25 µl of standard, controls or supernatants of cells treated with *M. bovis* BCG in the presence or absence of properdin and MBP-TSR4+5. 25 µl of magnetic beads coupled to analytes of interest was added in each well and incubated for 18 h at 4°C. The 96-well plate was washed with the assay buffer, and 25 µl of detection antibodies was incubated with the beads for 1 h at room temperature. 25 µl of streptavidin–phycoerythrin was then added to each well and incubated for 30 min at room temperature with shaking at 750 rpm. Following a washing step, 150 µl of sheath fluid was added to each well, and the plate was read using the Luminex Magpix instrument. Assays were conducted in duplicate.

Statistical Analysis

Analysis of data for statistical significance was conducted using GraphPad Prism 6 for Windows (GraphPad Software, Inc.). Statistical analyses were made using two-way ANOVA for mRNA expression data and a one-way ANOVA for the multiplex data. p Values < 0.05 were considered statistically significant, unless otherwise stated (non-significant).

RESULTS

Human Properdin and TSR4+5 Bind to Mycobacteria

Human properdin was purified from human plasma. SDS-PAGE, followed by western blotting using antihuman properdin polyclonal antibodies, showed a distinct band at 55 kDa (**Figure 1A**), which was the expected molecular weight of the glycosylated monomer. The two biologically active modules of properdin TSR4 and TSR5 were expressed together in tandem as previously described, fused to MBP (7), and is also shown on an SDS-PAGE gel, which has a molecular weight of 55 kDa (**Figure 1B**). Using gel filtration chromatography, we found that human properdin eluted as a mixture of monomer, dimer and trimer; a negligible amount probably formed aggregates. Nearly 60% of MBP-TSR4+5 appeared as a monomer while nearly 40% was found to migrate as a dimer (data not shown).

The binding of properdin to *M. bovis* BCG was observed to be in a dose-dependent manner; BSA was used as a negative control that showed almost no binding (**Figure 2A**). TSR4+5 binding was also observed to be in a dose-dependent manner. MBP was used as a negative control (**Figure 2B**). The two binding curves cannot be compared quantitatively, as different detection antibodies were used. Because the MBP-TSR4+5 recombinant protein and properdin monomer have about the same molecular weight, 5 µg of TSR4+5 corresponds in molar terms to about 5 µg of properdin monomer (**Figures 1A,B**). The binding of a mixture of the two separately expressed TSR4, and TSR5 is much lower than that of the combined expressed TSR4+5 (**Figure 2B**). For this comparison, the same detection antibody was used. These results suggest that both TSR4 and TSR5 modules contribute to the interaction with *M. bovis* BCG, and that TSR4+5 binds

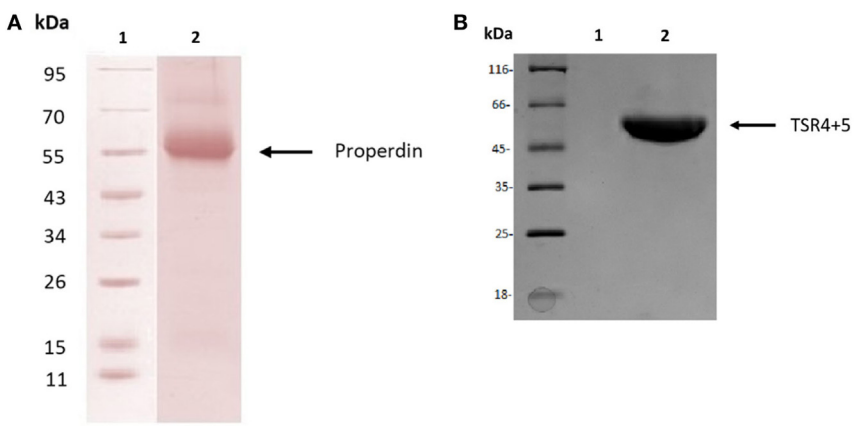

FIGURE 1 | Purified human properdin and recombinant maltose-binding protein (MBP)-thrombospondin repeats (TSR) 4+5. **(A)** Properdin was purified from human plasma. Filtered plasma was applied to a non-immune IgG-Sepharose column, then to a mouse monoclonal anti-properdin Sepharose column; properdin was eluted with 3 M $MgCl_2$. The eluted samples were dialyzed against HEPES buffer (10 mM HEPES, 140 mM NaCl, 0.5 mM EDTA, pH 7.4) overnight at 4°C. Contaminants were removed by applying the protein to a Q Sepharose column, and the product appears as a single band on SDS-PAGE and western blot at about 55 kDa. **(B)** MBP-TSR4+5 was purified *via* an amylose resin column, and the purified fusion protein also appears on SDS-PAGE as a band of about 55 kDa.

with similar characteristics to that of whole properdin on *M. bovis* BCG surface. These results were further confirmed using microscopy where TSR4+5 specifically bound to *M. bovis* BCG in a dose-dependent manner (**Figure 2C**).

Properdin Inhibits Uptake of *M. bovis* BCG by THP-1 Cells

Properdin inhibited the uptake of *M. bovis* BCG by THP-1 cells. At a concentration of 20 μg/ml, uptake of *M. bovis* BCG was significantly reduced by properdin (**Figure 3A**). TSR4+5 was also able to substantially inhibit uptake of *M. bovis* BCG by THP-1 cells (**Figure 3B**). The effect of properdin and

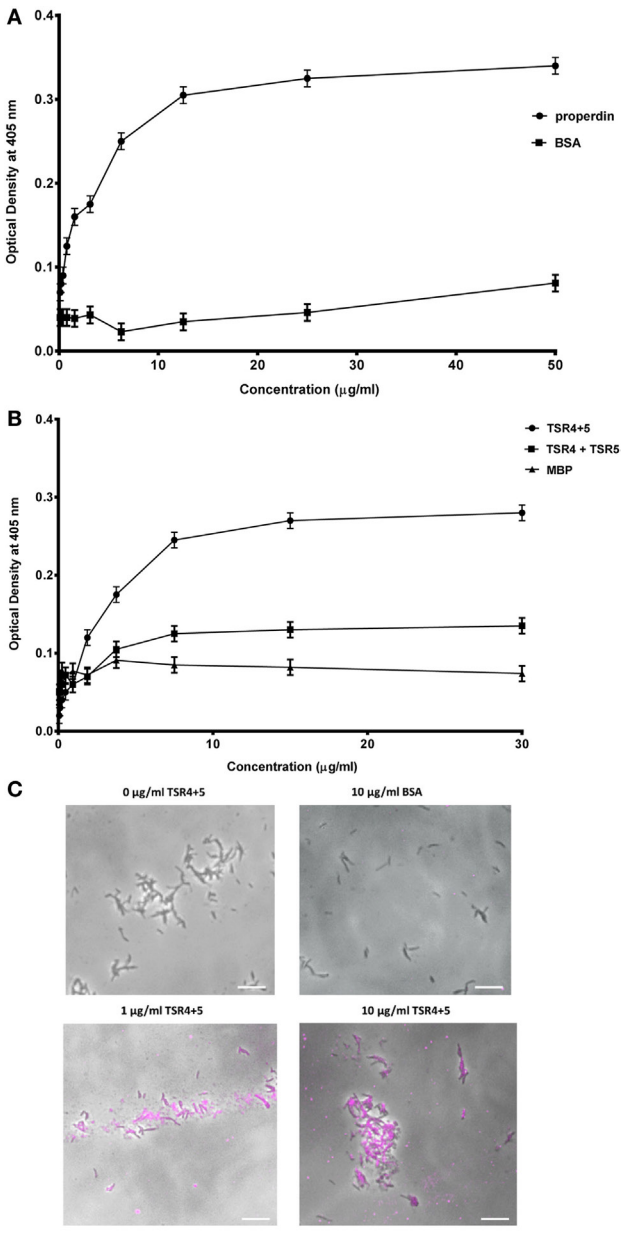

FIGURE 2 | Continued

FIGURE 2 | Human properdin binds mycobacteria *via* thrombospondin repeats (TSR) 4+5. **(A)** Properdin binding to mycobacteria; BSA was used as a negative control protein. **(B)** Comparison between TSR4+5 and individual TSR4 and TSR5 binding to mycobacteria; maltose-binding protein (MBP) as negative control. Assays were conducted in 10 mM HEPES, 140 mM NaCl, 0.5 mM $CaCl_2$ + 0.5 mM $MgCl_2$, 100 μg/ml hen ovalbumin, and pH 7.5. Serial dilutions of properdin were incubated in mycobacteria coated wells followed by incubation with mouse anti-properdin monoclonal antibody and mouse anti-BSA monoclonal antibody, respectively; serial dilutions of TSR4+5, TSR4 or TSR5 were incubated in another set of mycobacteria coated wells followed by incubation with mouse anti-MBP monoclonal antibody. Anti-mouse IgG conjugated with alkaline phosphatase and substrate *p*-nitrophenol phosphate were incubated in both sets of wells, and the color was measured at 405 nm using a plate reader. Assay was conducted in quadruplicate. Error bars represent SD. **(C)** Differential direct binding of 0, 1, and 10 μg/ml of TSR4+5 to *Mycobacterium bovis* BCG. 10 μg/ml of BSA was used as a negative control. Cells were incubated for 2 h with either TSR4+5 or BSA. Cells were washed, fixed, and stained with mouse anti-MBP monoclonal antibody followed by goat anti-mouse 1gG-conjugated with AlexaFluor488. Images are shown as single sections taken using a Leica DM4000 microscope; bar scale 10 μm.

TSR4+5 on the phagocytosis of *M. bovis* BCG was dose dependent. The input number of *M. bovis* BCG was about 7.8×10^6 CFU/ml, which was the total number of bacteria added to THP-1 cells. Without properdin or TSR4+5, 5.0×10^6 CFU/ml of *M. bovis* BCG was phagocytosed which was approximately 66% efficiency of phagocytosis compared with the input number. At the highest concentration tested, properdin showed an inhibition of uptake of approximately 60% compared with *M. bovis* BCG with no properdin (**Figure 3A**). For TSR4+5, the effect on *M. bovis* BCG was slightly lower at approximately 40% inhibition (**Figure 3B**). These results were also confirmed by microscopy, with TSR4+5 having a suppressive effect on the uptake of GFP-expressing *M. bovis* BCG by THP-1 cells (**Figure 3C**). PMA stimulation was used to induce differentiation of THP-1 cells before incubation with *M. bovis* BCG. PMA has been shown to activate protein kinase C and increase cell adherence and expression of surface markers associated with macrophage differentiation (30). These data show that (i) properdin has an anti-opsonic effect on *M. bovis* BCG, inhibiting phagocytosis; and (ii) TSR4+5 modules play a major role in this interaction of *M. bovis* BCG and macrophages. These observations demonstrate, for the first time, a novel, non-complement-related role for properdin in host–pathogen interactions in tuberculosis.

Properdin Induces a Pro-Inflammatory Response During the Early Phase of Phagocytosis of *M. bovis* BCG by THP-1 Cells

The effect of properdin on the inflammatory response during the phagocytosis of *M. bovis* BCG was measured. The gene expression of key pro- and anti-inflammatory cytokines in tuberculosis was determined using quantitative real-time PCR. Our data showed that properdin significantly enhanced the upregulation of pro-inflammatory cytokines TNF-α, IL-1β, and IL-6 from THP-1 cells challenged by *M. bovis* BCG (**Figure 4A**), particularly at the

initial stage of uptake (within the first hour of phagocytosis), which decreased gradually toward the later stages of phagocytosis. The increase in TNF-α transcript was particularly striking as TNF-α is well known for activating macrophages for killing of intracellular mycobacteria. In addition, TNF-α is a key mediator in the early stages of granuloma formation. By contrast, the anti-inflammatory cytokines measured from THP-1 cells (IL-10 and TGF-β) were shown to be downregulated in the presence of properdin, when challenged by *M. bovis* BCG (**Figure 4B**). IL-12 also appeared to be downregulated (**Figure 4A**). Properdin, therefore, appears to play an important role in pro-inflammatory cytokine production by macrophages infected by *M. bovis* BCG, which may have significant implications in shaping the adaptive immune response during *M. tuberculosis* infection.

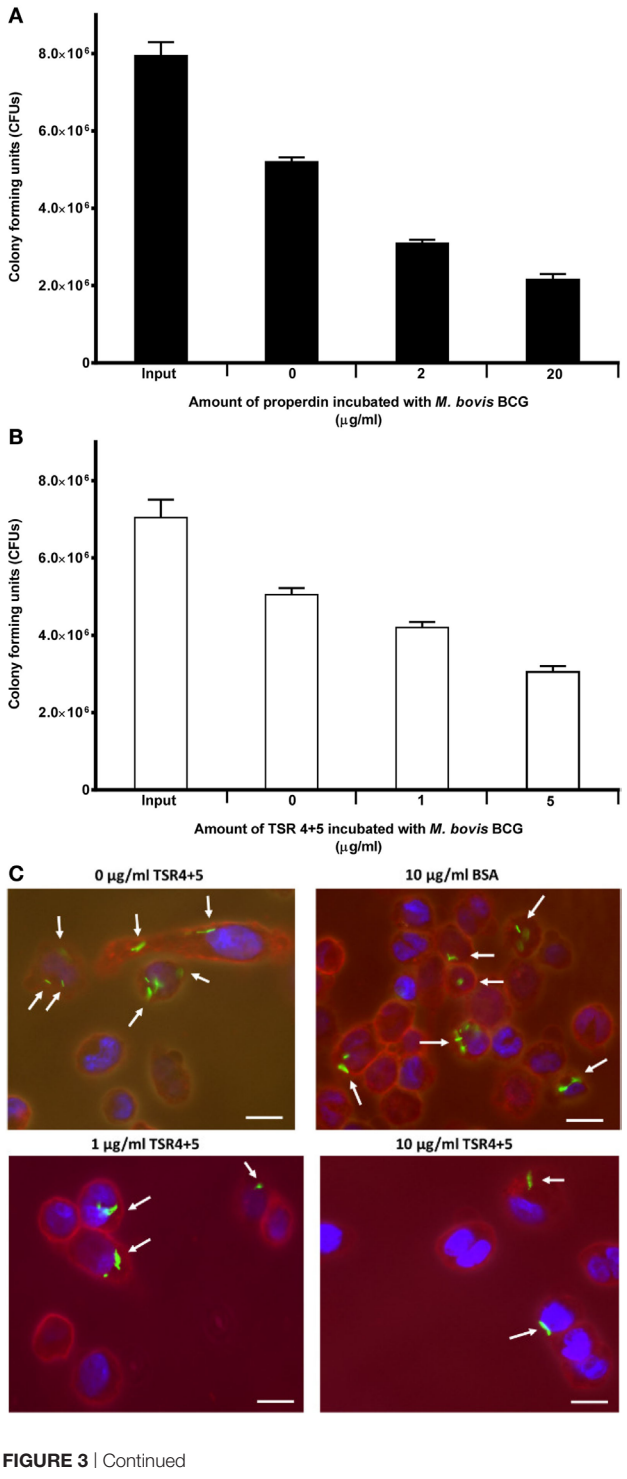

FIGURE 3 | Continued

FIGURE 3 | Effect of properdin and thrombospondin repeats (TSR) 4+5 on the phagocytosis of *Mycobacterium bovis* BCG by THP-1 cells. **(A)** *M. bovis* BCG was treated with properdin at concentrations of 0, 2, and 20 μg/ml or with **(B)** TSR4+5 at concentrations 0, 1, and 5 μg/ml. The mycobacteria were incubated with macrophage for 2 h. After THP-1 cell lysis, surviving internalized *M. bovis* BCG were measured by plating lysates on 7H10 media to obtain colony-forming units (CFUs). The input value is the starting number of *M. bovis* BCG added to the THP-1 cells, before phagocytosis. A one-way ANOVA test was performed on the data to determine significant differences in CFU count by properdin or TSR4+5. All comparisons were significant ($p < 0.05$), unless where shown (ns, not significant, $p > 0.05$). Samples were analyzed in triplicate. **(C)** Differential uptake of GFP-*M. bovis* BCG by THP-1 macrophages after treatment with 0, 1, and 10 μg/ml of TSR4+5, or 10 μg/ml of BSA, used as a negative control. Cells were incubated for 2 h. Cells were then washed, fixed, and stained with AlexaFluor546-conjugated wheat germ agglutinin to reveal the plasma membrane (red), and the nucleus was stained with DAPI (blue). Images are shown as single sections, taken using a Leica DM4000 microscope; bar scale 10 μm.

Cytokine gene expression by THP-1 cells infected with *M. bovis* BCG were also studied in the presence of TSR4+5, which revealed that TSR4+5 also has a significant effect on the pro-inflammatory response. TNF-α was upregulated (**Figure 5A**), while IL-10 was found to be downregulated (**Figure 5B**), during the first hour of phagocytosis. IL-12 was also shown to be significantly downregulated (**Figure 5A**). These data mirror the observations for properdin, and hence, validate the importance of TSR4+5 in the binding of properdin to *M. bovis* BCG and in its modulation of the inflammatory response. These data are also similar to recent published observations of another complement regulatory protein, factor H (19), thus offering potentially novel insights into the involvement of these proteins in host–pathogen interactions in tuberculosis.

Multiplex Analysis of Cytokine Secretion

The inflammatory response during the phagocytosis of *M. bovis* BCG by THP-1 cells was further determined by measuring the secretion of cytokines, chemokines, and other growth factors using the Multiplex analysis of supernatants collected at 24 and 48 h post phagocytosis (**Figures 6A–D**). The secretion of pro-inflammatory cytokines TNF-α, IL-1β, and IL-1α was significantly enhanced by treatment with properdin or TSR4+5 at the 24 h time point (**Figure 6A**). The enhancement of these pro-inflammatory cytokines can be critical for controlling mycobacterial infection, particularly in the formation of the granuloma. However, by 48 h, there was a decrease in the production of pro-inflammatory cytokines (IL-6, IL-12p40, IL-12p70, IL-1α, IL-1β, TNF-α, IL-13, IL-15, and IL-9) in the presence of properdin- and TSR4+5-treated *M. bovis* BCG (**Figure 6A**). Properdin and TSR4+5 also downregulated the

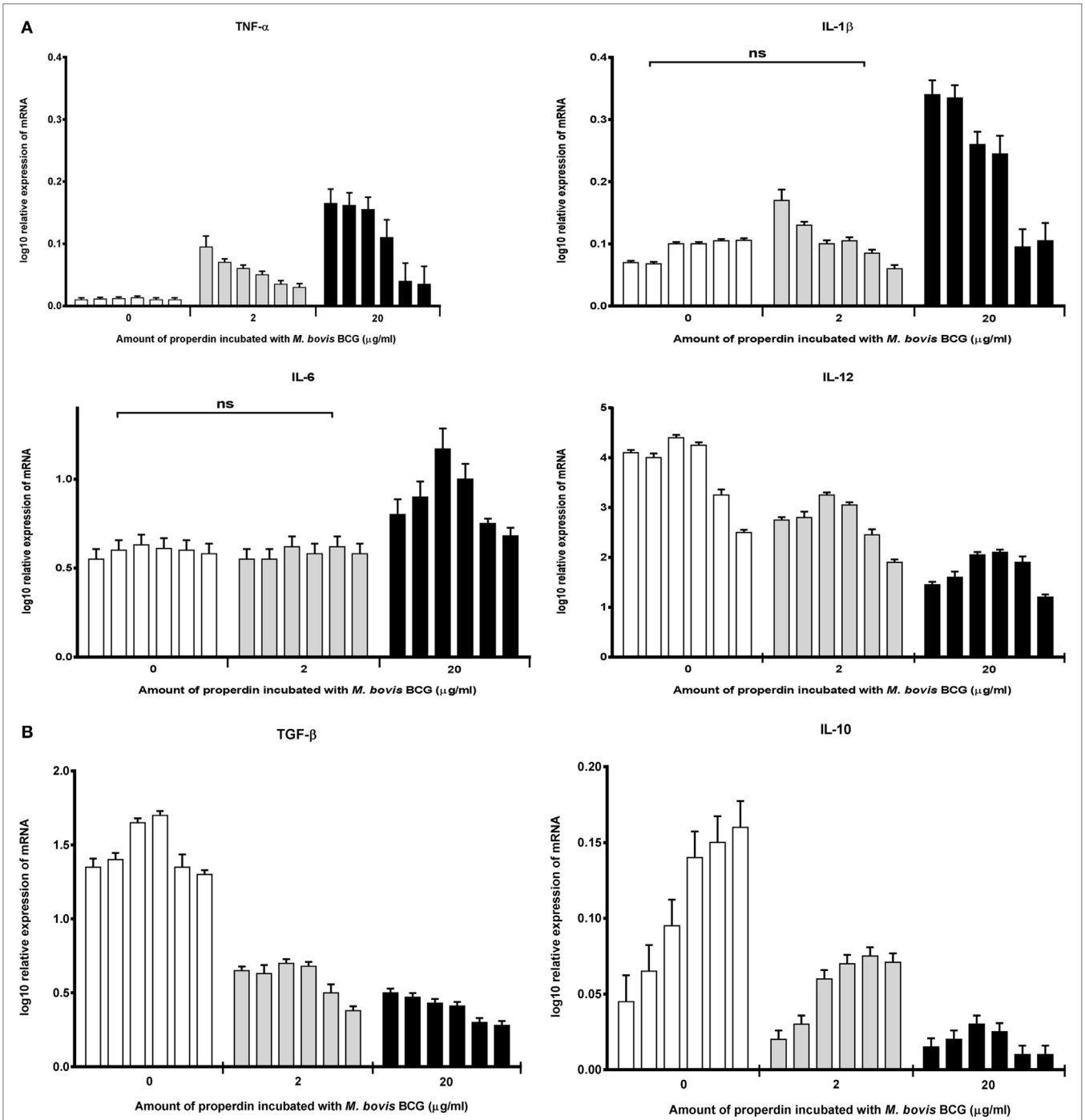

FIGURE 4 | Temporal mRNA expression profile of cytokines produced by THP-1 cells incubated with different concentrations of properdin and *Mycobacterium bovis* BCG. **(A)** Pro-inflammatory cytokines: TNF-α, IL-1β, IL-6, and IL-12; **(B)** anti-inflammatory cytokines: TGF-β and IL-10. The expression of each cytokine was measured using qPCR, and the relative expression [relative quantification (RQ)] calculated by normalizing the data using human 18S rRNA expression as a control. The RQ value was calculated using the formula: $RQ = 2^{-\Delta\Delta Ct}$. Assays were conducted twice in triplicates. Error bars represent SD. A two-way ANOVA test was performed on the data to determine significant differences in expression of cytokine production by properdin. All comparisons were significant ($p < 0.05$), unless where shown (ns, not significant, $p > 0.05$).

anti-inflammatory response such as IL-10 after 24 and 48 h of phagocytosis, although this was less pronounced for IL-12 at 48 h (**Figure 6A**). These observations again mirror the initial responses observed in cytokine gene expression of during the first few hours of phagocytosis, in the presence of properdin or TSR4+5 (**Figures 5A,B**). The effect of properdin and TSR4+5 also led to marked downregulation of a number of growth factors MCP-3 (24 h), MDC, Eotaxin, Fractalkine (24 h), GRO

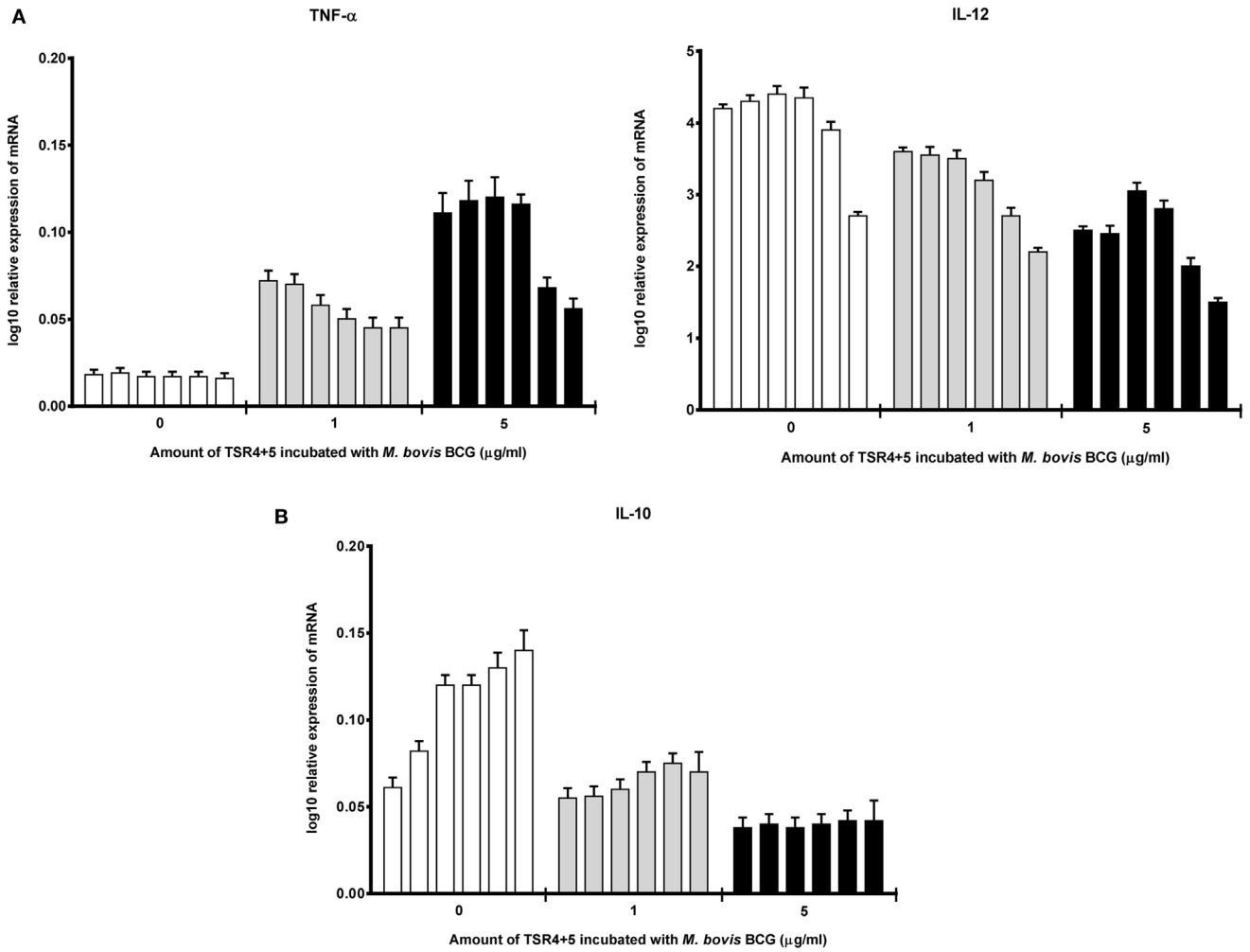

FIGURE 5 | Temporal mRNA expression profile of cytokines produced by THP-1 cells incubated with different concentrations of thrombospondin repeats (TSR) 4+5 and *Mycobacterium bovis* BCG. **(A)** Pro-inflammatory cytokines: TNF-α and IL-12; **(B)** anti-inflammatory cytokine: IL-10. The expression of each cytokine was measured using qPCR, and the relative expression [relative quantification (RQ)] calculated by normalizing the data using human 18S rRNA expression as a control. The RQ value was calculated using the formula: $RQ = 2^{-\Delta\Delta Ct}$. Assays were conducted twice in triplicates. Error bars represent SD. A two-way ANOVA test was performed on the data to determine significant differences in expression of cytokine production by TSR4+5. All comparisons were significant ($p < 0.05$), unless where shown (ns, not significant, $p > 0.05$).

(24 h), IP-10, MCP-1, MIP-1, VEGF, G-CSF (48 h), GM-CSF (48 h), and VEGF (24 h) (**Figures 6B,C**). Additional ligands and receptors (IFN-α2, IFN-γ, FLT-3L, IL-1RA, and sCD40L) did not show any significant changes (**Figure 6D**).

DISCUSSION

We have previously shown that a complement regulatory protein, factor H, can bind to *M. bovis* BCG and inhibit its uptake by THP-1 macrophages (19). Factor H can also enhance the pro-inflammatory response during this host–pathogen interaction (19). This study highlighted a novel complement-independent property of factor H as an anti-opsonin and in the modulation of the inflammatory response against a pathogen. With the goal of further elucidating the role of complement control proteins in the early stages of mycobacterial infection, this study looked at the role of properdin, an upregulator of the alternative complement pathway. Properdin and thrombospondin repeat (TSR) modules TSR4+5 were shown to bind to *M. bovis* BCG and inhibit bacterial uptake by THP-1 cells, augmenting the inflammatory response. These observations are similar to what has been observed previously with factor H (19), which is intriguing, since properdin and factor H have opposing effects on the regulation of complement activation (3). These findings were also consistent with previous reports, which have demonstrated that properdin deficient mice have a reduced M1 (IL-1β) and increased M2 (arginase-1, MCP-1, IL-10) profile, crucial for the tumor microenvironment (31). This suggests that the production of IL-1β and reduction in IL-10 mediated by properdin may be required for protection against *M. tuberculosis* in the initial phase of infection.

The functions of properdin have been extensively investigated within the remit of the complement alternative pathway, and

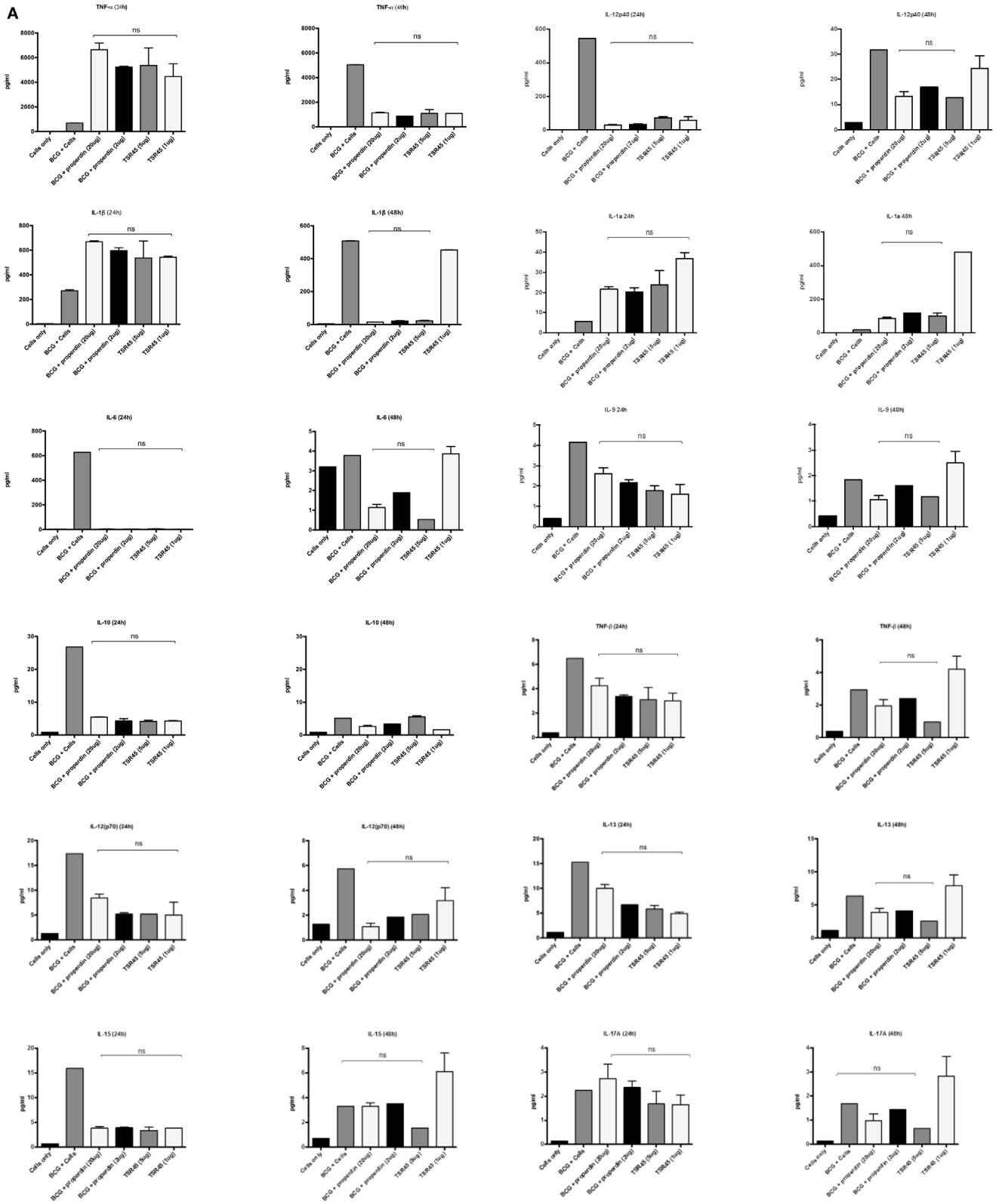

FIGURE 6 | Continued

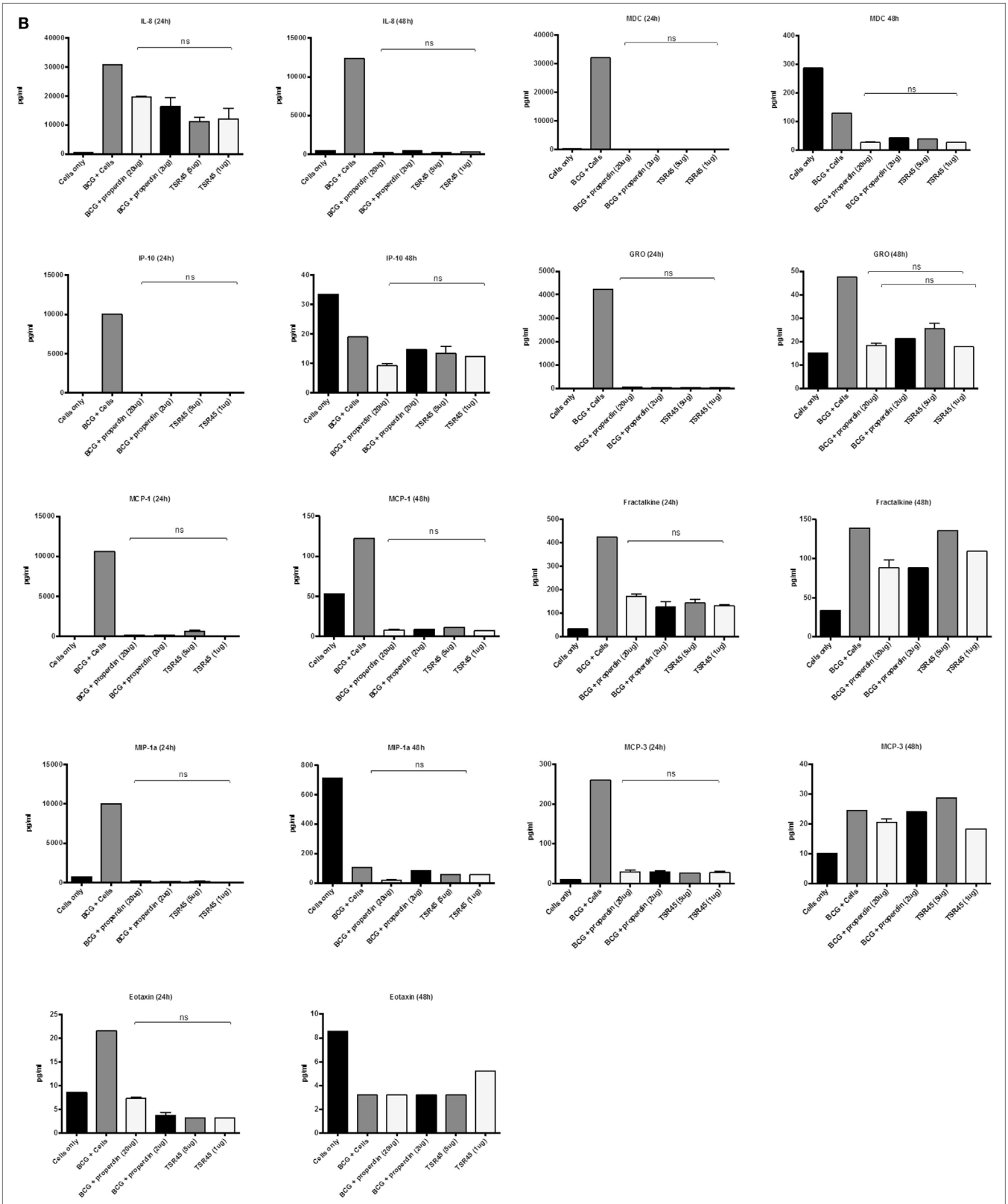

FIGURE 6 | Continued

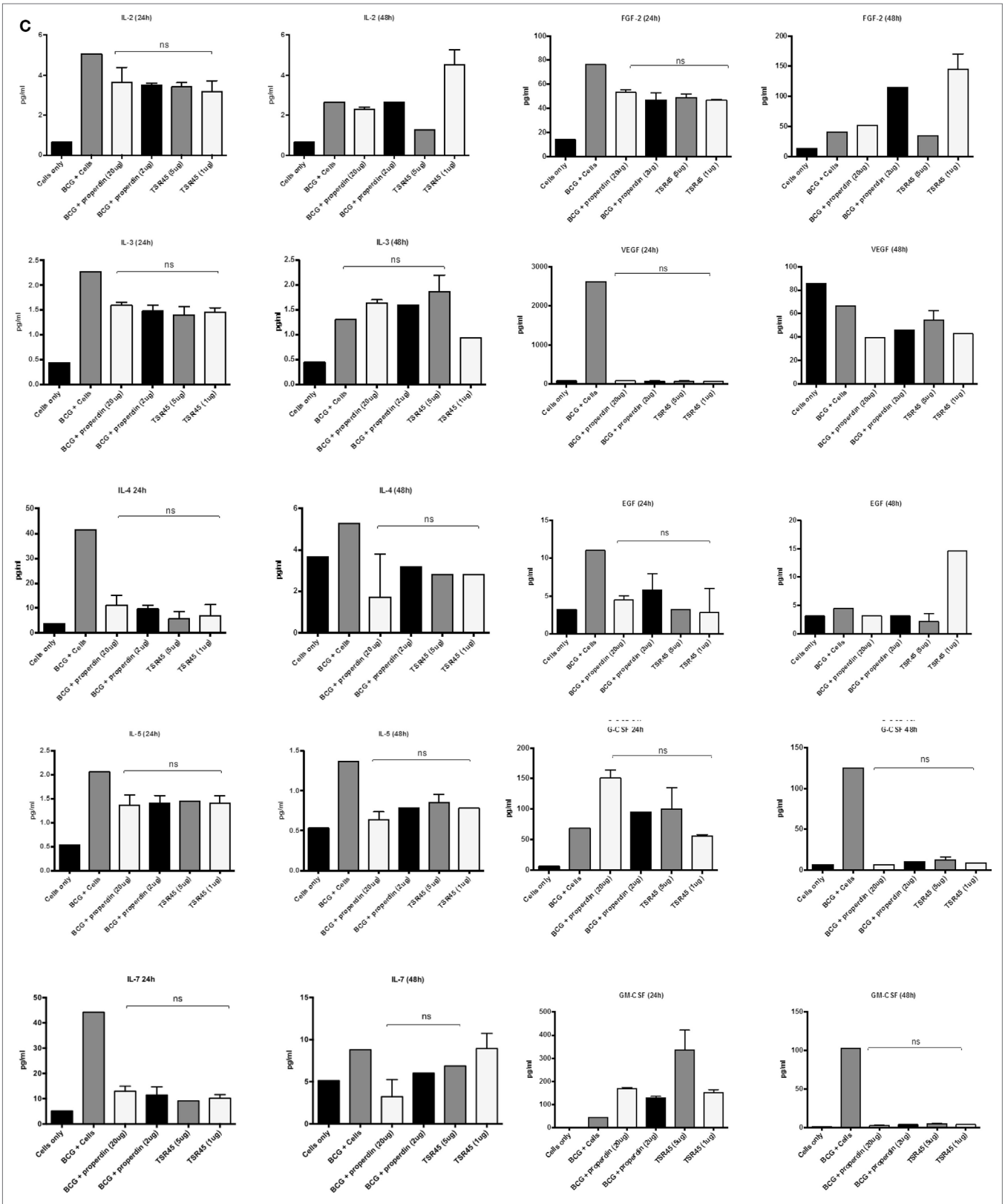

FIGURE 6 | Continued

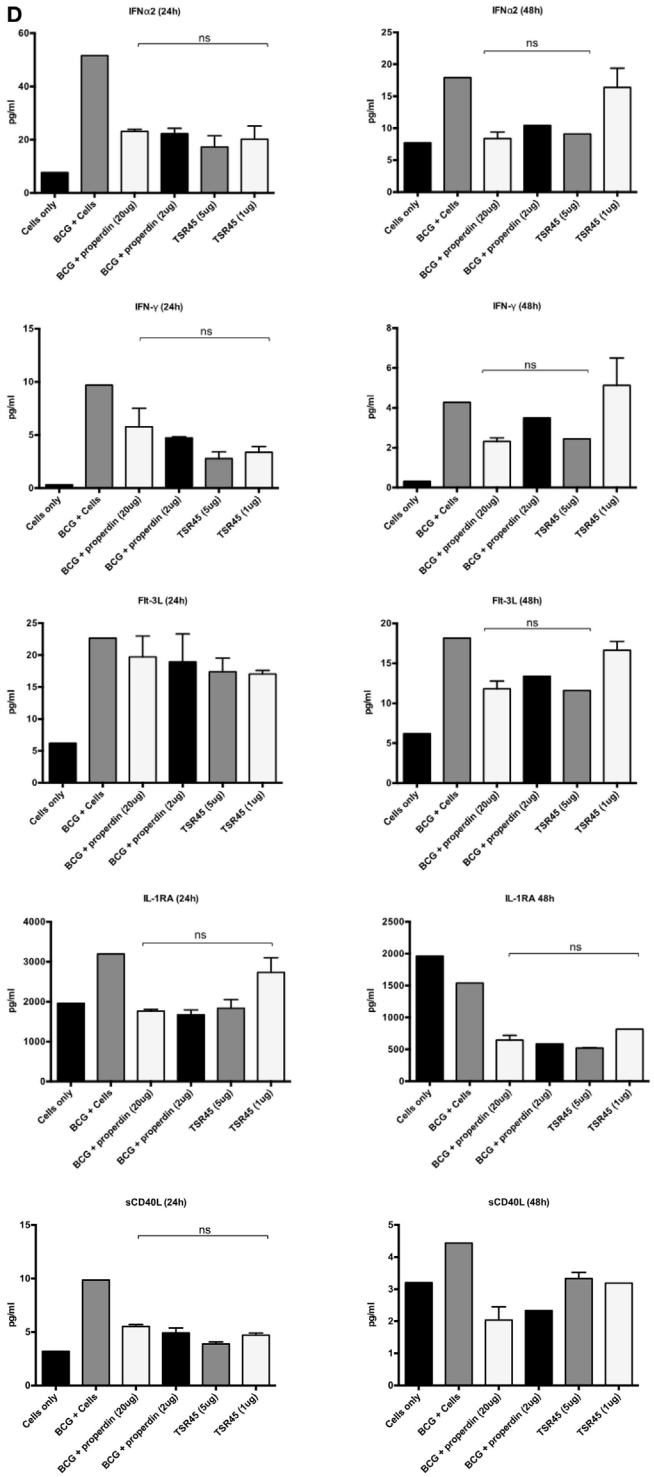

FIGURE 6 | Multiplex cytokine analysis of supernatants collected at 24 and 48 h phagocytosis of *Mycobacterium bovis* BCG by THP-1 cells incubated with or without properdin and thrombospondin repeats (TSR) 4+5. The supernatants were collected from phagocytosis assay of *M. bovis* BCG in the presence or absence of properdin and TSR4+5 at 24 and 48 h time point. The levels of cytokine production were measured for **(A)** (IL-6, IL-10, IL-12p40, IL-12p70, IL-1α, IL-1β, TNF-α, IL-13, IL-15, IL-17A, IL-9, and TNF-β), **(B)** chemokines (MCP-3, MDC, Eotaxin, Fractalkine, GRO, IL-8, IP-10, MCP-1, and MIP-1α), **(C)** growth factors (IL-9, IL-2, EGF, FGF-2, G-CSF, GM-CSF, IL-3, IL-4, IL-5, IL-7, and VEGF), and **(D)** related ligands and receptors (IFN-α2, IFN-γ, FLT-3L, IL-1RA, and sCD40L) using multiplex analysis. Error bars represent SD. A one-way ANOVA test was performed on the data to determine significant differences in expression of cytokine production by properdin or TSR4+5. All comparisons were significant ($p < 0.05$), unless where shown (ns, not significant, $p > 0.05$). Supernatants were analyzed in duplicate.

its involvement with pathogens has largely been characterized as complement dependent. In this study, we aimed to look at the complement-independent interaction of properdin with mycobacteria (i.e., effects in the absence of other complement proteins), with a view to examining its possible role in the pathogenesis of tuberculosis. The role of complement in tuberculosis has been examined, but little is understood about the role of the individual complement proteins in tuberculosis infection, especially complement control proteins. Properdin has been shown to play a role in a number of pathogenic infections such as those by *C. pneumoniae*, in which properdin promotes complement C3b deposition and opsonization (12). A recent study also demonstrated that a low dose of properdin, which is highly polymerized, is able to protect against *N. meningitidis* and *Streptococcus pneumoniae*, by assembling the alternative complement pathway (16). The central premise in these recent studies is that properdin is an upregulator of the complement alternative pathway, and thus, when in contact with pathogens, the alternative pathway is triggered and stabilized by properdin.

Properdin has also been shown to enhance the uptake of apoptotic T cells by dendritic cells (DCs) and macrophages, thus promoting phagocytosis (27). Properdin may also bind to the DNA found to be exposed on apoptotic and necrotic cells, suggesting that this may also be a crucial site for alternative pathway activation (32). There is recent evidence to suggest that properdin, locally produced by tolerogenic DCs, binds to necrotic cells, confirming its role a pattern recognition molecule of the innate immunity. In addition, properdin is also involved in the interaction of DC and T cell responses. Interestingly, silencing of properdin by treating DCs with siRNA in the presence/absence of IFN-γ reduced the proliferation of allogenic T cells (33). Properdin binds to early apoptotic cells via sulfated GAGs, resulting in C3b deposition and uptake by phagocytes. Activation of neutrophils drives the deposition of properdin, which binds apoptotic T cells. Since properdin has been shown to bind apoptotic cells via GAGs (27) or DNA, it remains unclear what other ligands and receptors are involved in properdin–apoptotic cell interaction. It is likely that properdin as a soluble factor is acting as an adaptor molecule. Furthermore, properdin also binds to NKp46 expressed on natural killer cells, innate lymphoid cells (ILC)1 and ILC3. This study demonstrated that the control of meningococcal infection was dependent on NKp46 and group 1 ILCs, further elucidating the role of properdin as an independent pattern recognition molecule (34).

In our study, we show that purified native properdin and TSR4+5 bind to *M. bovis* BCG in a dose-dependent manner, suggesting that the binding of properdin to *M. bovis* BCG may be *via* TSR4+5. The physiological concentration of properdin in serum is about 25 μg/ml (35). We also demonstrate that coating of *M. bovis* BCG with properdin inhibits the uptake of the bacterium by THP-1 cells; however, only about 60% inhibition was achieved at the highest dose of native properdin. TSR4+5 was also able to mirror the effects of properdin, in inhibiting the uptake of *M. bovis* BCG by macrophages by up to 40%.

The recruitment of properdin by mycobacteria may be particularly crucial in the initial stages of tuberculosis infection, when after inhalation, the first host cell *M. tuberculosis* encounters is the alveolar macrophage.

In the lungs, mycobacteria are phagocytosed by alveolar macrophages, which are unable to completely eliminate them, and so produce crucial chemoattractants (36), which recruit inflammatory cells such as neutrophils, macrophages, γδ-T cells, and natural killer cells that stimulate inflammation and tissue remodeling (36–38). Our findings may be indicative of the early inflammatory processes *in vivo*, involved in granuloma formation, which are nodular-type lesions that cordon-off *M. tuberculosis* infection, and provide an environment for the bacilli to persist and survive as a latent infection. TNF-α and IFN-γ are involved in recruitment of cells in the granuloma (39, 40). Thus, properdin may play a role in granuloma formation by promoting pro-inflammatory cytokines. Inflammatory balance is essential particularly of Th2/Th1 cytokines, which are required to maintain a protective granuloma (41). This is determined by the balance in IFN-γ/TNF-α versus IL-4/IL-10/TGF-β within the granuloma. Properdin and TSR4+5 may be implicated in maintaining this balance. It is not known whether complement proteins reside in the granuloma; however, during infection, complement proteins may be produced locally at sites of infection. Properdin may be secreted by neutrophils, monocytes and T cells locally at the site of infection (3). Thus, innate immune molecules residing in or being recruited at sites of infection may play a role in the balance of Th1/Th2, which may cause granuloma necrosis and replication of *M. tuberculosis* (41–43).

TNF-α was dramatically increased in the first 24 h of phagocytosis in the presence of properdin and TSR4+5, compared to non-treated mycobacteria. TNF-α plays a major role in granuloma formation and our results suggest that properdin may have a role in potentiating the pro-inflammatory response that results in granuloma formation. These observations are further strengthened by the concurrent increase in IL-1α levels over 24 h which have been shown to be key in macrophage proliferation and maturation during granuloma formation (44).

During phagocytosis, pro- and anti-inflammatory cytokines were produced by THP-1 cells when treated with properdin or TSR4+5. In the initial stages of infection by *M. bovis* BCG, pretreated with properdin, during phagocytosis, the expression of TNF-α was significantly enhanced. Other pro-inflammatory responses that were also elevated in the presence of properdin at initial stages of infection are IL-1β and IL-6. IL-1β is a mediator of inflammation and is required for host resistance to *M. tuberculosis* infection (45). IL-6 is a biomarker for tuberculosis, as increased levels are observed in patients with tuberculosis (46) that is required for a T cell response against *M. tuberculosis* infection (47, 48). Conversely, IL-10, IL-12, and TGF-β were downregulated by properdin, thus suppressing the anti-inflammatory response. The downregulation of IL-12 by properdin *in vivo* may suppress the Th1 response. TSR4+5 was also able to mimic the cytokine response like properdin, suggesting that the modules responsible for the major part of the interaction with *M. bovis* BCG may be TSR4+5.

Macrophages play a significant role in the innate immune response to pathogens and so are also crucial for an adaptive immune response (49). However, *M. tuberculosis* can evade the innate immune defense, inhibiting phagosome maturation (36), resisting anti-microbial agents damaging the bacterial cell wall

and facilitating replication within the host and escaping early immune recognition. Thus, these pathogens interfere with the early immune response and the induction of pro-inflammatory cytokines (49).

IL-10 and TGF-β suppression by properdin may enhance the clearance of mycobacteria by the host during the early stages of *M. tuberculosis* infection. After phagocystosis of *M. tuberculosis*, IL-10 has been shown to block phagolysosome maturation and antigen presentation by macrophages, thus aiding the survival of the pathogen (50, 51). Furthermore, IL-10 can inhibit the generation of reactive oxygen and nitrogen intermediates in IFN-γ activated macrophages, which are required for intracellular killing (52, 53). The enhanced levels of IL-10 and TGF-β in the lungs of active tuberculosis patients demonstrate a weakened immune response to *M. tuberculosis*, and hence, a role in the pathogenesis and disease progression (54, 55). VEGF was also found to be at a significantly higher level in tuberculosis patients with extrapulmonary tuberculosis (EPTB) than those with pulmonary disease (56). In our study, properdin and TSR4+5 seems to result in a marked elevation of VEGF after 48 h. Since our data also shows that mycobacteria have a reduced phagocytosis by macrophages, the resulting extracellular bacteria may be encouraged by VEGF to disseminate. The beneficial effect of properdin may be to inhibit the mechanisms involved in evasion and, thus, facilitate a protective response against mycobacterial infection.

The downregulation of IL-12 by properdin or TSR4+5 may be due to the reduced phagocytosis of *M. bovis* BCG, thus, downregulating the Th1 response. This may be necessary for the Th1/Th2 homeostasis in the protective granuloma (41, 57, 58). Both IL-10 and TGF-β levels were supressed, whilst TNF-α was elevated during the first 24 h after phagocytosis.

Although *M. bovis* BCG shares 99% genome homology to *M. tuberculosis*, there are some genetic differences which lead to its avirulence. The major difference between *M. bovis* BCG and *M. tuberculosis* is the large genomic deletion RD1, which causes the loss of various virulent genes coding for proteins such as ESAT-6, CFP-10 and also a bacterial secretion system (59, 60). Therefore the findings in our study will need to be validated using virulent strains of *M. tuberculosis*.

Properdin deficiency renders the host susceptible to a range of bacterial infections, especially *Neisseria* species. Three types of properdin deficiency have been reported: type I (absence of the properdin protein), type 2 (low level of properdin about 1–10% found in the serum), and type 3 deficiency (normal levels of protein being produced, but functionally defective). The most commonly reported deficiency is the type I properdin deficiency that exhibits fulminant infections. The incidence of tuberculosis has not been reported in properdin deficient subjects, possibly due to the majority of studies being in Scandinavia or western Europe, in populations where there is a low incidence of tuberculosis.

The data in this study suggest that properdin, *via* TSR4+5, may help in the clearance of mycobacterial infection by circumventing pathogen immune evasion strategies by upregulating the pro-inflammatory response. Properdin may also promote the formation and maintenance of the protective granuloma. The data in this study give further insights into the involvement of complement regulatory proteins in shaping the cellular immune response against mycobacteria in a complement activation-independent manner. Further studies are needed to fully characterize the nature and extent of involvement of properdin in tuberculosis pathogenesis, particularly in the early stages of infection.

The complement-independent interaction between human properdin and mycobacteria is a novel observation, which is independent of C3b deposition and aggregation of properdin (61). This is consistent with our recent study where we have shown that properdin can recognize chemical patterns on nanoparticles *via* TSR4+5 and modulate immune response by THP-1 cells (26) without involving complement activation/deposition. In conclusion, properdin may be involved in modulating host-pathogen interactions in tuberculosis. However, further studies are needed on pathogenic *M. tuberculosis* and *in vivo*, to understand the precise role of this complement regulatory protein in pathogenesis, which may give new insights into therapies against this formidable disease.

AUTHOR CONTRIBUTIONS

MA-M, AT, MA-A, and LK carried out crucial experiments. SA, MNA-A, AAP, VM, EMG, AK, and RBS provided crucial reagents and expertise. UK, AT and LK wrote the manuscript in addition to designing the experiments.

FUNDING

MA-A has been supported by the Ministry of Higher Education, Malaysia and the Universiti Sains Malaysia.

REFERENCES

1. Pangburn MK, Muller-Eberhard HJ. The C3 convertase of the alternative pathway of human complement. Enzymic properties of the bimolecular proteinase. *Biochem J* (1986) 235:723–30. doi:10.1042/bj2350723
2. Pillemer L, Blum L, Lepow IH, Ross OA, Todd EW, Wardlaw AC. The properdin system and immunity. I. Demonstration and isolation of a new serum protein, properdin, and its role in immune phenomena. *Science* (1954) 120:279–85. doi:10.1126/science.120.3112.279
3. Kouser L, Abdul-Aziz M, Nayak A, Stover CM, Sim RB, Kishore U. Properdin and factor h: opposing players on the alternative complement pathway "see-saw". *Front Immunol* (2013) 4:93. doi:10.3389/fimmu.2013.00093
4. Smith CA, Pangburn MK, Vogel CW, Muller-Eberhard HJ. Molecular architecture of human properdin, a positive regulator of the alternative pathway of complement. *J Biol Chem* (1984) 259:4582–8.
5. Higgins JM, Wiedemann H, Timpl R, Reid KB. Characterization of mutant forms of recombinant human properdin lacking single thrombospondin type I repeats identification of modules important for function. *J Immunol* (1995) 155:5777–85.
6. Goundis D, Reid KB. Properdin, the terminal complement components, thrombospondin and the circumsporozoite protein of malaria parasites contain similar sequence motifs. *Nature* (1988) 335:82–5.
7. Kouser L, Abdul-Aziz M, Tsolaki AG, Singhal D, Schwaeble WJ, Urban BC, et al. A recombinant two-module form of human properdin is an

inhibitor of the complement alternative pathway. *Mol Immunol* (2016) 73:76–87. doi:10.1016/j.molimm.2016.03.005
8. Pangburn MK. Analysis of the natural polymeric forms of human properdin and their functions in complement activation. *J Immunol* (1989) 142:202–7.
9. Alcorlo M, Tortajada A, Rodriguez de Cordoba S, Llorca O. Structural basis for the stabilization of the complement alternative pathway C3 convertase by properdin. *Proc Natl Acad Sci U S A* (2013) 110:13504–9. doi:10.1073/pnas.1309618110
10. Gulati S, Agarwal S, Vasudhev S, Rice PA, Ram S. Properdin is critical for antibody-dependent bactericidal activity against *Neisseria gonorrhoeae* that recruit C4b-binding protein. *J Immunol* (2012) 188:3416–25. doi:10.4049/jimmunol.1102746
11. Kimura Y, Miwa T, Zhou L, Song WC. Activator-specific requirement of properdin in the initiation and amplification of the alternative pathway complement. *Blood* (2008) 111:732–40. doi:10.1182/blood-2007-05-089821
12. Cortes C, Ferreira VP, Pangburn MK. Native properdin binds to *Chlamydia pneumoniae* and promotes complement activation. *Infect Immun* (2011) 79:724–31. doi:10.1128/IAI.00980-10
13. Ferreira VP, Cortes C, Pangburn MK. Native polymeric forms of properdin selectively bind to targets and promote activation of the alternative pathway of complement. *Immunobiology* (2010) 215:932–40. doi:10.1016/j.imbio.2010.02.002
14. Saggu G, Cortes C, Emch HN, Ramirez G, Worth RG, Ferreira VP. Identification of a novel mode of complement activation on stimulated platelets mediated by properdin and C3(H_2O). *J Immunol* (2013) 190:6457–67. doi:10.4049/jimmunol.1300610
15. Carroll MV, Lack N, Sim E, Krarup A, Sim RB. Multiple routes of complement activation by *Mycobacterium bovis* BCG. *Mol Immunol* (2009) 46:3367–78. doi:10.1016/j.molimm.2009.07.015
16. Ali YM, Hayat A, Saeed BM, Haleem KS, Alshamrani S, Kenawy HI, et al. Low-dose recombinant properdin provides substantial protection against *Streptococcus pneumoniae* and *Neisseria meningitidis* infection. *Proc Natl Acad Sci U S A* (2014) 111:5301–6. doi:10.1073/pnas.1401011111
17. Tsolaki AG. Innate immune recognition in tuberculosis infection. *Adv Exp Med Biol* (2009) 653:185–97. doi:10.1007/978-1-4419-0901-5_13
18. Rooijakkers SH, van Strijp JA. Bacterial complement evasion. *Mol Immunol* (2007) 44:23–32. doi:10.1016/j.molimm.2006.06.011
19. Abdul-Aziz M, Tsolaki AG, Kouser L, Carroll MV, Al-Ahdal MN, Sim RB, et al. Complement factor H interferes with *Mycobacterium bovis* BCG entry into macrophages and modulates the pro-inflammatory cytokine response. *Immunobiology* (2016) 221:944–52. doi:10.1016/j.imbio.2016.05.011
20. Ferguson JS, Weis JJ, Martin JL, Schlesinger LS. Complement protein C3 binding to *Mycobacterium tuberculosis* is initiated by the classical pathway in human bronchoalveolar lavage fluid. *Infect Immun* (2004) 72:2564–73. doi:10.1128/IAI.72.5.2564-2573.2004
21. Ramanathan VD, Curtis J, Turk JL. Activation of the alternative pathway of complement by mycobacteria and cord factor. *Infect Immun* (1980) 29:30–5.
22. Cywes C, Godenir NL, Hoppe HC, Scholle RR, Steyn LM, Kirsch RE, et al. Nonopsonic binding of *Mycobacterium tuberculosis* to human complement receptor type 3 expressed in Chinese hamster ovary cells. *Infect Immun* (1996) 64:5373–83.
23. Hu C, Mayadas-Norton T, Tanaka K, Chan J, Salgame P. *Mycobacterium tuberculosis* infection in complement receptor 3-deficient mice. *J Immunol* (2000) 165:2596–602. doi:10.4049/jimmunol.165.5.2596
24. Schlesinger LS, Bellinger-Kawahara CG, Payne NR, Horwitz MA. Phagocytosis of *Mycobacterium tuberculosis* is mediated by human monocyte complement receptors and complement component C3. *J Immunol* (1990) 144:2771–80.
25. Cywes C, Hoppe HC, Daffé M, Ehlers MR. Nonopsonic binding of Mycobacterium tuberculosis to complement receptor type 3 is mediated by capsular polysaccharides and is strain dependent. *Infect Immun* (1997) 65:4258–66.
26. Kouser L, Paudyal B, Kaur A, Stenbeck G, Jones LA, Abozaid SM, et al. Human properdin opsonizes nanoparticles and triggers a potent pro-inflammatory response by macrophages without involving complement activation. *Front Immunol* (2018) 9:131. doi:10.3389/fimmu.2018.00131
27. Kemper C, Hourcade DE. Properdin: new roles in pattern recognition and target clearance. *Mol Immunol* (2008) 45:4048–56. doi:10.1016/j.molimm.2008.06.034
28. Kemper C, Atkinson JP, Hourcade DE. Properdin: emerging roles of a pattern-recognition molecule. *Annu Rev Immunol* (2010) 28:131–55. doi:10.1146/annurev-immunol-030409-101250
29. Perdikoulis MV, Kishore U, Reid KB. Expression and characterisation of the thrombospondin type I repeats of human properdin. *Biochim Biophys Acta* (2001) 1548:265–77. doi:10.1016/S0167-4838(01)00238-2
30. Daigneault M, Preston JA, Marriott HM, Whyte MK, Dockrell DH. The identification of markers of macrophage differentiation in PMA-stimulated THP-1 cells and monocyte-derived macrophages. *PLoS One* (2010) 5:e8668. doi:10.1371/journal.pone.0008668
31. Al-Rayahi IA, Browning MJ, Stover C. Tumour cell conditioned medium reveals greater M2 skewing of macrophages in the absence of properdin. *Immun Inflamm Dis* (2017) 5:68–77. doi:10.1002/iid3.142
32. Xu W, Berger SP, Trouw LA, de Boer HC, Schlagwein N, Mutsaers C, et al. Properdin binds to late apoptotic and necrotic cells independently of C3b and regulates alternative pathway complement activation. *J Immunol* (2008) 180:7613–21. doi:10.4049/jimmunol.180.11.7613
33. Dixon KO, O'Flynn J, Klar-Mohamad N, Daha MR, van Kooten C. Properdin and factor H production by human dendritic cells modulates their T-cell stimulatory capacity and is regulated by IFN-gamma. *Eur J Immunol* (2017) 47:470–80. doi:10.1002/eji.201646703
34. Narni-Mancinelli E, Gauthier L, Baratin M, Guia S, Fenis A, Deghmane AE, et al. Complement factor P is a ligand for the natural killer cell-activating receptor NKp46. *Sci Immunol* (2017) 2(10):eaam9628. doi:10.1126/sciimmunol.aam9628
35. Agarwal S, Specht CA, Haibin H, Ostroff GR, Ram S, Rice PA, et al. Linkage specificity and role of properdin in activation of the alternative complement pathway by fungal glycans. *MBio* (2011) 2(5):e00178-11. doi:10.1128/mBio.00178-11
36. Russell DG. *Mycobacterium tuberculosis*: here today, and here tomorrow. *Nat Rev Mol Cell Biol* (2001) 2:569–77. doi:10.1038/35085034
37. Feng CG, Kaviratne M, Rothfuchs AG, Cheever A, Hieny S, Young HA, et al. NK cell-derived IFN-gamma differentially regulates innate resistance and neutrophil response in T cell-deficient hosts infected with *Mycobacterium tuberculosis*. *J Immunol* (2006) 177:7086–93. doi:10.4049/jimmunol.177.10.7086
38. Eum SY, Kong JH, Hong MS, Lee YJ, Kim JH, Hwang SH, et al. Neutrophils are the predominant infected phagocytic cells in the airways of patients with active pulmonary tuberculosis. *Chest* (2010) 137:122–8. doi:10.1378/chest.09-0903
39. Smith D, Hansch H, Bancroft G, Ehlers S. T-cell-independent granuloma formation in response to *Mycobacterium avium*: role of tumour necrosis factor-alpha and interferon-gamma. *Immunology* (1997) 92:413–21. doi:10.1046/j.1365-2567.1997.00384.x
40. Algood HM, Chan J, Flynn JL. Chemokines and tuberculosis. *Cytokine Growth Factor Rev* (2003) 14:467–77. doi:10.1016/S1359-6101(03)00054-6
41. Ehlers S, Schaible UE. The granuloma in tuberculosis: dynamics of a host-pathogen collusion. *Front Immunol* (2012) 3:411. doi:10.3389/fimmu.2012.00411
42. Dannenberg AM Jr. Delayed-type hypersensitivity and cell-mediated immunity in the pathogenesis of tuberculosis. *Immunol Today* (1991) 12:228–33. doi:10.1016/0167-5699(91)90035-R
43. Sanghi S, Grewal RS, Vasudevan B, Lodha N. Immune reconstitution inflammatory syndrome in leprosy. *Indian J Lepr* (2011) 83:61–70.
44. Huaux F, Lo Re S, Giordano G, Uwambayinema F, Devosse R, Yakoub Y, et al. IL-1α induces CD11b(low) alveolar macrophage proliferation and maturation during granuloma formation. *J Pathol* (2015) 235(5):698–709. doi:10.1002/path.4487
45. Mayer-Barber KD, Barber DL, Shenderov K, White SD, Wilson MS, Cheever A, et al. Caspase-1 independent IL-1beta production is critical for host resistance to *Mycobacterium tuberculosis* and does not require TLR signaling in vivo. *J Immunol* (2010) 184:3326–30. doi:10.4049/jimmunol.0904189
46. Correia JW, Freitas MV, Queiroz JA, PereiraPerrin M, Cavadas B. Interleukin-6 blood levels in sensitive and multiresistant tuberculosis. *Infection* (2009) 37:138–41. doi:10.1007/s15010-008-7398-3
47. Leal IS, Smedegard B, Andersen P, Appelberg R. Interleukin-6 and interleukin-12 participate in induction of a type 1 protective T-cell response during vaccination with a tuberculosis subunit vaccine. *Infect Immun* (1999) 67:5747–54.

48. Appelberg R, Castro AG, Pedrosa J, Minoprio P. Role of interleukin-6 in the induction of protective T cells during mycobacterial infections in mice. *Immunology* (1994) 82:361–4.
49. Bhatt K, Salgame P. Host innate immune response to *Mycobacterium tuberculosis*. *J Clin Immunol* (2007) 27:347–62. doi:10.1007/s10875-007-9084-0
50. Shaw TC, Thomas LH, Friedland JS. Regulation of IL-10 secretion after phagocytosis of *Mycobacterium tuberculosis* by human monocytic cells. *Cytokine* (2000) 12:483–6. doi:10.1006/cyto.1999.0586
51. O'Leary S, O'Sullivan MP, Keane J. IL-10 blocks phagosome maturation in *Mycobacterium tuberculosis*-infected human macrophages. *Am J Respir Cell Mol Biol* (2011) 45:172–80. doi:10.1165/rcmb.2010-0319OC
52. Moore KW, de Waal Malefyt R, Coffman RL, O'Garra A. Interleukin-10 and the interleukin-10 receptor. *Annu Rev Immunol* (2001) 19:683–765. doi:10.1146/annurev.immunol.19.1.683
53. Gazzinelli RT, Oswald IP, James SL, Sher A. IL-10 inhibits parasite killing and nitrogen oxide production by IFN-gamma-activated macrophages. *J Immunol* (1992) 148:1792–6.
54. Almeida AS, Lago PM, Boechat N, Huard RC, Lazzarini LC, Santos AR, et al. Tuberculosis is associated with a down-modulatory lung immune response that impairs Th1-type immunity. *J Immunol* (2009) 183:718–31. doi:10.4049/jimmunol.0801212
55. Barnes PF, Lu S, Abrams JS, Wang E, Yamamura M, Modlin RL. Cytokine production at the site of disease in human tuberculosis. *Infect Immun* (1993) 61:3482–9.
56. Ranaivomanana P, Raberahona M, Rabarioelina S, Borella Y, Machado A, Randria MJD. Cytokine biomarkers associated with human extra-pulmonary tuberculosis clinical strains and symptoms. *Front Microbiol* (2018) 9:275. doi:10.3389/fmicb.2018.00275
57. Aly S, Mages J, Reiling N, Kalinke U, Decker T, Lang R, et al. Mycobacteria-induced granuloma necrosis depends on IRF-1. *J Cell Mol Med* (2009) 13:2069–82. doi:10.1111/j.1582-4934.2008.00470.x
58. Rook GA. Th2 cytokines in susceptibility to tuberculosis. *Curr Mol Med* (2007) 7:327–37. doi:10.2174/156652407780598557
59. Gordon SV, Brosch R, Billault A, Garnier T, Eiglmeier K, Cole ST. Identification of variable regions in the genomes of tubercle bacilli using bacterial artificial chromosome arrays. *Mol Microbiol* (1999) 32:643–55. doi:10.1046/j.1365-2958.1999.01383.x
60. Brodin P, Majlessi L, Marsollier L, de Jonge MI, Bottai D, Demangel C, et al. Dissection of ESAT-6 system 1 of *Mycobacterium tuberculosis* and impact on immunogenicity and virulence. *Infect Immun* (2006) 74:88–98. doi:10.1128/IAI.74.1.88-98.2006
61. Harboe M, Johnson C, Nymo S, Ekholt K, Schjalm C, Lindstad JK, et al. Properdin binding to complement activating surfaces depends on initial C3b deposition. *Proc Natl Acad Sci U S A* (2017) 114(4):E534–9. doi:10.1073/pnas.1612385114

Conflict of Interest Statement: The authors declare that the research was conducted in the absence of any commercial or financial relationships that could be construed as a potential conflict of interest.

frontiers in Immunology

ORIGINAL RESEARCH
published: 04 June 2018
doi: 10.3389/fimmu.2018.01126

A Recombinant Fragment of Human Surfactant Protein D induces Apoptosis in Pancreatic Cancer Cell Lines *via* Fas-Mediated Pathway

*Anuvinder Kaur[1], Muhammad Suleman Riaz[1], Valarmathy Murugaiah[1], Praveen Mathews Varghese[1], Shiv K. Singh[2] and Uday Kishore[1]**

[1] Biosciences, College of Health and Life Sciences, Brunel University London, Uxbridge, United Kingdom,
[2] Department of Gastroenterology and Gastrointestinal Oncology, University Medical Center, Goettingen, Germany

OPEN ACCESS

Edited by:
Janos G. Filep, Université de Montréal, Canada

Reviewed by:
Taruna Madan, National Institute for Research in Reproductive Health (ICMR), India
Soren Werner Karlskov Hansen, University of Southern Denmark Odense, Denmark
Kenneth Reid, University of Oxford, United Kingdom

***Correspondence:**
Uday Kishore
uday.kishore@brunel.ac.uk, ukishore@hotmail.com

Specialty section:
This article was submitted to Molecular Innate Immunity, a section of the journal Frontiers in Immunology

Received: *13 October 2017*
Accepted: *03 May 2018*
Published: *04 June 2018*

Citation:
Kaur A, Riaz MS, Murugaiah V, Varghese PM, Singh SK and Kishore U (2018) A Recombinant Fragment of Human Surfactant Protein D induces Apoptosis in Pancreatic Cancer Cell Lines via Fas-Mediated Pathway. Front. Immunol. 9:1126. doi: 10.3389/fimmu.2018.01126

Human surfactant protein D (SP-D) is a potent innate immune molecule, which is emerging as a key molecule in the recognition and clearance of altered and non-self targets. Previous studies have shown that a recombinant fragment of human SP-D (rfhSP-D) induced apoptosis *via* p53-mediated apoptosis pathway in an eosinophilic leukemic cell line, AML14.3D10. Here, we report the ability of rfhSP-D to induce apoptosis *via* TNF-α/Fas-mediated pathway regardless of the p53 status in human pancreatic adenocarcinoma using Panc-1 ($p53^{mt}$), MiaPaCa-2 ($p53^{mt}$), and Capan-2 ($p53^{wt}$) cell lines. Treatment of these cell lines with rfhSP-D for 24 h caused growth arrest in G1 cell cycle phase and triggered transcriptional upregulation of pro-apoptotic factors such as TNF-α and NF-κB. Translocation of NF-κB from the cytoplasm into the nucleus of pancreatic cancer cell lines was observed *via* immunofluorescence microscopy following treatment with rfhSP-D as compared to the untreated cells. The rfhSP-D treatment caused upregulation of pro-apoptotic marker Fas, as analyzed *via* qPCR and western blot, which then triggered caspase cascade, as evident from cleavage of caspase 8 and 3 analyzed *via* western blot at 48 h. The cell number following the rfhSP-D treatment was reduced in the order of Panc-1 (~67%) > MiaPaCa-2 (~60%) > Capan-2 (~35%). This study appears to suggest that rfhSP-D can potentially be used to therapeutically target pancreatic cancer cells irrespective of their p53 phenotype.

Keywords: pancreatic cancer, innate immunity, surfactant protein D, apoptosis, immune surveillance

INTRODUCTION

Human surfactant protein D (SP-D), a member of soluble C-type lectin family called Collectins, plays a vital role in linking the innate and adaptive immunity to protect against infection, allergy, and inflammation (1). Although its homeostatic role in lungs has been widely studied, its specific functions at extra-pulmonary tissues such as kidney, human trachea, brain, testis, heart, prostate, kidneys, and pancreas are poorly understood (1–3). SP-D deficiency in animal models has been shown to be associated with considerable pathophysiological consequences (4–6). SP-D gene knockout mice showed chronic inflammation and fibrosis due to accumulation of surfactant phospholipids in the lungs, monocytes infiltration, and activation of pro-inflammatory alveolar macrophages (5, 6). The absence of SP-D in children makes them more susceptible to frequent pneumonia as compared to

SP-D sufficient children (7). *SFTPD* (SP-D gene) polymorphisms increase the susceptibility to chronic and infectious lung diseases (8), pneumococcal lung disease (9), emphysema (10), tuberculosis (11, 12), Crohn's disease, and ulcerative colitis (12).

SP-D has been shown to be a potent innate immune molecule at pulmonary as well as extra-pulmonary mucosal surfaces by virtue of its ability to control inflammatory response and helper T cell polarization (3). The first clue came *via* a murine model of allergic hypersensitivity, when therapeutic treatment with a recombinant fragment of human SP-D (rfhSP-D) lowered peripheral and pulmonary eosinophilia, in addition to specific IgE levels and Th2 cytokines in the spleen (13, 14). It turned out that rfhSP-D selectively induced apoptosis in sensitized eosinophils derived from allergic patients (15). Using an eosinophilic cell line, AML14.3D10 (a model cell line for leukemia), it was established, *via* proteomics analysis, that apoptosis induction by rfhSP-D involved upregulation of p53 (16, 17). Another crucial study by Pandit et al. (18) revealed that rfhSP-D was able to induce apoptosis in activated human PBMCs, but not in resting, non-activated PBMCs. These studies, for the first time, raised the possibility that SP-D can have a function of immune surveillance against activated self and perhaps altered self. Recently, human lung adenocarcinoma cells (A549 cell line), when exogenously treated with SP-D, showed suppressed epidermal growth factor (EGF) signaling by reducing the EGF binding to EGFR, which subsequently reduced the cell proliferation, invasion, and migration of cancer cells (19).

Here, we set out to examine a possible pro-apoptotic role of SP-D in pancreatic cancer. Pancreatic cancer is the fourth leading cause of cancer-related mortality in the western world (20, 21) and its 5-year survival rate is ~5% (22). The poor prognosis has been attributed to the silent nature of the tumor in early stages, aggressive phenotype, surgical complications, and lack of targeted efficacious therapies (23). In this study, we show that rfhSP-D, composed of 8 Gly-X-Y repeats, homotrimeric neck and carbohydrate recognition domains (CRDs) (1), induces cell growth arrest in G1 phase and subsequent apoptosis in human pancreatic adenocarcinoma cells using Panc-1, MiaPaCa-2, and Capan-2 cell lines. The apoptosis induction appears to involve TNF-α, NF-κB, and Fas axis, revealing a p53 independent route of apoptosis induction in the p53 mutated Panc-1 and MiaPaCa-2 cell lines and p53-dependent apoptosis in p53 wild type Capan-2 cell line by rfhSP-D.

MATERIALS AND METHODS

Cell Culture and Treatments

Human pancreatic cancer cells lines, Panc-1 (CRL-1469), MiaPaCa-2 (CRL-1420), and Capan-2 (HTB-80), were obtained from ATCC and used as an *in vitro* model in this study. All cell lines were cultured at 37°C under 5% v/v CO_2 using DMEM-F12 media (Thermo Fisher) containing 10% v/v fetal calf serum with 2 mM L-glutamine, and penicillin (100 U/ml)/streptomycin (100 μg/ml) (Thermo Fisher) until 80–90% confluency was reached.

Expression and Purification of rfhSP-D

Plasmid pUK-D1 (containing cDNA sequences for 8 Gly-X-Y repeats, neck, and CRD region of human SP-D), transformed into *Escherichia coli* BL21 (λDE3) pLysS (Invitrogen), was used to express rfhSP-D, as described earlier (15, 16). The expression cassette included a short stretch of eight N-terminal Gly–X–Y triplets with substitution of S for P in position 2 (residue 180), followed by the α-helical coiled-coil neck region (residues 203–235) and the globular CRD region (residues 236–355). Endotoxin levels were determined using the QCL-1000 Limulus amebocyte lysate system (Lonza) and the assay was found to be linear over a range of 0.1–1.0 EU/ml (10 EU = 1 ng of endotoxin). The amount of endotoxin levels were <4 pg/μg of the rfhSP-D. Full length native SP-D (FL-SP-D) was purified form lung washings of alveolar proteinosis patients using methods previously described by Strong et al. (24).

Fluorescence Microscopy

All cell lines used in this study (Panc-1, MiaPaCa-2, and Capan-2) were grown on coverslips using 0.5×10^5 cells overnight. Next day, cells were washed three times with PBS before being incubated with rfhSP-D (20 μg/ml) in a serum-free DMEM-F12 medium. For rfhSP-D and FL-SP-D binding analysis, the coverslips were incubated for 1 h with mouse anti-human SP-D (rfhSP-D) and rabbit anti-human SP-D (FL-SP-D) (MRC Immunochemistry Unit, Oxford; 1:200), followed by goat anti-mouse IgG H&L (Cy5) and Goat anti-Rabbit IgG H&L Alexa Fluor 488 (1:500; Abcam), respectively, and Hoechst (1:10,000; Thermo Fisher) for fluorescence microscopy analysis. For apoptosis analysis *via* fluorescence microscopy using an FITC annexin V apoptosis detection kit with propidium iodide (PI) (BioLegend), the cells were incubated with rfhSP-D (20 μg/ml) for 48 h. After 48 h, the cells were incubated with annexin V binding buffer containing FITC annexin V (1:200), PI (1:200), and Hoechst (1:10,000) for 15 min, and washed twice with PBS before mounting on the slides to visualize under a HF14 Leica DM4000 microscope.

Flow Cytometry

Cell lines were plated in a 6-well plate (0.1×10^7) and incubated with rfhSP-D (20 μg/ml), FL-SP-D (10 and 20 μg/ml), and an

TABLE 1 | Target genes and terminal primers used in the qPCR analysis.

Target gene	Forward primer	Reverse primer
18S	5′-ATGGCCGTTCT TAGTTGGTG-3′	5′-CGCTGAGCCAG TCAGTGTAG-3′
Fas	5′-ACACTCACCAG CAACACCAA-3′	5′-TGCCACTGTTTC AGGATTTAA-3′
mTOR	5′-TGCCAACTATCT TCGGAACC-3′	5′-GCTCGCTTCACC TCAAATTC-3′
TNF-α	5′-GTATCGCCAGG AATTGTTGC-3′	5′-AGCCCATGTTGT AGCAAACC-3′
NF-κB	5′-TGAGGTACAGGC CCTCTGAT-3′	5′-GTATTTCAACCAC AGATGGCACT-3′
P53	5′-AGCACTGTCCAA CAACACCA-3′	5′-CTTCAGGTGGCT GGAGTGAG-3′

untreated control, for 24 and 48 h, followed by cell detachment using 5 mM EDTA, pH 8, and centrifugation at 1,200 × *g* for 5 min. For cell cycle analysis, the cells were fixed in 70% v/v ethanol for 30 min at 4°C, followed by PBS wash twice at 850 × *g*. The cells were then treated with ribonuclease (100 µg/ml) to ensure DNA staining without RNA contamination before staining with PI (50 µg/ml). 10,000 cells were then acquired for both treated and untreated samples and the PI histograms were plotted using the set markers within the analysis program of Novocyte Flow Cytometer. For apoptosis analysis *via* FACS, FITC annexin V apoptosis detection kit with PI (BioLegend) was used, as per manufacturer's instructions. Compensation parameters were acquired using unstained, untreated FITC stained, and untreated PI stained cells.

MTT Assay

MTT (3-[4,5-dimethylthiazol-2-yl]-2,5-diphenyltetrazolium bromide) (Thermo Fisher) assay was performed by incubating pancreatic cancer cells (0.1×10^5) in a 96-well microtiter plate with rfhSP-D, FL-SP-D (10 and 20 µg/ml), and an untreated control in serum-free DMEM-F12 medium for 48 h, followed by incubation with 50 µg/µl MTT (5 mg/ml stock) per well for 4 h at 37°C. Majority of the media was removed leaving behind 25 µl per well, which was mixed thoroughly with 50 µl of dimethyl

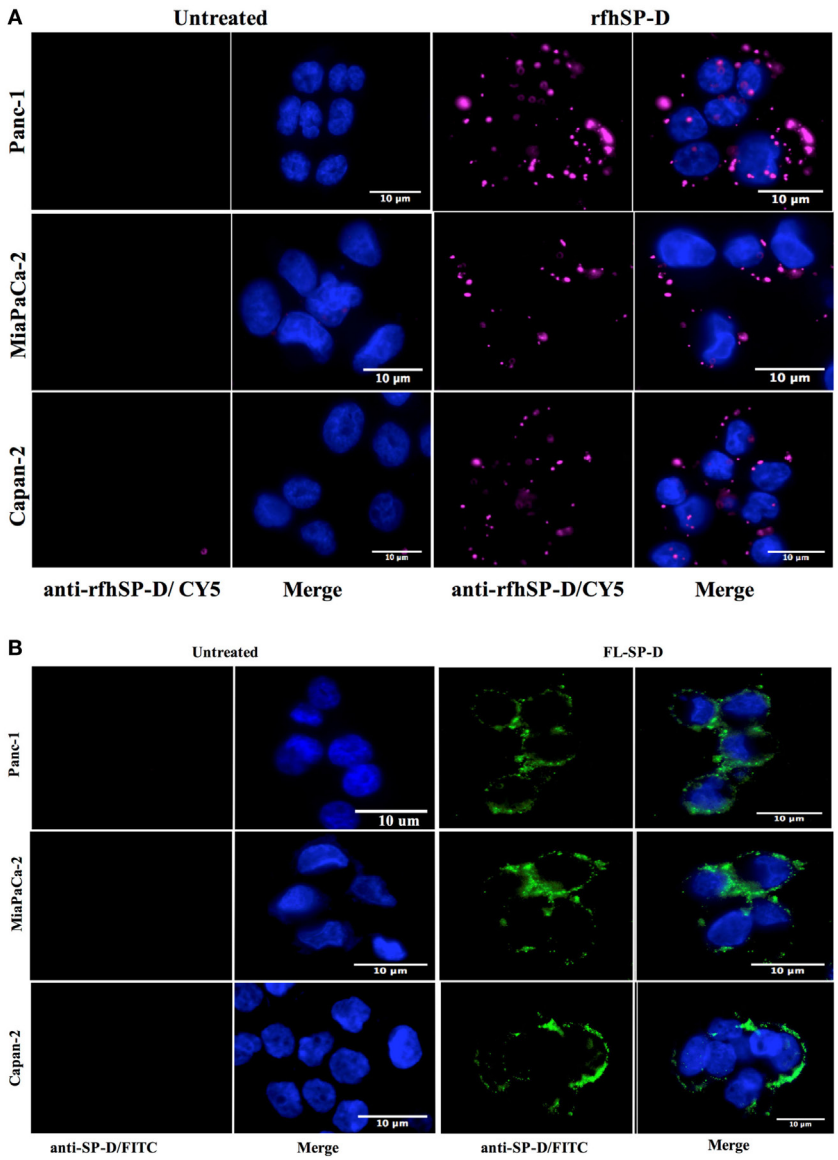

FIGURE 1 | **(A)** Fluorescence microscopy showing binding of rfhSP-D and **(B)** FL-SP-D (10 µg/ml; 1 h incubation) to Panc-1, MiaPaCa-2, and Capan-2 cells. The nucleus of the cells was stained with Hoechst. Cells were probed with mouse anti-human SP-D/CY5 (rfhSP-D) and rabbit anti-human/FITC (FL-SP-D); the bound proteins are visible on the cell membrane in the treated cells. No CY5 or FITC fluorescence was detected in the untreated control cells.

sulfoxide and incubated for another 10 min at 37°C. The absorbance was read at 570 nm using a plate reader.

Western Blot

Cell lines (0.1×10^7 cells) were seeded in a 6-well plate (Nunc) and incubated with rfhSP-D (20 µg/ml), together with an untreated control, in a serum-free DMEM-F12 medium. The cells were lysed within the wells using treatment buffer (50 mM Tris-HCl pH 6.8, 2% v/v β-mercaptoethanol, 2% v/v SDS, 0.1% w/v bromophenol blue, and 10% v/v glycerol) and transferred to pre-cooled microcentrifuge tubes followed by sonication for 15 s. The samples were heated at 100°C for 10 min and subjected to SDS-PAGE (12% w/v) for 90 min at 120 V. The SDS-PAGE separated proteins were then electrophoretically transferred onto a nitrocellulose membrane (Thermo Fisher) using an iBLOT (Thermo Fisher). The membrane was then blocked using 5% w/v dried milk powder (Sigma) in 100 ml PBS for 2 h on a rotatory shaker at room temperature. The membrane was incubated with rabbit anti-human caspase primary antibodies (anti-cleaved caspase 3; anti-cleaved caspase 8; Cell Signaling) at 4°C overnight, followed by incubation with secondary Goat anti-rabbit IgG HRP-conjugate (1:1,000; Promega) for 1 h at room temperature. The membrane was washed with PBST (PBS + 0.05% Tween 20) three times, 10 min each time. The color was developed using 3,3′-diaminobenzidine substrate kit (Thermo Fisher).

Quantitative RT-PCR

Panc-1, MiaPaCa-2, and Capan-2 cells were incubated with and without rfhSP-D (20 µg/ml) for various time points. The cell pellet

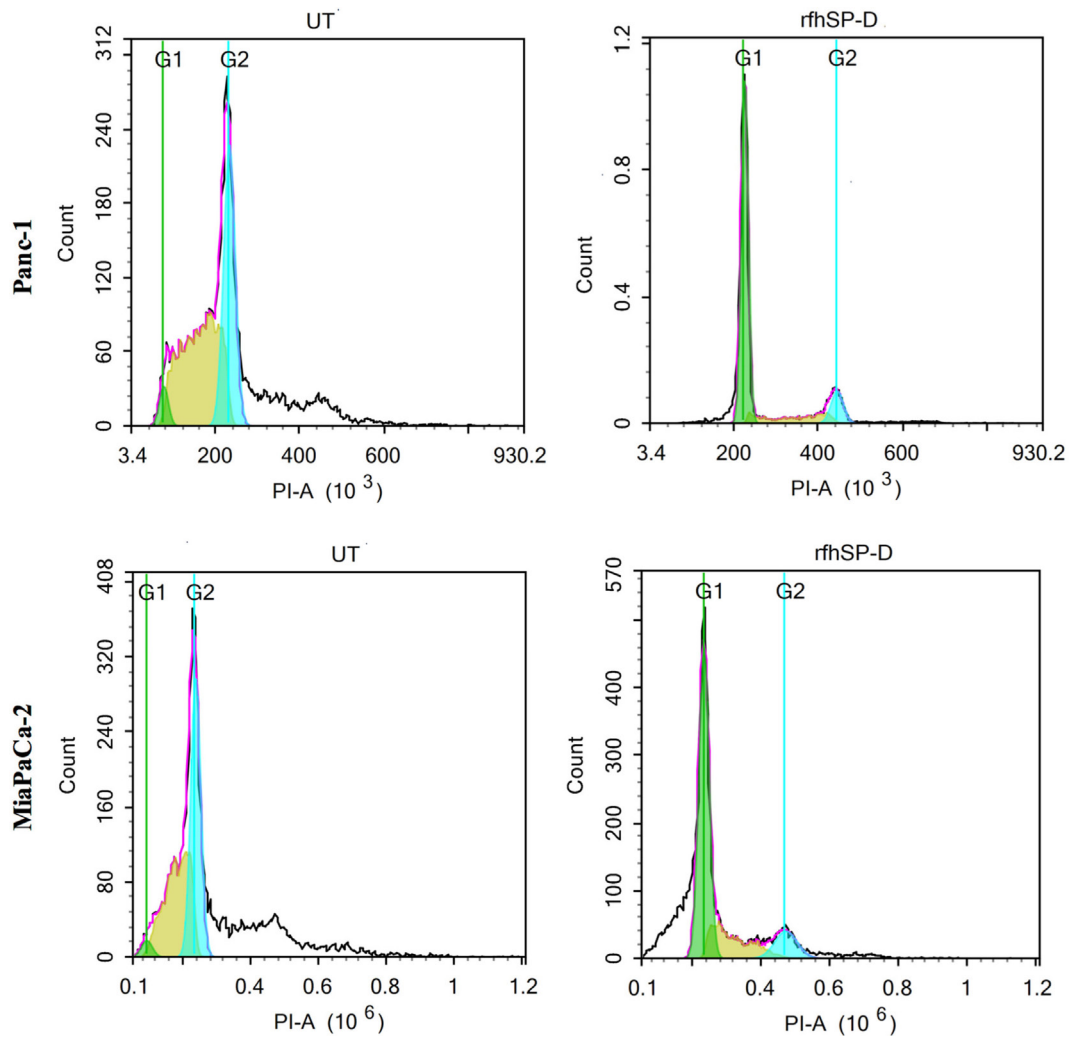

FIGURE 2 | Cell cycle analysis following 24 h treatment of pancreatic cancer cell lines with rfhSP-D. Propidium iodide (PI) was used to stain DNA. PI histograms were plotted using set markers within the analysis program of Novocyte Flow cytometer. The rfhSP-D treated pancreatic cancer cells show arrest in G1 phase in the case of Panc-1 (G1 phase: 68%; S phase: 13%; G2 phase: 11%) and MiaPaCa-2 (G1 phase: ~50%; S phase: 17%; G2 phase: 10%) cell line at 24 h, whereas untreated Panc-1 cells (G1 phase: 3%; S phase: 42%; G2 phase: 32%) and MiaPaCa-2 cells (G1 phase: 2%; S phase: 32%; G2 phase: 33%) progressed to the next cell cycle phases.

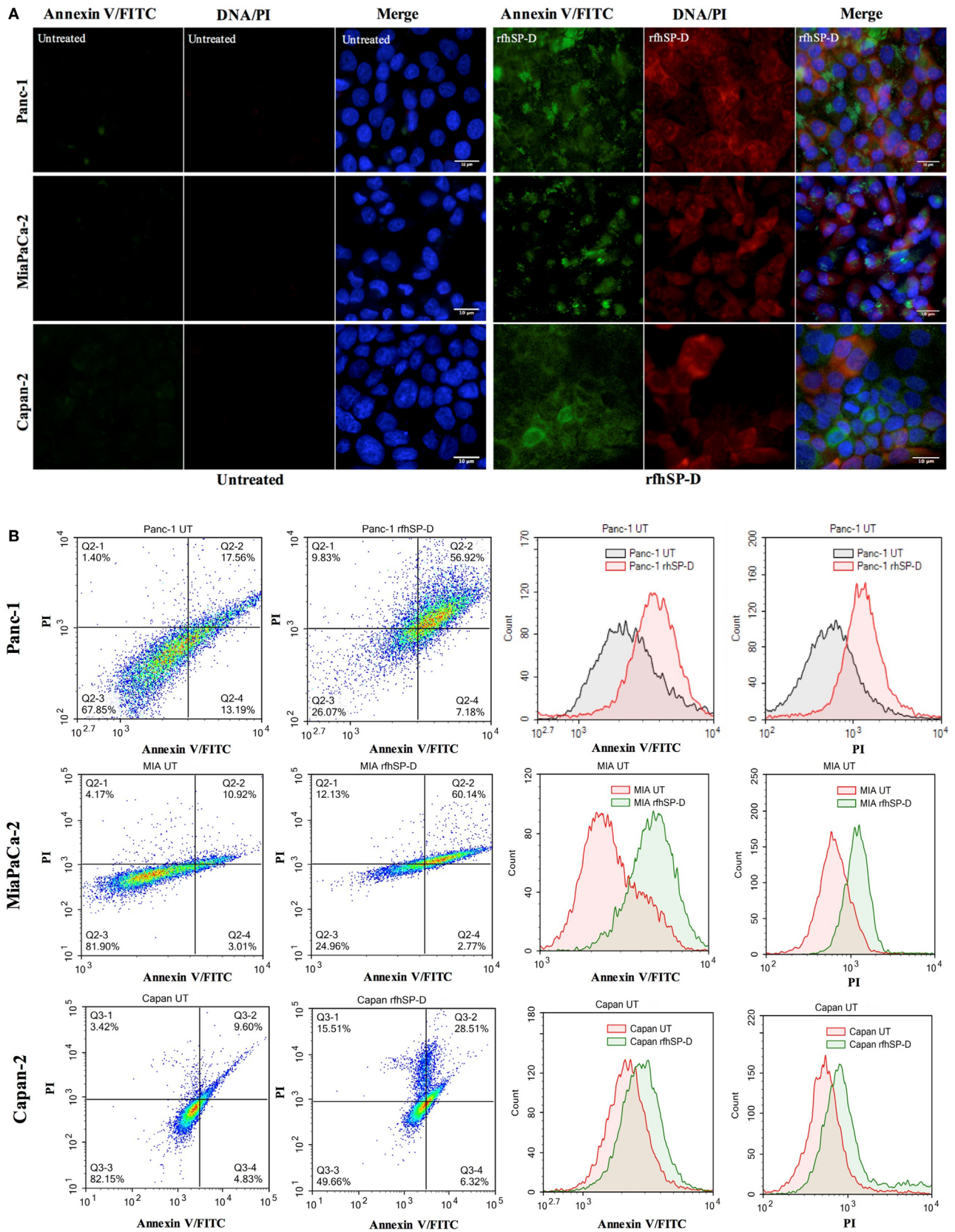

FIGURE 3 | Continued

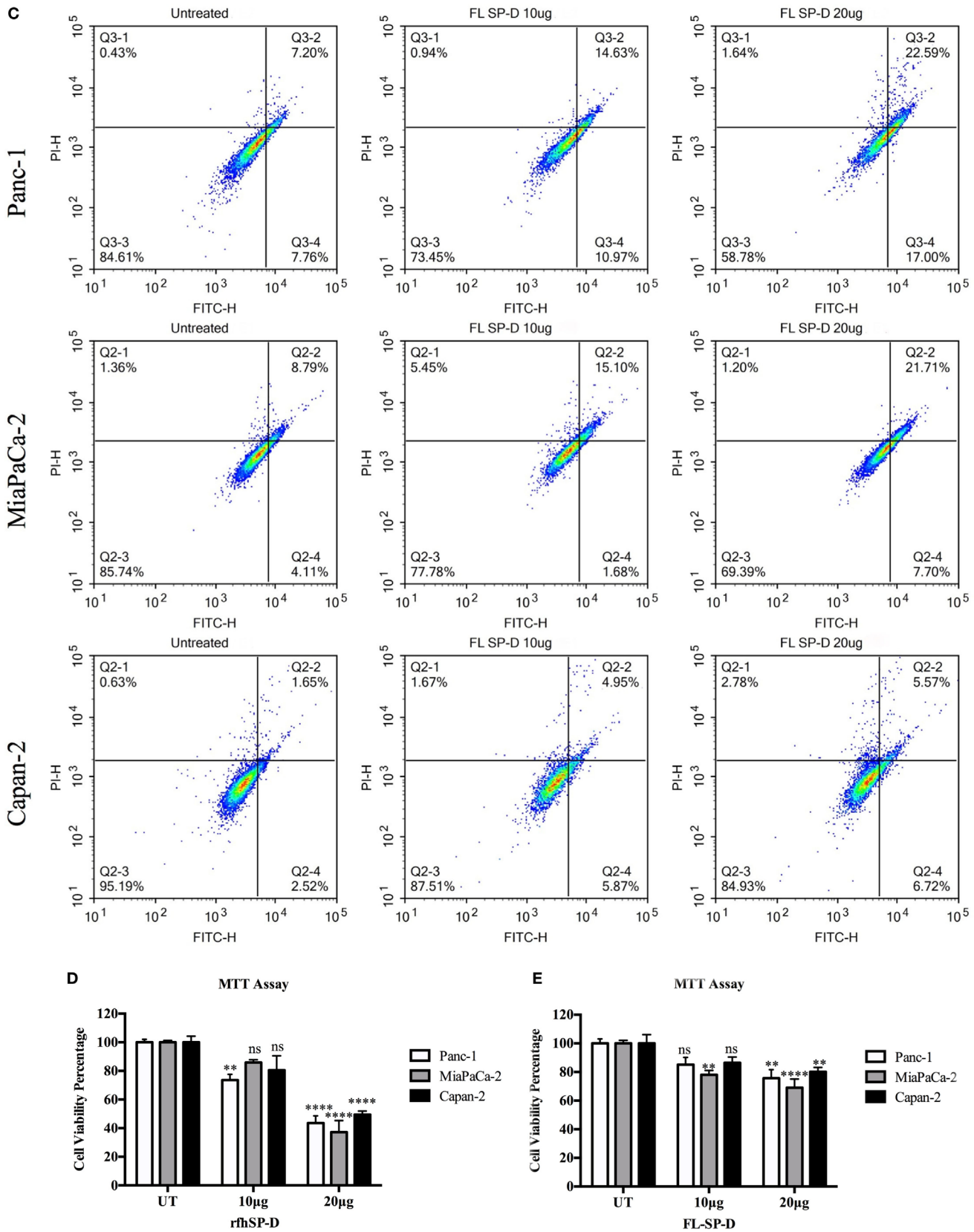

FIGURE 3 | Continued

FIGURE 3 | **(A)** Fluorescence microscopy to analyze apoptosis in pancreatic cancer cell lines following treatment with rfhSP-D. Cells were treated with rfhSP-D for 48 h and apoptosis was analyzed using an annexin V/propidium iodide (PI) staining kit. The cell membrane was positively stained for annexin V and the DNA staining is visible in the treated cells indicating that the cells underwent apoptosis turning the membrane inside out, thus making phosphatidylserine available for annexin V binding; due to the porous membrane, PI was taken in which stained the DNA of apoptotic cells. No such staining was seen in the untreated cells. The nucleus was stained with Hoechst for both treated and untreated cells. **(B,C)** Quantitative analysis of apoptosis using Flow Cytometer. Cells were treated with rfhSP-D or FL-SP-D for 48 h and apoptosis was analyzed using annexin V with PI kit. 10,000 cells were acquired and plotted for both annexin V/FITC and DNA/PI staining, which showed a shift in the fluorescence intensity of both FITC and PI between treated and untreated cells. Approximately 67% of Panc-1 cells, ~60% MiaPaCa-2 cells, and ~35% Capan-2 cells underwent apoptosis following rfhSP-D treatment and ~25% Panc-1 and MiaPaCa-2 cells following FL-SP-D treatment as compared to untreated cells. No significant difference was seen in Capan-2 cells following FL-SP-D treatment. **(D,E)** MTT assay to assess cell viability following treatment with rfhSP-D and FL-SP-D (10 and 20 μg/ml) and untreated for 48 h (±SEM, of three independent experiments). Cell numbers were reduced by approximately 70% in the rfhSP-D-treated Panc-1, 60% in MiaPaCa-2, and 45% in Capan-2 cells, as compared to untreated cells. Cell numbers were reduced by approximately 25% in the Panc-1 and MiaPaCa-2 and less than 10% in Capan-2 cells treated with FL-SP-D as compared to untreated cells. Significance was established using the unpaired two-way ANOVA test (**$p < 0.01$, ****$p < 0.0001$, ns: non-significant) ($n = 3$).

for each time-point was centrifuged and stored at −80°C. RNA was extracted using GenElute Mammalian Total RNA Purification Kit (Sigma-Aldrich, UK), as per manufacturer's instructions, followed by treatment with DNase I (Sigma-Aldrich, UK). The absorbance at 260 and 260:280 nm ratio was used to determine the concentration and purity of total RNA, respectively, using NanoDrop 2000/2000c (Thermo-Fisher Scientific). Total RNA (2 μg) was used for cDNA synthesis using High Capacity RNA to cDNA Kit (Applied Biosystems). The forward and reverse primers used in this study were designed using the web based Basic Local Alignment Search Tool and Primer-BLAST (http://blast.ncbi.nlm.nih.gov/Blast.cgi) are given in **Table 1**.

Relative mRNA expression was determined by qPCR reactions performed in triplicates consisting of 10 μl final volume per well [5 μl Power SYBR Green MasterMix (Applied Biosystems), 75 nM of forward and reverse primers, and 500 ng cDNA], using the 7900HT Fast Real-Time PCR System (Applied Biosystems). Samples were initially incubated at 50°C (2 min) and 95°C (10 min), followed by 40 cycles (each cycle for 15 s at 95°C and 1 min at 60°C) for amplification of the template. Human 18S rRNA, an endogenous control, was used to normalize the gene expression. Relative quantification (RQ) value and formula: $RQ = 2^{-\Delta\Delta Ct}$ was used to calculate the relative expression of each target.

Statistical Analysis

Graphs were made and statistically analyzed using Graphpad Prism 6.0 by applying an unpaired two-way ANOVA test. Significance of values is based on *$p < 0.05$, **$p < 0.01$, ***$p < 0.001$, ****$p < 0.0001$ between treated and untreated samples. Error bars represent the SD or SEM, as indicated in the figure legends.

RESULTS

rfhSP-D Binds to a Range of Pancreatic Cell Lines

The fluorescence microscopy analysis of rfhSP-D and FL-SP-D binding to Panc-1, MiaPaCa-2, and Capan-2 cells revealed its membrane localization following 1 h incubation at 4°C (**Figure 1**). The rfhSP-D probed with mouse anti-human SP-D-CY5 antibody and FL-SP-D probed with rabbit anti-human SP-D-FITC appeared evenly bound in clusters on the cell membrane, along with nucleus stained positively with Hoechst. All cell lines showed a similar rfhSP-D and FL-SP-D binding pattern. No CY5 or FITC fluorescence was detected in the untreated controls, probed with primary and secondary antibodies, for each cell line, suggesting the rfhSP-D and FL-SP-D binding observed in the treated cell lines was protein-specific.

rfhSP-D Induces Cell Cycle Arrest in G1 Phase in Panc-1 and MiaPaCa-2

Panc-1, MiaPaCa-2, and Capan-2 cell lines were individually treated with rfhSP-D for 24 h to assess whether rfhSP-D induced growth arrest. DNA binding dye, PI, was used to analyze the cell cycle for both treated and untreated cells *via* DNA quantitation. rfhSP-D induced inhibition of DNA synthesis in treated Panc-1 (68%) and MiaPaCa-2 (50%) in comparison to untreated Panc-1 (3%) and MiaPaCa-2 (2%) cells, respectively, as the cells were arrested in G1 phase (**Figure 2**). DNA synthesis was unaffected in the untreated cells for both cell lines since Panc-1 (43%) and MiaPaCa-2 (31%) were seen in S phase and Panc-1 (32%) and MiaPaCa-2 (33%) in the G2 phase of cell cycle. The growth arrest was, however, not seen in Capan-2 cell line following the rfhSP-D treatment (data not shown). Growth arrest at 24 h following rfhSP-D treatment prompted the determination of cell fate at a later time point; therefore, all cell lines were analyzed for likely apoptosis at 48 h.

rfhSP-D Induces Apoptosis Induction in Pancreatic Cancer Cells by 48 h

The qualitative apoptosis analysis of Panc-1, MiaPaCa-2, and Capan-2 treated with FL-SP-D or rfhSP-D for 48 h using immunofluorescence microscopy (**Figure 3A**) showed that the cell membrane was disoriented and the PI bound to DNA in the treated cells as compared to untreated cells, where no florescence was detected, indicating that cells were undergoing apoptosis at 48 h.

The flow cytometry analysis to quantify apoptosis showed significant reduction in the viable cell percentage of Panc-1, MiaPaCa-2, and Capan-2. The rfhSP-D induced apoptosis in ~67% of Panc-1 cells at 48 h, out of which, ~57% Panc-1 cells were both FITC and PI positive and ~7% were FITC alone positive, suggesting annexin V/FITC binding to phosphatidylserine, a cell membrane phospholipid, which is externalized during early apoptotic stage and the passage of PI, a DNA stain, through the porous cell membrane into the nucleus in order to intercalate the DNA. Approximately, 10% cells were PI alone positive, which

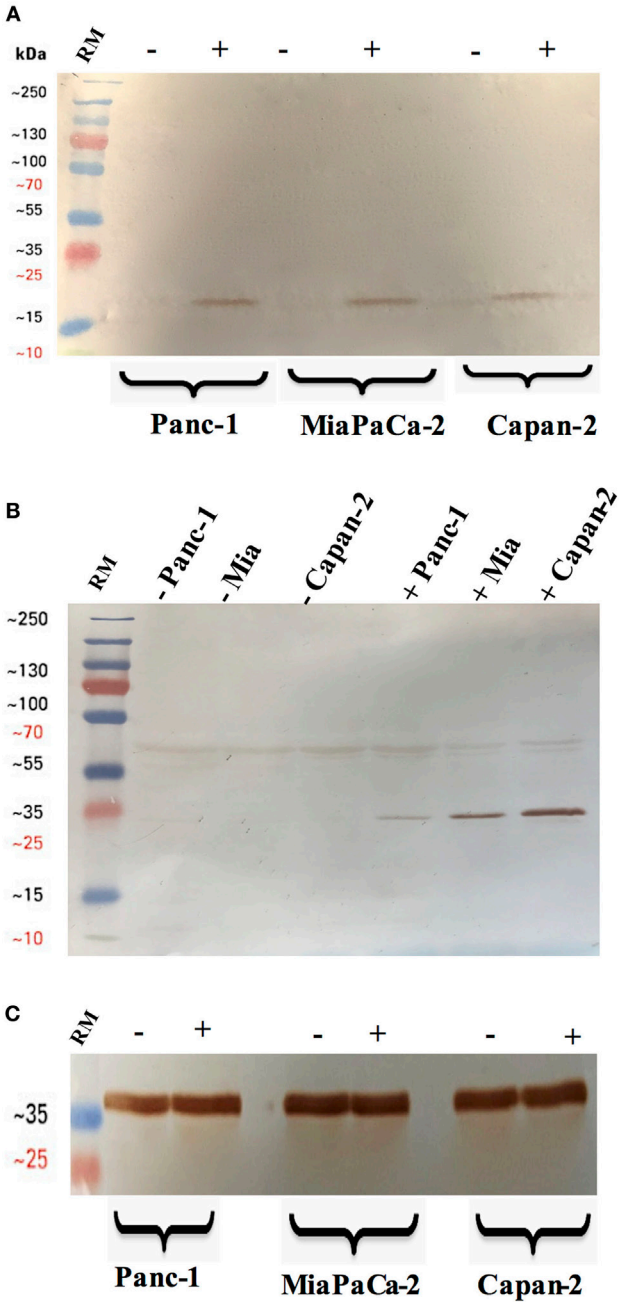

FIGURE 4 | Cleavage of caspase 3 **(A)** and 8 **(B)** in pancreatic cancer cell lines following rfhSP-D treatment. Pancreatic cancer cell lines were analyzed for caspase 8 and 3 activation *via* western blot using anti-rabbit cleaved caspase 3 and 8 (1:1,000) at 4°C overnight, followed by incubation with secondary anti-rabbit IgG HRP-conjugate (1:1,000) for 1 h at room temperature. The membrane was washed with PBST (PBS + 0.05% Tween 20) three times, 10 min each between each step. The bands were developed using 3,3′-diaminobenzidine substrate kit. The cleaved caspase 3 and 8 were detected only in the rfhSP-D treated samples of all cell lines, whereas no bands appeared in the untreated cell samples. Full-length caspase 8 bands are visible around 43 kDa. **(C)** Anti-GAPDH was used as a loading control.

suggested that these cells were either dead or in late apoptotic stage. The percentage of viable cells, i.e., unstained, in the untreated sample was significantly higher (70%) as compared to treated (26%) (**Figure 3B**). The rfhSP-D induced apoptosis in MiaPaCa-2 was ~60%. However, rfhSP-D induced apoptosis in Capan-2 (~35%) cell line, which was not as much as in Panc-1 and MiaPaCa-2 cell lines (**Figure 3B**). The treatment with FL-SP-D (20 μg/ml) for 48 h induced apoptosis in approximately 25% of Panc-1 and MiaPaCa-2 cell lines, and less than 10% in Capan-2 cell line. No significant difference was seen with FL-SP-D (10 μg/ml)

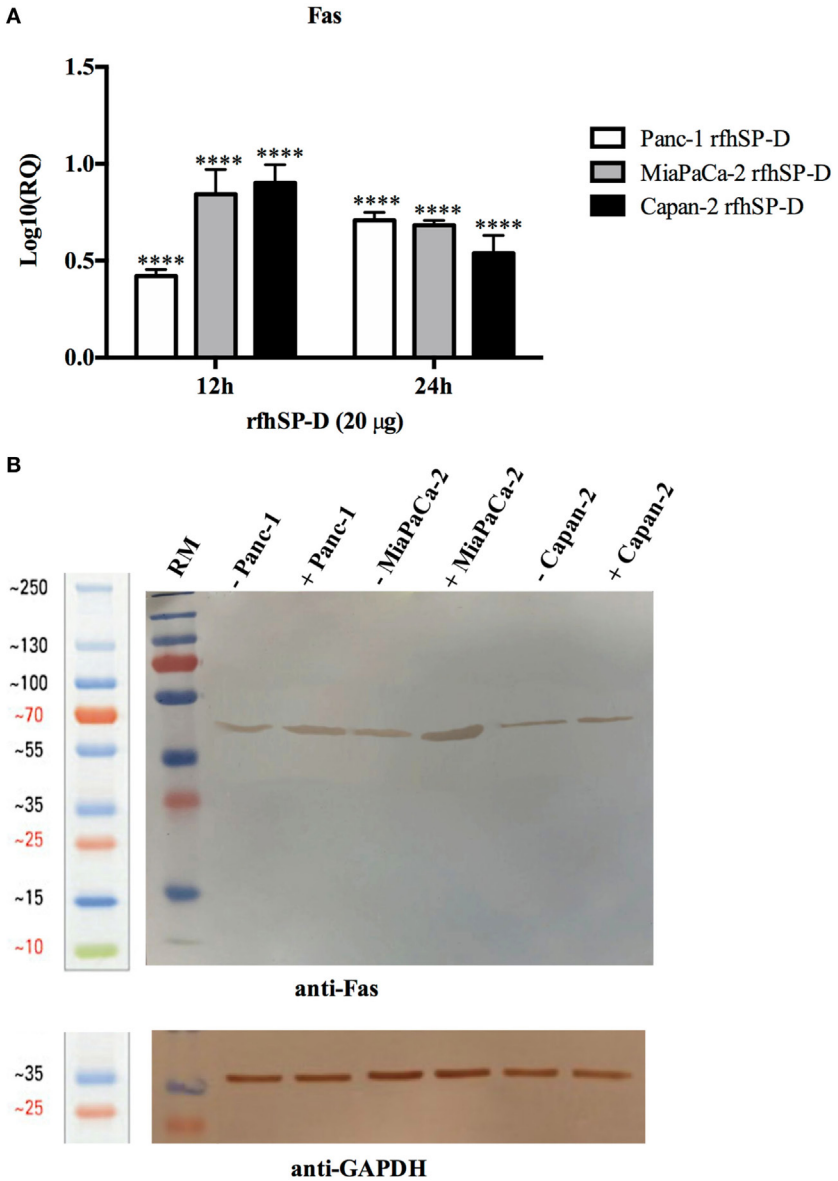

FIGURE 5 | Relative quantification (RQ) of Fas mRNA expression in Panc-1, MiaPaCa-2, and Capan-2 cell lines treated with rfhSP-D (20 μg/ml) for 12 and 24 h. **(A)** Fas expression was upregulated in the treated samples at 12 and 24 h as compared to untreated cells. Significance was determined using the unpaired two-way ANOVA test (****$p < 0.0001$) ($n = 3$). **(B)** Fas expression *via* western blot analysis in pancreatic cell lines treated with rfhSP-D for 24 h using rabbit anti-human Fas (1:1,000) at 4°C overnight, followed by incubation with secondary anti-rabbit IgG HRP-conjugate (1:1,000) for 1 h at room temperature. The bands were developed using diaminobenzidine substrate kit. Fas expression at ~50 kDa was upregulated in the treated samples at 24 h for all cells as compared to untreated. Anti-GAPDH used as a loading control.

treatment for 48 h in all the cell lines investigated in this study (**Figure 3C**).

The cell viability analysis *via* MTT assay following rfhSP-D treatment showed ~60% decrease in the cell viability of Panc-1 and MiaPaCa-2 and 45% in Capan-2 as compared to untreated (**Figure 3D**) and BSA (10 and 20 μg/ml; data not shown) controls. The cell viability analysis *via* MTT assay following FL-SP-D treatment also showed consistent reduction as seen in flow cytometer analysis (**Figure 3E**). Apoptosis was further confirmed by analyzing the activation of caspase to determine the pathway involved.

rfhSP-D Activates Cleavage of Caspase 8 and 3

Western blot analysis revealed that caspase 8 and 3 were cleaved in all the cell lines following treatment with rfhSP-D for 48 h (**Figure 4**). The cleavage of caspase 3, however, was not seen in the untreated cells and faint bands appeared for caspase 8 in

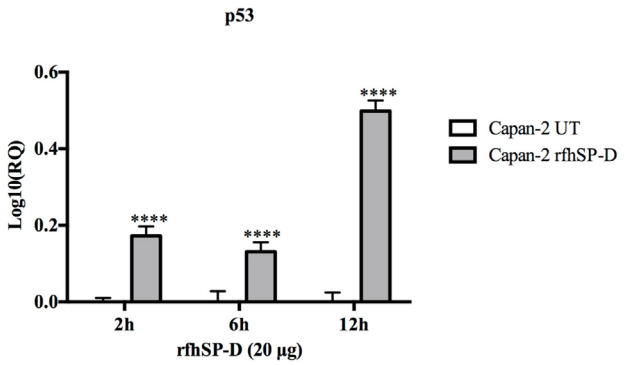

FIGURE 6 | Relative quantification (RQ) of p53 mRNA expression in Capan-2 cell line treated with rfhSP-D (20 µg/ml) for 2, 6, and 12 h. p53 expression was significantly upregulated in the rfhSP-D-treated samples at 2, 6, and 12 h as compared to the untreated. Significance was determined using the unpaired two-way ANOVA test (****$p < 0.0001$) ($n = 3$).

the untreated cells (**Figure 4**), which further confirmed that cell death occurred *via* apoptosis. Interestingly, although Capan-2 cell line appeared unaffected in terms of cell cycle arrest at 24 h; yet, the cleaved bands for caspase 8 and 3 were seen in Capan-2 treated cells too, which suggested that rfhSP-D can affect the cancer cells *via* multiple pathways. Caspase 9 was tested as a marker for intrinsic apoptosis pathway; however, no difference was noted between treated and untreated cells (data not shown). Therefore, gene expressions were assessed for pro-apoptotic genes such as Bax, an intrinsic pathway marker, and Fas, an extrinsic pathway marker, to further determine the apoptotic pathway.

rfhSP-D Upregulates the Expression of Pro-Apoptotic Marker, Fas

Human pancreatic cancer cells often escape apoptosis by down-regulating apoptosis stimulators such as FasL/FasR (25), or pro-apoptotic proteins such as Bax (26). These pro-apoptotic genes, Bax and Fas, for time-points ranging from 2 to 24 h in all the cell lines, were analyzed. Bax was unaffected following the treatment with rfhSP-D in Panc-1 and MiaPaCa-2 cell lines at all time-points (data not shown), which, in addition to unaffected caspase 9, suggested that intrinsic pathway may not have been involved in causing the cell death in these cell lines. Fas expression was unaffected at earlier time-points up to 6 h (data not shown); however, it was upregulated at 12 and 24 h in Panc-1 ($\log_{10}$ ~0.5), MiaPaCa-2 ($\log_{10}$ ~1), and Capan-2 ($\log_{10}$ ~1) cell lines (**Figure 5A**), which indicated that apoptosis induction by rfhSP-D is likely to take place *via* the extrinsic pathway. Western blot analysis also showed upregulation of Fas at the protein level in rfhSP-D treated cells as compared to untreated cells (**Figure 5B**). Since TNF-α and NF-κB are crucial factors in the apoptotic pathway and they can regulate Fas expression (27), the effect of rfhSP-D on the gene expression of TNF-α and NF-κB as well as translocation of NF-κB from the cytoplasm to nucleus was investigated.

rfhSP-D Upregulates p53 Expression in Capan-2 Cell Line

The p53 transcript levels were measured by qPCR following the treatment with rfhSP-D at 2, 6, and 12 h in Capan-2 cells and compared with the p53 levels in untreated cells for each time-point. Interestingly, the levels of p53 were upregulated, most significantly at 12 h, which suggested that p53 may also have contributed to the apoptosis in Capan-2 cells (**Figure 6**).

rfhSP-D Upregulates the Expression of TNF-α and Causes Nuclear Translocation of NF-κB

Following treatment with rfhSP-D, the analysis of TNF-α mRNA expression levels showed a significant upregulation in Panc-1 ($\log_{10}$ ~0.5), MiaPaCa-2 ($\log_{10}$ ~1), and Capan-2 ($\log_{10}$ ~1) at 12 and 24 h; however, no difference was observed at earlier time-points. Similar transcriptional upregulation was noted for NF-κB for Panc-1 ($\log_{10}$ ~0.4), MiaPaCa-2 ($\log_{10}$ ~0.8), and Capan-2 ($\log_{10}$ ~0.6) at 12 and 24 h (**Figure 7A**). Immunofluorescence microscopy of Panc-1, MiaPaCa-2, and Capan-2 cell lines showed that NF-κB was translocated to the nucleus at 24 h, which was not seen in the untreated cells (**Figure 7B**). This further confirmed that NF-κB could play a key role in deciding the apoptotic fate of the pancreatic cancer cells following the rfhSP-D treatment.

rfhSP-D Downregulates the Survival Pathway, mTOR

The mTOR is often deregulated in the pancreatic cancer (28) and its activation is associated with poor prognosis (29). Upon treatment with rfhSP-D, mRNA expression of mTOR was downregulated in Panc-1 and MiaPaCa-2 cell line at 12 h (**Figure 8A**), however, no difference was seen in Capan-2 (data not shown). In addition, immunofluorescence analysis revealed that in comparison to the untreated cells, a significant decrease in the cytoplasmic levels and an increased accumulation of mTOR in the nucleus of MiaPaCa-2 cells was evident (**Figure 8B**), where it has been shown to be present in its inactive form (30).

DISCUSSION

In this study, we show that a recombinant fragment of human surfactant protein D (rfhSP-D) induces apoptosis in a range of pancreatic cancer cell lines. We show that rfhSP-D induces apoptosis regardless of p53 status using two p53 mutated, aggressive cell lines, Panc-1 (derived from head of the pancreas), MiaPaCa-2 (derived from the body and tail of the pancreas), and a p53 wild type, non-aggressive cell line, Capan-2 (derived from head of the pancreas) (31).

Following the treatment with rfhSP-D, Panc-1 and MiaPaCa-2 cells were arrested in G1 phase at 24 h, whereas untreated cells progressed to S and G2 phase. In addition, upregulation of Fas, an apoptosis stimulator, and pro-apoptotic TNF-α (and associated transcription factor, NF-κB) at 24 h was consistent with the cleavage of caspase 8 and 3 at 48 h. These findings indicated that cell death is likely to occur *via* TNF-α/

Fas-mediated apoptosis pathway (32–34). The cell viability after 48 h of rfhSP-D treatment was reduced in the order of Panc-1 > MiaPaCa-2 > Capan-2, which coincided with the approximate growth arrested percentage of Panc-1 and MiaPaCa-2 at 24 h. Although Capan-2 cells were not arrested in the cell cycle, yet they underwent apoptosis at 48 h, which may be attributed to their increased sensitivity to Fas-mediated apoptosis as compared to other two cell lines (25) and upregulation of p53 transcripts following the treatment with rfhSP-D, as reported previously (16). Treatment with FL-SP-D induced apoptosis in approximately 25% of Panc-1 and MiaPaCa-2, compared to Panc-1 (~67%) > MiaPaCa-2 (~60%) > Capan-2 (~35) by rfhSP-D. This quantitative difference is likely to be due to difference in the molar ration of the two proteins at the same concentration.

Fas is a type I membrane protein that belongs to TNF superfamily (35, 36) that undergoes trimerization upon binding to its physiological ligand, FasL, to form a Fas-associated death domain protein (FADD) *via* its cytoplasmic domain (37, 38). It then activates downstream caspase cascade, which subsequently causes cleavage of caspase 3 as the terminal molecular event during apoptosis (39, 40). When the Panc-1, MiaPaCa-2, and Capan-2 cell lines were treated with rfhSP-D, Fas remained unaffected up to 12 h. Upregulation of Fas transcripts as well as protein was seen at 24 h, indicating that TNF-α (41) and NF-κB (33) might also be affected since they are well known to tightly regulate the Fas-mediated apoptosis pathway. TNF-α, another member of TNF superfamily, acts *via* TNFR2 to increase the susceptibility of the target cells to Fas-mediated death; in addition, it stimulates the downstream NF-κB signaling (42) by recruitment and activation

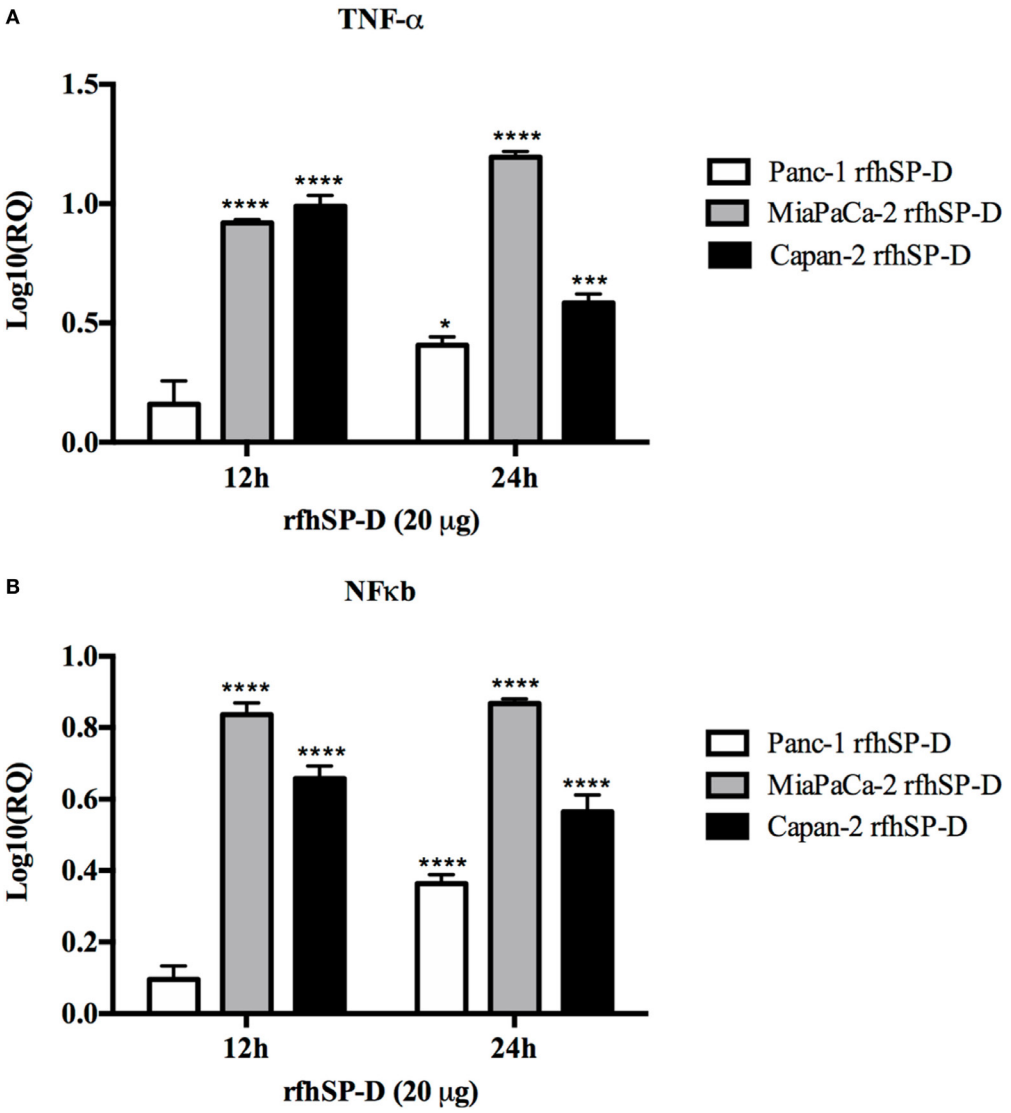

FIGURE 7 | Continued

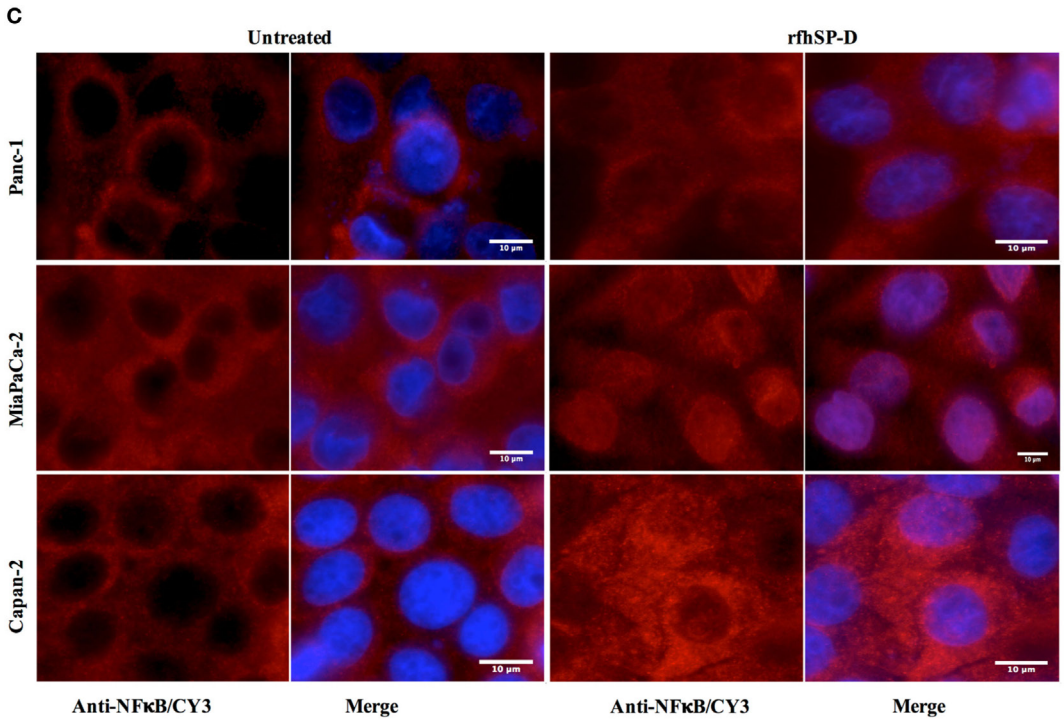

FIGURE 7 | Relative quantification (RQ) comparisons of TNF-α **(A)** and NF-κB **(B)** mRNA expression in Panc-1, MiaPaCa-2, and Capan-2 cell lines treated with rfhSP-D (20 µg/ml) for 12 and 24 h. The transcriptional expressions of both TNF-α and NF-κB were upregulated in the treated samples at 12 and 24 h as compared to untreated. Significance was determined using the unpaired two-way ANOVA test (*$p < 0.05$, ***$p < 0.001$, ****$p < 0.0001$) ($n = 3$). **(C)** Immunofluorescence microscopy to determine the translocation of NF-κB into nucleus following rfhSP-D treatment. Anti-NF-κB stained positively in the nucleus of treated cells as compared to untreated in all cell lines at 24 h.

of inhibitor of IκB kinases (IKK), which in turn enables its translocation to the nucleus where transcription of NF-κB-dependent genes such as Fas occurs (33, 43).

In this study, transcriptional levels of both NF-κB and TNF-α were upregulated at the same time-point as Fas, which was largely anticipated (33). In addition, the immunofluorescence microscopy revealed NF-κB translocation to nucleus at 24 h in the rfhSP-D-treated cells as compared to the untreated counterpart, which suggested that TNF-α induced canonical NF-κB pathway (44). NF-κB can regulate both pro- as well as anti-apoptotic genes, depending upon its canonical or non-canonical signaling (43, 44). Interestingly, canonical NF-κB has been shown to bind directly to the Fas promoter to facilitate cell death *via* Fas-mediated pathway (33). NF-κB plays an important role in deciding the cell fate as its canonical activation acts a transcription factor of Fas, which upon stimulation induces apoptosis signaling (32, 33). However, SP-D has been shown to regulate steady-state NF-κB activation in alveolar macrophages of SP-D deficient mice (45). Interestingly, SP-D has also been shown to trigger TNF-α production in human $CCR2^+$ inflammatory monocytes (46). These studies present an interesting central role of SP-D and their interdependent regulation, which could be important in deciding the cell viability/apoptosis. Moreover, cleaved caspase 8 and 3 were seen at 48 h, whereas intrinsic apoptosis markers such as caspase 9 and Bax remained unaffected (27), in all rfhSP-D-treated pancreatic cancer cell lines as compared to untreated cells, which further confirmed the cell death *via* Fas-mediated pathway alone. In addition, mTOR pathway was downregulated following the treatment with rfhSP-D, which is crucial for cell survival and proliferation, and thus, to protect the cancer cells from apoptosis (47). These findings are also supported by studies such as targeting mTOR pathway using rapamycin (48), or its regulating component RICTOR knockdown (49), significantly reduces the pancreatic cancer cell growth. Interestingly, immunofluorescence microscopy showed that rfhSP-D causes nuclear accumulation of mTOR in the treated cells, which may have a transcriptional role. However, the nuclear versions do not form an intact mTORC1 required for regulatory signaling pathways (30).

rfhSP-D bound all the pancreatic cell lines tested in this study: Panc-1, MiaPaCa-2, and Capan-2 (**Figure 1A**). However, the putative SP-D receptor or the ligand on the pancreatic cancer cell surface is not yet known. Recently, an interaction between the CRD region of human SP-D and N-glycans of EGFR has been reported which led to downregulated EGF signaling in human lung adenocarcinoma, A549 cell line cells (19).

In conclusion, rfhSP-D upregulates pro-apoptotic factors such as TNF-α, NF-κB, and Fas to activate caspase cascade to induce apoptosis in pancreatic cancer cell lines, which needs further exploration in orthotropic murine models. Majority of the conventional anti-cancer therapies only target the rapidly proliferating cancer cells, therefore, new strategies involving immune molecules such as rfhSP-D that target the signaling pathways to reduce the cell growth merit further investigation as these would

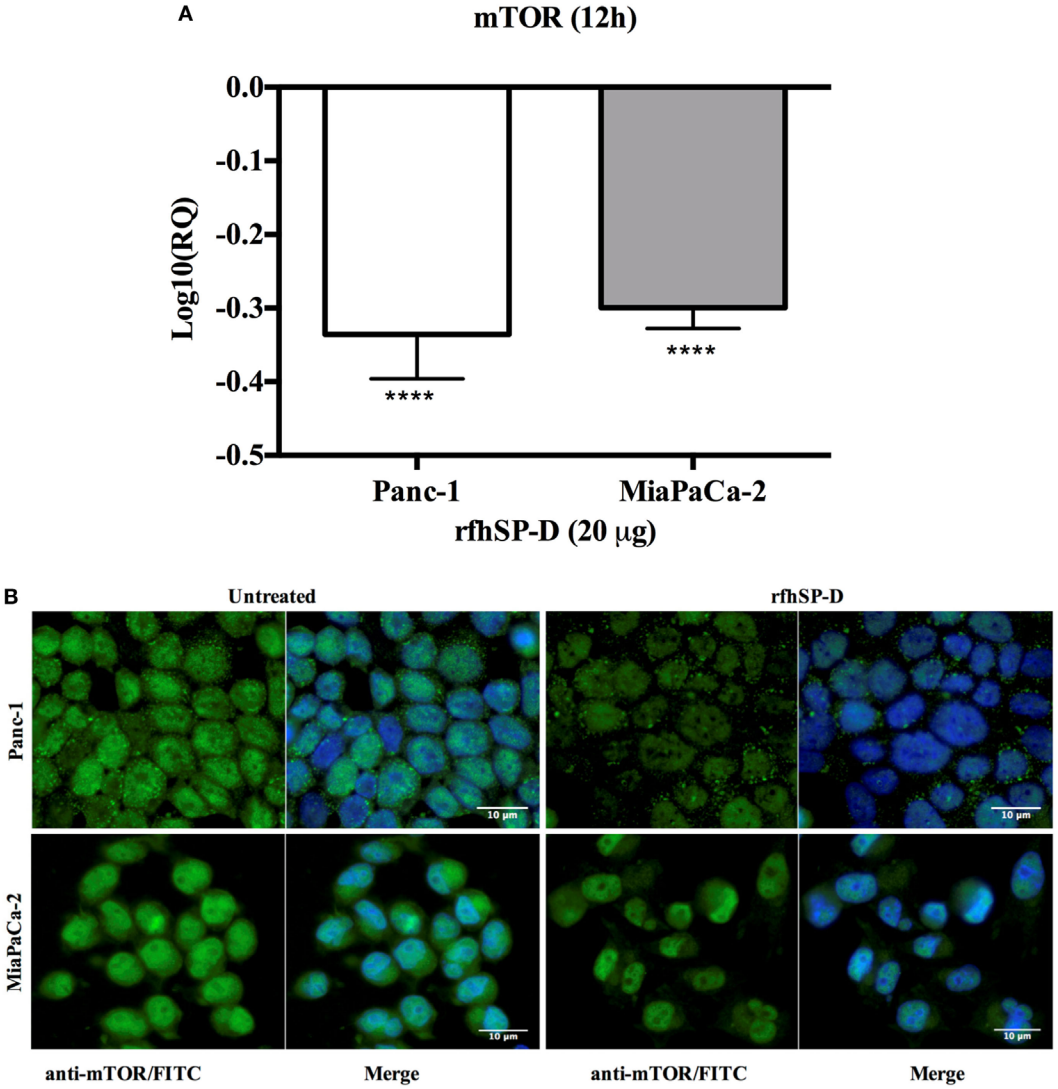

FIGURE 8 | rfhSP-D downregulated the survival pathway, mTOR. **(A)** rfhSP-D treatment of Panc-1 and MiaPaCa-2 cells downregulated the mRNA expression of mTOR (****$p < 0.0001$). **(B)** Immunofluorescence microscopy showed reduced cytoplasmic levels of mTOR following treatment as compared to the untreated. Nuclear accumulation is clearly visible in the rfhSP-D treated cells.

not only help eliminate the tumor but could also influence recurrence or migratory capacity of the tumor cells.

AUTHOR CONTRIBUTIONS

AK carried out most crucial experiments and was supported by MR, VM, and PV. SS provided ideas for crucial experiments and offered important reagents. AK wrote the first draft. UK led the study and helped with the manuscript preparation.

FUNDING

SS is supported by a Max-Elder Research Grant.

REFERENCES

1. Kishore U, Greenhough TJ, Waters P, Shrive AK, Ghai R, Kamran MF, et al. Surfactant proteins SP-A and SP-D: structure, function and receptors. *Mol Immunol* (2006) 43:1293–315. doi:10.1016/j.molimm.2005.08.004
2. Ujma S, Horsnell WG, Katz AA, Clark HW, Schafer G. Non-pulmonary immune functions of surfactant proteins A and D. *J Innate Immun* (2017) 9:3–11. doi:10.1159/000451026
3. Nayak A, Dodagatta-Marri E, Tsolaki AG, Kishore U. An insight into the diverse roles of surfactant proteins, SP-A and SP-D in innate and adaptive immunity. *Front Immunol* (2012) 3:131. doi:10.3389/fimmu.2012.00131
4. Schaub B, Westlake RM, He H, Arestides R, Haley KJ, Campo M, et al. Surfactant protein D deficiency influences allergic immune responses. *Clin Exp Allergy* (2004) 34:1819–26. doi:10.1111/j.1365-2222.2004.02068.x
5. Wert SE, Yoshida M, LeVine AM, Ikegami M, Jones T, Ross GF, et al. Increased metalloproteinase activity, oxidant production, and emphysema in surfactant

protein D gene-inactivated mice. *Proc Natl Acad Sci U S A* (2000) 97:5972–7. doi:10.1073/pnas.100448997
6. Ikegami M, Na CL, Korfhagen TR, Whitsett JA. Surfactant protein D influences surfactant ultrastructure and uptake by alveolar type II cells. *Am J Physiol Lung Cell Mol Physiol* (2005) 288:L552–61. doi:10.1152/ajplung.00142.2004
7. Griese M, Steinecker M, Schumacher S, Braun A, Lohse P, Heinrich S. Children with absent surfactant protein D in bronchoalveolar lavage have more frequently pneumonia. *Pediatr Allergy Immunol* (2008) 19:639–47. doi:10.1111/j.1399-3038.2007.00695.x
8. Foreman MG, Kong X, DeMeo DL, Pillai SG, Hersh CP, Bakke P, et al. Polymorphisms in surfactant protein-D are associated with chronic obstructive pulmonary disease. *Am J Respir Cell Mol Biol* (2011) 44:316–22. doi:10.1165/rcmb.2009-0360OC
9. Lingappa JR, Dumitrescu L, Zimmer SM, Lynfield R, McNicholl JM, Messonnier NE, et al. Identifying host genetic risk factors in the context of public health surveillance for invasive pneumococcal disease. *PLoS One* (2011) 6:e23413. doi:10.1371/journal.pone.0023413
10. Ishii T, Hagiwara K, Ikeda S, Arai T, Mieno MN, Kumasaka T, et al. Association between genetic variations in surfactant protein D and emphysema, interstitial pneumonia, and lung cancer in a Japanese population. *COPD* (2012) 9:409–16. doi:10.3109/15412555.2012.676110
11. Silveyra P, Floros J. Genetic variant associations of human SP-A and SP-D with acute and chronic lung injury. *Front Biosci (Landmark Ed)* (2012) 17:407–29. doi:10.2741/3935
12. Tanaka M, Arimura Y, Goto A, Hosokawa M, Nagaishi K, Yamashita K, et al. Genetic variants in surfactant pulmonary-associated protein D (SFTPD) and Japanese susceptibility to ulcerative colitis. *Inflamm Bowel Dis* (2009) 15:918–25. doi:10.1002/ibd.20936
13. Madan T, Kishore U, Singh M, Strong P, Clark H, Hussain EM, et al. Surfactant proteins A and D protect mice against pulmonary hypersensitivity induced by *Aspergillus fumigatus* antigens and allergens. *J Clin Invest* (2001) 107:467–75. doi:10.1172/JCI10124
14. Singh M, Madan T, Waters P, Parida SK, Sarma PU, Kishore U. Protective effects of a recombinant fragment of human surfactant protein D in a murine model of pulmonary hypersensitivity induced by dust mite allergens. *Immunol Lett* (2003) 86:299–307. doi:10.1016/S0165-2478(03)00033-6
15. Mahajan L, Madan T, Kamal N, Singh VK, Sim RB, Telang SD, et al. Recombinant surfactant protein-D selectively increases apoptosis in eosinophils of allergic asthmatics and enhances uptake of apoptotic eosinophils by macrophages. *Int Immunol* (2008) 20:993–1007. doi:10.1093/intimm/dxn058
16. Mahajan L, Pandit H, Madan T, Gautam P, Yadav AK, Warke H, et al. Human surfactant protein D alters oxidative stress and HMGA1 expression to induce p53 apoptotic pathway in eosinophil leukemic cell line. *PLoS One* (2013) 8:e85046. doi:10.1371/journal.pone.0085046
17. Mahajan L, Gautam P, Dodagatta-Marri E, Madan T, Kishore U. Surfactant protein SP-D modulates activity of immune cells: proteomic profiling of its interaction with eosinophilic cells. *Expert Rev Proteomics* (2014) 11:355–69. doi:10.1586/14789450.2014.897612
18. Pandit H, Thakur G, Koippallil Gopalakrishnan AR, Dodagatta-Marri E, Patil A, Kishore U, et al. Surfactant protein D induces immune quiescence and apoptosis of mitogen-activated peripheral blood mononuclear cells. *Immunobiology* (2016) 221(2):310–22. doi:10.1016/j.imbio.2015.10.004
19. Hasegawa Y, Takahashi M, Ariki S, Asakawa D, Tajiri M, Wada Y, et al. Surfactant protein D suppresses lung cancer progression by downregulation of epidermal growth factor signaling. *Oncogene* (2015) 34:4285–6. doi:10.1038/onc.2014.20
20. Malvezzi M, Bertuccio P, Rosso T, Rota M, Levi F, La Vecchia C, et al. European cancer mortality predictions for the year 2015: does lung cancer have the highest death rate in EU women? *Ann Oncol* (2015) 26:779–86. doi:10.1093/annonc/mdv001
21. Siegel RL, Miller KD, Jemal A. Cancer statistics, 2016. *CA Cancer J Clin* (2016) 66:7–30. doi:10.3322/caac.21332
22. Wolfgang CL, Herman JM, Laheru DA, Klein AP, Erdek MA, Fishman EK, et al. Recent progress in pancreatic cancer. *CA Cancer J Clin* (2013) 63:318–48. doi:10.3322/caac.21190
23. Ansari D, Tingstedt B, Andersson B, Holmquist F, Sturesson C, Williamsson C, et al. Pancreatic cancer: yesterday, today and tomorrow. *Future Oncol* (2016) 12:1929–46. doi:10.2217/fon-2016-0010
24. Strong P, Kishore U, Morgan C, Lopez Bernal A, Singh M, Reid KB. A novel method of purifying lung surfactant proteins A and D from the lung lavage of alveolar proteinosis patients and from pooled amniotic fluid. *J Immunol Methods* (1998) 220:139–49. doi:10.1016/S0022-1759(98)00160-4
25. von Bernstorff W, Spanjaard RA, Chan AK, Lockhart DC, Sadanaga N, Wood I, et al. Pancreatic cancer cells can evade immune surveillance via nonfunctional Fas (APO-1/CD95) receptors and aberrant expression of functional Fas ligand. *Surgery* (1999) 125:73–84. doi:10.1016/S0039-6060(99)70291-6
26. Friess H, Lu Z, Graber HU, Zimmermann A, Adler G, Korc M, et al. Bax, but not Bcl-2, influences the prognosis of human pancreatic cancer. *Gut* (1998) 43:414–21. doi:10.1136/gut.43.3.414
27. Fulda S, Debatin KM. Extrinsic versus intrinsic apoptosis pathways in anti-cancer chemotherapy. *Oncogene* (2006) 25:4798–811. doi:10.1038/sj.onc.1209608
28. Semba S, Moriya T, Kimura W, Yamakawa M. Phosphorylated Akt/PKB controls cell growth and apoptosis in intraductal papillary-mucinous tumor and invasive ductal adenocarcinoma of the pancreas. *Pancreas* (2003) 26:250–7. doi:10.1097/00006676-200304000-00008
29. Kennedy AL, Morton JP, Manoharan I, Nelson DM, Jamieson NB, Pawlikowski JS, et al. Activation of the PIK3CA/AKT pathway suppresses senescence induced by an activated RAS oncogene to promote tumorigenesis. *Mol Cell* (2011) 42:36–49. doi:10.1016/j.molcel.2011.02.020
30. Betz C, Hall MN. Where is mTOR and what is it doing there? *J Cell Biol* (2013) 203:563–74. doi:10.1083/jcb.201306041
31. Deer EL, Gonzalez-Hernandez J, Coursen JD, Shea JE, Ngatia J, Scaife CL, et al. Phenotype and genotype of pancreatic cancer cell lines. *Pancreas* (2010) 39:425–35. doi:10.1097/MPA.0b013e3181c15963
32. Kaur A, Sultan SH, Murugaiah V, Pathan AA, Alhamlan FS, Karteris E, et al. Human C1q induces apoptosis in an ovarian cancer cell line via tumor necrosis factor pathway. *Front Immunol* (2016) 7:599. doi:10.3389/fimmu.2016.00599
33. Liu F, Bardhan K, Yang D, Thangaraju M, Ganapathy V, Waller JL, et al. NF-κB directly regulates Fas transcription to modulate Fas-mediated apoptosis and tumor suppression. *J Biol Chem* (2012) 287:25530–40. doi:10.1074/jbc.M112.356279
34. Ashkenazi A, Dixit VM. Death receptors: signaling and modulation. *Science* (1998) 281:1305–8. doi:10.1126/science.281.5381.1305
35. Armitage RJ. Tumor necrosis factor receptor superfamily members and their ligands. *Curr Opin Immunol* (1994) 6:407–13. doi:10.1016/0952-7915(94)90119-8
36. Schulze-Osthoff K, Ferrari D, Los M, Wesselborg S, Peter ME. Apoptosis signaling by death receptors. *Eur J Biochem* (1998) 254:439–59. doi:10.1046/j.1432-1327.1998.2540439.x
37. Boldin MP, Varfolomeev EE, Pancer Z, Mett IL, Camonis JH, Wallach D. A novel protein that interacts with the death domain of Fas/APO1 contains a sequence motif related to the death domain. *J Biol Chem* (1995) 270:7795–8. doi:10.1074/jbc.270.14.7795
38. Chinnaiyan AM, O'Rourke K, Tewari M, Dixit VM. FADD, a novel death domain-containing protein, interacts with the death domain of Fas and initiates apoptosis. *Cell* (1995) 81:505–12. doi:10.1016/0092-8674(95)90071-3
39. Janicke RU, Sprengart ML, Wati MR, Porter AG. Caspase-3 is required for DNA fragmentation and morphological changes associated with apoptosis. *J Biol Chem* (1998) 273:9357–60. doi:10.1074/jbc.273.16.9357
40. Zheng TS, Schlosser SF, Dao T, Hingorani R, Crispe IN, Boyer JL, et al. Caspase-3 controls both cytoplasmic and nuclear events associated with Fas-mediated apoptosis in vivo. *Proc Natl Acad Sci U S A* (1998) 95:13618–23. doi:10.1073/pnas.95.23.13618
41. Elzey BD, Griffith TS, Herndon JM, Barreiro R, Tschopp J, Ferguson TA. Regulation of Fas ligand-induced apoptosis by TNF. *J Immunol* (2001) 167:3049–56. doi:10.4049/jimmunol.167.6.3049
42. Micheau O, Tschopp J. Induction of TNF receptor I-mediated apoptosis via two sequential signaling complexes. *Cell* (2003) 114:181–90. doi:10.1016/S0092-8674(03)00521-X

43. Oeckinghaus A, Ghosh S. The NF-kappaB family of transcription factors and its regulation. *Cold Spring Harb Perspect Biol* (2009) 1:a000034. doi:10.1101/cshperspect.a000034
44. Perkins ND. Integrating cell-signalling pathways with NF-κB and IKK function. *Nat Rev Mol Cell Biol* (2007) 8:49–62. doi:10.1038/nrm2083
45. Yoshida M, Korfhagen TR, Whitsett JA. Surfactant protein D regulates NF-κB and matrix metalloproteinase production in alveolar macrophages via oxidant-sensitive pathways. *J Immunol* (2001) 166:7514–9. doi:10.4049/jimmunol.166.12.7514
46. Barrow AD, Palarasah Y, Bugatti M, Holehouse AS, Byers DE, Holtzman MJ, et al. OSCAR is a receptor for surfactant protein D that activates TNF-alpha release from human CCR2$^+$ inflammatory monocytes. *J Immunol* (2015) 194:3317–26. doi:10.4049/jimmunol.1402289
47. Laplante M, Sabatini DM. mTOR signaling at a glance. *J Cell Sci* (2009) 122:3589–94. doi:10.1242/jcs.051011
48. Matsubara S, Ding Q, Miyazaki Y, Kuwahata T, Tsukasa K, Takao S. mTOR plays critical roles in pancreatic cancer stem cells through specific and stemness-related functions. *Sci Rep* (2013) 3:3230. doi:10.1038/srep03230
49. Schmidt KM, Hellerbrand C, Ruemmele P, Michalski CW, Kong B, Kroemer A, et al. Inhibition of mTORC2 component RICTOR impairs tumor growth in pancreatic cancer models. *Oncotarget* (2017) 8:24491–505. doi:10.18632/oncotarget.15524

Conflict of Interest Statement: The authors declare that the research was conducted in the absence of any commercial or financial relationships that could be construed as a potential conflict of interest.

frontiers in Immunology

ORIGINAL RESEARCH
published: 30 July 2018
doi: 10.3389/fimmu.2018.01586

Entry Inhibition and Modulation of Pro-Inflammatory Immune Response Against Influenza A Virus by a Recombinant Truncated Surfactant Protein D

Mohammed N. Al-Ahdal[1], Valarmathy Murugaiah[2], Praveen M. Varghese[2], Suhair M. Abozaid[1], Iram Saba[1], Ahmed Ali Al-Qahtani[1], Ansar A. Pathan[2], Lubna Kouser[2,3], Béatrice Nal[2] and Uday Kishore[2]*

[1] Department of Infection and Immunity, King Faisal Specialist Hospital and Research Centre, Riyadh, Saudi Arabia, [2] Biosciences, College of Health and Life Sciences, Brunel University London, Uxbridge, United Kingdom, [3] Allergy & Clinical Immunology Inflammation, Repair and Development, Imperial College London, London, United Kingdom

OPEN ACCESS

Edited by:
Francesca Granucci, Università degli studi di Milano Bicocca, Italy

Reviewed by:
Luisa Martinez-Pomares, University of Nottingham, United Kingdom
Junji Xing, Houston Methodist Research Institute, United States

***Correspondence:**
Mohammed N. Al-Ahdal
ahdal@kfshrc.edu.sa

Specialty section:
This article was submitted to Molecular Innate Immunity, a section of the journal Frontiers in Immunology

Received: *13 February 2018*
Accepted: *26 June 2018*
Published: *30 July 2018*

Citation:
Al-Ahdal MN, Murugaiah V, Varghese PM, Abozaid SM, Saba I, Al-Qahtani AA, Pathan AA, Kouser L, Nal B and Kishore U (2018) Entry Inhibition and Modulation of Pro-Inflammatory Immune Response Against Influenza A Virus by a Recombinant Truncated Surfactant Protein D. Front. Immunol. 9:1586. doi: 10.3389/fimmu.2018.01586

Surfactant protein D (SP-D) is expressed in the mucosal secretion of the lung and contributes to the innate host defense against a variety of pathogens, including influenza A virus (IAV). SP-D can inhibit hemagglutination and infectivity of IAV, in addition to reducing neuraminidase (NA) activity via its carbohydrate recognition domain (CRD) binding to carbohydrate patterns (N-linked mannosylated) on NA and hemagglutinin (HA) of IAV. Here, we demonstrate that a recombinant fragment of human SP-D (rfhSP-D), containing homotrimeric neck and CRD regions, acts as an entry inhibitor of IAV and downregulates M1 expression considerably in A549 cells challenged with IAV of H1N1 and H3N2 subtypes at 2 h treatment. In addition, rfhSP-D downregulated mRNA levels of TNF-α, IFN-α, IFN-β, IL-6, and RANTES, particularly during the initial stage of IAV infection of A549 cell line. rfhSP-D also interfered with IAV infection of Madin Darby canine kidney (MDCK) cells through HA binding. Furthermore, rfhSP-D was found to reduce luciferase reporter activity in MDCK cells transduced with H1+N1 pseudotyped lentiviral particles, where 50% of reduction was observed with 10 µg/ml rfhSP-D, suggestive of a critical role of rfhSP-D as an entry inhibitor against IAV infectivity. Multiplex cytokine array revealed that rfhSP-D treatment of IAV challenged A549 cells led to a dramatic suppression of key pro-inflammatory cytokines and chemokines. In the case of pH1N1, TNF-α, IFN-α, IL-10, IL-12 (p40), VEGF, GM-CSF, and eotaxin were considerably suppressed by rfhSP-D treatment at 24 h. However, these suppressive effects on IL-10, VEGF, eotaxin and IL-12 (p40) were not so evident in the case of H3N2 subtype, with the exception of TNF-α, IFN-α, and GM-CSF. These data seem to suggest that the extent of immunomodulatory effect of SP-D on host cells can vary considerably in a IAV subtype-specific manner. Thus, rfhSP-D treatment can downregulate pro-inflammatory milieu encouraged by IAV that otherwise causes aberrant inflammatory cell recruitment leading to cell death and lung damage.

Keywords: innate immunity, influenza A virus, surfactant protein D, pseudotyped lentiviral particles, inflammation

INTRODUCTION

The innate immune system is composed of both cellular and humoral players to encounter invading pathogens. It is also an important component in the initiation and modulation of the adaptive immunity. To distinguish self from non-self, the innate immune system has evolved to recognize pathogen-associated molecular patterns through a number of pattern recognition receptors, including toll like receptors and C-type lectin receptors. Collectins are collagenous lectins, representing a crucial group of calcium-dependent pattern recognition molecules present in pulmonary secretions and mammalian serum (1). They play a crucial role in the first line of defense against a diverse range of pathogens by interacting with specific glycoconjugates and lipid moieties present on the surface of microorganisms. A significant number of *in vitro and in vivo* studies have focused on the immunomodulatory functions of a lung collectin, human surfactant protein D (SP-D). SP-D is primarily organized into four regions: a cysteine-linked N-terminal region involved in multimerization, a triple-helical collagen region composed of Gly-X-Y repeats, an α-helical, coiled-coil trimerizing neck region, and the C-terminal carbohydrate recognition domains (CRDs) or C-type lectin domain (2). Human SP-D is primarily synthesized by alveolar type II and Clara cells, in addition to being present in several extra-pulmonary tissues. SP-D triggers a range of anti-microbial defense mechanisms, including agglutination/aggregation, phagocytosis, and direct growth inhibition (1). SP-D is also capable of controlling pulmonary inflammation including allergy and asthma, and thus, linking innate with adaptive immunity *via* modulation of dendritic cell maturation, and polarization of helper T cells (1).

The direct nature of interaction between SP-D and Influenza A Virus (IAV) has been reported (3, 4), which often results in virus neutralization and enhanced phagocytosis (5, 6). Anti-viral roles of SP-D during IAV infection have been well-documented, principally by Hartshorn group. IAV is an enveloped RNA virus and a member of Orthomyxoviridae family that possesses eight single-stranded RNA segments with negative orientation. These RNA segments can encode up to 13 viral proteins, including two surface glycoproteins, an ion channel protein, nucleocapsid protein, structural scaffolding protein, a tripartite polymerase complex, two non-structural proteins, and three non-essential proteins (7). IAV is subtyped based on their surface glycoproteins, such as hemagglutinin (HA) and neuraminidase (NA); to date, there are 19 HA and 9 NA protein subtypes that have been well established. Both HA and NA play an important role in the host range, viral replication, and pathogenicity (8). Among the three genera of influenza viruses reported, infection by IAV is the most common and severe in humans, swine, and avian species. It is also known to cause pandemic infections, being diverse in host specificity. IAV is considered as a major human respiratory pathogen following 1918 H1N1 influenza pandemic (Spanish Flu) (9), which is believed to have resulted in the zoonotic transmission of an avian virus to a human host and has rapidly dispersed (10).

Binding of IAV to target cells is mediated *via* the globular head of HA to sialic acid (SA) receptors present on the host cell surface (11, 12). IAV subtypes have adapted to human preferentially *via* binding with α (2–6) linkage of SA receptors (13). Following IAV–SA receptor interaction, virus particles are internalized *via* clathrin, resulting in clathrin-mediated endocytosis, or *via* caveolin/clathrin-independent mechanism (14, 15). Thus, acidic environment triggers M2 ion channel and transfers protons and potassium into the interior portion of the virion to dissociate M1 protein from the ribonucleoprotein (RNP) (16). Acidification also initiates HA-mediated conformational changes, which leads to viral fusion and RNPs release into the cytoplasm, resulting in viral transcription and replication. It is, therefore, suggested that SA and its linkage are crucial for the initiation of IAV infection of both epithelial and immune cells. Thus, inhibition of SA receptor binding or enzymatic switching of SA-mediated linkages can confer cell resistance, and/or alter susceptibility to IAV infection. Hence, cell surface SA is considered as an important primary receptor and determinant of IAV tropism, contributing to induction of immune responses as well as to viral pathogenesis.

It is crucial to understand the molecular mechanisms of host defense against IAV in order to design novel anti-IAV strategies. SP-D binding to HA leads to a direct inhibition of cellular infection by preventing HA–SA receptor interaction (4). SP-D has been shown to bind HA-mediated glycosylation sites, identified as β-type inhibitor of IAV. This interaction is calcium dependent, and binding of SP-D to NA inhibits the release of progeny virions from infected cells (17, 18). It has been reported that recombinant full-length porcine SP-D has a potent antiviral activity against a wide range of IAV by similar mechanisms, more than human SP-D due to structural differences, such as an additional loop in its CRD, an additional glycosylation site, and an additional cysteine in the collagen domain (19). In this study, we have used a well-characterized recombinant homotrimeric fragment of human SP-D comprising neck and CRD region (rfhSP-D), and examined its ability to act as an entry inhibitor of IAV and pseudotyped viral particles, and modulate subsequent immunological response *in vitro*.

MATERIALS AND METHODS

Reagents

Viruses and Reagents

The A/England/2009 (pH1N1) and the A/HK/99 (H3N2) strains were gifted by Wendy Barclay from the Imperial College, London and Leo Poon from the University of Hong Kong, respectively. The plasmids used to produce the H1+N1 pseudotyped lentiviral particles were obtained from Addgene. The pHIV-Luciferase plasmid was a gift from Bryan Welm (Addgene plasmid # 21375); psPAX2 was a gift from Didier Trono (Addgene plasmid # 12260); and Vesicular Stomatitis Virus (VSV-G) was offered by Bob Weinberg (Addgene plasmid #8454). Monoclonal Anti-Influenza Virus H1 HA, A/California/04/2009 (H1N1)pdm09, Clone 5C12 (produced *in vitro*), NR-42019 and Polyclonal Anti-Influenza Virus H3 HA, A/Hong Kong/1/1968 (H3N2) (antiserum, Goat), NR-3118 were obtained from BEI Resources, NIAID, NIH, USA.

Cell Culture

Adenocarcinomic human alveolar basal epithelial cells (A549), Madin Darby Canine Kidney (MDCK), and human embryonic kidney (HEK) 293T cell lines were cultured in Dulbecco's Modified

Eagle's Medium (DMEM) (Sigma-Aldrich), supplemented with 10% v/v fetal bovine serum (FBS), 2 mM L-glutamine, 100 U/ml penicillin (Sigma-Aldrich), 100 µg/ml streptomycin (Sigma-Aldrich) and 1 mM sodium pyruvate (Sigma-Aldrich), and left to grow at 37°C in the presence of 5% v/v CO_2 for approximately 3 days before passaging. Since these cells were adherent, they were detached using 2× Trypsin-EDTA (0.5%) (Fisher Scientific) for 10 min at 37°C. Cells were then centrifuged at 1,200 rpm for 5 min, followed by re-suspension in complete DMEM with FBS, penicillin, and streptomycin, as described above. To determine the cell count and viability, an equal volume of the cell suspension and Trypan Blue (0.4% w/v) (Fisher Scientific) solution were vortexed, followed by cell count using a hemocytometer with Neubauer rulings (Sigma-Aldrich). Cells were then re-suspended in complete DMEM for further use.

Purification of IAV Subtypes

MDCK cells at 80–90% confluency were washed with sterile PBS twice before infection. Diluted pH1N1 (2×10^4) or H3N2 (3.3×10^4) (600 µl/flask) was transferred to the flask containing 20 ml of complete DMEM, and incubated at 37°C for 1 h. Unbound viruses were removed by washing three times with sterile PBS. 25 ml of infection medium [DMEM with 1% penicillin/streptomycin, 0.3% bovine serum albumin (BSA), and 1 µg/ml of L-1-Tosylamide-2-phenylethyl chloromethyl ketone (TPCK)—Trypsin] (Sigma-Aldrich) were added to the flasks, and incubated at 37°C for 3 days. The virus particles were then harvested *via* centrifugation of the infection medium at 3,000 × *g* at 4°C for 15 min. The supernatant obtained was centrifuged at 10,000 × *g* for 30 min at 4°C. 26 ml of supernatant was added slowly to new ultra-clear centrifuge tubes containing 30% w/v sucrose (8 ml/tube) (Sigma-Aldrich), and centrifuged at 25,000 × *g* at 4°C for 90 min. The upper phase of the medium and the sucrose phase were carefully removed; IAV particles at the bottom were re-suspended in 100 µl of sterile PBS. Virus suspension (15 µl) was subsequently analyzed by SDS-PAGE and ELISA.

Tissue Culture Infectious Dose 50% ($TCID_{50}$) Assay

Purified pH1N1 or H3N2 virus stocks were prepared with a starting dilution of 10^{-2} in DMEM and 146 µl of the diluted virus was added to all wells; uninfected MDCK cells were used as a control. 46 µl of pH1N1 or H3N2 was then serially diluted ($1/2\log_{10}$ up to 10^{-7}) and incubated at 37°C for 1 h in a microtiter plate. 1×10^5 MDCK cells, earlier trypsinised and re-suspended in 2× infection medium, were added to each well and incubated for 3 days at 37°C under 5% v/v CO_2 until cytopathic effect (CPE) was observed. After 5 days, each well was observed under microscope, and the number of wells that were positive and negative for CPE at each dilution was recorded.

Expression and Purification of a Recombinant Fragment of Human SP-D Containing Neck and CRD Regions

A recombinant fragment of human SP-D (rfhSP-D) was expressed under bacteriophage T7 promoter in *Escherichia coli* BL21 (λDE3) pLysS (Invitrogen), transformed with plasmid pUK-D1 containing cDNA sequences for the 8 Gly-X-Y repeats, neck and CRD regions of human SP-D, as described previously (20). Briefly, a primary inoculum of 25 ml bacterial culture was inoculated into 500 ml of LB containing 100 µg/ml ampicillin and 34 µg/ml chloramphenicol (Sigma-Aldrich), grown to OD_{600} of 0.6, and then induced with 0.5 mM isopropyl β-D-1-thiogalactopyranoside (IPTG) (Sigma-Aldrich) for 3 h. The bacterial cell pellet was re-suspended in lysis buffer (50 mM Tris–HCl pH7.5, 200 mM NaCl, 5 mM EDTA pH 8, 0.1% v/v Triton X-100, 0.1 mM phenyl-methyl-sulfonyl fluoride, 50 µg/ml lysozyme) and sonicated (five cycles, 30 s each). The sonicate was harvested at 12,000 × *g* for 30 min, followed by solubilization of inclusion bodies in refolding buffer (50 mM Tris–HCl pH 7.5, 100 mM NaCl, 10 mM 2-Mercaptoethanol) containing 8 M urea. The solubilized fraction was then dialyzed stepwise against refolding buffer containing 4 M, 2 M, 1 M, and no urea. The clear dialysate was loaded onto a maltose agarose column (5 ml; Sigma-Aldrich) and the bound rfhSP-D was eluted using 50 mM Tris–HCl, pH 7.5, 100 mM NaCl, and 10 mM EDTA. The eluted fractions were then passed through PierceTM High Capacity Endotoxin Removal Resin (Qiagen) to remove endotoxin. The endotoxin levels were measured *via* QCL-1000 Limulus amebocyte lysate system (Lonza), and found to be <5 pg/µg of rfhSP-D.

Direct Binding ELISA

Maxisorp 96-well microtiter plates were coated with rfhSP-D (5, 2.5, 1.25, and 0.625 µg/well) in carbonate-bicarbonate buffer (CBC), pH 9.6, and incubated overnight at 4°C. After removing the CBC buffer, microtiter wells were washed with PBS three times, blocked with 2% w/v BSA in PBS for 2 h at 37°C, and then washed three times with PBST (PBS + 0.05% Tween 20). 20 µl of concentrated pH1N1, H3N2 virus (1.36×10^6 pfu/ml), or purified recombinant HA (2.5 µg/ml) was diluted in 200 µl of PBS, 10 µl of diluted virus was added to each well, and incubated at room temperature (RT) for 2 h in buffer containing 5 mM $CaCl_2$. VSV-G pseudotyped lentivirus was used as a negative control. The microtiter wells were washed with PBST three times and the binding was probed with primary antibody: monoclonal anti-influenza virus H1 (BEI-Resources) and polyclonal anti-influenza virus H3 (BEI-Resources) antibody (1:5,000 dilution in PBS) for 1 h at 37°C. The wells were washed again with PBST and incubated with anti-mouse IgG-Horseradish peroxidase (HRP)-conjugate (1:5,000) (Fisher Scientific) and Protein A-HRP-conjugate (Fisher Scientific) in PBS (100 µl/well), respectively, for 1 h at 37°C. Color was developed using 3,3′, 5,5′-Tetramethylbenzidine (TMB) substrate (Sigma-Aldrich). The reaction was stopped using 2 N H_2SO_4 and the absorbance was read at 450 nm using iMark™ microplate absorbance reader (Bio-Rad).

Far Western Blotting

rfhSP-D (5 µg) or 10 µl of concentrated pH1N1/H3N2 (1.36×10^6 pfu/ml) were run separately on a 12% (w/v) SDS-PAGE, and then electrophoretically transferred onto a nitrocellulose membrane (320 mA for 2 h) in 1× transfer buffer (25 mM Tris–HCl pH 7.5, 190 mM glycine, and 20% methanol), followed

by blocking overnight in 5% w/v dried milk powder in PBS (Sigma-Aldrich) at 4°C on a rotatory shaker. The membrane was then washed with PBST three times, 10 min each. For far western blotting, the nitrocellulose membrane was incubated with 5 μg/ml of rfhSP-D in PBS containing 5 mM $CaCl_2$ for 1 h at RT and 1 h at 4°C. Following PBST wash, the membrane was incubated with primary antibodies, polyclonal rabbit anti-human SP-D, monoclonal anti-influenza virus H1 (BEI-Resources), or polyclonal anti-influenza virus H3 (BEI-Resources) in PBS (1:1,000) for 1 h at RT. Following washing, the membrane was probed with secondary antibodies: protein-A-HRP-conjugate, or rabbit anti-mouse IgG HRP conjugate (1:1,000) (Fisher Scientific) in PBS (100 μl/well) for 1 h at RT. After PBST wash, the blot was developed either using 3,3′-diaminobenzidine (DAB) or enhanced chemiluminescence substrate. For M1 detection, following 6 h incubation, both untreated (cells + virus) and treated samples (cells + virus + 10 μg/ml rfhSP-D) were run on the 12% (w/v) SDS-PAGE, and transferred onto a nitrocellulose membrane, as described above. The M1 expression was detected using anti-M1 monoclonal antibody (BEI-Resources).

Cell-Binding Assay

A549 cells were seeded in microtiter wells using complete DMEM (1×10^5 cells/well) and incubated overnight at 37°C. The wells were washed with PBS three times, and then rfhSP-D (10, 5, 2.5, and 1.25 μg/ml) was pre-incubated with pH1N1 or H3N2 virus (1.36×10^6 pfu/ml) diluted in 200 μl of PBS + 5 mM $CaCl_2$; 10 μl of diluted virus was added to the corresponding wells, and incubated at RT for 2 h. Maltose-binding protein (MBP) was used as a negative control. The microtiter wells were then washed with PBS three times, and fixed with 4% paraformaldehyde (Fisher Scientific) for 10 min at RT. The wells were washed again with PBS three times, and blocked with 2% w/v BSA in PBS for 2 h at 37°C. Monoclonal anti-influenza virus H1 (BEI-Resources) and polyclonal anti-influenza virus H3 (BEI-Resources) in PBS (1:5,000) were added to each well and incubated for 1 h at 37°C. After washing with PBST three times, the corresponding wells were probed with goat anti-mouse IgG-HRP-conjugate (Thermo-Fisher), or Protein A-HRP conjugate (1:5,000) in PBS for 1 h at 37°C. The wells were washed again with PBST three times and the color was developed using TMB substrate. The reaction was stopped using 2 M H_2SO_4, followed by absorbance reading at 450 nm.

Titration Assay

Maxisorp 96-well plates were coated with 0.01% collagen (Sigma-Aldrich) and incubated at RT for 3 h. After removing the excess collagen, the wells were washed with PBS twice. 75,000 A549 cells were seeded and grown overnight at 37°C in the presence of 5% v/v CO_2, until 75–80% confluency. Cells were washed with 1× PBS twice, pH1N1 or H3N2 virus (MOI of 1) diluted in pure DMEM with 10 μg/ml rfhSP-D was added to cells, respectively. The plates were incubated at 37°C for 1 h. The wells were then washed with PBS twice and 200 μl of infection medium was added to the cells, and incubated for 24 h at 37°C with 5% v/v CO_2. The media of the infected cells in the presence or absence of rfhSP-D was collected and virus titer was estimated by $TCID_{50}$.

Infection Assay Using pH1N1 and H3N2

A549 cells were cultured in complete DMEM with usual supplements at 37°C in CO_2 incubator until about 70–80% confluence. Cells, washed with PBS twice, trypsinised, and adjusted to 5×10^5 cells in 12-well plates (Fisher Scientific), were left to adhere overnight at 37°C in serum-free complete DMEM. Cells were washed in PBS before the addition of rfhSP-D (10 μg/well) in pure DMEM containing 5 mM $CaCl_2$ with MOI 1 of pH1N1 or H3N2 virus (1 h at RT and 1 h at 4°C). The pre-incubated virus and protein mix was then added onto the cells in a circular motion and incubated at 37°C for 1 h in DMEM only. Medium containing unabsorbed virus and rfhSP-D protein was removed, cells were washed with PBS twice, infection medium was added, and then left to incubate 2 and 6 h. The infected cells were detached by scrapping with a sterile cell scrapper, centrifuged at $1{,}500 \times g$ for 3 min, and frozen at −80°C until further analysis *via* qPCR.

Real-Time Quantitative PCR Analysis

The infected A549 cells were lysed using a lysis solution (50 mM Tris–HCl pH 7.5, 200 mM NaCl, 5 mM EDTA pH 8, 0.1% v/v Triton X-100). Total RNA was extracted using RNase Mini Kit (Qiagen). Contaminating DNA was removed by DNase I treatment, followed by heat-inactivation at 70°C of DNase I and RNase. A260 nm was used to quantify the amount of RNA using NanoDrop 2000/2000c (Sigma-Aldrich), and the RNA purity was assessed using A260/A280 ratio between 1.8 and 2.1. The isolated RNA was then converted into cDNA using SuperScript II Reverse Transcriptase (Thermo-Fisher Scientific). Oligo-dT primers were added to initiate cDNA synthesis and to avoid labeling of the rRNA and tRNA. cDNA was synthesized using high capacity RNA to cDNA Kit (Thermo-Fisher Scientific) using 1–2 μg of total RNA. Primer sequences were designed for specificity using the Primer-BLAST software (Basic Local Alignment Search Tool) (http://blast.ncbi.nlm.nih.gov/Blast.cgi) (**Table 1**). The qRT-PCR was performed using the Light Cycler system (Applied Biosciences). The amplification program used was at 95°C for 5 min, followed by 45 cycles of 95°C for 10 s, 60°C for 10 s, and 72°C for 10 s. The specificity of the assay was established by melting-curve analysis.

Multiplex Cytokine Array Analysis

Supernatant from A549 cells, incubated with IAV with or without rfhSP-D for 24 h were collected for measuring secreted cytokines [TNF-α, IL-6, IL-10, IL-1α, interferon (IFN)-α, and IL-12p40], chemokine (eotaxin) and growth factors (GM-CSF and VEGF). The analytes were measured using MagPixMilliplex kit (EMD Millipore). 25 μl of assay buffer was added to each well of a 96-well plate, followed by addition of 25 μl of standard, control, or supernatant from A549 cells infected with pH1N1 or H3N2 (with or without rfhSP-D). 25 μl of magnetic beads, coupled to analytes, were added to each well, and incubated for 18 h at 4°C. The plate was washed with the assay buffer and 25 μl of detection antibodies were incubated with the beads for 1 h at RT. 25 μl of Streptavidin–Phycoerythrin was then added to each well and incubated for 30 min at RT. Following a washing step, 150 μl

TABLE 1 | Target genes, forward primers, and reverse primers used for qPCR.

Target	Forward primer	Reverse primer
18S	5′-ATGGCCGTTC TTAGTTGGTG-3′	5′-CGCTGAGCCA GTCAGTGTAG-3′
IL-6	5′-GAAAGCAGCA AAGAGGCACT-3′	5′-TTTCACCAGG CAAGTCTCCT-3′
IL-12	5′-AACTTGCAGC TGAAGCCATT-3′	5′-GACCTGAACG CAGAATGTCA-3′
TNF-α	5′-AGCCCATGTT GTAGCAAACC-3′	5′-TGAGGTACAG GCCCTCTGAT-3′
M1	5′AAACATATGTCTGATAAC GAAGGAGAACAGTTCTT-3′	5′GCTGAATTCTACCT CATGGTCTTCTTGA-3′
RANTES	5′-GCGGGTACCAT GAAGATCTCTG-3′	5′-GGGTCAGAATC AAGAAACCCTC-3′
IFN-α	5′-TTT CTC CTG CC T GAA GGA CAG-3′	5′-GCT CAT GAT TTC TGC TCT GAC A-3′
IFN-β	5′-AAA GAA GCA G CA ATT TTC AGC-3′	5′-CCT TGG CCT TCA GGT AAT GCA-3′

of sheath fluid was added to each well and the plate was read using the Luminex Magpix instrument. Assays were conducted in duplicate.

Production of H1+N1 Pseudotyped Lentiviral Particles

HEK293T cells were co-transfected with 20 μg of pcDNA3.1-swineH1-flag (H1 from swine H1N1 A/California/04/09) (Invitrogen), pcDNA3.1-swine N1-flag (N1 from swine H1N1 A/California/04/09) (Invitrogen), pHIV-Luciferase backbone (Addgene), which carries a modified proviral HIV-1 genome with *env* deleted and designed to express the firefly luciferase reporter, and psPAX2 (Addgene). psPAX2 is a second-generation lentiviral packaging plasmid and can be used with second or third generation lentiviral vectors and envelope expressing plasmid. VSV-G lentivirus was produced in a similar way as described above, without H1+N1 plasmids. Supernatant containing the released H1+N1 pseudotyped and VSV-G lentiviral particles were harvested at 24 and 48 h and centrifuged at 5,000 × *g* for 10 min to remove any debris, and concentrated *via* ultra-centrifugation. The transfected HEK293T cells were lysed using lysis buffer (50 mM Tris–HCl pH 7.5, 200 mM NaCl, 5 mM EDTA, 0.1% v/v Triton X-100). The filtered supernatant and the cell lysate were analyzed *via* western blotting and luciferase reporter activity assay.

Luciferase Reporter Activity Assay

MDCK cells were cultured in supplemented DMEM as described earlier, until about 70–80% confluency. The harvested H1+N1 pseudotyped particles at 24 and 48 h were used to perform luciferase reporter activity using luciferase one-step assay kit (Thermo Scientific). rfhSP-D (5 and 10 μg/ml) was used to determine its effect on the luciferase reporter activity; cells only, and cells + H1+N1 particles were used as controls. Readings were measured using a GloMax 96 Microplate Luminometer (Promega).

Statistical Analysis

Graphs were generated using GraphPad Prism 6.0 software and the statistical analysis was performed using a two-way ANOVA test. Significant values were considered based on $^{*}p < 0.1$, $^{**}p < 0.05$, $^{***}p < 0.01$, and $^{****}p < 0.001$ between treated and untreated conditions. Error bars show the SD or SEM, as indicated in the figure legends.

RESULTS

rfhSP-D Binds Directly to IAV Subtypes

Escherichia coli BL21 (λDE3) pLysS containing pUK-D1 construct (20) expressed a ~20 kDa protein following IPTG induction, compared to the un-induced bacterial cells (**Figure 1A**). The overexpressed insoluble rfhSP-D as inclusion bodies was refolded *via* denaturation and renaturation cycle. The soluble rfhSP-D fractions were affinity purified using maltose–agarose column, which appeared as a single band on 12% SDS-PAGE (v/v) under reducing condition (**Figure 1B**). The immunoreactivity of purified rfhSP-D was confirmed *via* western blotting using rabbit polyclonal anti-human SP-D antibody that was raised against native human SP-D purified from lung lavage of alveolar proteinosis patients (**Figure 1C**). The ability of pH1N1 and H3N2 subtypes to bind microtiter-coated rfhSP-D was examined *via* ELISA. As shown in **Figure 2**, rfhSP-D bound both IAV subtypes in a dose- and calcium-dependent manner. VSV-G pseudotyped lentivirus was used as a negative control RNA virus, where no significant binding was seen with all rfhSP-D concentrations tested. For cell-binding assay, A549 cells were challenged with purified pH1N1 or H3N2 pre-incubated with a range of rfhSP-D concentrations (**Figure 3**). The maximum inhibition (50%) of cell binding was seen at 10 μg/ml. MBP was used as a negative control protein.

rfhSP-D Binds to HA and Restricts Replication of IAV in A549 Cells

Previous studies have shown that SP-D binds to the glycosylation site of HA1 domain on IAV (18). Far western blotting revealed that rfhSP-D bound to HA (70 kDa) and M1 (27 kDa) of pH1N1 (**Figure 4A**) and H3N2 (**Figure 4B**) subtypes. As shown in **Figure 4C**, rfhSP-D was able to bind purified recombinant HA protein in a concentration-dependent manner. The binding of rfhSP-D may inhibit cellular viral infection by restricting the interaction of HA with SA containing receptors, and HA-mediated fusion in endosomes. The interaction between rfhSP-D and HA appears to offer another dimension at which rfhSP-D may suppress target cell infection and intracellular replication. The mechanism of direct inhibition of IAV by rfhSP-D was thus investigated *via* infection assay. A549 cells infected with pH1N1 and H3N2 revealed an upregulation of M1 expression at 2 and 6 h time points (**Figure 5**). However, A549 cells, pre-treated with rfhSP-D showed downregulation of viral M1 expression when compared to untreated cells challenged with virus (**Figure 5**). The downregulation of M1 expression due to rfhSP-D pre-incubation was more effective in the case of pH1N1 compared to H3N2, where -8 $\log_{10}$ fold downregulation was seen at 2 h (**Figure 5A**). This was validated *via* western blotting, where a low M1 expression was detected

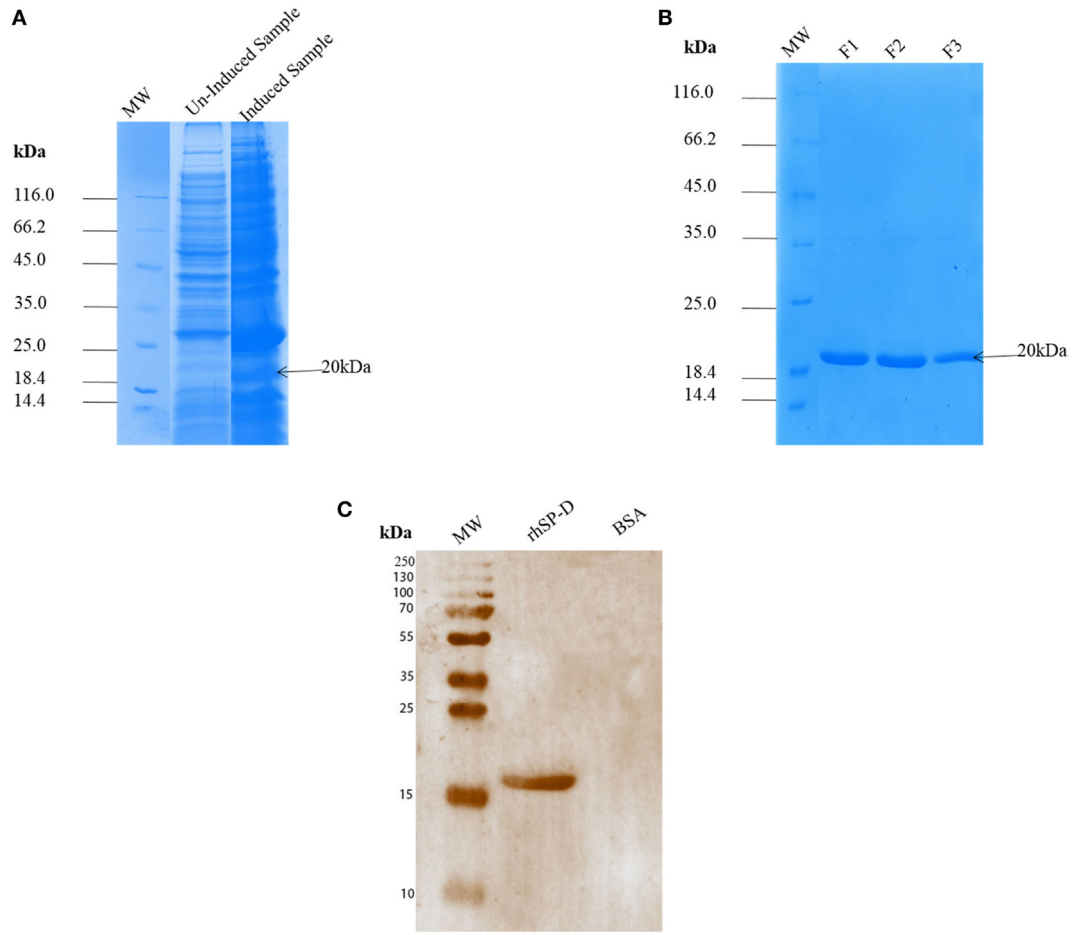

FIGURE 1 | SDS-PAGE (12% v/v) under reducing conditions showing expression and purification of a recombinant surfactant protein D (rfhSP-D). The neck and carbohydrate recognition domain regions were expressed in *Escherichia coli* BL21 (λDE3) pLysS. **(A)** Following induction with 0.5 mM IPTG, a ~20 kDa band appeared being overexpressed compared to uninduced sample. Following denaturation–renaturation cycle, the rfhSP-D was purified on an affinity column to homogeneity after elution with EDTA as fractions F1, F2 and F3 **(B)**. A rabbit polyclonal antibody raised against full-length SP-D purified from human bronchoalveolar lavage **(C)** recognized the purified rfhSP-D, but not BSA that was used as a negative control protein.

in rfhSP-D (10 μg/ml) treated sample following 6 h incubation, when compared to untreated samples (cells + virus) (**Figure 5C**). Furthermore, anti-IAV activity of rfhSP-D was confirmed *via* virus titration assay (**Figures 5D,E**). Approximately 40% titer reduction was seen in 10 μg rhfSP-D treated cells compared to untreated samples, suggesting the ability of rfhSP-D to act as an entry inhibitor. Differential inhibitory effects of rfhSP-D on IAV subtypes may reflect on the glycosylation of the HA protein of IAV, suggesting a correlation between HA-glycan attachment and susceptibility of IAV strains to inhibition by rfhSP-D that involves specific interaction sites on HA.

rfhSP-D Modulates Pro-Inflammatory Cytokine/Chemokine Immune Responses Following Virus Challenge to A549 Cells

The qPCR analysis revealed that there was an upregulation of pro-inflammatory cytokines TNF-α and IL-6 by H3N2 strain, which were brought down slightly by rfhSP-D at 2 h (**Figure 6A**). However, both TNF-α and IL-6 in the case of pH1N1 were found to be downregulated considerably by rfhSP-D at 2 h, which gradually recovered by 6 h (**Figure 6B**). IL-6, which is crucial for the resolution of IAV infection, acts by inducing neutrophil mediated viral clearance. An elevated level of IL-6 in lung and serum has been reported in patients infected with pH1N1 (21). TNF-α and IL-6 are the key contributors to IAV-mediated respiratory diseases and acute lung injury. By contrast, there was a broad level of downregulation of IL-12 in the case of both IAV subtypes incubated with rfhSP-D, suggesting a likely reduction of Th1 response and suppression of IFN-γ production by $CD4^+$ T cells. Suppressed transcript level of RANTES (1 $\log_{10}$ fold) by rfhSP-D was observed at 2 h treatment in the case of pH1N1. However, in the case of H3N2 strain, RANTES was downregulated by 0.5-fold ($\log_{10}$) (**Figure 6B**) at 2 h following treatment with rfhSP-D compared to untreated A549 cells. Furthermore, suppression of IFN-α and IFN-β were also seen with rfhSP-D treatment at both 2 and 6 h time points (**Figure 6C**). Both of these type I IFN cytokines play a crucial anti-viral role against IAV, and

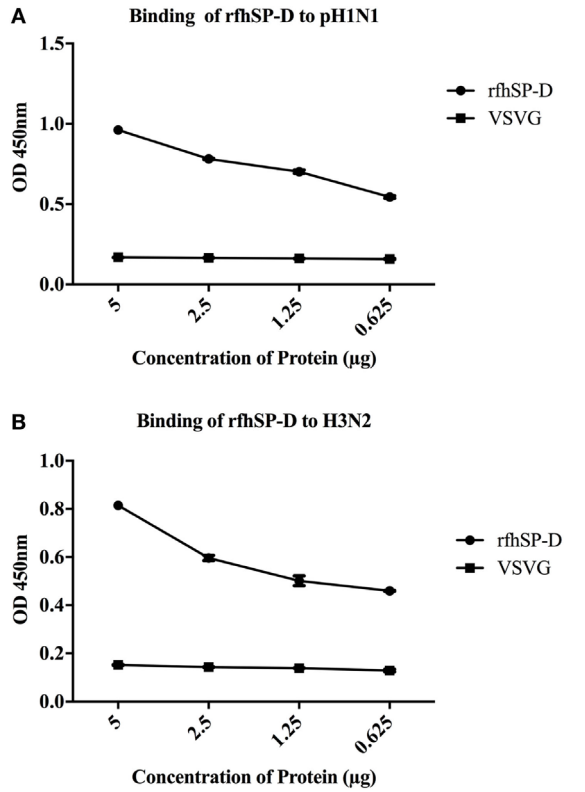

FIGURE 2 | ELISA to show binding of rfhSP-D to **(A)** pH1N1 and **(B)** H3N2: microtiter wells were coated with different concentrations of rfhSP-D (5, 2.5, 1.25, and 0.625 µg/ml). 20 µl of concentrated pH1N1 or H3N2 virus (1.36×10^6 pfu/ml) was diluted in 200 µl of PBS + 5 mM $CaCl_2$ and 10 µl of diluted virus was added to all the wells, and probed with either monoclonal anti-influenza virus H1 or polyclonal anti-influenza virus H3 antibody. VSV-G pseudotyped lentivirus was used as a negative RNA virus control. The data were expressed as mean of three independent experiments done in triplicates ± SEM.

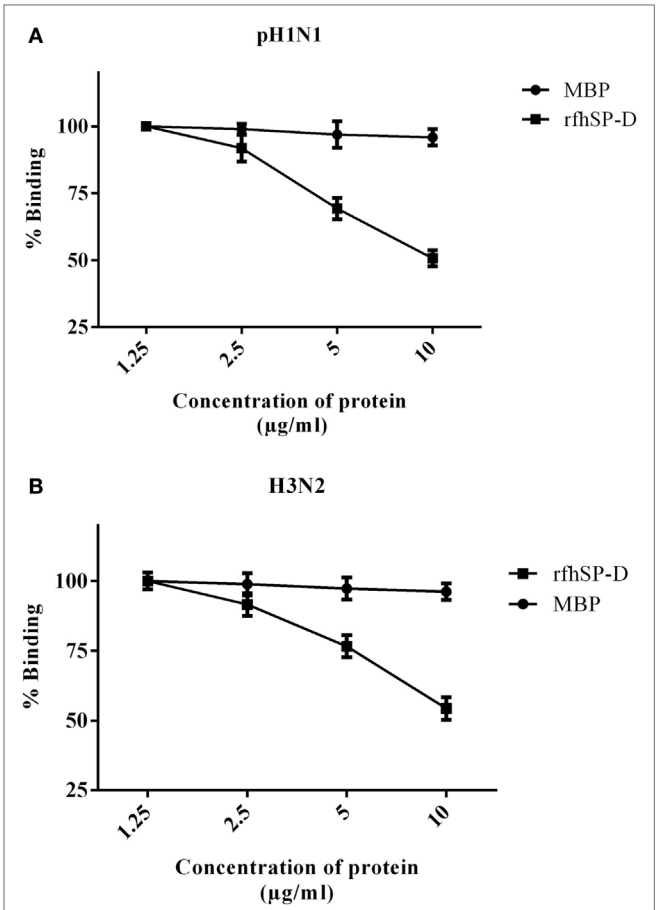

FIGURE 3 | Cell-binding assay to show binding of **(A)** pH1N1 and **(B)** H3N2 pre-incubated with rfhSP-D to A549 cells. Microtiter wells were coated with A549 cells (1×10^5 cells/ml) and incubated overnight at 37°C. Varied concentrations of pre-incubated rfhSP-D (10, 5, 2.5, and 1.25 µg/ml) with pH1N1 and H3N2 virus were added to the corresponding wells, followed by incubation at room temperature for 1–2 h. After fixing the cells with 4% paraformaldehyde solution, monoclonal anti-influenza virus H1, or polyclonal anti-influenza virus H3 were added to corresponding well. Maltose-binding protein (MBP) was used as a negative control protein. The data were expressed as mean of three independent experiments done in triplicates ± SEM.

determine the rate of viral replication in the initial stages of infection. Suppression of type I IFN levels suggests the ability of rfhSP-D to reduce the rate of viral replication, thereby reducing the levels of INF produced by the innate immune system.

Multiplex Cytokine Array Analysis Reveals a Differential Ability of rfhSP-D to Downregulate Pro-Inflammatory Cytokines and Chemokines

To assess secretion of cytokines, chemokines, and growth factors over a period of 24 h post rfhSP-D treatment, a multiplex cytokine array was performed using supernatants of the IAV challenged and rfhSP-D treated A549 cells. rfhSP-D induced a dramatic suppression of some of the key pro-inflammatory cytokines and chemokines in the virus infected A549 cells. In the case of pH1N1, TNF-α, IFN-α, IL-10, IL-12 (p40), VEGF, GM-CSF, and eotaxin were considerably suppressed by rfhSP-D treatment at 24 h (**Figure 7A**). However, these suppressive effects on IL-10, VEGF, eotaxin, and IL-12 (p40) were not so evident in the case of H3N2 subtype, with the exception of TNF-α, IFN-α, and GM-CSF (**Figure 7**). These data seem to suggest that the extent of immunomodulatory effect of rfhSP-D on host cells can vary considerably in a IAV subtype-specific manner.

rfhSP-D Binds to H1+N1 Pseudotyped Lentivirus and Reduces Luciferase Reporter Activity

H1+N1 pseudotyped lentiviral particles were produced as a safe strategy to study the differential or combinatorial involvement of HA or NA viral glycoproteins in the recognition and neutralization of IAV by rfhSP-D. The production of lentiviral particles pseudotyped with envelope proteins H1+N1 was carried out by co-transfecting HEK293T cells with plasmid containing the coding sequence of the indicated H1+N1, pHIV-Luciferase backbone, and psPAX2. Purified H1+N1 pseudotyped particles

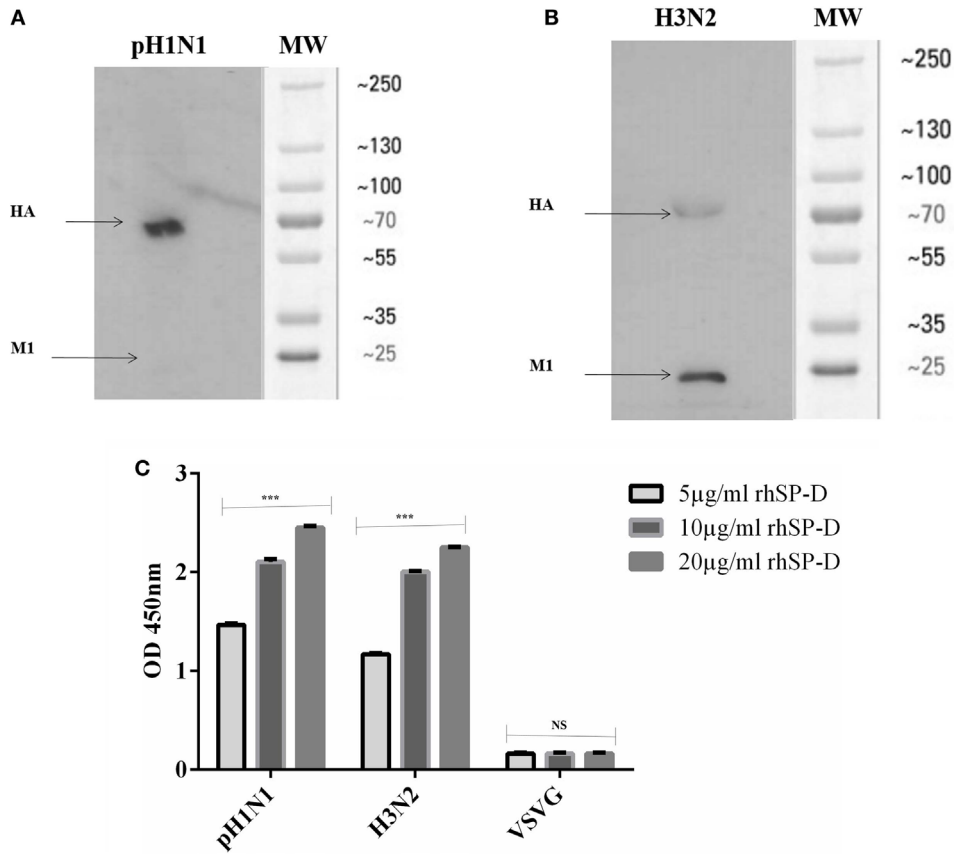

FIGURE 4 | Far western blot analysis to show rfhSP-D binding to purified **(A)** pH1N1 and **(B)** H3N2: 10 µl of concentrated virus (1.36×10^6 pfu/ml) was first run on the SDS-PAGE under reducing conditions, and then transferred onto a nitrocellulose membrane and incubated with 5 µg of rfhSP-D. The membrane was probed with anti-rabbit SP-D polyclonal antibodies. rfhSP-D bound to HA (70 kDa) and M1 (27 kDa) in the case of both pH1N1 and H3N2 subtypes. **(C)** ELISA to show the binding of rfhSP-D to purified recombinant hemagglutinin (HA) (µg/ml). VSV-G was used as a negative control. The data were expressed as mean of three independent experiments carried out in triplicates ± SEM. Significance was determined using the unpaired one-way ANOVA test (***$p < 0.0001$) ($n = 3$).

and cell lysate harvested at 24 and 48 h were analyzed *via* western blotting, and the expression level of HA was determined using anti-H1 monoclonal antibody (**Figure 8A**); HA was evident at 70 kDa. Far western blotting revealed binding of rfhSP-D to HA at 70 kDa (**Figure 8B**), suggesting that the binding of rfhSP-D to HA is crucial for the inhibition of viral infectivity. Purified H1+N1 pseudotyped particles harvested at 24 and 48 h were used to transduce MDCK cells to measure the luciferase reporter activity assay. Higher levels of luciferase reporter activity were observed at 24 h when compared to 48 h post-transfection (**Figure 8C**). Thus, pseudotyped particles harvested at 24 h were used to transduce MDCK cells with or without rfhSP-D (5 and 10 µg/ml) (**Figure 8D**). Nearly 50% reduction in the luciferase reporter activity was observed with 10 µg/ml of rfhSP-D compared to cells challenged with H1+N1 pseudotyped particles. This suggested an entry inhibitory role of rfhSP-D against IAV.

DISCUSSION

Respiratory tract infection caused by IAV is associated with up to half a million mortality rates worldwide and five million cases of morbidity per year. A new swine-origin H1N1 IAV, identified in April 2009, spread worldwide, and was officially declared pandemic in June 2009. There are concerns that H1N1 or H3N2 viruses reassort with existing H5N1 virus using bird or pig as intermediate hosts, giving rise to more pathogenic IAV. Thus, it is important to understand molecular mechanisms of host's first line of defense against IAV in order to design and develop novel and effective anti-IAV strategies. SP-D expressed at the mucosal sites including lungs plays an important role during IAV infection (22). SP-D has been shown to have a wide range of innate immune roles including neutralization, agglutination, opsonization and clearance of viruses including IAV. The binding ability of rfhSP-D to HIV-1 gp120 was reported, primarily in a dose- and calcium-dependent manner (23). Human SP-D has also been shown to bind IAV-HA and NA, resulting in the inhibition of viral attachment and entry into the host cells (24). However, the mechanism of direct inhibition of IAV and pseudotyped viral particles by SP-D and subsequent immune response is not fully explored.

Using two different IAV subtypes (pH1N1 and H3N2), we have shown that the entry inhibitory capability of rfhSP-D is not limited

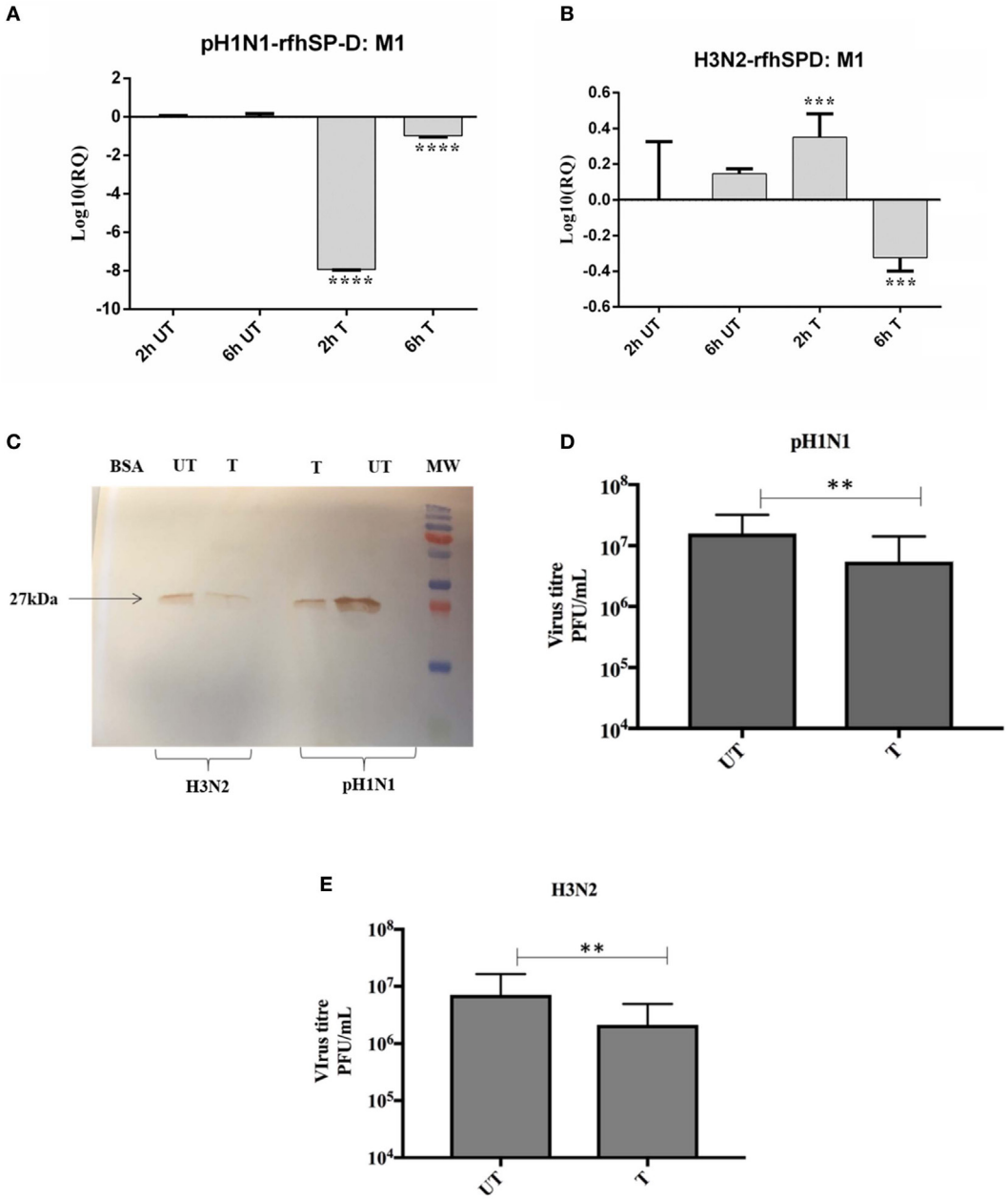

FIGURE 5 | rfhSP-D restricts replication of **(A)** pH1N1 and **(B)** H3N2 in target human A549 cells. M1 expression of both pH1N1 and H3N2 influenza A virus (IAV) (MOI 1) after infection of A549 cells at differential time points at 2 and 6 h. A549 cells were incubated either with pre-incubated pH1N1 and H3N2 with (10 μg) or without purified rfhSP-D. Cell pellets were harvested at 2 and 6 h to analyze the M1 expression of IAV. Cells were lysed, and purified RNA extracted was converted into cDNA. Infection was measured *via* qRT-PCR using M1 primers and 18S was used as an endogenous control. Results shown are normalized to M1 levels at 2 h untreated. Significance was determined using the unpaired one-way ANOVA test (**$p < 0.01$, ***$p < 0.001$, and ****$p < 0.0001$) ($n = 3$). **(C)** Western blotting to shown M1 expression in both untreated (cells + virus) and treated (cells + virus + 10 μg/ml rfhSP-D) following 6 h incubation. Titration assay to show the anti-IAV activity of rfhSP-D (10 μg/ml), using both pH1N1 **(D)** and H3N2 **(E)** subtypes. A549 cells were infected with pH1N1/H3N2 (MOI 1) for 24 h. Then, the supernatants were collected and virus titers measured using a TCID50 assay. Treatment with rfhSP-D reduced viral titers by approximately 40%, suggesting that rfhSP-D acts as an entry inhibitor.

to a particular IAV subtype. To identify the interaction of rfhSP-D with IAV viral proteins, protein–protein interaction studies were carried out *via* ELISA, cell-binding assay, and far western blot. The ELISA (**Figure 2**) and cell-binding assay (**Figure 3**) revealed the maximal binding of rfhSP-D to both pH1N1 and H3N2 IAV subtypes at 5 μg/ml, and the maximum inhibition of cell binding was seen at 10 μg/ml of rfhSP-D. Furthermore, rfhSP-D bound purified recombinant HA protein in a concentration- and calcium-dependent manner (**Figure 4C**). rfhSP-D bound HA (70 kDa) and M1 (25 kDa) (**Figure 4**). N-linked oligosaccharides

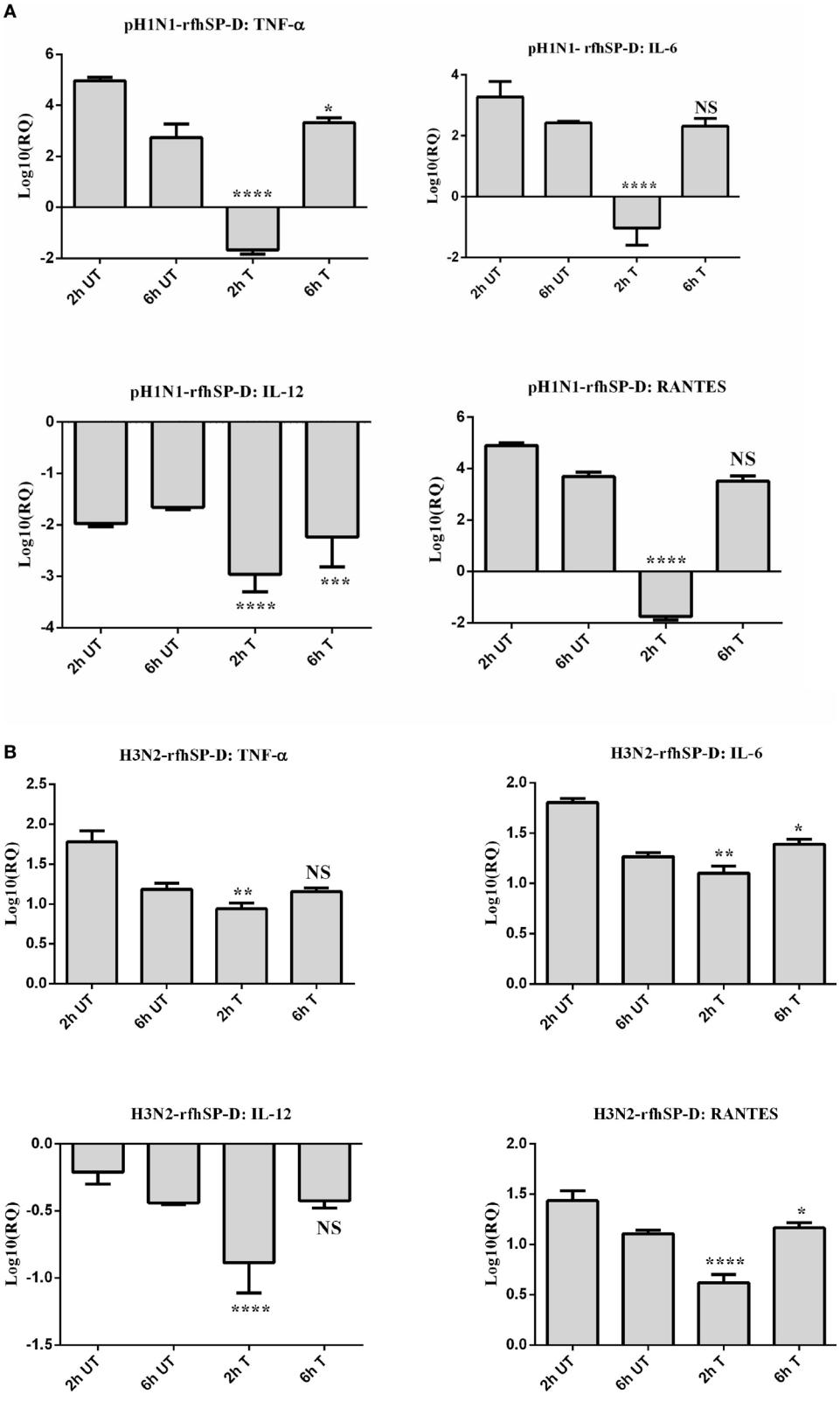

FIGURE 6 | Continued

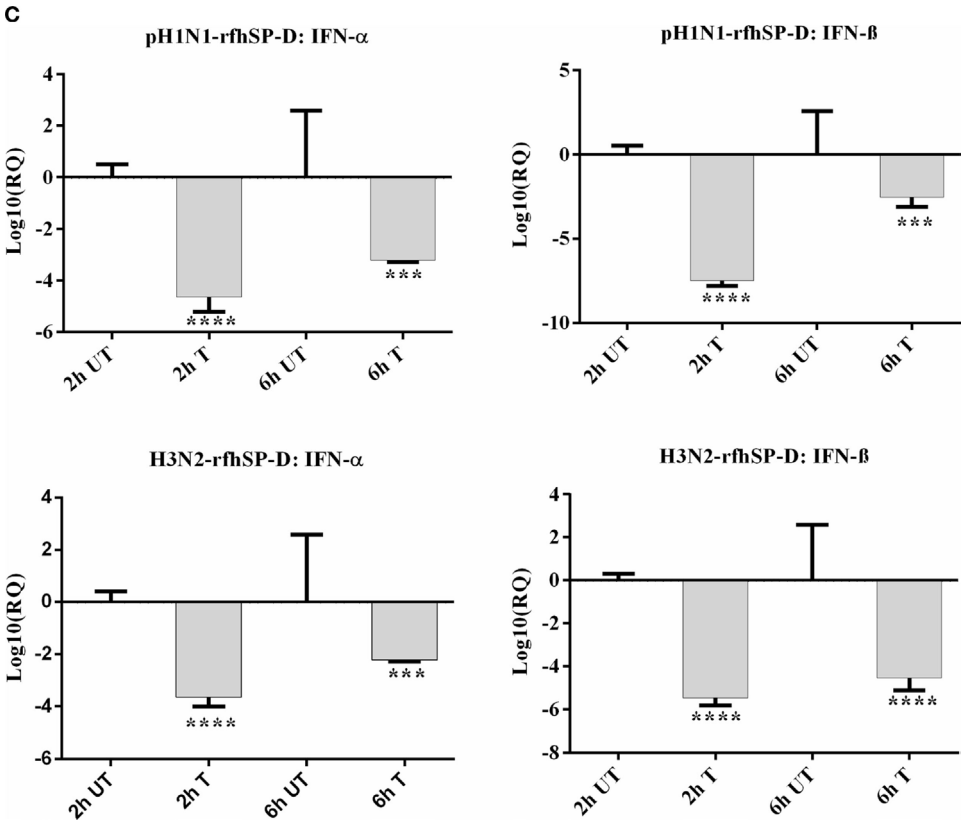

FIGURE 6 | Differential mRNA expression profile of A549 cells challenged with pre-incubated **(A)** pH1N1, **(B)** H3N2 with rfhSP-D, and **(C)** expression levels of type I interferon (IFN) subtypes in both untreated and treated samples. The expression levels of cytokines and chemokine were measured using qRT-PCR and the data were normalized *via* 18S rRNA expression as a control. The relative expression (RQ) was calculated by using cells only time point as the calibrator. The RQ value was calculated using the formula: $RQ = 2^{-\Delta\Delta Ct}$. Assays were conducted in triplicates and error bars represents ± SEM. Significance was determined using the unpaired one-way ANOVA test (*$p < 0.05$, **$p < 0.01$, ***$p < 0.001$, and ****$p < 0.0001$) ($n = 3$).

found on the IAV envelope glycoproteins (HA and NA) are known to be recognized by the CRD region of SP-D. Thus, HA-exposed glycans differing in location and numbers between IAV subtypes may be responsible for this interaction. rfhSP-D is likely to inhibit IAV infection by preventing the HA interaction with SA containing receptors. A reverse genetic approach has been used to analyze the role of N-glycosylation sites on the head of H1 in modulating sensitivity to SP-D *in vitro* and *in vivo* (25). It was found that HA Asn-144 was a critical factor in sensitivity to SP-D (25).

We also examined the immune response of A549 lung epithelial cells following IAV challenge in the presence or absence of rfhSP-D, which can impact upon cellular infection and viral replication. Therefore, the ability of rfhSP-D to modulate viral replication as well as inflammatory immune response following IAV challenge was examined *via* infection assay, qPCR, and multiplex cytokine array. The key aspect of host–pathogen interaction arising out of this study is the ability of rfhSP-D-bound pH1N1 and H3N2 to undergo suppressed replication, as evident by the expression of M1 gene. M1 is a matrix protein of IAV that lies beneath the lipid layer and is the most abundant protein, which is essential for viral stability and integrity. Thus, it plays a critical role in the recruitment and assembly of viral sites, nuclear export of viral RNPs, and thus, establishing the host components for viral budding (26). rfhSP-D suppressed the expression of M1 in pH1N1 (**Figure 5A**) at 2 h, while downregulating at 6 h in the case of H3N2 (**Figure 5B**). In addition, a lowered M1 expression was detected *via* western blot in the rfhSP-D treated sample compared to untreated sample following 6 h incubation (**Figure 5C**). Viral replication was also reduced in the presence of rfhSP-D as evident in **Figures 5D,E**. This suggests that rfhSP-D could act as an entry inhibitor against the subtypes tested (pH1N1 and H3N2). It is known that HA undergoes N-linked glycosylation, leading to modulation of antigenicity, fusion activity, receptor-binding specificity, and immune evasion of IAV. Therefore, SP-D can play an important role in innate defense against IAV as entry inhibitor by interfering with glycosylation sites and binding to glycans on the viral HA. It has been reported that the combinatorial substitutions of D325A/S+R343V in a trimeric neck and CRD fragment of human SP-D markedly increased anti-viral activity against pandemic IAV. This is because of the increased ability of the mutant to block the SA binding sites, aggregate the virus and reduce viral uptake (27).

Our qPCR data demonstrated an increased expression level of TNF-α and IL-6 in the case of H3N2 subtype (**Figure 6B**)

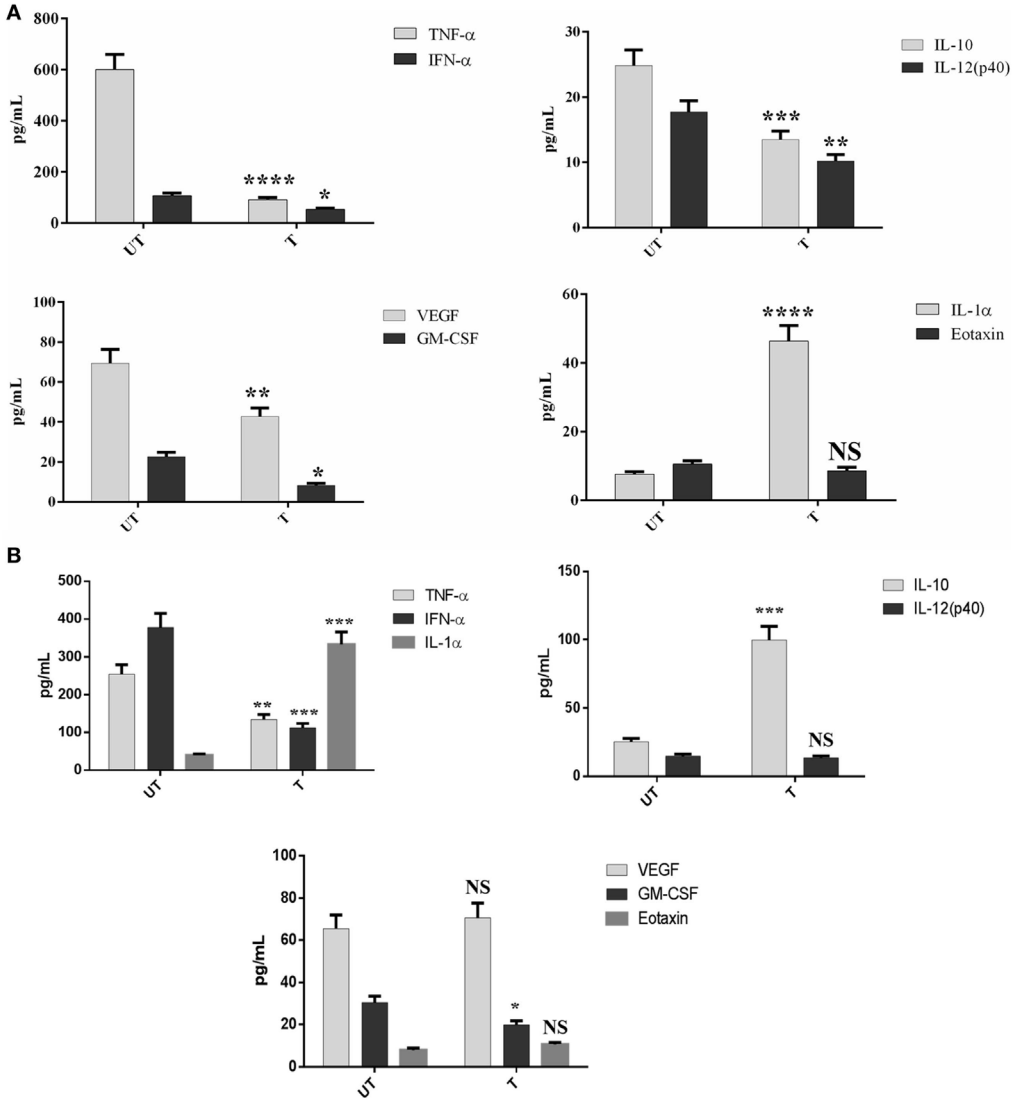

FIGURE 7 | Multiplex cytokine array analysis of supernatants that were collected at 24 h time point. A549 cells were infected with pH1N1 **(A)** and H3N2 **(B)**, treated with 10 μg/ml of rfhSP-D. Cytokines (TNF-α, IL-6, IL-10, IL-1α, IFN-α, and IL-12p40), chemokine (eotaxin), and growth factors (GM-CSF and VEGF) were measured using a commercially available MagPix Milliplex kit (EMD Millipore). Assays were conducted in triplicates and error bars represent ± SEM ($n = 3$); significance was determined using unpaired one-way ANOVA test (*$p < 0.05$, **$p < 0.01$, ***$p < 0.001$ and ****$p < 0.0001$).

compared to pH1N1. However, when pH1N1 was treated with rfhSP-D, TNF-α and IL-6 were suppressed at 2 h (**Figure 6A**), which recovered later (6 h). Elevated TNF-α and IL-6 levels can contribute to virus-mediated respiratory diseases or acute lung injury. IL-12 was considerably downregulated by rfhSP-D in the case of both IAV subtypes, suggesting the likely suppression of Th1 immune response. mRNA expression of RANTES was 10-fold ($log_{10}1$ fold) downregulated in the presence of rfhSP-D at 2 h time point in pH1N1 compared to A549 cells challenged with IAV. However, cells, challenged with H3N2 and treated with rfhSP-D, were seen to have log_{10} one-fold downregulation of RANTES expression. In this study, we also report the ability of rfhSP-D (10 μg/ml) to downregulate both IFN-α and IFN-β expression (**Figure 6C**) at 2 and 6 h. Higher expression levels of IFN-α and IFN-β were detected in the untreated (cells + virus) sample, which was threefold (log10 fold) downregulated in the presence of rfhSP-D at 6 h. This suggests that when cells were incubated with pH1N1/H3N3 (MOI 1), higher levels of both IFN-α and IFN-β were produced by A549 cells to clear the virions. Since addition of rfhSP-D caused inhibition of viral replication, lower levels of INF were detected. Recently, the E3 ubiquitin ligase, TRIM29, has been shown to be a negative regulator of type I IFN responses in the lungs post-IAV challenge *in vivo*. TRIM29 acts by inhibiting IFN-regulatory factors and signaling *via* NF-κB, leading to degradation of NF-κB essential modulator (28). Whether rfhSP-D works *via* similar mechanisms is worth further investigation using SP-D gene-deficient mice (29). In addition, cytokine array analysis using supernatants that were collected at

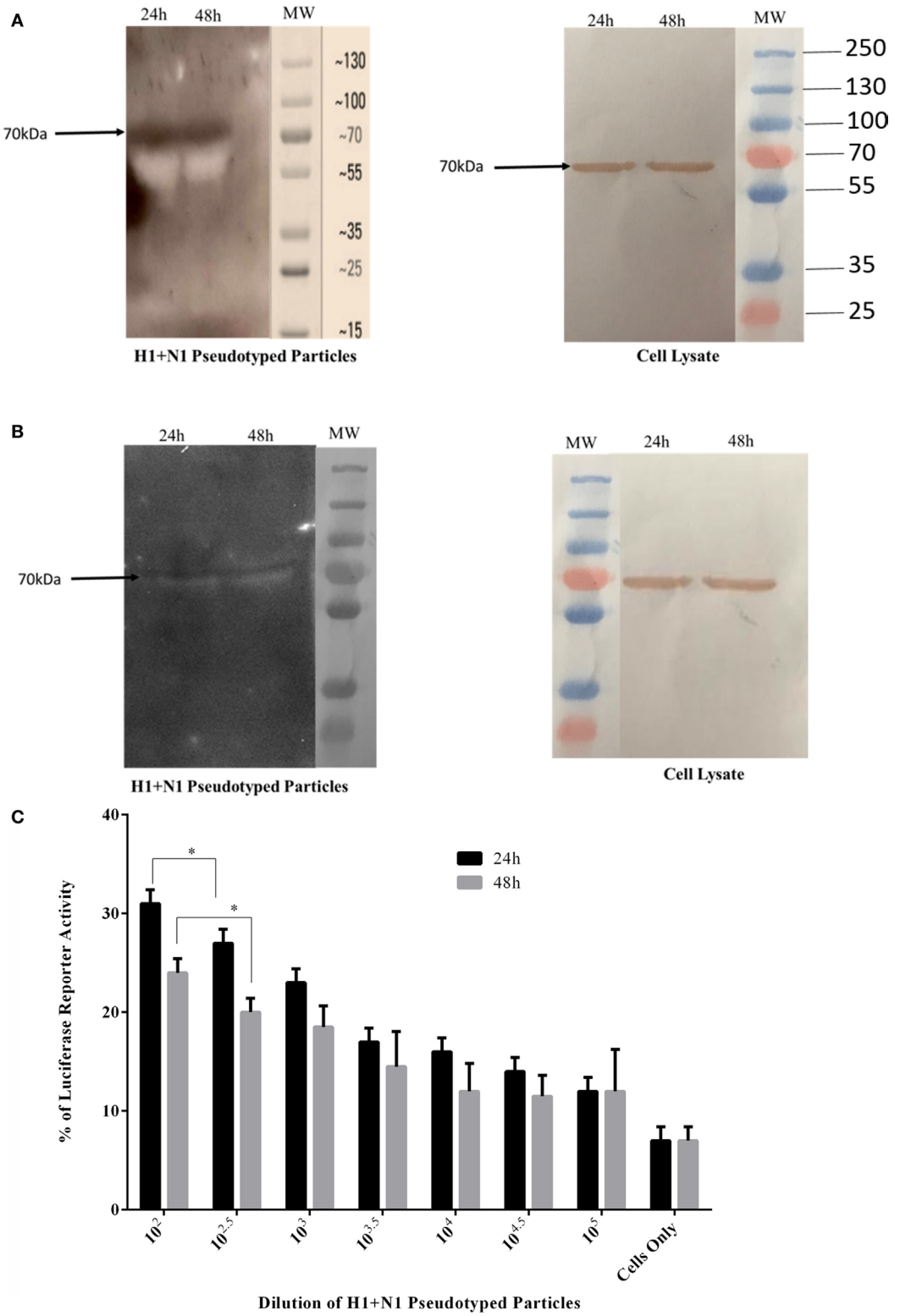

FIGURE 8 | Continued

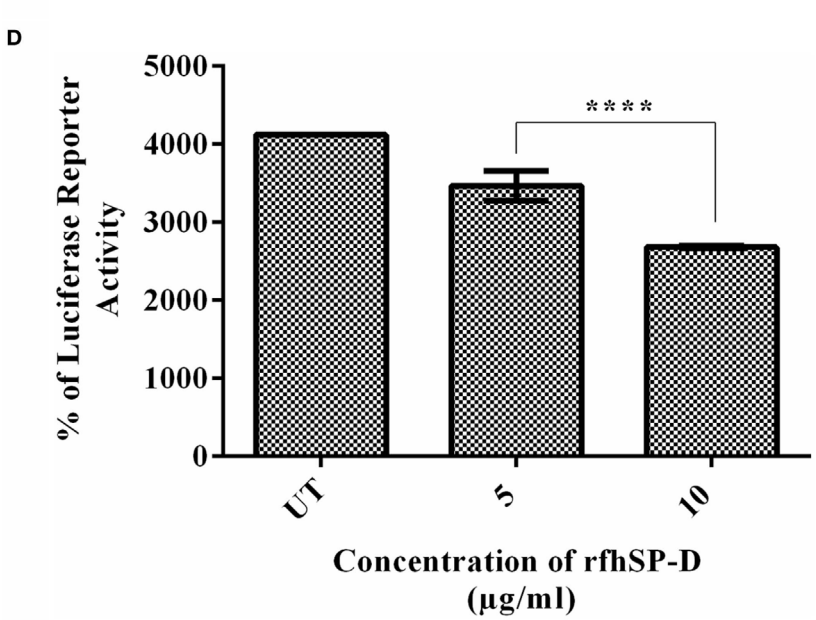

FIGURE 8 | **(A)** Western blotting to show the expression of influenza A virus-hemagglutinin (HA) protein in purified H1+N1 pseudotyped lentiviral particles and cell lysate at 24 and 48 h. The presence of HA was identified at 70 kDa. **(B)** Far western blotting to show rfhSP-D binding in both purified H1+N1 pseudotyped lentiviral particles and cell lysate at 24 and 48 h. HA was evident at 70 kDa when probed with rfhSP-D. **(C)** Luciferase reporter activity of purified H1+N1 pseudotyped lentiviral particles at 24 and 48 h, and **(D)** Luciferase reporter activity of rfhSP-D treated MDCK cells transduced with these lentiviral particles. Significance was determined using the unpaired one-way ANOVA test (*$p < 0.05$ and ****$p < 0.0001$) ($n = 3$).

24 h showed considerable downregulation of some of the key pro-inflammatory cytokines, chemokines, and other soluble factors in the presence of rfhSP-D. The downregulation of various humoral factors by rfhSP-D treatment could also facilitate the prevention of life-threatening secondary bacterial infections that may be caused by aberrant virus-mediated immune modulation.

In this study, we have produced the second-generation lentiviral vectors pseudotyped for H1+N1 of IAV. This system contains a single packaging plasmid (psPAX2) encoding genes including Gag, Pol, and Tat. pHIV-Luciferase was used as a lentiviral transfer plasmid, which is flanked with long terminal repeat (LTR) sequences, and designed to express the firefly luciferase reporter. Thus, pHIV-Luciferase is "replication incompetent" which contains an additional sequence deletion in the 3′ LTR leading to viral "self-inactivation" post-integration. This was selected as a safe alternative method to mimic the structure and surfaces of IAV, and to prove rfhSP-D as an entry inhibitor in cells transduced with pseudotyped IAV particles that are restricted to only one replicative cycle. The lentiviral particles pseudotyped with H1+N1 were analyzed *via* SDS-PAGE and western blotting. Expression of HA in purified H1+N1 pseudotyped lentiviral particles from transfected HEK293T cells was assessed by western blotting using anti-H1 monoclonal antibody (**Figure 8A**). H1+N1 pseudotyped lentiviral particles, purified *via* ultra-centrifugation, were used to investigate the combinatorial or differential involvement of viral envelope glycoproteins in the recognition and neutralization of HA by rfhSP-D. Incubation of rfhSP-D with these H1+N1 pseudotyped lentiviral particles was found to facilitate its binding to HA that appeared at 70 kDA in the far western blot (**Figure 8B**). To validate the effectiveness of rfhSP-D as an entry inhibitor of IAV, luciferase reporter activity assay was performed. Nearly 50% luminescent signal was seen with 10 µg/ml of rfhSP-D when compared to MDCK cells challenged with H1+N1 pseudotyped lentiviral particles alone. This, therefore, suggested the ability of rfhSP-D to inhibit viral infectivity through binding to cell surface bound HA found on the infected MDCK cells.

In summary, suppression of M1 expression, pro-inflammatory cytokine response, as well as luciferase reporter activity in target A549 cells by rfhSP-D highlight its potential as a therapeutic molecule in an entry inhibitory role against IAV.

AUTHOR CONTRIBUTIONS

MA-A, BN, and UK led the project; VM, PV, LK, and AP carried out crucial experiments; SA, IS, and AA-Q provided important reagents. VM, UK, and MA-A wrote the manuscript.

ACKNOWLEDGMENTS

This work is part of a project funded by the Biotechnology program of the King Abdulaziz City for Science and Technology (14-MED258-20) and approved by the Research Advisory Council of the King Faisal Specialist Hospital and Research Centre, Riyadh (2150031). We thank Maureene Delos Reyes and Hanan Shaarawi for secretarial and logistic assistance.

REFERENCES

1. Nayak A, Dodagatta-Marri E, Tsolaki AG, Kishore U. An insight into the diverse roles of surfactant proteins, SP-A and SP-D in innate and adaptive immunity. *Front Immunol* (2012) 3:131. doi:10.3389/fimmu.2012.00131
2. Kishore U, Greenhough TJ, Waters P, Shrive AK, Ghai R, Kamran MF, et al. Surfactant proteins SP-A and SP-D: structure, function and receptors. *Mol Immunol* (2006) 43(9):1293–315.
3. Crouch E, Hartshorn K, Horlacher T, McDonald B, Smith K, Cafarella T, et al. Recognition of mannosylated ligands and influenza A virus by human surfactant protein D: contributions of an extended site and residue 343. *Biochemistry* (2009) 48:3335–45. doi:10.1021/bi8022703
4. Hartshorn KL, Webby R, White MR, Tecle T, Pan C, Boucher S, et al. Role of viral hemagglutinin glycosylation in anti-influenza activities of recombinant surfactant protein D. *Respir Res* (2008) 9:65–9921–9–65. doi:10.1186/1465-9921-9-65
5. Hartshorn KL, Crouch EC, White MR, Eggleton P, Tauber AI, Chang D, et al. Evidence for a protective role of pulmonary surfactant protein D (SP-D) against influenza A viruses. *J Clin Invest* (1994) 94:311–9. doi:10.1172/JCI117323
6. Hartshorn KL, Sastry K, White MR, Anders EM, Super M, Ezekowitz RA, et al. Human mannose-binding protein functions as an opsonin for influenza A viruses. *J Clin Invest* (1993) 91:1414–20. doi:10.1172/JCI116345
7. Roberts KL, Manicassamy B, Lamb RA. Influenza A virus uses intercellular connections to spread to neighboring cells. *J Virol* (2015) 89:1537–49. doi:10.1128/JVI.03306-14
8. Mitnaul LJ, Matrosovich MN, Castrucci MR, Tuzikov AB, Bovin NV, Kobasa D, et al. Balanced hemagglutinin and neuraminidase activities are critical for efficient replication of influenza A virus. *J Virol* (2000) 74:6015–20. doi:10.1128/JVI.74.13.6015-6020.2000
9. Morens DM, Taubenberger JK, Harvey HA, Memoli MJ. The 1918 influenza pandemic: lessons for 2009 and the future. *Crit Care Med* (2010) 38:e10–20. doi:10.1097/CCM.0b013e3181ceb25b
10. Taubenberger JK, Morens DM. 1918 influenza: the mother of all pandemics. *Emerg Infect Dis* (2006) 12:15–22. doi:10.3201/eid1209.05-0979
11. Skehel JJ, Wiley DC. Receptor binding and membrane fusion in virus entry: the influenza hemagglutinin. *Annu Rev Biochem* (2000) 69:531–69. doi:10.1146/annurev.biochem.69.1.531
12. Wilson IA, Cox NJ. Structural basis of immune recognition of influenza virus hemagglutinin. *Annu Rev Immunol* (1990) 8:737–71. doi:10.1146/annurev.iy.08.040190.003513
13. Glaser L, Stevens J, Zamarin D, Wilson IA, Garcia-Sastre A, Tumpey TM, et al. A single amino acid substitution in 1918 influenza virus hemagglutinin changes receptor binding specificity. *J Virol* (2005) 79:11533–6. doi:10.1128/JVI.79.17.11533-11536.2005
14. Lakadamyali M, Rust MJ, Zhuang X. Ligands for clathrin-mediated endocytosis are differentially sorted into distinct populations of early endosomes. *Cell* (2006) 124:997–1009. doi:10.1016/j.cell.2005.12.038
15. de Vries E, Tscherne DM, Wienholts MJ, Cobos-Jimenez V, Scholte F, Garcia-Sastre A, et al. Dissection of the influenza A virus endocytic routes reveals macropinocytosis as an alternative entry pathway. *PLoS Pathog* (2011) 7:e1001329. doi:10.1371/journal.ppat.1001329
16. Stauffer S, Feng Y, Nebioglu F, Heilig R, Picotti P, Helenius A. Stepwise priming by acidic pH and a high K^+ concentration is required for efficient uncoating of influenza A virus cores after penetration. *J Virol* (2014) 88:13029–46. doi:10.1128/JVI.01430-14
17. Tecle T, White MR, Crouch EC, Hartshorn KL. Inhibition of influenza viral neuraminidase activity by collectins. *Arch Virol* (2007) 152:1731–42. doi:10.1007/s00705-007-0983-4
18. Hartshorn KL, White MR, Voelker DR, Coburn J, Zaner K, Crouch EC. Mechanism of binding of surfactant protein D to influenza A viruses: importance of binding to haemagglutinin to antiviral activity. *Biochem J* (2000) 351(Pt 2):449–58. doi:10.1042/bj3510449
19. Hillaire ML, van Eijk M, Vogelzang-van Trierum SE, Fouchier RA, Osterhaus AD, Haagsman HP, et al. Recombinant porcine surfactant protein D inhibits influenza A virus replication ex vivo. *Virus Res* (2014) 181:22–6. doi:10.1016/j.virusres.2013.12.032
20. Singh M, Madan T, Waters P, Parida SK, Sarma PU, Kishore U. Protective effects of a recombinant fragment of human surfactant protein D in a murine model of pulmonary hypersensitivity induced by dust mite allergens. *Immunol Lett* (2003) 86:299–307. doi:10.1016/S0165-2478(03)00033-6
21. Paquette SG, Banner D, Zhao Z, Fang Y, Huang SS, Leomicronn AJ, et al. Interleukin-6 is a potential biomarker for severe pandemic H1N1 influenza A infection. *PLoS One* (2012) 7:e38214. doi:10.1371/journal.pone.0038214
22. Ng WC, Tate MD, Brooks AG, Reading PC. Soluble host defense lectins in innate immunity to influenza virus. *J Biomed Biotechnol* (2012) 2012:732191. doi:10.1155/2012/732191
23. Dodagatta-Marri E, Mitchell DA, Pandit H, Sonawani A, Murugaiah V, Idicula-Thomas S, et al. Protein-protein interaction between surfactant protein D and DC-SIGN via C-type lectin domain can suppress HIV-1 transfer. *Front Immunol* (2017) 8:834. doi:10.3389/fimmu.2017.00834
24. Yang J, Li M, Shen X, Liu S. Influenza A virus entry inhibitors targeting the hemagglutinin. *Viruses* (2013) 5:352–73. doi:10.3390/v5010352
25. Tate MD, Brooks AG, Reading PC. Specific sites of N-linked glycosylation on the hemagglutinin of H1N1 subtype influenza A virus determine sensitivity to inhibitors of the innate immune system and virulence in mice. *J Immunol* (2011) 187:1884–94. doi:10.4049/jimmunol.1100295
26. Rossman JS, Lamb RA. Influenza virus assembly and budding. *Virology* (2011) 411:229–36. doi:10.1016/j.virol.2010.12.003
27. Nikolaidis NM, White MR, Allen K, Tripathi S, Qi L, McDonald B, et al. Mutations flanking the carbohydrate binding site of surfactant protein D confer antiviral activity for pandemic influenza A viruses. *Am J Physiol Lung Cell Mol Physiol* (2014) 306:L1036–44. doi:10.1152/ajplung.00035.2014
28. Xing J, Weng L, Yuan B, Wang Z, Jia L, Jin R, et al. Identification of a role for TRIM29 in the control of innate immunity in the respiratory tract. *Nat Immunol* (2016) 17(12):1373–80. doi:10.1038/ni.3580
29. Madan T, Reid KB, Singh M, Sarma PU, Kishore U. Susceptibility of mice genetically deficient in the surfactant protein (SP)-A or SP-D gene to pulmonary hypersensitivity induced by antigens and allergens of *Aspergillus fumigatus*. *J Immunol* (2005) 174(11):6943–54. doi:10.4049/jimmunol.174.11.6943

Conflict of Interest Statement: The authors declare that the research was conducted in the absence of any commercial or financial relationships that could be construed as a potential conflict of interest.

Immunobiology 224 (2019) 408–418

Contents lists available at ScienceDirect

Immunobiology

journal homepage: www.elsevier.com/locate/imbio

Full-length human surfactant protein A inhibits influenza A virus infection of A549 lung epithelial cells: A recombinant form containing neck and lectin domains promotes infectivity

Ahmed A. Al-Qahtani[a,b,1], Valarmathy Murugaiah[c,1], Hani A. Bashir[c], Ansar A. Pathan[c], Suhair M. Abozaid[a], Evgeny Makarov[c], Beatrice Nal-Rogier[c], Uday Kishore[c], Mohammed N. Al-Ahdal[a,b,*]

[a] Department of Infection and Immunity, King Faisal Specialist Hospital and Research Centre, Riyadh, Saudi Arabia
[b] Alfaisal University College of Medicine, Riyadh, Saudi Arabia
[c] Biosciences, College of Health and Life Sciences, Brunel University London, Uxbridge, UB8 3PH, United Kingdom

ARTICLE INFO

Keywords:
Innate immunity
Influenza A virus
Pulmonary collectins
Surfactant protein A

ABSTRACT

Hydrophilic lung surfactant proteins have emerged as key immunomodulators which are potent at the recognition and clearance of pulmonary pathogens. Surfactant protein A (SP-A) is a surfactant-associated innate immune molecule, which is known to interact with a variety of pathogens, and display anti-microbial effects. SP-A, being a carbohydrate pattern recognition molecule, has a wide range of innate immune functions against respiratory pathogens, including influenza A virus (IAV). Some pandemic pH1N1 strains resist neutralization by SP-A due to differences in the N-glycosylation of viral hemagglutinin (HA). Here, we provide evidence, for the first time, that a recombinant form of human SP-A (rfhSP-A), composed of α-helical neck and carbohydrate recognition domains, can actually promote the IAV replication, as observed by an upregulation of M1 expression in lung epithelial cell line, A549, when challenged with pH1N1 and H3N2 IAV subtypes. rfhSP-A (10 μg/ml) bound neuraminidase (NA) (~60 kDa), matrix protein 1 (M1) (~25 kDa) and M2 (~17 kDa) in a calcium dependent manner, as revealed by far western blotting, and direct binding ELISA. However, human full length native SP-A downregulated mRNA expression levels of M1 in A549 cells challenged with IAV subtypes. Furthermore, qPCR analysis showed that transcriptional levels of TNF-α, IL-12, IL-6, IFN-α and RANTES were enhanced following rfhSP-A treatment by both IAV subtypes at 6 h post-IAV infection of A549 lung epithelial cells. In the case of full length SP-A treatment, mRNA expression levels of TNF-α and IL-6 were downregulated during the mid-to-late stage of IAV infection of A549 cells. Multiplex cytokine/chemokine array revealed enhanced levels of both IL-6 and TNF-α due to rfhSP-A treatment in the case of both IAV subtypes tested, while no significant effect was seen in the case of IL-12. Enhancement of IAV infection of pH1N1 and H3N2 subtypes by truncated rfhSP-A, concomitant with infection inhibition by full-length SP-A, appears to suggest that a complete SP-A molecule is required for protection against IAV. This is in contrast to a recombinant form of trimeric lectin domains of human SP-D (rfhSP-D) that acts as an entry inhibitor of IAV.

1. Introduction

The initial response to an infection in a host is the activation of its innate immune system. Understanding how innate immune mechanisms restrict the spread of respiratory infections is crucial to designing therapeutic strategies. Influenza virus is a major infectious respiratory pathogen, and remains a serious global health concern, resulting in up to half a million deaths annually (WHO, 2018). There are four distinct types of Influenza virus, cause infections in humans; influenza virus A (IAV) represents the most common cause of significant health threat. IAV is responsible for approximately 70% of all influenza related deaths, and has caused highly pathogenic pandemics (WHO, 2009). IAV is further classified into different subtypes, depending on the combination of their surface glycoproteins, hemagglutinin (HA) and neuraminidase (NA) (Bouvier and Palese, 2008). IAV exerts a greater selective pressure on the host, with a complex pathogenesis, characterised

* Corresponding author.
E-mail address: profahdal@gmail.com (M.N. Al-Ahdal).
[1] AAQ and VM are joint first authors.

https://doi.org/10.1016/j.imbio.2019.02.006
Received 12 December 2018; Received in revised form 5 February 2019; Accepted 5 February 2019
Available online 11 February 2019

by rapid viral replication and viral distribution within the lungs, while evoking cellular and humoral immunity (Fukuyama and Kawaoka, 2011). Although IAV has evolved numerous molecular strategies to avoid and escape the host's immune response to promote its continuous survival within the host, a range of immune responses could potentially target any stage of IAV.

The pulmonary surfactant system is composed of abundant proteins and lipids that lower the surface tension of the alveoli, and play important roles in innate immunity. Its hydrophilic proteins, also called collectins, are soluble collagenous lectins that serve multiple antimicrobial functions against influenza viruses by binding to oligosaccharide structures via conserved carbohydrate recognition domains (CRDs) on the surface of viral particles (van de Wetering et al., 2004). The interaction between IAV and collectins (found within the mammalian serum and pulmonary fluids) leads to anti-viral activity *in vitro* (Reading et al., 1997). Bovine conglutinin and mannose binding lectin (MBL) cause inhibition of IAV hemagglutination and neutralisation (Hartley et al., 1992). Other collectins, including surfactant protein A (SP-A) and SP-D, expressed in the lungs, mucosal and epithelial surfaces in the body, are involved in a number of immune functions involving neutralization, agglutination, opsonisation and clearance of pathogens.

SP-A is a collagenous calcium-dependent defense lectins, composed of N-terminal domain rich in cysteine, collagen domain, an α-helical coiled-coil neck, and a C-terminal carbohydrate recognition domain (CRD) (Kishore et al., 2006; Nayak et al., 2012). The overall structure of SP-A is made up six of these subunits, which look like a bouquet (Kishore et al., 2006). The trimeric CRD region recognises pathogens by engaging terminal monosaccharide residues or charged patterns on microorganisms, serving as soluble pattern recognition receptors (PRRs). Thus, collagen like region is crucial for the interaction with immune cell-mediated receptors such as calreticulin-CD91 complex to bring about removal of pathogens (Kishore et al., 2006; Gardai et al., 2003).

Direct interaction between SP-A and various viruses results in viral neutralisation and induction of phagocytosis *in vitro*. SP-A can interact with glycoprotein 120 of HIV-1 and suppress infection of $CD4^+$ T cells, and enhance HIV-1 transfer via dendritic cells, serving as a dual modulator of HIV-1 infection (Gaiha et al., 2008). SP-A has also been shown to interact with herpes simplex virus type 1 (HSV-1), and mediate phagocytosis of HSV-1 by alveolar macrophages (van Iwaarden et al., 1991). SP-A can bind to the F2 subunit of respiratory syncytial virus (RSV) and neutralise its infectivity (Ghildyal et al., 1999). In the case of IAV, SP-A can bind HA and NA, and inhibit haemagglutination at initial stages. However, pH1N1 pandemic strains are not neutralised by SP-A due to variations in the N-linked glycosylation of HA (Job et al., 2010). We have recently shown a recombinant form of human surfactant protein D, containing homotrimeric neck and CRD region (rfhSP-D), binds HA and reduces M1 expression in A549 cells challenged with pH1N1 and H3N2 strains (Al-Ahdal et al., 2018). In addition, mRNA expression levels of TNF-α, IFN-α, IFN-β, IL-6 and RANTES were down-regulated following rfhSP-D treatment. Furthermore, rfhSP-D also reduced MDCK cell transduction by H1 + N1 pseudotyped lentiviral particles, suggesting a possible therapeutic potential against IAV infection. In this regards, this study was aimed at investigating the possible role of a well-characterised recombinant truncated form of human SP-A (rfhSP-A) made up of trimeric CRDs, using pH1N1 and H3N2 IAV subtypes.

2. Method and materials

2.1. Virus and antibodies

A/England/2009 (pH1N1) and the A/HK/99 (H3N2) influenza A subtypes were used for most experiments. Vesicular Stomatitis Virus (VSV-G) was used as a control for ELISA. Monoclonal Anti-Influenza Virus NA, A/California/04/2009 (pH1N1) pdm09, Clone 5C12 (produced *in vitro*), NR-42019 and A/Hong Kong/1/1968 (H3N2) (antiserum, Goat), NR-3118 and anti-M1 monoclonal antibody were obtained from BEI Resources, NIAID, NIH, USA. Monoclonal anti-influenza A virus M2 protein was obtained from Abcam.

2.2. Cell culture

Most reagents were purchased from Sigma unless mentioned otherwise. A549 and MDCK cell lines were cultured in complete DMEM containing FBS (10%), L-glutamine (2 mM), penicillin (100 U/ml), streptomycin (100 μg/ml) and sodium pyruvate (1 mM). Cells were cultured at 37 °C in a CO_2 incubator until they were 80% confluent. Cells were trypsinised (0.5%; 10 min), spun at 1000 rpm for 7′, and suspended in complete DMEM. Viable cells were counted via Trypan Blue (0.4%).

2.3. Virus purification and infection titre determination

Purification and production of pH1N1 and H3N2 subtypes were carried out as described earlier (Al-Ahdal et al., 2018). MDCK cells were infected with pH1N1 (2×10^4) or H3N2 (3.3×10^4) by incubation at 37 °C for 1 h. Post infection, the viral particles were pelleted via 3000 × g centrifugation at 4 °C for 10′. Supernatants containing virus particles were then subjected to ultracentrifugation (25,000 × g, 4 °C, 1 h 30′), followed by re-suspending virus in 100 μl of PBS. 15 μl of virus stock was assessed via reduced SDS-PAGE and ELISA. Tissue culture infectious dose ($TCID_{50}$) assay was performed to determine the infectious titre of the purified pH1N1 and H3N2 viral stocks, and to assess its cytopathic effects (CPE) using MDCK cells, as reported recently (Al-Ahdal et al., 2018). CPE effects of infected and non-infected cells were microscopically examined at each viral dilution.

2.4. Production of rfhSP-A

DNA sequences coding for trimeric neck and CRD region were cloned under T7 promoter and expressed in *Escherichia coli* BL21 (λDE3) pLysS using construct pUK-A1 (Karbani et al., 2014). *E. coli* cells were grown in LB medium, containing 100 μg/ml ampicillin and 34 μg/ml of chloramphenicol, at 37 °C until an OD_{600} reached 0.6. Following induction with 0.5 mM isopropyl β-D-thiogalactoside (IPTG), the bacterial culture was left to grow further for another 3 h on a shaker at 37 °C. The bacterial cell culture was then centrifuged (4500 rpm, 4 °C, 10′) and the pellet was re-suspended in lysis buffer (0.05 M Tris − HCL pH 7.5, 0.2 M NaCl, 0.005 M EDTA, 0.1% Triton X-100, 0.1 mM phenylmethane sulfonyl fluoride (PMSF), 50 μg lysozyme) for 1 h at 4 °C. The lysate was sonicated using a Soniprep 150 (MSE, London, UK) at 60 Hz for 30 s with an interval of 2 min (12 cycles), followed by centrifugation at 12,000 rpm for 15 min. The inclusion bodies were denatured fully in 50 ml of 0.5 M Tris − HCl, 0.1 M NaCl, pH7.5 and 8 M urea for 1 h at 4 °C. The soluble fraction was dialysed against the same buffer containing 4 M, 2 M, 1 M and no urea for 2 h at each urea concentration. The refolded material was then extensively dialysed against affinity buffer that contained 10 mM $CaCl_2$ instead of 5 mM EDTA for 2 h. The supernatant was loaded on a 5 ml of mannose-sepharose column, and bound rfhSP-A was eluted with buffer with 10 mM EDTA. Purified rfhSP-A was run on SDS-PAGE to assess its purity. LPS was removed using Endotoxin Removal Resin. LPS level was determined using QCL-1000 Limulus amebocyte lysate system (Lonza) and found to be ~5 pg/μg of rfhSP-A.

2.5. Extraction of full length native SP-A from human bronchoalveolar lavage fluid

Human full-length native SP-A (FLSP-A) was purified as published earlier (Strong et al., 1998). Bronchoalveolar lavage fluid (BAL) collected from pulmonary alveolar proteinosis patients was made up with

buffer I containing 20 mM Tris − HCl and 10 mM EDTA, pH 7.4, followed by centrifugation at 10,000 × g. The centrifuged cell pellet was extracted using buffer I with 6 M urea. The solubilised FLSP-A was centrifuged again at 10,000 × g and the soluble fraction was dialysed against 4, 2, and 1 M urea in buffer II (20 mM Tris − HCl, 100 mM NaCl, and 5 mM EDTA, pH 7.4). The supernatant was again dialysed against buffer II containing 15 mM $CaCl_2$, and loaded onto maltose agarose column, followed by elution with buffer II containing 10 mM EDTA.

2.6. SDS-PAGE

SDS-PAGE 12% (w/v) was performed to analyse and detect the purity of purified rfhSP-A and FLSP-A. Purified proteins were diluted in 1:1 (v/v) ratio in 2× Laemmli sample buffer (10 ml) (Bio-Rad, Hertfordshire) containing 1 M Tris − HCL (pH 6.8, 1 ml), 10% SDS (4 ml), 100% Glycerol (2 ml), 1% Bromophonol blue, β-mercaptoethanol (2.5 ml) and distilled water (d.H2O). The protein was then denatured for 10 min at 95 °C before loading. Standard pre-stained protein marker (Fisher Scientific) was also loaded to assess the size of the purified rfhSP-A. The SDS-PAGE gel was stained overnight using staining solution (1 g of Brilliant Blue, 50% v/v methanol, 10% acetic acid and 40 ml of D.H_2O). The stained gel was then de-stained using the de-staining solution 40% (v/v) methanol, 10% (v/v) acetic acid until the protein bands were visible.

2.7. Direct binding ELISA

FLSP-A, rfhSP-A, rfhSP-D and VSV-G (as a negative control protein) (10, 5, 2.5, and 1.25 μg/well) were coated on microtitre wells of a Maxisorp 96 well plate (Sigma-Aldrich) in carbonate/bicarbonate buffer, pH 9.6 and incubated at 4 °C overnight. After washing with PBS three times, the unoccupied sites on the wells were blocked with 2% w/v BSA for 2 h at 37 °C, followed by washing with PBST (PBS + 0.05% Tween 20). pH1N1/H3N2 virus (20 μl of 1.36×10^6 pfu/ml) was diluted 10 times using PBS, and 10 μl was incubated in the wells for 2 h at RT. After washing, monoclonal anti-H1 and polyclonal anti-H3 (both from BEI-Resources) in PBS (1:5000) were added to the appropriate wells and incubated at 37 °C for 1 h, followed by 1 h incubation with rabbit anti-mouse and protein A conjugated to HRP (1:5000), respectively (Fisher Scientific). TMB was used as a substrate and the plate was read at OD_{450}.

2.8. Far western blotting

Purified pH1N1/H3N2 (1.36×10^6pfu/ml) was run on SDS-PAGE and then separated proteins were transferred to a PVDF membrane using transfer buffer (0.25 M Tris, 0.19 M glycine and 20% methanol). After blocking the membrane with 5% w/v milk power in PBS at 4 °C and washing with PBST, the membrane was probed with monoclonal anti-NA, anti-M1 or anti-M2 (1:1000 dilutions) antibodies for 1 h at RT. For far-western blotting, the membrane was incubated with 5 μg/ml of rfhSP-A in 5 mM $CaCl_2$ buffer overnight at 4 °C. Binding was probed with rabbit anti-human SP-A polyclonal antibodies in PBS (1:1000) for 1 h at RT. Rabbit anti-mouse and Protein A conjugated to HRP (1:5000) (Fisher Scientific) were used as respective conjugates/secondary probes for monoclonal and polyclonal antibodies. The colour was developed using DAB as a substrate and H_2O_2.

2.9. Cell-binding assay

A549 cells (10,000 cells per well) were seeded in complete DMEM and incubated at 37 °C until 80% confluence was reached. After washing with different concentration of purified rfhSP-A (1.25–10 μg/ml) were pre-treated with pH1N1/H3N2 virus (1.36×10^6 pfu/ml). 10 μl of diluted virus stock was added to the appropriate wells, and incubated for 2 h at RT. After fixing the wells with 4% v/v paraformaldehyde (Fisher Scientific) for 10′ at RT, the blocking step was carried out using 2% w/v BSA. Anti-H1 and H3 antibodies and secondary probes were used, as described earlier, using TMB as a substrate.

2.10. Quantitative RT-PCR

rfhSP-A and FLSP-A (10 μg/ml) were added to A549 cells (0.5×10^6) in DMEM + 5 mM $CaCl_2$ with MOI 1 of H1N1/H3N2 virus and pelleted at different time points. Total RNA was extracted from the above-mentioned cells using GenElute Mammalian Total RNA Purification Kit (Sigma-Aldrich, UK). Total RNA was treated with DNase I (Sigma-Aldrich, UK) prior to assessing concentration and purity of total RNA via reading at OD_{260} and OD_{260}:OD_{280}(NanoDrop 2000/2000c; Thermo Fisher Scientific). 2 μg of RNA was converted into cDNA using cDNA Kit (Applied Biosystems). qRT-PCR was performed using the 7900 H T Fast Real-Time PCR System (Applied Biosciences). Each reaction was carried out in triplicates and included 5 μl Power SYBR Green MasterMix, 75 nM of FP and RP, and 500 ng cDNA. The amplification cycle involved 50 °C and 95 °C for 2′ and 10′, followed by 40 cycles of amplification. Human 18S rRNA was used to normalise gene expression and as an endogenous control. A list of primers have been provided in Table 1.

2.11. Multiplex cytokine array analysis

In order to measure the secreted cytokines and chemokines following rfhSP-A treatment, IAV treated A549 cells were incubated in the presence or absence of rfhSP-A (10 μg/ml) for 24 h. Subsequently, supernatants were collected for measuring IL-6, TNF-α, IL-8, IL12 (p40) and MCP-1. The expression levels of various analytes were measured using EMD Millipore multiplex kit. As per manufacture's instruction, 25 μl assay buffer was added to microtiter wells, plus 25 μl standard, control or supernatant of A549 cells. Magnetic beads (25 μl) linked-analytes were added to each well and incubated at 4 °C for 18 h. After assay buffer washing, detection antibodies (25 μl) were incubated with beads at RT for 1 h. 25 μl of Streptavidin-Phycoerythrin was then added to each well and incubated for 30 min. at RT. After another round of washing, 150 μl of sheath fluid was added to each well and the plate was read using the Luminex Magpix instrument.

Table 1
Target Genes, Forward and Reverse primers used for qPCR.

Target	Forward Primer	Reverse Primer
18S	5′-ATGGCCGTTCTTAGTTGGTG-3′	5′-CGCTGAGCCAGTCAGTGTAG-3′
IL-6	5′-GAAAGCAGCAAAGAGGCACT-3′	5′-TTTCACCAGGCAAGTCTCCT-3′
IL-12	5′-AACTTGCAGCTGAAGCCATT-3′	5′-GACCTGAACGCAGAATGTCA-3′
TNF-α	5′-AGCCCATGTTGTAGCAAACC-3′	5′-TGAGGTACAGGCCCTCTGAT-3′
M1	5′AAACATATGTCTGATAACGAAGGAGAACAGTTCTT-3′	5′GCTGAATTCTACCTCATGGTCTTCTTGA-3′
RANTES	5'-GCGGGTACCATGAAGATCTCTG-3'	5'-GGGTCAGAATCAAGAAACCCTC-3'
IFN-α	5'-TTT CTC CTG CCT GAA GGA CAG-3'	5'-GCT CAT GAT TTC TGC TCT GAC A-3'

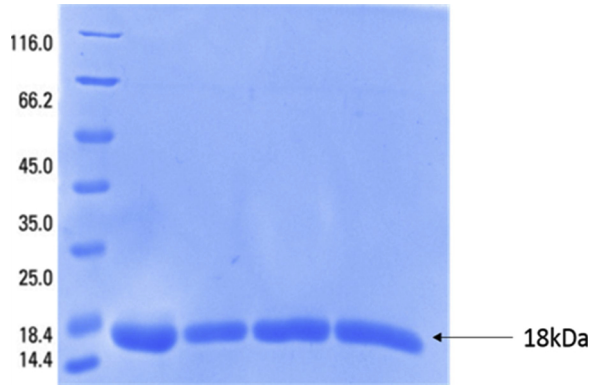

Fig. 1. SDS-PAGE (15% w/v) analysis of affinity purified recombinant fragment of Human Surfactant protein (rfhSP-A). pUK-A1 construct containing neck and CRD region was expressed under T7 bacteriophage in *Escherichia coli* BL21 (λDE3) pLysS. Following IPTG induction, the expressed bacterial cells show rfhSP-A overexpression at ~18 kDa. The inclusion bodies were refolded and affinity purified using a mannose-agarose column. Purified rfhSP-A appeared as a homogenous band of ~18 kDa.

2.12. Statistical analysis

GraphPad Prism 6.0 software was used to generate all the graphs. Two-way ANOVA test was used to perform the statistical analysis, and the significance values were considered between rfhSP-A treated and untreated conditions based on *p < 0.1, **p < 0.05, ***p < 0.01, and ****p < 0.001. Error bars show the SD or SEM (figure legends).

3. Results

3.1. Interaction of affinity purified rfhSP-A and FLSP-A with pH1N1/H3N3

The affinity purified and LPS-free rfhSP-A appeared as a single band at ~18 kDa on 15% SDS-PAGE (v/v) under reducing condition (Fig. 1). FLSP-A preparation appeared mostly as a ~32 kDa monomer, with a small proportion showing up as a non-reducible dimer of ~64 kDa (data not shown). The interaction of FLSP-A, rfhSP-A, and rfhSP-D with pH1N1/H3N2 viral particles was determined using direct binding ELISA. As shown in Fig. 2, FLSP-A, rfhSP-A and rfhSP-D bound IAV subtypes in a dose and calcium-dependent manner. No significant binding was observed with VSV-G pseudotyped lentivirus (negative control RNA virus). Cell binding assay was also performed to assess the interaction of rfhSP-A with A549 lung epithelial cells challenged with pH1N1 and H3N2 (Fig. 3). Maximum cell binding was seen at 10 µg/ml for both IAV subtypes, while a clear dose dependent binding was seen with H3N2, compared to pH1N1.

3.2. rfhSP-A interaction with NA, M1, and M2 proteins of pH1N1 and H3N2

Binding of rfhSP-A to NA (~60 kDa), M1 (~25 kDa) and M2 (~17 kDa) of purified pH1N1 and H3N2 was established using far western blotting (Fig. 4A). The ability of rfhSP-A to bind immobilised purified recombinant NA was assessed using ELISA. As shown in Fig. 4C, rfhSP-A interacted with NA dose- and calcium-dependently; VSV-G-pseudotyped particles did not show significant binding. Polymerization of M1 is suggested to provide a crucial mechanism for the elongation of filamentous IAV virions. In addition, rfhSP-A was also found to bind matrix protein 2 (M2) migrating at ~17 kDa, as evident from western blotting (Fig. 4A). Binding of rfhSP-A to M2 protein may suggest enhancement of viral replication by stabilising the viral budding site, enabling M2 polymerization leading to formation of filamentous viral particles.

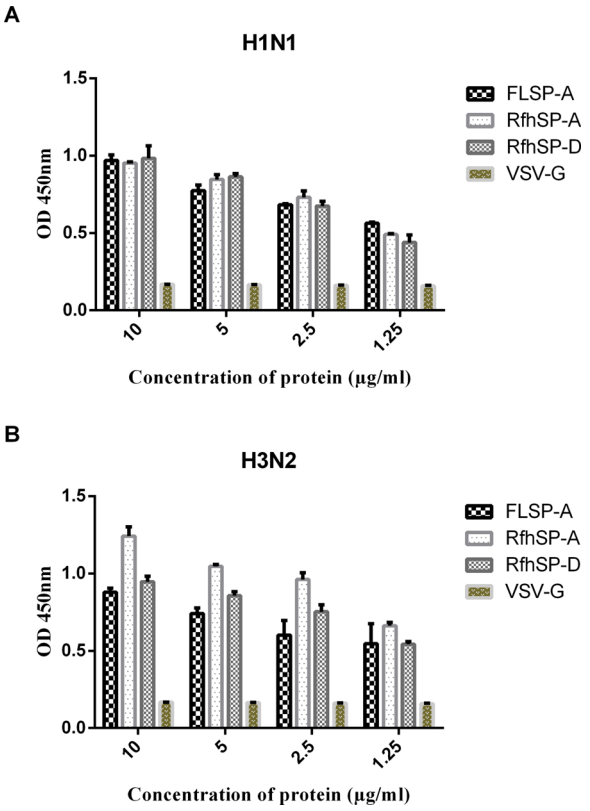

Fig. 2. Binding of rfhSP-A to (A) pH1N1 and (B) H3N2 via ELISA. Microtiter wells were coated with varied concentrations of FLSP-A, rfhSP-A and rfhSP-D (10, 5, 2.5, and 1.25 µg/ml). 20 µl of concentrated pH1N1 or H3N2 virus (1.36×10^6 pfu/ml) was diluted in 200 µl of PBS + 5 mM $CaCl_2$ and 10 µl of the diluted virus was added to all the wells, and probed with either monoclonal anti-influenza virus H1 or polyclonal anti-influenza virus H3 antibody. VSV-G pseudotyped lentivirus was used as a negative RNA virus control. The data were expressed as mean of three independent experiments done in triplicates ± SEM.

3.3. rfhSP-A promotes, while FLSP-A inhibits, infection of A549 cells by IAV

Infection assay was performed to determine the ability of IAV to infect A549 cells in the presence or absence of FLSP-A and rfhSP-A (10 µg/ml). rfhSP-A treatment up-regulated M1 expression in infected A549 cells when compared to untreated cells challenged only with virus (Fig. 5). In the case of both IAV subtypes, rfhSP-A treatment upregulated M1 expression at 2 and 6 h. The up-regulation of M1 expression was more pronounced for H3N2 than pH1N1, where $7\log_{10}$ fold up-regulation was noted at 6 h (Fig. 5A). M1 is known to bind cytoplasmic ends of HA and NA of IAV, allowing M1 association with lipid raft membrane, and inducing change in its conformation and polymerization at the site of virus budding (Gómez-Puertas et al., 2000). However, FLSP-A caused downregulation of M1 expression at 2 h and 6 h in the case of both IAV subtypes. The suppression of M1 following FLSP-A treatment was more evident in the case of pH1N1 when compared to H3N2, where -5 $\log_{10}$ fold reduction was seen at 6 h (Fig. 5B). This data is using rfhSP-A is in contrast to a recent study using rfhSP-D, where -8 $\log_{10}$ fold downregulation of M1 expression was seen with pH1N1 at 2 h (Al-Ahdal et al., 2018).

3.4. qRT-PCR analysis of modulation of immune responses by rfhSP-A on A549 challenged with IAV subtypes

The mRNA levels of pro-inflammatory cytokines and chemokines were determined via qPCR. The relative mRNA levels of TNF-α, IL-12,

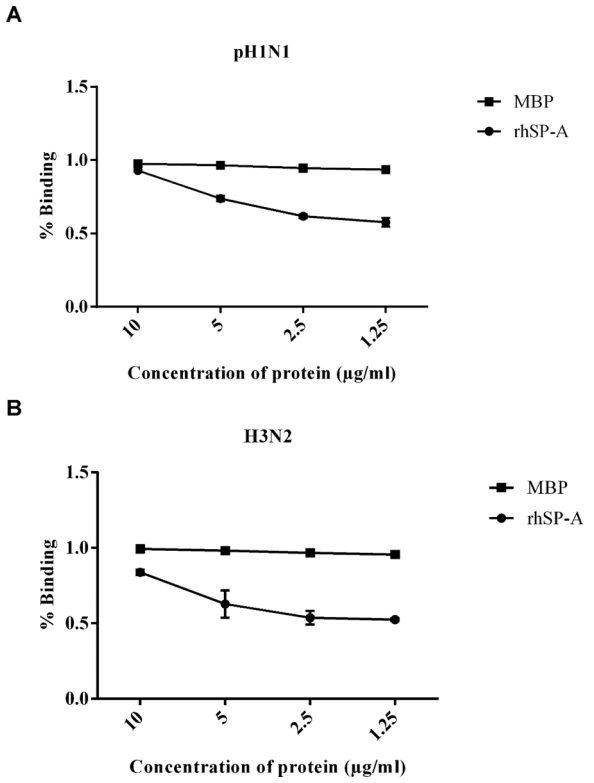

Fig. 3. Cell-binding assay to show binding of (A) pH1N1 and (B) H3N2, pre-incubated with rfhSP-A, to A549 cells. Microtiter wells were coated with A549 cells (1×10^5 cells/ml) and incubated overnight at 37 °C. Different concentrations of rfhSP-A (10, 5, 2.5, and 1.25 µg/ml), pre-incubated with pH1N1 and H3N2 virus were added to the corresponding wells, followed by incubation at room temperature for 2 h. After fixing the cells with 4% paraformaldehyde, monoclonal anti-influenza virus H1, or polyclonal anti-influenza virus H3 antibodies were added to the corresponding wells. Maltose-binding protein (MBP) was used as a negative control protein. The data were expressed as mean of three independent experiments carried out in triplicates ± SEM.

IFN-α, and RANTES were upregulated by both IAV strains, following rfhSP-A treatment at 6 h time point. However, IL-6 was $2\log_{10}$ fold upregulated by pH1N1 at 6 h by rfhSP-A treatment (Fig. 6A), but no significant change was obeserved with H3N2 strain at 6 h. Furthermore, enhancement of IFN-α was also evident with rfhSP-A treatment at 2 h, which gradually declined by $2\log_{10}$ fold at 6 h (Fig. 7A). Upregulation of type I interferon may suggest that rfhSP-A can enhance viral replication, and thus, increase the levels of interferon type I response to alert other immune cells to mobilise mechanisms towards viral clearance. In the case of FLSP-A treatment, pro-inflammatory cytokines such as TNF-α and IL-6 were downregulated at 6 h treatment for both pH1N1 and H3N2 (Fig. 6C & D). Enhanced level of IL-6 has been reported in patients infected with pH1N1 (Paquette et al., 2012). IL-12 (-2 $\log_{10}$ fold) and RANTES (-6.5 $\log_{10}$ fold) were downregulated by FLSP-A treatment in pH1N1 subtype (Fig. 6C), while this upregulation was seen with H3N2 (Fig. 6D), suggesting the possible enhancement of Th1 immune response. In the case of type I interferons, FLSP-A induced upregulation of INF-α at 6 h for both IAV strains.

3.5. Multiplex analysis of cytokine/chemokine array following rfhSP-A treatment

Secretion of cytokines and chemokines, 24 h post rfhSP-A treatment, was assessed using a multiplex cytokine/chemokine array. rfhSP-A triggered enhancement of TNF-α, IL-6 and IL-8 in both IAV subtypes (Fig. 8). However, no significant change in the level of MCP-1 was seen with MCP-1 for both IAV subtypes. Increased IL-6 level has been linked with the severity of IAV infection based on a study involving pH1N1-infected mice (Paquette et al., 2012). Expression of TNF-α in lung epithelial cells is suggested to be the key targets of IAV, and is important for controlling IAV in the host respiratory tract. TNF-α is involved in recruiting monocytes, T and B lymphocytes to the site of infection, suggesting its role in clearing the viral particles in the respiratory tract prior to the induction of secondary immune response. Therefore, up-regulation of TNF-α and IL-6 by rfhSP-A can serve as a potential biomarker during IAV infection, similar to other diseases (Damas et al., 1992; Theoharides et al., 2002).

4. Discussion

Influenza A virus (IAV) is a contagious respiratory virus, causing substantial morbidity and mortality. Anders et al. first reported collectins as beta inhibitors derived from bovine and mouse. The calcium dependent mannose binding lectin (MBL) was shown to bind glycans found on the globular region of HA, thus, inhibiting HA from binding to sialic acid-decorated cell-surface receptors (Anders et al., 1990). Collectins can orchestrate a number of anti-IAV mechanisms such as inhibition of HA and NA (Hartshorn et al., 1994, 2008; Al-Ahdal et al., 2018), virus neutralisation, virus aggregation, IAV uptake by neutrophils, and viral opsonisation. SP-A is a calcium-dependent hydrophilic C-type collectin, involved in pulmonary surfactant homeostasis (Weaver and Whitsett, 1991), and reported to be a potent innate immune molecule in the lungs. SP-A can bind various self and non-self-ligands in a calcium- dependent manner, mostly via CRD region on the target surface. Thus, recruitment and activation of immune cells occurs via collagen domain for the clearance of microorganisms (Kishore et al., 2006). SP-A can bind a diverse group of pathogens, acting as opsonins leading to direct and indirect biological consequences (Crouch, 2000; Lawson and Reid, 2000; Crouch and Wright, 2001). Specific interaction of SP-A with a number of respiratory viruses has been reported, which requires interaction with viral glycoproteins and complex oligosaccharides. Recently, we described a protective effect of rfhSP-D that was able to inhibit entry of IAV into A549 cells challenged with pH1N1 and H3N2 subtypes (Al-Ahdal et al., 2018). Therefore, this study was aimed at examining the direct interaction of a truncated recombinant fragment of human SP-A (rfhSP-A) with IAV, and subsequent immunological consequences.

In this study, plasmid pUK-A1, containing cDNA sequences for neck and CRD region of human SP-A (Karbani et al., 2014) was transformed in *Escherichia coli* BL21 (λDE3) pLysS strain under T7 bacteriophage promoter. rfhSP-A, recovered from inclusion bodies via denaturation-renaturation cycles, was affinity purified on a mannose-agarose column, which appeared as a ~18 kDa band on a 15% SDS-PAGE gel electrophoresis (Fig. 1). rfhSP-A eluted as a trimer on a gel filtration column and was recognised by rabbit polyclonal and mouse monoclonal antibodies raised against full length SP-A purified from lung lavage of an alveolar proteinosis patient (data not shown). Affinity purified rfhSP-A, made free from endotoxin, was then examined for its respective interaction with IAV subtypes (pH1N1 and H3N2) via direct ELISA (Fig. 2). The ability of rfhSP-A to bind IAV subtypes is consistent with an earlier study using a recombinant form of truncated human SP-D (rfhSP-D) composed of trimeric neck and CRD region (Al-Ahdal et al., 2018).

Ten µg/ml of rfhSP-A bound best to both pH1N1 and H3N2 (Fig. 2). The ability of rfhSP-A to bind IAV bound A549 cells was measured via cell binding assay (Fig. 3). To understand whether interaction between rfhSP-A and IAV subtypes led to specific interaction with IAV glycoproteins, far western blotting analysis was carried out (Fig. 4A). rfhSP-A (10 µg/ml) bound to NA (~60 kDa), M1 (~25 kDa) and M2 (~17 kDa) of purified pH1N1 and H3N2 in a calcium-dependent manner. Furthermore, in order to validate the binding interaction rfhSP-A and NA, an ELISA was carried out using purified recombinant NA protein. As

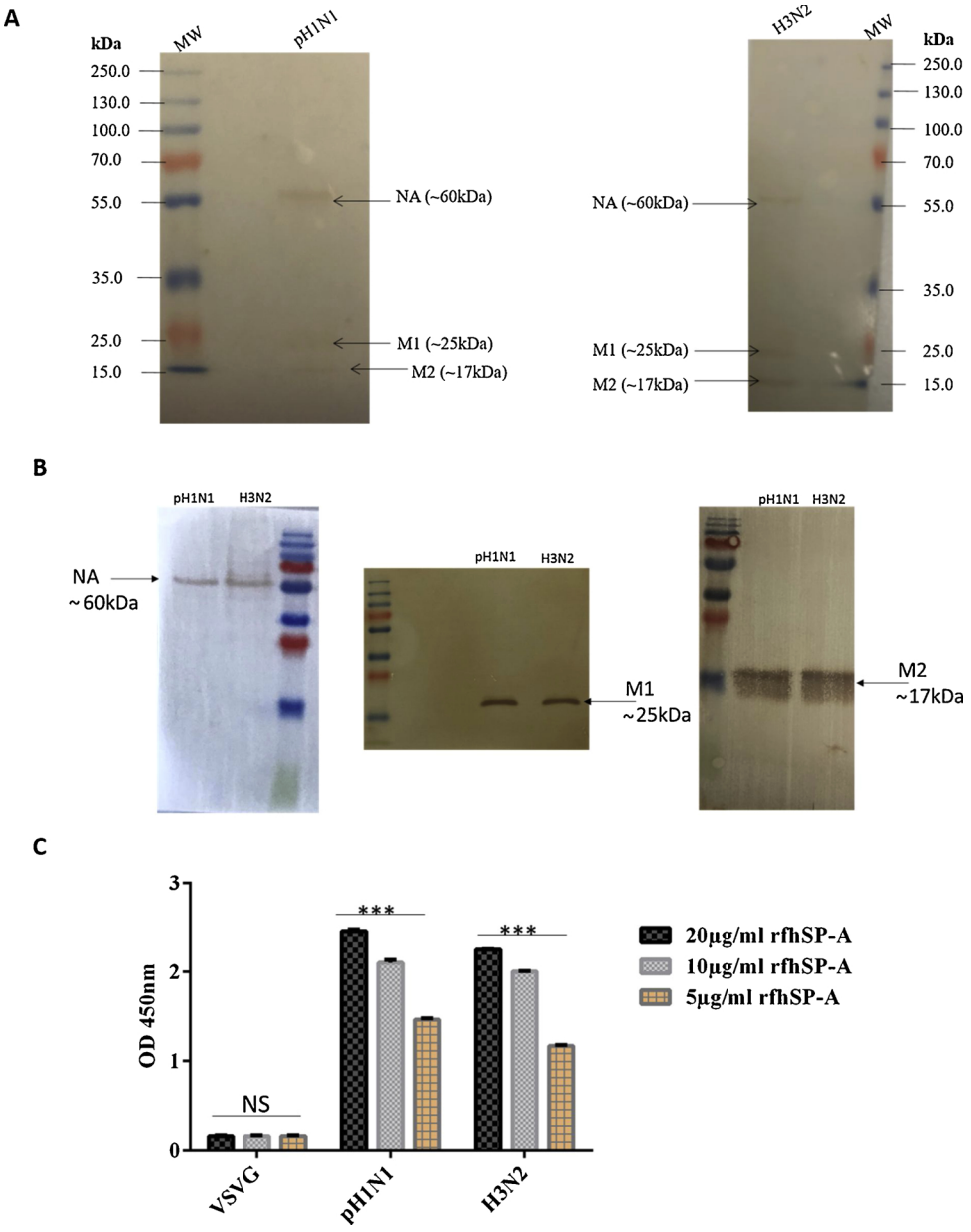

Fig. 4. (A) Far western blot analysis to show rfhSP-A binding to purified pH1N1 and H3N2. 10 µl of concentrated virus (1.36×10^6 pfu/ml) was first run on the SDS-PAGE under reducing conditions, transferred onto a nitrocellulose membrane, and incubated with 10 µg/ml of rfhSP-A. The membrane was probed with rabbit anti-human SP-A polyclonal antibody. rfhSP-A bound to NA (~60 kDa), M1 (~25 kDa) and M2 (~17 kDa) in the case of both pH1N1 and H3N2 subtypes. The identity of SP-A bound IAV proteins was validated using a separate blot that was directly probed with monoclonal anti-NA, M1 and M2 antibodies (B). (C) Direct ELISA to show the ability of rfhSP-A to bind purified recombinant neuraminidase (NA) of IAV. VSV-G was used as a negative control protein, where no significant binding was detected. The data were expressed as mean of three independent experiments carried out in triplicates ± SEM. Significance was determined using the unpaired one-way ANOVA test (***$p < 0.0001$)($n = 3$.

evident in Fig. 4B, rfhSP-A bound purified NA protein dose-dependently. Previous studies have also suggested that full length SP-A can bind to NA, and inhibit the release of viral particles from infected cells (Tecle et al., 2007). Thus, N-linked oligosaccharides found on NA are likely to be recognised by the CRD region of SP-A and SP-D (Tecle et al., 2007).

The ability of rfhSP-A to modulate viral replication and host immune response by IAV challenged A549 cells was also examined. IAV-bound rfhSP-A was found to induce enhanced viral replication, based on the expression levels of M1 gene. M1 is an abundant matrix protein of IAV, which plays dual roles in virion assembly and infection (Rossman and Lamb, 2011). Up-regulation of M1 expression was brought about by rfhSP-A treatment in IAV challenged A549 cells, compared to cells without rfhSP-A treatment but challenged with pH1N1 or H3N2 only (Fig. 5). M1 upregulation, following rfhSP-A treatment, was more pronounced in H3N2 infected cells compared to pH1N1, where 7$\log_{10}$ fold upregulation was seen at 6 h (Fig. 5). However, A549 cells, pre-treated with FLSP-A, caused downregulation of M1 expression when compared to cells only challenged with IAV subtypes (Fig. 5B). M1 downregulation by FLSP-A was found to be more effective against pH1N1 subtype, when compared to H3N2, where -5 $\log_{10}$ fold downregulation was evident at 6 h treatment (Fig. 5B). M1 can bind cytoplasmic ends of HA and NA, polymerize and form the interior structure of emerging viral particles (Rossman and Lamb, 2011). Additionally, as evident from the far western blotting, rfhSP-A was also able to bind Matrix protein 2 (M2) of IAV at ~17 kDa (Fig. 4). HA bound M1 serves as a docking site for the viral RNPs recruitment and may mediate M2 recruitment to the site of viral budding (Rossman and Lamb, 2011). M2 can stabilise the budding site, enabling polymerization of the matrix protein, leading to formation of viral particles. Furthermore, M2 has also been reported to change so as to facilitate release of the progeny viral particles. Binding of rfhSP-A to NA/M1/M2, and upregulation of M1 expression could explain the likely effect of rfhSP-A as a facilitator of IAV replication of subtypes tested in this study.

mRNA expression of pro-inflammatory cytokines and chemokines following rfhSP-A treatment was determined by qPCR, which showed an upregulation of TNF-α, IL-12 and RANTES in the case of both IAV subtypes at 6 h time point. However, an increased expression levels of IL-6 (2$\log_{10}$ fold) (Fig. 6A) was seen only with pH1N1 at 6 h, while H3N2 did not show any significant effect (Fig. 6B). In contrast,

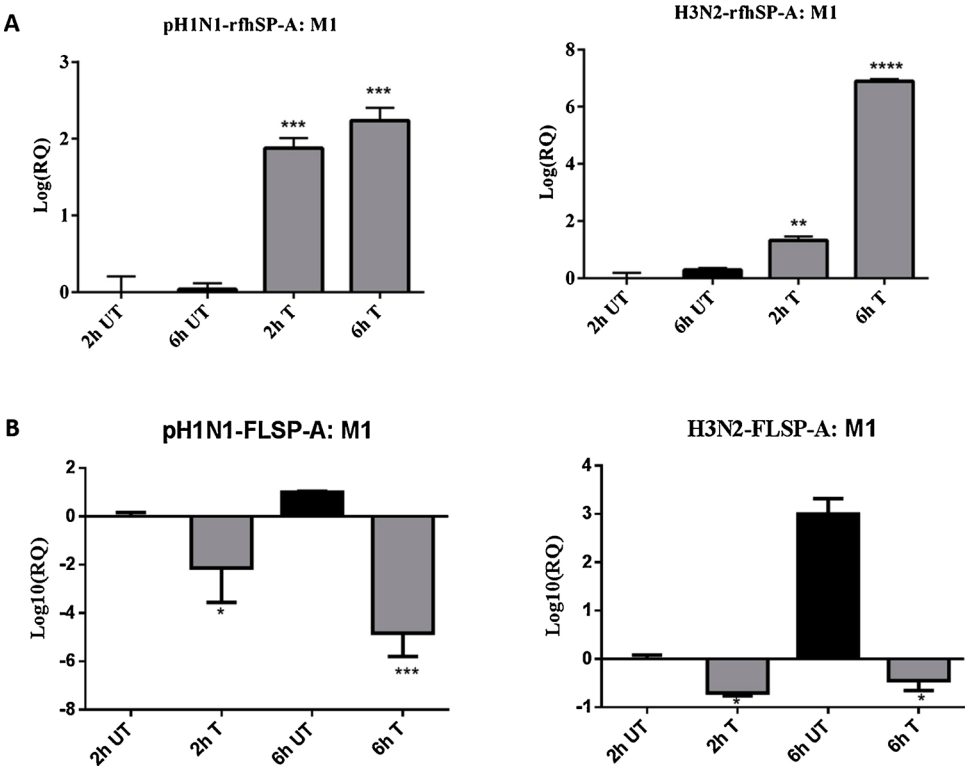

Fig. 5. rfhSP-A treatment promotes infection and replication (A), while suppression of M1 replication was seen with FLSP-A (B) of pH1N1 and (B) H3N2 in target human A549 cells. M1 mRNA expression of both pH1N1 and H3N2 influenza A virus (IAV) (MOI 1) after infection of A549 cells at 2 and 6 h was measured. A549 cells were incubated with pH1N1 and H3N2, pre-incubated with or without purified rfhSP-A and FLSP-A (10 μg/ml). Cell pellets were harvested at 2 and 6 h to analyze the M1 expression of IAV. Cells were lysed, and purified RNA extracted was converted into cDNA. Infection was measured via qRT-PCR using M1 primers; 18S was used as an endogenous control. Results shown are normalized to M1 levels at 2 h untreated. Significance was determined using the unpaired one-way ANOVA test (**$p < 0.01$, ***$p < 0.001$, and ****$p < 0.0001$) (n = 3). UT (un-treated sample), and T (treated sample).

downregulation of TNF-α (-4.5 $_{log10}$ fold) and IL-6 (-5 $_{log10}$ fold) was seen at 6 h following FLSP-A treatment (Fig. 6C & D). In the case of pH1N1, FLSP-A also caused downregulation of IL-12 and RANTES mRNA expression (Fig. 6C), while increased expression levels was observed with H3N2 IAV subtype (Fig. 6D). Enhanced levels of TNF-α and IL-6 have been reported during IAV infection, and it is also associated with severe lung pathology and worse outcome in IAV infected patients (La Gruta et al., 2007). However, these cytokines can also be protective during seasonal influenza infection. Studies also report an increased level of IL-6 in the lungs and serum of patients infected with influenza virus, including the outbreak 2009 pH1N1 pandemic subtype (Kaiser et al., 2001; Hagau et al., 2010a, 2010b). Therefore, increased levels of IL-6 following rfhSP-A treatment may be associated with facilitation of IAV infection.

Increased serum levels of TNF-α has been reported in most influenza infected patients, particularly with pH1N1 subtype (Hagau et al., 2010a, 2010b; Zúñiga et al., 2011; Bermejo-Martin et al., 2010; Morales-García et al., 2012). In this study, when pH1N1 and H3N2 were treated with rfhSP-A, TNF-α expression levels were enhanced at 6 h (Fig. 6), suggesting the ability of rfhSP-A to increase viral infection. Overexpression of TNF-α and IL-6 has been suggested as a hallmark of viral infection (Mogensen and Paludan, 2001). Elevated levels of these cytokines haven been observed in patients with both acute (Kaiser et al., 2001) and severe (Heltzer et al., 2009) seasonal IAV infection. Up-regulation of cytokine production upon H1N1 infection has been reported as an important crucial player in the pathogenesis of IAV infection. Thus, invasion of H1N1 strain into the lungs can trigger production of pro-inflammatory cytokine profile, resulting in the development of pneumonia.

rfhSP-A treatment caused increased levels of IL-12 by both pH1N1 and H3N2 in a time dependent manner (Fig. 6), suggesting the likely enhancement of viral replication and Th1 immune response. RANTES was down-regulated in the presence of rfhSP-A at 2 h, which recovered by 2.5log_{10} fold later at 6 h time point in pH1N1 treated cells. However, for H3N2, only 1log_{10} fold upregulation was seen following rfhSP-A treatment in a time-dependent manner (Fig. 6B). Lower expression levels of IFN-α was observed in the untreated sample, which was 3log_{10} fold up-regulated in the presence of rfhSP-A at 2 h (Fig. 7), suggesting that rfhSP-A can enhance the rate of viral replication, and thus, thereby enhance the levels of IFN produced by the innate immune cells in order to clear viral particles from infected host.

In conclusion, a truncated recombinant form of human SP-A, rfhSP-A, can promote pH1N1 and H3N2 subtypes of IAV instead of anticipated inhibition of infection. We have previously shown that its SP-D counterpart acts as an entry inhibitor (Al-Ahdal et al., 2018), suggesting that rfhSP-A may not have a therapeutic value. The effects of FLSP-A on IAV challenged A549 cells is similar to the effect seen by rfhSP-D, where downregulation of M1 and pro-inflammatory cytokines was seen with FLSP-A treatment. The observed restriction of M1 replication following FLSP-A treatment is likely to be due to the presence of collagen region, which could shift the way SP-A acts on IAV infectivity involving its putative receptor on the cell surface (Gardai et al., 2003). This study highlights a fundamental difference in the structure-function relationships between SP-A and SP-D. The literature is full of evidences where a recombinant truncated form of human SP-D (rfhSP-D) containing trimeric neck and CRD regions behaves like full-length SP-D *in vitro*, *in vivo* and *ex vivo*, including offering a protective effect against IAV (Madan et al., 2010; Al-Ahdal et al., 2018). In the case of SP-A and IAV interaction, it appears that only FLSP-A is capable of interfering with IAV entry into the target cells, highlighting the importance of the collagen domain and an intact SP-A molecule. It is also apparent that entry inhibition is coupled with an anti-inflammatory response, as evident from downregulation of TNF-α and IL-6. However, both FLSP-A as well as rfhSP-A upregulate type I interferon (IFN-α) response, raising the notion that FLSP-A creates an anti-inflammatory milieu during IAV infection. How rfhSP-A on its own enhances IAV infection remains an intriguing question. We are currently examining the mechanism of enhanced infectivity that may involve topological alterations in M1 and M2 proteins leading to an exaggerated budding.

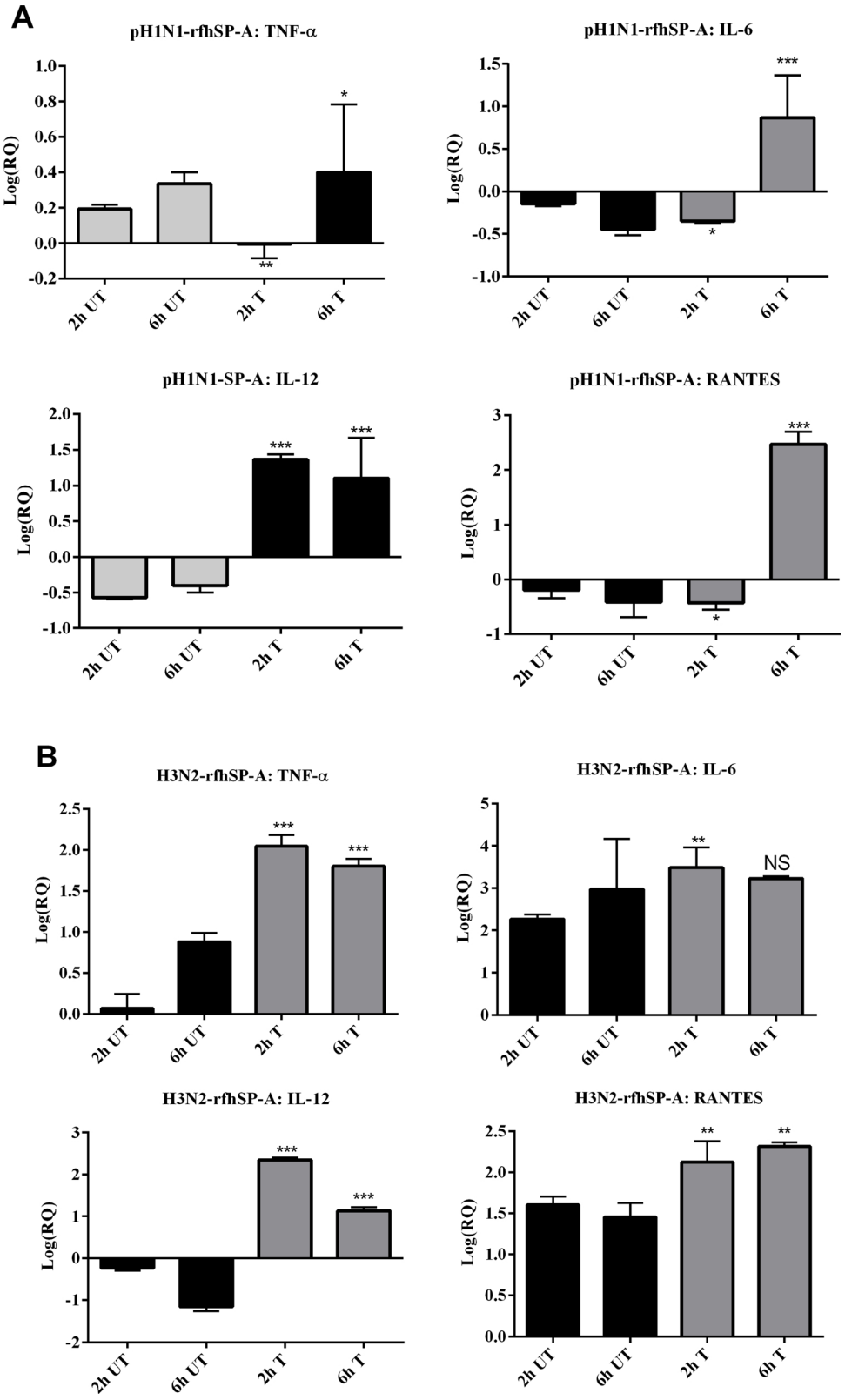

Fig. 6. Differential mRNA expression profile of selected cytokines/chemokines produced by A549 cells challenged with pH1N1 and H3N2 pre-incubated with rfhSP-A (A&B) and FLSP-A (C&D). The expression levels of selected cytokines and chemokine were measured using qRT-PCR and the data were normalized via 18S rRNA expression as a control. The relative expression (RQ) was calculated by using cells only time point as the calibrator. The RQ value was calculated using the formula: $RQ = 2-\Delta\Delta Ct$. Assays were conducted in triplicates and error bars represent ± SEM. Significance was determined using the unpaired one-way ANOVA test (**$p < 0.01$, ***$p < 0.001$, and ****$p < 0.0001$) (n = 3). UT (untreated sample), and T (treated sample).

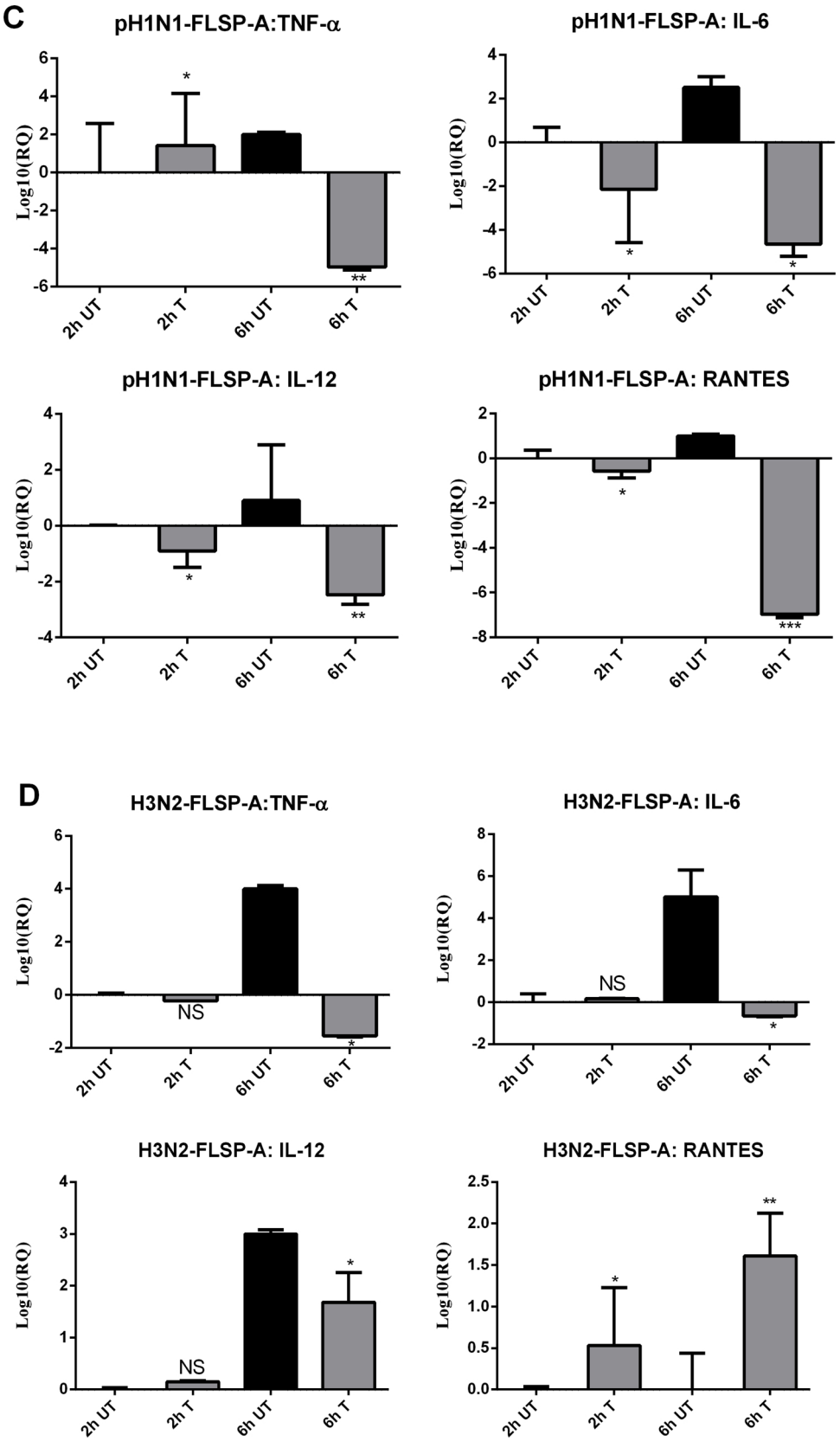

Fig. 6. (*continued*)

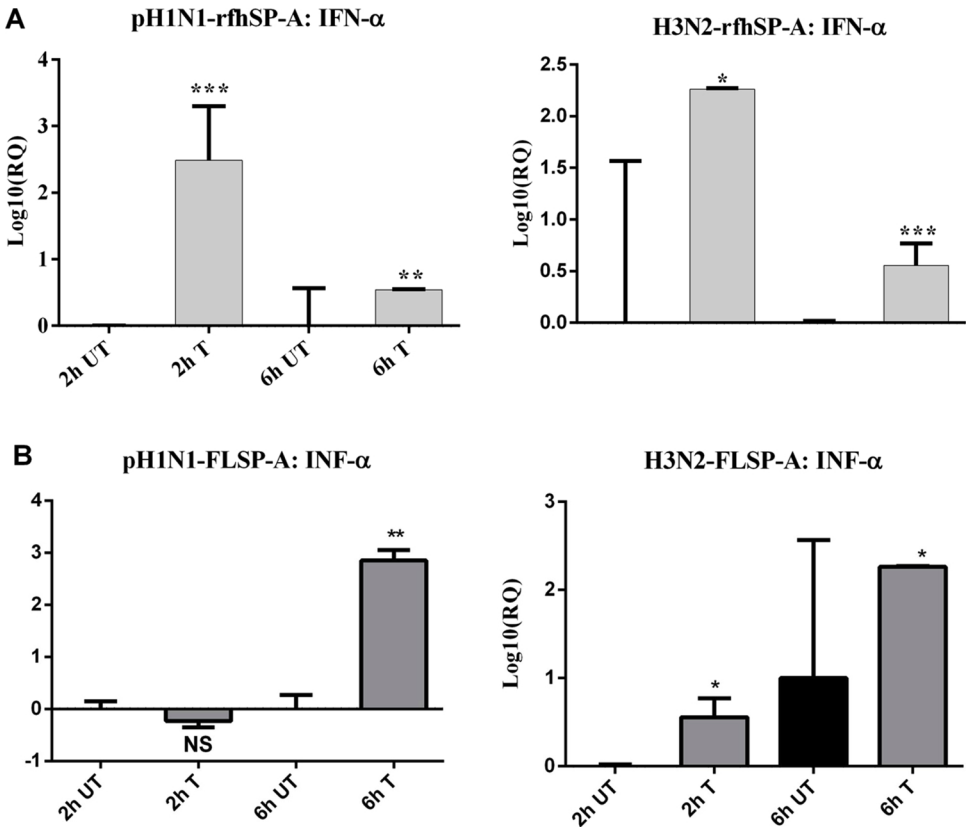

Fig. 7. mRNA expression levels of pro-inflammatory cytokine, interferon (IFN) α in untreated, rfhSP-A (A) and FLSP-A (B) treated pH1N1 and H3N2 subtype of IAV. The expression levels were measured using qRT-PCR and the data were normalized via 18S rRNA expression as an endogenous control. The relative expression (RQ) was calculated by using cells only time point as the calibrator. The RQ value was calculated using the formula: $RQ = 2-\Delta\Delta Ct$. Assays were conducted in triplicates and error bars represents ± SEM. Significance was determined using the unpaired one-way ANOVA test (*$p < 0.05$, **$p < 0.01$, ***$p < 0.001$, and ****$p < 0.0001$) (n = 3 UT (untreated sample), and T (treated sample).

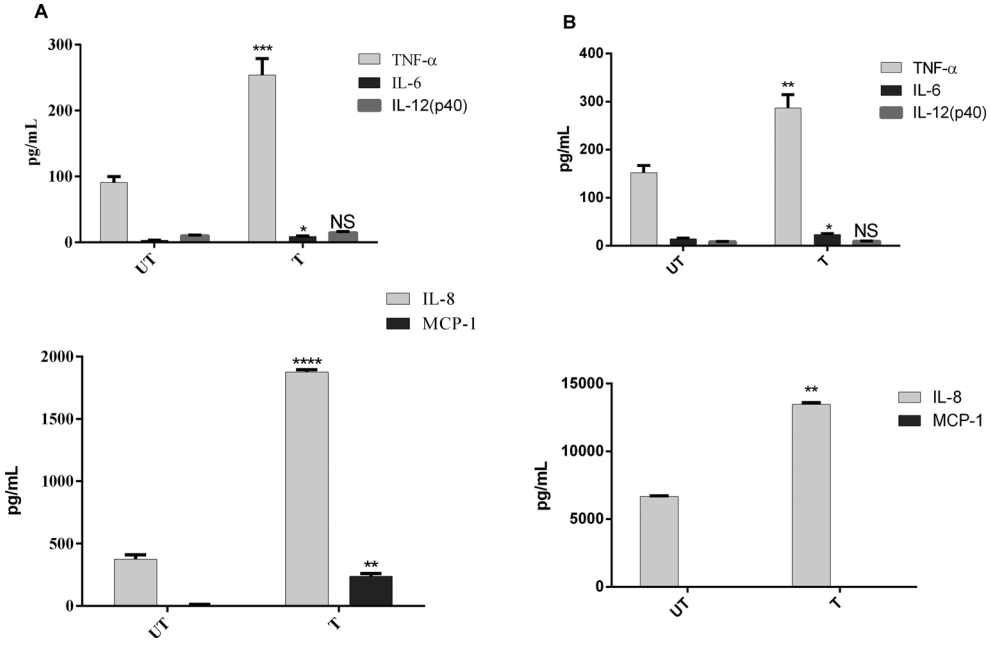

Fig. 8. Multiplex cytokine array analysis of supernatants collected at 24 h time point. A549 cells were challenged with (A) pH1N1 and (B) H3N2, followed by rfhSP-A (10 μg/ml) treatment. TNF-α, IL-6, IL-8, IL-12p40 and MCP-1 were measured using a commercially available MagPix Milliplex kit (EMD Millipore). Experiment was conducted in duplicates and error bars represent ± SEM (n = 3); significance was determined using unpaired one-way ANOVA test (*$p < 0.05$, **$p < 0.01$, ***$p < 0.001$ and ****$p < 0.0001$). UT (untreated sample), and T (treated sample).

Acknowledgements

This work was funded by the KACST (14-MED258-20) and approved by the RAC of the KFSHRC, Riyadh, Saudi Arabia (2150031). We are grateful to Maureene Delos Reyes and Hanan Shaarawi for secretarial help and administrative support. The A/England/195/2009 (pH1N1) and the A/Hong Kong/1774/99 (H3N2) strains were gifted by Wendy Barclay from the Imperial College London and Leo Poon from the University of Hong Kong, respectively. VSVG was offered by Bob Weinberg (Addgene plasmid #8454).

References

Al-Ahdal, M.N., Murugaiah, V., Varghese, P.M., Abozaid, S.M., Saba, I., Al-Qahtani, A.A., Pathan, A.A., Kouser, L., Nal, B., Kishore, U., 2018. Entry inhibition and modulation of pro-inflammatory immune response against influenza A virus by a recombinant truncated surfactant protein D. Front. Immunol. 30 (July (9)), 1586. https://doi.org/10.3389/fimmu.2018.01586. eCollection 2018.

Anders, E.M., Hartley, C.A., Jackson, D.C., 1990. Bovine and mouse serum beta inhibitors of influenza A viruses are mannose-binding lectins. Proc. Natl Acad. Sci. U. S. A. 87 (June (12)), 4485–4489.

Bermejo-Martin, J.F., Martin-Loeches, I., Rello, J., Antón, A., Almansa, R., Xu, L., Lopez-Campos, G., Pumarola, T., Ran, L., Ramirez, P., Banner, D., Ng, D.C., Socias, L., Loza,

A., Andaluz, D., Maravi, E., Gómez-Sánchez, M.J., Gordón, M., Gallegos, M.C., Fernandez, V., Aldunate, S., León, C., Merino, P., Blanco, J., Martin-Sanchez, F., Rico, L., Varillas, D., Iglesias, V., Marcos, M.Á, Gandía, F., Bobillo, F., Nogueira, B., Rojo, S., Resino, S., Castro, C., Ortiz de Lejarazu, R., Kelvin, D., 2010. Host adaptive immunity deficiency in severe pandemic influenza. Crit Care 14 (5), R167. https://doi.org/10.1186/cc9259. Epub 2010 Sep 14.

Bouvier, N.M., Palese, P., 2008. The biology of influenza viruses. Vaccine 26 (September Suppl 4), D49–53.

Crouch, E.C., 2000. Surfactant protein-D and pulmonary host defense. Respir. Res. 1 (2), 93–108 Epub 2000 Aug 25.

Crouch, E., Wright, J.R., 2001. Surfactant proteins A and D and pulmonary host defense. Annu. Rev. Physiol. 63, 521–554.

Damas, P., Ledoux, D., Nys, M., Vrindts, Y., De Groote, D., Franchimont, P., Lamy, M., 1992. Cytokine serum level during severe sepsis in human IL-6 as a marker of severity. Ann. Surg. 215 (April (4)), 356–362.

Fukuyama, S., Kawaoka, Y., 2011. The pathogenesis of influenza virus infections: the contributions of virus and host factors. Curr. Opin. Immunol. 23 (August (4)), 481–486. https://doi.org/10.1016/j.coi.2011.07.016. Epub 2011 Aug 11.

Gaiha, G.D., Dong, T., Palaniyar, N., Mitchell, D.A., Reid, K.B., Clark, H.W., 2008. Surfactant protein A binds to HIV and inhibits direct infection of CD4+ cells, but enhances dendritic cell-mediated viral transfer. J. Immunol. 181 (July (1)), 601–609.

Gardai, S.J., Xiao, Y.Q., Dickinson, M., Nick, J.A., Voelker, D.R., Greene, K.E., Henson, P.M., 2003. By binding SIRPalpha or calreticulin/CD91, lung collectins act as dual function surveillance molecules to suppress or enhance inflammation. Cell 115 (October (1)), 13–23.

Ghildyal, R., Hartley, C., Varrasso, A., Meanger, J., Voelker, D.R., Anders, E.M., Mills, J., 1999. Surfactant protein A binds to the fusion glycoprotein of respiratory syncytial virus and neutralizes virion infectivity. J. Infect. Dis. 180 (December (6)), 2009–2013.

Gómez-Puertas, P., Albo, C., Pérez-Pastrana, E., Vivo, A., Portela, A., 2000. Influenza virus matrix protein is the major driving force in virus budding. J. Virol. 74 (December (24)), 11538–11547.

Hagau, N., Slavcovici, A., Gonganau, D.N., Oltean, S., Dirzu, D.S., Brezoszki, E.S., Maxim, M., Ciuce, C., Mlesnite, M., Gavrus, R.L., Laslo, C., Hagau, R., Petrescu, M., Studnicska, D.M., 2010a. Clinical aspects and cytokine response in severe H1N1 influenza A virus infection. Crit Care 14 (6), R203. https://doi.org/10.1186/cc9324. Epub 2010 Nov 9.

Hagau, N., Slavcovici, A., Gonganau, D.N., Oltean, S., Dirzu, D.S., Brezoszki, E.S., Maxim, M., Ciuce, C., Mlesnite, M., Gavrus, R.L., Laslo, C., Hagau, R., Petrescu, M., Studnicska, D.M., 2010b. Clinical aspects and cytokine response in severe H1N1 influenza A virus infection. Crit. Care 14 (6), R203. https://doi.org/10.1186/cc9324. Epub 2010 Nov 9.

Hartley, C.A., Jackson, D.C., Anders, E.M., 1992. Two distinct serum mannose-binding lectins function as beta inhibitors of influenza virus: identification of bovine serum beta inhibitor as conglutinin. J. Virol. 66 (July (7)), 4358–4363.

Hartshorn, K.L., Crouch, E.C., White, M.R., Eggleton, P., Tauber, A.I., Chang, D., et al., 1994. Evidence for a protective role of pulmonary surfactant protein D (SPD) against influenza A viruses. J. Clin. Invest. 94, 311–319. https://doi.org/10.1172/JCI117323.

Hartshorn, K.L., Webby, R., White, M.R., Tecle, T., Pan, C., Boucher, S., et al., 2008. Role of viral hemagglutinin glycosylation in anti-influenza activities of recombinant surfactant protein D. Respir. Res. 9https://doi.org/10.1186/ 1465-9921-9-655. 65–9921–9–65.

Heltzer, M.L., Coffin, S.E., Maurer, K., Bagashev, A., Zhang, Z., Orange, J.S., Sullivan, K.E., 2009. Immune dysregulation in severe influenza. J. Leukoc. Biol. 85 (June (6)), 1036–1043. https://doi.org/10.1189/jlb.1108710.

Job, E.R., Deng, Y.M., Tate, M.D., Bottazzi, B., Crouch, E.C., Dean, M.M., Mantovani, A., Brooks, A.G., Reading, P.C., 2010. Pandemic H1N1 influenza A viruses are resistant to the antiviral activities of innate immune proteins of the collectin and pentraxin superfamilies. J. Immunol. 185 (October (7)), 4284–4291. https://doi.org/10.4049/jimmunol.1001613. Epub 2010 Sep 3.

Kaiser, L., Fritz, R.S., Straus, S.E., Gubareva, L., Hayden, F.G., 2001. Symptom pathogenesis during acute influenza: interleukin-6 and other cytokine responses. J. Med. Virol. 64 (July (3)), 262–268.

Karbani, N., Dodagatta-Marri, E., Qaseem, A.S., Madhukaran, P., Waters, P., Tsolaki, A.G., Madan, T., Kishore, U., 2014. Purification of native surfactant protein SP-A from pooled amniotic fluid and bronchoalveolar lavage. Methods Mol. Biol. 1100, 257–272. https://doi.org/10.1007/978-1-62703-724-2_21.

Kishore, U., Greenhough, T.J., Waters, P., Shrive, A.K., Ghai, R., Kamran, M.F., Bernal, A.L., Reid, K.B., Madan, T., Chakraborty, T., 2006. Surfactant proteins SP-A and SP-D: structure, function and receptors. Mol. Immunol. 43 (March (9)), 1293–1315 Epub 2005 Oct 5.

La Gruta, N.L., Kedzierska, K., Stambas, J., Doherty, P.C., 2007. A question of self-preservation: immunopathology in influenza virus infection. Immunol. Cell Biol. 85 (February-March (2)), 85–92 Epub 2007 Jan 9.

Lawson, P.R., Reid, K.B., 2000. The roles of surfactant proteins A and D in innate immunity. Immunol. Rev. 173 (February), 66–78.

Madan, T., Reid, K.B., Clark, H., Singh, M., Nayak, A., Sarma, P.U., Hawgood, S., Kishore, U., 2010. Susceptibility of mice genetically deficient in SP-A or SP-D gene to invasive pulmonary aspergillosis. Mol. Immunol. 47 (June (10)), 1923–1930. https://doi.org/10.1016/j.molimm.2010.02.027.

Morales-García, G., Falfán-Valencia, R., García-Ramírez, R.A., Camarena, Á, Ramirez-Venegas, A., Castillejos-López, M., Pérez-Rodríguez, M., González-Bonilla, C., Grajales-Muñíz, C., Borja-Aburto, V., Mejía-Aranguré, J.M., 2012. Pandemic influenza A/H1N1 virus infection and TNF, LTA, IL-1β, IL-6, IL-8, and CCL polymorphisms in Mexican population: a case-control study. BMC Infect. Dis. 13 (November 12), 299. https://doi.org/10.1186/1471-2334-12-299.

Nayak, A., Dodagatta-Marri, E., Tsolaki, A.G., Kishore, U., 2012. An insight into the diverse roles of surfactant proteins, SP-A and SP-D in innate and adaptive immunity. Front. Immunol. 7 (June (3)), 131. https://doi.org/10.3389/fimmu.2012.00131. eCollection 2012.

Paquette, S.G., Banner, D., Zhao, Z., Fang, Y., Huang, S.S., León, A.J., Ng, D.C., Almansa, R., Martin-Loeches, I., Ramirez, P., Socias, L., Loza, A., Blanco, J., Sansonetti, P., Rello, J., Andaluz, D., Shum, B., Rubino, S., de Lejarazu, R.O., Tran, D., Delogu, G., Fadda, G., Krajden, S., Rubin, B.B., Bermejo-Martin, J.F., Kelvin, A.A., Kelvin, D.J., 2012. Interleukin-6 is a potential biomarker for severe pandemic H1N1 influenza A infection. PLoS One 7 (6), e38214. https://doi.org/10.1371/journal.pone.0038214. Epub 2012 Jun 5.

Reading, P.C., Morey, L.S., Crouch, E.C., Anders, E.M., 1997. Collectin-mediated antiviral host defense of the lung: evidence from influenza virus infection of mice. J. Virol. 71 (November (11)), 8204–8212.

Rossman, J.S., Lamb, R.A., 2011. Influenza virus assembly and budding. Virology 411 (March (2)), 229–236. https://doi.org/10.1016/j.virol.2010.12.003. Epub 2011 Jan 14.

Strong, P., Kishore, U., Morgan, C., Lopez Bernal, A., Singh, M., Reid, K.B., 1998. A novel method of purifying lung surfactant proteins A and D from the lung lavage of alveolar proteinosis patients and from pooled amniotic fluid. J. Immunol. Methods 220 (November (1-2)), 139–149.

Tecle, T., White, M.R., Crouch, E.C., Hartshorn, K.L., 2007. Inhibition of influenza viral neuraminidase activity by collectins. Arch. Virol. 152 (9), 1731–1742 Epub 2007 May 22.

Theoharides, T.C., Boucher, W., Spear, K., 2002. Serum interleukin-6 reflects disease severity and osteoporosis in mastocytosis patients. Int. Arch. Allergy Immunol. 128 (August (4)), 344–350.

Van de Wetering, J.K., van Golde, L.M., Batenburg, J.J., 2004. Collectins: players of the innate immune system. Eur. J. Biochem. 271 (April (7)), 1229–1249.

Van Iwaarden, J.F., van Strijp, J.A., Ebskamp, M.J., Welmers, A.C., Verhoef, J., van Golde, L.M., 1991. Surfactant protein A is opsonin in phagocytosis of herpes simplex virus type 1 by rat alveolar macrophages. Am. J. Physiol. 261 (August (2 Pt 1)), L204–9.

Weaver, T.E., Whitsett, J.A., 1991. Function and regulation of expression of pulmonary surfactant-associated proteins. Biochem. J. 273 (January (Pt 2)), 249–264.

Zúñiga, J., Torres, M., Romo, J., Torres, D., Jiménez, L., Ramírez, G., Cruz, A., Espinosa, E., Herrera, T., Buendía, I., Ramírez-Venegas, A., González, Y., Bobadilla, K., Hernández, F., García, J., Quiñones-Falconi, F., Sada, E., Manjarrez, M.E., Cabello, C., Kawa, S., Zlotnik, A., Pardo, A., Selman, M., 2011. Inflammatory profiles in severe pneumonia associated with the pandemic influenza A/H1N1 virus isolated in Mexico city. Autoimmunity 44 (November (7)), 562–570. https://doi.org/10.3109/08916934.2011.592885.

frontiers in Oncology

ORIGINAL RESEARCH
published: 09 July 2019
doi: 10.3389/fonc.2019.00542

Surfactant Protein D as a Potential Biomarker and Therapeutic Target in Ovarian Cancer

Juhi Kumar[1†], Valamarthy Murugaiah[1†], Georgios Sotiriadis[1], Anuvinder Kaur[1], Jeyarooban Jeyaneethi[1], Isotta Sturniolo[1], Fatimah S. Alhamlan[2], Jayanta Chatterjee[3], Marcia Hall[1,4], Uday Kishore[1] and Emmanouil Karteris[1,5*]*

[1] Department of Life Sciences, College of Health and Life Sciences, Brunel University London, Uxbridge, United Kingdom, [2] Department of Infection and Immunity, King Faisal Specialist Hospital and Research Centre, Riyadh, Saudi Arabia, [3] Faculty of Health and Medical Sciences, School of Biosciences and Medicine, University of Surrey, Guildford, United Kingdom, [4] Mount Vernon Cancer Centre, Northwood, United Kingdom, [5] Institute of Environment, Health and Societies, Brunel University London, Uxbridge, United Kingdom

Surfactant protein D (SP-D) is an important innate immune molecule that is involved in clearing pathogens and regulating inflammation at pulmonary as well as extra-pulmonary sites. Recent studies have established the role of SP-D as an innate immune surveillance molecule against lung and pancreatic cancer, but little is known about its involvement in signaling pathways it can potentially activate in ovarian cancer. We focused our study on ovarian cancer by performing bioinformatics analysis (Oncomine) of datasets and survival analysis (Kaplan-Meier plotter), followed by immunohistochemistry using ovarian cancer tissue microarrays. SP-D mRNA was found to be expressed widely in different types of ovarian cancer irrespective of stage or grade. These *in silico* data were further validated by immunohistochemistry of clinical tissues. High transcriptional levels of SP-D were associated with unfavorable prognosis (overall and progression-free survival). We also detected SP-D protein in Circulating Tumor Cells of three ovarian cancer patients, suggesting that SP-D can also be used as a potential biomarker. Previous studies have shown that a recombinant fragment of human SP-D (rfhSP-D) induced apoptosis in pancreatic cancer cells via Fas-mediated pathway. In this study, we report that treatment of SKOV3 cells (an ovarian cancer cell line) with rfhSP-D led to a decrease in cell motility and cell proliferation. This was followed by an inhibition of the mTOR pathway activity, increase in caspase 3 cleavage, and induction of pro-apoptotic genes Fas and TNF-α. These data, suggesting a likely protective role of rfhSP-D against ovarian cancer, together with the observation that the ovarian cancer microenvironment overexperesses SP-D leading to poor prognosis, seems to suggest that the tumor microenvironment components manipulate the protective effect of SP-D *in vivo*.

Keywords: surfactant protein, SP-D, innate immunity, ovarian cancer, biomarker, circulating tumor cells

OPEN ACCESS

Edited by:
Jian-Jun Wei,
Northwestern University, United States

Reviewed by:
Kenneth Reid,
University of Oxford, United Kingdom
Ahmad R. Safa,
Indiana University, United States

***Correspondence:**
Uday Kishore
ukishore@hotmail.com
Emmanouil Karteris
emmanouil.karteris@brunel.ac.uk

†Joint first authors

Specialty section:
This article was submitted to Women's Cancer, a section of the journal Frontiers in Oncology

Received: *22 March 2019*
Accepted: *04 June 2019*
Published: *09 July 2019*

Citation:
Kumar J, Murugaiah V, Sotiriadis G, Kaur A, Jeyaneethi J, Sturniolo I, Alhamlan FS, Chatterjee J, Hall M, Kishore U and Karteris E (2019) Surfactant Protein D as a Potential Biomarker and Therapeutic Target in Ovarian Cancer. Front. Oncol. 9:542. doi: 10.3389/fonc.2019.00542

INTRODUCTION

Surfactant protein D (SP-D) is an innate immune molecule involved in clearing a range of pathogens and apoptotic/necrotic cells at pulmonary as well as extra-pulmonary mucosal sites (1, 2). SP-D interacts with infectious microbes using its C-type lectic domains and brings about effector mechanisms via agglutination, enhanced phagocytosis and oxidative burst, and direct

cytostatic properties (1); SP-D is also considered to be involved in controlling allergic sensitization in the lungs (3) where it exerts anti-lymphoproliferative effect following allergen challenge (4). In mouse models of Aspergillus fumigatus-induced allergic hypersensivity, immunopathological parameters of type I and III hypersensitivity improved considerably following therapeutic delivery of full-length human SP-D and its recombinant fragment containing trimeric neck and lectin domains (rfhSP-D) (5). SP-D can also induce apoptosis in activated eosinophilic and T cells via p53 pathway (6–9). In addition to several extrapulmonary sites, SP-D has also been found in various parts of the reproductive tract, including the ovaries (2, 10).

Emerging evidence seems to suggest that tumor cells are affected by the inflammatory environment, which can influence tumor proliferation and metastasis (11). Recent studies have focused on lung cancer, as it is the primary production site of SP-D where it plays a crucial role in surfactant and immunological homeostasis. SP-D can downregulate the EGF pathway by directly binding to EGFR and inhibit cell proliferation, invasion and metastasis of the A549 lung cancer cell line (12). A clinical study in 71 patients showed that low levels of SP-D were associated with increased incidence of lung cancer and that SP-D levels in bronchoalveolar lavage fluid could be used as a biomarker (13). Moreover, single nucleotide polymorphisms within the SP-D gene have been correlated with lung cancer, pneumonia and emphysema (14, 15). In pancreatic cancer, a recombinant fragment of human SP-D (rfhSP-D) induced apoptosis *in vitro* via Fas-mediated pathway (16). Furthermore, rfhSP-D inhibited TGF-β expression in a range of pancreatic cancer cell lines, thereby reducing their invasive potential by suppressing the Epithelial-to-Mesenchymal Transition (17).

In a recent study, it has been demonstrated that SP-D mRNA is overexpressed in ovarian cancer and can be of a potential prognostic value (18). Ovarian cancer affects over 65,500 women every year in Europe alone, and within 5 years, nearly 70% (42,716) of sufferers are predicted to die; it is the 6th leading cause of death in women worldwide. Ovarian cancer is known as the silent killer as it causes no symptoms in the early stages, so it is difficult to detect. Even at its advanced stage, the symptoms are very vague. Approximately, 70% of patients are diagnosed at advanced stage III (where ovarian cancer has spread into the upper part of the abdomen), or IV (where ovarian cancer cells are outside the abdominal cavity), with nearly 85% expected mortality. If ovarian cancer is diagnosed/detected early (Stage I–in the ovary only), its treatment is much more successful with the survival rates up to 90% (19, 20). In this study, we carried out a bioinformatic analysis to ascertain the potential prognostic role of SP-D in ovarian cancer. We also used a tissue microarray to validate these data and circulating tumor cells from ovarian cancer patients to measure/detect SP-D levels in liquid biopsies.

Given its pro-apoptotic and anti-invasive potential in a few *in vitro* cancer models, we hypothesized that rfhSP-D might be a novel therapeutic agent in ovarian cancer. Thus, in this study, we also investigated the effect of rfhSP-D on ovarian cancer signaling, using the SKOV3 cell line as an *in vitro* model- with emphasis to mTOR pathways. The mTOR pathway is a central regulator of growth, proliferation, apoptosis and angiogenesis providing balance between cellular resources. mTOR and one of its substrates, S6 kinase, are activated in ovarian cancer cells and inhibition of the mTOR pathways has anti-proliferative effects (21).

MATERIALS AND METHODS

In silico Analyses

The expression level of SFTPD gene in various types of ovarian cancer was analyzed using Oncomine, a cancer microarray database and web-based data mining platform from genome-wide expression analyses (22, 23). We compared the differences in mRNA level between normal and ovarian cancer tissues. The prognostic significance of SP-D mRNA expression and survival in ovarian cancer was analyzed by Kaplan–Meier plotter as described recently (18).

Immunohistochemistry

Ovarian carcinoma tissue microarrays, containing 10 cases of ovarian tumor with 2 non-neoplastic tissues, duplicated cores per case (Biomax, U.S.), were used to examine the expression of SP-D. The slides were deparaffinised following a series of washing in histoclear (National Diagnostics) and ethanol. Slides were boiled in sodium citrate for 20 min, washed with Tris-buffered Saline (TBS) with 0.025% v/v Triton-X 100, and then incubated with 3% v/v hydrogen peroxide in PBS for 30 min before being washed again in TBS with 0.025% Triton X 100. After blocking the slides using 5% v/v goat serum in PBS + 0.025% Triton-X 100 in a humidity chamber, the slides were incubated overnight with rabbit anti-human SP-D polyclonal antibodies (MRC immunochemistry unit, Oxford) diluted in PBS + 0.025% Triton-X 100. After a series of washing with TBS + 0.025% Triton X 100, the slides were incubated with Goat anti-rabbit IgG-HRP conjugate (Zytomed Systems, Germany) diluted in PBST, for 1 h at room temperature. DAB (3,3′-diaminobenzidine) substrate solution (Vector Laboratories) containing hydrogen peroxide was loaded on the slides for 5 min. Slides were washed in H_2O for 5 min and then incubated with Harris' haematoxylin for 30 s. Slides were stained with 0.1% w/v sodium bicarbonate for 30 s before dehydration in ethanol and histoclear. Images were captured using an EOS 1200D Brunel Microscope Ltd.

Liquid Biopsies

Patients with advanced ovarian cancer included in this study were enrolled at Mount Vernon Cancer Centre (East and North Hertfordshire NHS Trust) in the prospective CICATRIx clinical study that allows collection of blood samples for biomarker studies. All patients provided written informed consent for participation in the study and subsequent use of their tissue and blood specimens for research. The CICATRIx study was approved by the West Midlands—South Birmingham Ethics Committee (reference 16/WM/0196).

ImageStreamx Mark II Flow Cytometry

Whole blood (1 ml) from ovarian cancer patient samples (n = 3) was mixed with 9 ml of red blood cell lysis (RBC) buffer (G Biosciences, St. Louis, MO, USA), followed by incubation for 10 min at room temperature with gentle agitation. Following centrifugation at 1,260 × g for 10 min at 4°C, the supernatant was aspirated and 3 ml of RBC lysis buffer for second wash. This was followed by another incubation for 10 min at room temperature with gentle agitation, followed by centrifugation. The resultant pellet was resuspended in 1.5 ml of PBS and then centrifuged at 1,450 × g for 3 min. The cell pellet was resuspended in 1 ml of ice-cold 4% v/v paraformaldehyde for 7 min on ice and then centrifuged for 5 min at 250 × g. Subsequent immunostaining using specific polyclonal antibodies against human SP-D diluted in FBS-PBS (1:200) was used as previously described in the solution containing CTCs (and some white blood cells) (24, 25).

Cell Culture and Treatments

SKOV3 (human ovarian clear cell adenocarcinoma) cell line was purchased from the American Type Culture Collection (ATCC, Rockville, MD, USA) and used as an *in vitro* cell model for epithelial ovarian cancer. SKOV3 cells were cultured in DMEM supplemented with 10% v/v FBS, 1% v/v penicillin/streptomycin and 1% L-glutamine (Gibco, MA, USA). Cells were grown under standard culture conditions (37°C, 5% v/v CO_2). At approximately 80–90% confluency, the media was discarded, and cells were washed with fresh PBS. Seeded SKOV3 cells in 6-well plates were treated with rfhSP-D in a dose- (5, 10, 20 μg/ml) and time- (12, 24, 48 h) dependent manner in triplicates.

Expression of a Recombinant Fragment of Human SP-D (rfhSP-D)

A recombinant fragment of human SP-D containing trimeric neck and C-type lectin domains was expressed in *E.coli* and purified, as previously described (26, 27). Its three-dimensional crystallographic structures are well-established (28, 29). The affinity purified fractions were passed through a Pierce High Capacity endotoxin removal resin column to remove lipopolysaccharides (LPS) (Thermo Scientific). The endotoxin levels were measured using a QCL-1000 Limulus amebocyte lysate system (BioWhittaker, Walkersville, MD, USA) and were approximately 5 pg per μg of rfhSP-D.

Immunofluorescence Microscopy for SP-D

SKOV3 cells were grown in a 24-well plate on the top of coverslips. Cells were fixed with 4% paraformaldehyde (PFA; Sigma-Aldrich) for 10 min at room temperature, and then permeabilised with 0.5% v/v Triton X 100 (Sigma-Aldrich) for 5 min on ice. Next, cells were blocked using 5% v/v FBS diluted in PBS for 45 min and then incubated for another 45 min with rabbit anti-human SP-D polyclonal antibody diluted in 5% FBS-PBS. Cells were washed and incubated with a staining buffer containing Alexafluor 568 secondary conjugated goat anti-rabbit antibody, phalloidin 488 and Hoechst (Invitrogen, Life Technologies). This incubation was performed in the dark for 45 min. After washing with 5% FBS-PBS, the coverslips were mounted on slides and visualized under a HF14 Leica DM4000 microscope.

Live Cell Imaging

SKOV3 cells were grown in a Petri dish and allowed to reach ∼30–40% confluency. Cells were treated with rfhSP-D at a final concentration of 10 μg/ml. Cells were then placed under a Zeiss Axiovert 200M microscope attached to an incubator in order to examine cell survival and visualize cell motility. Images of the cells were recorded every 5 min for 15 h. X and Y coordinates were generated through ImageJ software for 25 cells for the first 8 h. Using Pythagoras' theorem, the distance, the velocity and the displacement were established.

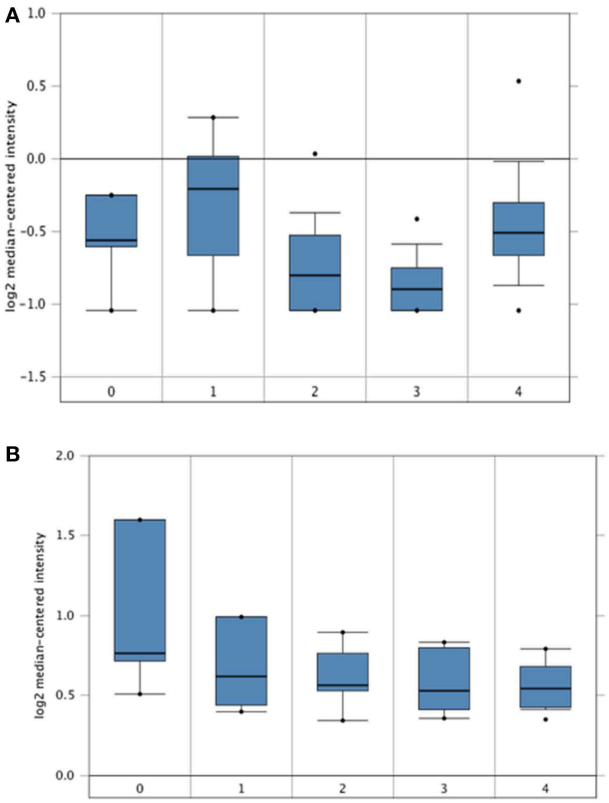

FIGURE 1 | *In silico* analyses of SP-D (SFTPD) expression in different subsets of ovarian cancer patients. SP-D gene expression from the Hendrix et al. (31) dataset plotted by Oncomine. **(A)** Mean SP-D gene expression in control normal ovaries (0), ovarian clear cell adenocarcinoma (1), ovarian endometrioid adenocarcinoma (2), ovarian mucinous adenocarcinoma (3), and ovarian serous adenocarcinoma (4). Boxes represent the 25th-75th percentile (with median line), bars show the 10th−90th percentile and dots show the complete spread of data. Fold change in SP-D expression was 1: 1.217 (p = 0.123), 2: −1.109 (p = 0.782), 3: −1.201 (p = 0.897) and 4: 1.086 (p = 0.266) when compared to normal, respectively. SP-D gene expression from the Lu et al. dataset **(B)**. Mean SP-D gene expression in control normal ovaries (0), ovarian clear cell adenocarcinoma (1), ovarian endometrioid adenocarcinoma (2), ovarian mucinous adenocarcinoma (3), and ovarian serous adenocarcinoma (4). Fold change in SP-D expression was 1: −1.179 (p = 0.855), 2: −1.214 (p = 0.893), 3: −1.255 (p = 0.922) and 4: −1.257 (p = 0.924) when compared to normal, respectively.

Wound Healing Assay

SKOV3 cells were assessed for their ability to close an artificially created gap in a cell growth area in the presence or absence of rfhSP-D. SKOV3 cells were cultured in a petri dish and allowed to reach 100% confluency. Using a 20 µl pipette tip, the bottom of the dish was scratched to create an artificial gap. Cells were placed under a Zeiss Axiovert 200M microscope and images were recorded every 5 min for up to 48 h.

Flow Cytometry

SKOV3 (0.1 × 107) cells were grown in a 6-well plate and incubated with rfhSP-D (5, and 10 µg/ml), along with an untreated control, for 48 h. The cells were then detached using 2 × Trypsin-EDTA (0.5%) (Fisher Scientific) and centrifuged at 1,500 × g for 5 min. Annexin V apoptosis detection kit with PI (Abcam) was used, according to the manufacturer's instructions. After extensive washing with PBS, apoptosis was measured using Novocyte Flow Cytometer. Compensation parameters were acquired using unstained, untreated FITC stained, and untreated PI stained. 12,000 SKOV3 cells were acquired for each experiment and compensated before plotting the acquired data.

Fluorescence Microscopy

SKOV3 cells were cultured in DMEM-F12 medium, supplemented with 10% v/v FBS, penicillin (100 U/ml)/streptomycin (100 µg/ml), and 2 mM L-glutamine (Fisher Scientific). Cells were grown at 37°C in the presence of 5% v/v CO_2 until 85% confluency was reached. For apoptosis analysis, 0.5 × 10^5 cells were grown on microscopy coverslips, and incubated with rfhSP-D (10 µg/ml) in serum free medium for 48 h. The cells were then washed with PBS three times, and incubated with FITC Annexin V (1:200), and PI (1:200) diluted in Annexin V-binding buffer, for 15 min at room temperature in dark. After washing again with PBS, the coverslips were mounted on the slides, and visualized under a HF14 Leica DM4000 microscope. For mTOR analysis, the cells were incubated with rfhSP-D (10 µg/ml) for 15 h, and washed gently with PBS three times. The cells were permeablized and fixed with ice-cold 100% methanol for 10 min at −20°C. Following 1 h incubation with rabbit anti-human mTOR (1:500) (Sigma-Aldrich) primary antibody, the cells were washed again with PBS, and incubated with Hoechst (1:10,000) and Goat anti-rabbit Alexa Fluor® 488 (1:500) (Abcam) secondary antibody. The mounted coverslips were visualized on a HF14 Leica DM4000 microscope.

RNA Extraction and Quantitative RT-PCR

RNA was extracted from SKOV3 cells treated and untreated with rfhSP-D using the Nucleospin kit (Macherey-nagel, Bethlehem, USA) and the quantity was estimated using nanodrop. Two microgram of total RNA was used to synthesize cDNA using the Precision nanoScript 2 Reverse Transcription kit (Primer design). Relative expression levels of mTOR, DEPTOR, Rictor and Raptor (19) were assessed by quantitative PCR (Q-PCR) on an ABI FAST HT9000 PCR instrument, using SYBR green mastermix (Primer Design). Gene expression levels were normalized to GAPDH levels. All samples were analyzed in triplicates (19). RT-qPCR data was analyzed using the ΔCq method whereby the Cq of the endogenous control was subtracted from the Cq of the gene of interest and an RQ (relative quantity) value was calculated by finding 2-ΔCq (30).

Western Blotting

Proteins were extracted from SKOV3 cells treated with rfhSP-D for 24 and 48 h (21) and separated on a 10% v/v SDS-PAGE. The separated proteins were then electrophoretically transferred

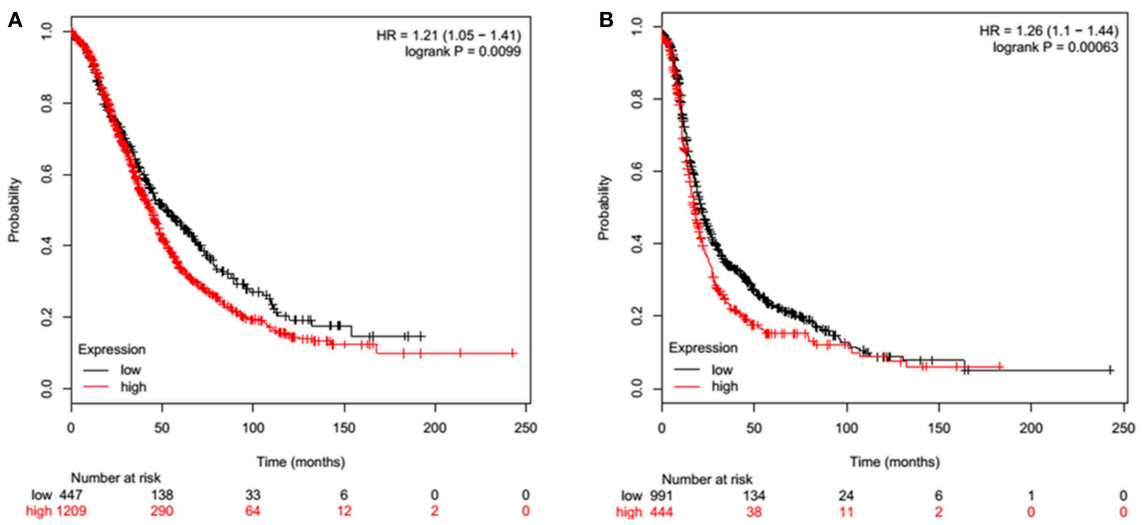

FIGURE 2 | Overall Survival (OS) of ovarian cancer patients expressing high (red) and low (black) SP-D **(A)**. High ($n = 1209$) and low ($n = 447$) expression of SP-D is shown over a 250 month (20 year) period. Low SP-D expression shows a significant improvement in survival than high SP-D expression ($p = 0.0099$). Progression-Free Survival (PFS) of ovarian cancer patients expressing high (red) and low (black) SP-D **(B)**. High ($n = 444$) and low ($n = 991$) expression of SP-D is shown over a 250 month (20 year) period. There is greater overall survival in low SP-D expression compared to high SP-D expression ($p = 0.00063$).

onto a nitrocellulose membrane (Thermo Scientific) in Wet-Transfer Buffer. The membrane was incubated in TBS containing 5% w/v dried milk powder and 0.1% v/v Tween Tween-20, for 1 h at room temperature to block non-specific binding. The membrane was then incubated with primary anti-human SP-D polyclonal antibodies (raised in rabbit), caspases 3 and 9, and phospho (Thr389) p70S6K (Cell Signaling Technology) at 4°C overnight. The membranes were washed in TBS + 0.1% Tween-20 (3 times, 15 min each) before incubation with the secondary goat anti-rabbit IgG-HRP-conjugated antibody for 1 h at room temperature. Proteins were visualized as previously described (21).

Statistical Analysis

Graphpad Prism 5.0 was used to generate the graphs and perform the statistical analysis. When data were of equal variance, an unpaired student's *t*-test was performed. When the data was of unequal variance, the Mann-Whitney U test was performed. Values were considered significant when $^{*}p < 0.05$, $^{*}p < 0.01$ and $^{***}p < 0.001$. Significance was identified between control and treated samples, as well as between treated samples. Error bars represent the standard deviation or standard error of the mean, where specified. Survival curves were generated by the Kaplan–Meier plots. All results are displayed with *p*-values from a logrank test. $p < 0.05$ were considered significant. Similarly, with Oncomine, the statistical significance of data (p-values) was provided by the program.

RESULTS

SP-D Is Expressed in Ovarian Cancer and Predicts Survival

A recent study using a bioinformatic approach and RT-qPCR validation indicated that SP-D is overexpressed in ovarian cancer patients (serous cystadenocarcinoma) compared to healthy controls (18). In the current study, we performed an extended

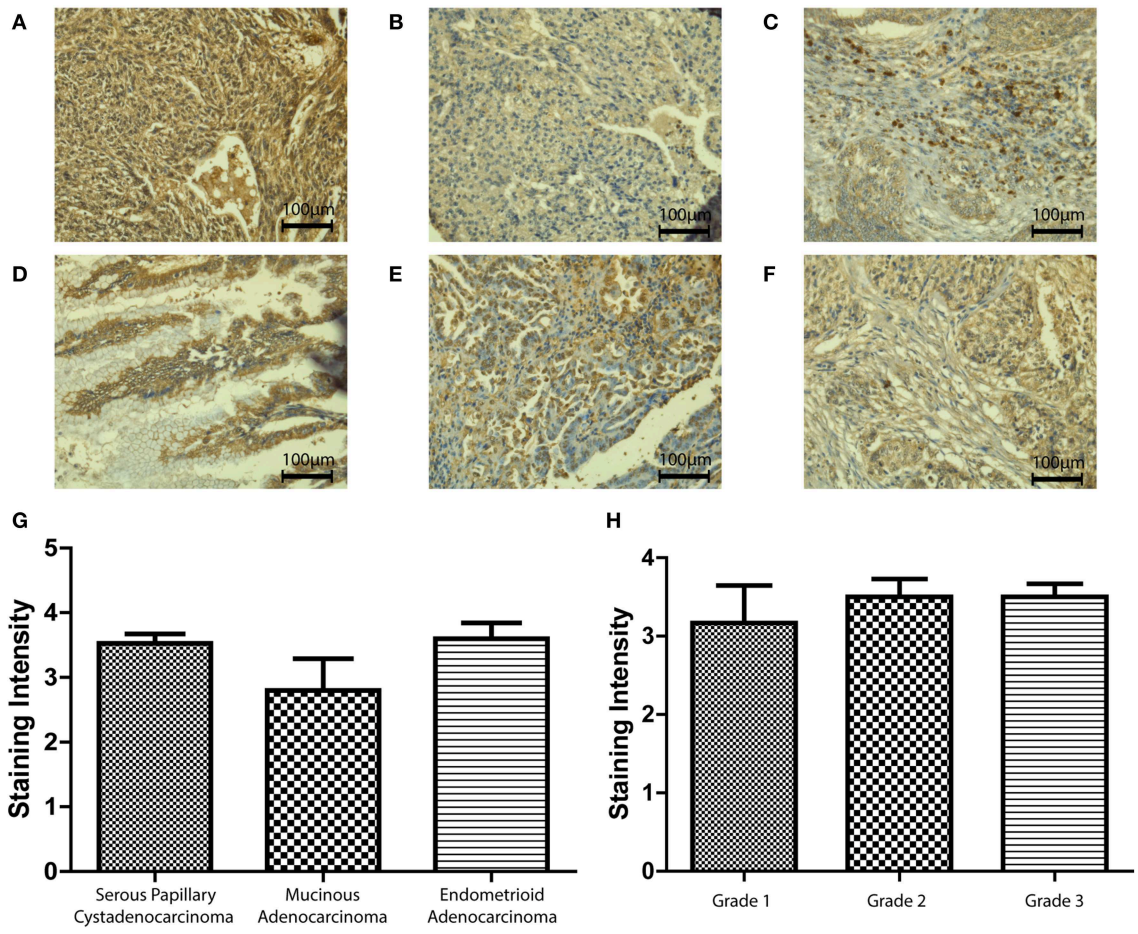

FIGURE 3 | Immunohistochemistry for SP-D expression in different pathologies of ovarian tissue array clinical samples (40x magnification): serous papillary cystadenocarcinoma **(A)**, mucinous adenocarcinoma **(B)** and endometrioid adenocarcinoma **(C)**. No significant change was seen between different types of OC ($p = 0.2235$; **G**). Immunohistochemistry for SP-D expression in different grades of ovarian tissue array clinical samples: mucinous cystadenocarcinoma grade 1 **(D)**, serous papillary cystadenocarcinoma grade 2 **(E)** and serous papillary cystadenocarcinoma grade 3 **(F)**. No significant change was seen between different grades of disease ($p = 0.7055$, **H**).

bioinformatics analysis in order to investigate whether SP-D is differentially expressed in various types of ovarian cancer and whether it can serve as a potential prognostic marker for the disease. We used the Oncomine™ dataset and the survival analysis platforms Kaplan–Meier plotter.

The Hendrix dataset (31) demonstrated that SP-D (SFTPD) is expressed in a wide range of ovarian cancers such as: clear cell adenocarcinoma ($n = 8$), endometrioid adenocarcinoma ($n = 37$), mucinous adenocarcinoma ($n = 13$), serous adenocarcinoma ($n = 41$) and normal ovaries ($n = 4$). Some subtle changes were noted amongst these groups, but they did not reach significance compared to healthy controls (**Figure 1A**). Similarly, when the Lu dataset was accessed (32), a similar picture emerged with the expression of SP-D mRNA (SFTPD) in normal ovaries ($n = 5$), clear cell adenocarcinoma ($n = 7$), endometrioid adenocarcinoma ($n = 9$), mucinous adenocarcinoma ($n = 9$) and serous adenocarcinoma ($n = 20$; **Figure 1B**).

Overall Survival (OS) in ovarian cancer was measured by Kaplan-Meier plots. In a cohort of 1656 ovarian cancer patients, high ($n = 1209$) and low ($n = 447$) mRNA expression of SP-D was measured over a 250-month (20 year) period. Low SP-D expression shows a significant improvement in survival than high SP-D expression ($p = 0.0099$; **Figure 2A**). Similarly, Progression-Free Survival (PFS) was also studied in 1435 ovarian cancer patients of which 444 had high expression of SP-D and 991 low. There was a significant progression-free survival (PFS) improvement in low SP-D cohort compared to patients with high SP-D expression ($p = 0.00063$; **Figure 2B**).

Ovarian Cancer Tissue Microarray Analysis Corroborates Bioinformatics Data

We then used an ovarian cancer tissue microarray to perform immunohistochemistry in a number of clinical samples in order to validate the *in-silico* data and identify any changes in protein expression with respect to type, grade, or stage of the disease. SP-D was expressed in serous papillary cystadenocarcinoma, mucinous adenocarcinoma and endometrioid adenocarcinoma (**Figures 3A–C**). Scoring of immunostaining did not reveal any

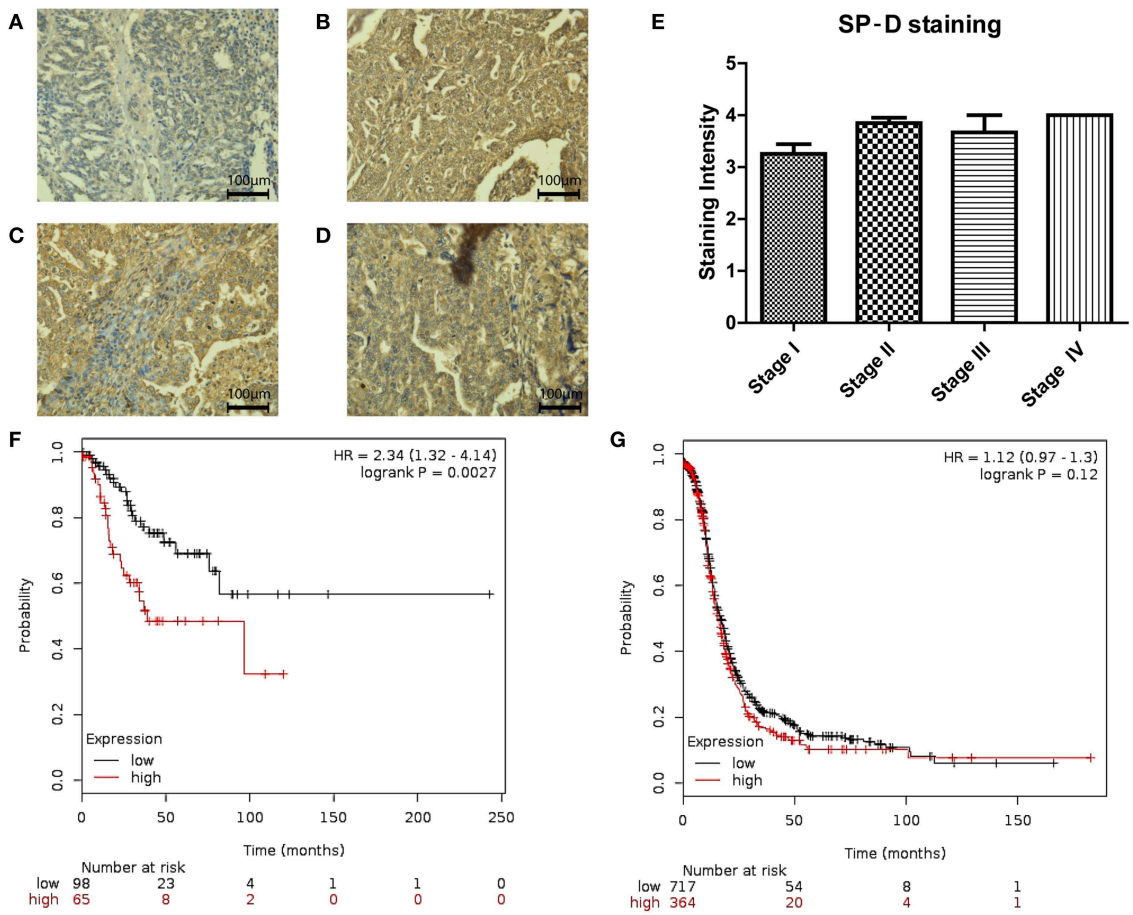

FIGURE 4 | Immunohistochemistry for SP-D expression in different stages of ovarian tissue array clinical samples (40 x magnification): serous papillary cystadenocarcinoma stage I **(A)**, serous papillary cystadenocarcinoma stage II **(B)**, serous papillary cystadenocarcinoma stage III **(C)** and serous papillary cystadenocarcinoma stage IV **(D)**. A nearly significant up-regulation of SP-D was observed in stage II OC compared to stage I OC ($p = 0.053$; **E**). Stratification of PFS in Stages I and II **(F)** against stages III and IV **(G)**. There was a significant survival improvement in low SP-D cohort compared to patients with high SP-D expression only in Stages I and II ($p = 0.0027$, and $p = 0.12$, respectively).

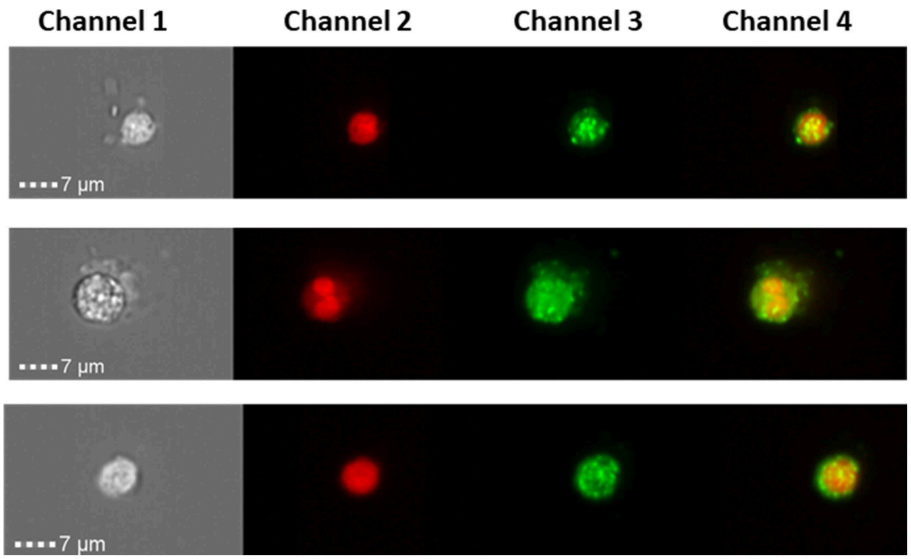

FIGURE 5 | ImageStream analysis showing expression SP-D in circulating tumor cells of 3 ovarian cancer patients, magnification x 40. Channel 1 shows the brightfield pictures of cells, channel 2 shows the nucleus stained with DRAQ5 (red), channel 3 shows SP-D expression using an Alexa Fluor® secondary antibody (green) and channel 4 is the merged image of channels 1 and 2. SP-D is localized in the cytoplasm, with strong fluorescence intensity.

apparent differences in the SP-D expression (**Figure 3G**), thus corroborating the gene expression Oncomine data. We then measured SP-D expression in clinical samples of different grades: Grade 1 ($n = 6$), Grade 2 ($n = 14$) and Grade 3 ($n = 28$) (**Figures 3D–F**). No apparent differences amongst grades were noted (**Figure 3H**).

We also measured SP-D protein expression in different stages (I-IV) of ovarian cancer ($n = 48$; **Figures 4A–D**). No differences were noted between stages III and IV. However, when Stages I and II were compared, SP-D was over-expressed in Stage II compared to Stage I ($p = 0.053$; **Figure 4E**). When we stratified, PFS in Stages I and II (**Figure 4F**; $n = 163$) against stages III and IV (**Figure 4G**; $n = 1081$), there was a significant survival improvement in low SP-D cohort compared to patients with high SP-D expression only in Stages I and II. These results are consistent with Mangogna et al who reported correlation between SP-D expression in ovarian cancer tissues and poor survival prognosis (18).

SP-D Is Expressed in Circulating Tumor Cells (CTCs) From Ovarian Cancer Patients

Liquid biopsies offer a promising alternative to tissue samples, providing a non-invasive diagnostic approach or serial monitoring of the disease evolution. Here, we measured SP-D protein expression in CTCs from three Stage III ovarian cancer patients (**Figure 5**) using a novel imaging flow-cytometry (ImageStream). CTCs were selected based on being positive for cytokeratin markers, WT-1 and negative for CD45 (a white blood cell marker). CTCs from all three patients were positive for SP-D (**Figure 5**).

rfhSP-D Compromises Migratory Capacity of SKOV3 Ovarian Cancer Cells *in vitro*

In view of the abundance of SP-D in ovarian cancer tissues, we wished to investigate how SP-D can affect ovarian cancer cells *in vitro*. We used a well-established rfhSP-D, which has been shown to induce apopotosis in pancreatic cell lines, to treat cultured SKOV3 cells.

Wound healing assay was used to have a visual assessment of cell proliferative and migratory capacity spatially *in vitro*. Using a fine pipette tip, an artificial wound was created on a confluent cell surface followed by treatment with 10 µg/ml of rfhSP-D. Images acquired from the wound healing assay over 48 h showed that untreated SKOV3 cells closed the gap at 24 h, whereas SP-D treated cells closed the artificially-created gap after 34 h (**Figures 6A–F**). Therefore, there was a marked inhibition of growth in the treated cells.

We expanded on these observations by locating an area with approximately 25–30 cells where images were captured every 5 min for up to 12 h. Using ImageJ, the coordinates for 25 cells were acquired. Using Pythagora's theorem for each point for each of the cells, the distance, velocity and displacement for all 25 cells were calculated. Cells treated with rfhSP-D moved significantly less and slower compared to untreated cells; there was a significant decrease in distance (**Figure 6G**), velocity (**Figure 6H**) and displacement (**Figure 6I**) of rfhSP-D treated SKOV3 cells compared to untreated cells.

rfhSP-D Induces Apoptosis in SKOV3 Ovarian Cancer Cells

Fluorescence microscopy analysis of rfhSP-D treated SKOV3 cells revealed a positive staining for cell membrane integrity

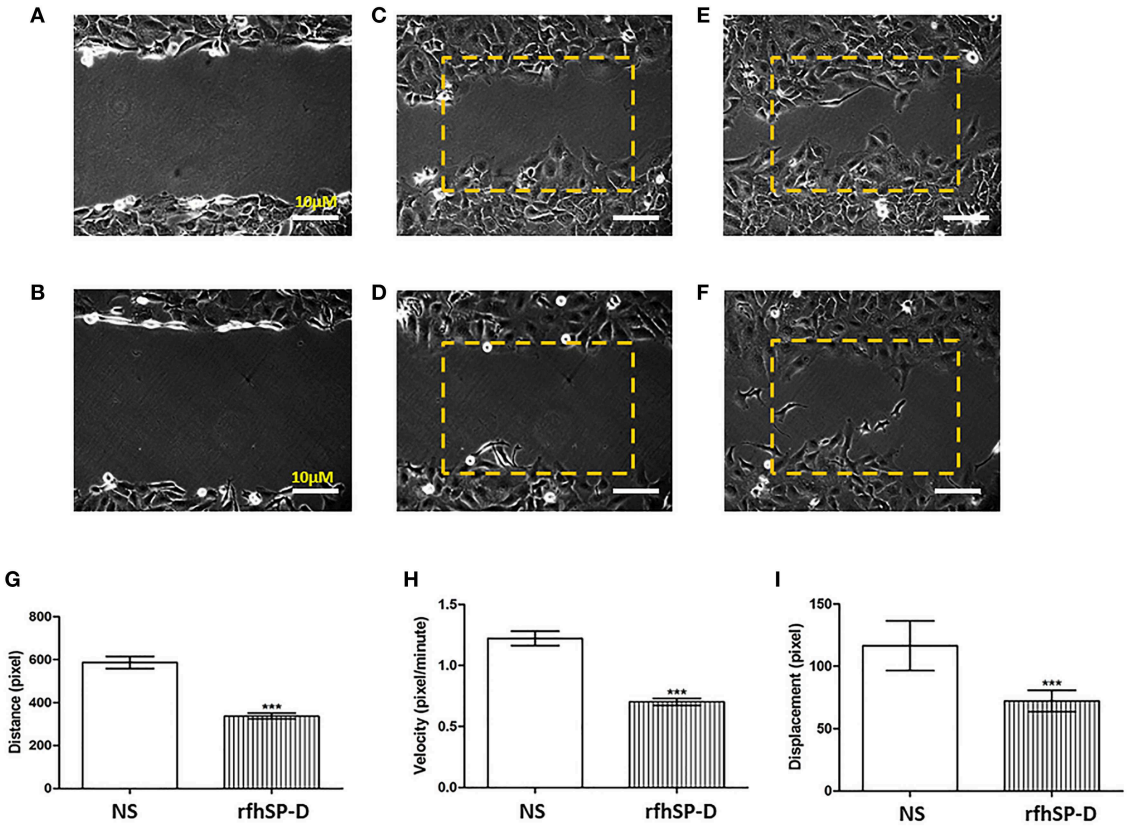

FIGURE 6 | Wound healing assay. The artificial wound created on the cell surface in untreated cells **(A)** and rh-SPD treated cells **(B)** at 0 h. Untreated cells **(C)** or treated cells with rfhSP-D **(D)** did not appear to close the gap after 12 h. At 24 h untreated cells managed to close the gap **(E)** whereas rfhSP-D treated cells did so after 30 h **(F)**. rfhSP-D treated SKOV3 cells have their distance **(G)**, velocity **(H)**, and displacement **(I)** reduced, compared to control SKOV3 cells. 25 cells were counted for each experiment. Comparisons ±SEM between untreated (NS) and treated SKOV3 cells with rfhSP-D at 10 μg/ml (***$p < 0.001$).

marker, Annexin V (conjugated to FITC), and disoriented cell membrane morphology was observed. Thus, PI positive staining was seen in rfhSP-D treated cells compared to un-treated controls (**Figure 7A**), suggesting induction of apoptosis by the protein.

The quantitative as well as qualitative analyses of apoptosis induction in SKOV3 cells were performed using immunofluorescence microscopy and flow cytometry. A significant proportion of SKOV3 cells following rfhSP-D treatment showed apoptosis at 48, as revealed by FACS analysis. 20 μg/ml of rfhSP-D was effective in inducing the maximum apoptosis in this cell line at 48 h; i.e., ∼68%. Approximately 31% cells were FITC and PI positive, suggesting that annexin V/FITC was able to bind to phosphatidylserine (PS) found on the cell surface of cells undergoing apoptosis. However, the percentage of SKOV3 cells stained for PI alone was higher (∼46%), suggesting that these cells were either at the late stage of apoptosis or undergoing necrosis. The percentage of viable cells in the untreated sample (90%) was significantly higher as compared to treated sample, suggesting that apoptosis induction was protein-specific, where the integrity of the cell membrane was intact in the untreated cells, and hence, the cells were still viable (**Figure 7B**).

In view of these findings, we sought to investigate the effects of rfhSP-D on the cleavage of caspase-3, a critical mediator of apoptosis. Cleaved caspase-3 compared to total caspase-3 expression was increased after 48 h at 20 μg/ml rfhSP-D treatment (**Figure 7C**).

Moreover, changes in the expression of pro-apoptotic genes, Bax, Fas and TNF-α following treatment with rfhSP-D (20 μg/ml) at 24 and 48 h were assessed. We chose to include TNF-α since it is a key mediator of the apoptotic pathway and has been shown to modulate Fas expression. Bax was unaffected following the treatment with rfhSP-D in SKOV3 cells at both time-points (**Figures 8A,B**), suggesting that the intrinsic apoptotic pathway may not be directly involved. Fas and TNF-α were significantly upregulated following treatment with rfhSP-D at 24 h compared to controls (**Figure 8A**). At 48 h, there was no apparent changes in the mRNA expression of TNF-α, but a clear trend in the over-expression of Fas was noted (**Figure 8B**).

Treatment of SKOV3 Cells With rfhSP-D Compromises mTOR Signaling

The mechanistic Target of Rapamycin (mTOR) has been linked with the pathogenesis of ovarian cancer, especially with its progression (33). Treatment of SKOV3 cells with rfhSP-D (5,

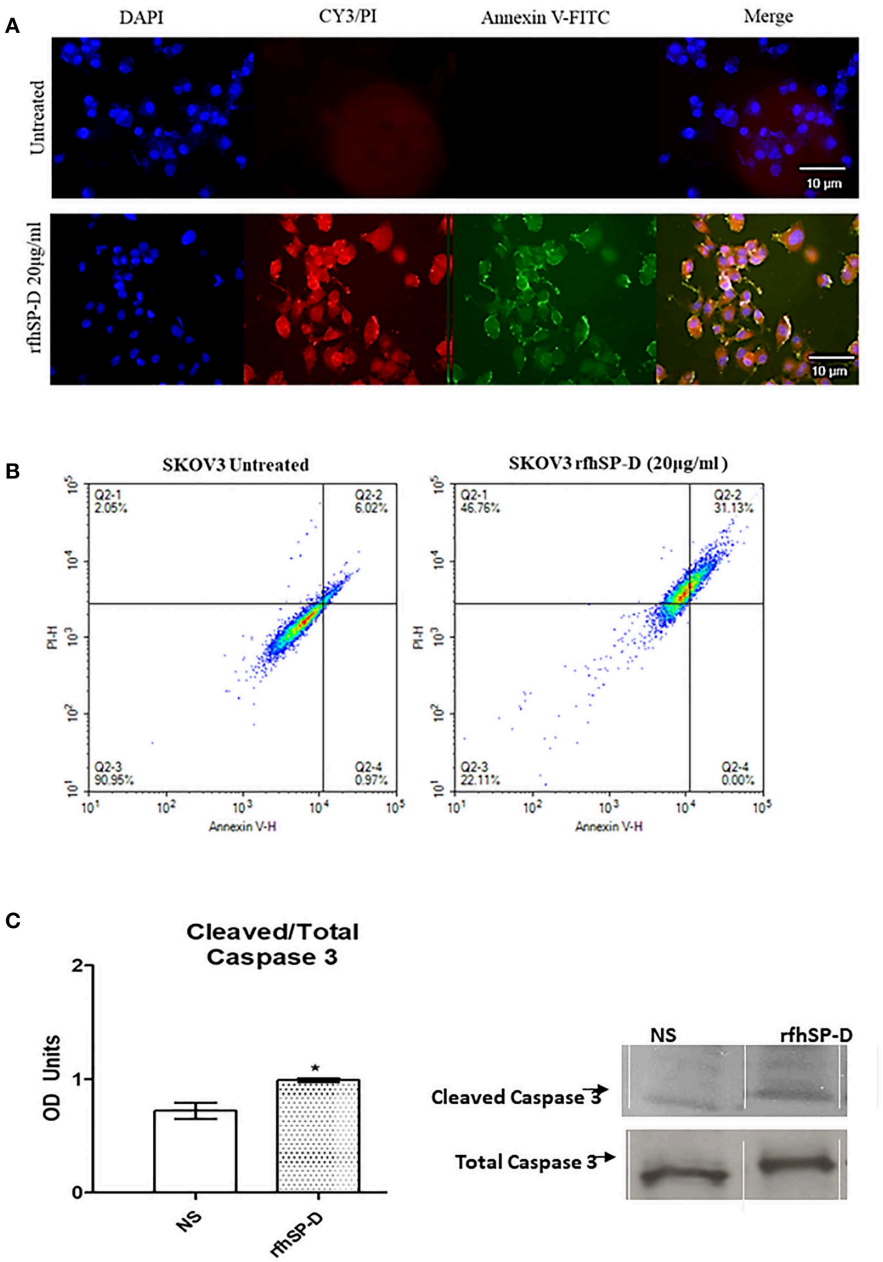

FIGURE 7 | Fluorescence microscopy to analyze apoptosis in SKOV3 cells treated with rfhSP-D for 48 h. Apoptosis was analyzed using an annexin V/propidium iodide (PI) staining kit **(A)**. The cell membrane was positively stained for annexin V and the DNA staining is visible in the treated cells indicating that the cells underwent apoptosis and PI was taken in which stained the DNA of apoptotic cells. No such staining was seen in the untreated cells. The nucleus was stained with Hoechst for both treated and untreated cells **(A)**. Quantitative analysis of apoptosis using Flow Cytometer **(B)**. SKOV3 cells were treated with rfhSP-D 48 h and apoptosis was analyzed using annexin V with PI kit. Cells were acquired and plotted for both annexin V/FITC, which showed a shift in the fluorescence intensity of in treated cells **(B)**. Effects of rfhSP-D on caspase 3 **(C)**. Scanning densitometry of protein expression of cleaved over total caspase 3 in SKOV3 cells treated with rfhSP-D ±SD at 48 h which were acquired from the western blotting analysis **(C)**. Cleaved Caspase 3 over total ratio was significantly increased after 48 h 20 µg/ml. $^*p < 0.05$.

10 and 20 µg/ml) for 12 h did not affect the gene or protein expression of mTOR (data not shown). However, mRNA levels of both key components of mTORC1 and mTORC2 complexes, namely Raptor and Rictor, were significantly down-regulated 12 h post-treatment (**Figures 9A,B**). Rictor downregulation was mirrored at protein level at 24 h as assessed by Western blotting (**Figure 9C**), whereas a reduction in Raptor expression was evident at 48 h post rfhSP-D (20 µg/ml) treatment (**Figure 9D**).

Fluorescence microscopy analysis following rfhSP-D (20 µg/ml) treatment of SKOV3 cells for 12 h showed

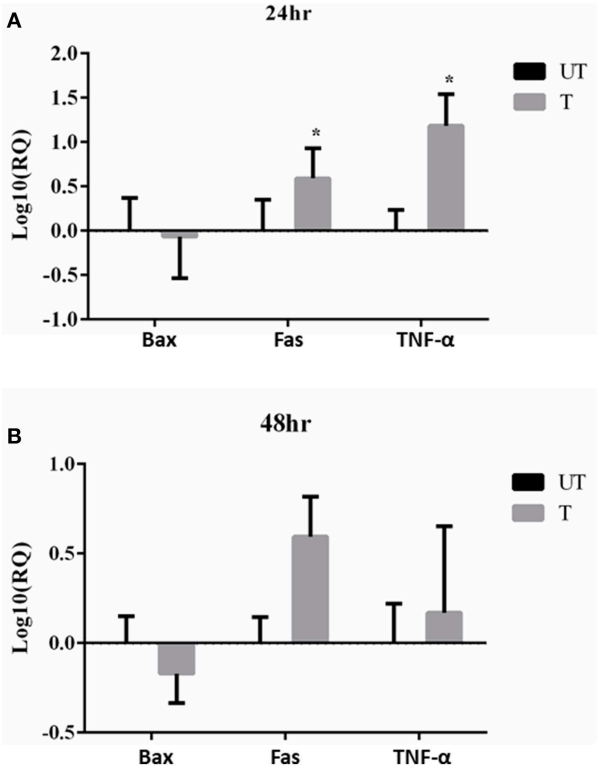

FIGURE 8 | Effects of rfhSP-D treated SKOV3 cells on Bax, Fas and TNF-α at 24 h **(A)** and 48 h **(B)**. Fas and TNF-α are significantly up-regulated at 24 h of treatment compared to controls *$P < 0.05$.

reduced cytoplasmic levels of mTOR compared to the untreated controls (**Figure 10A**). Nuclear accumulation of mTOR was seen in the treated cells, indicative of a potential shuttling.

Finally, we assessed the effect of rfhSP-D on mTORC1 activity by measuring the phosphorylation status of S6 Kinase (S6K) since an increase in S6K phosphorylation is a sign of an active mTOR pathway and has been evidenced in late stage ovarian cancer (19). There was a notable ($p = 0.05$) decrease in the phosphorylation level of (Thr389) p70S6K S6K protein following rfhSP-D (20 μg/ml) treatment (**Figure 10B**).

DISCUSSION

SP-D, which acts as an anti-microbial and anti-allergic humoral factor at the mucosal surface, has emerged as an innate immune surveillance molecule against cancer. Its transcriptional and protein levels have recently been associated with prognosis in a range of cancers (18). SP-D has been reported to be overexpressed in ovarian cancer patients (serous cystadenocarcinoma) compared to healthy controls (18). Here, we extended our observations by measuring the gene expression levels in different sub-types of ovarian cancer. We provide evidence that SP-D is widely expressed in clear cell adenocarcinomas, endometrioid adenocarcinomas, mucinous adenocarcinomas, and serous adenocarcinoma. We validated these observations by immunohistochemistry using tissue microarrays, where SP-D expression was unchanged in grade or type; however, there was a modest increase in the expression between Stage I to Stage II.

Low SP-D mRNA expression showed a significant improvement in overall survival and progression free survival than higher SP-D expression. A report on non-small cell lung cancers (NSCLC) revealed that an increased expression of SP-D in the lungs of NSCLC patients was correlated with metastasis and poor outcome (34). These data provide evidence for a higher order of complexity in the regulation and function of SP-D in cancer. Another study has recently reported that in lung, gastric, and breast cancers, there is a lower expression of SP-D compared to healthy controls; in lung cancer, the presence of SP-D could be associated with a favorable prognosis. On the contrary, in breast, and ovarian cancers, the presence of SP-D is associated with an unfavorable prognosis (18). It is possible that SP-D acts in a tissue- or cell-specific manner, depending on the composition of the tumor microenvironment. These observations require further investigation using a wider repertoire of cell lines and clinical samples. Nevertheless, SP-D emerges here as a potential biomarker for ovarian cancer.

Thus, we expanded on the clinical observations by measuring its expression in circulating tumor cells (CTCs) of 3 Stage III ovarian cancer patients. An abundant expression was noted using an imaging flow-cytometric approach. This is the first time that SP-D expression is being documented in CTCs. Blood based biomarkers such as "liquid biopsies" are becoming an increasingly attractive area of cancer research due to their non-invasive nature and importance in detecting the stage and the spread of the tumor (35). The detection of CTCs and appropriate biomarkers can, therefore, help not only in diagnosis but also in real-time therapy monitoring and more efficient personalized treatments (36).

We also demonstrate an involvement of SP-D in ovarian cancer and provide a novel insight into the signaling pathways that are involved using an ovarian cancer cell line *in vitro*. When SKOV3 cells were treated with rfhSP-D, there was a decrease, although moderate, in proliferation, suggesting a direct anti-proliferative effect of rfhSP-D. There was also a noticeable decrease in distance, velocity and displacement of SKOV3 cells treated with rfhSP-D, when compared to untreated cells. Thus, rfhSP-D could exert a cytostatic or cytotoxic effect, as evident from rfhSP-D induced Caspase 3 cleavage *in vitro*. Caspase-3 is a critical regulator of apoptosis, as it contributes to the proteolytic cleavage of many key proteins, such as poly adenosine diphosphate-ribose polymerase (PARP) (37). The rfhSP-D induced apoptosis in SKOV3 cells was further corroborated by an increase in annexin V staining, which is used to detect cell death by its ability to bind to PS, a marker of apoptosis when it is on the outer leaflet of the plasma membrane. Collectively, our study is in agreement with recent studies involving a number of malignancies. In a human lung epithelial cancer cell line (A549), SP-D inhibits cell progression and metastasis via inhibition of the EGF pathway through binding to EGFR and compromising the EGFR-EGF complex (12). rfhSP-D can also alter oxidative stress and high-mobility

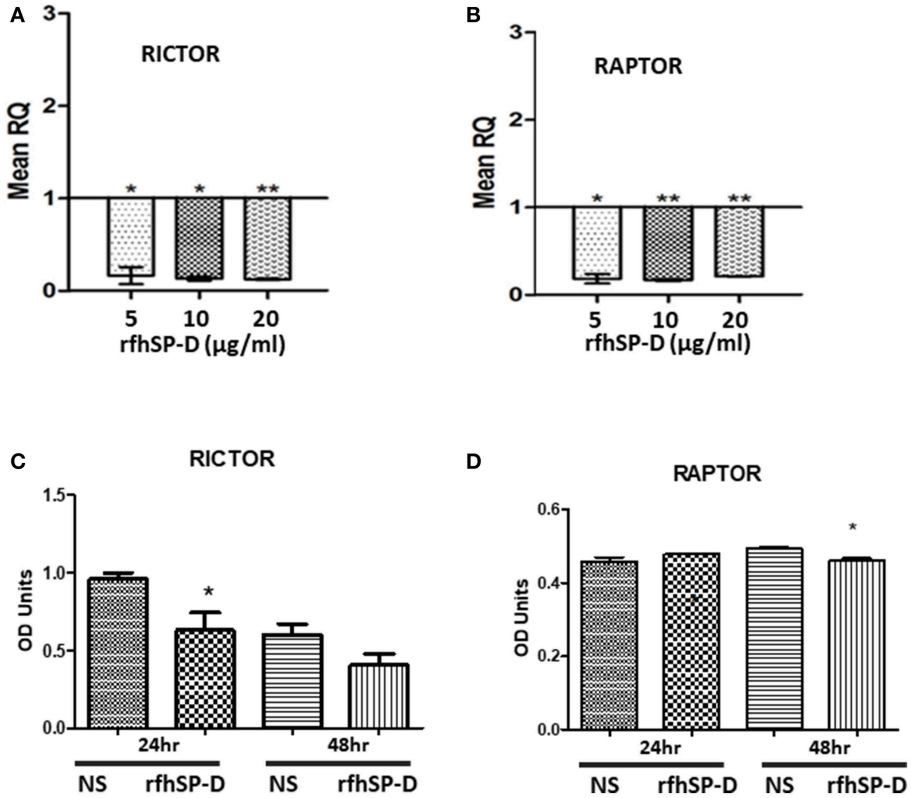

FIGURE 9 | Relative quantification of Rictor **(A)** and Raptor **(B)** mRNA expression in SKOV3 cells treated with 5, 10 and 20 µg/ml of rfhSPD after 12 h (*$p < 0.05$, **$p < 0.01$ compared to basal levels set at 1.0). Western blotting for Rictor **(C)** and Raptor **(D)** showed a downregulation at protein level at 24 and 48 h, respectively compared to controls; *$P < 0.05$.

group A factor 1 (HMGA1) expression leading to induction of the p53 apoptotic pathway in an eosinophil leukemic cell line (7, 8). In a more recent study, rfhSP-D induced apoptosis in pancreatic cancer cell lines via Fas-mediated pathway, followed by cleavage of caspases 8 and 3 (16).

In this study, we demonstrate that rfhSP-D exerts its anti-proliferative effects by compromising mTOR signaling and activating the pro-apoptotic genes, Fas and TNF-α, but not Bax. Fas belongs to TNF superfamily that can activate caspase cascade, which can lead to cleavage of caspase 3 as the terminal molecular event during apoptosis (38–40). TNF-α, another TNF superfamily member, exerts its effects via TNFR2 to increase the susceptibility of the target cells to Fas-mediated death (16, 41). With regards to Bax, this is not the first time that a modest gene expression is noted. When FSTL1 and RAD51AP1 genes were silenced in ovarian cancer cells, a decrease in proliferation was noted while the Bax gene expression remained unchanged (24, 42).

To this date, little is known about an association between SP-D and mTOR. The mTOR pathway has been shown as an important regulatory epicenter for cell growth, metabolism, autophagy, gene expression and protein synthesis (43). mTOR acts through two complexes, mTORC1 and mTORC2, and Raptor and Rictor are key components of these two complexes, respectively (4, 44). We, therefore, decided to examine the effects of rfhSP-D on the mTOR pathway. When we treated SKOV3 cells with rfhSP-D and measured the expression of key components of the mTOR pathway, the mRNA and protein levels of Rictor and Raptor were down-regulated compared to untreated controls, with a concomitant decrease in the phosphorylation of S6K (Ser).

Interestingly, although the mTOR protein expression remained largely unaltered following rfhSP-D treatment, its translocation from the cytoplasm to the nucleus was noted. mTOR primarily resides within the cytoplasm (45), but nuclear localization has also been documented in rhabdomyosarcomas, human fibroblasts and colon carcinoma cells (46). In a study using multiple myeloma cell lines, it was reported that treatment with pomalidomide (IMID®), an immunomodulatory FDA-approved drug for the treatment of multiple myeloma, increased nuclear mTOR and p-mTOR expression levels in the nucleus with a concomitant decrease of the cytoplasmic fractions (47). This shuttling correlated with a decrease in cell viability in this study. Moreover, it has been shown that the mTORC2 complex components, Rictor and Sin1, are dephosphorylated and dynamically distributed between the cytoplasm and the

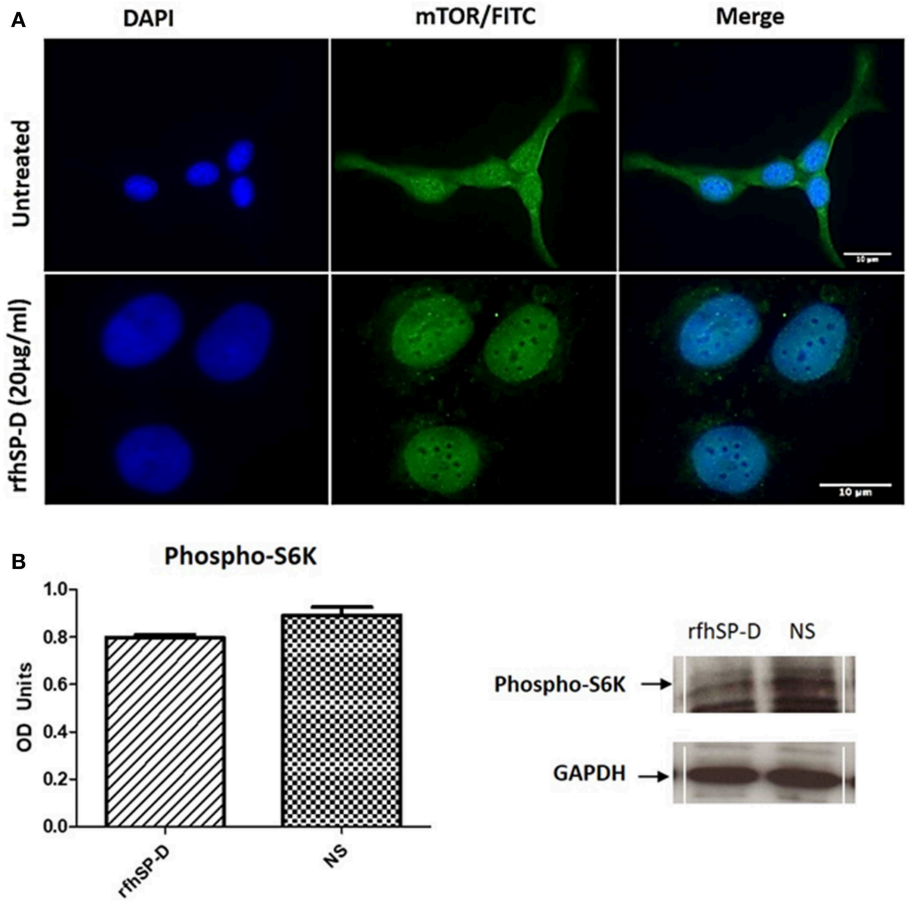

FIGURE 10 | Assessment of mTOR localization in SKOV3 cells. **(A)** rfhSP-D treatment downregulated the survival pathway, mTOR. Fluorescence microscopy analysis following rfhSP-D (20 ug/ml) treatment of SKOV3 cells showed reduced cytoplasmic levels of mTOR following treatment as compared to the untreated. Nuclear accumulation of mTOR was seen in the treated cells. **(B)** Effects of rfhSP-D on phospho (Thr389) p70S6K in SKOV3 cells treated with rfhSP-D (20 µg/ml).

nucleus upon long-term treatment with the mTOR-inhibitor rapamycin (48). Thus, rfhSP-D can compromise mTOR signaling via downregulation of Rictor and Raptor, shuttling of mTOR leading to dysfunction of the downstream signaling cascade (i.e., dephosphorylation of S6K), and subsequent inhibition of cell proliferation.

In conclusion, rfhSP-D treatment of SKOV3 cells downregulates Rictor and Raptor and upregulates pro-apoptotic factors such as TNF-α and Fas to activate caspase 3 cascade to induce apoptosis *in vitro*. New therapeutic strategies involving immune molecules such as rfhSP-D that target pro-apoptotic genes and the mTOR pathway merit further investigation. Finally, the emergence of SP-D as a potential biomarker needs to be verified in a large cohort of ovarian cancer patients. However, the prognostic value of SP-D in ovarian cancer, where high levels correlate with poor survival, together with the *in vitro* effects of rfhSP-D, is quite intriguing. One possibility is that the SP-D protein in ovarian cancer tissues is non-functional as we have recently observed in a triple-positive breast cancer cell line that secretes a non-functional variant of SP-D although the same cell line remains susceptible to apoptosis induction by rfhSP-D (Murugaiah et al., unpublished data). In case the ovarian tissue, SP-D is functionally active, it is possible it binds to components of tumor microenvironment (e.g., hyaluronic acid). This interaction is capable of negating the protective effect of SP-D *in vivo*. Further studies are required to delineate the relationship between SP-D, its ligand in the tumor microenviroment and SP-D receptors on the primary ovarian cancer cells.

DATA AVAILABILITY

Publicly available datasets were analyzed in this study. This data can be found here: www.oncomine.org.

ETHICS STATEMENT

Patients included in this study were enrolled in the prospective CICATRIx clinical study which collects blood samples for exploratory biomarkers from patients with advanced cancer attending Mount Vernon Cancer Centre (East and North

Hertfordshire NHS Trust). All patients provided written informed consent for participation in the study and for use of their donated tissue and blood specimens. The CICATRIx study was approved by the West Midlands – South Birmingham Ethics Committee (reference 16/WM/0196).

AUTHOR CONTRIBUTIONS

JK and VM carried out key experiments. GS, AK, JJ, and IS carried out supportive and validation experiments. FA, JC, and MH provided crucial reagents. UK and EK designed various experiments and wrote the manuscript.

FUNDING

This study has been funded by GRACE.

ACKNOWLEDGMENTS

We thank Periklis Katopodis for help with figures.

REFERENCES

1. Kishore U, Greenhough TJ, Waters P, Shrive AK, Ghai R, Kamran MF, et al. Surfactant proteins SP-A and SP-D: structure, function and receptors. *Mol Immunol*. (2006) 43:1293–315. doi: 10.1016/j.molimm.2005.08.004
2. Nayak A, Dodagatta-Marri E, Tsolaki AG, Kishore U. An insight into the diverse roles of surfactant proteins, SP-A and SP-D in innate and adaptive immunity. *Front Immunol*. (2012) 3:1–21. doi: 10.3389/fimmu.2012.00131
3. Qaseem AS, Singh I, Pathan AA, Layhadi JA, Parkin R, Alexandra F, et al. A recombinant fragment of human surfactant protein d suppresses basophil activation and T-helper type 2 and B-cell responses in grass pollen-induced allergic inflammation. *Am J Respir Crit Care Med*. (2017) 196:1526–34. doi: 10.1164/rccm.201701-0225OC
4. Wang JY, Shieh CC, You PF, Lei HY, Reid KBM. Inhibitory effect of pulmonary surfactant proteins A and D on allergen- induced lymphocyte proliferation and histamine release in children with asthma. *Am J Respir Crit Care Med*. (1998) 158:510–8. doi: 10.1164/ajrccm.158.2.9709111
5. Madan T, Kishore U, Singh M, Sarma PU, Strong P, Clark H, et al. Surfactant proteins A and D protect mice against pulmonary hypersensitivity induced by *Aspergillus fumigatus* antigens and allergens. *J Clin Invest*. (2001) 107:467–75. doi: 10.1172/JCI10124
6. Mahajan L, Gautam P, Dodagatta-Marri E, Madan T, Kishore U. Surfactant protein SP-D modulates activity of immune cells: proteomic profiling of its interaction with eosinophilic cells. *Expert Rev Proteom*. (2014) 11:355–69. doi: 10.1586/14789450.2014.897612
7. Mahajan L, Madan T, Kamal N, Singh VK, Sim RB, Telang SD, et al. Recombinant surfactant protein-D selectively increases apoptosis in eosinophils of allergic asthmatics and enhances uptake of apoptotic eosinophils by macrophages. *Int Immunol*. (2008) 20:993–007. doi: 10.1093/intimm/dxn058
8. Mahajan L, Pandit H, Madan T, Gautam P, Yadav AK, Warke H, et al. Human surfactant protein D alters oxidative stress and HMGA1 expression to induce p53 apoptotic pathway in eosinophil leukemic cell line. *PLoS ONE*. (2013) 8:1–16. doi: 10.1371/journal.pone.0085046
9. Pandit H, Thakur G, Koippallil Gopalakrishnan AR, Dodagatta-Marri E, Patil A, Kishore U, et al. Surfactant protein D induces immune quiescence and apoptosis of mitogen-activated peripheral blood mononuclear cells. *Immunobiology*. (2016) 221:310–22. doi: 10.1016/j.imbio.2015.10.004
10. Sotiriadis G, Dodagatta-Marri E, Kouser L, Alhamlan FS, Kishore U, Karteris E. Surfactant proteins SP-A and SP-D modulate uterine contractile events in ULTR myometrial cell line. *PLoS ONE*. (2015) 10:1–18. doi: 10.1371/journal.pone.0143379
11. Brigati C, Noonan DM, Albini A, Benelli R. Tumors and inflammatory infiltrates: friends or foes? *Clin Exp Metast*. (2002) 19:247–58. doi: 10.1023/A:1015587423262
12. Hasegawa Y, Takahashi M, Ariki S, Asakawa D, Tajiri M, Wada Y, et al. Surfactant protein D suppresses lung cancer progression by downregulation of epidermal growth factor signaling. *Oncogene*. (2015) 34:838–45. doi: 10.1038/onc.2014.20
13. Don D. S, Paul Man SF, McWilliams A, Lam S. Surfactant protein D and bronchial dysplasia in smokers at high risk of lung cancer. *Chest*. (2008) 134:582–8. doi: 10.1378/chest.08-0600
14. Lin Z, Thomas NJ, Bibikova M, Seifart C, Wang Y, Guo X, et al. DNA methylation markers of surfactant proteins in lung cancer. *Int J Oncol*. (2007) 31:181–91. doi: 10.3892/ijo.31.1.181
15. Takeo I, Hagiwara K, Ikeda S, Arai T, Meino MN, Kumasaka T, et al. Association between genetic variations in surfactant protein D and emphysema, interstitial pneumonia and lung cancer in a Japanese population. *J Chronic Obstr Pulm Dis*. (2012) 9:409–16. doi: 10.3109/15412555.2012.676110
16. Kaur A, Riaz MS, Murugaiah V, Varghese PM, Singh SK, Kishore U. A Recombinant fragment of human surfactant protein D induces apoptosis in pancreatic cancer cell lines via fas-mediated pathway. *Front Immunol*. (2018) 9:1126. doi: 10.3389/fimmu.2018.01126
17. Kaur A, Riaz MS, Singh SK, Kishore U. Human surfactant protein D suppresses epithelial-to-mesenchymal transition in pancreatic cancer cells by downregulating TGF-β. *Front Immunol*. (2018) 9:1–13. doi: 10.3389/fimmu.2018.01844
18. Mangogna A, Belmonte B, Agostinis C, Ricci G, Gulino A, Ferrara I, et al. Pathological significance and prognostic value of surfactant protein D in cancer. *Front Immunol*. (2018) 9:1–12. doi: 10.3389/fimmu.2018.01748
19. Rogers-Broadway KR, Chudasama D, Pados G, Tsolakidis D, Goumenou A, Hall M, et al. Differential effects of rapalogues, dual kinase inhibitors on human ovarian carcinoma cells *in vitro*. *Int J Oncol*. (2016) 49:133–43. doi: 10.3892/ijo.2016.3531
20. Cancer Research UK. *Cancer Research UK - Ovarian Cancer Statistics* (2012). Available online at: https://www.cancerresearchuk.org/health-professional/cancer-statistics-for-the-uk
21. Davies J, Chen J, Pink R, Carter D, Saunders N, Sotiriadis G, et al. Orexin receptors exert a neuroprotective effect in Alzheimer's disease (AD) via heterodimerization with GPR103. *Sci Rep*. (2015) 5:1–12. doi: 10.1038/srep12584
22. Rhodes DR, Yu J, Shanker K, Deshpande N, Varambally R, Ghosh D, et al. ONCOMINE: A cancer microarray database and integrated data-mining platform. *Neoplasia*. (2004) 6:1–6. doi: 10.1016/S1476-5586(04)80047-2
23. Rhodes DR, Kalyana-Sundaram S, Mahavisno V, Varambally R, Yu J, Briggs BB, et al. Oncomine 3.0: genes, pathways, and networks in a collection of 18,000 cancer gene expression profiles. *Neoplasia*. (2007) 9:166–80. doi: 10.1593/neo.07112
24. Chudasama D, Bo V, Hall M, Anikin V, Jeyaneethi J, Gregory J, et al. Identification of cancer biomarkers of prognostic value using specific gene regulatory networks (GRN): a novel role of RAD51AP1 for ovarian and lung cancers. *Carcinogenesis*. (2018) 39:407–17. doi: 10.1093/carcin/bgx122
25. Rogers-Broadway KR, Kumar J, Sisu C, Wander G, Mazey E, Jeyaneethi J, et al. Differential expression of mTOR components in endometriosis and ovarian cancer: effects of rapalogues and dual kinase inhibitors on mTORC1 and mTORC2 stoichiometry. *Int J Mol Med*. (2019) 43:47–56. doi: 10.3892/ijmm.2018.3967
26. Dodagatta-Marri E, Qaseem AS, Karbani N, Tsolaki AG, Waters P, Madan T, et al. Purification of surfactant protein D (SP-D) from pooled amniotic fluid and bronchoalveolar lavage. *Methods Mol Biol*. (2014) 1100:273–90. doi: 10.1007/978-1-62703-724-2_22
27. Singh M, Madan T, Waters P, Parida SK, Sarma PU, Kishore U. Protective effects of a recombinant fragment of human surfactant protein D in a murine

model of pulmonary hypersensitivity induced by dust mite allergens. *Immunol Lett*. (2003) 86:299–307. doi: 10.1016/S0165-2478(03)00033-6
28. Shrive AK, Martin C, Burns I, Paterson JM, Martin JD, Townsend JP, et al. Structural characterisation of ligand-binding determinants in human lung surfactant protein D: influence of Asp325. *J Mol Biol*. (2009) 394:776–88. doi: 10.1016/j.jmb.2009.09.057
29. Shrive AK, Tharia HA, Strong P, Kishore U, Burns I, Rizkallah PJ, et al. High-resolution structural insights into ligand binding and immune cell recognition by human lung surfactant protein D. *J Mol Biol*. (2003) 331:509–23. doi: 10.1016/S0022-2836(03)00761-7
30. Livak KJ, Schmittgen TD. Analysis of relative gene expression data using real-time quantitative PCR and the 2(-Delta Delta C(T)) Method. *Methods*. (2001) 25:402–8. doi: 10.1006/meth.2001.1262
31. Hendrix ND, Wu R, Kuick R, Schwartz DR, Fearon ER, Cho KR. Fibroblast growth factor 9 has oncogenic activity and is a downstream target of Wnt signaling in ovarian endometrioid adenocarcinomas. *Cancer Res*. (2006) 66:1354–62. doi: 10.1158/0008-5472.CAN-05-3694
32. Lu KH, Patterson AP, Wang L, Marquez RT, Atkinson EN, Baggerly KA, et al. Selection of potential markers for epithelial ovarian cancer with gene expression arrays and recursive descent partition analysis selection of potential markers for epithelial ovarian cancer with gene expression arrays and recursive descent partition anal. *Clin Cancer Res*. (2004) 10:3291–300. doi: 10.1158/1078-0432.CCR-03-0409
33. Zhou HY, Wong AST. Activation of p70S6K induces expression of matrix metalloproteinase 9 associated with hepatocyte growth factor-mediated invasion in human ovarian cancer cells. *Endocrinology*. (2006) 147:2557–66. doi: 10.1210/en.2005-1404
34. Chong IW, Chang MY, Chang HC, Yu YP, Sheu CC, Tsai JR, et al. Great potential of a panel of multiple hMTH1, SPD, ITGA11 and COL11A1 markers for diagnosis of patients with non-small cell lung cancer. *Oncol Rep*. (2006) 16:981–8. doi: 10.3892/or.16.5.981
35. Karachaliou N, Mayo-de-las-Casas C, Molina-Vila MA, Rosell R. Real-time liquid biopsies become a reality in cancer tratment. *Ann Transl Med*. (2015) 3:36. doi: 10.3978/j.issn.2305-5839.2015.01.16
36. Fan T, Zhao Q, Chen JJ, Chen WT, Pearl ML. Clinical significance of circulating tumor cells detected by an invasion assay in peripheral blood of patients with ovarian cancer. *Gynecol Oncol*. (2009) 112:185–91. doi: 10.1016/j.ygyno.2008.09.021
37. Huang Q, Li F, Liu X, Li W, Shi W, Liu FF, et al. Caspase 3-mediated stimulation of tumor cell repopulation during cancer radiotherapy. *Nat Med*. (2011) 17:860–6. doi: 10.1038/nm.2385
38. Janicke RU, Sprengart ML, Wati MR, Porter AG. Caspase-3 is required for DNA fragmentation and associated with apoptosis. *Biochemistry*. (1998) 273:9357–60. doi: 10.1074/jbc.273.16.9357
39. Zheng TS, Schlosser SF, Dao T, Hingorani R, Crispe IN, Boyer JL, et al. Caspase-3 controls both cytoplasmic and nuclear events associated with Fas-mediated apoptosis *in vivo*. *Proc Natl Acad Sci USA*. (1998) 95:13618–23. doi: 10.1073/pnas.95.23.13618
40. Armitage RJ. Tumour necrosis factor receptor superfamily members and their ligands. *Curr Opin Immunol*. (1994) 6:407–13.
41. Michaeu O, Tschopp J. Induction of TNF receptor I-mediated apoptosis via two sequential signaling complexes. *Cell*. (2003) 114:181–90. doi: 10.1016/S0092-8674(03)00521-X
42. Chan QKY, Ngan HYS, Ip PPC, Liu VWS, Xue WC, Cheung ANY. Tumor suppressor effect of follistatin-like 1 in ovarian and endometrial carcinogenesis - A differential expression and functional analysis. *Carcinogenesis*. (2009) 30:114–21. doi: 10.1093/carcin/bgn215
43. Gentilella A, Kozma SC, Thomas G. A liaison between mTOR signaling, ribosome biogenesis and cancer. *Biochim Biophys Acta Gene Regul Mech*. (2015) 1849:812–20. doi: 10.1016/j.bbagrm.2015.02.005
44. Beauchamp EM, Platanias LC. The evolution of the TOR pathway and its role in cancer. *Oncogene*. (2013) 32:3923–32. doi: 10.1038/onc.2012.567
45. Foster H, Coley HM, Goumenou A, Pados G, Hervey A, Karteris E. Differential expression of mTOR signalling components in drug resistance in ovarian cancer. *Anticancer Res*. (2010) 30:3529–54.
46. Zhang X, Shu L, Hosoi H, Gopal Murti K, Houghton PJ. Predominant nuclear localization of mammalian target of rapamycin in normal and malignant cells in culture. *J Biol Chem*. (2002) 277:28127–34. doi: 10.1074/jbc.M202625200
47. Guglielmelli T, Giugliano E, Brunetto V, Rapa I, Cappia S, Giorcelli J, et al. mTOR pathway activation in multiple myeloma cell lines and primary tumour cells: Pomalidomide enhances cytoplasmicnuclear shuttling of mTOR protein. *Oncoscience*. (2015) 2:382–94. doi: 10.18632/oncoscience.148
48. Rosner M, Hengstschlager M. Detection of cytoplasmic and nuclear functions of mTOR by fractionation. *Methods Mol Biol*. (2011) 821:105–24. doi: 10.1007/978-1-61779-430-8_8

Conflict of Interest Statement: The authors declare that the research was conducted in the absence of any commercial or financial relationships that could be construed as a potential conflict of interest.

frontiers in Oncology

ORIGINAL RESEARCH
published: 11 July 2019
doi: 10.3389/fonc.2019.00565

Human SP-D Acts as an Innate Immune Surveillance Molecule Against Androgen-Responsive and Androgen-Resistant Prostate Cancer Cells

*Gargi Thakur[1], Gagan Prakash[2], Vedang Murthy[2], Nilesh Sable[2], Santosh Menon[2], Salman H. Alrokayan[3], Haseeb A. Khan[3], Valarmathy Murugaiah[4], Ganesh Bakshi[2], Uday Kishore[4] and Taruna Madan[1]**

[1] Department of Innate Immunity, ICMR-National Institute for Research in Reproductive Health, Mumbai, India, [2] Tata Memorial Hospital, Homi Bhabha National Institute, Mumbai, India, [3] Department of Biochemistry, College of Science, King Saud University, Riyadh, Saudi Arabia, [4] Biosciences, College of Health and Life Sciences, Brunel University London, Uxbridge, United Kingdom

OPEN ACCESS

Edited by:
Massimiliano Berretta, Centro di Riferimento Oncologico di Aviano (IRCCS), Italy

Reviewed by:
Gaetano Facchini, National Cancer Institute G. Pascale Foundation (IRCCS), Italy
Giuseppe Palma, National Cancer Institute G. Pascale Foundation (IRCCS), Italy

***Correspondence:**
Taruna Madan
taruna_m@hotmail.com

Specialty section:
This article was submitted to Molecular and Cellular Oncology, a section of the journal Frontiers in Oncology

Received: 29 March 2019
Accepted: 10 June 2019
Published: 11 July 2019

Citation:
Thakur G, Prakash G, Murthy V, Sable N, Menon S, Alrokayan SH, Khan HA, Murugaiah V, Bakshi G, Kishore U and Madan T (2019) Human SP-D Acts as an Innate Immune Surveillance Molecule Against Androgen-Responsive and Androgen-Resistant Prostate Cancer Cells. Front. Oncol. 9:565. doi: 10.3389/fonc.2019.00565

Surfactant Protein D (SP-D), a pattern recognition innate immune molecule, has been implicated in the immune surveillance against cancer. A recent report showed an association of decreased SP-D expression in human prostate adenocarcinoma with an increased Gleason score and severity. In the present study, the SP-D expression was evaluated in primary prostate epithelial cells (PrEC) and prostate cancer cell lines. LNCaP, an androgen dependent prostate cancer cell line, exhibited significantly lower mRNA and protein levels of SP-D than PrEC and the androgen independent cell lines (PC3 and DU145). A recombinant fragment of human SP-D, rfhSP-D, showed a dose and time dependent binding to prostate cancer cells via its carbohydrate recognition domain. This study, for the first time, provides evidence of significant and specific cell death of tumor cells in rfhSP-D treated explants as well as primary tumor cells isolated from tissue biopsies of metatstatic prostate cancer patients. Viability of PrEC was not altered by rfhSP-D. Treated LNCaP ($p53^{+/+}$) and PC3 ($p53^{-/-}$) cells exhibited reduced cell viability in a dose and time dependent manner and were arrested in G2/M and G1/G0 phase of the cell cycle, respectively. rfhSP-D treated LNCaP cells showed a significant upregulation of p53 whereas a significant downregulation of pAkt was observed in both PC3 and LNCaP cell lines. The rfhSP-D-induced apoptosis signaling cascade involved upregulation of Bax:Bcl2 ratio, cytochrome c and cleaved products of caspase 7. The study concludes that rfhSP-D induces apoptosis in prostate tumor explants as well as in androgen dependent and independent prostate cancer cells via p53 and pAkt pathways.

Keywords: pattern recognition receptor, prostate tumor explants, LNCaP cells, PC3 cells, viability, apoptosis, p53, pAkt

INTRODUCTION

Prostate cancer, an adenocarcinoma of epithelial cell-origin, is the second most frequently diagnosed cancer among men (1). In its early stages, prostate cancer cells rapidly proliferate in an androgen dependent manner, and thus, are treated by androgen deprivation therapy (2). Conventional anti-cancer treatments such as chemotherapy and radiotherapy improve survival, but many patients encounter relapse and metastasis. Following the remittent stage, the cancer progresses to become androgen-independent where most therapeutic strategies fail.

Immunotherapy by stimulating pattern recognition receptors of the innate immune system such as toll-like receptors (TLRs) has shown promise as a preferred adjunct treatment against cancer (3). Imiquimod, a synthetic imidazoquinoline and an agonist that targets TLR-7 and induces the production of pro-inflammatory cytokines including IFN-α, IL-6, and TNF-α, inhibited cancer growth in the mouse prostate via apoptosis induction (4, 5).

Collectins are pattern recognition proteins belonging to the C-type lectin family. They are composed of an N-terminal cysteine-rich region, a triple-helical collagen domain, an α-helical coiled-coil neck region, and C-terminal carbohydrate recognition domain (CRD) (6). Surfactant Protein D (SP-D) is one of the most studied collectins with a vital role in host defense against pathogens and allergens, and modulation of inflammatory response (6). Although SP-D was historically shown to be lung-resident being produced by type II alveolar and Clara cells (7), studies during the last decade have established its extrapulmonary existence in a range of tissues (8). SP-D has also been shown to be expressed in the male reproductive tracts of human and mice (9, 10). Elevated levels of SP-D at inflamed sites in the prostate manifested protection against bacterial infection (11, 12). Kankavi et al. (13) observed differential expression of SP-D in glandular structures of inflamed malignant and non-malignant human prostate tissues. There was a significant correlation between decreased levels of SP-D and increased Gleason score, a grading system based on the histologic pattern of arrangement of carcinoma cells, and tumor volume.

Previously, we reported a novel anti-cancer role of human SP-D and its recombinant fragment (rfhSP-D) comprising 8 Gly-X-Y repeats neck and CRD region, wherein they reduced the viability of a range of human cancer cell lines including eosinophilic leukemia cell line (AML14.3D10) (14). Importantly, survival of peripheral blood mononuclear cells (PBMCs) derived from healthy individuals was found to be unaltered (14). rfhSP-D treated AML14.3D10 cells showed a significant increase in apoptosis with reduced HMGA1 levels and increased levels of activated p53 and caspase 9 (14). SP-D has recently been shown to inhibit the proliferation, migration and invasion of A549 human lung adenocarcinoma cells by binding to N-glycans of epidermal growth factor receptor (EGFR) via its CRD region, and interfering with EGF signaling (15). In UV treated apoptotic Jurkat T cells, SP-D enhanced membrane and nuclear blebbing, suggesting involvement of SP-D in induction of apoptosis (16). Exogenous treatment of SKOV3 cells (an ovarian cancer cell line) with rfhSP-D led to increased caspase 3 cleavage and induction of pro-apoptotic genes Fas and TNF-α (17).

To take the next logical step from the reported anti-cancer role of SP-D in tumorigenic cell lines, we examined anti-prostate cancer role of rfhSP-D using tumor explants and primary cells derived from tissue biopsies of metastatic prostate cancer patients. rfhSP-D induced apoptosis selectively in various prostate cancer cells including the two prostate cancer cell lines (LNCaP and PC3) in a dose- and time-dependent manner. Apoptotic signaling involved upregulation of p53 and downregulation of pAkt. Decreased levels of Bcl2, with a concomitant increase in Bax, cytochrome c and cleavage of caspase 7, confirmed rfhSP-D mediated induction of intrinsic apoptosis.

MATERIALS AND METHODS

Ethics Statement

The study was approved by the Institutional Ethics Committee for Clinical Studies, ICMR- National Institute for Research in Reproductive Health; (Project No.: 260/2014) and Institutional Ethics Committee, Tata Memorial Hospital (Study no: 1467). Tissue biopsy samples were collected from 9 suspected metastatic prostate cancer patients (treatment naïve) undergoing Transrectal Ultrasound guided multiple core needle biopsy, with written informed consent. Chemotherapy was initiated in the patients after confirmation of metastasized prostate cancer. Information regarding the androgen dependency of the prostate cancer in these patients was not available. Average age of the study participants was 67.4 ± 3.97 years with Mean PSA (Prostate- specific antigen) level of 190.04 ± 85.12 ng/ml and Median Gleason score of 8 ± 0.83.

Explant and Cell Culture

Prostate tissue biopsies were collected in cold Phosphate Buffer saline containing 10% v/v fetal bovine serum (FBS; GIBCO) and 2% v/v Pen-Strep solution (GIBCO) and immediately processed in sterile conditions. Biopsies were cut into 5 mm explants, placed in the scratched areas of 35 mm tissue culture plate (Nunc) and cultured in RPMI 1640 (GIBCO) supplemented with 10% FBS, 1% Pen-Strep solution, Glucose (1 mg/ml) (HiMedia) and 1% Sodium Pyruvate (GIBCO) (complete RPMI) for a week. Primary Cancer Epithelial Cells (PrCEC) isolated from the explants were sub-cultured using 5 mM EDTA (Sigma) in PBS and passaged further. Isolated PrCEC (Passage 2) were examined for Cytokeratin (an epithelial cell marker) via immunofluorescence microscopy (Anti-cytokeratin antibody, Dako, 1:500) and by Real time RT-PCR analysis for CD164 expression, a marker for metastatic epithelial cell cancer (18). Isolated PrCEC were stained for the presence of Alpha-methylacyl-CoA racemase (AMACR) expression, which is upregulated in prostate cancer with high-grade prostatic intraepithelial neoplasia (HGPIN) than in the normal human prostate (19). PrEC, PrCEC and PC3 cells were stained using mouse monoclonal antibodies to AMACR (Novus Biologicals, 1:100) or matched-isotype control IgG for 1 h at 4°C. Phycoerythrin-conjugated rat anti-mouse IgG (Molecular Probes, Eugene, USA) was used as secondary antibody. The gated cell population was determined using PE tagged anti-AMACR. Cells were analyzed via BD FACS Aria III (BD Biosciences, San Jose, California, USA) flow cytometer.

Human prostate cancer cell lines, LNCaP (androgen dependent, $p53^{+/+}$), DU145 (androgen independent $p53^{+/-}$) and PC3 (androgen independent, $p53^{-/-}$) (ATCC, Rockville, MD, USA) were cultured in complete RPMI 1640 medium. Human primary prostate epithelial cells (PrEC; LONZA) were maintained in Prostate epithelial growth medium (PrEGM Bulletkit) supplemented with Triiodothyronine (T3), Transferrin, Bovine Pituitary Extract (BPE), recombinant human Epidermal growth factor (rhEGF), GA-1000, Insulin, Hydrocortisone, Epinephrine, and retinoic acid (LONZA, Cat no. CC-3165). All experiments with Human PrEC were completed within first five passages. Cells were grown at 37°C under 5% v/v CO_2 until 70–80% confluency was attained.

rfhSP-D Preparation

The recombinant fragment of human SP-D (rfhSP-D) was expressed in *Escherichia coli* BL21 (λDE3) pLysS (Invitrogen), purified and characterized, as described previously (15). Endotoxin level in the rfhSP-D preparation was determined using the QCL-1000 Limulus amebocyte lysate system (BioWhittaker Inc., USA). The assay was linear over a range of 0.1–1.0 EU/ml (10 EU = 1 ng of endotoxin) and the amount of endotoxin present in the preparations was found to be <4 pg/μg of rfhSP-D.

Interaction Between FITC Labeled rfhSP-D and Prostate Cells

rfhSP-D was labeled with FITC dye (20) and incubated with prostate epithelial cells and prostate cancer cells at 5, 10, and 20 μg/ml concentration in staining buffer for 15, 30, 45, and 60 min at 4°C in the presence of 2 mM $CaCl_2$. Cells were washed to remove unbound rfhSP-D and fixed with 2% PFA for analysis via BD FACS Aria III (BD Biosciences, San Jose, California, USA). Data was analyzed using FCS Express 6 De Nova software. To assess the specificity of the interaction, PC3 cells were incubated with FITC labeled rfhSP-D in the presence of 5 mM $CaCl_2$, or 5 mM EDTA, or 5 mM Glucose in PBS, pH 7.4. Staining buffer was used as control for these experiments.

Cell Viability Assay

Human PrEC (passage no. 3–5), LNCaP, PC3, or PrCEC (passage no. 3–5) cells (5×10^3) were placed in 96-well tissue culture plates (Nunc) and grown overnight. Cells were then starved in cell appropriate serum free media (PrEC and PrCEC for 4 h; LNCaP cells for 12 h; PC3 cells for 18 h) and treated with rfhSP-D (5, 10, and 20 μg/ml) for 24, 48, and 72 h. Cells alone in the culture medium served as an untreated control. After incubation 10 μl MTT [3-(4, 5-dimethylthiazol-2-yl)-2, 5-diphenyltetrazolium bromide] (5 mg/ml stock) was added to each well and incubated at 37°C for 4 h. Formazan crystals were dissolved in acidified isopropanol and absorbance was read at 570 nm (Beckman Coulter).

Cell Cycle Analysis

LNCaP or PC3 cells (2×10^4) were plated in 12-well tissue culture plate, starved for 18 h in serum-free RPMI medium serum-free RPMI medium, and then treated with rfhSP-D (20 μg/ml) for 48 h. After incubation, cells were trypsinized, suspended in cold hypotonic solution containing 0.1% sodium citrate, 0.3 μl/mL of NP-40 (Sigma), 2 mg/mL RNaseA (Thermo Fisher Scientific), and 50 μg/mL Propidium Iodide (PI; Sigma) for 20 min, and then analyzed using BD FACS Aria III using BD FACS DIVA software (21).

Fluorescence Microscopy for Nuclear Morphology

PrEC, LNCaP, or PC3 cells (2×10^3) were grown on coverslips and incubated with rfhSP-D (20 μg/ml) for 48 h to analyze nuclear morphology following induction of apoptosis. Cells were fixed in 2% PFA and permeabilized using 1% v/v Triton X 100 (Sigma). Cells were incubated with Hoechst (1:10,000, Invitrogen) for 20 min in dark. Coverslips were mounted in vector shield (Vector laboratories, UK) and observed under confocal microscope (Zeiss, Germany).

TUNEL (Terminal Deoxynucleotidyl Transferase dUTP Nick end Labeling) Assay

Prostate tissue biopsies collected from metastatic prostate cancer patients were incubated with rfhSP-D (40 μg/ml) for 48 h in serum free RPMI medium at 37°C under 5% v/v CO_2. Five micrometer paraffin embedded sections of 10% NBF (neutral-buffered formalin) fixed prostate tissue biopsies were placed on poly L-lysine coated slides. The sections were fixed with chilled acetone followed by washing with PBS. Slides were incubated in TUNEL Mix (Roche Diagnostics), containing terminal deoxynucleotidyl transferase (TdT) and fluorescein labeled nucleotides for an hour in a moist chamber at 37°C. The slides were washed and counterstained with DAPI (4′,6-diamidino-2-phenylindole). TUNEL positive apoptotic cells (green-stained cells) were viewed under confocal microscope (Zeiss, Germany).

Annexin V Assay

For Annexin-V immunostaining, the manufacturer's protocol of Annexin V-FITC apoptosis detection kit (Calbiochem) was followed with some modifications. PrEC, LNCaP, or PC3 were treated with indicated concentrations of rfhSP-D and harvested at the end of 24 and 48 h. Cells were trypsinized and washed with ice cold PBS to remove culture supernatant, followed by incubation with FITC-tagged Annexin V for 20 min in dark. Subsequently, Annexin V was washed and 1 μl PI was added to stain the DNA. Cells were immediately analyzed via BD FACS Aria III.

Western Blot

PC3 or LNCaP cells (1×10^6) were plated in a six-well plate and incubated with or without rfhSP-D (20 μg/ml), in serum-free RPMI medium for 12 h and 24 h. The cells were lysed in lysis buffer (50 mM Tris-HCL, pH7.5, 150 mM NaCl, 1% Triton X, 1 mM Sodium orthovanadate, 10 mM β- glycerophosphate, 2 mM EDTA, 10 mM Sodium pyrophosphate) and analyzed by western blotting. Lysate proteins (30 μg) were separated on 15% SDS-PAGE polyacrylamide gel and electrophoretically transferred onto PVDF membranes (Pall Corporation, NY, USA). The blot

was probed with primary antibodies raised against human SP-D [a gift from Uffe Holmskov, (13)], Phosphorylated-p53 (Ser 15) (Cell Signaling Technology), pAKT (PathScan® Multiplex Western Cocktail I), pan Akt (ABclonal), phospho-Bad-S155 (ABclonal), Bcl-2 associated death promoter (Bad) (Apoptosis I sampler Kit), Bcl-2-associated X protein (Bax) (Apoptosis I sampler Kit), B-cell lymphoma 2 (Bcl2) (Apoptosis I sampler Kit) or caspase 7 (Cell Signaling Technology), followed by HRP-conjugated secondary antibodies. All western blot images were acquired by Syngene (Chem Genius) and quantified by Syngene Gene Tools.

Enzyme-Linked Immnosorbent Assay (ELISA) for SP-D and Cytochrome c

Cell lysates and culture supernatants were analyzed for SP-D levels (Duo Set Human SP-D, catlog no. DY1920, R & D Systems) and Cytochrome c (Human Cyt-C, catlog no. E1516Hu, BT Assay) using commercially available ELISA kits. Briefly, for quantification of cytochrome c, PrEC, LNCaP, PC3 cells, or Prostate tissue biopsies collected from metastatic prostate cancer patients were incubated with indicated concentrations of rfhSP-D for 48 h. Cell culture supernatant was analyzed for cytochrome c released by cells. Color development was stopped using 2N H_2SO_4 and optical density was determined at 450 nm using a microplate reader (Beckman Coulter).

Real Time PCR

PrEC, PrCEC, PC3, and LNCaP cells (1×10^6) were plated in a six-well plate and total RNA was isolated using Trizol (Takara) that was further treated with DNase I (Thermo Scientific, Rockford, USA) at 37°C for 30 min to eliminate genomic DNA contamination. One to two microgram of total RNA was reverse transcribed into cDNA using Superscript III first strand synthesis kit (Invitrogen, USA). One microliter of cDNA was used for real time PCR reactions using BioRad CFX96 TouchTM real-time PCR detection system and iQTM SYBR Green Supermix (Bio-Rad, Hercules, CA, USA). 18S was used as housekeeping control. Each qPCR experiment was performed in triplicates and each experiment was repeated 3 times. Primers were designed using NCBI Primer BLAST Software and their annealing temperatures and product sizes are mentioned in **Table 1**.

In silico Analysis of Human SP-D Promoter Region for Androgen Responsive Elements

In silico analysis was carried out to predict putative androgen responsive elements (ARE) in promoter regions of human SP-D gene using MatInspector Genomatix v3.4 Software, GmbH, Munchen (Germany). The transcription start site (TSS) for SP-D was determined from the Institute of Bioinformatics and Applied Biotechnology (IBAB) MGEx-Tdb database. Promoter regions −10,000 bp upstream and +1,000 bp downstream from the transcription start site (TSS sites) were submitted for analysis.

Statistical Analysis

GraphPad PRISM Software version 6.00 (GraphPad Software Inc., San Diego, CA) was used to plot the graphs and analyze the data using one-way ANOVA with Bonferroni corrections for comparison among prostate cells or unpaired two tailed Student's *t*-test for comparing the rfhSP-D treated groups with control. Data is represented as mean ± SD. Values of $p < 0.05$ were considered statistically significant.

RESULTS

Prostate Epithelial and Cancer Cells Expressed SP-D

Since it is known that prostate epithelial cells secrete SP-D (11, 13), we evaluated SP-D expression and its regulation in PrEC, LNCaP, DU145, and PC3. **Figure 1A** shows that SP-D is expressed by prostate epithelial cells and prostate tumor cells; SP-D expression in LNCaP cells is significantly lower in comparison with DU145 ($p < 0.05$), PC3 ($p < 0.05$), and PrEC ($p < 0.05$) by western blot and ELISA (PrEC-1.48 ± 0.31 pg of SP-D/μg of total protein; LNCaP-1.26 ± 0.28 pg/μg; DU145-1.50 ± 0.35 pg/μg, data not shown). SP-D was detectable in the cell culture supernatants of various prostate cells (Range-150 ± 21 to 260 ± 35 pg/ml), suggesting that SP-D is secreted, though not sufficient enough to induce apoptosis (10–20 μg/ml) (14). It is reported that androgen induces proliferation of prostate epithelial cells and LNCaP cells via androgen receptors (22). Furthermore, SP-D expression in rodent prostate is altered on castration (11). Hence, we evaluated levels of SP-D transcripts in Dihydrotestosterone (DHT) treated PrEC, LNCaP, and PC3 cells. Treatment with DHT (10 nM) significantly upregulated SP-D transcripts in both PrEC and LNCaP cells by 1.9 fold but not in PC3 cells (androgen independent) (**Figure 1B**). This suggests that SP-D expression is regulated by androgens (DHT) in androgen dependent cancer. Increased cell viability was observed in DHT treated PrEC (111.43 ± 4.69%) and LNCaP (119.23 ± 2.68%) cells as reported [**Figure 1B** (ii)]. *In silico* analysis of promoter region of human SP-D gene elucidated 10 putative Androgen Responsive Elements (AREs) (**Table 2**), suggesting that androgens may regulate SP-D expression. The functionality of identified ARE has not been evaluated in this study.

rfhSP-D Binds Differentially to Prostate Cancer Cells

FITC-labeled rfhSP-D showed a dose and time dependent binding to PrEC and prostate cancer cells (LNCaP, DU145, and PC3) (**Figure 2**). A significantly higher binding was observed with the androgen independent PC3 cells (MFI-743.86 ± 67.41) than the androgen dependent LNCaP cells (MFI-354.75 ± 54.11) ($p < 0.05$) (**Figure 2A**). PrEC (MFI-96.48 ± 21.07) showed comparatively less binding with the FITC-labeled rfhSP-D than any of the cancer cells (PC3, LNCaP, $p < 0.05$). Binding of rfhSP-D to all cell types was calcium- and carbohydrate-dependent that was inhibitable by EDTA and glucose (**Figures 2B,C** show representative binding to PC3 cells). DU145 cells showed results similar to that of PC3 cells (data not shown).

TABLE 1 | Primer sequences.

Transcripts	Forward primer (5′-3′)	Reverse primer (5′-3′)	Tm (°C)	Product size (in bp)
SP-D	AGGCTGCTTTCCTGAGCATGAC	CCATTGGTGAAGATCTCCACACAG	57.8	148
CD164	GACTTTAGCGCCCATCTCCA	GCCGTGGAAACGGAACAGAA	68	233
BCL2	GCGTCAACCGGGAGATGTCGCCC	TTTCTTAAACAGCCTGCAGCTTTG	66	208
BAX	AGTGACCCCTGACCTCACTG	GCAGGGGACTGAGATGAACG	68	296
BAD	GAGCTCCGGAGGATGAGTGA	CAAGTTCCGATCCCACCAGG	68	141
18S	GGAGAGGGAGCCTGAGAAAC	CCTCCAATGGATCCTCGTTA	64	174

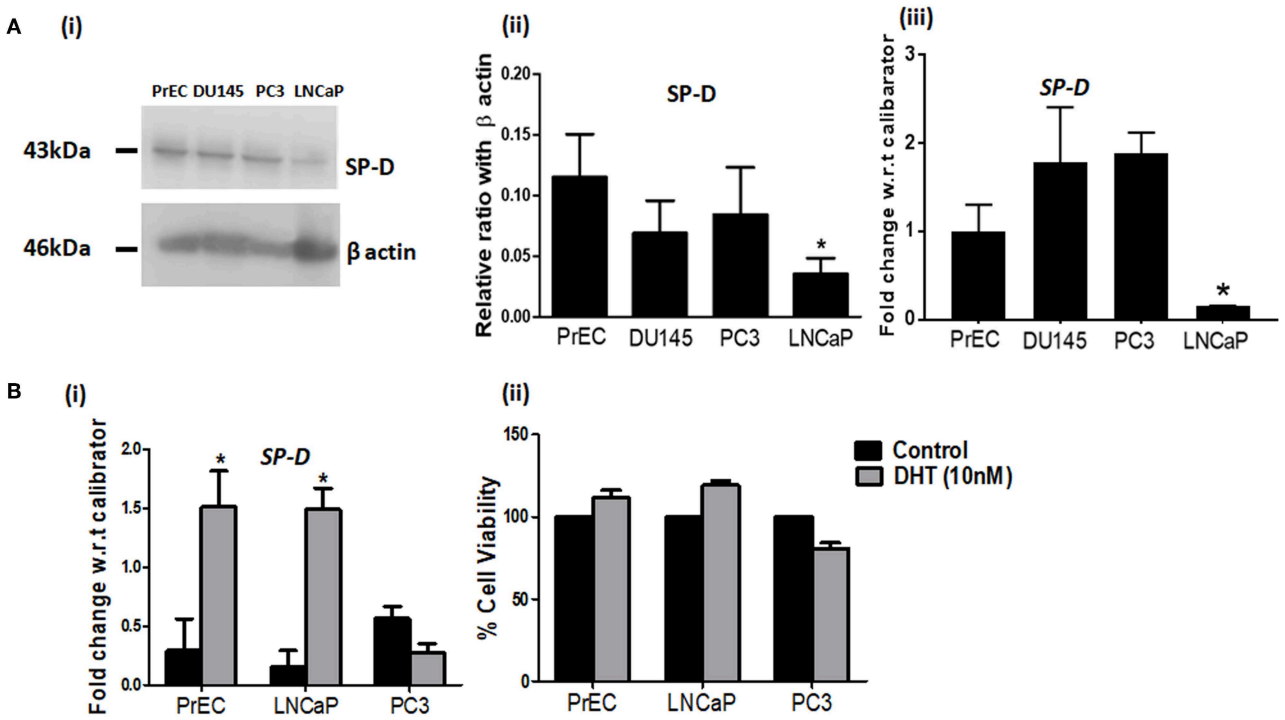

FIGURE 1 | SP-D expression is regulated by Dihydrotestosterone (DHT) in prostate cells. **(A)** Levels of SP-D protein by immunoblotting (i) and transcripts by real time RT-PCR (iii) in PrEC, DU145, PC3, and LNCaP cell lysates. Panel (ii) shows densitometric analysis for the SP-D expression in PrEC, DU145, PC3, and LNCaP cells; $n = 3$ independent experiments, error bar represents the S.D. $^*p < 0.05$. **(B)** (i) SP-D transcripts in PrEC, LNCaP, and PC3 cells treated with DHT (10 nM) for 48 h. $^*p < 0.05$ relative to untreated controls; $n = 3$ independent experiments, error bar represents the S.D. (ii) Cell viability of PrEC, LNCaP, and PC3 cells incubated with DHT (10 nM) for 48 h by MTT assay. Each bar represents % viability ± S.D of three independent experiments. $^*p < 0.05$, relative to untreated controls.

TABLE 2 | Putative Androgen Responsive Elements in the promoter region of human SP-D gene[a].

Sr.		Start	End	Anchor	Core Sim.	Matrix Sim.	Strand	Sequence
1	ARE	904	922	913	0.898	0.938	+	ataagacctcctGTGCtcc
2	ARE	2,339	2,357	2,348	1	0.895	–	gaaatgcttaaaGTTCtaa
3	ARE	3,787	3,805	3,796	1	0.912	–	ccaaagctttgtGTTCcct
4	ARE	5,430	5,448	5,439	0.878	0.901	+	ttttttctttcaGTACttt
5	ARE	5,851	5,869	5,860	1	0.912	+	ttttttctttttGTTCctc
6	ARE	7,481	7,499	7,490	1	0.941	+	gccataccttatGTTCtgc
7	ARE	7,589	7,607	7,598	1	0.8	+	caggtgctatcTGTTgttg
8	ARE	8,303	8,321	8,312	0.875	0.945	–	gctgcacccactGTCCtgc
9	ARE	8,366	8,384	8,375	0.869	0.896	–	ccctgacccctGTGCtct
10	ARE	9,883	9,901	9,892	0.959	0.907	–	ttctctctggctGTCCtta

[a]*MatInspector Genomatix v3.4 Software was used for in silico analysis of human SP-D gene promoter region −10,000 bp upstream to +1,000 bp downstream from the TSS site.*

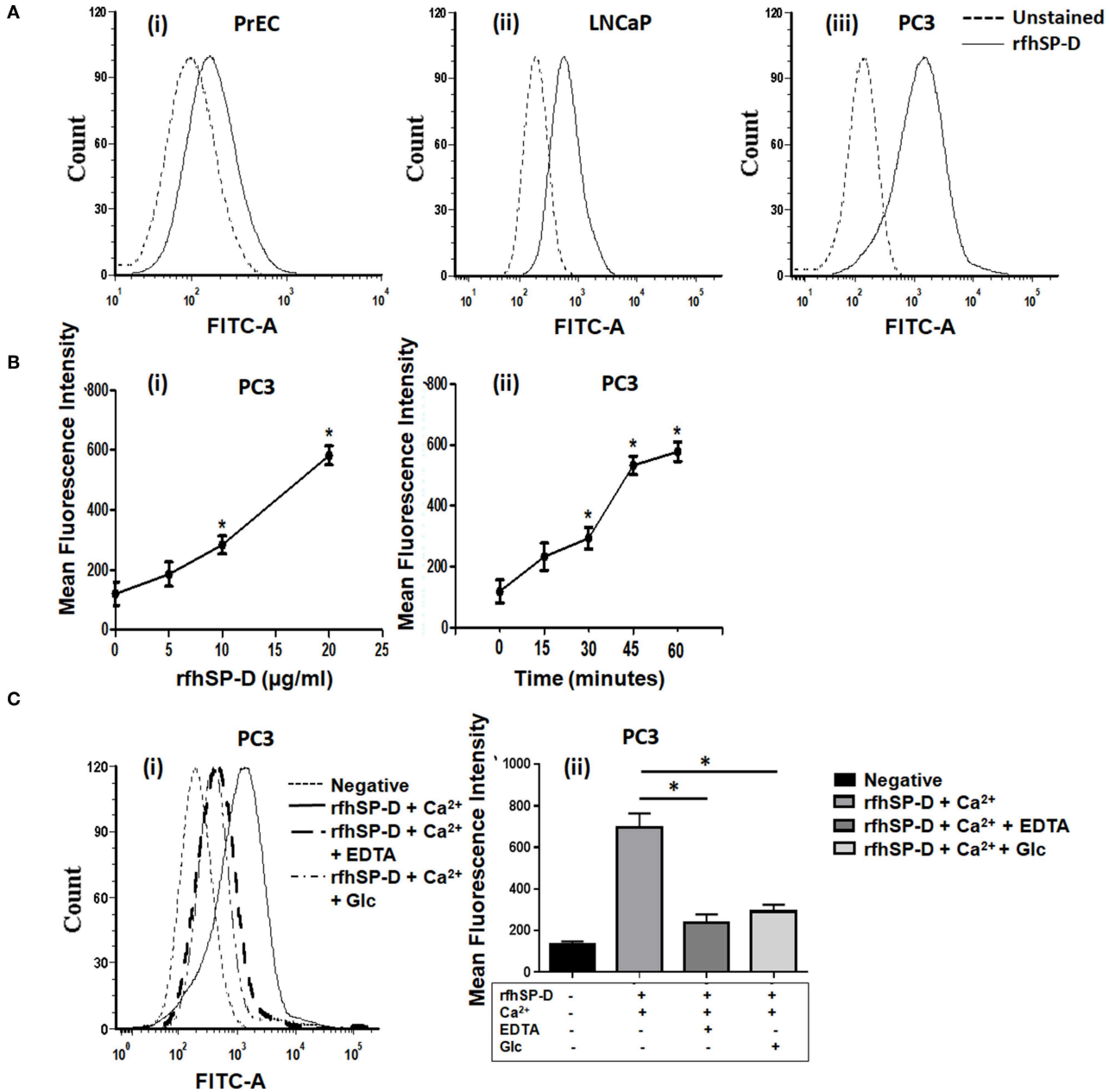

FIGURE 2 | rfhSP-D differentially binds to normal prostate epithelial cells and cancer cells. **(A)** Binding of FITC labeled rfhSP-D to normal prostate epithelial cells (PrEC) and cancer cell lines (LNCaP and PC3) (representative histograms). Black dotted line represents unstained cells, black line shows rfhSP-D (20 μg/ml) binding to (i) PrEC, (ii) LNCaP, (iii) PC3 in comparison to their respective unstained. Each experiment was repeated three times. **(B)** Mean Fluorescence Intensity (MFI) of FITC labeled rfhSP-D binding to PC3 cells (i) at different doses of rfhSP-D and, (ii) time intervals. Data represents mean ± S.D of three independent experiments. *$p < 0.05$, vs. unstained cells. **(C)** Involvement of CRD region of rfhSP-D in its interaction with PC3 cells. (i) PC3 cells were incubated with FITC labeled rfhSP-D alone and in the presence of 5 mM Calcium (Ca^{2+}) or 5 mM Ca^{2+} and 5 mM EDTA (EDTA) or 5 mM Ca^{2+} and 5 mM Glucose (Glc). A representative FACS histogram of PC3 cells with FITC-labeled rfhSP-D (20 μg/ml) showing decreased binding in presence of EDTA and glucose. (ii) Data are Mean ± S.D. of the mean fluorescence intensity of rfhSP-D binding to the PC3 cells relative to control; $n = 3$ independent experiments. *$p < 0.05$.

Anti-prostate Cancer Activity of rfhSP-D in PrCEC and Tumor Explants

We first carried out a pilot investigation on the effect of rfhSP-D on the primary cells derived from tissue biopsies of metastatic PCa patients ($n = 9$). Isolated PrCEC (Passage 2) showed positive staining for Cytokeratin (**Figure 3C**). Expression of AMACR (which is upregulated in prostate cancer with high-grade prostatic intraepithelial neoplasia) in PrCEC was not significantly

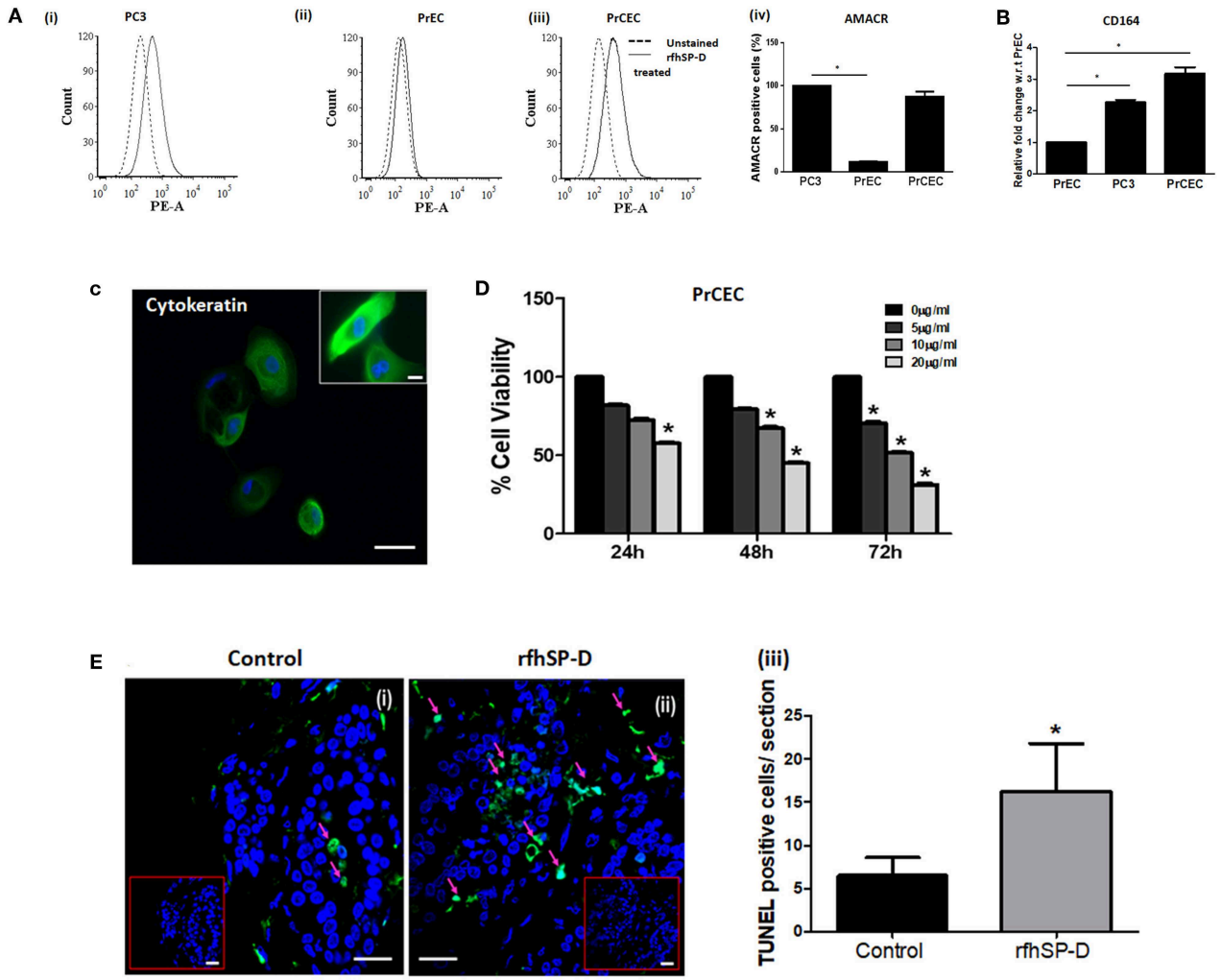

FIGURE 3 | rfhSP-D reduced viability of primary Cancer Epithelial Cells (PrCEC) isolated from the metastatic prostate cancer tissue biopsies and enhanced apoptosis in tumor explants. **(A)** FACS analysis of PE tagged anti-AMACR (prostate cancer marker) expression in PrEC ($n = 3$) (i), PC3 ($n = 3$) (ii), and isolated PrCEC ($n = 9$) (iii) cell population (representative histograms). Dotted black line histogram represents isotype control. The black line histogram indicates AMACR expression. Data (iv) represents mean of positively stained AMACR cell population (%), error bar represents the S.D. $^*p < 0.05$ vs. PC3. **(B)** Transcript levels of CD164 (marker for metastatic epithelial cell cancer) in PrEC ($n = 3$), PC3 ($n = 3$), and PrCEC ($n = 9$). Data represents the mean of three independent experiments, error bar represents the S.D. $^*p < 0.05$ vs. PrEC. **(C)** Positive immunofluorescence staining for FITC tagged anti-Cytokeratin, a marker for epithelial cells. Inset: Higher magnification, Scale bar = 20 µm. **(D)** PrCEC were incubated with different concentrations of rfhSP-D (5, 10, or 20 µg/ml) for the indicated time intervals (24, 48, and 72 h) ($n = 5$). Each bar represents % viability ± S.D, $^*p < 0.05$, relative to untreated controls. **(E)** TUNEL assay of tissue biopsies from metastatic prostate cancer patients exogenously treated with rfhSP-D (40 µg/ml) for 48 h. Untreated tissue biopsy (i) showed significantly less number of TUNEL positive cells when compared with the treated biopsy, (ii) from the same individual. Scale bar, 20 µm. (iii) TUNEL+ve cells were quantitated and are shown as the number of TUNEL+ve cells per section (six sections per tissue biopsy). $^*p < 0.05$, relative to untreated controls.

different than the PC3 cells whereas PrEC cells showed significantly decreased expression (**Figure 3A**). PrCEC and PC3 cells showed significantly upregulated expression of CD164 in comparison with PrEC (**Figure 3B**). PrCEC cells isolated from the metastatic PCa patients showed significantly reduced viability in a dose- and time-dependent manner following treatment with rfhSP-D (**Figure 3D**). Importantly, TUNEL assay confirmed increased apoptosis in rfhSP-D treated tissue biopsies of the same patients (**Figure 3E**). Since these metastatic PCa patients were not evaluated for androgen-dependency, we could not assess if rfhSP-D induced cancer cell death would vary with androgen resistance. Therefore, we pursued further studies to delineate the molecular mechanisms for rfhSP-D mediated apoptosis in androgen dependent (LNCaP) and independent (PC3) cancer cell lines.

rfhSP-D Selectively Reduced the Viability of Prostate Cancer Cells

Reduction in the viability of PCa cells following rfhSP-D treatment was dose- and time-dependent,

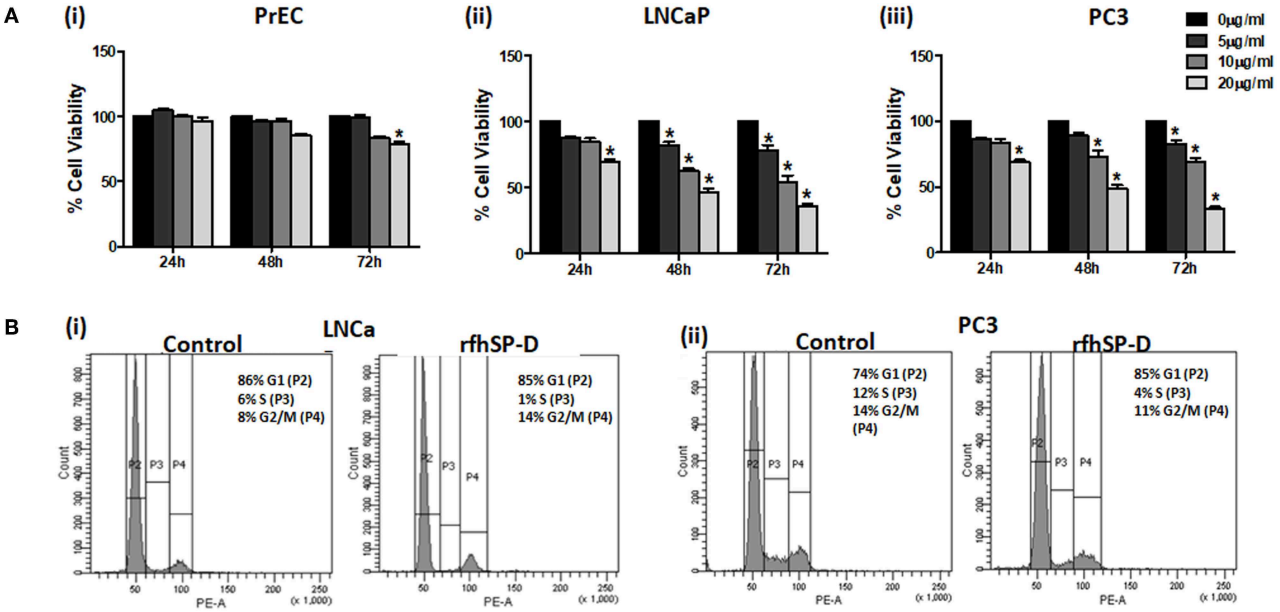

FIGURE 4 | rfhSP-D treated LNCaP and PC3 cells showed increased cell cycle arrest. **(A)** (i) Normal prostate epithelial cells (PrEC); prostate cancer cell lines, LNCaP (ii) and PC3 (iii) were incubated with different concentrations of rfhSP-D (5, 10, or 20 μg/ml) for the indicated time intervals (24, 48, and 72 h). Each bar represents % viability ± S.D. of three independent experiments. *$p < 0.05$, relative to untreated controls. **(B)** (i) LNCaP ($p53^{+/+}$) cells and (ii) PC3 ($p53^{-/-}$) cells were incubated in the presence of rfhSP-D (20 μg/ml) or in culture medium alone (control) for 48 h and were subjected to flowcytometric cell cycle analysis. The figure is a representative histogram of one of the three independent experiments. The total population of cells has been divided in the G1, S, and G2 phases and analyzed using BD FACS DIVA software. Treated LNCaP (p53+/+) cells showed growth arrest in G2/M phase (14.8 ± 1.7%) in comparison with the untreated cells (8.36 ± 1.58%) ($p < 0.05$). Treated PC3 ($p53^{-/-}$) cells showed growth arrest in G0/G1 phase (79.3 ± 3.02%) in comparison with the untreated cells (69.6 ± 4.50%) ($p < 0.05$).

TABLE 3 | IC_{50} values of rfhSP-D induced cell death in various prostate cancer cells at 48 h.

Prostate cancer cells	IC_{50} for rfhSP-D (μg/ml)
PrEC	94.54 ± 3.97
LNCaP	23.14 ± 3.70
PC3	31.98 ± 3.42
DU145	24.80 ± 2.94

irrespective of their androgen sensitivity whereas the viability of rfhSP-D treated PrEC was unaltered till 48 h (**Figure 4A**). The half-maximal inhibitory concentration (IC_{50}) of rfhSP-D against the PCa cells is tabulated as **Table 3**.

rfhSP-D Caused Blockade in the Cell Cycle of Prostate Cancer Cells

We further analyzed the effect of rfhSP-D on the percentage of cells in various phases of the cell cycle (**Figure 4B**). rfhSP-D treatment significantly reduced the S-phase peak with an accumulation of cancer cells in either G0/G1 or G2/M cell cycle phases. At 48 h, we observed growth arrest of LNCaP ($p53^{+/+}$) cells in G2/M (14.8 ± 1.7%) as compared to the untreated control (8.36 ± 1.58%) ($p < 0.05$). There was a significant increase (79.3 ± 3.02%) in G0/G1 population in the rfhSP-D treated PC3 ($p53^{-/-}$) cells, in comparison with the untreated cells (69.6 ± 4.50%) ($p < 0.05$). Cell cycle inhibition following treatment with rfhSP-D was consistent with the cell viability results. No cell cycle arrest was observed in the PrEC (data not shown), which confirmed that the rfhSP-D mediated cell cycle arrest was specific to cancer cells.

rfhSP-D Induced Apoptosis in LNCaP and PC3 Cells

Annexin-V, a classical marker of the apoptosis, was evaluated by flow cytometry. A significant increase in the annexin-V positive cells was observed post 48 h in rfhSP-D treated LNCaP (19.13 ± 2.69%[Q2] and 25.82 ± 1.14% [Q4]) ($p < 0.05$) and PC3 (40.32 ± 2.24% [Q2] and 7.405 ± 1.63% [Q4]) ($p < 0.05$) cells as compared to treated PrEC (2.63 ± 1.41% [Q2] and 3.9 ± 1.95% [Q4]) (**Figure 5A**). rfhSP-D promoted karyorrhexis (fragmentation of nucleus) of LNCaP and PC3 cells at 48 h, as seen in Hoechst stained cells (**Figure 5B**).

rfhSP-D Triggered Intrinsic Mitochondrial Apoptosis in the Prostate Cancer Cells

p53 and PI3K/Akt are involved in several cellular physiological processes including apoptosis and cell proliferation. Our previous study had shown involvement of p53 in the rfhSP-D mediated apoptosis of AML14.3D10 cells (12). Here, rfhSP-D treated LNCaP cells with a wild type p53, showed significant upregulation of p53 (**Figure 6A**). To understand the other likely mechanisms of apoptosis, p53 null PC3 cells were examined

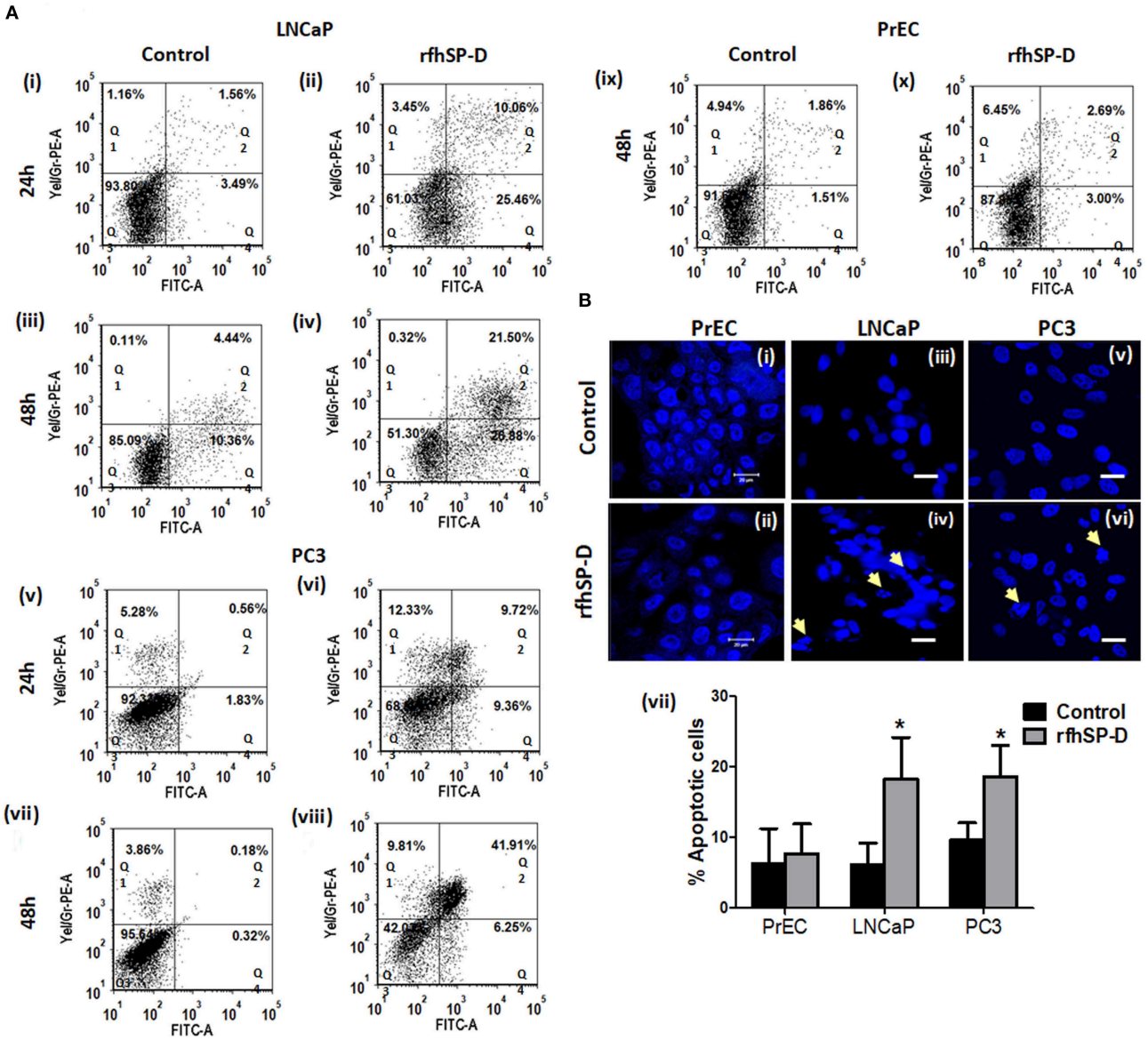

FIGURE 5 | Significant increase in apoptosis in rfhSP-D treated prostate cancer cells. **(A)** Dot blots showing Annexin V-FITC and PI staining of PrEC, LNCaP, and PC3 cells incubated with rfhSP-D (20 μg/ml) for 24 and 48 h. Q1 represents necrotic cells, Q2 show Annexin V FITC and PI double positive cells in late apoptosis, Q3 is unstained cells and Q4 represents Annexin V FITC positive cells in early apoptosis. (i) LNCaP 24 h control, (ii) LNCaP 24 h rfhSP-D treated, (iii) LNCaP 48 h control, (iv) LNCaP 48 h rfhSP-D treated, (v) PC3 24 h control, (vi) PC3 24 h rfhSP-D treated, (vii) PC3 48 h control, (viii) PC3 48 h rfhSP-D treated, (ix) PrEC 48 h control, (x) PrEC 48 h rfhSP-D treated. The figure shows representative histograms from one of the three independent experiments. The total cell population has been divided into four quadrants and analyzed using FCS Express 6 software. **(B)** Fluorescence microscopy images showed that rfhSP-D promotes karyorrhexis of LNCaP and PC3 cells at 48 h after staining with highly diluted Hoechst DNA stain (1 μg/ml). (i), (iii), and (v) represent normal nuclear morphology of PrEC, LNCaP, and PC3 cells; (ii), (iv), and (vi) represent effect of rfhSP-D on nuclear morphology of PrEC, LNCaP, and PC3 cells. "White arrows" indicate disintegrated nucleus. Scale bar, 20 μm. (vii) Percent apoptotic cells was recorded in all the cell types with and without rfhSP-D treatment, each bar represents the mean ± S.D. of three independent experiments. *$p <$ 0.05 relative to untreated controls.

(**Figure 6B**) for differential expression of several kinases (MAPK, JAK, Stat-1, ERK, and Akt). rfhSP-D significantly decreased the phospho-active forms of Akt in PC3 cells at 15 min (**Figure 6B** iii and iv). Interestingly, treated LNCaP cells also showed significantly decreased pAkt at 30 min (**Figure 6B** i and ii). Phosphorylated Akt leads to increased phosphorylation of Bad, an inactive form of Bad. The rfhSP-D induced decrease in pAkt sequentially led to a significant decrease in phosphorylated Bad in both the cell lines (**Figure 7A**). rfhSP-D treatment further led to a significantly decreased level of Bcl2 and an increased level of Bax at 24 h (**Figure 7B**). Both LNCaP and PC3 cells showed a significant increase in Bax to Bcl-2 ratio ($p < 0.05$) upon

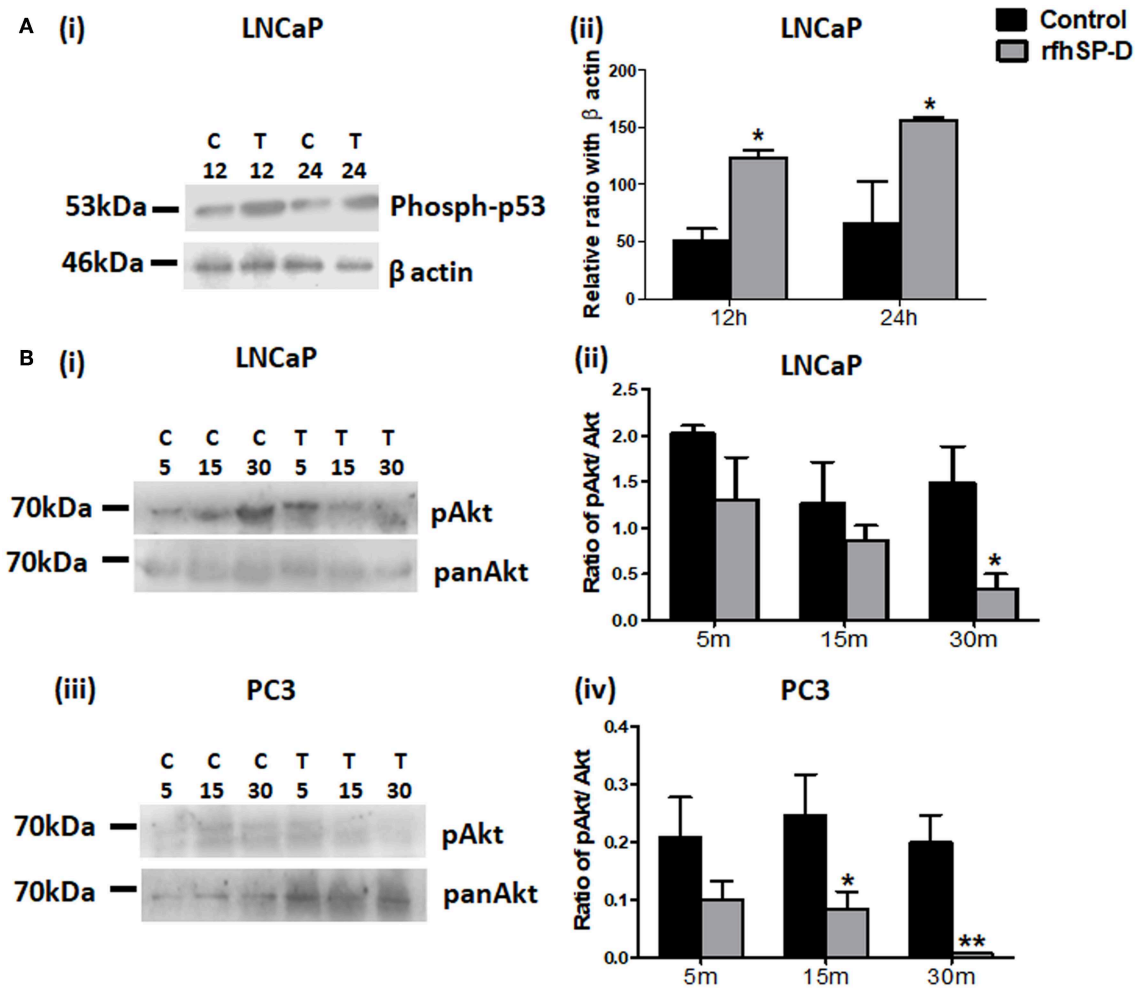

FIGURE 6 | Levels of p53 and pAkt were altered in rfhSP-D treated prostate cancer cells. **(A)** LNCaP cells (i) incubated with rfhSP-D (20 μg/ml) for 12 and 24 h were analyzed for the levels of anti-phosphorylated-p53(Ser 15) (Cell Signaling Technology) by immunoblotting. Densitometric analysis for the same is shown in panel, (ii) $n = 3$ independent experiments. *$p < 0.05$ vs. control. **(B)** LNCaP (i) and PC3 (iii) cells treated with rfhSP-D (20 μg/ml) for 5, 15, and 30 min were analyzed for anti-pAkt (PathScan Multiplex Western Cocktail I) and anti-pan Akt (ABclonal) expression by western blot. Their respective densitometric analysis is shown as pAkt/Akt ratio in (ii) and (iv). $n = 3$ independent experiments. *$p < 0.05$, **$p < 0.01$ vs. control. Full length western blots provided as **Supplementary Information**.

treatment with rfhSP-D. Similarly, transcripts for pro-apoptotic genes like BAX, BAD were upregulated and transcripts of BCL2 an anti-apoptotic gene was down regulated in a time dependent manner in LNCaP and PC3 cells (**Figure 8**). In LNCaP cells, transcripts for BAX (by 1.5 folds) were upregulated during 12 h of rfhSP-D incubation; in PC3 cells, transcripts for BAD (by 6 folds) were significantly upregulated at 6 h of rfhSP-D incubation.

To delineate the penultimate steps of apoptotic cascade, we assessed levels of cytochrome c and activation of caspases in rfhSP-D treated prostate cancer cells. At 48 h, rfhSP-D treatment induced release of cytochrome c attained significance in culture supernatant of cancer cells (LNCaP, PC3) and tissue biopsies of prostate cancer when compared to PrEC (**Figure 7D**). Cleaved products of the executioner caspase 7 were significantly increased after 24 h following rfhSP-D treatment (**Figure 7C**). From these observations, we infer that rfhSP-D triggers intrinsic mitochondrial pathway of apoptosis in prostate cancer cells.

DISCUSSION

The present study established the anti-prostate cancer activity of rfhSP-D via induction of intrinsic apoptosis in explants and primary tumor cells isolated from tissue biopsies of metastatic prostate cancer patients and prostate cancer cell lines: LNCaP (androgen responsive) and PC3 (androgen resistant). Various attributes of apoptosis like phosphatidylserine externalization (**Figure 5**), mitochondrial dysfunction (**Figure 7**), and DNA fragmentation (**Figure 5**) and various apoptotic markers (**Figure 7**) were observed in the rfhSP-D treated LNCaP and PC3 cells. Viability of the normal prostate epithelial cells (PrEC) was not altered in presence of rfhSP-D (**Figure 1**).

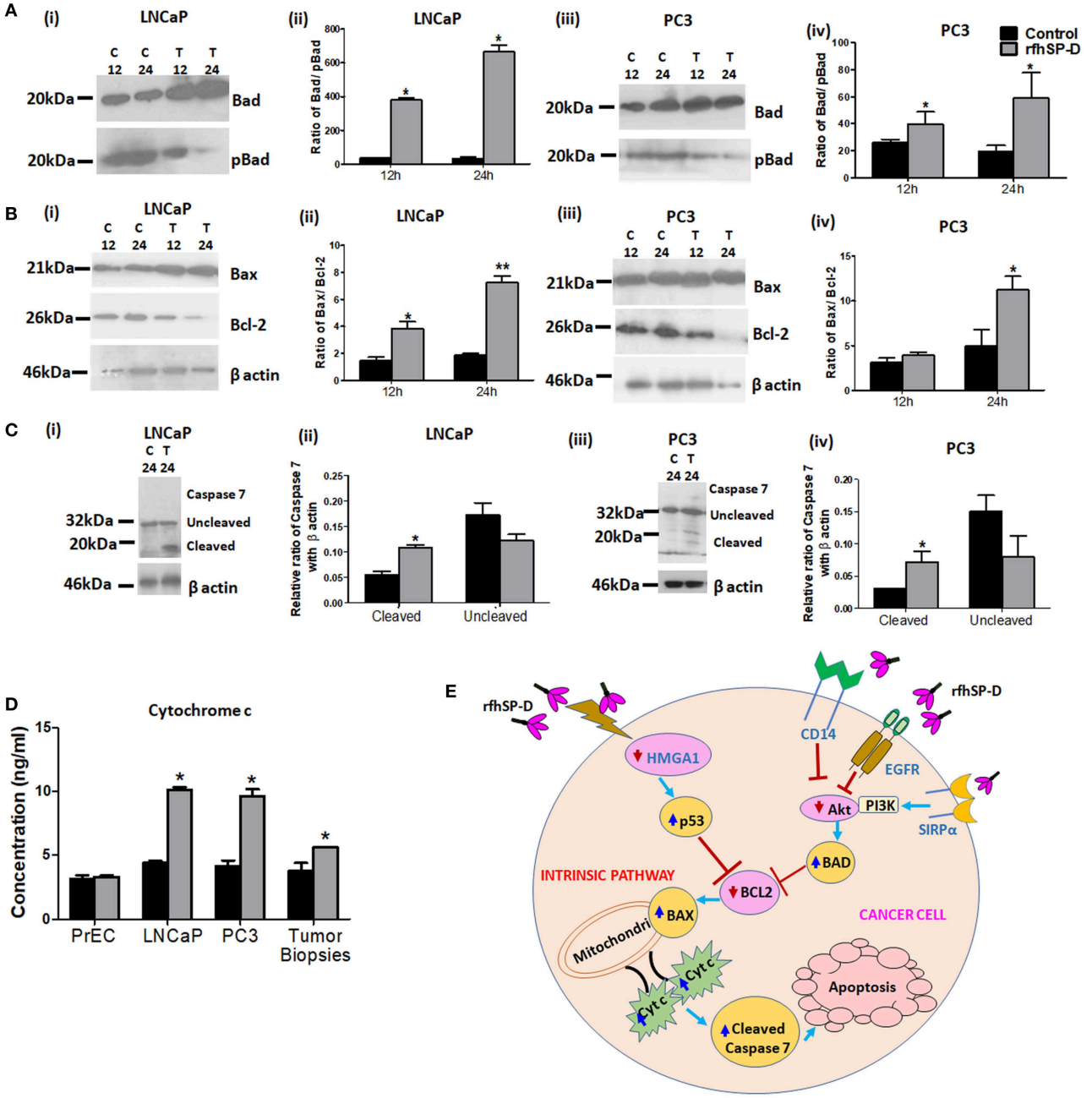

FIGURE 7 | rfhSP-D triggers intrinsic apoptotic pathway. **(A)** LNCaP (i) and PC3 (iii) cells treated with rfhSP-D (20 μg/ml) for 12 and 24 h were analyzed for anti-pBad (Ser 155) (ABclonal) and anti-Bad (Apoptosis I sampler Kit, Cell Signaling Technology) expression by immunoblotting. Panels (ii) and (iv) show densitometric analysis for the Bad/pBad ratio in LNCaP and PC3 cells respectively. $n = 3$ independent experiments. *$p < 0.05$ vs. control. **(B)** LNCaP (i) and PC3 (iii) cells treated with rfhSP-D (20 μg/ml) for 12 and 24 h were analyzed for anti-Bax (Apoptosis I sampler Kit, Cell Signaling Technology) and anti-Bcl-2 (Apoptosis I sampler Kit, Cell Signaling Technology) expression by immunoblotting. Panels (ii) and (iv) show densitometric analysis for the Bax/Bcl2 ratio in LNCaP and PC3 cells, respectively. $n = 3$ independent experiments. *$p < 0.05$ vs. control, **$p < 0.01$ vs. control. **(C)** Immunoblotting for uncleaved anti-Caspase 7(Cell Signaling Technology) and its cleaved products of molecular mass 32 kDa (upper panel; black arrow) and 20 kDa (lower panel; black arrow) respectively, in rfhSP-D (20 μg/ml) treated LNCaP (i) and PC3 (iii) cells for 24 h. Panels (ii) and (iv) show densitometric analysis for the cleaved caspase 7 and uncleaved caspase 7 in rfhSP-D treated LNCaP and PC3 cells, respectively. $n = 3$ independent experiments. *$p < 0.05$ vs. control. Full length western blots provided as **Supplementary Information**. **(D)** Measurement of Cytochrome c (Human Cyt-C, catalog no. E1516Hu, BT Assay) in cell culture supernatants of normal prostate epithelial cells (PrEC), cancer cell lines (LNCaP and PC3) and tumor tissue biopsies on exposure to rfhSP-D treatment for 48 h by ELISA. Data are presented as the mean ± S.D from three independent experiments. *$p < 0.05$ vs. control. **(E)** Proposed mechanisms for rfhSP-D mediated apoptosis in PCa cells. Treatment with rfhSP-D upregulates p53 and downregulates pAkt, resulting in upregulation of Bad, Bax, and release of cytochrome c leading to cleavage of caspase 7 in prostate cancer cells. SP-D interaction with some key molecules like HMGA1, CD14, SIRPα, and EGFR has been reported previously and may be relevant as part of the proposed mechanisms of p53 and Akt.

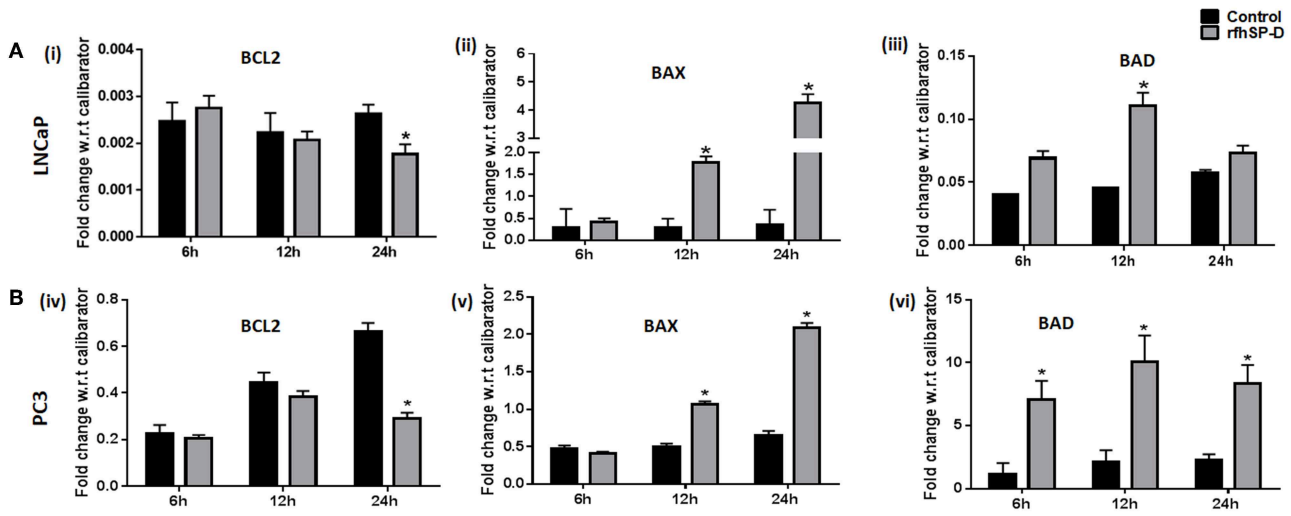

FIGURE 8 | rfhSP-D treatment induced alterations in the transcripts of anti and pro-apoptotic genes. **(A,B)** Real time RT-PCR analysis showed an upregulation of transcripts of BAX (ii, v) BAD (iii, vi) and downregulation of BCL2 (i, iv) in LNCaP and PC3 cells on treatment with rfhSP-D (20 μg/ml) for 6, 12, and 24 h. Each bar represents the mean ± S.D of three independent experiments. * indicates statistical significance and $^*p < 0.05$ relative to rfhSP-D untreated controls.

Human prostate cancer tissues frequently exhibit inactivation of the tumor suppressor gene p53 which is associated with therapeutic resistance (23). The p53 pathway plays a crucial role in the transmission of pro-apoptotic signals (24). Various therapeutic agents/candidates induce apoptosis of LNCaP ($p53^{+/+}$) cells by increasing the levels of phosphorylated p53 (25–27). Knockdown of p53 resulted in blockade of docetaxel induced apoptotic cell death in prostate cancer cells (28). Upregulation of activated p53 levels in a time-dependent manner by rfhSP-D treatment suggested involvement of the p53 pathway in the induction of apoptosis of LNCaP cells. Previously, activation of p53 was also observed in the eosinophilic leukemic cells (AML14.3D10) undergoing apoptosis upon treatment with rfhSP-D (14, 29). rfhSP-D treated AML14.3D10 cells showed significantly reduced levels of HMGA1, a survival protein (14). PC3 cells, a p53 null and highly metastatic prostate cancer cell line, also showed significant apoptosis following treatment with rfhSP-D, which suggested involvement of a p53 independent mechanism of apoptosis. Among 25% prostate cancer cases, diallelic deletion of the Phosphatase and tensin homolog (PTEN) gene and the associated increase in Akt phosphorylation correlates with hormone refractory prostate cancer (30). Decreased levels of activated Akt may lead to decreased levels of phosphorylated Bad (Bcl-2 associated death promoter). Dephosphorylated Bad interferes with interaction of activated Bcl2 with Bax. Thus, increased release of Bax triggers apoptosis (31, 32). Decreased ratio of transcripts of *Bcl-2* to *Bax* has been associated with cell death following an apoptotic stimulus (33, 34). Both LNCaP and PC3 cells, upon treatment with rfhSP-D, showed a significant increase in Bax to Bcl-2 ratio ($p < 0.05$), suggesting that besides activation of p53 pathway, rfhSP-D also inhibited Akt-PI3K pathway leading to induction of Bax mediated apoptosis. The present study unravels PI3K/Akt, an anti-apoptotic pathway, as a novel target of rfhSP-D mediated anti-prostate cancer activity.

Mitochondria plays a central role in the initiation of intrinsic apoptosis pathway (35). rfhSP-D treatment mediated disruption of the mitochondria was elucidated by its reduced ability to oxidize methyl tetrazolium to form formazan crystals (MTT assay; **Figure 4**). Breakdown of mitochondria is followed by the release of cytochrome c (**Figure 7**), a key initial step in the irreversible apoptotic process (35, 36). Culture supernatants from the rfhSP-D treated prostate cancer cells and cancer tissue biopsies showed significantly elevated levels of cytochrome c, confirming induction of intrinsic apoptosis. Once in the cytosol, the cytochrome c interacts with its adaptor molecule, Apaf-1, resulting in the processing and activation of pro-caspase-9 (37). Caspase-9, in turn, cleaves and activates pro-caspases−3 and−7, effector caspases responsible for the cleavage of various proteins leading to the biochemical and morphological features observed in apoptosis (38). Treatment of the prostate cancer cells with rfhSP-D resulted in the cleavage and activation of the effector caspase-7, thus leading to programmed cell death. Nuclear condensation, membrane and nuclear blebbing and flipping of phosphatidylserine (PS) on the cell membranes, the typical morphological characteristics of apoptotic cells, were observed in the rfhSP-D treated prostate cancer cells, confirming apoptotic cell death. The proposed mechanisms for the rfhSP-D mediated apoptosis in prostate cancer cells as revealed in this study along with some key molecules of these pathways interacting with/ induced by SP-D as reported previously have been depicted in **Figure 7E**.

Recent studies highlighted the suppressive role of SP-D in extrinsic apoptosis wherein native purified human SP-D interacted with Jurkat T cells and delayed the progression of Fas (CD95)-Fas ligand and TRAIL-TRAIL receptor induced, but not TNF-TNF receptor-mediated apoptosis (39). In a subsequent

study from the same group in UV irradiated Jurkat T cells, SP-D reduced the activation of caspase-8, executioner caspase-3 and exposure of phosphatidylserine (PS) on the membranes of dying cells, with a concomitant increase in the formation of nuclear and membrane blebs (16). The involvement of rfhSP-D in extrinsic apoptotic pathway in prostate cancer cells needs to be explored further.

rfhSP-D induced a cell cycle arrest in G2/M and G0/G1 phases of LNCaP and PC3 cells, respectively. We had previously shown that the rfhSP-D induced elevated p21 expression and inhibited Cdc2 phosphorylation resulting in reduced activity of Cdc2-cyclin B1 thus, leading to G2/M arrest in the AML14.3D10 cells (14). Several genes are common to the pathways involved in cell cycle regulation and apoptosis (40). The p53 protein plays a critical role both in the G1/S and G2/M checkpoint while Retinoblastoma (Rb) protein is a potent inhibitor of the G1 to S phase transition in the cell cycle (41, 42). Following rfhSP-D treatment, PC3 cells, which are null p53 but express the wild type Rb gene, showed an arrest in the G1-phase with significant reduction in the S-phase cell population. This alluded to the involvement of a p53 independent mechanism in the rfhSP-D induced apoptosis in PC3 cells.

Increased interaction of rfhSP-D with the prostate cancer cells as compared to PrEC, could be due to differential expression of the receptors. Similar to our previous study with eosinophilic leukemic cells, rfhSP-D showed interaction with the prostate cancer cells via carbohydrate recognition domain (CRD) (14). CRD domain of SP-D is known to interact with CD14, TLR-2, TLR-4, EGFR, and SIRPα that are reported to be present on prostate cancer cells and normal prostate tissues (15, 43, 44). Binding of SP-D with pattern recognition receptors CD14, TLR-2, and TLR-4 may lead to blockade of their downstream pro-inflammatory and pro-survival signaling (**Figure 7E**). Interaction with SIRPα, involved in the negative regulation of receptor tyrosine kinase-coupled signaling processes, may result in recruitment of PI3K, leading to a reduction in the activity of the downstream kinase Akt (45) (**Figure 7E**). A recent study showed that SP-D reduced EGF -EGFR binding through the interaction between CRD of SP-D and N-glycans of EGFR, thus, leading to downregulation of EGF signaling in the A549 human lung adenocarcinoma cells (15) (**Figure 7E**). Further studies are needed to elucidate the involvement of CRD and its interacting partners in downstream signaling of rfhSP-D in the prostate cancer cells.

Oncogenic mutations disturb the normal cellular functions, thus, allowing the tumor cells to undergo dysregulated proliferation, resist pro-apoptotic insults, invade normal tissues, and most importantly, escape apoptosis. Therefore, induction of apoptosis in the malignant tumors has evolved as a successful adjunct anti-cancer strategy. We report that rfhSP-D selectively triggered intrinsic apoptosis in androgen-dependent as well as androgen-independent prostate cancer cells, without affecting normal epithelial cells (PrEC). rfhSP-D also induced apoptotic cell death in the tissue biopsies from metastatic prostate cancer patients. Thus, SP-D is likely to act as an integral component of the human innate immune surveillance against cancer cells. A great advantage associated with the anti-cancer activity of rfhSP-D is induction of apoptosis by simultaneous targeting of multiple cellular signaling pathways including transcription factors, tumor cell survival factors, protein kinases resulting in the efficient and selective killing of prostate cancer cells. Murine models of prostate cancer including the patient-derived xenograft (PDX) mouse models that mimic human disease and 3D cell cultures derived from PDX are going to be valuable tools for the evaluation of therapeutic strategies using rfhSP-D (46).

DATA AVAILABILITY

The raw data supporting the conclusions of this manuscript will be made available by the authors, without undue reservation, to any qualified researcher.

ETHICS STATEMENT

The study was approved by the Institutional Ethics Committee for Clinical Studies, ICMR-National Institute for Research in Reproductive Health (Project No.: 260/2014) and Tata Memorial Hospital (Study no: 1467). Tissue biopsy samples were collected from 9 metastatic prostate cancer patients (treatment naïve) using Trans-rectal Ultrasound guided multiple core needle, with written informed consent. Chemotherapy was started in the case of patients following confirmation of metastasized prostate cancer. Information regarding the androgen dependency of the prostate cancer in these patients was not available. Average age of the study participants was 67.4 ± 3.97 years with Mean PSA (Prostate-specific antigen) level of 190.04 ± 85.12 ng/ml and Median Gleason score of 8 ± 0.83.

AUTHOR CONTRIBUTIONS

GT conceived and co-ordinated the study, designed, performed and analyzed the experiments, and wrote the paper. GP, VM, and GB designed and co-ordinated the study. GP recruited and screened the study participants. NS screened the study participants and collected tissue biopsies. SM interpreted the laboratory investigations of study participants. SA, HK, VM, and UK expressed, purified and characterized rfhSP-D for the study. UK provided purified and characterized rfhSP-D for the study and critical suggestions for the manuscript. TM conceived and co-ordinated the study, procured the intra-mural grant support, mediated the clinical collaboration, defended the protocol for IEC approval, analyzed the data, and edited the paper. All authors reviewed the results and approved the final version of the manuscript.

FUNDING

This work was financially supported by the Institutional Grant provided by ICMR-NIRRH (Accession no. 614). GT was supported with ICMR-NIRRH-Junior Research Fellowship and ICMR-Senior Research Fellowship.

ACKNOWLEDGMENTS

We thank Dr. Smita Mahale, Director, ICMR- National Institute for Research in Reproductive Health (ICMR-NIRRH), Mumbai, for her support. We are grateful to Ms. Sushma Gadkar and Dr. Geetanjali Sachdeva for the guidance in cell culture and maintenance. We sincerely acknowledge Dr. Sushama Rokade for the *in silico* analysis of steroid responsive elements in the promoter of SP-D gene. We also thank Ms. Sushma Khavale, Ms. Gayatri Shinde, and Dr. Srabani Mukherjee for their help in flow cytometry experiments and Ms. Shobha Banage, Ms. Reshma Gaonkar, and Dr. Nafisa Balasinor for helping us with confocal microscopy. We thank Mr. Vaibhav Shinde for his help in improving figure resolution. We also acknowledge the International Scientific Partnership Program (ISPP) at the King Saud University for funding via ISPP.

SUPPLEMENTARY MATERIAL

The Supplementary Material for this article can be found online at: https://www.frontiersin.org/articles/10.3389/fonc.2019.00565/full#supplementary-material

REFERENCES

1. Ferlay J, Shin H, Bray F, Forman D, Mathers C, Parkin D. Estimates of worldwide burden of cancer in 2008: GLOBOCAN 2008. *Int J Cancer.* (2010) 127:2893–917. doi: 10.1002/ijc.25516
2. Sooriakumaran P, Nyberg T, Akre O, Haendler L, Heus I, Olsson M, et al. Comparative effectiveness of radical prostatectomy and radiotherapy in prostate cancer: observational study of mortality outcomes. *Br Med J.* (2014) 348:g1502. doi: 10.1136/bmj.g1502
3. Disis M. Mechanism of action of immunotherapy. *Semin Oncol.* (2014) 5:S3–13. doi: 10.1053/j.seminoncol.2014.09.004
4. Hennessy E, Parker A, O'Neill L. Targeting Toll-like receptors: emerging therapeutics? *Nat Rev Drug Discovery.* (2010) 9:293–307. doi: 10.1038/nrd3203
5. Han J, Park S, Kim J, Cho S, Kim B, Kim B, et al. TLR7 expression is decreased during tumour progression in transgenic adenocarcinoma of mouse prostate mice and its activation inhibits growth of prostate cancer cells. *Am J Reprod Immunol.* (2013) 70:317–26. doi: 10.1111/aji.12146
6. Kishore U, Greenhough T, Waters P, Shrive A, Ghai R, Kamran M, et al. Surfactant proteins SP-A and SP-D: structure, function and receptors. *Mol Immunol.* (2006) 43:1293–315. doi: 10.1016/j.molimm.2005.08.004
7. Voorhout WF, Veenendaal T, Kuroki Y, Ogasawara Y, van Golde LM, Geuze HJ. Immunocytochemical localization of surfactant protein D (SP-D) in type II cells, Clara cells, and alveolar macrophages of rat lung. *J Histochem Cytochem.* (1992) 40:1589–97. doi: 10.1177/40.10.1527377
8. Madsen J, Kliem A, Tornøe I, Skjødt K, Koch C, Holmskov U. Localization of lung surfactant protein D on mucosal surfaces in human tissues. *Am J Respir Cell Mol Biol.* (2003) 29:591–7. doi: 10.1165/rcmb.2002-0274OC
9. Beileke S, Claassen H, Wagner W, Matthies C, Ruf C, Hartmann A, et al. Expression and localization of lung surfactant proteins in human testis. *PLoS ONE.* (2015) 24:e0143058. doi: 10.1371/journal.pone.0143058
10. Rokade S, Madan T. Testicular expression of SP-A, SP-D and MBL-A is positively regulated by testosterone and modulated by lipopolysaccharide. *Immunobiology.* (2016) 221:975–85. doi: 10.1016/j.imbio.2016.05.005
11. Oberley R, Goss K, Dahmoush L, Ault K, Crouch E, Snyder J. A role for surfactant protein D in innate immunity of the human prostate. *Prostate.* (2005) 65:241–51. doi: 10.1002/pros.20292
12. Quintar A, Leimgruber C, Pessah O, Doll A, Maldonado CA. Androgen depletion augments antibacterial prostate host defences in rats. *Int J Androl.* (2012) 35:845–59. doi: 10.1111/j.1365-2605.2012.01288.x
13. Kankavi O, Baykara M, ErenKaranis MI, Bassorgun CI, Ergin H, Ciftcioglu MA. Evidence of surfactant protein A and D expression decrement and their localizations in human prostate adenocarcinomas. *Renal Failure.* (2014) 36:258–65. doi: 10.3109/0886022X.2013.846831
14. Mahajan L, Pandit H, Madan T, Gautam P, Yadav AK, Warke H, et al. Human surfactant protein D alters oxidative stress and HMGA1 expression to induce p53 apoptotic pathway ineosinophil leukemic cell line. *PLoS ONE.* (2013) 8:e85046. doi: 10.1371/journal.pone.0085046
15. Hasegawa Y, Takahashi M, Ariki S, Asakawa D, Tajiri M, Wada Y, et al. Surfactant protein D suppresses lung cancer progression by downregulation of epidermal growth factor signaling. *Oncogene.* (2015) 34:838–45. doi: 10.1038/onc.2014.20
16. Djiadeu P, Farmakovski N, Azzouz D, Kotra LP, Sweezey N, Palaniyar N. Surfactant protein D regulates caspase-8-mediated cascade of the intrinsic pathway of apoptosis while promoting bleb formation. *Mol Immunol.* (2017) 92:190–8. doi: 10.1016/j.molimm.2017.10.016
17. Kumar J, Murugaiah V, Sotiriadis G, Kaur A, Jeyaneethi J, Sturniolo I, et al. Surfactant protein D as a potential biomarker and therapeutic target in ovarian cancer. *Front Oncol.* (2019) doi: 10.3389/fonc.2019.00542. [Epub ahead of print].
18. Havens A, Jung Y, Sun Y, Wang J, Shah R, Bühring H, et al. The role of sialomucin CD164 (MGC-24v or endolyn) in prostate cancer metastasis. *Biomed Central Cancer.* (2006) 6:195. doi: 10.1186/1471-2407-6-195
19. Ananthanarayanan V, Deaton R, Yang X, Pins M, Gann P. Alpha-methylacyl-CoA racemase (AMACR) expression in normal prostatic glands and high-grade prostatic intraepithelial neoplasia (HGPIN): association with diagnosis of prostate cancer. *Prostate.* (2005) 63:341–6. doi: 10.1002/pros.20196
20. Mahajan L, Madan T, Kamal N, Singh VK, Sim R, Telang SD, et al. Recombinant surfactant protein-D selectively increases apoptosis in eosinophils of allergic asthmatics and enhances uptake of apoptotic eosinophils by macrophages. *Int Immunol.* (2008) 20:993–1007. doi: 10.1093/intimm/dxn058
21. Shaikh A, Nagvenkar P, Pethe P, Hinduja I, Bhartiya D. Molecular and phenotypic characterization of CD133 and SSEA4 enriched very small embryonic-like stem cells in human cord blood. *Leukemia.* (2015) 29:1909–17. doi: 10.1038/leu.2015.100
22. Kokontis J, Hay N, Liao S. Progression of LNCaP prostate tumor cells during androgen deprivation: hormone-independent growth, repression of proliferation by androgen, and role for p27Kip1 in androgen-induced cell cycle arrest. *Mol Endocrinol.* (1998) 12:941–53. doi: 10.1210/mend.12.7.0136
23. Ecke T, Schlechte H, Schiemenz K, Sachs M, Lenk S, Rudolph B, et al. TP53 gene mutations in prostate cancer progression. *Anticancer Res.* (2010) 30:1579–86.
24. Gottlieb T, Leal J, Seger R, Taya Y, Oren M. Cross-talk between Akt, p53 and Mdm2: possible implications for the regulation of apoptosis. *Oncogene.* (2002) 21:1299–303. doi: 10.1038/sj.onc.1205181
25. Chappell W, Lehmann B, Terrian D, Abrams S, Steelman L, McCubrey J. p53 expression controls prostate cancer sensitivity to chemotherapy and the MDM2 inhibitor Nutlin-3. *Cell Cycle.* (2012) 11:4579–88. doi: 10.4161/cc.22852
26. Jiang C1, Hu H, Malewicz B, Wang Z, Lü J. Selenite-induced p53 Ser-15 phosphorylation and caspase-mediated apoptosis in LNCaP human prostate cancer cells. *Mol Cancer Therapeut.* (2004) 3:877–84.
27. Zhang ZW, Yang ZM, Zheng YC, Chen ZD. Transgelin induces apoptosis of human prostate LNCaP cells through its interaction with p53. *Asian J Androl.* (2010) 12:186–95. doi: 10.1038/aja.2009.76
28. Liu C, Zhu Y, Lou W, Nadiminty N, Chen X, Zhou Q, et al. Functional p53 determines docetaxel sensitivity in prostate cancer cells. *Prostate.* (2013) 73:418–27. doi: 10.1002/pros.22583
29. Mahajan L, Gautam P, Dodagatta-Marri E, Madan T, Kishore U. Surfactant protein SP-D modulates activity of immune cells: proteomic profiling of its interaction with eosinophilic cells. *Expert Rev Proteomics.* (2014) 11:355–69. doi: 10.1586/14789450.2014.897612

30. Sircar K, Yoshimoto M, Monzon F, Koumakpayi I, Katz R, Khanna A, et al. PTEN genomic deletion is associated with p-Akt and AR signalling in poorer outcome, hormone refractory prostate cancer. *J Pathol.* (2009) 218:505–13. doi: 10.1002/path.2559
31. Ruvolo PP, Deng X, May WS. Phosphorylation of Bcl2 and regulation of apoptosis. *Leukemia.* (2001) 15:515–22. doi: 10.1038/sj.leu.2402090
32. Oltvai Z, Milliman C, Korsmeyer S. Bcl-2 heterodimerizes *in vivo* with a conserved homolog, Bax, that accelerates programmed cell death. *Cell.* (1993) 74:609–19.
33. Paul-Samojedny M, Kokocinska D, Samojedny A, Mazurek U, Partyka R, Lorenz Z, et al. Expression of cell survival/death genes: Bcl-2 and Bax at the rate of colon cancer prognosis. *Biochim Biophys Acta.* (2005) 1741:25–9. doi: 10.1016/j.bbadis.2004.11.021
34. Perlman H, Zhang X, Chen MW, Walsh K, Buttyan R. An elevated bax/bcl-2 ratio corresponds with the onset of prostate epithelial cell apoptosis. *Cell Death Differ.* (1999) 6:48–54. doi: 10.1038/sj.cdd.4400453
35. Green D, Reed J. Mitochondria and apoptosis. *Science.* (1998) 281:1309–12.
36. Shawgo M, Shelton S, Robertson J. Caspase-mediated Bak activation and cytochrome c release during intrinsic apoptotic cell death in jurkat cells. *J. Biol Chem.* (2008) 283:35532–8. doi: 10.1074/jbc.M807656200
37. Li P, Nijhawan D, Budihardjo I, Srinivasula SM, Ahmad M, Alnemri ES, et al. Cytochrome c and dATP-dependent formation of Apaf-1/caspase-9 complex initiates an apoptotic protease cascade. *Cell.* (1997) 91:479–89.
38. Robertson JD, Orrenius S, Zhivotovsky B. Review: nuclear events in apoptosis. *J Struct Biol.* (2000) 129:346–58. doi: 10.1006/jsbi.2000.4254
39. Djiadeu P, Kotra LP, Sweezey N, Palaniyar N. Surfactant protein D delays Fas- and TRAIL-mediated extrinsic pathway of apoptosis in T cells. *Apoptosis.* (2017) 22:730–40. doi: 10.1007/s10495-017-1348-4
40. Vemeulen K, Berneman ZN, Bockstaele DR. Cell cycle and apoptosis. *Cell Proliferation.* (2003) 36:165–75. doi: 10.1046/j.1365-2184.2003.00267.x
41. Senturk E, Manfredi J. p53 and cell cycle effects after DNA damage. *Methods Mol Biol.* (2013) 962:49–61. doi: 10.1007/978-1-62703-236-0_4
42. Bertoli C, Skotheim J, deBruin R. Control of cell cycle transcription during G1 and S phases. *Nat Revi Mol Cell Biol.* (2013) 14:518–28. doi: 10.1038/nrm3629
43. Ohya M, Nishitani C, Sano H, Yamada C, Mitsuzawa H, Shimizu T, et al. Human pulmonary surfactant protein D binds the extracellular domains of Toll-like receptors 2 and 4 through the carbohydrate recognition domain by a mechanism different from its binding to phosphatidylinositol and lipopolysaccharide. *Biochemistry.* (2006) 45:8657–64. doi: 10.1021/bi060176z
44. Janssen WJ, McPhillips KA, Dickinson MG, Linderman DJ, Morimoto K, Xiao YQ, et al. Surfactant proteins A and D suppress alveolar macrophage phagocytosis via interaction with SIRP alpha. *Am J Respir Crit Care Med.* (2008) 178:158–67. doi: 10.1164/rccm.200711-1661OC
45. Dong LW, Kong XN, Yan HX, Yu LX, Chen L, Yang W, et al. Signal regulatory protein alpha negatively regulates both TLR3 and cytoplasmic pathways in type I interferon induction. *Mol Immunol.* (2008) 45:3025–35. doi: 10.1016/j.molimm.2008.03.012.2
46. Rea D, Del Vecchio V, Palma G, Barbieri A, Falco M, Luciano A, et al. Mouse models in prostate cancer translational research: from xenograft to PDX. *Biomed Res Int.* (2016) 2016:9750795. doi: 10.1155/2016/9750795

Conflict of Interest Statement: The authors declare that the research was conducted in the absence of any commercial or financial relationships that could be construed as a potential conflict of interest.

Immunobiology 224 (2019) 625–631

Contents lists available at ScienceDirect

Immunobiology

journal homepage: www.elsevier.com/locate/imbio

Secretion of functionally active complement factor H related protein 5 (FHR5) by primary tumour cells derived from Glioblastoma Multiforme patients

Syreeta DeCordova[a], Amr Abdelgany[b,c], Valarmathy Murugaiah[a], Ansar A. Pathan[a], Annapurna Nayak[a], Tom Walker[b], Abhishek Shastri[a,d], Salman H. Alrokayan[e], Haseeb A. Khan[e], Shiv K. Singh[f], Nick De Pennington[b], Robert B. Sim[g], Uday Kishore[a,*]

[a] Biosciences, College of Health and Life Sciences, Brunel University London, Uxbridge, UB8 3PH, UK
[b] Nuffield Department of Clinical Neuroscience, John Radcliffe Hospital, University of Oxford, Headington, OX3 9DS, UK
[c] Department of Oncology, University of Oxford, Roosevelt Drive, Oxford, OX3 7DQ, UK
[d] Westminster Community Mental Health Team, Central and North-West London NHS Foundation Trust, London SW1V 1DX, UK
[e] Department of Biochemistry, College of Science, King Saud University, Riyadh 11451, Saudi Arabia
[f] Department of Gastroenterology and Gastrointestinal Oncology, University Medical Centre, Goettingen, Germany
[g] Department of Biochemistry, University of Oxford, South Parks Road, Oxford, OX1 3QU, UK

ARTICLE INFO

Keywords:
FHR5
FH
Glioblastoma and complement

ABSTRACT

The complement system is an important humoral immune surveillance mechanism against tumours. However, many malignant tumours are resistant to complement mediated lysis. Here, we report secretion of complement factor H related protein 5 (FHR5) by primary tumour cells derived from Glioblastoma multiforme (GBM) patients. We investigated whether the secreted FHR5 exhibited functional activity similar to factor H, including inhibition of complement mediated lysis, acting as a co-factor for factor I mediated cleavage of C3b, and decay acceleration of C3 convertase. Immunoblotting analysis of primary GBM cells (B30, B31 and B33) supernatant showed the active secretion of FHR5, but not of Factor H. ELISA revealed that the secretion of soluble GBM-FHR5 by cultured GBM cells increased in a time-dependent manner. Primary GBM-FHR5 inhibited complement mediated lysis, possessed co-factor activity for factor I mediated cleavage and displayed decay acceleration of C3 convertase. In summary, we detected the secretion of FHR5 by primary GBM cells B30, B31 and B33. The results demonstrated that GBM-FHR5 shares biological function with FH as a mechanism primary GBM cells potentially use to resist complement mediated lysis.

1. Introduction

Glioblastoma multiforme (GBM) is the most lethal brain tumour in adults with a median survival of less than 15 months (Ohgaki et al., 2004). One of the biggest clinical challenges in the treatment of GBM is the highly aggressive behaviour of cells that prevent complete surgical resection and enhance resistance to conventional radio- and chemotherapy (Ohgaki et al., 2004; Furnari et al., 2007). Even with complete surgical resection, the long-term survival of GBM patients remains very poor due to a high recurrence rate (Ohgaki et al., 2004). Recent findings from The Cancer Genome Atlas confirmed that the immune microenvironment significantly contributes to therapy resistance and is associated with worse survival in GBM (Iglesia et al., 2016). In addition, glioma cells have the capacity to escape immune surveillance, and are involved in immune suppressive activities to promote the malignant transformation of GBM tumours (Chang et al., 2016; Mieczkowski et al., 2015).

GBM is a grade IV astrocytoma, characterised by uncontrolled cellular proliferation, diffuse infiltration, extensive genomic instability, tendency for necrosis, angiogenesis, and resistance to apoptosis. The tumour is characterised by high inter- and intra- morphological heterogeneity, hence the term “multiforme” (Furnari et al., 2007; Liu et al., 2012). GBM is a robust malignant tumour distinguished by its local invasion pattern (Gabrusiewicz et al., 2014; Hermanson et al., 1992). Clinical symptoms may include progressive headaches, seizures and focal neurological deficit (Pace et al., 2009; Faithfull et al., 2005; Oberndorfer et al., 2008; Hermanson et al., 1992). GBM is most often *de novo* (primary GBM), which develops quickly within a three-month

* Corresponding author.
E-mail addresses: uday.kishore@brunel.ac.uk, ukishore@hotmail.com (U. Kishore).

https://doi.org/10.1016/j.imbio.2019.07.006
Received 18 March 2019; Received in revised form 11 June 2019; Accepted 30 July 2019
Available online 05 August 2019

period before the initial symptoms indicate the onset of the tumour. Primary GBM accounts for approximately 90% of the cases and is predominately found in patients older than 45. The tumour may also develop from a lower grade tumour to a higher malignancy (secondary GBM) over 5-10-years, which is more commonly observed in patients below the age of 45. These subtypes have distinct genetic aberrations but are histologically indistinguishable (Furnari et al., 2007; Maher et al., 2006; Fujisawa et al., 1999). GBM is resistant to destruction by the immune system. Despite aggressive treatment including surgical resection and radiotherapy with concomitant chemotherapy, prognosis remains poor due to GBM recurrence, with a median survival of 14.6 months (Stupp et al., 2005).

The complement system is one of the most potent humoral innate immune protective mechanisms. Complement is activated via three pathways (classical, alternative and lectin). The recognition molecules of each pathway identify non-self and altered self, and the activities of the complement system eventually eliminate the targets (Kohl, 2006). All the three complement pathways converge on the generation of C3 convertase, leading to terminal membrane attack complex (MAC), which is lytic to target cells. The resistance to complement mediated killing by both normal tissue and human malignancies is due to membrane-bound inhibitors including complement receptor 1 (CR1; CD35), membrane cofactor protein (MCP; CD46), decay-accelerating factor (DAF; CD55), and protectin (CD59) (Morgan and Meri, 1994; Gorter and Meri, 1999). CR1 and MCP act as a co-factor for factor I mediated degradation of C3b (Fearon, 1979; Seya et al., 1986), while DAF and CR1 promote the decay of C3 and C5 convertases. Protectin inhibits the formation of the MAC on cell membranes (Sugita et al., 1988; Meri et al., 1990).

In addition to membrane bound regulators, the activity of the complement system is efficiently controlled by soluble factor H (FH), which is predominantly synthesised by the liver (Davies et al., 1989; Weiler et al., 1976). FH regulates the alternative pathway by acting as a cofactor for factor I-mediated cleavage of C3b, competes with factor B to bind to C3b, and promotes the dissociation of C3 convertase, C3bBb (Fearon and Austen, 1977; Whaley and Ruddy, 1976). FH is a 150 kDa soluble protein consisting of 20 complement control protein modules (CCPs) (also called short consensus repeats; SCR), each composed of about 60 amino acids (Ripoche et al., 1988). The complement regulatory activity is located in CCP1–4 (Jokiranta et al., 2000; Sharma and Pangburn, 1996; Gordon et al., 1995; Kuhn and Zipfel, 1996), which is also one of the three C3b binding sites. A second C3b binding site may be localised on CCP 8–15 and the third binding site exists on CCP 19–20 (Jokiranta et al., 2000, 2005).

FHR5 is a protein of the FH family, which includes FH, FH like protein 1 (FHL-1), and FHR1-5, which are structurally and immunologically related. FHL-1 is an alternatively-spliced product of the FH gene, whereas FHR1-5 are each encoded by separate genes. FHR5 exists as a glycosylated protein with a plasma concentration of approximately 5 μg/mL (Skerka et al., 2013) The FHR5 gene is located downstream of the FH gene on a distinct segment of human chromosome 1q32 within the Regulation of Complement Activation (RCA) gene cluster (Jokiranta et al., 2005; Clark and Bishop, 2015). FHR5 is the largest human FHR protein (~65 kDa) and is composed of 9 CCPs. All FHR proteins contain CCPs which are similar in sequence to CCP 6, 19 and 20 of FH (Ohgaki et al., 2004; Furnari et al., 2007; Iglesia et al., 2016; Chang et al., 2016; Mieczkowski et al., 2015). However, FHR5 is the only FHR to contain additional CCPs, which are similar to CCP10–14 of FH. CCP3-7 of FHR5 show 46%, 75%, 57%, 48% and 71% amino acid identity with CCP10–14 of FH, respectively (Jokiranta et al., 2005). The extensive sequence similarities between FHR1-5 and FH allow FHRs to be recognised by polyclonal anti-FH antibodies. The C-terminal FHR5 CCP8 and 9 share sequence identity of 64% with CCP19 and 42% with CCP 20 of FH whereas there is a more distant sequence homology between FHR5 CCP1-2 and CCP6 and CCP7 of FH (Medjeral-Thomas and Pickering, 2016; McRae et al., 2001). FHR5 has the ability to bind to C3b, heparin, C-reactive protein, and iC3b (the cleavage product of C3b). The function of FHR5 is not well understood (Csincsi et al., 2015). Weak co-factor activity for cleavage of C3b by factor I and decay-acceleration activity of C3bBb convertase have been attributed to FHR5 (Jokiranta et al., 2005; McRae et al., 2005). However, studies have also reported that FHR5 can deregulate complement by competing with FH for binding to surface polyanions and C3b (Csincsi et al., 2015; Goicoechea de Jorge et al., 2013).

Here, we report that primary tumour cells, directly isolated from GBM patients post-surgery, secrete FHR5 in culture (GBM-FHR5). Our results show that the primary GBM-FHR5 is functionally active and regulates complement by acting as a co-factor for factor I mediated cleavage of C3b, and degrading (decaying) C3 convertase.

2. Materials and methods

2.1. Isolation of primary GBM Cells from tumour samples

Primary GBM cells were obtained directly from surgical resections of three patients at the John Radcliffe Hospital, Oxford, UK following local ethical board approval. Briefly, a small piece of each tumour tissue was removed and placed into Accutase (Sigma-Aldrich) for 15 min to dissociate into single cells. All primary cells used in this study, namely B30, B31 and B33, were grown in DMEM-F12 medium (Life Technologies) supplemented with 10% v/v heat inactivated fetal calf serum (FCS; Life Technologies), and 1% penicillin/streptomycin (Life Technologies) at 37 °C in 5% v/v CO_2. The cells were passaged up to three times.

2.2. FHR5 purification from B30, B31 and B33 cells

2×10^6 B30, B31, or B33 cells were grown in 75 cm^3 culture flasks in serum free DMEM/F12 with penicillin/streptomycin until the cells were 80% confluent. The culture supernatant was centrifuged for 5 min at 2000 rpm to remove cells in suspension. The supernatant was dialysed overnight against buffer containing 25 mM Tris−HCl pH 7.5, 140 mM NaCl, 0.5 mM EDTA, pH 7.5 and passed through an anti-FH Sepharose column (CNBr-activated Sepharose to which rabbit anti-human FH IgG fraction was coupled) (MRC Immunochemistry Unit, Oxford) (Soames and Sim, 1997).

The column was then washed with 10 bed volumes of the same buffer. Bound protein was eluted with 3 M $MgCl_2$, adjusted to pH 6.8. The eluted fractions were dialysed overnight against distilled water followed by 4 h dialysis against 10 mM potassium phosphate, 140 mM NaCl, 0.5 mM EDTA, pH 7.5. The final protein concentration was measured with a nanodrop spectrophotometer, reading at 280 nm. FH was purified as a control protein from normal human serum using the same technique. Procedures are based on those in Yu et al. (2014), although a different antibody preparation was used.

2.3. SDS-PAGE

SDS-PAGE was performed using the Laemmli (1970) method to observe the proteins purified from primary GBM cells and to assess the purity of human FH. The samples were added to 2 x treatment buffer with or without the reducing agent i.e. beta mercaptethanol (Sigma-Aldrich) in a 1:1 v/v ratio and were denatured for 10 min at 100 °C. Standard Protein markers (Thermo-Scientific) and the denatured samples were loaded onto the gel and separated via electrophoresis for 90 min at 120 V. The gel was stained overnight on a rotary shaker with Coomassie blue stain solution (0.1% w/v Coomassie blue (Sigma-Aldrich), 10% v/v acetic acid, 20% v/v methanol, followed by de-staining for 2 h using de-stain solution (10% v/v acetic acid, 20% v/v methanol) to visualise the bands.

2.4. Western blot

0.2×10^6 cells/mL of primary GBM cells B30, B31, B33 and cell line H2 (control: glioblastoma cell line; Gasque et al. (1992) (kindly provided by Prof Seppo Merri from University of Helsinki) were plated in 12 well plates in the presence of DMEM-F12 and 1% penicillin/streptomycin to obtain serum-free culture supernatant. Cells were grown at 37 °C in 5% CO_2 until 80% confluency was reached. The culture supernatant was centrifuged for 5 min at 10,000 rpm. Each supernatant was run on a 12% SDS-PAGE gel under reducing conditions. The protein bands were transferred to a nitrocellulose membrane in 1 x transfer buffer (25 mM Tris-HCl, 190 mM glycine, 20% v/v methanol pH 8.3) at 70 V for 2 h at 4 °C. After blocking non-specific binding sites overnight with 2% w/v bovine serum albumin (BSA) at 4 °C, the membrane was incubated for 1 h at room temperature (RT) with primary polyclonal rabbit anti-human FH (10 μg/mL IgG; MRC Immunochemistry Unit, Oxford) in 1 x PBS (Thermo-Scientific). The membrane was washed using 1 x PBS + 0.05% Tween20 (PBST) and incubated with secondary anti-rabbit IgG-horseradish peroxidase (HRP) conjugate (5 μg/mL) (Sigma Aldrich) for 1 h at RT. After washing, bound antibodies were detected and visualised using 3,3′diaminobenzidine (DAB; Sigma Aldrich). A similar blot was also probed with goat anti-FHR5 polyclonal antibodies (R&D; cat. no. AF3845-SP).

2.5. ELISA

The culture supernatant (100 μL) from 0.2×10^6 B30, B31 or B33 primary cells/mL grown in serum free media was dispensed in triplicates in a microtiter plate, with the addition of another 100 μL of carbonate bicarbonate buffer (Sigma-Aldrich) to each well. Human FH and BSA (100 μg/mL) were added to separate wells as positive and negative control proteins. After overnight incubation at 4 °C, the wells were washed with 1 x PBST and non-specific binding sites were blocked by incubation with 2% BSA for 2 h at 37 °C. The wells were washed again, the primary polyclonal rabbit anti-human FH antibody (10 μg/mL IgG) in PBS was added, and incubated for 1 h at 37 °C. After washing, bound antibodies were detected using anti-rabbit IgG-HRP secondary antibody (5 μg/mL) in PBS for 1 h at 37 °C. Wells were washed and o-Phenylenediamine (Sigma-Aldrich) was added in the dark. The A_{450} nm was measured using a microplate absorbance reader (Bio-Rad).

2.5.1. Haemolytic assay

Sheep erythrocytes (TCS Bioscience) were washed with PBS-5 mM EDTA. The cell concentration was adjusted to 1×10^9 cells/mL using DGVB-Mg-EGTA (2.5 mM sodium barbital, 71 Mm NaCl, 7 mM $MgCl_2$, 10 mM EGTA, 0.1% w/v gelatin, 2.5% w/v glucose pH 7.4). The presence of EGTA and $MgCl_2$ allows activation of the complement alternative pathway only. Serum depleted of FH family proteins (FH, FHL-1, and FHR1-5) was made by passing normal human serum (TCS Bioscience) through a polyclonal anti-FH Sepharose column in the presence of 0.1 mM EDTA at 4 °C and freezing the flow-through immediately at −80 °C (McRae et al., 2005). A dot blot was performed on the serum that had been passed through the column using polyclonal anti-human FH and anti-rabbit IgG-HRP (1:1000) antibodies to ensure FH family proteins were absent. 40 μL of FH family depleted serum was diluted in 160 μL of DGVB-Mg-EGTA followed by a 2-fold serial dilution on a microtiter plate on ice and 100 μL of sheep erythrocytes were added to each well. Following incubation for 30 min at 37 °C and centrifugation (5000 rpm, 10 min, 4 °C), the supernatants were removed, and the absorbance was measured at 541 nm. To determine percentage haemolysis, 100 μL of sheep erythrocytes with 100 μL of water was included separately to determine total cell lysis and 100 μL of sheep erythrocytes with 100 μL of DGVB-Mg-EGTA was included as a blank.

On ice, 20 μL of depleted serum that caused 50% haemolysis, was mixed with varying concentrations of GBM-FHR5 (0.2–4 μM), 100 μL of sheep erythrocytes and sufficient DGVB-Mg-EGTA (to bring the mix to 200 μL). Human FH (0.2–4 μM) was used instead of FHR5 as a control. The samples were incubated for 30 min at 37 °C followed by immediate centrifugation at 4 °C. The absorbance at 541 nm was measured for each supernatant and the percentage haemolysis was calculated.

2.6. Co-factor assay

The Factor I co-factor activity assay was adapted from Brandstatter et al. (2012). Briefly, 3 μg of C3b (0.55 μM)(Complement Technology), 45 ng of factor I (4 nM)(Complement Technology) and 0.39–78 μg (0.2–4 μM) of FHR5 or 0.9–18 μg (0.2-4μM) FH were added to 10 mM sodium phosphate, pH 6.0 to a final volume of 30 μL. Samples without FH or FHR5 were included as controls. The samples were incubated at 37 °C for 10 min and separated under reducing conditions via SDS-PAGE and subjected to Coomassie blue staining.

2.7. Decay acceleration activity

The decay acceleration assay was modified from Brandstatter et al. (2012). Briefly, a microtiter plate was coated with 50 μL containing 250 ng of C3b in 50 mM carbonate bicarbonate buffer, pH 9.6 overnight at 4 °C. Generation of nickel chloride stabilised C3 convertase was achieved by the addition of 400 ng of Factor B (Complement Technology) and 25 ng of factor D (Complement Technology), in the presence of 2 mM nickel chloride (Sigma-Aldrich), 25 mM NaCl and 4% w/v BSA to a total volume of 150 μL. The samples were incubated for 2 h at 37 °C. After extensive washing with PBS, varying concentrations of FHR5 (1.3 to 26μg, resulting in concentration 0.2–4 μM) were diluted in PBS to a total volume of 100 μL and added directly to each well then incubated for 30 min at 37 °C. Samples with and without FH or FHR5 were included as controls. After extensive washing, intact complexes (not decayed) were detected with goat anti-human factor B antibody (40 μg/mL; Complement Technology) in PBS for 1 h at 37 °C. The wells were washed and rabbit anti-goat IgG-HRP (1.5 μg/mL) (Thermo-Scientific) in PBS was added to each well and incubated for 1 h at 37 °C, followed by washing. To each well, o-Phenylenediamine was added for 5 min in the dark and the A450 nm was measured.

3. Results

3.1. Secretion of FHR5 by B30, B31 and B33 GBM cells

We first examined the presence of FH family proteins in the culture supernatant of B30, B31 and B33 primary GBM cells. Using western blot analysis, we were able to detect FHR5 in serum free culture supernatant of primary GBM cells, demonstrating that these cells secreted FHR5, migrating at ~65 kDa under reducing conditions (Fig. 1A). H2 supernatant (Fig.1B) differed from the primary cells supernatant as bands were displayed for FH at 150 kDa and FH like -1 (FHL-1) at 42 kDa. FH, FHL-1 and FHR1–4 were undetectable in B30, B31 and B33 culture supernatant. The identity of FHR5 was a established by use of an anti-FHR5 polyclonal antibody (Fig. 1C). Subsequently, we affinity-purified the protein using a polyclonal anti-human factor H Sepharose column (Fig. 2). In order to eliminate interference with the presence of FH in fetal calf serum, the culture supernatant was obtained from cells grown in serum-free media. A prominent band was visualised at ~65 kDa under reducing conditions, the molecular weight for FHR5. No higher or lower bands were present, indicating that there were no impurities or other FH family proteins eluted. The lack of additional bands also confirmed that the protein was not a cleaved product of full length FH. In addition, the purified protein continued to migrate at ~65 kDa even under non-reducing conditions (Fig. 2B), ruling out the possibility of the purified protein being C4b binding protein (with which polyclonal anti-FH also cross-reacts). A protein yield of 400 μg for B30, 300 μg for B31 and 300 μg for B33 was obtained from 50 mL serum-free DMEM/F12 with penicillin/streptomycin collected from the cells at 80%

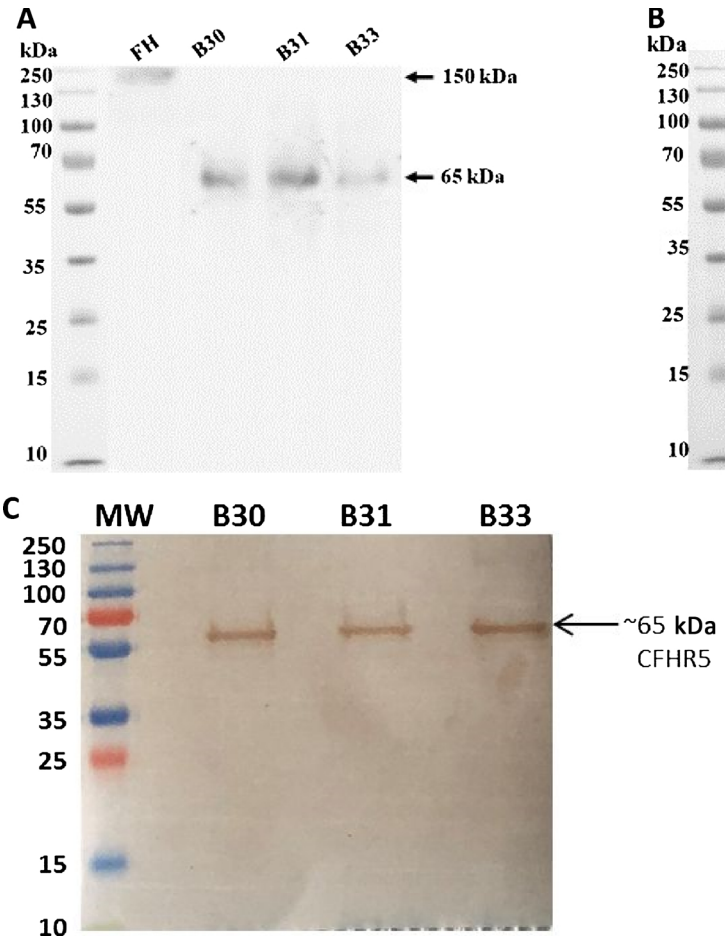

Fig. 1. Western blot analysis of serum free primary GBM supernatant. 0.2×10^6 (A) B30, B31, B33 (B) and H2 cells (control) Cells were grown for 48 h at 37 °C with 5% v/v CO_2 in the absence of fetal calf serum. The culture supernatant was collected and an SDS-PAGE was run (reduced samples). FH was included as a control. The samples were transferred onto nitrocellulose membrane and probed with polyclonal rabbit polyclonal anti-FH (10 µg IgG/mL) and anti-rabbit IgG-HRP (5 µg/mL) antibodies for 1 h. The detected protein band was visualised using 3,3′diaminobenzidine. (c) The purified proteins were also probed with goat anti-FHR5 polyclonal antibodies (1:1000; R&D: cat. no. AF3845-SP).

confluence. Using ELISA, we analysed the protein secretion at regular intervals of cell growth. There was a significant time dependent increase in FHR5 secretion over 48 h of growth (Fig. 3). These data show that FHR5 is secreted by primary GBM cells B30, B31 and B33, but FH and other members of the FH family are not.

3.2. GBM-FHR5 inhibits complement-mediated lysis of sheep erythrocytes

Sheep erythrocytes have cell surfaces rich in sialic acid and are used as the standard non-activator for human complement analysis. The ability of FHR5 from B30, B31 and B33 cells to recognise sialic acids and inhibit activation of the complement system was assessed by replacing serum depleted of FH family proteins (confirmed by dot blot) with purified GBM-FHR5. We first carried out the haemolytic assay in serum depleted of FH family proteins which demonstrated that sheep erythrocytes were lysed in a dose dependent manner. When sheep erythrocytes were incubated with varying concentrations of FHR5, haemolysis was reduced dose dependently (Fig. 4). 4 µM of FHR5 was needed to achieve complete inhibition of cell haemolysis, whereas 1 µM of FH was needed to reduce lysis to zero.

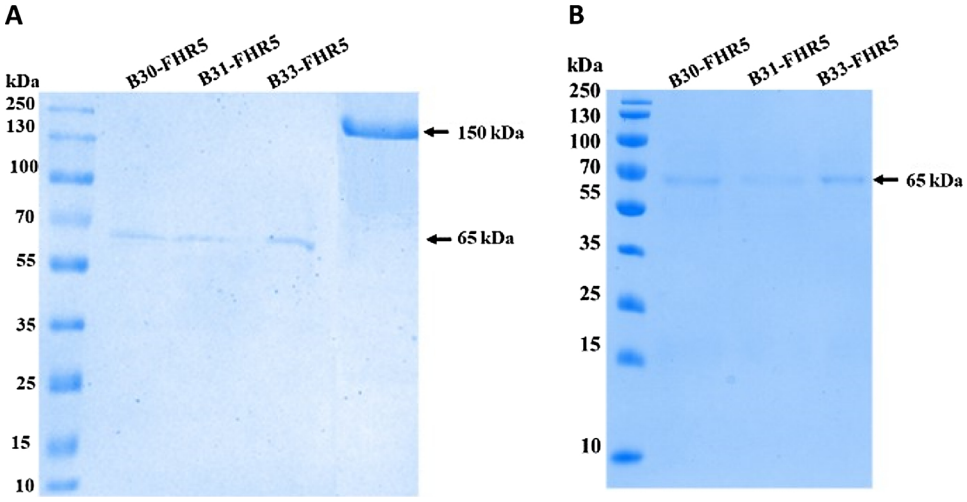

Fig. 2. Purification of FHR5 from primary GBM cells. The supernatant from cultured B30, B31 and B33 cells were dialysed against wash buffer I overnight. The dialysate was passed through a polyclonal anti-human FH Sepharose column. The bound protein was eluted and dialysed against distilled water over night and dialysis buffer I for 4 h. (A) A reduced SDS-PAGE. (B) A non-reduced SDS-PAGE. FH is shown as a control in A.

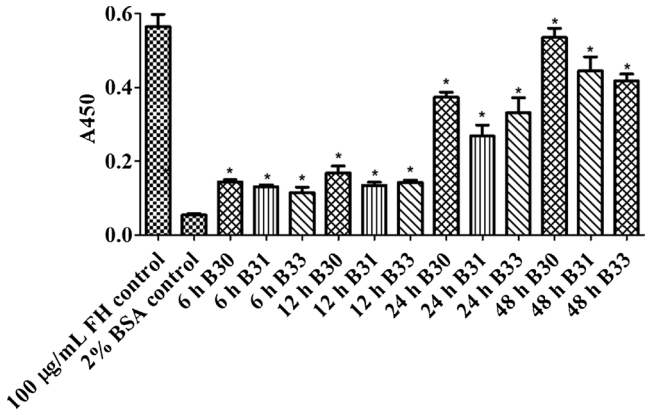

Fig. 3. FHR5 secreted by primary GBM cells. 0.2 × 10 (Liu et al., 2012) primary GBM cells B30, B31 and B33 were grown in the absence of fetal calf serum for 6 h, 12 h, 24 h and 48 h. The culture supernatants were coated onto microtitre plates in 0.05 M carbonate bi-carbonate buffer, wells were blocked with 2% BSA and probed with polyclonal anti-FH (10 µg IgG/mL) and anti-rabbit IgG-HRP (5 µg/mL) antibodies. FH (100 ug/mL) and 2% w/v BSA were coated on plates as controls. The experiments were carried out in triplicates. Data were analysed between the mean A450 for culture supernatants and the mean A450 for 2% BSA. *P < 0.05, error bars represent standard deviation.

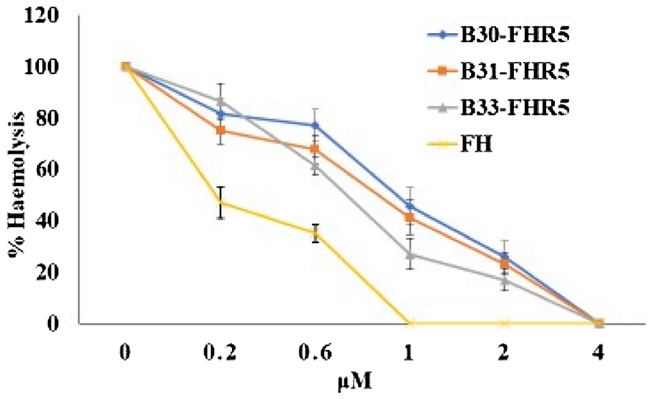

Fig. 4. Inhibition of haemolysis by FHR5. The volume 20 µL of FH family depleted serum capable of giving 50% haemolysis was mixed with DGVB-Mg-EGTA, sheep erythrocytes and varying concentrations of FHR5 or FH (0.2–4 µM). Haemolysis observed is displayed as percentage of the lysis of FH family depleted serum without additions. The experiments were carried out in triplicates. Error bars represent standard deviation.

3.3. GBM-FHR5 shows co-factor activity for factor I-mediated cleavage of C3b

A co-factor assay was performed to measure the ability of FHR5 to act as a co-factor for factor I-mediated cleavage of C3b. Factor I, C3b and GBM-FHR5 or FH were mixed and incubated to allow FHR5 or FH to bind to C3b and enable factor I mediated cleavage. Co-factor activity for factor I was visualised by SDS-PAGE analysis through the loss of or reduced intensity of C3b α- chain and the appearance of two cleaved inactivated C3b (iC3b) fragments at 68 kDa and 43 kDa (Fig. 5A-D). Reactions containing 0.6–4 µM of GBM-FHR5 mediated factor I cleavage of C3b. However, at 0.2 µM (Fig. 5A-C) cleavage was not detected whereas reactions containing 0.2 µM of FH did display C3b cleavage in the presence of factor I (Fig. 5D). In the absence of FHR5 and FH, factor I alone was unable to cleave C3b.

3.4. GBM-FHR5 has decay acceleration activity for C3 convertase

To establish whether GBM-FHR5 had decay acceleration activity as a mechanism to inhibit the alternative pathway, a dissociation assay was carried out. A modified ELISA technique was used to determine the ability of FHR5 to exert decay acceleration activity. Nickel chloride-stabilised C3 convertase was formed and subsequently treated with FHR5 and the control protein, FH. The addition of GBM-FHR5 was successful in dissociating Bb fragment from C3bBb(Ni^{2+}) in a dose-dependent manner (Fig. 6), as shown by the inverse correlation between FHR5 concentration and intact C3 convertase.

4. Discussion

The function of human FHR5 is currently controversial and only limited data is available. There are studies which show that FHR5 has a complement "activating" role (by competing with the down-regulatory effect of FH) (Goicoechea de Jorge et al., 2013) whereas it is also reported that FHR5 can inhibit complement (McRae et al., 2005). An earlier study by Junnikkala et al demonstrated the expression of FH and FHL-1 in GBM H2 cell line, which were found to regulate complement activation (Junnikkala et al., 2000). We therefore investigated whether primary GBM cells would express the same factor H family proteins and if the endogenous product would inhibit or activate complement.

To our knowledge, this is the first study to show that primary GBM cells (B30, B31 and B33), obtained directly from three different GBM patients who underwent brain surgery, were found to secrete FHR5, but not FH. We were able to detect the presence of FHR5 through western blot as the polyclonal anti-FH antibody detected a band at 65 kDa, which corresponds to FHR5. The primary anti-FH polyclonal antibody used can detect FH family proteins as they all share high sequence homology, especially FHR5, as it is the only FHR to share sequence homology with CCP 10-14 of FH (Skerka et al., 2013). FH, FHL-1 and CFHR1–4 were not detected in the culture supernatant of the three primary GBM cells examined in this study. The secretion of FH family proteins was also studied in the H2 cell line to compare the difference between primary cells and a cell line. As expected, H2 cells were found to secrete FH and FHL-1 as previously demonstrated by Junnikkala et al. (2000). The difference in FH family expression between both cell types, highlight the importance of studying primary cancer cells. The absence of FH from primary GBM culture is of interest as it is known to be the most abundant soluble complement inhibitor. We were able to rule out the possibility of the detected protein being a cleaved product of FH as the purification process only produced a single band at 65 kDa for each primary GBM cell (Fig. 2) whereas a cleaved product would show up as having more than one band. Since the purified protein continued to run at 65 kDa on SDS-PAGE under non-reducing conditions, it became evident that the isolated protein was not C4BP (Fig. 2B).

Protein production of FHR5 was supported by an ELISA, which demonstrated that over a 48-h growth period, the concentration of FHR5 gradually increased: with more primary GBM cells present, the greater the quantity of FHR5 secreted. The significant increase in FHR5 secretion over 48 h as well as the lack of FH suggested FHR5 may have a role in the control of complement activation in tumour cells. A previous study by Gasque et al demonstrated that certain glioma cells express FH mRNA; however, its role in complement resistance was not studied (Gasque et al., 1992). They had also shown that an oligodendrocyte cell line (HOG) was able to secrete FH upon IFN-α cytokine stimulation. However, in our study, we observed that primary GBM B30, B31 and B33 produced FHR5 without the addition of cytokines. As FHR5 has a high sequence homology with FH, we wanted to establish whether it was functionally active and could potentially inhibit activation of the complement alternative pathway.

We have demonstrated, via in vitro assays, that purified FHR5 from primary GBM cells is biologically active and our study support a function of FHR5 as a down-regulator of complement. The functional activity was assessed using various techniques including the haemolytic assay. The assay revealed that all three primary GBM-FHR5 exhibited dose-dependent inhibition of sheep erythrocyte lysis (Fig. 4). It is likely

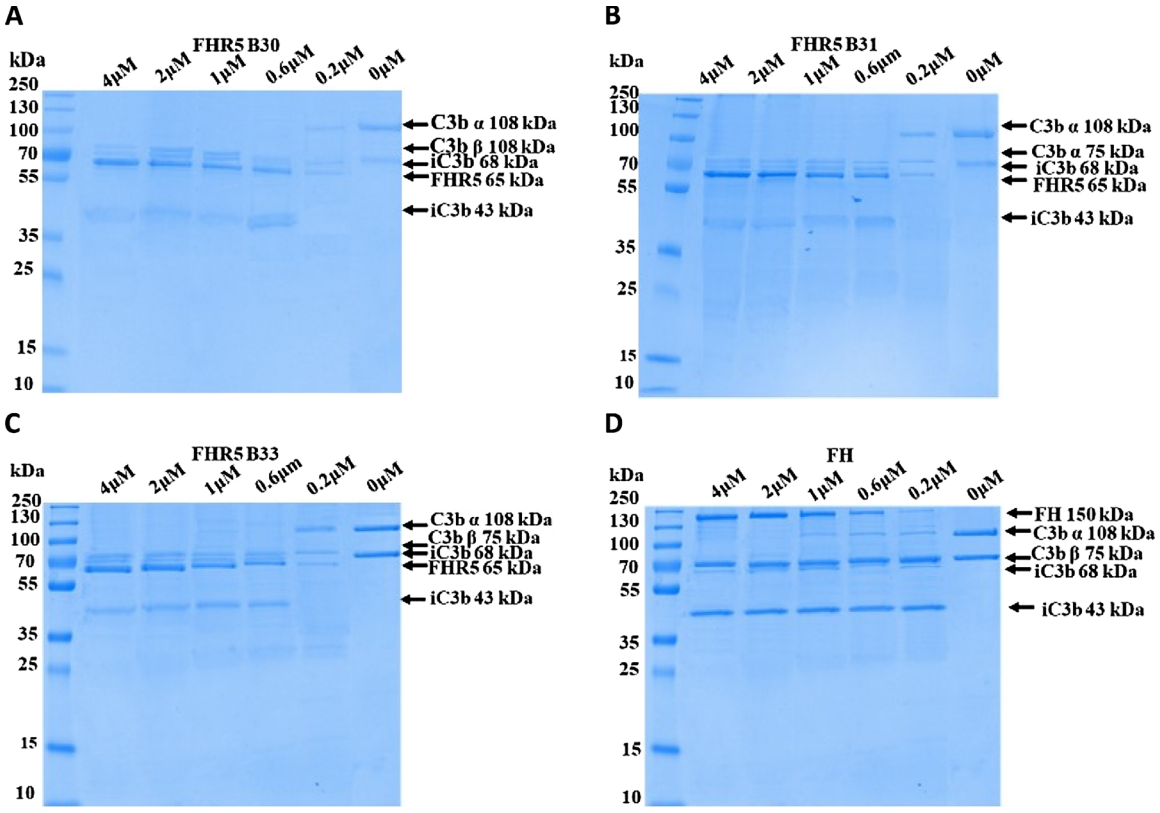

Fig. 5. GBM-FHR5 has factor I-cofactor activity. Varying doses between 0.2–4 μM of GBM-FHR5 were incubated with 3 μg of C3b, 45 ng of Factor I in 10 mM sodium phosphate (pH 6.0) for 10 min at 37 °C. Reactions without GBM-FHR5 or FH and were included as controls. Cleavage of C3b was analysed by SDS-PAGE using Coomassie blue staining.

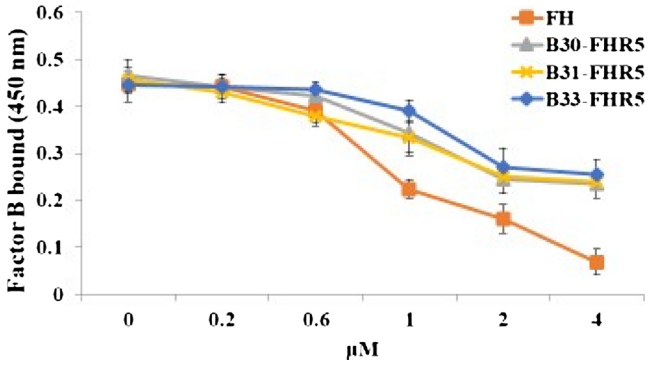

Fig. 6. FHR5 promotes decay acceleration activity on C3 convertase. C3 convertase was generated in microtiter plates with 250 ng of C3b, 400 ng of factor B, 25 ng of factor D, 2 mM nickel chloride, 25 mM NaCl and 4% BSA for 2 h at 37 °C. Varying concentrations of FHR5 (0.2–4 μM) were added and incubated for 30 min at 37 °C. FH and samples without FH and FHR5 were included as controls. Intact C3 convertase was detected by goat anti-human factor B and rabbit anti-goat IgG-HRP antibody. The colour was developed with o-Phenylenediamine. The experiment was repeated in triplicates. Error bars represent standard deviation.

that the implication of FHR5 inhibiting complement activity is to promote tumour survival as tumour cells readily exploit many strategies to overcome immune attack (Jurianz et al., 1999).

Since GBM-FHR5 down-regulated complement lysis of sheep erythrocytes, we wanted to investigate the mechanism through which this inhibitory effect was brought about. Co-factor activity of recombinant FHR5 has been reported (McRae et al., 2005). Therefore, we wanted to study whether this activity was present in GBM-FHR5. GBM-FHR5 was able to act as a co- factor for factor I mediated cleavage of C3b (Fig. 5).

It was clear from SDS-PAGE analysis that the presence of FHR5 had enabled factor I to cleave C3b into inactive iC3b fragments of 68 and 43 kDa. This demonstrated that co-factor activity is a mechanism by which primary GBM-FHR5 can inhibit complement activation.

Human FH displays decay accelerating activity as a mechanism to inhibit activation of the alternative pathway (Brandstatter et al., 2012). We therefore examined the ability of GBM-FHR5 to decay C3 convertase. The inverse correlation depicted on the graph between FHR5 concentration and intact C3 convertase showed that FHR5 was able to decay C3 convertase dose dependently although the activity was less than that of FH (Fig. 6). This was interesting as McRae et al. (2005) were unable to demonstrate recombinant FHR5 decay acceleration activity using the solid phase assay; however, primary GBM-FHR5 were able to show decay acceleration using this assay (McRae et al., 2005).

It is interesting that GBM FHR5 downregulates activation of complement lysis, acts as a co-factor for factor I mediated cleavage of C3b and accelerates the decay of C3 convertase as these functions had been attributed to CCPs 1–4 of FH. FHR5 does not share homology with FH CCP 1-4 which suggests these biological activities may also be associated with CCPs 10–14 or 19–20 of FH as these CCPs share high sequence homology with FHR5.

In summary, our study shows that primary GBM cells B30, B31 and B33 secrete FHR5, which share biological function with human FH. Primary GBM-FHR5 is biologically active and can inhibit complement activation, act as a cofactor for factor I mediated cleavage and degrade C3 convertase in-vitro. These findings warrant additional studies to evaluate the relevance in in-vivo immune surveillance. The elucidation of FHR5 functional activity would potentially help to design efficient complement mediated immunotherapies against GBM.

Acknowledgement

We thank the International Scientific Partnership Program (ISPP) at the King Saud University for funding via ISPP No. 145.

References

Brandstatter, H., Schulz, P., Polunic, I., Kannicht, C., Kohla, G., Romisch, J., 2012. Purification and biochemical characterization of functional complement factor H from human plasma fractions. Vox Sang. 103 (3), 201–212.

Chang, A.L., Miska, J., Wainwright, D.A., Dey, M., Rivetta, C.V., Yu, D., Kanojia, D., Pituch, K.C., Qiao, J., Pytel, P., Han, Y., Wu, M., Zhang, L., Horbinski, C.M., Ahmed, A.U., Lesniak, M.S., 2016. CCL2 produced by the glioma microenvironment is essential for the recruitment of regulatory t cells and myeloid-derived suppressor cells. Cancer Res. 76 (19), 5671–5682.

Clark, S.J., Bishop, P.N., 2015. Role of factor H and related proteins in regulating complement activation in the Macula, and relevance to age-related macular degeneration. J. Clin. Med. 4 (1), 18–31.

Csincsi, A.I., Kopp, A., Zoldi, M., Banlaki, Z., Uzonyi, B., Hebecker, M., Caesar, J.J., Pickering, M.C., Daigo, K., Hamakubo, T., Lea, S.M., Goicoechea de Jorge, E., Jozsi, M., 2015. Factor H-related protein 5 interacts with pentraxin 3 and the extracellular matrix and modulates complement activation. J. Immunol. 194 (10), 4963–4973.

Davies, A., Simmons, D.L., Hale, G., Harrison, R.A., Tighe, H., Lachmann, P.J., Waldmann, H., 1989. CD59, an LY-6-like protein expressed in human lymphoid cells, regulates the action of the complement membrane attack complex on homologous cells. J. Exp. Med. 170 (3), 637–654.

Faithfull, S., Cook, K., Lucas, C., 2005. Palliative care of patients with a primary malignant brain tumour: case review of service use and support provided. Palliat. Med. 19 (7), 545–550.

Fearon, D.T., Austen, K.F., 1977. Activation of the alternative complement pathway with rabbit erythrocytes by circumvention of the regulatory action of endogenous control proteins. J. Exp. Med. 146 (1), 22–33.

Fearon, D.T., 1979. Regulation of the amplification C3 convertase of human complement by an inhibitory protein isolated from human erythrocyte membrane. Proc. Natl. Acad. Sci. U.S.A. 76 (11), 5867–5871.

Fujisawa, H., Kurrer, M., Reis, R.M., Yonekawa, Y., Kleihues, P., Ohgaki, H., 1999. Acquisition of the glioblastoma phenotype during astrocytoma progression is associated with loss of heterozygosity on 10q25-qter. Am. J. Pathol. 155 (2), 387–394.

Furnari, F.B., Fenton, T., Bachoo, R.M., Mukasa, A., Stommel, J.M., Stegh, A., Hahn, W.C., Ligon, K.L., Louis, D.N., Brennan, C., Chin, L., DePinho, R.A., Cavenee, W.K., 2007. Malignant astrocytic glioma: genetics, biology, and paths to treatment. Genes Dev. 21 (21), 2683–2710.

Gabrusiewicz, K., Liu, D., Cortes-Santiago, N., Hossain, M.B., Conrad, C.A., Aldape, K.D., Fuller, G.N., Marini, F.C., Alonso, M.M., Idoate, M.A., Gilbert, M.R., Fueyo, J., Gomez-Manzano, C., 2014. Anti-vascular endothelial growth factor therapy-induced glioma invasion is associated with accumulation of Tie2-expressing monocytes. Oncotarget 5 (8), 2208–2220.

Gasque, P., Julen, N., Ischenko, A.M., Picot, C., Mauger, C., Chauzy, C., Ripoche, J., Fontaine, M., 1992. Expression of complement components of the alternative pathway by glioma cell lines. J. Immunol. 149 (4), 1381–1387.

Goicoechea de Jorge, E., Caesar, J.J., Malik, T.H., Patel, M., Colledge, M., Johnson, S., Hakobyan, S., Morgan, B.P., Harris, C.L., Pickering, M.C., Lea, S.M., 2013. Dimerization of complement factor H-related proteins modulates complement activation in vivo. Proc. Natl. Acad. Sci. U.S.A. 110 (12), 4685–4690.

Gordon, D.L., Kaufman, R.M., Blackmore, T.K., Kwong, J., Lublin, D.M., 1995. 'Identification of complement regulatory domains in human factor H. J. Immunol. 155 (1), 348–356.

Gorter, A., Meri, S., 1999. Immune evasion of tumor cells using membrane-bound complement regulatory proteins. Immunol. Today 20 (12), 576–582.

Hermanson, M., Funa, K., Hartman, M., Claesson-Welsh, L., Heldin, C.H., Westermark, B., Nister, M., 1992. Platelet-derived growth factor and its receptors in human glioma tissue: expression of messenger RNA and protein suggests the presence of autocrine and paracrine loops. Cancer Res. 52 (11), 3213–3219.

Iglesia, M.D., Parker, J.S., Hoadley, K.A., Serody, J.S., Perou, C.M., Vincent, B.G., 2016. Genomic analysis of immune cell infiltrates across 11 tumor types. J. Natl. Cancer Inst. 108 (11). https://doi.org/10.1093/jnci/djw144.

Jokiranta, T.S., Hellwage, J., Koistinen, V., Zipfel, P.F., Meri, S., 2000. Each of the three binding sites on complement factor H interacts with a distinct site on C3b. J. Biol. Chem. 275 (36), 27657–27662.

Jokiranta, T.S., Cheng, Z.Z., Seeberger, H., Jozsi, M., Heinen, S., Noris, M., Remuzzi, G., Ormsby, R., Gordon, D.L., Meri, S., Hellwage, J., Zipfel, P.F., 2005. 'Binding of complement factor H to endothelial cells is mediated by the carboxy-terminal glycosaminoglycan binding site. Am. J. Pathol. 167 (4), 1173–1181.

Junnikkala, S., Jokiranta, T.S., Friese, M.A., Jarva, H., Zipfel, P.F., Meri, S., 2000. 'Exceptional resistance of human H2 glioblastoma cells to complement-mediated killing by expression and utilization of factor H and factor H-like protein 1. J. Immunol. 164 (11), 6075–6081.

Jurianz, K., Ziegler, S., Garcia-Schuler, H., Kraus, S., Bohana-Kashtan, O., Fishelson, Z., Kirschfink, M., 1999. Complement resistance of tumor cells: basal and induced mechanisms. Mol. Immunol. 36 (13–14), 929–939.

Kohl, J., 2006. Self, non-self, and danger: a complementary view. Adv. Exp. Med. Biol. 586, 71–94.

Kuhn, S., Zipfel, P.F., 1996. Mapping of the domains required for decay acceleration activity of the human factor H-like protein 1 and factor H. Eur. J. Immunol. 26 (10), 2383–2387.

Laemmli, U.K., 1970. Cleavage of structural proteins during the assembly of the head of bacteriophage T4. Nature 227 (5259), 680–685.

Liu, K.Q., Liu, Z.P., Hao, J.K., Chen, L., Zhao, X.M., 2012. Identifying dysregulated pathways in cancers from pathway interaction networks. BMC Bioinformatics 13 (126), 11.

Maher, E.A., Brennan, C., Wen, P.Y., Durso, L., Ligon, K.L., Richardson, A., Khatry, D., Feng, B., Sinha, R., Louis, D.N., Quackenbush, J., Black, P.M., Chin, L., DePinho, R.A., 2006. Marked genomic differences characterize primary and secondary glioblastoma subtypes and identify two distinct molecular and clinical secondary glioblastoma entities. Cancer Res. 66 (23), 11502–11513.

McRae, J.L., Cowan, P.J., Power, D.A., Mitchelhill, K.I., Kemp, B.E., Morgan, B.P., Murphy, B.F., 2001. Human factor H-related protein 5 (FHR-5). A new complement-associated protein. J. Biol. Chem. 276 (9), 6747–6754.

McRae, J.L., Duthy, T.G., Griggs, K.M., Ormsby, R.J., Cowan, P.J., Cromer, B.A., McKinstry, W.J., Parker, M.W., Murphy, B.F., Gordon, D.L., 2005. Human factor H-related protein 5 has cofactor activity, inhibits C3 convertase activity, binds heparin and C-reactive protein, and associates with lipoprotein. J. Immunol. 174 (10), 6250–6256.

Medjeral-Thomas, N., Pickering, M.C., 2016. The complement factor H-related proteins. Immunol. Rev. 274 (1), 191–201.

Meri, S., Morgan, B.P., Wing, M., Jones, J., Davies, A., Podack, E., Lachmann, P.J., 1990. Human protectin (CD59), an 18-20-kD homologous complement restriction factor, does not restrict perforin-mediated lysis. J. Exp. Med. 172 (1), 367–370.

Mieczkowski, J., Kocyk, M., Nauman, P., Gabrusiewicz, K., Sielska, M., Przanowski, P., Maleszewska, M., Rajan, W.D., Pszczolkowska, D., Tykocki, T., Grajkowska, W., Kotulska, K., Roszkowski, M., Kostkiewicz, B., Kaminska, B., 2015. Down-regulation of IKKbeta expression in glioma-infiltrating microglia/macrophages is associated with defective inflammatory/immune gene responses in glioblastoma. Oncotarget 6 (32), 33077–33090.

Morgan, B.P., Meri, S., 1994. Membrane proteins that protect against complement lysis. Springer Semin. Immunopathol. 15 (4), 369–396.

Oberndorfer, S., Lindeck-Pozza, E., Lahrmann, H., Struhal, W., Hitzenberger, P., Grisold, W., 2008. The end-of-life hospital setting in patients with glioblastoma. J. Palliat. Med. 11 (1), 26–30.

Ohgaki, H., Dessen, P., Jourde, B., Horstmann, S., Nishikawa, T., Di Patre, P.L., Burkhard, C., Schuler, D., Probst-Hensch, N.M., Maiorka, P.C., Baeza, N., Pisani, P., Yonekawa, Y., Yasargil, M.G., Lutolf, U.M., Kleihues, P., 2004. Genetic pathways to glioblastoma: a population-based study. Cancer Res. 64 (19), 6892–6899.

Pace, A., Di Lorenzo, C., Guariglia, L., Jandolo, B., Carapella, C.M., Pompili, A., 2009. End of life issues in brain tumor patients. J. Neurooncol. 91 (1), 39–43.

Ripoche, J., Day, A.J., Harris, T.J., Sim, R.B., 1988. 'The complete amino acid sequence of human complement factor H. Biochem. J. 249 (2), 593–602.

Seya, T., Turner, J.R., Atkinson, J.P., 1986. Purification and characterization of a membrane protein (gp45-70) that is a cofactor for cleavage of C3b and C4b. J. Exp. Med. 163 (4), 837–855.

Sharma, A.K., Pangburn, M.K., 1996. Identification of three physically and functionally distinct binding sites for C3b in human complement factor H by deletion mutagenesis. Proc. Natl. Acad. Sci. U.S.A. 93 (20), 10996–11001.

Skerka, C., Chen, Q., Fremeaux-Bacchi, V., Roumenina, L.T., 2013. Complement factor H related proteins (CFHRs). Mol. Immunol. 56 (3), 170–180.

Soames, C.J., Sim, R.B., 1997. Interaction between human complement components Factor H, factor I and C3b. Biochem. J. 326, 553–561.

Stupp, R., Mason, W.P., van den Bent, M.J., Weller, M., Fisher, B., Taphoorn, M.J., Belanger, K., Brandes, A.A., Marosi, C., Bogdahn, U., Curschmann, J., Janzer, R.C., Ludwin, S.K., Gorlia, T., Allgeier, A., Lacombe, D., Cairncross, J.G., Eisenhauer, E., Mirimanoff, R.O., European Organisation for Research and Treatment of Cancer Brain Tumor and Radiotherapy Groups and National Cancer Institute of Canada Clinical Trials Group, 2005. Radiotherapy plus concomitant and adjuvant temozolomide for glioblastoma. N. Engl. J. Med. 352 (10), 987–996.

Sugita, Y., Nakano, Y., Tomita, M., 1988. Isolation from human erythrocytes of a new membrane protein which inhibits the formation of complement transmembrane channels. J. Biochem. 104 (4), 633–637.

Weiler, J.M., Daha, M.R., Austen, K.F., Fearon, D.T., 1976. Control of the amplification convertase of complement by the plasma protein beta1H. Proc. Natl. Acad. Sci. U.S.A. 73 (9), 3268–3272.

Whaley, K., Ruddy, S., 1976. Modulation of the alternative complement pathways by beta 1 H globulin. J. Exp. Med. 144 (5), 1147–1163.

Yu, B.B., Moffatt, B.E., Fedorova, M., Villiers, C.G., Arnold, J.N., Du, E., Swinkels, A., Li, M.C., Ryan, A., Sim, R.B., 2014. Purification, quantification, and functional analysis of Complement Factor H. Methods Mol. Biol. 1100, 207–223.

frontiers in Immunology

ORIGINAL RESEARCH
published: 25 March 2020
doi: 10.3389/fimmu.2020.00355

Complement-Independent Modulation of Influenza A Virus Infection by Factor H

*Valarmathy Murugaiah[1], Praveen M. Varghese[1,2], Soad M. Saleh[3], Anthony G. Tsolaki[1], Salman H. Alrokayan[4], Haseeb A. Khan[4], Kate S. Collison[3], Robert B. Sim[5], Béatrice Nal[1], Futwan A. Al-Mohanna[3] and Uday Kishore[1]**

[1] Biosciences, College of Health and Life Sciences, Brunel University London, Uxbridge, United Kingdom, [2] School of Biosciences and Technology, Vellore Institute of Technology, Vellore, India, [3] Department of Cell Biology, King Faisal Specialist Hospital and Research Centre, Riyadh, Saudi Arabia, [4] Department of Biochemistry, College of Science, King Saud University, Riyadh, Saudi Arabia, [5] Department of Biochemistry, University of Oxford, Oxford, United Kingdom

The complement system is an ancient innate immune defense mechanism that can recognize molecular patterns on the invading pathogens. Factor H, as an inhibitor of the alternative pathway, down-regulates complement activation on the host cell surface. Locally synthesized factor H at the site of infection/injury, including lungs, can act as a pattern recognition molecule without involving complement activation. Here, we report that factor H, a sialic acid binder, interacts with influenza A virus (IAV) and modulates IAV entry, as evident from down-regulation of matrix protein 1 (M1) in H1N1 subtype-infected cells and up-regulation of M1 expression in H3N2-infected A549 cells. Far-western blot revealed that factor H binds hemagglutinin (HA, ∼70 kDa), neuraminidase (NA, ∼60 kDa), and M1 (∼25 kDa). IAV-induced transcriptional levels of IFN-α, TNF-α, IL-12, IL-6, IFN-α, and RANTES were reduced following factor H treatment for the H1N1 subtype at 6 h post-infection. However, for the H3N2 subtype, mRNA levels of these pro-inflammatory cytokines were enhanced. A recombinant form of vaccinia virus complement control protein (VCP), which like factor H, contains CCP modules and has complement-regulatory activity, mirrored the results obtained with factor H. Both factor H (25%), and VCP (45%) were found to reduce luciferase reporter activity in MDCK cells transduced with H1N1 pseudotyped lentiviral particles. Factor H (50%) and VCP (30%) enhanced the luciferase reporter activity for H3N2, suggesting an entry inhibitory role of factor H and VCP against H1N1, but not H3N2. Thus, factor H can modulate IAV infection and inflammatory responses, independent of its complement-related functions.

Keywords: innate immunity, complement, factor H, vaccinia virus complement control protein, influenza A virus, pseudotyped lentiviral particles, cytokine storm

OPEN ACCESS

Edited by:
Jagadeesh Bayry, Institut National de la Santé et de la Recherche Médicale (INSERM), France

Reviewed by:
Kenneth Reid, University of Oxford, United Kingdom
Lubka T. Roumenina, INSERM U1138 Centre de Recherche des Cordeliers, France

***Correspondence:**
Uday Kishore
Uday.Kishore@brunel.ac.uk

Specialty section:
This article was submitted to Molecular Innate Immunity, a section of the journal Frontiers in Immunology

Received: *15 January 2020*
Accepted: *13 February 2020*
Published: *25 March 2020*

Citation:
Murugaiah V, Varghese PM, Saleh SM, Tsolaki AG, Alrokayan SH, Khan HA, Collison KS, Sim RB, Nal B, Al-Mohanna FA and Kishore U (2020) Complement-Independent Modulation of Influenza A Virus Infection by Factor H. Front. Immunol. 11:355. doi: 10.3389/fimmu.2020.00355

INTRODUCTION

Influenza A virus (IAV) is a severe respiratory pathogens, belonging to the Orthomyxoviridae family and responsible for outbreaks with high morbidity, and mortality in both humans and animals (1). IAV exhibits antigenic variations within viral surface glycoproteins, including hemagglutinin (HA), and neuraminidase (NA) (2). HA is the most important viral glycoprotein that can bind to sialic acid on host cells, enabling cellular fusion and viral entry (3). HA

epitopes are also known to trigger synthesis of neutralizing antibodies by B cells, allowing IAV to escape from immune surveillance, leading to seasonal epidemics (4). NA cleaves sialic acid moieties, which enables release of virions, and promotes IAV dispersion (5). There are around 16 antigenic variants of HA and 9 of NA, which are found in numerous combinations and subtypes (2, 6). Among all subtypes of IAV, H1N1 and H3N2 are the predominant IAV subtypes for seasonal flu in humans, with annual epidemics estimated to result in ∼5 million cases of severe illness and half a million respiratory deaths (7). Current circulating human IAV strains are likely to continue acquiring mutations resulting in antigenic drift and shift of HA and NA glycoproteins (8, 9), which enhance the virus' ability to evade host immune system, promoting rapid viral invasion and replication.

Airway and alveolar epithelial cells are the primary targets for IAV, which uses sialic acid as receptors, causing damage to the alveolar epithelium (10, 11). Individuals infected with IAV may become susceptible to acute respiratory distress syndrome (ARDS) (12, 13). Lung epithelial cells express mucin glycoproteins, such as MUC5AC, MUC5B, and MUC1, which play an important role in restricting IAV infectivity (14–16). These mucins are rich in sialic acid, serve as viral receptors, and restrict viral binding to the target cells (16–18). However, NA can attenuate the biological activity of these mucins (18, 19). The D151G mutation is a well-known mutation in NA glycoprotein, which is responsible for its interaction with human α2-6 and avian α2-3 linked sialic acid, mediating the H3N2 viral association with sialic acid receptors. However, this mutation is reported to reduce the enzymatic action of NA that is required for HA detachment from its receptors (19, 20). Early defense against invading IAV by the innate immune system is crucial in limiting viral replication and invasion. The complement system, a major humoral wing of innate immunity, offers a crucial protective mechanism against IAV infection (21). This includes neutralization, aggregation, opsonization and lysis of viral particles, and induction of phagocytosis via complement receptors (22, 23). A number of *in vitro* and *in vivo* studies have established the protective role of the complement system against IAV (24–27).

In the alternative pathway of the complement system, factor H is an important negative regulator that interacts with negatively charged surfaces containing sialic acids and glycosaminoglycans, and protects cellular structures from C3 convertase formation, hence diminishing complement activation. Factor H is a soluble, 155 kDa glycoprotein present at a concentration of 128–654 μg/ml in human plasma (28). It is composed of 20 complement control protein (CCP) modules with different ligand binding properties. There is plenty of evidence of the local extrahepatic synthesis of factor H [reviewed in (30)]. Factor H binds to many pathogens via charge interactions (29), and for pathogens, surface-bound factor H may be of benefit for their survival. Factor H binds to sialic acids on *Neisseria gonorrhoeae* (30) and the outer surface of OspE of *Borrelia burgdorferi*, providing complement resistance to these pathogenic microbes. Its interaction with soluble West Nile virus NS1 protein has also been described (31). Furthermore, *Plasmodium falciparum* binds factor H and factor H-like protein 1 (FHL-1) to prevent complement-mediated lysis in the mosquito midgut via the plasmodial transmembrane gliding-associated protein 50 (GAP50) (32). Factor H can also bind to the surface of mycobacteria, restrict their uptake by macrophages, and modulate pro-inflammatory cytokine responses (33).

Viruses employ diverse strategies to protect their viral lipid envelopes from complement lysis by encoding or recruiting complement inhibitors, with structural and functional similarities to complement control proteins (CCP). Vaccinia virus complement control protein (VCP) is a well-known complement inhibitor, secreted by vaccinia virus infected cells. VCP has inhibitory activity for both classical and alternative pathways (34). Further examples of viral regulation of complement includes binding of West Nile virus non-structural protein (NS1) to factor H, or association of Nipah virions with factor I, thus restricting complement activation (31, 35). In addition, NS1 serves as a key inhibitor of innate immunity as it blocks the synthesis and signaling of type 1 interferons (IFNs) (36). NS1 also induces apoptosis in human airway epithelial cells during IAV infection via caspase-dependent mechanisms (37).

Since factor H can bind to sialic acids, a natural ligand for IAV, it is of interest to examine potential influence of factor H in competitively inhibiting IAV interaction with host cell surfaces. This study was designed to investigate the complement independent functions of factor H in the regulation of IAV infection *in vitro*. Here, we report the ability of human factor H and recombinant VCP to act as entry inhibitors of IAV.

MATERIALS AND METHODS

Viruses and Reagents

The IAV subtypes used in this study, including the pH1N1 (A/England/2009) and H3N2 (A/HK/1999), were provided by Wendy Barclay (Imperial College, London) and Leo Poon (University of Hong Kong), respectively. The plasmids used for the production of H1N1 and H3N2 pseudo-typed viral particles were obtained from Addgene; pHIV-Luciferase (Addgene plasmid #21375); psPAX2 (Addgene plasmid # 12260); and Vesicular Stomatitis Virus (VSV-G) (Addgene plasmid #8454). pcDNA3.1-swineH1-flag (H1 from swine H1N1 A/California/04/09) (Invitrogen), pcDNA3.1-swine N1-flag (N1 from swine H1N1 A/California/04/09), and pCDNA H3 (from A/Denmark/70/03 (H3N2) (Invitrogen) were obtained commercially. pI.18-N2 [N2 from A/Texas/50/2012/(H3N2)] plasmid was a gift from Nigel Temperton (University of Kent). Anti-influenza antibodies used were obtained from BEI Resources, NIAID, NIH, USA, and used as previously described (38); these include polyclonal anti-influenza Virus H3 HA, A/Hong Kong/1/1968 and monoclonal anti-influenza virus H1 HA, A/California /04/2009.

Purification of Human Complement Factor H

Complement factor H was purified from human plasma, as described previously (39), using an affinity column made up of a monoclonal antibody against human factor H (MRCOX23)

coupled to CNBr-activated Sepharose (GE healthcare, UK). Freshly thawed human plasma (Fisher Scientific) was adjusted to 5 mM EDTA, pH 8, and dialyzed overnight against Buffer I (25 mM Tris-HCL, 140 mM NaCl, and 0.5 mM EDTA, pH 7.5). MRCOX23 Sepharose column was washed with three bed volumes of buffer I, and dialyzed plasma was passed through the column. The column was then washed again with the same buffer and factor H was eluted using 3 M $MgCl_2$, pH 6.8. The eluted fractions were dialyzed against H_2O overnight, followed by 10 mM potassium phosphate pH 7.4. The samples were then analyzed for purity by 12% v/v SDS-PAGE.

Purification of Recombinant Vaccinia Virus Complement Control Protein Expressed in HEK293 Cell Line

The VCP gene (accession X13166.1) was codon-optimized for expression in human embryonic kidney (HEK) cells by GeneArt® using GeneOptimizer® (Geneart GmbH, Regensburg). For lentiviral expression, amplified VCP cDNA was ligated into the pLenti6/V5-D-TOPO vector, using the ViraPower Lentiviral Directional TOPO Expression kit, according to the manufacturer's instructions (K4950-00 Invitrogen Corp, Carlsbad CA). Following transformation into DH5α chemically competent *E. coli* cells, a number of colonies were analyzed for correct insertion and orientation using colony PCR. Transient transfection of the plasmid pLenti6/V5/VCP in HeLa cells and indirect immunofluorescence using anti-V5 antibody (Invitrogen # R960-25) was performed to verify the VCP expression. Replication-incompetent lentiviral stock was made by co-transfection with the ViraPower™ Packaging Mix (pLP1, pLP2, and pLP/VSVG: K4975-00, Invitrogen Corp) in HEK 293FT cells (ATCC CRL-1573) cells using Lipofectamine 2000® reagent (Life Technologies Inc.), according to the manufacturer's instructions. Forty-eight hours after co-transfection, viral supernatant was collected, concentrated by centrifugation, and the titer was determined using standard procedures. A number of stable HEK 293FT cell lines expressing VCP were generated under neomycin selection (0.5 g/L) and screened for VCP expression by Western blot analysis. Three clones of HEK-293 cells secreting high levels of the VCP were selected and cultured. Secreted VCP was purified using a heparin column. Column-bound proteins were eluted with a linear salt gradient (0–0.5 M NaCl). Fractions were collected and analyzed via SDS-PAGE and western blotting.

Cell Culture and Treatments

Madin Darby Canine Kidney (MDCK) and Adenocarcinomic human alveolar basal epithelial cells (A549) cells (ATCC, Rockville, MD, USA) were cultured in complete DMEM media, supplemented with 10% v/v fetal calf serum, 2 mM L-glutamine, and penicillin (100 U/ml)/streptomycin (100 μg/ml) (Thermo Fisher), at 37°C under 5% v/v CO_2, with fresh complete medium added every 2–3 days until 80% confluence was reached. Cell lines used in this study were subjected to a maximum of 7 passages for *in vitro* experiments.

Production of IAV Subtypes and Pseudotyped Viral Particles, and TCID50 (Median Tissue Culture Infectious Dose) Assay

50,000 MDCK cells at 80% confluency were infected either with pH1N1 (2×10^4) or H3N2 (3.3×10^4) particles and incubated in complete DMEM medium at 37°C for 1 h. Unbound viral particles were removed and replaced with infection medium, composed of DMEM with 0.3% bovine serum albumin (BSA), 1% penicillin/streptomycin, and 1 μg/ml of l-1-tosylamido-2-phenylethyl chloromethyl ketone (TPCK)— Trypsin (Sigma –Aldrich), and incubated for 3 days under culture conditions, as mentioned above. Post infection, supernatant was subjected to ultra-centrifugation (25,000 × g) for 90 min at 4°C. Purified viral particles were then re-suspended in PBS, and purity of the virus was analyzed by SDS-PAGE and western blotting. Production of pseudotyped particles was carried out, as described earlier (38). Briefly, HEK293T cells were co-transfected with 20 μg of respective IAV pCDNAs, including pcDNA3.1-swineH1-flag (H1 from swine H1N1 A/California/04/09) (Invitrogen), pcDNA3.1-swine N1-flag (N1 from swine H1N1 A/California/04/09) (Invitrogen), pcDNA-H3 [H3 from A/Denmark/70/03/(H3N2)], pI.18-N2 [N2 from A/Texas/50/2012/(H3N2)], pHIV-Luciferase backbone (Addgene), and psPAX2 (Addgene). VSV-G was generated similarly, without H1N1 and H3N2 pcDNAs. The released H1N1, H3N2, and VSV-G pseudotyped lentiviral particles were harvested in the supernatant at 48 h. Harvested supernatant was centrifuged at 5,000 × g for 20 min, and the clear supernatant without any debris was concentrated using ultra centrifugation (25,000 × g) for 90 min. The ultra-centrifuged lentiviral particles were re-suspended in sterile PBS and analyzed via TCID50, western blotting and luciferase activity assay. TCID50 assay was carried out to determine the viral titer and cytopathic effects of infected cells (40). Briefly, MDCK cells (1×10^5) were infected with either purified pH1N1 and H3N2 viral parties or pseudotyped lentiviral particles, incubated at 37°C for 3 days under 5% v/v CO_2, until a cytopathic effect was observed in terms of structural changes in MDCK cells caused by viral invasion.

Hemagglutination Inhibition Assay

In a 96 microtiter well plate, 25 μl of PBS was added to each well. In the first column, a starting concentration (total volume 50 μl) of 20 μg of factor H was serially diluted (25 μl) to achieve final quantities of 20, 10, 5, and 2.5 μg of factor H per well. Twenty-five microliters of respective IAV subtype particles were added to wells, except for PBS control wells, at the dilutions corresponding to their respective HA titer to initiate hemagglutination. Plates were gently mixed and incubated at 37°C for 1 h. Fifty microliter of 0.75% v/v guinea pig RBCs was added to each well; plates were gently mixed and incubated at room temperature for 1 h. Inhibition of hemagglutination appeared as a halo or circle of settled cells in the center of round-bottomed wells. Absence of inhibition was observed as a uniform red color across the well (hemagglutination).

ELISA to Detect Interaction of Factor H and VCP With IAV Subtypes

Factor H or VCP (5, 2.5, 1.25, and 0.625 μg/well in 100 μl volume) were coated onto 96-well microtiter plates using carbonate-bicarbonate buffer (CBC), pH 9.6, and incubated at 4°C overnight. After washing the microtiter wells with PBS, the wells were blocked with 2% w/v BSA in PBS and incubated at 37°C for 2 h, followed by three PBST (PBS + 0.05% v/v Tween 20) washes. Twenty microliters of H1N1 or H3N2 virus (1.36×10^6 pfu/ml) in PBS were added to each well and incubated at 37°C for 2 h in the presence of 5 mM $CaCl_2$. VSV-G pseudotyped lentivirus was used as a negative control. Following PBST washes, the corresponding wells were incubated with primary antibodies (100 μl/well): polyclonal anti-influenza virus H3 and monoclonal anti-influenza virus H1 (1:5,000) (BEI-Resources). The wells were again washed with PBST three times and probed with Protein A-HRP-conjugate, or goat anti-mouse IgG-horseradish peroxidase (HRP)-conjugate (1:5,000) (Fisher Scientific), followed by incubation at 37°C for 1 h. Color was developed using 3,3′, 5,5′-tetramethylbenzidine (TMB) substrate (Sigma-Aldrich), and reaction was stopped using 1M H_2SO_4, followed by measuring absorbance at 450 nm, using iMark™ microplate absorbance reader (Bio-Rad).

Cell Binding Assay to Detect IAV Interference With Factor H and VCP

A549 cells (1×10^5 cells/well) were seeded in 96 microtiter wells and incubated at 37°C overnight in 5% v/v CO_2. Once 80% confluency was reached, the cells were washed twice with sterile PBS. Factor H or VCP (10, 5, 2.5, 1.25 μg/ml), pre-incubated with H1N1 and H3N2 (1.36×10^6 pfu/ml) IAV subtypes, were added to the wells (in 5 mM $CaCl_2$) and incubated at room temperature for 2 h. BSA was used as a negative control. Following washes with PBS three times, the corresponding wells were fixed with 4% v/v paraformaldehyde (Fisher Scientific) for 5 min at room temperature. The wells were then blocked with 2% w/v BSA for 2 h at 37°C. Polyclonal anti-influenza virus H3 (BEI-Resources) and monoclonal anti-influenza H1 (BEI-Resources) were added to the appropriate wells and incubated at 37°C for 1 h. After gentle washes with PBSST, the wells were probed with protein A-HRP conjugate or goat anti-mouse IgG-HRP-conjugate (Thermo-Fisher) diluted in PBS in 1:5,000 dilution and incubated at 37°C for 1 h. The wells were washed again with PBST; the color was developed by adding TMB substrate and the reaction was stopped by using 1M H_2SO_4. The absorbance was read at 450 nm using an ELISA plate reader.

Far-Western Blotting

Purified H1N1/H3N2 (1.36×10^6 pfu/ml) virus particles were run on a 12% (w/v) SDS-PAGE, and transferred onto a PVDF membrane for 2 h at 320 mA in transfer buffer (25 mM Tris–HCl, pH 7.5, 20% v/v methanol, and 190 mM glycine). Membrane was blocked with PBS+5% w/v BSA (Sigma-Aldrich) at room temperature, followed by PBST washes. The membrane was then incubated with 10 μg/ml of factor H or VCP overnight at 4°C, and probed appropriately with either monoclonal mouse anti-human factor H (MRCOX23) (MRC Immunochemistry Unit, Oxford) (1 mg/ml) or rabbit anti-VCP polyclonal antibody (0.5 mg/ml) (King Faisal Specialist Hospital and Research Center, Saudi Arabia) at room temperature for 1 h. Following PBST washes (three times, 10 min each), the membrane was incubated with secondary antibody, rabbit anti-mouse IgG HRP conjugate (1:1,000) (Sigma-Aldrich) or Protein A-HRP-conjugate for 1 h at room temperature. The secondary antibody was removed, followed by PBST washes; then the membrane was developed using 3,3′-diaminobenzidine (DAB).

Infection Assay for Extracting RNA

A549 (5×10^5/well) cells were cultured in complete DMEM and grown overnight at 37°C in a CO_2 incubator. Once 85% cell confluency was reached, the cells were washed gently with fresh PBS and replaced with DMEM without FBS. Forty μg/ml of factor H or VCP was added to corresponding wells, with a MOI = 1:1 of pH1N1, and H3N2 or pseudotyped viral particles (333 μl/ml) at room temperature for 1 h and at 4°C for another hour. The unbound virus and protein were removed by pipetting out the supernatant. The cells were washed gently again with PBS, and placed in 1 ml of infection medium to initiate viral infection of the host cells being incubated for 2 and 6 h. After removing the supernatant, the infected cells were washed with PBS and detached using 2 × Trypsin-EDTA (0.5%) (Fisher Scientific), centrifuged at 1,500 x g for 5 min, and the cell pellet was frozen at −80°C for RNA extraction.

Quantitative RT-PCR Analysis

The virus infected cell pellets were lysed using lysis buffer (50 mM Tris–HCl, pH 7.5, 200 mM NaCl, 5 mM EDTA pH 8, 0.1% v/v Triton X-100). GenElute Mammalian Total RNA Purification Kit (Sigma-Aldrich) was used to extract the total RNA, as per the manufacturer's instructions. Once RNA was extracted, DNase I (Sigma-Aldrich) treatment was performed to remove any DNA contaminants, followed by quantifying the amount of RNA at A260 nm using a NanoDrop 2000/2000c (Fisher-Scientific). The purity of RNA was assessed using the ratio A260/A280. Two micrograms of total RNA was used to synthesize cDNA, using High Capacity RNA to cDNA Kit (Applied Biosystems) and cDNA conversion was performed. The primer BLAST software (Basic Local Alignment Search Tool) was used to design primer sequences as listed in **Table 1**. The qRT-PCR assay was performed using the StepOne Plus system (Applied Biosciences). Each qPCR reaction was conducted in triplicates, containing 75 nM of forward and reverse primers, 5 μl Power SYBR Green MasterMix (Applied Biosystems), and 500 ng of cDNA. qPCR samples were run for 50°C and 95°C for 2 and 10 min, followed by running the amplification template for 40 cycles, each cycle involving 15 s at 95°C and 1 min at 60°C. Eighteen seconds RNA was used as an endogenous control to normalize the gene expression.

Statistical Analysis

The graphs were generated using the GraphPad Prism 6.0 software, A one-way ANOVA test was carried out for statistical

significance. Significant values were considered based on $^{*}p < 0.05$, $^{**}p < 0.01$, and $^{***}p < 0.001$, between treated and untreated conditions. Error bars show the SD or SEM, as indicated in the figure legends.

RESULTS

Factor H Inhibits Hemagglutination of Guinea Pig Red Blood Cells by IAV

Factor H was purified from human plasma, using monoclonal MRCOX23 Sepharose affinity column (39). The purity of the eluted protein was confirmed by SDS-PAGE; the molecular weight of factor H was evident at ∼155 kDa (**Figure 1A**). Recombinant VCP appeared pure and migrated at ∼35 kDa (**Figure 1B**). Guinea pig RBCs were used to determine if addition of factor H would inhibit hemagglutination by IAV subtypes (**Figure 2**). Five IAV strains of H3N2 or H1N1 subtypes were tested. The basic principle of this assay relies on the specific feature of envelope viral glycoproteins that can interact with sialic acid on RBCs. In the absence of viral particles, RBCs sedimented under gravity, forming a distinct red halo at the bottom of the microtiter well (**Figure 2**). However, in the presence of viral particles, glycoproteins of virus (HA or NA in this case) interact and bind with sialic acid on RBCs, forming clumps, leading to a lattice formation, where RBCs remain in suspension. Factor H partially inhibited the hemagglutination of IAV strains. Low concentration of factor H (2.5 μg/ml) was more potent in inhibiting hemagglutination of H1N1 than H3N2 strains. Hemagglutination of all strains was effective using 10 μg/ml of factor H. It is possible that factor H binds to the IAV particles, restricting the binding of virus to RBCs, allowing them to form a halo at the bottom of the wells. PBS alone, in the absence of IAV particles, led to the formation of a halo at the bottom of the microtiter well, suggesting no hemagglutination.

TABLE 1 | Primers used for target genes in qPCR.

Target	Forward primer	Reverse primer
18S rRNA	5′-ATGGCCGTTCTTAGTT GGTG-3′	5′-CGCTGAGCCAGTCAGTG TAG-3′
IL-6	5′-GAAAGCAGCAAAGAG GCACT-3′	5′-TTTCACCAGGCAAGT CTCCT-3′
IL-12	5′-AACTTGCAGCTGAAGC CATT-3′	5′-GACCTGAACGCAGAAT GTCA-3′
TNF-α	5′-AGCCCATGTTGTAGCAA ACC-3′	5′-TGAGGTACAGGCCCTC TGAT-3′
M1	5′AAACATATGTCTGATAACG AAGGAGAACAGTTCTT-3′	5′GCTGAATTCTACCTCATGG TCTTCTTGA-3′
RANTES	5'-GCGGGTACCATGAAGA TCTCTG-3'	5'-GGGTCAGAATCAAGAAAC CCTC-3'
IFN-α	5′-TTT CTC CTG CCT GAA GGA CAG-3′	5′-GCT CAT GAT TTC TGC TCT GAC A-3′

Factor H and VCP Bind IAV Envelope Glycoproteins

Since factor H was able to inhibit hemagglutination by H1N1 and H3N2 IAV subtypes, a direct ELISA was set up with factor H -coated plates to establish possible interaction with IAV viruses (**Figure 3**). We also examined, for the first time, the likely interaction between IAV and VCP, which contains CCP modules (4) like human factor H. A/England/2009 (H1N1) and A/Hong Kong/1999 (H3N2) strains were used in this study. A comparable dose-dependent binding by factor H and VCP was evident with H1N1 (**Figure 3A**) and H3N2 (**Figure 3B**) subtypes. VSV-G pseudotyped lentivirus was used as a negative control,

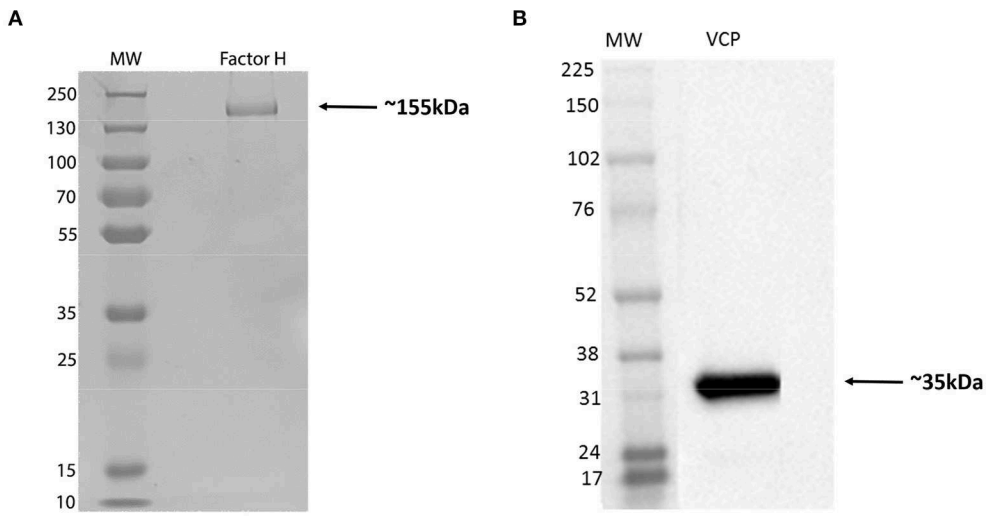

FIGURE 1 | 12% (w/v) SDS-PAGE analysis of complement factor H purified from human plasma **(A)**, and a recombinant form of vaccinia virus complement control protein (VCP) expressed in HEK 293FT cells **(B)**. The purified protein was run under reducing conditions: Factor H appears as ∼155 kDa band, and VCP was observed at ∼35 kDa.

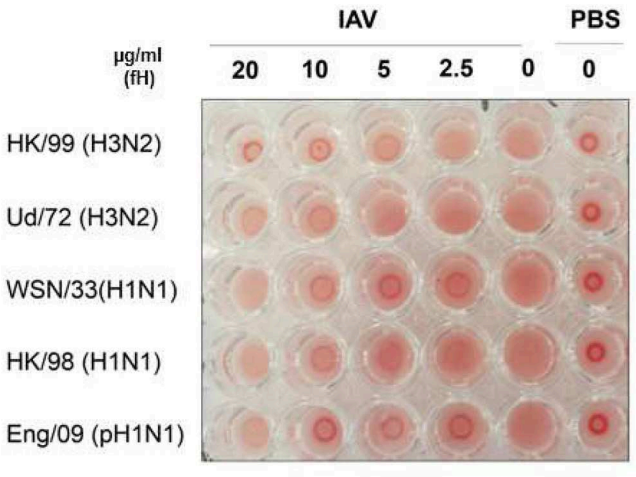

µg/ml (fH)	IAV 20	10	5	2.5	0	0 (PBS)
HK/99 (H3N2)	X	X	X	X	✓	X
Ud/72 (H3N2)	X	X	✓	✓	✓	X
WSN/33(H1N1)	✓	X	X	X	✓	X
HK/98 (H1N1)	✓	X	X	✓	✓	X
Eng/09 (pH1N1)	✓	X	X	X	✓	X

FIGURE 2 | Hemagglutination assay. Inhibition of hemagglutination by purified human factor H was tested on human IAV subtypes. Guinea pig red blood cells were incubated with either PBS or IAV subtypes with and without various concentrations of factor H (20, 10, 5, and 2.5 µg).

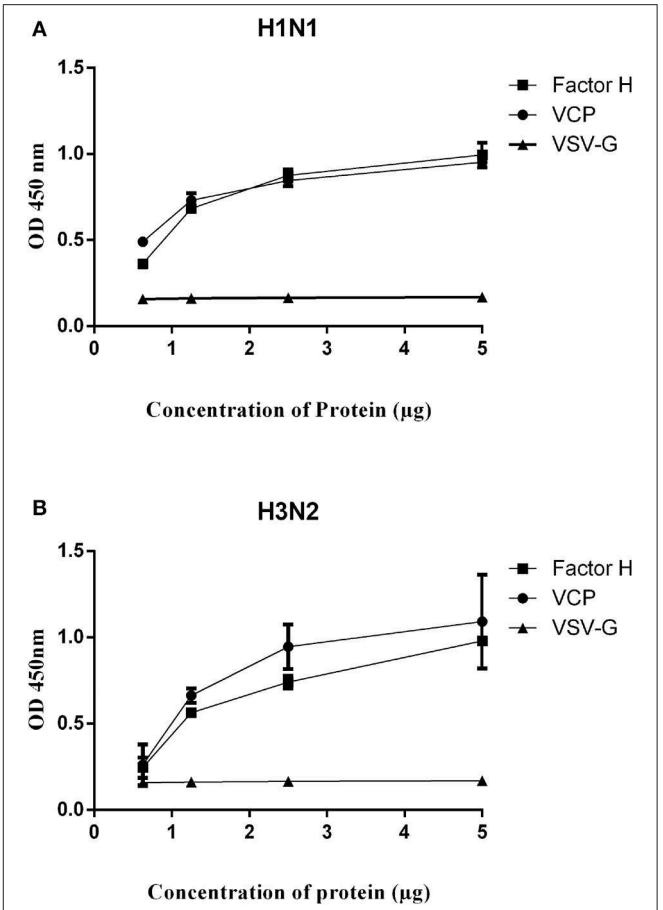

FIGURE 3 | Binding between factor H or VCP with H1N1 **(A)**, and H3N2 **(B)** IAV subtypes were determined via ELISA. Microtiter wells were coated with various concentrations of factor H, VCP or VSV-G (0.625, 1.25, 2.5, and 5 µg/well) in carbonate bicarbonate buffer, pH 9.6 overnight at 4°C. H1N1 or H3N2 virus (1.36×10^6 pfu/ml) was added to each well in the presence of 5 mM $CaCl_2$ and probed with either monoclonal anti-influenza virus H1 or polyclonal anti-influenza virus H3 antibody. VSV-G pseudotyped particles were used as a negative RNA virus control. The data were expressed as mean of three independent experiments done in triplicates ± SEM.

which did not show any binding with either factor H or VCP. The ability of factor H and VCP to interfere with IAV binding to A549 cells was then assessed via the cell binding assay (**Figure 4**). An increase of IAV binding in presence of factor H and VCP was seen at the concentration of 10 µg/ml for both H1N1 and H3N2 IAV subtypes, and the binding occurred in a dose and calcium dependent manner (**Figure 4**), suggesting that factor H and VCP enhance binding of IAV to target cells, which in turn interferes with viral infection in a complement-independent manner. The binding of factor H and VCP was more effective in the case of H1N1 than H3N2. We then set up a far western blot to identify viral particles binding to factor H and VCP (**Figure 5**). In this assay, virus subtypes (H1N1 and H3N2) separated on SDS-PAGE were transferred to a nitrocellulose membrane and were probed with either 10 µg/ml factor H or VCP. The far western blot also revealed the binding of factor H and VCP to HA (∼70 kDa), and M1 (∼25 kDa) of both H1N1 and H3N2 IAV subtypes (**Figure 5**). Furthermore, factor H also bound to NA (∼55 kDa) of H3N2 strain more strongly compared to H1N1 strain.

Modulation of IAV Infectivity by Factor H and VCP in A549 Cells

In view of factor H and VCP binding to key IAV proteins, an infection assay was set up to assess the impact of this interaction on viral infectivity and replication by factor H and VCP. A549 lung epithelial cells, infected with H1N1 and H3N2 with and without factor H or VCP (40 µg/ml), showed differential expression of M1 mRNA levels at 2 and 6 h post-infection (**Figure 6**). In the case of H1N1, both factor H and VCP led to the down-regulation ($-4\ \log_{10}$) of viral M1 transcription at 6 h. However, an up-regulation was seen with H3N2 ($2\log_{10}$) subtype following factor H and VCP treatment, suggesting that the inhibitory effect by these proteins is strain specific (**Figure 6A**).

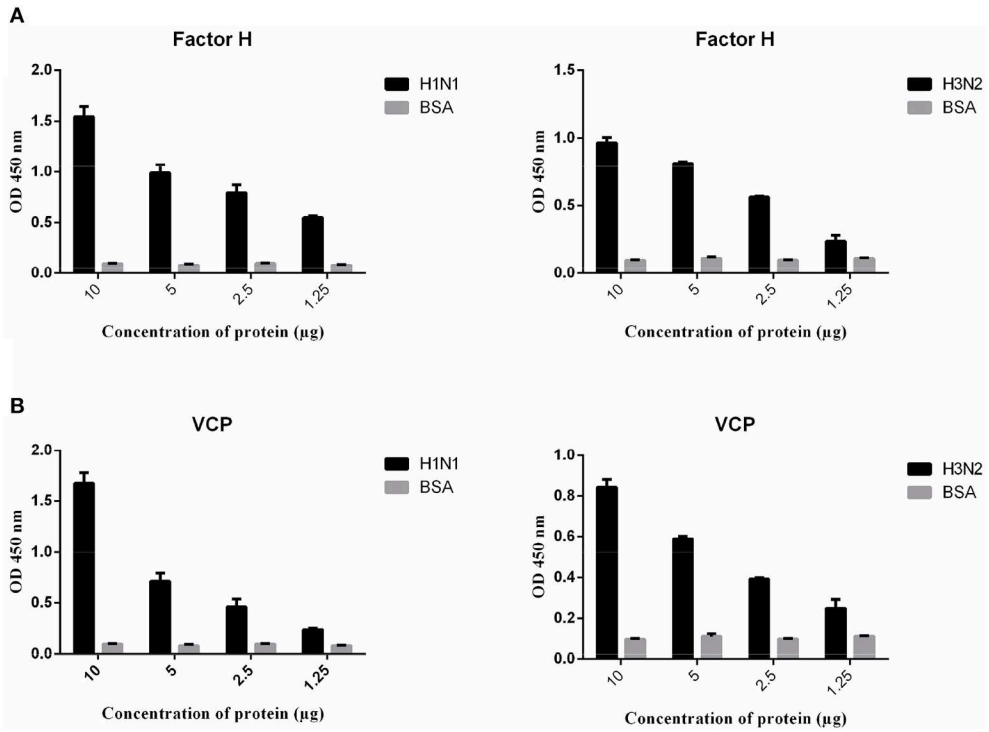

FIGURE 4 | Cell-binding assay to show binding of factor H **(A)** and VCP **(B)** to A549 cells challenged with H1N1 and H3N2. A549 cells (1×10^5 cells/ml) were seeded in a 96-well microtiter plate and incubated at 37°C overnight. Decreasing concentrations of factor H and VCP (10, 5, 2.5, and 1.25 µg), pre-incubated with IAV subtypes, were added to the corresponding wells, and incubated at room temperature for 1 h. After removing unbound protein and viral particles, the wells were fixed with 4% v/v paraformaldehyde, and probed with monoclonal anti-influenza virus H1 or polyclonal anti-influenza virus H3 antibodies. BSA was used as a negative control protein. Three independent experiments were carried out in triplicates and error bars expressed as ± SEM.

Factor H and VCP Trigger an Anti-inflammatory Response in the Case of H1N1

qPCR data revealed that factor H and VCP treatment resulted in the modulation of both pro and anti-inflammatory responses (**Figures 6B,C**). Following factor H treatment of IAV-challenged A549 cells, the mRNA levels of TNF-α were down-regulated at 2 h ($-5\log_{10}$) and 6 h ($-8\log_{10}$) in H1N1 infected cells (**Figure 6B**). However, an opposite effect was seen with H3N2 infected cells; the expression level of TNF-α was up-regulated, although not dramatically, at 2 h ($3\log_{10}$), as well as at 6 h ($3.5\log_{10}$) (**Figure 6B**). In H1N1 challenged cells, the mRNA levels of IL-6 ($-3.5\log_{10}$) and RANTES ($-0.5\log_{10}$) were also down-regulated at 2 h time point in the presence of factor H. Conversely, IL-6 ($2.5\log_{10}$) and RANTES ($1.5\log_{10}$) levels were up-regulated in H3N2 challenged cells at 2 and 6 h (IL-6/$3\log_{10}$) (RANTES/$2.5\log_{10}$) treatment with factor H. Factor H also down-regulated IL-12 levels in H1N1 ($1\log_{10}$) subtype at 6 h, but enhanced in H3N2 challenged cells at both 2 and 6 h. We also show here, for the first time, the effect of VCP, which contains 4 CCP modules like human factor H, on IAV infection; it mirrored the results obtained with factor H (**Figure 6B**). A greater down-regulation of TNF-α ($-5\log_{10}$), IL-6 ($-3.5\log_{10}$) and IL-12 ($-1.5\log_{10}$) levels were seen at 6 h following VCP treatment when compared to untreated control (cells + H1N1) (**Figure 6B**). VCP treated H1N1 challenged A549 cells showed a reduced level of RANTES at 2 h ($-0.7\log_{10}$), which was raised slightly at 6 h. In the case of H3N2, effects similar to factor H were observed (**Figure 6B**). TNF-α, IL-6, IL-12, and RANTES were increased at 6 h VCP treatment. Higher levels of pro-inflammatory cytokines, including TNF-α, IL-6, and IFN-α have been detected in IAV infected patients (41), and correlate with severe infectivity. H1N1 infected patients have higher levels of IL-6 in their lungs and serum (42, 43). Therefore, down-regulation of IL-6 by both factor H and VCP in H1N1 infected A549 cells suggests a possible anti-inflammatory role of these two proteins in a strain specific manner. In addition, the ability of factor H ($-2\log_{10}$) and VCP ($-2.5\log_{10}$) to down-regulate type 1 IFN-α (**Figure 6C**) at 6 h was also seen in H1N1. However, higher expression levels of IFN-α were detected in the case of H3N2 in the presence of factor H ($2\ \log_{10}$) and VCP ($1.7\ \log_{10}$) (**Figure 6C**).

Factor H and VCP Act as Entry Inhibitors of H1N1 Viral Infection

In this study, lentiviral pseudotypes were generated to determine cell entry strategies of H1N1 and H3N2 subtypes of IAV.

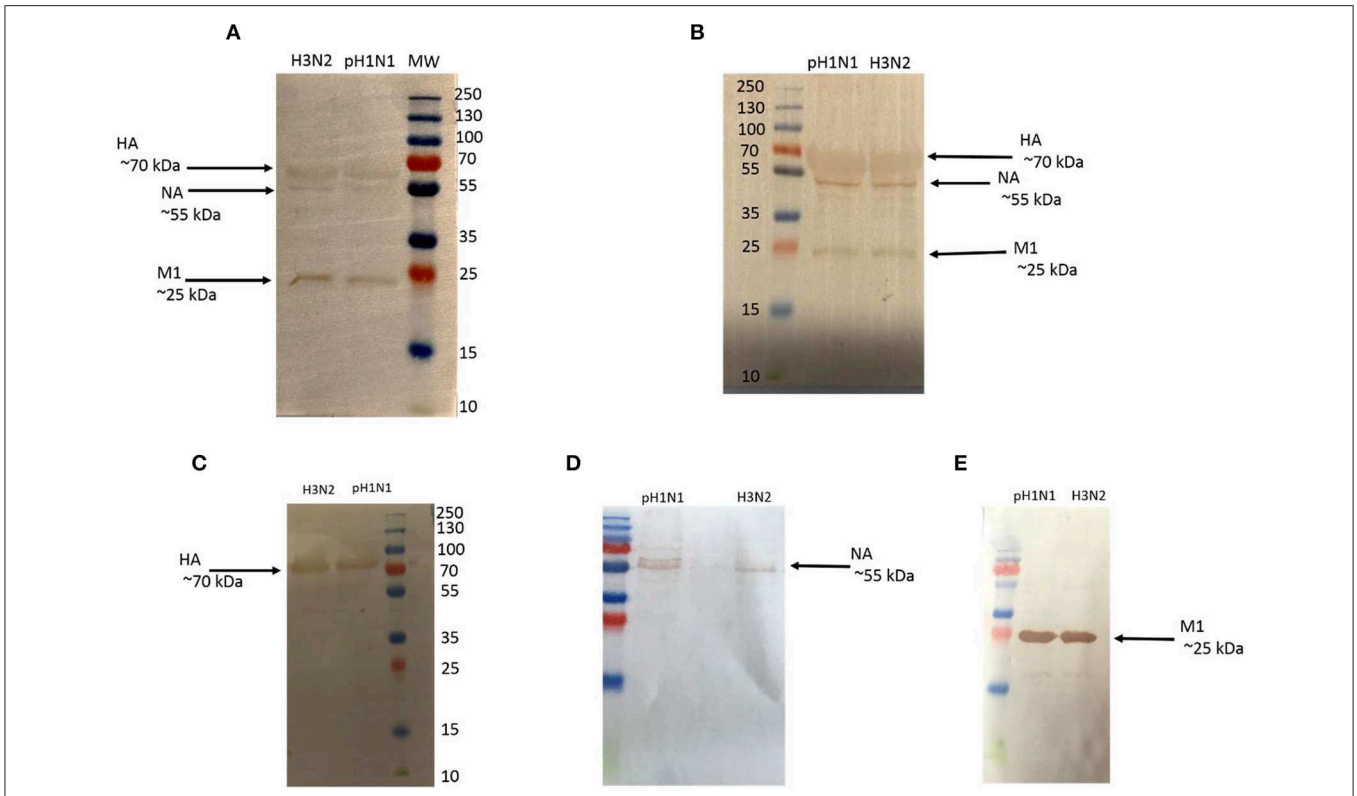

FIGURE 5 | Far western blot analysis to show factor H **(A)** and VCP **(B)** binding with purified H1N1 and H3N2. IAV subtypes (1.36×10^6pfu/ ml) were first run on the SDS-PAGE under reducing conditions and transferred onto a nitrocellulose membrane. The transferred membrane was then incubated with 10 μg/ml of factor H or VCP. The membrane was probed with either monoclonal mouse anti-human factor H or polyclonal rabbit anti-VCP antibody. Factor H and VCP bound to HA (~70 kDa), NA (~55 kDa), and M1 (~25 kDa) in the case of both IAV subtypes. The identities of factor H and VCP bound IAV glycoproteins were validated using a separate blot that was directly probed with monoclonal anti-HA **(C)**, anti-NA **(D)**, and anti-M1 **(E)** antibodies.

Production of lentiviral pseudotypes was carried out by co-transfecting HEK293T cells with plasmid containing the coding sequence of IAV glycoprotein combinations such as H1+N1 and H3+N2, pHIV-Luciferase backbone, and psPAX2 plasmids via a calcium phosphate transfection method. Post transfection, H1N1 and H3N2 pseudotyped particles were harvested at 48 h, purified, and analyzed via western blotting. The HA expression level was detected using anti-H1 polyclonal antibody; HA was evident around ~70 kDa (**Figure 7A**). MDCK cells were transduced with purified H1N1 and H3N2 pseudotyped particles to measure the luciferase reporter activity, with and without factor H or VCP (40 μg/ml). Nearly 25% reduction in the luciferase reporter activity was observed for factor H compared to cells only, challenged with H1N1 pseudotyped particles (**Figure 7B**). However, factor H enhanced the luciferase activity by 50% in cells transduced with H3N2 pseudotyped particles. In the case of VCP, ~45% reduction of luciferase activity for cells transduced with H1N1-pseudotyped particles was noted, whereas it caused ~30% increase of luciferase activity in cells transduced with H3N2 pseudotyped particles (**Figure 7B**). Thus, factor H and VCP seem to act as entry inhibitors only in the case of H1N1.

DISCUSSION

Pathogens have evolved a range of defense mechanisms to overcome the immune response modifying their infectivity and dissemination in the host (44, 45). The complement system, a major arm of the innate immune system, consists of several soluble factors and cell surface receptors that interact with and react to invading pathogens. Some pathogens mimic and recruit complement inhibitors, such as factor H and C4b binding protein (C4BP) to escape complement (46–48).

Factor H is an abundant plasma protein, which has a regulatory function in the homeostasis of the complement system and in the protection of bystander host cells and tissues from injury via the complement activation of the alternative pathway (31). The most important point in the complement activation is the regulation of C3 convertase, which is monitored by factor H, a well-established sialic acid binder. A number of bacteria can recruit factor H via the presentation of specific binding proteins, including factor H binding proteins (fHbp) of *Neisseria meningitidis* (49), CspA and outer surface protein E of *Borrelia burgdorferi* (50, 51), staphylococcal binder of IgG from *Staphylococcus aureus* (52), and pneumococcal surface

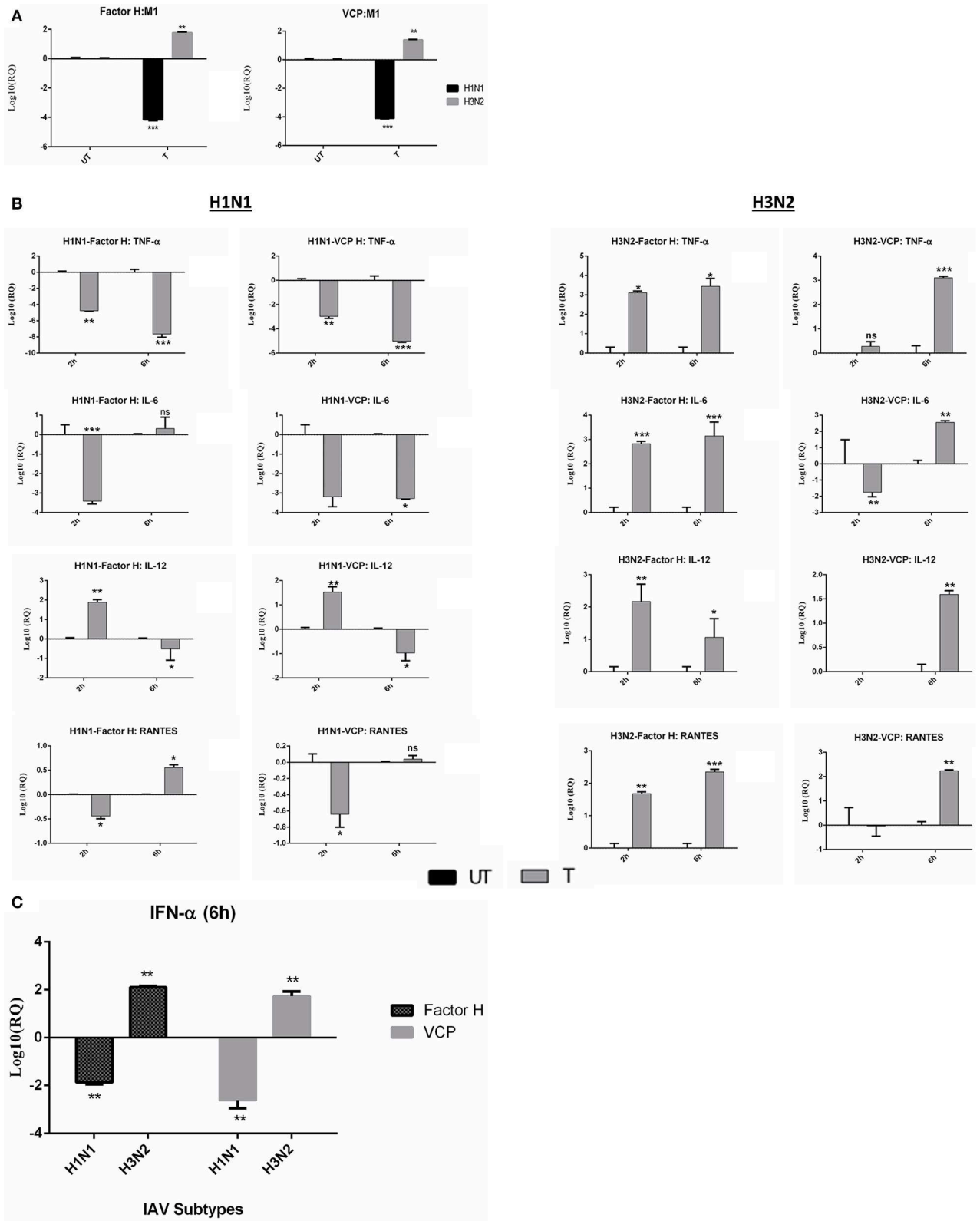

FIGURE 6 | Replication of IAV subtypes and inflammatory responses of A549 cells. **(A)** Following entry inhibition, replication of IAV subtypes (H1N1 and H3N2) is affected by factor H and VCP in human A549 cells. M1 expression was monitored in A549 cells challenged with either H1N1 or H3N2 IAV subtypes (MOI 1) at 6 h. A549 cells were challenged with H1N1 and H3N2 pre-incubated with or without factor H and VCP (40 μg/ml). Cell pellets were harvested at 6 h post-infection.

(Continued)

FIGURE 6 | 18S rRNA was used as an endogenous control. Significance was determined using the unpaired one-way ANOVA test (**$p < 0.01$, and ***$p < 0.001$) ($n = 3$). **(B)** Transcription expression profile of cytokines and chemokines produced by A549 in response to H1N1 and H3N2 challenge with and without factor H. 18S rRNA expression was used as an endogenous control. Cells only was used as a calibrator sample to calculate relative quantitation (RQ); $RQ = 2^{-\Delta\Delta Ct}$. Experiments were conducted in triplicates, and error bars represents ± SEM. Unpaired one-way ANOVA test was used calculate the significance (*$p < 0.05$, **$p < 0.01$, and ***$p < 0.001$) ($n = 3$). (UT, untreated sample; T, treated sample). **(C)** Expression levels of type I interferon alpha (IFN-α) following 6 h treatments with factor H and VCP. 18S rRNA was used as an endogenous control. $RQ = 2^{-\Delta\Delta Ct}$ was used to calculate the RQ value. Significance was determined using the unpaired one-way ANOVA test (**$p < 0.01$) ($n = 3$).

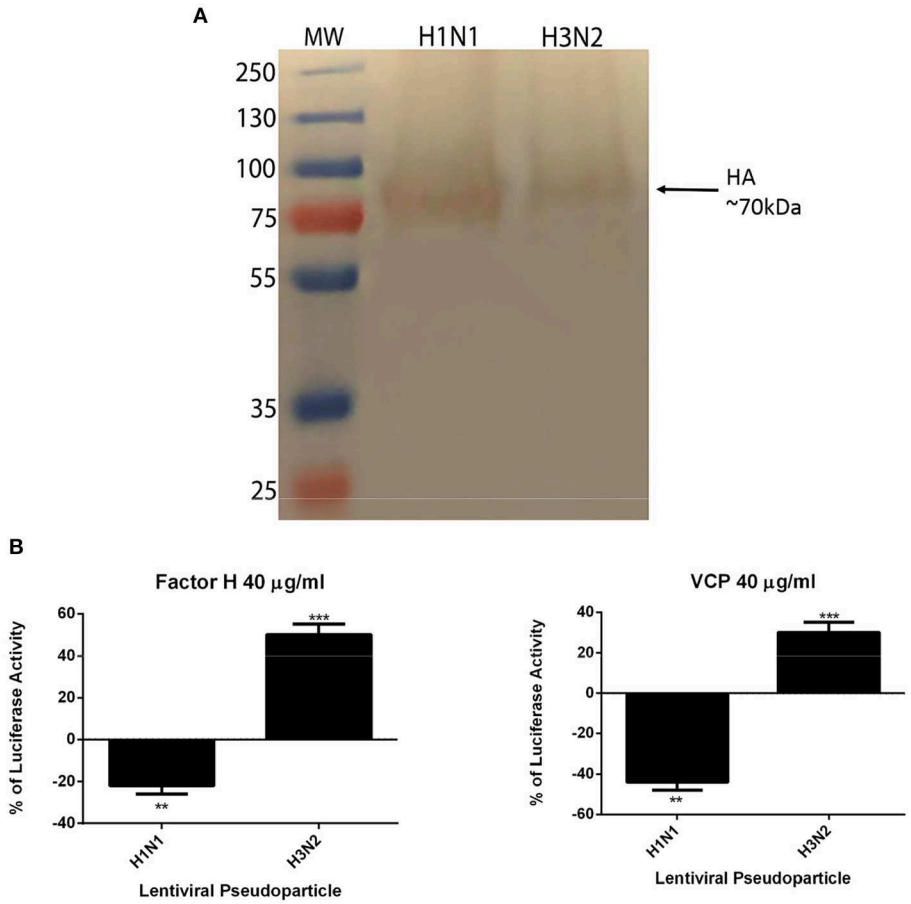

FIGURE 7 | Factor H and VCP inhibit transduction of MDCK cells by H1N1-pseudotyped lentiviral particles. Western blotting to show expression of hemagglutinin (HA) in purified H1N1 and H3N2 pseudotyped lentiviral particles **(A)**. HA expression was evident at ∼70 kDa. Luciferase reporter activity of H1N1 and H3N2 pseudotyped lentiviral particles-transduced cells with factor H and VCP **(B)**. Significance was determined using the unpaired one-way ANOVA test (**$p < 0.01$ and ***$p < 0.001$) ($n = 3$).

protein C of *Streptococcus pneumoniae* (53). The factor H ligands, expressed by pathogens, are structurally distinct from each other, but they share the related binding site on factor H that can be localized on a common site of the CCP20 module (45). These interactions increase the binding ability of CCP 19-20 modules to C3b, resulting in a stable complex between factor H, C3b and microbial targets, with an enhanced co-factor activity. *Pseudomonas aeruginosa* express sialic acid on their surfaces, which reduces complement deposition via probable factor H recruitment. Sialic acid also recruits siglec-7/9 leading to immune escape (54). In addition, factor H binds to ApoE on High Density Lipoprotein (HDL) via CCP 5-7 modules, and is used by the bacteria to mimic the plasma HDL to increase their survival in the blood (35).

Here, we investigated the complement-independent function of factor H in the regulation of IAV infection. Since VCP is an efficient complement inhibitor and a homolog of factor H (34), we included it in the present study. VCP is a ∼35 kDa secretory protein of vaccinia virus, encoded by the C3L open reading frame (ORF), and contains four CCP modules (34). VCP has been shown to inhibit complement lysis of sheep RBCs, by binding to C3b and C4b (34), and serves as a cofactor in the factor I-mediated cleavage of C3b and C4b (34). Additionally, VCP has been shown to inhibit formation of C3 convertase

and accelerate the decay of the alternative pathway (55). In the present study, a direct and complement independent interaction of factor H and VCP with H1N1 and H3N2 IAV subtypes were examined via hemagglutination assay, ELISA, cell binding, and far western blotting. In the hemagglutination assay, factor H inhibited hemagglutination of both H1N1 and H3N2 IAV subtypes; 10 μg/ml being the most effective with H1N1 and H3N2 subtypes.

VCP 4 modules contain a heparin binding site, as does factor H (56). It is possible that in a manner similar to factor H (57, 58), the heparin binding site found within the VCP protein enhances its decay-accelerating action against C3 convertase. SRBCs have high surface sialic acid. Factor H binds to this and protects them from the complement alternative pathway. On removal of the sialic acid with neuraminidase, SRBCs become susceptible to complement lysis. However, other studies suggest that the decay activity rate of VCP does not reduce following neuraminidase-treatment of SRBCs (57, 58), indicating a difference in reaction with sialic acids. Furthermore, a weaker decay rate was seen with CCP 2–4 mutants of VCP. Factor H and VCP seem to bind H1N1 and H3N2 via HA (∼70 kDa) and NA (∼55 kDa) in addition to recognizing M1. It is well-known that the viral HA can bind to sialic acid residues on surface glycoprotein and its receptor binding depends on the nature of the glycosidic linkage (59). The binding of HA to sialic acids, like factor H, is the initial event in the virus association with human epithelial cells. In addition, the resulting disruption of the neuraminic acid residues can enable the virus to cross over the epithelial cells, thus entering new cells to initiate viral replication.

The immune response of A549 cells following IAV challenge in the presence and absence of factor H or VCP was examined using qRT-PCR. The ability of factor H and VCP to modulate viral replication, due to entry inhibition, was determined using M1 mRNA expression levels between protein treated and untreated A549 cells challenged with H1N1 or H3N2 subtypes. Both factor H and VCP modulated the IAV replication in a strain dependent manner. In the case of H1N1, both factor H and VCP showed reduced viral M1 expression; however, an increased M1 expression was seen for H3N2, suggesting that the inhibitory effect of these proteins is strain-dependent. This suggests that both factor H and VCP could act as entry inhibitors against H1N1 subtype, but not H3N2.

Several studies have demonstrated both direct and indirect correlation between cytokine levels and viral replication (60, 61). IAV targets lung epithelial cells, and following initial exposure, progeny viral particles proliferate to infect other cells, including alveolar macrophages (62). Thus, an acute inflammatory response is triggered by the activation of pro-inflammatory cytokines and chemokines (62, 63), where higher levels lead to a dramatic cytokine storm; altered levels of TNFs, IFNs, interleukins and chemokines have been detected in IAV infected patients (41). Over-synthesis of IFN levels during early stages of IAV infection causes irreversible lung damage in mice infected with H5N1; however, IFN signaling may also be crucial in preventing H5N1 dissemination (64, 65). TNFs are key soluble factors in the cytokine storm; H5N1 infected mice deficient in TNF receptors, as well as H5N1 infected mice treated with anti-TNF-α antibodies, show no change in survival rate compared to healthy controls (66). Furthermore, IL-6 and IL-1 are the crucial pro-inflammatory cytokines produced by the host during influenza infection. Expression of IL-1 is detected in the early stage of IAV infection, followed by an increased IL-6 expression (67). H5N1 infected mice lacking in IL-6 receptor have demonstrated a poor survival outcome, suggesting the protective role of IL-6 pathway in the cytokine storm (67). Therefore, an unbalanced cytokine storm can also lead to damage in the vascular barrier, causing tissue oedema, capillary leakage, failure of multiple organs, and death (67). However, no specific singular mechanism is reported when it comes to triggering a cytokine storm with respect to influenza strains.

In this study, alterations of cytokine levels were observed in H1N1 and H3N2 challenged A549 cells in the presence of factor H and VCP. Factor H treatment resulted in down-regulation of TNF-α at 2 and 6 h in H1N1 infected cells. In the case of H3N2 infected cells, expression of TNF-α was up-regulated at 2 and 6 h after treatment. Reduced mRNA levels of IL-6 and RANTES were also seen at 2 h treatment with factor H, which slightly increased at 6 h. Conversely, enhanced levels of IL-6 and RANTES were observed in H3N2 infected cells following 2 and 6 h treatment with factor H.

In the case of VCP, TNF-α IL-6, and IL-12 levels were found to be down-regulated at 6 h treatment. H1N1 infected cells treated with VCP also showed reduced levels of RANTES at 2 h. H3N2 infected A549 cells following VCP treatment revealed similar effects as factor H. Up-regulation of TNF-α, IL-6, IL-12, and RANTES were observed at 6 h following VCP treatment. Previous studies have reported enhanced serum levels of pro-inflammatory cytokines, including TNF-α, IL-6, and IFN-α in individuals infected with IAV (68). IL-6 and TNF-α may be the key contributors to virus mediated respiratory diseases, including Acute Respiratory Distress syndrome (ARDS) and acute lung injury (69). During IAV infection, alveolar macrophages are activated, which are the primary phagocytic cells that produce robust amounts of IL-6 and TNF-α (70). Macrophages infected with IAV have also been shown to produce chemokines such as RANTES and monocytes chemotactic protein-1 (MCP-1). This further recruits mononuclear cells to the lungs and facilitates viral clearance (71), and enhances production of those cytokines (e.g., TNF-α, IL-6, RANTES, and IL-8) that are also implicated in the pathogenesis of influenza virus. RANTES, IL-1β, IL-6, and TNF-α induced by influenza result in pro-inflammatory Th1-type immune responses in the infected host (71). Dysregulation of cytokine and chemokine levels during influenza has been demonstrated to promote tissue injury and impaired viral clearance. Additionally, suppression of IFN-α was also evident with factor H and VCP in H1N1 challenged A549 cells. In the case of H3N2, both factor H and VCP increased the expression of IFN-α, which may possibly induce protection of A549 cells against H3N2 viral particles in neighboring as well as non-infected cells. Thus, increased IFN-α by factor H and VCP may also suggest that in the infected A549 cells, factor H and VCP may cause digestion of viral RNA and viral proteins. Down-regulation of IFN-α levels in H1N1

infected cells may suggest the possibility of factor H and VCP treatment to reduce the rate of viral replication. Thus, treatments with factor H and VCP may elicit an anti-viral response, restricting the activation of innate immune cells and associated lung pathology.

Targeting viral entry into a host cell is an emerging approach for developing anti-viral therapy as viral propagation can be either restricted or blocked at an early stage of viral cycle, minimizing drug resistance by released virions. In this study, we have generated lentiviral pseudotypes, a safe surrogate model to mimic the structure and surfaces of IAV in order to determine if factor H and VCP act as an entry inhibitors in cells transduced with pseudotyped IAV particles that are restricted to only one replicative cycle. Factor H treatment resulted in 25% reduction of luciferase reporter activity in MDCK cells transduced with H1N1 pseudotyped particles. However, the addition of factor H increased the luciferase activity by 50% in cells challenged with H3N2 pseudotyped particles. VCP was found to reduce luciferase reporter activity of H1N1 transduced MDCK cells by 45%. As is the case with factor H, VCP also enhanced the reporter activity of MDCK cells transduced with H3N2 pseudotyped lentiviral particles by 30%, suggesting the ability of factor H and VCP to enhance viral infectivity through binding to cell surface bound HA found on infected MDCK cells. Our results are consistent with a previous study showing anti-viral activity of Stachyflin, which was found to be resistant against H3N2 due to differences in potential binding pockets for Stachyflin on HA molecule (72).

In conclusion, data from restriction of M1 mRNA levels, pro-inflammatory cytokine responses, and luciferase reporter activity highlights the potential of factor H and VCP as cell entry inhibitors against the H1N1 IAV subtype. It appears that factor H and VCP restrict viral entry for H1N1, whilst conversely promoting H3N2 entry, which may be due to the inherent antigenic variations in binding sites for HA or NA. Further studies are required to pinpoint the specific molecular interactions of factor H and VCP against HA and NA by investigating a range of IAV strains with antigenic variability. This will not only provide further data on the pathogenesis of IAV infection, but also the utility of factor H and VCP, and their recombinant CCP modules, as possible cell entry inhibitors against IAV.

DATA AVAILABILITY STATEMENT

The datasets generated for this study are available on request to the corresponding author.

AUTHOR CONTRIBUTIONS

VM and PV carried out the key experiments. SS and AT carried out supporting experiments. SA, HK, and KC provided crucial reagents and expertise. RS provided factor H and MRCOX23 hybridoma clones. BN provided viral expertise. FA-M produced VCP. UK led the project. VM and PV prepared the first draft of the manuscript. RS, FA-M, AT, BN, and UK carried out extensive editing and review of the manuscript.

ACKNOWLEDGMENTS

The authors acknowledge the International Scientific Partnership Programme (ISPP) at King Saud University, Riyadh for funding via ISPP -145.

REFERENCES

1. Cox R, Brokstad K, Ogra P. Influenza virus: immunity and vaccination strategies. Comparison of the immune response to inactivated and live, attenuated influenza vaccines. *Scand J Immunol.* (2004) 59:1–15. doi: 10.1111/j.0300-9475.2004.01382.x
2. Webster RG, Bean WJ, Gorman OT, Chambers TM, Kawaoka Y. Evolution and ecology of influenza A viruses. *Microbiol Mol Biol Rev.* (1992) 56:152–79. doi: 10.1128/MMBR.56.1.152-179.1992
3. Zhang H, Hale B, Xu K, Sun B. Viral and host factors required for avian H5N1 influenza A virus replication in mammalian cells. *Viruses.* (2013) 5:1431–46. doi: 10.3390/v5061431
4. Wang X, Sun Q, Ye Z, Hua Y, Shao N, Du Y, et al. Computational approach for predicting the conserved B-cell epitopes of hemagglutinin H7 subtype influenza virus. *Exp Ther Med.* (2016) 12:2439–46. doi: 10.3892/etm.2016.3636
5. Wang S, Li H, Chen Y, Wei H, Gao GF, Liu H, et al. Transport of influenza virus neuraminidase (NA) to host cell surface is regulated by ARHGAP21 and Cdc42 proteins. *J Biol Chem.* (2012) 287:9804–16. doi: 10.1074/jbc.M111.312959
6. Fouchier RA, Munster V, Wallensten A, Bestebroer TM, Herfst S, Smith D, et al. Characterization of a novel influenza A virus hemagglutinin subtype (H16) obtained from black-headed gulls. *J Virol.* (2005) 79:2814–22. doi: 10.1128/JVI.79.5.2814-2822.2005
7. Hussain M, Galvin HD, Haw TY, Nutsford AN, Husain M. Drug resistance in influenza A virus: the epidemiology and management. *Infect Drug Resist.* (2017) 10:121–34. doi: 10.2147/IDR.S105473
8. Medina RA, García-Sastre A. Influenza A viruses: new research developments. *Nat Rev Microbiol.* (2011) 9:590–603. doi: 10.1038/nrmicro2613
9. Tscherne DM, García-Sastre A. Virulence determinants of pandemic influenza viruses. *J Clin Invest.* (2011) 121:6–13. doi: 10.1172/JCI44947
10. van Riel D, den Bakker MA, Leijten LM, Chutinimitkul S, Munster VJ, de Wit E, et al. Seasonal and pandemic human influenza viruses attach better to human upper respiratory tract epithelium than avian influenza viruses. *Am J Pathol.* (2010) 176:1614–8. doi: 10.2353/ajpath.2010.090949
11. Shinya K, Ebina M, Yamada S, Ono M, Kasai N, Kawaoka Y. Avian flu: influenza virus receptors in the human airway. *Nature.* (2006) 440:435–6. doi: 10.1038/440435a
12. Herold S, Becker C, Ridge KM, Budinger GS. Influenza virus-induced lung injury: pathogenesis and implications for treatment. *Eur Respir J.* (2015) 45:1463–78. doi: 10.1183/09031936.00186214
13. Hogan BL, Barkauskas CE, Chapman HA, Epstein JA, Jain R, Hsia CC, et al. Repair and regeneration of the respiratory system: complexity, plasticity, and mechanisms of lung stem cell function. *Cell Stem Cell.* (2014) 15:123–38. doi: 10.1016/j.stem.2014.07.012
14. Roy MG, Livraghi-Butrico A, Fletcher AA, McElwee MM, Evans SE, Boerner RM, et al. Muc5b is required for airway defence. *Nature.* (2014) 505:412–6. doi: 10.1038/nature12807
15. Ehre C, Worthington EN, Liesman RM, Grubb BR, Barbier D, O'Neal WK, et al. Overexpressing mouse model demonstrates the protective role of Muc5ac in the lungs. *Proc Natl Acad Sci USA.* (2012) 109:16528–33. doi: 10.1073/pnas.1206552109
16. McAuley J, Corcilius L, Tan H, Payne R, McGuckin M, Brown L. The cell surface mucin MUC1 limits the severity of influenza A

virus infection. *Mucosal immunol.* (2017) 10:1581–93. doi: 10.1038/mi.2017.16
17. Duez J-M, Sixt N, Péchinot A. Influenza virus infection: don't forget the role of the mucociliary system! *JAntimicrob Chemother.* (2009) 63:421–2. doi: 10.1093/jac/dkn468
18. Cohen M, Zhang X-Q, Senaati HP, Chen H-W, Varki NM, Schooley RT, et al. Influenza A penetrates host mucus by cleaving sialic acids with neuraminidase. *Virol J.* (2013) 10:321. doi: 10.1186/1743-422X-10-321
19. Yang J, Liu S, Du L, Jiang S. A new role of neuraminidase (NA) in the influenza virus life cycle: implication for developing NA inhibitors with novel mechanism of action. *Rev Med Virol.* (2016) 26:242–50. doi: 10.1002/rmv.1879
20. Gulati S, Smith DF, Cummings RD, Couch RB, Griesemer SB, George KS, et al. Human H3N2 influenza viruses isolated from 1968 to 2012 show varying preference for receptor substructures with no apparent consequences for disease or spread. *PLoS ONE.* (2013) 8:e66325. doi: 10.1371/journal.pone.0066325
21. Rattan A, Kasbe R, Mullick J, Sahu A. The complement system as a viral target for immune evasion. In: Kishore U, Nayak A, editors. *Microbial Pathogenesis: Infection and Immunity, Landes Bioscience*. New York, NY: Springer (2013). p. 1–27.
22. Cooper N. *Complement and Viruses. The Human Complement System in Health and Disease*. New York, NY: Marcel Dekker (1998). p. 393–407.
23. Pyaram K, Kieslich CA, Yadav VN, Morikis D, Sahu A. Influence of electrostatics on the complement regulatory functions of Kaposica, the complement inhibitor of Kaposi's sarcoma-associated herpesvirus. *J Immunol.* (2010) 184:1956–67. doi: 10.4049/jimmunol.0903261
24. Kopf M, Abel B, Gallimore A, Carroll M, Bachmann MF. Complement component C3 promotes T-cell priming and lung migration to control acute influenza virus infection. *Nat Med.* (2002) 8:373–8. doi: 10.1038/nm0402-373
25. Hicks JT, Ennis FA, Kim E, Verbonitz M. The importance of an intact complement pathway in recovery from a primary viral infection: influenza in decomplemented and in C5-deficient mice. *J Immunol.* (1978) 121:1437–45.
26. Kandasamy M, Ying PC, Ho AW, Sumatoh HR, Schlitzer A, Hughes TR, et al. Complement mediated signaling on pulmonary CD103+ dendritic cells is critical for their migratory function in response to influenza infection. *PLoS Pathog.* (2013) 9:e1003115. doi: 10.1371/journal.ppat.1003115
27. Carroll MC, Isenman DE. Regulation of humoral immunity by complement. *Immunity.* (2012) 37:199–207. doi: 10.1016/j.immuni.2012.08.002
28. Ansari M, Mckeigue PM, Skerka C, Hayward C, Rudan I, Vitart V, et al. Genetic influences on plasma CFH and CFHR1 concentrations and their role in susceptibility to age-related macular degeneration. *Hum Mol Genet.* (2013) 22:4857–69. doi: 10.1093/hmg/ddt336
29. Lambris JD, Ricklin D, Geisbrecht BV. Complement evasion by human pathogens. *Nat Rev Microbiol.* (2008) 6:132–42. doi: 10.1038/nrmicro1824
30. Ferluga J, Kouser L, Murugaiah V, Sim RB, Kishore U. Potential influences of complement factor H in autoimmune inflammatory and thrombotic disorders. *Mol Immunol.* (2017) 84:84–106. doi: 10.1016/j.molimm.2017.01.015
31. Kouser L, Abdul-Aziz M, Nayak A, Stover CM, Sim RB, Kishore U. Properdin and factor h: opposing players on the alternative complement pathway "see-saw". *Front Immunol.* (2013) 4:93. doi: 10.3389/fimmu.2013.00093
32. Simon N, Lasonder E, Scheuermayer M, Kuehn A, Tews S, Fischer R, et al. Malaria parasites co-opt human factor H to prevent complement-mediated lysis in the mosquito midgut. *Cell Host Microbe.* (2013) 13:29–41. doi: 10.1016/j.chom.2012.11.013
33. Abdul-Aziz M, Tsolaki AG, Kouser L, Carroll MV, Al-Ahdal MN, Sim RB, et al. Complement factor H interferes with *Mycobacterium bovis* BCG entry into macrophages and modulates the pro-inflammatory cytokine response. *Immunobiology.* (2016) 221:944–52. doi: 10.1016/j.imbio.2016.05.011
34. Kotwal GJ, Isaacs SN, McKenzie R, Frank MM, Moss B. Inhibition of the complement cascade by the major secretory protein of vaccinia virus. *Science.* (1990) 250:827–30. doi: 10.1126/science.2237434
35. Haapasalo K, van Kessel K, Nissilä E, Metso J, Johansson T, Miettinen S, et al. Complement factor H binds to human serum apolipoprotein E and mediates complement regulation on high density lipoprotein particles. *J Biol Chem.* (2015) 290:28977–87. doi: 10.1074/jbc.M115.669226
36. Qian W, Wei X, Guo K, Li Y, Lin X, Zou Z, et al. The C-terminal effector domain of non-structural protein 1 of influenza A virus blocks IFN-β production by targeting TNF receptor-associated factor 3. *Front Immunol.* (2017) 8:779. doi: 10.3389/fimmu.2017.00779
37. Lam W, Tang JW, Yeung AC, Chiu LC, Sung JJ, Chan PK. Avian influenza virus A/HK/483/97 (H5N1) NS1 protein induces apoptosis in human airway epithelial cells. *J Virol.* (2008) 82:2741–51. doi: 10.1128/JVI.01712-07
38. Al-Ahdal MN, Murugaiah V, Varghese PM, Abozaid SM, Saba I, Al-Qahtani AA, et al. Entry inhibition and modulation of pro-inflammatory immune response against Influenza A Virus by a recombinant truncated surfactant protein D. *Front Immunol.* (2018) 9:1586. doi: 10.3389/fimmu.2018.01586
39. Sim R, Day A, Moffatt B, Fontaine M. [1] Complement factor I and cofactors in control of complement system convertase enzymes. *Methods Enzymol.* (1993) 223:13–35. doi: 10.1016/0076-6879(93)23035-L
40. Hollý J, Fogelová M, Jakubcová L, Tomčíková K, Vozárová M, Varečková E, et al. Comparison of infectious influenza A virus quantification methods employing immuno-staining. *J Virol Methods.* (2017) 247:107–13. doi: 10.1016/j.jviromet.2017.06.004
41. Beigel J, Farrar J, Han A, Hayden F, Hyer R, de Jong M, et al. Writing Committee of the World Health Organization (WHO) Consultation on human influenza A/H5: Avian influenza A (H5N1) infection in humans. *New Engl J Med.* (2005) 353:1374–85. doi: 10.1056/NEJMra052211
42. Kaiser L, Fritz RS, Straus SE, Gubareva L, Hayden FG. Symptom pathogenesis during acute influenza: interleukin-6 and other cytokine responses. *J Med Virol.* (2001) 64:262–8. doi: 10.1002/jmv.1045
43. Hagau N, Slavcovici A, Gonganau DN, Oltean S, Dirzu DS, Brezoszki ES, et al. Clinical aspects and cytokine response in severe H1N1 influenza A virus infection. *Crit Care.* (2010) 14:R203. doi: 10.1186/cc9324
44. Meri S, Jördens M, Jarva H. Microbial complement inhibitors as vaccines. *Vaccine.* (2008) 26:113–17. doi: 10.1016/j.vaccine.2008.11.058
45. Meri T, Amdahl H, Lehtinen M, Hyvärinen S, McDowell J, Bhattacharjee A, et al. Microbes bind complement inhibitor factor H via a common site. *PLoS Pathog.* (2013) 9:e1003308. doi: 10.1371/journal.ppat.1003308
46. Vogl G, Lesiak I, Jensen D, Perkhofer S, Eck R, Speth C, et al. Immune evasion by acquisition of complement inhibitors: the mould Aspergillus binds both factor H and C4b binding protein. *Mol Immunol.* (2008) 45:1485–93. doi: 10.1016/j.molimm.2007.08.011
47. Herbert AP, Makou E, Chen ZA, Kerr H, Richards A, Rappsilber J, et al. Complement evasion mediated by enhancement of captured factor H: implications for protection of self-surfaces from complement. *J Immunol.* (2015) 195:4986–98. doi: 10.4049/jimmunol.1501388
48. Kennedy AT, Schmidt CQ, Thompson JK, Weiss GE, Taechalertpaisarn T, Gilson PR, et al. Recruitment of factor H as a novel complement evasion strategy for blood-stage Plasmodium falciparum infection. *J Immunol.* (2016) 196:1239–48. doi: 10.4049/jimmunol.1501581
49. Pizza M, Donnelly J, Rappuoli R. Factor H-binding protein, a unique meningococcal vaccine antigen. *Vaccine.* (2008) 26:146–18. doi: 10.1016/j.vaccine.2008.11.068
50. Kraiczy P, Hartmann K, Hellwage J, Skerka C, Kirschfink M, Brade V, et al. Immunological characterization of the complement regulator factor H-binding CRASP and Erp proteins of *Borrelia burgdorferi. Int J Med Microbiol Suppl.* (2004) 293:152–7. doi: 10.1016/S1433-1128(04)80029-9
51. Hellwage J, Meri T, Heikkilä T, Alitalo A, Panelius J, Lahdenne P, et al. The complement regulator factor H binds to the surface protein OspE of borrelia burgdorferi. *J Biol Chem.* (2001) 276:8427–35. doi: 10.1074/jbc.M007994200
52. Haupt K, Reuter M, van den Elsen J, Burman J, Hälbich S, Richter J, et al. The staphylococcus aureus protein Sbi acts as a complement inhibitor and forms a tripartite complex with host complement Factor H and C3b. *PLoS Pathog.* (2008) 4:e1000250. doi: 10.1371/journal.ppat.1000250
53. Janulczyk R, Iannelli F, Sjöholm AG, Pozzi G, Björck L. Hic, a novel surface protein of *Streptococcus pneumoniae* that interferes with complement function. *J Biol Chem.* (2000) 275:37257–63. doi: 10.1074/jbc.M004572200
54. Khatua B, Ghoshal A, Bhattacharya K, Mandal C, Saha B, Crocker PR, et al. Sialic acids acquired by *Pseudomonas aeruginosa* are involved in reduced complement deposition and siglec mediated host-cell recognition. *FEBS Lett.* (2010) 584:555–61. doi: 10.1016/j.febslet.2009.11.087
55. McKenzie R, Kotwal GJ, Moss B, Hammer C, Frank M. Regulation of complement activity by vaccinia virus complement-control protein. *J Infect Dis.* (1992) 166:1245–50. doi: 10.1093/infdis/166.6.1245

56. Ganesh VK, Smith SA, Kotwal GJ, Murthy KH. Structure of vaccinia complement protein in complex with heparin and potential implications for complement regulation. *Proc Natl Acad Sci USA*. (2004) 101:8924–9. doi: 10.1073/pnas.0400744101
57. Sahu A, Panoburn MK. Identification of multiple sites of interaction between heparin and the complement system. *Mol Immunol*. (1993) 30:679–84. doi: 10.1016/0161-5890(93)90079-Q
58. Meri S, Pangburn MK. Discrimination between activators and nonactivators of the alternative pathway of complement: regulation via a sialic acid/polyanion binding site on factor H. *Proc Natl Acad Sci USA*. (1990) 87:3982–6. doi: 10.1073/pnas.87.10.3982
59. Stencel-Baerenwald JE, Reiss K, Reiter DM, Stehle T, Dermody TS. The sweet spot: defining virus–sialic acid interactions. *Nat Rev Microbiol*. (2014) 12:739–49. doi: 10.1038/nrmicro3346
60. Oslund KL, Baumgarth N. Influenza-induced innate immunity: regulators of viral replication, respiratory tract pathology, & adaptive immunity. *Future Virol*. (2011) 6:951–62. doi: 10.2217/fvl.11.63
61. Mogensen TH, Paludan SR. Molecular pathways in virus-induced cytokine production. *Microbiol Mol Biol Rev*. (2001) 65:131–50. doi: 10.1128/MMBR.65.1.131-150.2001
62. La Gruta NL, Kedzierska K, Stambas J, Doherty PC. A question of self-preservation: immunopathology in influenza virus infection. *Immunol Cell Biol*. (2007) 85:85–92. doi: 10.1038/sj.icb.7100026
63. Shinya K, Gao Y, Cilloniz C, Suzuki Y, Fujie M, Deng G, et al. Integrated clinical, pathologic, virologic, and transcriptomic analysis of H5N1 influenza virus-induced viral pneumonia in the rhesus macaque. *J Virol*. (2012) 86:6055–66. doi: 10.1128/JVI.00365-12
64. Muramoto Y, Shoemaker JE, Le MQ, Itoh Y, Tamura D, Sakai-Tagawa Y, et al. Disease severity is associated with differential gene expression at the early and late phases of infection in nonhuman primates infected with different H5N1 highly pathogenic avian influenza viruses. *J Virol*. (2014) 88:8981–97. doi: 10.1128/JVI.00907-14
65. Cilloniz C, Pantin-Jackwood MJ, Ni C, Goodman AG, Peng X, Proll SC, et al. Lethal dissemination of H5N1 influenza virus is associated with dysregulation of inflammation and lipoxin signaling in a mouse model of infection. *J Virol*. (2010) 84:7613–24. doi: 10.1128/JVI.00553-10
66. Peiris JSM, Cheung CY, Leung CYH, Nicholls JM. Innate immune responses to influenza A H5N1: friend or foe? *Trends Immunol*. (2009) 30:574–84. doi: 10.1016/j.it.2009.09.004
67. Tisoncik JR, Korth MJ, Simmons CP, Farrar J, Martin TR, Katze MG. Into the eye of the cytokine storm. *Microbiol Mol Biol Rev*. (2012) 76:16–32. doi: 10.1128/MMBR.05015-11
68. Duvigneau S, Sharma-Chawla N, Boianelli A, Stegemann-Koniszewski S, Nguyen VK, Bruder D, et al. Hierarchical effects of pro-inflammatory cytokines on the post-influenza susceptibility to pneumococcal coinfection. *Sci Rep*. (2016) 6:37045. doi: 10.1038/srep37045
69. Cheng X-W, Lu J, Wu C-L, Yi L-N, Xie X, Shi X-D, et al. Three fatal cases of pandemic 2009 influenza A virus infection in shenzhen are associated with cytokine storm. *Respir Physiol Neurobiol*. (2011) 175:185–7. doi: 10.1016/j.resp.2010.11.004
70. Dawson TC, Beck MA, Kuziel WA, Henderson F, Maeda N. Contrasting effects of CCR5 and CCR2 deficiency in the pulmonary inflammatory response to influenza A virus. *Am J Pathol*. (2000) 156:1951–9. doi: 10.1016/S0002-9440(10)65068-7
71. Kaufmann A, Salentin R, Meyer RG, Bussfeld D, Pauligk C, Fesq H, et al. Defense against influenza A virus infection: essential role of the chemokine system. *Immunobiology*. (2001) 204:603–13. doi: 10.1078/0171-2985-00099
72. Motohashi Y, Igarashi M, Okamatsu M, Noshi T, Sakoda Y, Yamamoto N, et al. Antiviral activity of stachyflin on influenza A viruses of different hemagglutinin subtypes. *Virol J*. (2013) 10:118. doi: 10.1186/1743-422X-10-118

Conflict of Interest: The authors declare that the research was conducted in the absence of any commercial or financial relationships that could be construed as a potential conflict of interest.

frontiers in Immunology

ORIGINAL RESEARCH
published: 08 July 2020
doi: 10.3389/fimmu.2020.01171

Hyaluronic Acid Present in the Tumor Microenvironment Can Negate the Pro-apototic Effect of a Recombinant Fragment of Human Surfactant Protein D on Breast Cancer Cells

Valarmathy Murugaiah[1], Chiara Agostinis[2], Praveen M. Varghese[1,3], Beatrice Belmonte[4], Salvatore Vieni[5], Fanan A. Alaql[1], Salman H. Alrokayan[6], Haseeb A. Khan[6], Anuvinder Kaur[1], Terry Roberts[1], Taruna Madan[7], Roberta Bulla[8] and Uday Kishore[1]**

[1] Biosciences, College of Health and Life Sciences, Brunel University London, Uxbridge, United Kingdom, [2] Institute for Maternal and Child Health, Istituto di Ricovero e Cura a Carattere Scientifico (IRCCS) Burlo Garofolo, Trieste, Italy, [3] School of Biosciences and Technology, Vellore Institute of Technology, Vellore, India, [4] Tumor Immunology Unit, Human Pathology Section, Department of Health Sciences, University of Palermo, Palermo, Italy, [5] Division of General and Oncological Surgery, Department of Surgical, Oncological and Oral Sciences, University of Palermo, Palermo, Italy, [6] Department of Biochemistry, College of Science, King Saud University, Riyadh, Saudi Arabia, [7] Department of Innate Immunity, ICMR—National Institute for Research in Reproductive Health, Mumbai, India, [8] Department of Life Sciences, University of Trieste, Trieste, Italy

Human surfactant protein D (SP-D) belongs to the family of collectins that is composed of a characteristic amino-terminal collagenous region and a carboxy-terminal C-type lectin domain. Being present at the mucosal surfaces, SP-D acts as a potent innate immune molecule and offers protection against non-self and altered self, such as pathogens, allergens, and tumor. Here, we examined the effect of a recombinant fragment of human SP-D (rfhSP-D) on a range of breast cancer lines. Breast cancer has four molecular subtypes characterized by varied expressions of estrogen (ER), progesterone (PR), and epidermal growth factor (EGF) receptors (HER2). The cell viability of HER2-overexpressing (SKBR3) and triple-positive (BT474) breast cancer cell lines [but not of a triple-negative cell line (BT20)] was reduced following rfhSP-D treatment at 24 h. Upregulation of p21/p27 cell cycle inhibitors and p53 phosphorylation (Ser15) in rfhSP-D-treated BT474 and SKBR3 cell lines signified G2/M cell cycle arrest. Cleaved caspases 9 and 3 were detected in rfhSP-D-treated BT474 and SKBR3 cells, suggesting an involvement of the intrinsic apoptosis pathway. However, rfhSP-D-induced apoptosis was nullified in the presence of hyaluronic acid (HA) whose increased level in breast tumor microenvironment is associated with malignant tumor progression and invasion. rfhSP-D bound to solid-phase HA and promoted tumor cell proliferation. rfhSP-D-treated SKBR3 cells in the presence of HA showed decreased transcriptional levels of p53 when compared to cells treated with rfhSP-D only. Thus, HA appears to negate the anti-tumorigenic properties of rfhSP-D against HER2-overexpressing and triple-positive breast cancer cells.

Keywords: innate immunity, surfactant protein D, immune surveillance, breast cancer, hyaluronic acid

OPEN ACCESS

Edited by:
Jagadeesh Bayry, Institut National de la Santé et de la Recherche Médicale (INSERM), France

Reviewed by:
Lalit Kumar Dubey, University of Lausanne, Switzerland
Kenneth Reid, University of Oxford, United Kingdom
Cordula M. Stover, University of Leicester, United Kingdom

***Correspondence:**
Roberta Bulla
rbulla@units.it
Uday Kishore
uday.kishore@brunel.ac.uk; ukishore@hotmail.com

Specialty section:
This article was submitted to Molecular Innate Immunity, a section of the journal Frontiers in Immunology

Received: *02 April 2020*
Accepted: *12 May 2020*
Published: *08 July 2020*

Citation:
Murugaiah V, Agostinis C, Varghese PM, Belmonte B, Vieni S, Alaql FA, Alrokayan SH, Khan HA, Kaur A, Roberts T, Madan T, Bulla R and Kishore U (2020) Hyaluronic Acid Present in the Tumor Microenvironment Can Negate the Pro-apototic Effect of a Recombinant Fragment of Human Surfactant Protein D on Breast Cancer Cells. Front. Immunol. 11:1171. doi: 10.3389/fimmu.2020.01171

INTRODUCTION

The immune surveillance of transformed cells by innate and adaptive immunity remains one of the targeted areas of research for developing therapeutic strategies (1, 2). *In vivo* and *in vitro* studies using cancer models have demonstrated compelling involvement of effector immune cells, soluble factors, and signaling pathways in anti-tumor immune responses. However, the immune system can also aid in the progression of transformed cells by triggering immunosuppression and promoting angiogenesis and metastasis of tumor cells (3, 4).

Human surfactant protein D (SP-D) is a potent innate immune molecule found at pulmonary and non-pulmonary mucosal surfaces (5). It is a member of the collectin family that is involved in the clearance of pathogens and apoptotic/necrotic cells and in the modulation of inflammatory responses (6). SP-D is composed of an N-terminal cysteine-rich domain, a triple-helical collagenous region, an α-helical coiled neck region, and a C-terminal C-type lectin or carbohydrate recognition domain (CRD) (7). The trimeric CRDs recognize carbohydrate or charged patterns on pathogens and allergens, while the collagen region is involved in interactions with receptor molecules present on immune cells in order to trigger clearance mechanisms such as agglutination, enhanced phagocytosis, and oxidative burst (6). SP-D is primarily synthesized and secreted into the airspace of the lungs by alveolar type II and Clara cells, with a key role in surfactant homeostasis by reducing surface tension (6). However, its extrapulmonary existence is well-established now, ranging from the mucosa of the gastrointestinal and reproductive tracts (including ovaries) and nasal cavity to the brain and in various exocrine ducts (8, 9), conjunctiva, cornea, lacrimal gland, nasolacrimal ducts (8), and synovial fluid (10). Protective effects of SP-D against a range of pathogens (6, 11) and allergens (12–16) are well-documented in the literature. However, recent studies have raised the possibility that SP-D may have an important defense role against tumor.

A direct interaction of SP-D with a number of cancer cells (leukemia, lung, prostate, and pancreatic) has been reported to result in the suppression of cancer progression, migration, and invasion, as well as enhanced apoptosis (17–21). The rfhSP-D-treated acute myeloid leukemia (AML) cells were shown to result in cell cycle arrest via activation of G2/M checkpoints, with an increased level of p21 and Try15 phosphorylation of cdc2. rfhSP-D treatment in AML cells also caused activation of pro-apoptotic markers, such as cleaved caspase 9 and downregulation of pro-survival protein HMGA1 (21, 22). Exogenous SP-D treatment has been shown to downregulate epidermal growth factor (EGF) signaling by preventing the binding of EGF to the EGF receptor (EGFR), hence suppressing the cell proliferation, invasion, and migration of A549 human lung adenocarcinoma cells (23). Recently, rfhSP-D has been shown to induce apoptosis in p53 mutant (mt) and wild-type (wt) pancreatic adenocarcinoma (PDAC) cell lines (Panc-1p53 mt, MiaPaCa-2p53 mt, and Capan-2p53wt), via the TNF/Fas-mediated extrinsic pathway (17). Furthermore, rfhSP-D can also suppress epithelial–mesenchymal transition (EMT) and related gene signatures (Vimentin, Zeb1, and Snail) and cell invasiveness in Panc-1 and MiaPaCa-2 cells via downregulation of TGF-β (24). In an ovarian cell line, SKOV3, rfhSP-D again triggered apoptosis via the Fas-mediated pathway (18). In both pancreatic and ovarian cancer cell lines, rfhSP-D treatment caused activation of caspase 3 cleavage and induction of pro-apoptotic genes such as Fas and TNF-α. Furthermore, the mTOR pathway was also affected by rfhSP-D treatment in both ovarian and pancreatic cancer cell lines. rfhSP-D-treated SKOV3 cells show downregulation of Rictor and Raptor mRNA levels, suggesting inhibition of cell proliferation (17, 18). Additionally, the anti-tumor role of rfhSP-D has been reported in androgen-resistant and androgen-responsive prostate cancer cells via p53 and pAkt pathways (19). In a recent bioinformatics study, a higher expression of SP-D in ovarian and lung cancer was found to be associated with a favorable prognosis (20). These studies therefore suggest that SP-D has an immune surveillance function against tumor cells. In this context, this study was aimed at investigating the role of SP-D in breast cancer.

Breast cancer is the most common cancer diagnosed in women worldwide, contributing to almost 60% mortality rate in lower-income countries (25). There is a large variation in the survival rates worldwide, with an estimated 5-year survival rate of 80% in developed countries and below ∼40% in low-income countries (26). Designing effective treatments are crucial to improve the survival rates and to ensure the best possible quality of life for cancer survivors. After lung cancer, breast carcinomas are the second most leading cause of mortality (27); ∼17.5 million new cases of breast cancer are diagnosed globally, and 8.7 million deaths documented (28). As per GLOBOCAN 2018, ∼2 million new cases were identified, and 6.6% of cancer-related deaths were caused by breast cancer. Furthermore, the 5-year prevalence rate of breast cancer was found to be ∼6.8 million (25). Breast cancer is characterized by an abnormal growth of malignant cells in the mammary glands. The physiological conditions that lead to breast tumorigenesis include inherited genetic mutation and epigenetic modifications, which can lead to premalignant transformation of mammary cells (29). The development of advanced breast tumor is a consequence of immune selection and immune evasion (30). Breast cancer is subdivided into different molecular subtypes: luminal A, luminal B, triple negative, human EGF receptor (HER)2-enriched, basal, and normal-like tumors (31, 32). The development and metastasis of cancer, including breast cancer, appear to be influenced by innate immune surveillance molecules and associated inflammatory mediators in the tumor microenvironment (33, 34).

Here, we examined possible protective effects of rfhSP-D in triple-negative ($ER^-/PR^-/HER2^-$), triple-positive ($ER^+/PR^+/HER2^+$), and $HER2^+$-overexpressing breast cancer cell lines. We also examined a possible interaction between SP-D and hyaluronic acid (HA; polymeric nonsulfated glycosaminoglycan), the most abundant component of the extracellular matrix (ECM), which plays an important role in inflammation, angiogenesis, fibrosis, and cancer progression (35). The interaction of breast cancer cells with HA can sustain tumor growth and promote malignant progression. The altered synthesis of HA in early and late stages of ductal breast carcinoma *in situ* (DCIS) microenvironment is correlated with tumor stage

progression and invasion (36). Several studies provide strong evidence that HA participates in the regulation of breast tumor cell migration and invasion *in vitro* and tumor growth and progression *in vivo* (37–39). We report, for the first time, that rfhSP-D interacts with HA that negates its anti-tumor properties; i.e., in the presence of HA, rfhSP-D is unable to induce apoptosis in triple-positive and HER2-overexpressing breast cancer cell lines. Therefore, neutralizing the negative effect of HA on rfhSP-D can have crucial implications for the development of therapeutic strategies.

MATERIALS AND METHODS

Expression and Purification of rfhSP-D

Expression and purification of rfhSP-D were performed as published earlier (19). Briefly, *Escherichia coli* BL21 (λDE3) pLysS bacterial strain (Invitrogen) was transformed with plasmid pUK-D1, composed of cDNA sequences for α-helical neck and CRD region of human SP-D. Twenty-five milliliters of bacterial primary inoculum was inoculated into 500 ml of Luria-Bertani medium containing 100 μg/ml ampicillin and 34 μg/ml chloramphenicol (Sigma-Aldrich) and grown to an OD600 of 0.6. The bacterial cells were then induced with 0.5 mM isopropyl β-D-1-thiogalactopyranoside (IPTG) (Sigma-Aldrich) for 3 h. The IPTG-induced bacterial cell pellet was treated with lysis buffer (50 mM Tris–HCl pH 7.5, 200 mM NaCl, 5 mM EDTA pH 8, 0.1% v/v Triton X-100, 0.1 mM phenyl-methyl-sulfonyl fluoride, 50 μg/ml lysozyme) and subsequently sonicated (five cycles, 30 s each). The sonicated was centrifuged at 12,000 × g for 30 min, followed by denaturation and renaturation of rfhSP-D inclusion bodies using refolding buffer (50 mM Tris–HCl pH 7.5, 100 mM NaCl, 10 mM 2-mercaptoethanol) containing 8 M urea. The dialysate was then loaded onto a maltose–agarose affinity column (5 ml; Sigma-Aldrich), and rfhSP-D was eluted using 10 mM EDTA buffer containing 50 mM Tris–HCl pH 7.5 and 100 mM NaCl. Eluted rfhSP-D fractions were then tested for endotoxin levels using a QCL-1000 Limulus amebocyte lysate system (Lonza). The endotoxin levels were found to be ∼5 pg/μg of rfhSP-D. The purity of protein was analyzed via 15% w/v SDS-PAGE, and its immunoreactivity was assessed via western blotting.

Cell Culture and Treatments

Human breast cancer cell lines, triple-negative BT20 ($ER^-/PR^-/HER2^-$) (ATCC-HTB19), triple-positive BT474 ($ER^+/PR^+/HER2^+$) (ATCC-HTB20), and HER2-positive SKBR3 ($ER^-/PR^-/HER2^+$) (ATCC-HTB30), were cultured in complete RPMI medium (Sigma-Aldrich), supplemented with 10% v/v fetal bovine serum (FBS), 2 mM L-glutamine, 100 U/ml penicillin (Sigma-Aldrich), 100 μg/ml streptomycin (Sigma-Aldrich), and 1 mM sodium pyruvate (Sigma-Aldrich) and left to grow at 37°C under 5% v/v CO_2. Since these cell lines were adherent, cells were detached using 2× trypsin–EDTA (0.5%) (Fisher Scientific) for 10 min at 37°C, then centrifuged at 1,500 rpm for 5 min, and resuspended in complete RPMI. Cell number and viability were assessed by mixing an equal volume of the cell suspension and Trypan Blue (0.4% w/v) (Fisher Scientific) and by counting using a hemocytometer with a Neubauer chamber (Sigma-Aldrich).

Fluorescence Microscopy

BT20, BT474, and SKBR3 (50,000) cells were grown on coverslips and incubated with rfhSP-D (10 μg/ml) in serum-free RPMI medium for 1 h for cell binding analysis and 24 h for apoptosis induction. For binding experiments, the coverslips were washed three times with phosphate-buffered saline (PBS) and incubated with polyclonal anti-rabbit human SP-D antibody (1:200) (Medical Research Council Immunochemistry Unit, Oxford) for 1 h at room temperature (RT). Following washes with PBS, the cells were incubated with goat anti-rabbit IgG conjugated to Alexa Fluor® 488 (1:200) (Abcam) and Hoechst (1:10,000) (Sigma-Aldrich) for immunofluorescence analysis. For apoptosis induction analysis, the cells were incubated with FITC Annexin V (1:200) and propidium iodide (PI) (1:200) diluted in Annexin V-binding buffer for 15 min at RT in dark. After washing with PBS three times, the coverslips were mounted on slides and viewed under an HF14 Leica DM4000 microscope.

Flow Cytometry

BT20, BT474, and SKBR3 (0.4×10^6) cells were grown in a six-well-plate and incubated with rfhSP-D (20 μg/ml), along with an untreated control, for 24 h. The cells were then detached using 2 × trypsin–EDTA (0.5%) (Fisher Scientific) and centrifuged at 1,500 × *g* for 5 min. Staurosporine (1 μM/ml; Sigma-Aldrich) was used as a positive control of apoptosis. Following washes with PBS, the cells were incubated for 15 min with goat anti-rabbit IgG conjugated to Alexa Fluor® 488 (1:200) (Abcam) and Hoechst (1:10,000) (Sigma-Aldrich) for apoptosis analysis. After washing with PBS three times, apoptosis was measured using a NovoCyte flow cytometer. Compensation parameters were acquired using unstained, untreated FITC-stained, and untreated PI-stained cells for all three cell lines. For solid-phase studies, six-well-plates were coated with HA (20 μg/ml) (a kind gift from Prof. Ivan Donati, Department of Life Sciences, University of Trieste) overnight at 4°C with and without rfhSP-D (20 μg/ml). The wells were washed with PBS, and 0.4×10^6 cells were added to the HA/rfhSP-D-coated wells and incubated 37°C for 24 h. For proliferative studies, the cells were washed with PBS and incubated with anti-mouse Ki-67 (BioLegend) diluted in a permeabilization reagent of the FIX&PERM kit (Fisher Scientific) for 30 min at RT. After PBS washes, the cells were probed with a goat anti-mouse-FITC conjugate (1:200) (Fisher Scientific) for 30 min at RT in the dark. Cells (12,000) were acquired for each experiment and compensated before plotting the acquired data.

Purification of Full-Length SP-D From Breast Cancer Cell Lines

BT20, BT474, and SKBR3 (0.4×10^6) culture media were collected and centrifuged at 5,000 rpm for 10 min. The supernatants were passed through a maltose–agarose affinity column. The bound full-length SP-D was eluted using an elution buffer, containing 50 mM Tris–HCl pH 7.5, 100 mM NaCl, and 10 mM EDTA. Full-length SP-D protein yield of 1 μg/ml

was obtained from 100 ml of culture medium. The purity of eluted fractions (10 μg/ml) was analyzed via 15% w/v SDS-PAGE, and its immunoreactivity was determined via western blotting. For western blotting analysis, the eluted full-length SP-D was heated for 10 min at 100°C and subjected to SDS-PAGE (12% v/v). The proteins were then electrophoretically transferred onto a nitrocellulose membrane (320 mA for 2 h) in 1× transfer buffer (25 mM Tris–HCl pH 7.5, 190 mM glycine, and 20% methanol). The membrane was blocked using 5% w/v dried milk powder (Sigma-Aldrich) in PBS overnight at 4°C, followed by washing with PBS three times for 5 min each. The membrane was then incubated with polyclonal anti-rabbit human SP-D antibody (MRC Immunohistochemistry Unit, Oxford) (1:1,000), followed by probing with protein A–HRP (Sigma-Aldrich) (1:1,000). Following washing with PBST, the membrane was developed using a 3′-diaminobenzidine (DAB) substrate kit.

Apoptosis Analysis of Breast Cancer Cells Treated With BT474-Derived Full-Length SP-D

The purified full-length SP-D from breast cancer culture was subjected to apoptosis assay using an Annexin V/FITC kit (BioLegend). BT20, BT474, and SKBR3 cells (0.4×10^6) were incubated with 20 μg/ml of culture-purified SP-D and incubated for 24 h. The cells were then detached using 2 × trypsin–EDTA (0.5%) (Fisher Scientific) and centrifuged at 1,500 × g for 5 min. Following washes, the cells were then incubated with both FITC and PI dye (1:200) for 15 min in the dark. After washing with PBS, the cells were subjected to flow cytometric analysis. Compensation parameters were acquired using unstained, untreated FITC-stained, and untreated PI-stained cells for all three cell lines.

Immunohistochemical Analysis

Surgical breast cancer tissues and adjacent peritumoral mammary parenchymas were selected following ethical approval by the University Hospital of Palermo Ethical Review Board (approval number 09/2018). TNBC, HER2+, luminal B, and luminal A breast cancer tissues were used, while normal breast tissue was used as a control. Immunohistochemistry (IHC) was performed using a polymer detection method. Briefly, tissue samples were fixed in 10% v/v buffered formalin and paraffin embedded. Four-micrometer-thick tissue sections were deparaffinized and rehydrated. The antigen unmasking technique was carried out using Novocastra Epitope Retrieval Solutions, pH 6 EDTA based (Leica Biosystems), in a thermostatic bath at 98°C for 30 min. Sections were brought to RT and washed in PBS. After neutralization of the endogenous peroxidase with 3% v/v H_2O_2 and Fc blocking (Novocastra, Leica Biosystems), the samples were incubated overnight at 4°C with mouse anti-human SP-D monoclonal antibody (1:800) (Abcam). Staining was revealed via a polymer detection kit (Novocastra, Leica Biosystems) and 3-amino-9-ethylcarbazole (AEC, Dako, Denmark) substrate chromogen. Slides were counterstained with Harris hematoxylin (Novocastra, Leica Biosystems). Alcian blue staining was carried out to detect the presence of mucins in breast cancer tissue sections, according to the manufacturer's kit Bioptica (04-160802). Slides were analyzed under the Axio Scope A1 optical microscope (Zeiss) and microphotographs were collected through the Axiocam 503 color digital camera (Zeiss) using the Zen 2 software.

Adhesion Assay

BT20, BT474, and SKBR3 (0.5×10^5) cells were labeled with FAST DiI fluorescent dye (Molecular Probes, Invitrogen) and allowed to adhere to 96 microtiter wells pre-coated with 20 μg/ml of HA, rfhSP-D, and bovine serum albumin (BSA). The adhesion of cells was measured after 35 min of incubation at 37°C under 5% CO_2. The non-adhered cells were washed off with PBS, and the remaining cells were lysed using 10 mM Tris–HCl pH 7.4 + 0.1% v/v SDS. The plate was read at 544 nm using Infinite 200 (Tecan). Results were expressed as adhesion percentage with reference to a standard curve established using an increasing number of FAST DiI-labeled cells.

Intracellular Signaling Analysis

Signaling pathway was analyzed using the PathScan Intracellular Signaling Array Kit (Cell Signaling Technology). Briefly, 0.5×10^6 breast cancer cell lines were grown in a six-well-plate in serum-free RPMI medium. Cells were then left to adhere to HA and rfhSP-D (20 μg/ml) pre-coated plates and incubated at 37°C for 25 min. The unbound cells were then washed with cold PBS and lysed in ice-cold cell lysis buffer containing a cocktail of protease inhibitors (Roche Diagnostics). The Array Diluent Blocking buffer was added to each well on the multi-well gasket at RT for 15 min. After decanting the Array Blocking Buffer, 75 μl of the total lysate (0.8 mg/ml) was added to each well and incubated for 2 h at RT on an orbital shaker. The well contents were decanted and washed with 100 μl of 1× Array Wash Buffer three times (5 min each wash). The wells were then incubated with biotinylated detection cocktail antibody for 1 h at RT, followed by incubation with streptavidin-conjugated DyLight 680 for 30 min. The fluorescence readout was measured via LI-COR Biosciences Infrared Odyssey imaging system (Millennium Science), and data were processed by the software Image Studio 5.0.

Western Blotting

BT20, BT474, and SKBR3 (0.4×10^6) cells were seeded in a six-well-plate and treated with rfhSP-D (20 μg/ml) for 24 h, along with an untreated control, in a serum-free RPMI medium. After removing the medium, the cells were lysed using a lysis buffer (50 mM Tris–HCl pH 6.8, 2% v/v SDS, 2% v/v β-mercaptoethanol, 10% v/v glycerol and 0.1% w/v bromophenol blue). The lysed cells were then sonicated for 15 s, and the sonicated samples were heated for 10 min at 100°C and subjected to SDS-PAGE (12% v/v). The proteins were then electrophoretically transferred onto a nitrocellulose membrane (320 mA for 2 h) in 1× transfer buffer (25 mM Tris–HCl pH 7.5, 190 mM glycine, and 20% v/v methanol). The membrane was blocked using 5% w/v dried milk powder (Sigma-Aldrich) in PBS overnight at 4°C, followed by washing with PBS three times (5 min each). For apoptosis studies, the membrane was incubated with rabbit anti-human caspase primary antibodies (anti-cleaved

caspase 9 and anti-cleaved caspase 3; Cell Signaling) at RT for 1 h. The membrane was washed with PBST (PBS + 0.05% Tween 20) three times, 10 min each, followed by incubation with secondary goat anti-rabbit IgG horseradish peroxidase (HRP) conjugate (1:1,000; Fisher Scientific) for 1 h at RT. Following washes with PBST, the membrane was developed using a DAB substrate kit (Thermo Fisher).

ELISA

For HA (1,500 kDa) binding analysis, a constant concentration of HA (20 μg/ml) was coated overnight at 4°C using carbonate/bicarbonate (CBC) pH 9.6 buffer, followed by blocking with 2% w/v BSA at 37°C. Recombinant maltose binding protein (MBP) was used as a negative control in this experiment. After three washes with PBST, rfhSP-D (5, 10, or 20 μg/ml) was incubated in buffer containing 5 mM $CaCl_2$ for 2 h at 37°C. After washing with PBST three times, the binding was assessed by polyclonal anti-rabbit human SP-D antibody (1:5,000) and incubated at 37°C for 1 h. The wells were washed again with PBST three times and incubated with protein A–HRP secondary conjugate (1:5,000) (Sigma-Aldrich) for 1 h at 37°C. After washes with PBST, the binding was detected using 3,3′,5,5′-tetramethylbenzidine (TMB) substrate (Sigma-Aldrich). The reaction was stopped using 2 N H_2SO_4, and the absorbance was read at 450 nm using an iMark™ microplate absorbance reader (Bio-Rad).

Quantitative RT-PCR

BT20, BT474, and SKBR3 (0.4×10^6) cells were added to six-well-plate pre-coated with HA (20 μg/ml), HA + rfhSP-D (20 μg/ml), and rfhSP-D (20 μg/ml) and incubated at 37°C for various time points. The cell pellet for each time point was subjected to RNA extraction using GenElute Mammalian Total RNA Purification Kit (Sigma-Aldrich). RNA samples were then treated with DNase I (Sigma-Aldrich), and the total RNA concentration and purity were determined using a 260:280 nm ratio using NanoDrop 2000/2000c (Thermo Fisher Scientific). Two micrograms of total RNA was used for cDNA synthesis using High Capacity RNA to cDNA kit (Applied Biosystems). Primer sequences used in this study were designed for specificity using the Primer-BLAST software (Basic Local Alignment Search Tool) (http://blast.ncbi.nlm.nih.gov/Blast.cgi). p21 and p27 mRNA levels were estimated by quantitative RT-PCR (qRT-PCR) using the following primers: 5′-TGGAGACTCTCAGGG TCGAAA-3′ and 5′-CGGCGTTTGGAGTGGTAGAA-3′ for p21, and 5′-CCGGTGGACCACGAAGAGT-3′ and 5′-GCTCGCCTC TTCCATGTCTC-3′ for p27. Briefly, the qPCR reaction consisted of 5 μl of iQ SYBR Green Supermix (Bio-Rad, Milan, Italy), 75 nM of forward and reverse primers, and 500 ng template cDNA in a 10 μl final reaction volume. qRT-PCR was performed on a Rotor-Gene 6000 (Corbett, Explera, Ancona, Italy). The melting curve of the reactions was recorded between 55 and 99°C with a hold every 2 s. The comparative quantification (CQ) method was used to determine the relative amount of gene expression in each sample, and the data analyzed using Rotor-Gene 1.7 software (Corbett Research) (40). The CQ method is specific in calculating the efficiencies of each gene for each individual PCR and is based on the second differential maximum method. The samples were normalized using the expression of human TATA binding protein (TBP) rRNA. Assays were conducted in triplicates.

Statistical Analysis

Graphs were generated using GraphPad Prism 6.0; the statistical analysis was carried out using an unpaired one-way ANOVA test. Error bars represent SD or SEM ($n = 3$), as indicated in the figure legends. The significant values were measured based on $^{*}p < 0.05$, $^{**}p < 0.01$, $^{***}p < 0.001$, and $^{****}p < 0.0001$ between treated and untreated samples.

RESULTS

A Recombinant Form of Truncated Human SP-D Binds Breast Cancer Cell Lines

rfhSP-D comprising the eight Gly-X-Y repeats and the neck and CRD regions of human SP-D was affinity-purified and migrated at ∼20 kDa on SDS-PAGE under reducing conditions (**Figure 1A**). The immunoreactivity of purified rfhSP-D was confirmed via western blotting using polyclonal anti-human SP-D antibody raised in rabbit against native human SP-D purified from lung lavage (**Figure 1B**). BSA was used as a negative control protein. Purified rfhSP-D (5 μg/ml) bound breast cancer cell lines, triple-negative BT20 ($ER^-/PR^-/HER2^-$), triple-positive BT474 ($ER^+/PR^+/HER2^+$), and HER2-positive SKBR3 ($ER^-/PR^-/HER2^+$) (**Figure 1D**). The nucleus of the cell was stained with Hoechst dye, while the membrane localization of the bound rfhSP-D was revealed using green FITC/anti-human SP-D conjugate. All rfhSP-D-treated breast cancer cell lines showed a similar "cluster"-like binding pattern on the cell membrane (**Figure 1D**). No FITC was detected in the untreated controls (**Figure 1C**), probed with both primary and secondary antibodies, suggesting the specificity of rfhSP-D binding.

Apoptosis Induction by rfhSP-D in Breast Cancer Cell Lines

The quantitative and qualitative analyses of apoptosis induction by rfhSP-D were performed using flow cytometry (**Figures 2A,B**) and immunofluorescence microscopy (**Figures 2C,D**). A significant proportion of BT474 and SKBR3 breast cancer cells treated with rfhSP-D (20 μg/ml) underwent apoptosis at 24 h as revealed by FACS analysis (**Table 1**). BT474 (∼61%) and SKBR3 (∼68%) cell lines were more susceptible to apoptosis induction when immobilized rfhSP-D (20 μg/ml) (**Figure 2A**) was used; there was no effect on the BT20 cell line. rfhSP-D in solution also induced apoptosis in BT474 (∼34%) and SKBR3 (∼53%) (**Figure 2B**); again, rfhSP-D had no significant effect on the BT20 cell line (**Figure 2A**, **Table 1**). The integrity of the cell membrane was intact in untreated cells, and hence, the cells were still viable, blocking the translocation of phosphatidylserine (PS) from the inner cell membrane to outer plasma membrane and preventing the PS–Annexin V interaction. Nearly 56% BT474 and SKBR3 cells were both stained positive for FITC and PI, suggesting that annexin V/FITC was able to bind to PS found on the cell surface of the cells undergoing apoptosis. However, there were more BT474 cells that stained for PI alone than the SKBR3 cell line, suggesting that BT474 cells were either at the

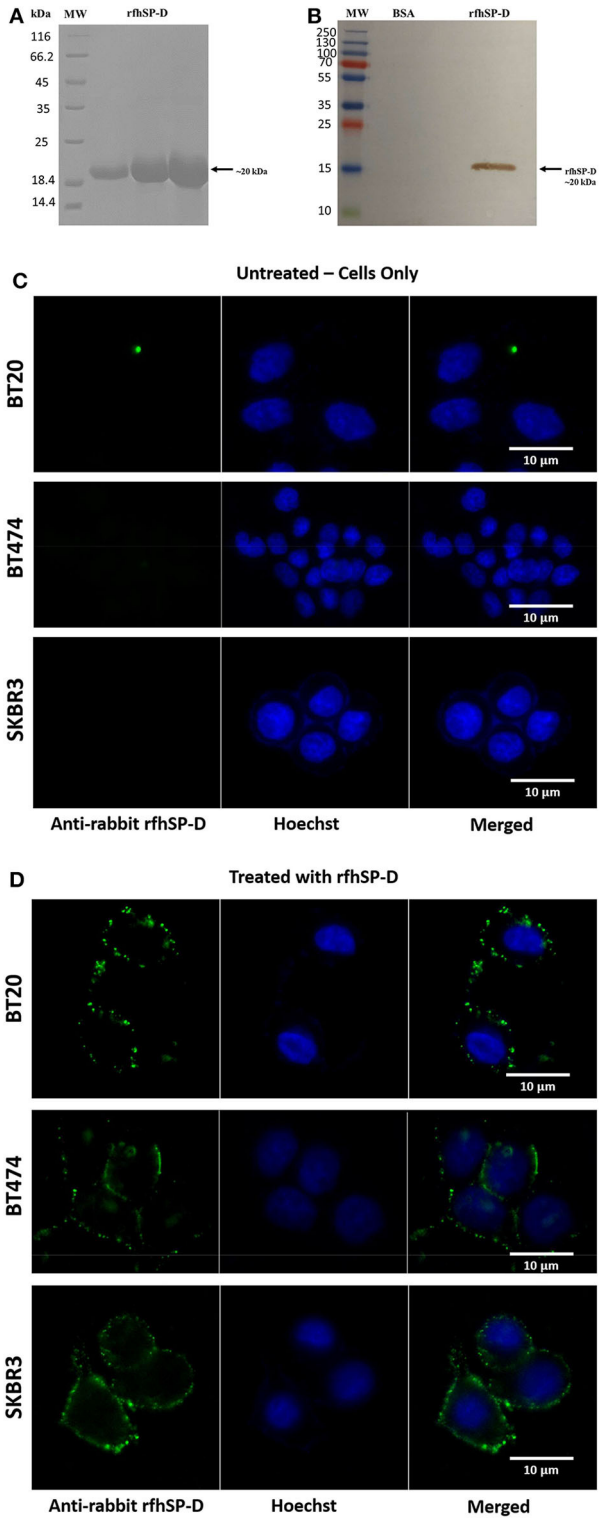

FIGURE 1 | SDS-PAGE **(A)** and immunoblot profile **(B)** of the purified recombinant form of human surfactant protein D (rfhSP-D). Expression of rfhSP-D under the bacteriophage T7 promoter, expressed as ~20 kDa insoluble protein. Eluted fractions were passed through a maltose–agarose column, which appeared as a single band at ~20 kDa. Immunoreactivity of

(Continued)

FIGURE 1 | affinity-purified rfhSP-D was examined via western blotting; lane 1: BSA as a negative control; lane 2: purified rfhSP-D (5 µg/ml). Binding of rfhSP-D (10 µg/ml) to breast cancer cell lines using fluorescence microscopy, following 1 h incubation at 4°C **(C,D)**. The nucleus of the cells was stained with Hoechst (1:10,000), and both untreated (cells only) **(C)** and rfhSP-D-treated **(D)** cells were probed with polyclonal anti-human SP-D/FITC antibody (1:200). Membrane localization of the bound proteins was only detected in the treated cells, while no FITC was detected in the untreated control (cells only).

late stage of apoptosis or undergoing necrosis. The percentage of viable cells in the untreated (cells only) sample was significantly higher as compared to the treated sample, BT474 (~92%) and SKBR3 (~96%), suggesting that apoptosis induction was a rfhSP-D protein-specific effect (**Figure 2A**). Staurosporine (1 µM/ml) was used as a positive control for apoptosis studies. Staurosporine-treated BT20, BT474, and SKBR3 showed ~70% of apoptosis induction at 24 h (**Figures 2A,B**). Staurosporine is a well-known therapeutic, potent apoptosis inducer, which is suggested to inhibit tumor cell growth and proliferation by triggering cell death via an intrinsic apoptotic pathway (41). Fluorescence microscopy analysis in BT474 and SKBR3 cell lines treated with rfhSP-D revealed a positive staining for cell membrane integrity marker, Annexin V (conjugated to FITC), and disoriented cell membrane morphology (**Figures 2C,D**). Thus, PI-positive staining was seen only in treated cell lines (**Figure 2D**) compared to untreated control cells (**Figure 2C**), indicating no occurrence of late apoptotic or necrosis. In contrast, no positive staining of Annexin V or PI was detected in BT20 treated cells, which were similar to the untreated control.

rfhSP-D Induces Apoptosis in BT474 and SKBR3 Cell Lines via Intrinsic Pathway

Since rfhSP-D caused apoptosis in BT474 and SKBR3 cells, we further examined the likely apoptotic pathway being triggered following rfhSP-D treatment. Apoptosis can be initiated through intrinsic or extrinsic pathways. Expression of caspases was tested in rfhSP-D-treated breast cancer cell lines. Western blotting analysis of rfhSP-D-treated BT474 and SKBR3 cells at 24 h revealed cleavage of caspase 9 (~37 kDa) and 3 (~17 kDa), suggesting the involvement of the intrinsic apoptosis pathway (**Figure 3**). As expected, cleavage of caspases 3 (**Figure 3A**) and 9 (**Figure 3B**) was not detected in BT20 and untreated (cells only) controls. Furthermore, cleaved caspase 8 was tested as a marker for the extrinsic pathway, but no difference was observed between rfhSP-D-treated cell lines and untreated controls (data not shown).

Expression of Human SP-D and HA in Breast Cancer Tissues

The expression of human SP-D was analyzed in eight cases of invasive ductal carcinoma, no special type (NSP), comprising two cases for each molecular class (luminal A, luminal B, Her2-Neu, and triple negative) based on the expression of the estrogen receptor (ER), the progesterone receptor (PR), and the human EGF receptor 2 (Her2-Neu) status. Among biological variables considered, besides the different molecular class, the

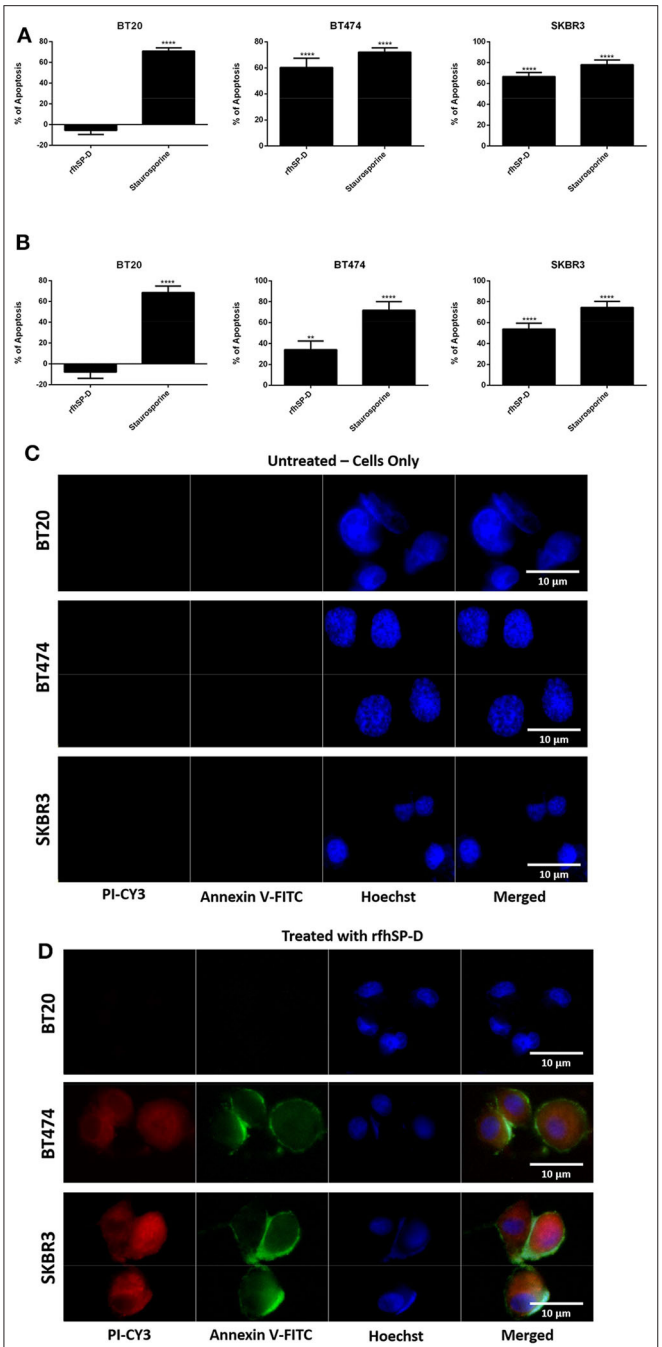

FIGURE 2 | Flow cytometric analysis of apoptosis induction in breast cancer cells treated with 20 μg/ml of immobilized **(A)** and solution-phase **(B)** rfhSP-D for 24 h. For both Annexin V/FITC and DNA/PI staining, 12,000 cells were acquired and plotted. A significant difference was seen among treated and untreated (cells only) samples, as evident by the shift in the fluorescence intensity. The data were expressed as the mean of three independent experiments ($n = 3$) done in triplicates ± SEM. Statistical significance was established using the unpaired one-way ANOVA test (**$p < 0.01$ and ****$p < 0.0001$). The percentage of apoptosis was calculated by normalizing the treated cells with their untreated counterparts. Fluorescence microscopy analysis of apoptosis induction in breast cancer cells treated with rfhSP-D (20 μg/ml) for 24 h, using an Annexin V with a propidium iodide (PI) staining kit; untreated (cells only) controls **(C)** and rfhSP-D-treated cells **(D)**. The nucleus was stained with Hoechst (1:10,000), and the cell membrane was stained positively with Annexin V and PI (1:200) in treated cell lines, suggesting that cells treated with rfhSP-D induced apoptosis at 24 h, where translocation of PS to the outer plasma membrane was able to bind Annexin V due to loss of membrane integrity and PI stain was taken, which stained the DNA of apoptotic cells. No Annexin V/PI staining was detected in untreated cells.

neoplastic tissues presented a different grade tumor, computed with the Nottingham score, varying from moderate (G2) to undifferentiated (G3). Indeed, the molecular classification allows us to identify four different classes based on the expression of the ER and PR and the human EGF receptor 2 (Her2-Neu) status and called luminal A, luminal B, Her2-Neu, and triple negative, respectively. The molecular subtypes reflect the neoplastic heterogeneity of breast cancer and differ in gene expression patterns, clinical and morphological features, response to treatment, and outcome. Our aim was to evaluate the presence and distribution of SP-D in all molecular subtypes of breast cancer to dissect its biological role in neoplastic progression and to consider a potential predictive and/or prognostic marker of mammary carcinoma. Our data appear to suggest heterogeneous inter-tumor and intra-tumor expressions of SP-D within the molecular subtypes. IHC staining for SP-D highlighted its cytoplasmic expression in both the neoplastic tissue and the healthy peritumoral mammary parenchyma, as previously demonstrated (20). Indeed, the presence of SP-D was evident in cytoplasmic labeling and was highly expressed by the ductal epithelium of peritumoral mammary parenchyma and the neoplastic subclones of luminal A type, while its reduced expression was evident in triple-negative breast cancer (TBNC) (**Figure 4A**). For the luminal B and HER2 groups, a heterogeneous expression of SP-D was observed (**Figures 4i**,**ii**). We also examined serial sections for the localization of HA within the tumor microenvironment following histochemical analysis of normal and breast cancer tissue specimens. As shown in **Figure 4i**, Alcian blue staining highlighted the presence of acid mucins, containing HA and sialic acid (42–44), in the tumor stroma, around the tumor cells and was very faint in the peritumoral mammary parenchyma in all the molecular classes of breast cancer considered. The luminal B and HER2 specimens were characterized by a variable SP-D expression within the tumor. In the luminal B and HER2 groups, Alcian blue staining also showed a greatly heterogeneous expression of HA. Thus, a stronger staining for Alcian blue was evident where a lower presence of SP-D was detected, suggesting that a modification of ECM might be associated with a variable distribution of SP-D (**Figures 4A,G–L**).

rfhSP-D Binds to High-Molecular-Weight HA

Confirmation of the presence of HA in the breast cancer tissues prompted us to examine if rfhSP-D binds to HA and can modulate the nature of rfhSP-D–breast cancer cell interaction. In direct binding ELISA, rfhSP-D bound to solid-phase high-molecular-weight (1,500 kDa) HA in a dose-dependent manner (**Figure 5A**). Immobilized rfhSP-D (20 μg/ml) alone as

TABLE 1 | Flow cytometric analysis of apoptosis induction in breast cancer cells treated with 20 μg/ml of immobilized and solution-phase rfhSP-D for 24 h.

	Immobilized phase			Solution phase		
	Background apoptosis (%)	Normalized apoptosis with rfhSP-D (%)	Normalized apoptosis with staurosporine (%)	Background apoptosis (%)	Normalized apoptosis with rfhSP-D (%)	Normalized apoptosis with staurosporine (%)
BT20	5	7	70	5	12	70
BT474	8	61	70	8	34	70
SKBR3	4	68	70	4	53	70

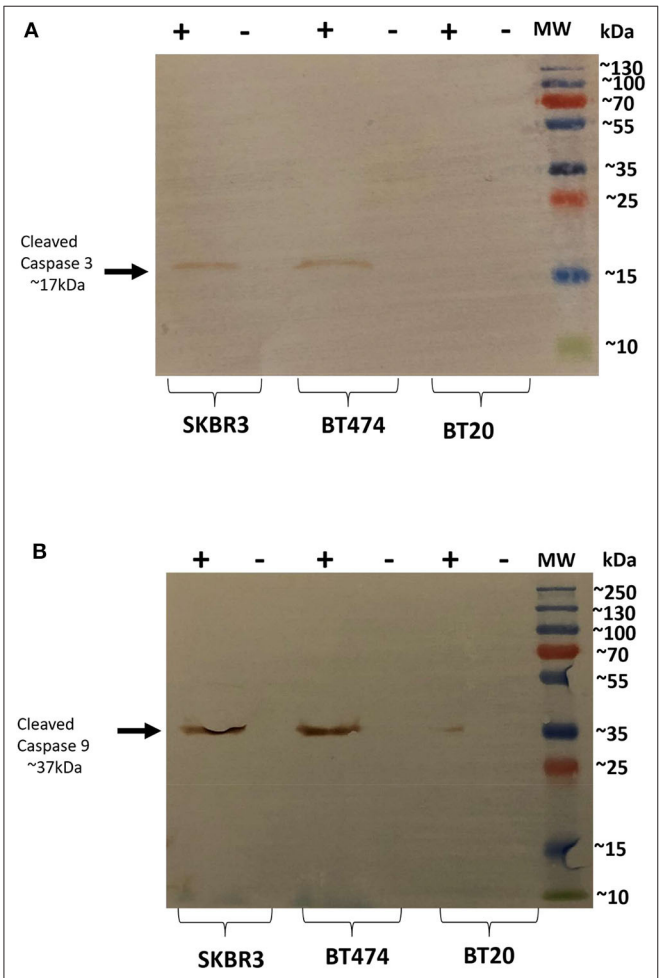

FIGURE 3 | Caspase activation in breast cancer cell lines following rfhSP-D treatment at 24 h. Western blot analysis showed presence of cleaved caspase 3 at 17kDa in the cells treated with rfhSP-D for 24 h. **(A)** Western blot analysis showed presence of cleaved caspase 9 at 37kDa **(B)**, suggesting induction of the intrinsic pathway.

well as HA (20 μg/ml)-bound rfhSP-D were then allowed to interact with breast cancer cell lines. Cell adhesion assay was performed by labeling the cells with the fluorescent probe FAST DiI (**Figure 5B**). All three breast cancer cell lines (BT20, BT474, and SKBR3) were able to adhere to HA, to rfhSP-D, and to HA-bound rfhSP-D. rfhSP-D enticed a greater cell adhesion when compared to HA alone or HA-bound rfhSP-D; all three cell lines bound to similar extent (**Figure 5B**).

HA Binding Modulates the Ability of rfhSP-D to Induce Apoptosis

The implication of HA–rfhSP-D interaction on apoptosis induction in breast cancer cells was investigated (**Figure 6A**). Breast cancer cells incubated with pre-coated HA, HA + rfhSP-D, and rfhSP-D-only wells, along with untreated (cells only) cells, were stained after 24 h with Annexin V/FITC; the quantification of apoptosis was carried out using flow cytometry (**Figure 6A**). Addition of HA to rfhSP-D reduced apoptosis induction by ∼45%. Since we noticed a reduced apoptosis induction by HA+ rfhSP-D, we considered if rfhSP-D induced a proliferative response in combination with HA. Thus, HA + rfhSP-D-treated breast cancer cells were stained with mouse anti- Ki-67 antibody to detect the percentage proliferation (**Figure 6B**). Ki-67 is a well-known nuclear protein associated with active cell proliferation and is expressed throughout the active cell cycle, including G1, S, G2, and M phases. Addition of HA in rfhSP-D-treated SKBR3 cells resulted in ∼30% cell proliferation (**Figure 6B**), suggesting that HA negated pro-apoptotic effects of rfhSP-D in breast cancer cell lines. In the case of BT474, only ∼47% of proliferative cells were seen among rfhSP-D-treated BT474 cells, while HA + rfhSP-D-treated BT474 cells showed a higher proliferation (∼95%) (**Figure 6B**). HA-only-treated BT474 cells showed ∼88% of Ki-67-positive cells, while ∼66% of proliferative cells were seen in HA-treated SKBR3 cells. However, proliferation of BT20 cells was not affected by rfhSP-D or HA treatment, suggesting that these cells continue to grow. These percentage proliferations are compared to untreated control (cells only). Given the presence of SP-D in the breast cancer tissues, we made an attempt to purify SP-D from the culture supernatants of the breast cancer cells on the assumption that breast cancer cells can also be a likely source of SP-D in the tumor microenvironment. We could purify SP-D only from BT474 cell culture (**Figure 6C**). However, the purified SP-D was not able to induce apoptosis in BT474 cells (**Figure 6D**).

rfhSP-D Treatment Upregulated Cell Cycle Inhibitors and Induced p53-Dependent Apoptosis

Activated p53 is a known mediator of DNA damage, oxidative burst, cell cycle arrest, and induction of apoptosis. Therefore, we analyzed the levels of activated p53 in rfhSP-D-treated breast cancer cells. Increased levels of p53 phosphorylation at Ser15 was detected in rfhSP-D-treated SKBR3 cells (**Figure 7A**), while downregulation was seen in the BT20 cell line (**Figure 7A**), suggesting that p53

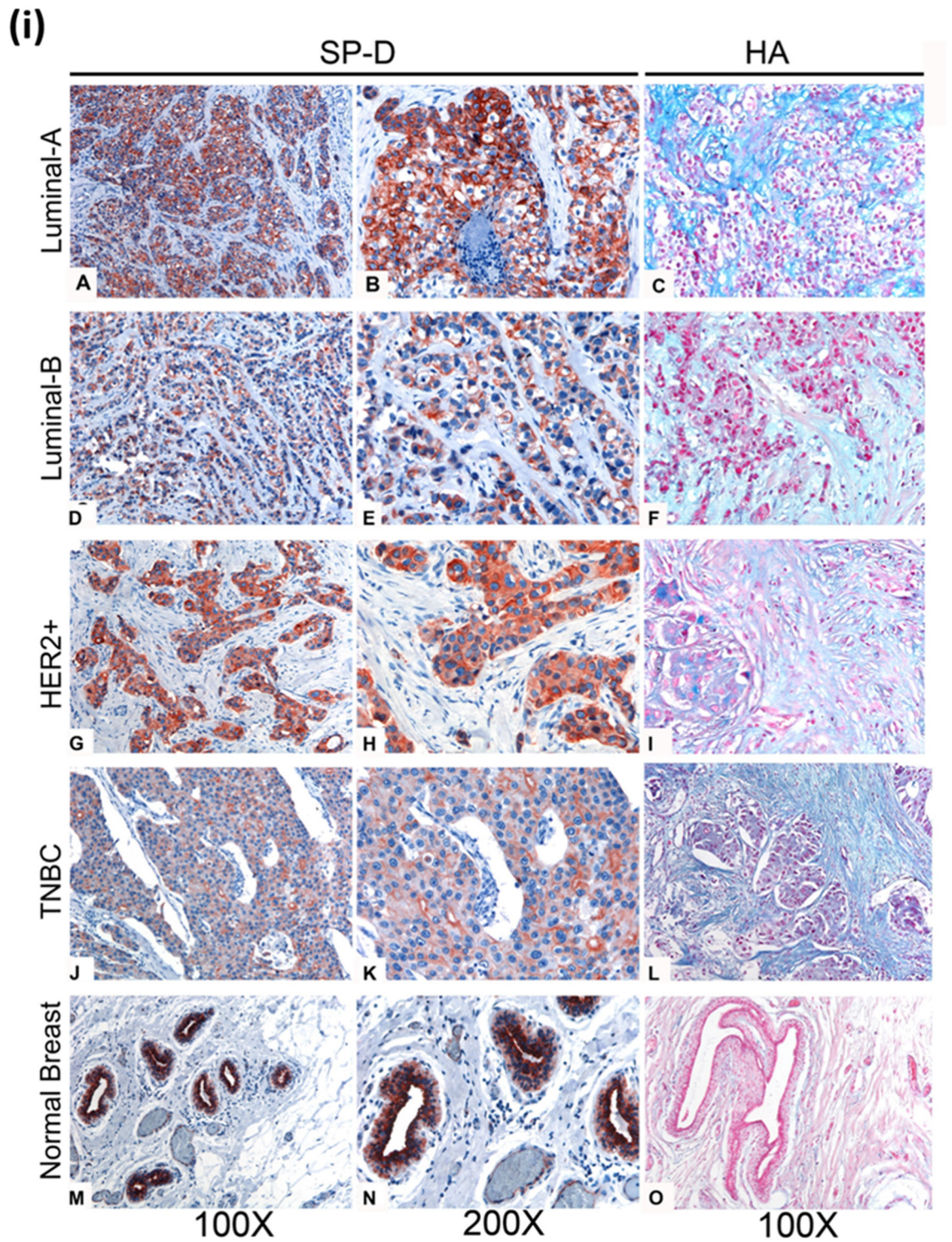

FIGURE 4 | (Continued)

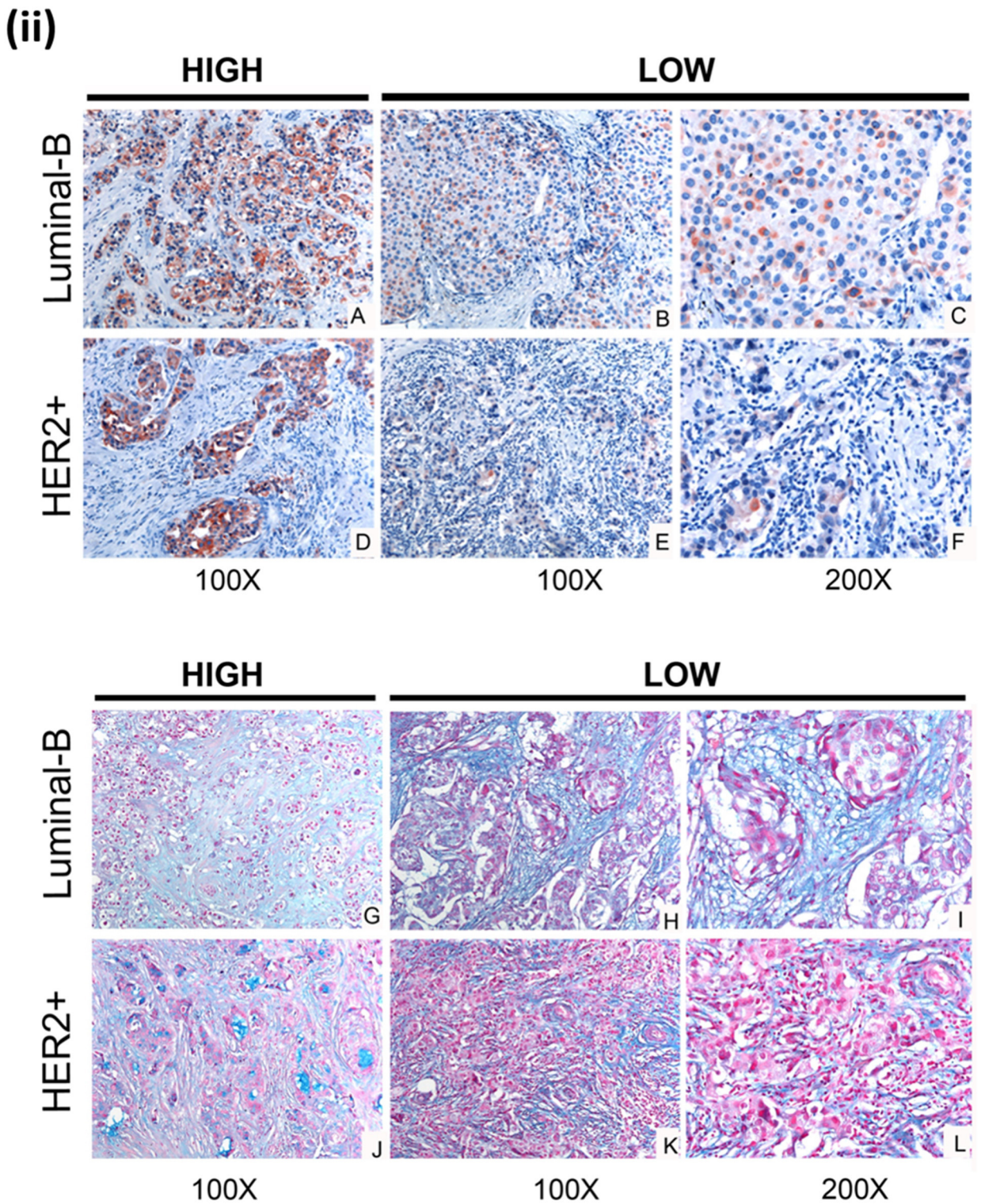

FIGURE 4 | (i) SP-D and Hyaluronic acid (HA) presence in different histotypes of neoplastic breast **(A–L)**, and normal ductal mammary epithelium **(M–O)**. **(A,D,G,J)**. A high variability of SP-D expression between different histotypes is shown, although the positivity of the signal is always attributable to neoplastic cells, as can be observed from the higher- resolution images in the right part of the figure **(B,E,H,K)**. AEC (red) chromogen was used to visualize the binding of anti-human SP-D antibodies. **(C,F,I,L,O)** Histochemical staining with Alcian Blue highlighted HA distribution in breast cancer and normal tissue sections; in particular, the staining was visible in tumor-associated stroma. (ii) Immunohistochemical and histochemical analysis in Luminal-B and Her2+/ER-/PR- breast carcinoma sections of SP-D **(A–F)** and HA **(G–L)** expression, respectively **(B)**. A high variability of SP-D and HA expression within the same isotypes is shown. It is possible to notice a slight inverse correlation between SP-D and HA expression. AEC (red) chromogen was used to visualize the binding of anti-human SP-D antibodies, whereas histochemical staining with Alcian Blue highlighted HA distribution.

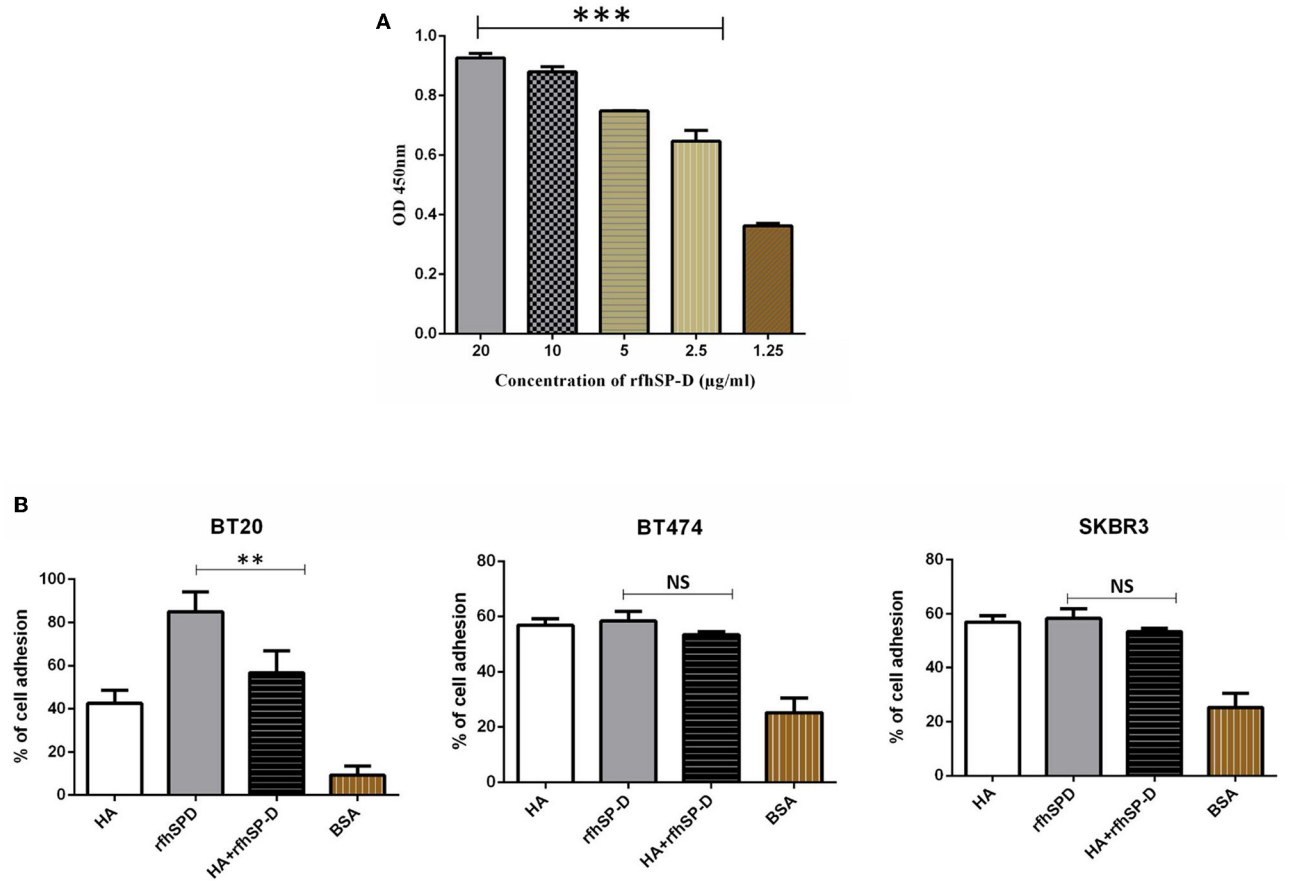

FIGURE 5 | Interaction of rfhSP-D with HA. Binding of varied concentrations of rfhSP-D to HA (20 µg/ml) by ELISA **(A)**. The effects of rfhSP-D on Breast cancer cell lines adhesion **(B)**. Breast cancer cells were labeled with the FAST DiI fluorescent dye and allowed to adhere to 96 microtiter wells pre-coated with HA, rfhSP-D, and BSA. The data is expressed as the mean of three independent experiments. The adhesion of cells was measured after 35 minutes of incubation at 37°C under 5% CO_2. Results are expressed as adhesion percentage with reference to a standard curve established using an increasing number of FAST DiI -labeled cells. The data is expressed as the mean of three independent experiments (n = 3) done in triplicates ± SEM. Statistical significance was established using the unpaired one-way ANOVA test (**$p < 0.01$ and ***$p < 0.001$). The statistical analysis was performed between rfhSP-D and HA + rfhSP-D -treated breast cancer cells.

upregulation may also have contributed to p53-dependent apoptosis induction in SKBR3 cells. In addition, increased transcript levels of p21 and p27 were observed in rfhSP-D-treated BT474 and SKBR3 cell lines (**Figure 7B**) at 12-h time point, suggesting the possibility of cdc2–cyclin B1 reduction leading to G2/M cell cycle arrest. Reduced levels of phosphorylated p53, caspase 3, p21, and p27 were observed in HA + rfhSP-D-treated SKBR3 and BT474 cells (**Figures 7A,B**), suggesting reduced apoptosis induction by the addition of HA. In the case of BT20, no significant difference was found in terms of p21 and p27 mRNA expression levels between rfhSP-D- and HA + rfhSP-D-treated BT20 cells.

DISCUSSION

In this study, we show that rfhSP-D binds to all breast cancer cell lines tested: BT20 ($ER^-/PR^-/HER2^-$), BT474 ($ER^+/PR^+/HER2^+$), and SKBR3 ($ER^-/PR^-/HER2^+$). However, the receptor, SP-D is binding to on the cancer cell surface, is not yet known. Exogenous treatment with rfhSP-D reduced cell viability of BT474 and SKBR3 cell lines and induced apoptosis at 24 h. Cell viability and apoptosis assays were carried out using varied concentrations of rfhSP-D (5, 10, and 20 µg/ml) and different time points (12, 24, and 48 h), but only 20 µg/ml concentration of rfhSP-D was effective in inducting the optimal cell viability reduction and apoptosis induction at 24 h. rfhSP-D-treated BT474 and SKBR3 cells showed a significant reduction in viable cells compared to untreated control (cells only), as evident from Trypan blue exclusion and MTT assay (data not shown). However, no effect of rfhSP-D was seen on the triple-negative (BT20) cell line in terms of cell viability. Recent studies have shown the ability of the CRD region of human SP-D to interact with N-glycans of EGFR, resulting in downregulation of EGF signaling in A549 cell line (23). It is likely that rfhSP-D-mediated apoptosis is due to HER2 expression on BT474 and SKBR3 cells; a lack of it seems to increase BT20 cells resistant

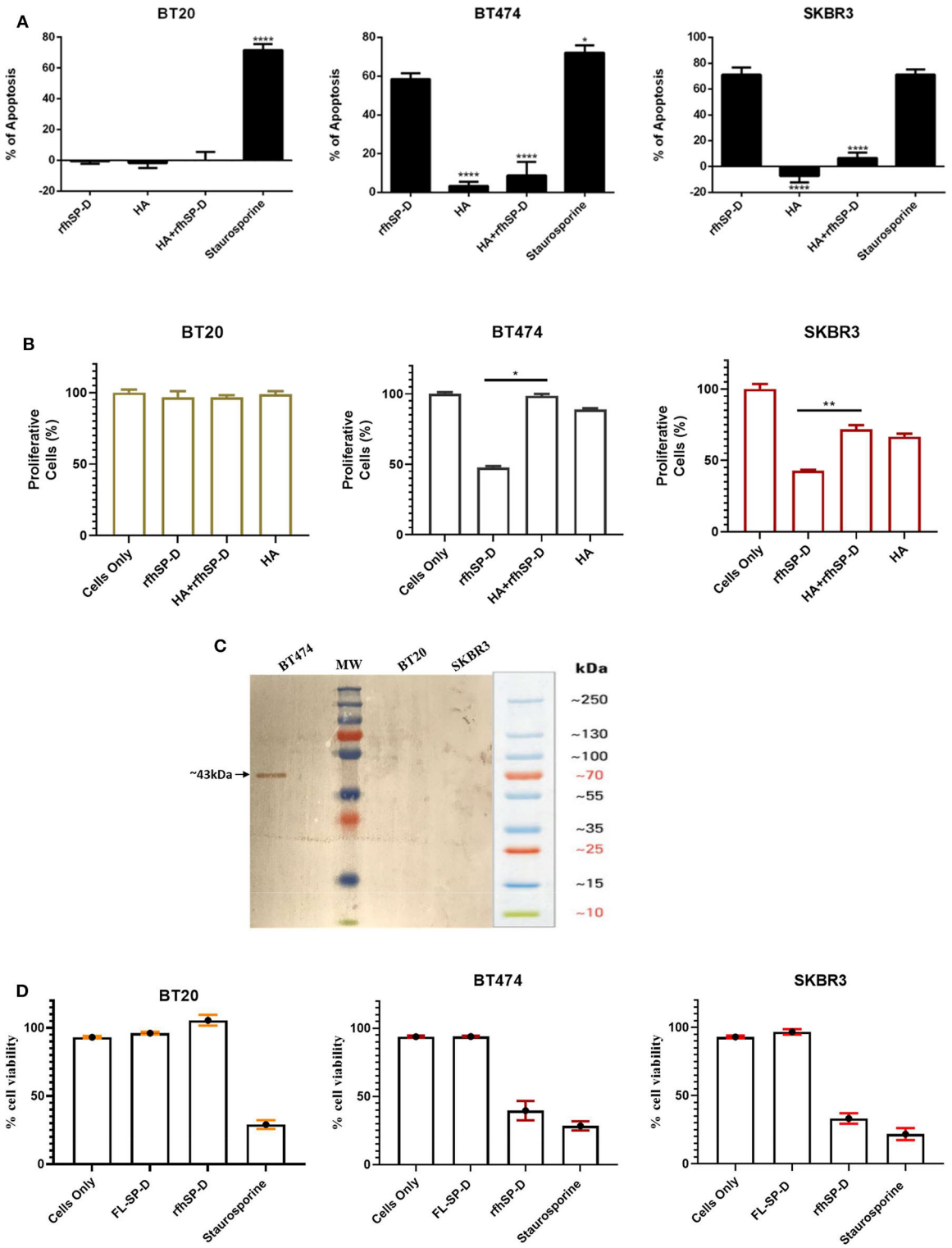

FIGURE 6 | Apoptosis induction in BT20, BT474, and SKBR3 cell lines following HA challenge in the presence and absence of rfhSP-D **(A)**. The data were expressed as the mean of three independent experiments ($n = 3$). A significant difference was seen among treated and untreated samples, as made evident by the shift in the fluorescence intensity. Staurosporine (1 μM/ml) was used as a positive control. Proliferative effects of rfhSP-D treatment on BT474 and SKBR3 breast cancer cell lines **(B)**. BT474 and SKBR3 cells were seeded in wells pre-coated with HA, HA + rfhSP-D, and rfhSP-D alone. The percentage of proliferative cells was evaluated by staining with mouse anti-human KI-67 antibody, and KI-67-stained cells were measured via flow cytometry. The data were generated from at least three independent

(Continued)

FIGURE 6 | experiments ($n = 3$) and presented as mean ± SD (*$p < 0.1$, **$p < 0.01$, and ****$p < 0.0001$). The statistical analysis was performed between rfhSP-D and HA + rfhSP-D-treated breast cancer cells. The secretion levels of FL-SP-D were confirmed and analyzed via western blotting **(C)**. Culture medium collected from BT20, BT474, and SKBR3 cell lines was passed through a maltose Agarose column, and the eluted fractions were validated via western blotting; FL-SP-D was detected at ∼43 kDa only for BT474. Both BT20 and SKBR3 cell lines did not secrete any FL-SP-D. Secreted FL-SP-D by BT474 was tested for its ability to induce apoptosis **(D)**. No effect of secreted FL-SP-D was seen in terms of cell viability and apoptosis induction.

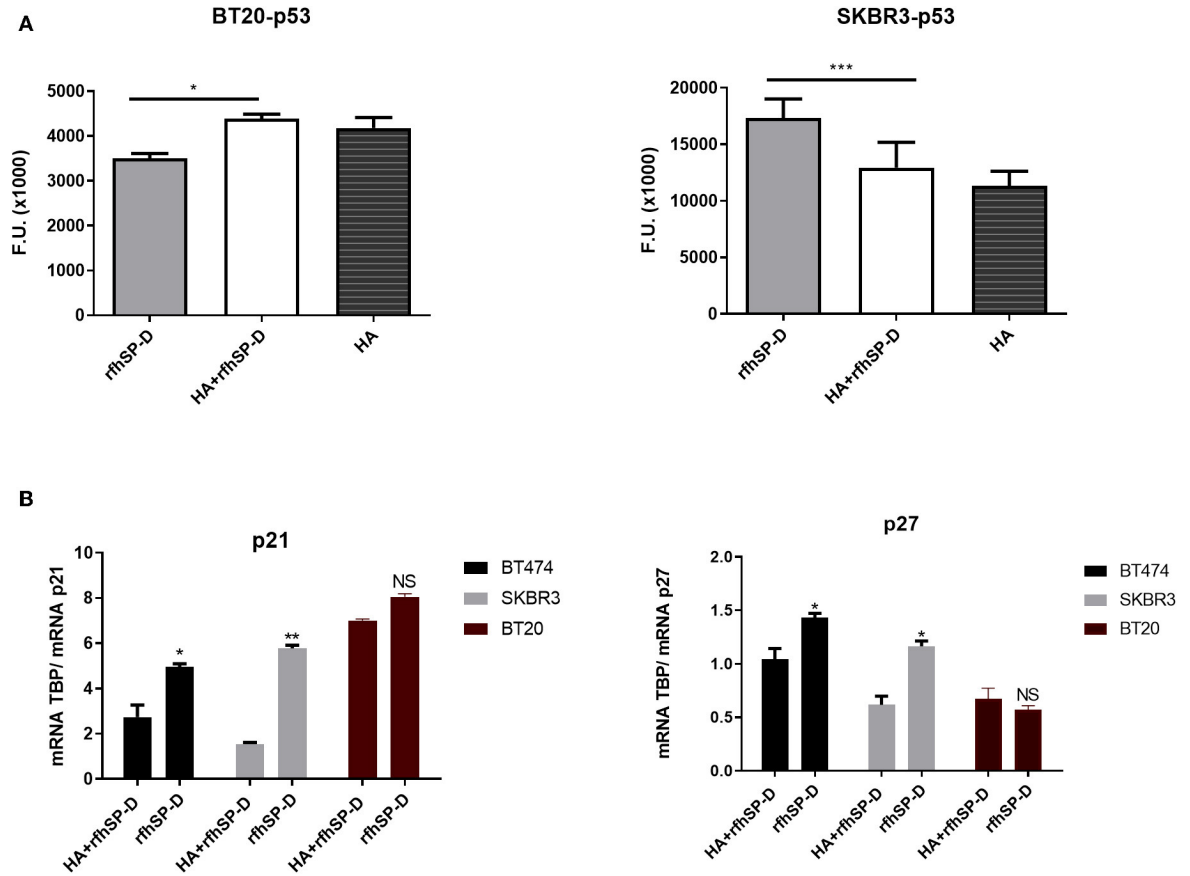

FIGURE 7 | Intracellular signaling to show phosphorylation of p53 in rfhSP-D-treated BT20 and SKBR3 cell lines **(A)**. Breast cancer cell lines were allowed to adhere to HA or HA-bound rfhSP-D, and the phosphorylation status of p53 was evaluated using total cell lysates with a PathScan Antibody Array Kit (Cell Signaling). Data were generated from at least three independent experiments and presented as mean ± SD. rfhSP-D treatment resulted in upregulation of p21 and p27 cell cycle inhibitors **(B)**. BT20, BT474, and SKBR3 (0.4×10^6) cells were seeded in a six-well-plate pre-coated with rfhSP-D and HA + rfhSP-D. The treated cells were lysed and pelleted down. The pelleted cells were subjected to RNA isolation, followed by cDNA synthesis and qPCR. The comparative quantification method was performed to calculate the efficiencies of each gene for each individual PCR and is based on the second differential maximum method or takeoff analysis. The takeoff results obtained with p21/p27 primers were normalized with the housekeeping gene TBP. qPCR assay was conducted in triplicates, and error bars represent ± SEM. Unpaired one-way ANOVA test was used to determine the significance; *$p < 0.05$, **$p < 0.01$, and ***$p < 0.001$ ($n = 3$). The statistical analysis was performed between rfhSP-D and HA + rfhSP-D-treated breast cancer cells.

to the rfhSP-D effect. Whether HER2 is implicated in mediating rfhSP-D-induced apoptosis is under investigation.

The ability of rfhSP-D to induce apoptosis at 24 h in SKBR3 and BT474 cell lines was evident from a significant increase in the number of Annexin V-/PI-positive breast cancer cells examined via flow cytometry and fluorescence microscopy. The cell surface of the healthy cells is composed of asymmetrically distributed lipids on the inner and outer surfaces of the plasma membrane. PS is one of these lipids, which is restricted to the inner surface of the plasma membrane and, thus, is only exposed to the cytoplasm of the cell. However, when apoptosis is triggered by stress factors, lipid asymmetry is lost, and PS translocates to the outer leaflet of the plasma membrane (45). Annexin V is a 36-kDa calcium-binding intracellular protein that binds to PS (45). Thus, Annexin V can also stain cells undergoing necrosis due to a ruptured membrane that permits the access of Annexin V to the entire plasma membrane. Western blotting analysis of rfhSP-D-treated BT474 and SKBR3 breast cancer cells revealed cleavage of caspases 9 and 3 at 12-h treatment. Caspases are well-known cysteine-aspartic proteases that play a crucial role in apoptosis;

caspase 9 is triggered by cellular stress (e.g., DNA damage), via its binding to apoptotic protease-activating factor 1 (Apaf-1). Apaf-1/procaspase 9, in turn, triggers executioner caspases 3 and 7 (46). Caspase 3 is an essential apoptotic executor, triggered by endoproteolytic cleavage at Asp175, which leads to inactivation of PARP (a known marker of apoptosis) (45, 47). These findings indicated that rfhSP-D-mediated apoptosis induction in SKBR3 and BT474 cell lines is likely to occur via the intrinsic apoptotic pathway (48). Recently, an integral role of rfhSP-D in innate immune surveillance against prostate cancer has been reported. rfhSP-D-mediated apoptosis has been suggested to take place by two distinct mitochondrial apoptotic mechanisms (19). It is also possible that p53 upregulation in rfhSP-D-treated BT474 and SKBR3 cell lines may lead to downregulation of the pAkt pathway, resulting in increased levels of Bad and Bax, triggering the release of cytochrome c, caspase 9 cleavage, and apoptosis induction. Furthermore, previous studies have also reported the interaction of SP-D with HMGA1, CD14, CD91–calreticulin complex, SIRPα, and EGFR (19, 22, 23, 49). The involvement of SP-D with these key molecules is likely to be relevant as a part of a possible mechanism/receptor through which rfhSP-D is likely mediating its apoptotic functions on breast cancer cells. As reported in previous studies, the CRD of SP-D can interact with pattern recognition receptors TLR-2, TLR-4 (50), and CD14 (22), which may block pro-inflammatory and pro-survival downstream signaling on breast cancer cells. However, further investigation is crucial to understand the involvement of CRD and its possible interacting partners involved in triggering the downstream mechanism of apoptosis induction.

During the development of breast tumorigenesis, the tumor cells interact with surrounding stroma to create a tumor microenvironment, supporting the growth, survival, and invasion of cancer cells. The ECM is an essential constituent of the niche, leading to progression of malignant tumor formation and proliferation. ECM is composed of a wide range of proteoglycans and glycosaminoglycans, which offers a structural support and promotes tissue organization, thus contributing to cell survival, proliferation, invasion, angiogenesis, and immune cell infiltration (35, 51). HA is one of the specific components of ECM, which is synthesized as a large linear anionic polymer at the cell surface. The role of HA during inflammation-mediated breast cancer has been established (52, 53). *In vitro* studies have reported the ability of HA to regulate tumor cell migration and invasion and tumor growth and progression using *in vivo* models (39). Synthesis and accumulation of HA have been detected in invasive breast cancer cells compared to normal breast epithelial tissues (39). Additionally, HA synthase 2 facilitates invasion in breast cancer cells (51). Furthermore, tumor cells overexpressing HA synthase 2 have been shown to enhance angiogenesis and stromal cell recruitment, suggesting that increased levels of HA in the tumor stroma support breast carcinoma (51). Pro-tumorigenic roles of increased HA expression in breast tumors and possible mechanisms through which HA might trigger tumor proliferation are areas of great interest. Therefore, we examined the interaction between rfhSP-D and HA and its implication on the adhesion and proliferation of BT20, BT474, and SKBR3 breast cancer cells.

Direct binding ELISA revealed that rfhSP-D bound to HA in a dose-dependent manner. The ability of breast cancer cells to interact with HA-bound rfhSP-D was examined via a cell adhesion assay. Cell adhesion assay was performed to assess the effect of rfhSP-D or HA treatment on the ability of breast cancer cells to adhere. A greater cell adhesion binding pattern was observed with rfhSP-D alone, when compared to HA-bound rfhSP-D or HA alone. This may be due to the interaction of rfhSP-D-treated cells with apoptotic-related receptors and pathways leading to apoptosis induction. Apoptotic and proliferative assays were also performed to investigate the effect of HA-bound rfhSP-D in comparison to rfhSP-D alone. SKBR3 cells seeded on HA-bound rfhSP-D resulted in an increased cell proliferation (1.7-fold), when compared to rfhSP-D alone. In the case of rfhSP-D-treated BT474 cells, addition of HA resulted in a two-fold increase of proliferative cells. However, the percentage of proliferating cells in the presence of HA-bound rfhSP-D was not significantly different from that in HA alone or untreated SKBR3 and BT474 cells. Therefore, these findings suggest that pro-apoptotic effects of rfhSP-D are modulated by HA addition. However, there was no significant difference in the proliferation of BT20 cells among all the conditions, suggesting that these cells continue to grow and are not affected by rfhSP-D treatment alone or in conjunction with HA. It is also possible that addition of HA may modulate the interaction of rfhSP-D-treated cells with pro-apoptotic signaling pathways, thereby restricting the possibility of apoptosis induction. Thus, addition of HA could facilitate cell proliferation by interacting with proliferative signaling cascades (e.g., Ras-ERK and PI3K-Akt). Even though breast cancer tissues express SP-D (**Figures 4i**,**ii**), the presence of HA within the breast tumor microenvironment seems to provide a self-protective coat, thus negating the anti-tumorigenic properties of SP-D. Since BT474 and SKBR3 cells treated with rfhSP-D undergo apoptosis and addition of HA to rfhSP-D enhances cell proliferation, it is likely that breast cancer cells can use HA in their tumor microenvironment as an escape mechanism from apoptosis induction triggered by rfhSP-D.

To further understand the mechanism of apoptosis induction by rfhSP-D treatment, the likely signaling pathways involved in tumor adhesion, proliferation, and cell death were analyzed. rfhSP-D treatment resulted in increased levels of p53 phosphorylation (at Ser15), possibly mediated by oxidative stress caused by rfhSP-D (17, 49). p53 is an essential transcriptional modulator of apoptosis and plays a crucial role in cellular response to DNA damage as well as other genomic alterations. Phosphorylated p53 and increased levels of P21/P27 expression may cause inactivation of cyclin B–cdc2 complexes that are crucial in regulating G2/M cell cycle transition, causing DNA repair or induction of apoptosis (17). However, decreased levels of caspase 3 and p53 were detected in HA + rfhSP-D-treated cells, possibly suggesting its resistance to apoptosis by addition of HA. Although the p21 trigger is p53 dependent in certain events such as DNA damage, there are several scenarios in which p21 expression is independent of p53 status, such as normal tissue development and differentiation. p21 can lead to tumor evolution directed toward tumor growth by slowing down the accumulation of DNA damage. Induction of p21 expression has

been shown to be crucial for promoting motility of tumor cells and tumorigenesis. Due to controversial roles of p21, it can be considered as an oncogenic protein and/or tumor suppressor, depending on its cytoplasmic localization. The dual roles of p21 as an oncogenic or tumor suppressor make it difficult to study the mechanisms involved in p53–p21-mediated apoptosis induction or cancer progression.

Targeting HA synthesis, accumulation, degradation, or HA–receptor interaction represents a potential therapeutic approach for treatment of breast and other cancers. The use of 4-MU to inhibit HA synthesis has been shown to reduce breast cancer proliferation and migration (54–57). 4-MU treatment has also been shown to inhibit intracellular and cell surface HA (57), in addition to suppression of Akt phosphorylation. Use of hyaluronidases to degrade HA in the tumor microenvironment has also been considered as a potential therapeutic approach for cancer. Bacteriophage hyaluronidase has been shown to effectively inhibit growth, migration, and invasion of breast cancer cells (58). Hyaluronidase treatment has also shown promising outcomes in pancreatic cancer in clinical trials (59–61). Furthermore, recombinant human hyaluronidase (rHUPH20) has been shown to improve drug delivery of antibody-based trastuzumab targeted therapy in $HER2^{+}$ breast cancer (62). A recent study has shown that HA degradation by pegvorhyaluronidase (PVHA) can remodel the TME in a murine model of breast cancer so as to increase the uptake of anti-Programmed Death-Ligand 1 (PD-L1) therapeutic antibody. PVHA treatment coincided with a dramatic effectiveness of anti-PD-L1 antibody in reducing the tumor growth (63).

Involvement of rfhSP-D and its associated pro-apoptotic properties in cancer models might be a novel therapeutic agent to target multiple cellular signaling pathways, including tumor cell survival factors, transcriptional factors, protein kinases, and pro-apoptotic gene signatures. The mechanism which enables rfhSP-D to induce apoptosis and inhibit tumor cell proliferation is tumor specific due to the differential effects on the cell types and probably expression of putative receptors. The nature of interaction between HA + rfhSP-D and cellular receptors is currently under investigation. The function of SP-D in the biology of cancer is complex and is strongly dependent on the tumor microenvironment. As SP-D and HA are overexpressed in breast cancer and other carcinomas, targeting both HA and SP-D is clinically relevant to inhibit HA-mediated intracellular signaling that negates the pro-apoptotic role of rfhSP-D. It is important to note that FL-SP-D purified from BT474 was not able to induce apoptosis in any of the three breast cancer cell lines. The plausible reasons could be that the tumor cells produce a dysfunctional protein owing to mutations, protein misfolding, and/or altered oligomerization.

In conclusion, rfhSP-D treatment was able to induce apoptosis in BT474 and SKBR3 cell lines involving the intrinsic apoptotic pathway, while having no effect on the triple-negative BT20 cell line. In addition, HA-bound rfhSP-D was able to restore cell growth, suggesting that these breast cancer cells may use HA as an escape mechanism to overcome pro-apoptotic effects of rfhSP-D. The mechanisms by which HA-bound rfhSP-D restores cell proliferation are yet to be elucidated.

DATA AVAILABILITY STATEMENT

The raw data supporting the conclusions of this article will be made available by the authors, without undue reservation.

ETHICS STATEMENT

Surgical breast cancer tissues and adjacent peritumoral mammary parenchymas were selected following ethical approval by the University Hospital of Palermo, Italy (approval number 09/2018).

AUTHOR CONTRIBUTIONS

Data curation: CA, PV, and TM; formal analysis: HK, TM, and RB; investigation: SA and AK; methodology: VM, PV, BB, and TR; resources: SV; supervision: RB and UK; validation: FA; writing—original draft: VM; writing—review and editing: UK. All authors contributed to the article and approved the submitted version.

ACKNOWLEDGMENTS

The authors acknowledge the International Scientific Partnership Program (ISPP) at King Saud University, Riyadh for funding via ISPP-145 and the Institute for Maternal and Child Health, IRCCS Burlo Garofolo, Trieste, Italy, for funding via RC20/16 and 5MILLE15D to CA.

REFERENCES

1. Swann JB, Smyth MJ. Immune surveillance of tumors. *J Clin Invest.* (2007) 117:1137–46. doi: 10.1172/JCI31405
2. Kim R, Emi M, Tanabe K. Cancer immunoediting from immune surveillance to immune escape. *Immunology.* (2007) 121:1–14. doi: 10.1111/j.1365-2567.2007.02587.x
3. Vesely MD, Kershaw MH, Schreiber RD, Smyth MJ. Natural innate and adaptive immunity to cancer. *Annu Rev Immunol.* (2011) 29:235–71. doi: 10.1146/annurev-immunol-031210-101324
4. Palucka AK, Coussens LM. The basis of oncoimmunology. *Cell.* (2016) 164:1233–47. doi: 10.1016/j.cell.2016.01.049
5. Lu J, Teh C, Kishore U, Reid KBM. Collectins and ficolins: sugar pattern recognition molecules of the mammalian innate immune system. *Biochim Biophys Acta.* (2002) 1572:387–400. doi: 10.1016/S0304-4165(02)00320-3
6. Kishore U, Greenhough TJ, Waters P, Shrive AK, Ghai R, Kamran MF, et al. Surfactant proteins SP-A and SP-D: Structure, function and receptors. *Mol Immunol.* (2006) 43:1293–315. doi: 10.1016/j.molimm.2005.08.004
7. Nayak A, Dodagatta-Marri E, Tsolaki AG, Kishore U. An insight into the diverse roles of surfactant proteins, SP-A and SP-D in innate and adaptive immunity. *Front Immunol.* (2012) 3:131. doi: 10.3389/fimmu.2012.00131
8. Madsen J, Kliem A, Tornøe I, Skjødt K, Koch C, Holmskov U. Localization of lung surfactant protein D on mucosal surfaces in human tissues. *J Immunol.* (2000) 164:5866–70. doi: 10.4049/jimmunol.164.11.5866

9. Sotiriadis G, Dodagatta-Marri E, Kouser L, Alhamlan FS, Kishore U, Karteris E. Surfactant proteins SP-A and SP-D modulate uterine contractile events in ULTR myometrial cell line. *PLoS One.* (2015) 10:e0143379. doi: 10.1371/journal.pone.0143379
10. Christensen AF, Sorensen GL, Junker K, Revald PH, Varnum C, Sorensen FB, et al. Localization of surfactant protein-D in the rheumatoid synovial membrane. *Apmis.* (2018) 126:9–13. doi: 10.1111/apm.12785
11. Wright JR. Immunomodulatory functions of surfactant. *Physiol Rev.* (1997) 77:931–2. doi: 10.1152/physrev.1997.77.4.931
12. Madan T, Kishore U, Shah A, Eggleton P, Strong P, Wang JY, et al. Lung surfactant proteins A and D can inhibit specific IgE binding to the allergens of *Aspergillus fumigatus* and block allergen-induced histamine release from human basophils. *Clin Exp Immunol.* (2007) 110:241–9. doi: 10.1111/j.1365-2249.1997.tb08323.x
13. Wang JY, Kishore U, Lim BL, Strong P, Reid KBM. Interaction of human lung surfactant proteins A and D with mite (*Dermatophagoides pteronyssinus*) allergens. *Clin Exp Immunol.* (1996) 106:367–73. doi: 10.1046/j.1365-2249.1996.d01-838.x
14. Madan T, Kishore U, Singh M, Strong P, Clark H, Hussain EM, et al. Surfactant proteins A and D protect mice against pulmonary hypersensitivity induced by *Aspergillus fumigatus* antigens and allergens. *J Clin Invest.* (2001) 107:467–75. doi: 10.1172/JCI10124
15. Madan T, Reid KBM, Singh M, Sarma PU, Kishore U. Susceptibility of mice genetically deficient in the surfactant protein (SP)-A or SP-D gene to pulmonary hypersensitivity induced by antigens and allergens of *Aspergillus fumigatus*. *J Immunol.* (2005) 174:6943–54. doi: 10.4049/jimmunol.174.11.6943
16. Mahajan L, Madan T, Kamal N, Singh VK, Sim RB, Telang SD, et al. Recombinant surfactant protein-D selectively increases apoptosis in eosinophils of allergic asthmatics and enhances uptake of apoptotic eosinophils by macrophages. *Int Immunol.* (2008) 20:993–1007. doi: 10.1093/intimm/dxn058
17. Kaur A, Riaz MS, Murugaiah V, Varghese PM, Singh SK, Kishore U. A Recombinant fragment of human surfactant protein D induces apoptosis in pancreatic cancer cell lines via fas-mediated pathway. *Front Immunol.* (2018) 9:1126. doi: 10.3389/fimmu.2018.01126
18. Kumar J, Murugaiah V, Sotiriadis G, Kaur A, Jeyaneethi J, Sturniolo I, et al. Surfactant protein D as a potential biomarker and therapeutic target in ovarian cancer. *Front Oncol.* (2019) 9:542. doi: 10.3389/fonc.2019.00542
19. Thakur G, Prakash G, Murthy V, Sable N, Menon S, Alrokayan SH, et al. Human SP-D Acts as an innate immune surveillance molecule against androgen-responsive and androgen-resistant prostate cancer cells. *Front Oncol.* (2019) 9:565. doi: 10.3389/fonc.2019.00565
20. Mangogna A, Belmonte B, Agostinis C, Ricci G, Gulino A, Ferrara I, et al. Pathological significance and prognostic value of surfactant protein D in cancer. *Front Immunol.* (2018) 9:1748. doi: 10.3389/fimmu.2018.01748
21. Mahajan L, Gautam P, Dodagatta-Marri E, Madan T, Kishore U. Surfactant protein SP-D modulates activity of immune cells: proteomic profiling of its interaction with eosinophilic cells. *Expert Rev Proteomics.* (2014) 11:355–69. doi: 10.1586/14789450.2014.897612
22. Mahajan L, Pandit H, Madan T, Gautam P, Yadav AK, Warke H, et al. Human surfactant protein D alters oxidative stress and HMGA1 expression to induce p53 apoptotic pathway in eosinophil leukemic cell line. *PLoS One.* (2013) 8:e85046. doi: 10.1371/journal.pone.0085046
23. Hasegawa Y, Takahashi M, Ariki S, Asakawa D, Tajiri M, Wada Y, et al. Surfactant protein D suppresses lung cancer progression by downregulation of epidermal growth factor signaling. *Oncogene.* (2015) 34:838–45. doi: 10.1038/onc.2014.20
24. Kaur A, Riaz MS, Singh SK, Kishore U. Human surfactant protein D suppresses epithelial-to-mesenchymal transition in pancreatic cancer cells by downregulating TGF-β. *Front Immunol.* (2018) 9:1844. doi: 10.3389/fimmu.2018.01844
25. Ferlay J, Shin HR, Bray F, Forman D, Mathers C, Parkin DM. Estimates of worldwide burden of cancer in 2008: GLOBOCAN 2008. *Int J Cancer.* (2010) 127:2893–917. doi: 10.1002/ijc.25516
26. Coleman RE, Collinson M, Gregory W, Marshall H, Bell R, Dodwell D, et al. Benefits and risks of adjuvant treatment with zoledronic acid in stage II/III breast cancer. 10 years follow-up of the AZURE randomized clinical trial (BIG 01/04). *J Bone Oncol.* (2018) 13:123–35. doi: 10.1016/j.jbo.2018.09.008
27. Sun YS, Zhao Z, Yang ZN, Xu F, Lu HJ, Zhu ZY, et al. Risk factors and preventions of breast cancer. *Int J Biol Sci.* (2017) 13:1387–97. doi: 10.7150/ijbs.21635
28. Azamjah N, Soltan-Zadeh Y, Zayeri F. Global trend of breast cancer mortality rate: a 25-year study. *Asian Pacific J Cancer Prev.* (2019) 20:2015–20. doi: 10.31557/APJCP.2019.20.7.2015
29. Baxter E, Windloch K, Gannon F, Lee JS. Epigenetic regulation in cancer progression. *Cell Biosci.* (2014) 4:45. doi: 10.1186/2045-3701-4-45
30. Bates JP, Derakhshandeh R, Jones L, Webb TJ. Mechanisms of immune evasion in breast cancer. *BMC Cancer.* (2018) 18:556. doi: 10.1186/s12885-018-4441-3
31. Fragomeni SM, Sciallis A, Jeruss JS. Molecular subtypes and local-regional control of breast cancer. *Surg Oncol Clin N Am.* (2018) 27:95–120. doi: 10.1016/j.soc.2017.08.005
32. Dai X, Li T, Bai Z, Yang Y, Liu X, Zhan J, et al. Breast cancer intrinsic subtype classification, clinical use and future trends. *Am J Cancer Res.* (2015) 5:2929–43.
33. Ben-Baruch A. Host microenvironment in breast cancer development. Inflammatory cells, cytokines and chemokines in breast cancer progression: Reciprocal tumor-microenvironment interactions. *Breast Cancer Res.* (2003) 5:31–6. doi: 10.1186/bcr554
34. Goldberg JE, Schwertfeger KL. Proinflammatory cytokines in breast cancer: mechanisms of action and potential targets for therapeutics. *Curr Drug Targets.* (2010) 11:1133–46. doi: 10.2174/138945010792006799
35. Heldin P, Basu K, Olofsson B, Porsch H, Kozlova I, Kahata K. Deregulation of hyaluronan synthesis, degradation and binding promotes breast cancer. *J Biochem.* (2013) 154:395–408. doi: 10.1093/jb/mvt085
36. Corte MD, González LO, Junquera S, Bongera M, Allende MT, Vizoso FJ. Analysis of the expression of hyaluronan in intraductal and invasive carcinomas of the breast. *J Cancer Res Clin Oncol.* (2010) 136:745–50. doi: 10.1007/s00432-009-0713-2
37. Tolg C, McCarthy JB, Yazdani A, Turley EA. Hyaluronan and RHAMM in wound repair and the "cancerization" of stromal tissues. *Biomed Res Int.* (2014) 2014:103923. doi: 10.1155/2014/103923
38. Bourguignon LYW, Wong G, Earle C, Krueger K, Spevak CC. Hyaluronan-CD44 interaction promotes c-Src-mediated twist signaling, microRNA-10b expression, and RhoA/RhoC up-regulation, leading to Rho-kinase-associated cytoskeleton activation and breast tumor cell invasion. *J Biol Chem.* (2010) 285:36721–35. doi: 10.1074/jbc.M110.162305
39. Li Y, Li L, Brown TJ, Heldin P. Silencing of hyaluronan synthase 2 suppresses the malignant phenotype of invasive breast cancer cells. *Int J Cancer.* (2007) 120:2557–67. doi: 10.1002/ijc.22550
40. McCurdy RD, McGrath JJ, Mackay-Sim A. Validation of the comparative quantification method of real-time PCR analysis and a cautionary tale of housekeeping gene selection. *Gene Ther Mol Biol.* (2008) 12:15–24. Available online at: https://research-repository.griffith.edu.au/handle/10072/25877
41. Antonsson A, Persson JL. Induction of apoptosis by staurosporine involves the inhibition of expression of the major cell cycle proteins at the G2/M checkpoint accompanied by alterations in Erk and Akt kinase activities. *Anticancer Res.* (2009) 29:2893–8.
42. Zugibe FT. *Diagnostic Histochemistry*. *Mosby* St. Louis, MO (1970).
43. Pearse AGE, Stoward PJ. *Histochemistry, Theoretical and Applied, Histochemistry, Theoretical and Applied.* London: Churchill Livingstone (1980).
44. Lillie RD, Conn HJ, Commission BS, Stotz EH, Emmel VM. *H. J. Conn's Biological Stains: A Handbook on the Nature and Uses of the Dyes Employed in the Biological Laboratory.* Edinburg: Williams & Wilkins (1977).
45. Porter AG, Jänicke RU. Emerging roles of caspase-3 in apoptosis. *Cell Death Differ.* (1999) 6:99–104. doi: 10.1038/sj.cdd.4400476
46. Li P, Zhou L, Zhao T, Liu X, Zhang P, Liu Y, et al. Caspase-9: structure, mechanisms and clinical application. *Oncotarget.* (2017) 8:23996–4008. doi: 10.18632/oncotarget.15098
47. Walsh JG, Cullen SP, Sheridan C, Lüthi AU, Gerner C, Martin SJ. Executioner caspase-3 and caspase-7 are functionally distinct proteases. *Proc Natl Acad Sci U S A.* (2008) 105:12815–9. doi: 10.1073/pnas.0707715105

48. Elmore S. Apoptosis: a review of programmed cell death. *Toxicol Pathol.* (2007) 35:495–516. doi: 10.1080/01926230701320337
49. Janssen WJ, McPhillips KA, Dickinson MG, Linderman DJ, Morimoto K, Xiao YQ, et al. Surfactant proteins A and D suppress alveolar macrophage phagocytosis via interaction with SIRP alpha. *Am J Respir Crit Care Med.* (2008) 178:158–67. doi: 10.1164/rccm.200711-1661OC
50. Ohya M, Nishitani C, Sano H, Yamada C, Mitsuzawa H, Shimizu T, et al. Human pulmonary surfactant protein D binds the extracellular domains of Toll-like receptors 2 and 4 through the carbohydrate recognition domain by a mechanism different from its binding to phosphatidylinositol and lipopolysaccharide. *Biochemistry.* (2006) 45:8657–64. doi: 10.1021/bi060176z
51. Bernert B, Porsch H, Heldin P. Hyaluronan synthase 2 (HAS2) promotes breast cancer cell invasion by suppression of tissue metalloproteinase inhibitor 1 (TIMP-1). *J Biol Chem.* (2011) 286:42349–59. doi: 10.1074/jbc.M111.278598
52. Soria G, Ben-Baruch A. The inflammatory chemokines CCL2 and CCL5 in breast cancer. *Cancer Lett.* (2008) 267:271–85. doi: 10.1016/j.canlet.2008.03.018
53. Ponting J, Howell A, Pye D, Kumar S. Prognostic relevance of serum hyaluronan levels in patients with breast cancer. *Int. J. Cancer.* (1992) 52:873–6. doi: 10.1002/ijc.2910520607
54. Bohrer LR, Chuntova P, Bade LK, Beadnell TC, Leon RP, Brady NJ, et al. Activation of the FGFR-STAT3 pathway in breast cancer cells induces a hyaluronan-rich microenvironment that licenses tumor formation. *Cancer Res.* (2014) 74:374–86. doi: 10.1158/0008-5472.CAN-13-2469
55. Nagy N, Kuipers HF, Frymoyer AR, Ishak HD, Bollyky JB, Wight TN, Bollyky PL. 4-Methylumbelliferone treatment and hyaluronan inhibition as a therapeutic strategy in inflammation, autoimmunity, and cancer. *Front Immunol.* (2015) 6:123. doi: 10.3389/fimmu.2015.00123
56. Saito T, Tamura D, Nakamura T, Makita Y, Ariyama H, Komiyama K, Oshihara T, Asano R. 4-Methylumbelliferone leads to growth arrest and apoptosis in canine mammary tumor cells. *Oncol Rep.* (2013) 29:335–42. doi: 10.3892/or.2012.2100
57. Urakawa H, Nishida Y, Wasa J, Arai E, Zhuo L, Kimata K, et al. Inhibition of hyaluronan synthesis in breast cancer cells by 4-methylumbelliferone suppresses tumorigenicity *in vitro* and metastatic lesions of bone *in vivo*. *Int J Cancer.* (2012) 130:454–66. doi: 10.1002/ijc.26014
58. Lee JH, Moore LD, Kumar S, Pritchard DG, Ponnazhagan S, Deivanayagam C. Bacteriophage hyaluronidase effectively inhibits growth, migration and invasion by disrupting hyaluronan-mediated Erk1/2 activation and RhoA expression in human breast carcinoma cells. *Cancer Lett.* (2010) 298:238–49. doi: 10.1016/j.canlet.2010.07.011
59. Whatcott CJ, Han H, Posner RG, Hostetter G, Von Hoff DD. Targeting the tumor microenvironment in cancer: why hyaluronidase deserves a second look. *Cancer Discov.* (2011) 1:291–6. doi: 10.1158/2159-8290.CD-11-0136
60. Provenzano PP, Cuevas C, Chang AE, Goel VK, Von Hoff DD, Hingorani SR. Enzymatic targeting of the stroma ablates physical barriers to treatment of pancreatic ductal adenocarcinoma. *Cancer Cell.* (2012) 21:418–29. doi: 10.1016/j.ccr.2012.01.007
61. Jacobetz MA, Chan DS, Neesse A, Bapiro TE, Cook N, Frese KK, et al. Hyaluronan impairs vascular function and drug delivery in a mouse model of pancreatic cancer. *Gut.* (2013) 62:112–20. doi: 10.1136/gutjnl-2012-302529
62. Shpilberg O, Jackisch C. Subcutaneous administration of rituximab (MabThera) and trastuzumab (Herceptin) using hyaluronidase. *Br J Cancer.* (2013) 109:1556–61. doi: 10.1038/bjc.2013.371
63. Clift R, Souratha J, Garrovillo SA, Zimmerman S, Blouw B. Remodeling the tumor microenvironment sensitizes breast tumors to anti-programmed death-ligand 1 immunotherapy. *Cancer Res.* (2019) 79:4149–59. doi: 10.1158/0008-5472.CAN-18-3060

Conflict of Interest: The authors declare that the research was conducted in the absence of any commercial or financial relationships that could be construed as a potential conflict of interest.

frontiers in Immunology

ORIGINAL RESEARCH
published: 08 January 2021
doi: 10.3389/fimmu.2020.585361

C4b Binding Protein Acts as an Innate Immune Effector Against Influenza A Virus

*Praveen M. Varghese[1,2], Valarmathy Murugaiah[1], Nazar Beirag[1], Nigel Temperton[3], Haseeb A. Khan[4], Salman H. Alrokayan[4], Mohammed N. Al-Ahdal[5], Beatrice Nal[1], Futwan A. Al-Mohanna[6], Robert B. Sim[7] and Uday Kishore[1]**

[1] Biosciences, College of Health and Life Sciences, Brunel University London, Uxbridge, United Kingdom, [2] School of Biosciences and Technology, Vellore Institute of Technology, Vellore, India, [3] Viral Pseudotype Unit, Medway School of Pharmacy, University of Kent and Greenwich, Kent, United Kingdom, [4] Department of Biochemistry, College of Science, King Saud University, Riyadh, Saudi Arabia, [5] Department of Cell Biology, King Faisal Specialist Hospital and Research Centre, Riyadh, Saudi Arabia, [6] Department of Infection and Immunity, King Faisal Specialist Hospital and Research Center, Riyadh, Saudi Arabia, [7] Department of Biochemistry, University of Oxford, Oxford, United Kingdom

OPEN ACCESS

Edited by:
Cordula M. Stover,
University of Leicester,
United Kingdom

Reviewed by:
Kenneth Reid,
University of Oxford, United Kingdom
Jean van den Elsen,
University of Bath, United Kingdom

***Correspondence:**
Uday Kishore
uday.kishore.brunel.ac.uk;
ukishore@hotmail.com

Specialty section:
This article was submitted to Molecular Innate Immunity, a section of the journal Frontiers in Immunology

Received: 20 July 2020
Accepted: 20 November 2020
Published: 08 January 2021

Citation:
Varghese PM, Murugaiah V, Beirag N, Temperton N, Khan HA, Alrokayan SH, Al-Ahdal MN, Nal B, Al-Mohanna FA, Sim RB and Kishore U (2021) C4b Binding Protein Acts as an Innate Immune Effector Against Influenza A Virus. Front. Immunol. 11:585361. doi: 10.3389/fimmu.2020.585361

C4b Binding Protein (C4BP) is a major fluid phase inhibitor of the classical and lectin pathways of the complement system. Complement inhibition is achieved by binding to and restricting the role of activated complement component C4b. C4BP functions as a co-factor for factor I in proteolytic inactivation of both soluble and cell surface-bound C4b, thus restricting the formation of the C3-convertase, C4b2a. C4BP also accelerates the natural decay/dissociation of the C3 convertase. This makes C4BP a prime target for exploitation by pathogens to escape complement attack, as seen in Streptococcus *pyogenes* or Flavivirus. Here, we examined whether C4BP can act on its own in a complement independent manner, against pathogens. C4BP bound H1N1 and H3N2 subtypes of Influenza A Virus (IAV) most likely *via* multiple sites in Complement Control Protein (CCP) 1-2, 4-5, and 7-8 domains of its α-chain. In addition, C4BP CCP1-2 bound H3N2 better than H1N1. C4BP bound three IAV envelope proteins: Haemagglutinin (~70 kDa), Neuraminidase (~55 kDa), and Matrix protein 1 (~25kDa). C4BP suppressed H1N1 subtype infection into the lung epithelial cell line, A549, while it promoted infection by H3N2 subtype. C4BP restricted viral entry for H1N1 but had the opposite effect on H3N2, as evident from experiments using pseudo-typed viral particles. C4BP downregulated mRNA levels of pro-inflammatory IFN-α, IL-12, and NFκB in the case of H1N1, while it promoted a pro-inflammatory immune response by upregulating IFN- α, TNF-α, RANTES, and IL-6 in the case of H3N2. We conclude that C4BP differentially modulates the efficacy of IAV entry, and hence, replication in a target cell in a strain-dependent manner, and acts as an entry inhibitor for H1N1. Thus, CCP containing complement proteins such as factor H and C4BP may have additional defense roles against IAV that do not rely on the regulation of complement activation.

Keywords: complement, C4BP, influenza A virus, inflammation, pseudo-typed lentiviral particles

INTRODUCTION

The complement system plays a crucial role in our early response against invading pathogens, including viruses. The complement system is activated *via* three pathways—Classical, Alternative, and Lectin. The classical pathway is activated through the binding of C1q to IgG or IgM-containing immune complexes or other non-immunoglobulin targets. Non-self-carbohydrate targets are recognized by Mannose Binding Lectin (MBL) or ficolins triggering the lectin pathway. The activation of classical or lectin pathways leads to the cleavage of C4 and C2, yielding C3 convertase (C4b2a), which then cleaves C3 to form C3b. For the alternative pathway, C3 is spontaneously hydrolyzed to a C3b-like form [C3(H_2O)] due to the hydrolysis of the internal thioester bond. The C3(H_2O) binds to Factor B, which enables Factor D to cleave Factor B to Bb. This then forms C3(H_2O)Bb, which is homologous to the C3 convertase, C4b2a. C3(H_2O)Bb then cleaves C3 to C3b, and C3b can bind covalently to target surfaces, on which it forms more convertase, C3bBb. The binding of the C3b to C4b2a or C3bBb converts them into classical or alternative pathway C5 Convertases, respectively. The subsequent cleavage of C5 by the C5 convertases initiates the formation of the Membrane Attack Complex (C5b-C9). This complex binds to the microbial surface and can cause lysis of lipid bilayer membranes (1).

The complement system is kept in check by various regulatory proteins to prevent runaway reactions leading to unnecessary inflammation and death of healthy cells. One such humoral regulator is C4b Binding Protein (C4BP). C4BP, like other complement regulators Factor H, CR1, CD46, CD55, and the Factor H-related family, is encoded by a gene present in the long arm of chromosome 1 and is synthesized and secreted mainly by hepatocytes (2). The normal range of C4BP in human plasma is estimated to be approximately 150–300 μg/ml (3). C4BP regulates complement activation by controlling C4b mediated reactions (4). C4BP, a 570 kDa glycoprotein, functions as a primary fluid phase regulator of the classical and lectin pathways (5). It consists of seven identical 70 kDa α-chains and a 45 kDa β-chain that are linked at their carboxy-terminal ends by short amphipathic helices further stabilized by disulfide bonds (6). The α- chains and β-chain contain eight and three Complement Control Protein (CCP) domains, each of ~60 amino acids, respectively. The polymerization of the polypeptide chains of C4BP occurs *via* a short C-terminal region, downstream of CCP8 (7). Each molecule of C4BP can bind only four molecules of C4b due to steric hindrance, although each of the seven α- chains has a C4b binding site (8). The binding site for C4b has been localized to CCP1-3, especially within a cluster of positively charged residues at the interface of CCP1 and CCP2 (9, 10). C4BP has been shown to inhibit the formation of C3 and C5 convertases, accelerate the decay of the convertases, and act as a co-factor for Factor I which cleaves and thereby inactivates fluid phase and cell-bound C4b (9–12). The co-factor activity of the protein has been linked to CCP1-4 (13).

Consistent with its role as an immunomodulator, C4BP also engages with pathogens. Flaviviruses limit complement activation by binding C4BP through their NS1 protein: the bound C4BP inactivates soluble or membrane-bound C4b (5). *Streptococcus pyogenes* uses its Protein H to recruit C4BP in order to facilitate the invasion of endothelial cells and reduce the chances of its opsonization by bound C3b, or attack by the MAC (14). C4BP probably is also recruited by other pathogens to limit C3 opsonization, MAC mediated lysis, and immune system activation by C3a/C5a (15).

C4BP has been reported to have properties that are independent of its involvement in complement regulation. For example, C4BP is known to facilitate the uptake of adenoviruses by hepatocytes *via* its interaction with heparin-sulfate proteoglycans found on cell surfaces (16). C4BP induces proliferation and activation of B lymphocytes by binding with CD40 (17). Interaction between CD40, CD154, and C4BP inhibits apoptosis in epithelial cells. C4BP has also been implicated in inhibiting DNA release from necrotic cells in conjunction with Protein S by binding to phosphatidylserine (18–20). C4BP also have an association with the clotting system as the β-chain binds the vitamin K-dependent anticoagulant protein S (21).

In this study, we investigated potential complement-independent defense functions of C4BP against Influenza A Virus (IAV). Influenza virus causes an upper respiratory tract infection affecting the nose, throat, bronchi, and sometimes the lungs. Of the three genera of Influenza virus that belong to the Orthomyxoviridae family, IAV is known to cause pandemics. IAV causes Influenza in birds and a few species of mammals, including humans and pigs. Its wide host range has led to pandemics such as the 1918 Spanish flu, which caused 20–50 million deaths (22). It has several subtypes based on variants of two proteins on the surface of the viral envelope. These proteins are Hemagglutinin (HA), which causes RBCs to agglutinate, and Neuraminidase (NA), which breaks the glycoside bonds of neuraminic acid (23). Currently, there are 18 known variations of HA, and 11 known variations of NA, theoretically allowing 198 different combinations (24, 25). Some of the well-known combinations are H1N1 that caused the 1918 Spanish flu, 1977 Russian flu, and 2009 flu Pandemic, H3N2 that caused the 1968 Hong Kong flu and H2N2 that caused 1957 Asian flu (26).

Human infection by IAV is achieved through oral or nasal cavities, where the viral HA binds sialic acids in order to attach to lung epithelial cells (27). The HA protein of the human-infecting IAV has increased specificity for α-2,6-linked sialic acid (28). Sialic acid, a nine-carbon acidic monosaccharide, is commonly found with α-2,6-linkages and a few α-2,3-linkages on human tracheal epithelial cells (29). Once bound to the cell surface, the viral particle undergoes receptor-mediated endocytosis. We show here that IAV interacts with the α chain of C4BP mainly *via* CCP domains 4–5, CCP domains 7–8, and to a lesser extent CCP domains 1–2. C4BP acts as an entry inhibitor for H1N1 subtype when challenged against A549 (lung epithelial) cells and suppresses the pro-inflammatory cytokine storm induced by IAV.

MATERIALS AND METHODS

Purification of Native C4BP

C4BP was isolated from human plasma as described previously (30). Briefly, C4BP was purified from neutral euglobulin

precipitate by affinity chromatography using C4c-Sepharose, equilibrated in 5 mM EDTA/25 mM potassium phosphate buffer, pH 7.0. The column was washed in the same buffer and then bound protein was eluted by a linear gradient of NaCl from 0 to 2 M; C4BP was eluted at 0.8 M NaCl. The peak fractions were run on 12% w/v acrylamide SDS-PAGE to assess purity and adjusted to 1 mg/ml concentration. The immunoreactivity of this plasma purified C4BP was assessed *via* western blotting.

Expression and Purification of Recombinant Complement Control Protein Deletants of C4BP α-Chain

Recombinant α-chain of C4BP (rC4BP) and C4BP α-chain CCP deletants (**Table 1**) were provided by Prof. Anna Blom, Lund University, Malmo, Sweden. Briefly, CCP deletant constructs were expressed in Human Embryonic Kidney (HEK) 293 cells (ATCC number 1573-CRL). The transfected cells were selected using neomycin analogue G418 (400 μg/ml), and colonies expressing the highest amount of CCP deletants were assessed by immunoblotting. The medium collected from transfected cells was subjected to the purification of CCP deletants using mAb 104 affinity columns (directed against CCP1) or mAb 67 (directed against CCP4) coupled to Affi-Gel 10 (2.6 × 12 cm column; Bio-Rad) (10). The recombinant CCP deletants were eluted using 3M guanidinium chloride, and the purified fractions were subjected to SDS-PAGE with 12% w/v acrylamide/bisacrylamide (10).

Preparation of Viral Stocks and Titration

A/England/2009 (H1N1) was a gift from Wendy Barclay, Department of Infectious Disease, Imperial College London, and the A/HK/99 (H3N2) was a gift from Leo Poon, Division of Public Health Laboratory Sciences, University of Hong Kong. Madin Darby Canine Kidney (MDCK) (ATCC® CCL-34™) cells, grown to 70% confluence in a 175 cm^2 flask (Fisher Scientific) in growth medium (DMEMF/12 with GlutaMAX™ Supplement (Gibco), + 10% v/v Heat Inactivated Fetal Bovine Serum (FBS) (Gibco) + 1% v/v Penicillin-Streptomycin (PS) (Gibco) at 37°C under 5% v/v CO_2, were washed with PBS twice to remove any residual serum-complemented DMEM media. H1N1 and H3N2 IAV subtypes were added to the MDCK cells diluted in serum-free DMEM (Gibco) and allowed to incubate for 1 h at 37°C. The medium was removed, and cells were washed with Phosphate-buffered saline (PBS) (0.01M sodium phosphate, 0.0027M KCl, and 0.137M NaCl, pH 7.4 at 25°C) (Fisher Bioreagents) to remove any unbound viruses. The cells were then incubated for 3 days at 37°C in the infection medium [DMEM + 1% penicillin/streptomycin + 0.3% w/v bovine serum albumin (BSA) + 1 μg/ml of l-1-Tosylamide-2-phenylethyl chloromethyl ketone (TPCK)-Trypsin] (Sigma-Aldrich)]. TPCK treated Trypsin mediates the cleavage of HA0 into two subunits HA1 and HA2, which are required to make HA fusion competent. After the incubation, the medium was collected and centrifuged in sealed containers at 3,000 × g at 4°C for 15 min. The supernatant containing the viral particles was harvested, and the titer of the particles was determined *via* 50% Tissue culture Infective Dose ($TCID_{50}$) Assay. Purified virus stocks were serially diluted in a 96-well plate up to 10^{-7}-fold with ½ $\log_{10}$ increments. 1×10^5 MDCK cells were added to each well and incubated for 3 days at 37°C under 5% v/v CO_2. Uninfected MDCK cells were used as negative control. The titter of the virus was determined to be 1×10^6 PFU/ml by TCID50 using the Reed–Muench method (31).

TABLE 1 | C4BP deletants used in this study.

Mutants	Deleted regions within the α-chain of C4BP
ΔCCP1	Asn^1–Tyr^{62}
ΔCCP2	Lys^{63}–Ile^{124}
ΔCCP3	Val^{125}–Lys^{188}
ΔCCP4	Lys^{188}–Asn^{249}
ΔCCP5	Asn^{249}–Ala^{314}
ΔCCP6	Leu^{315}–Gly^{375}
ΔCCP7	Asp^{376}–Lys^{433}
ΔCCP8	Cys^{436}–Trp^{492}

Production of Pseudo-Typed Lentiviral Particles

Pseudo-typed Lentiviral Particles were produced as previously described by Murugaiah et al., 2020 (32). Briefly, HEK 293T cells were cultured in RPMI 1640 (Gibco), supplemented with 10% v/v heat inactivated Fetal Bovine Serum (FBS) (Gibco), 1% v/v Penicillin-Streptomycin (Gibco) at 37°C under 5% v/v CO_2. Cells were co-transfected using 20 μg of the Envelope Protein-Coding plasmids that yield the viral envelope proteins [H1 and N1 or H3 and N2 or Vesicular Stomatitis Virus G protein (VSV-G)], an HIV-backbone containing a modified pro-viral HIV-1 genome with the *env* deleted and designed to express the firefly luciferase reporter and second or third-generation lentiviral vector packaging plasmid (**Table 2**). The culture supernatant was collected after 48 h (by centrifugation at 1,500 × g for 5 min).

TABLE 2 | Plasmids used for pseudo-typed lentivirus particle production.

	H1N1	H3N2	VSV-G
Envelope Protein-Coding Plasmid	pcDNA3.1-swineH1-flag (H1 from swine H1N1 A/California/04/09) (Codon optimized H1 (Genecust))	pcDNA-H3 [H3 from A/Denmark/70/03/(H3N2)] (Codon optimized H3 (Geneart))	pCMV-VSV-G (Addgene plasmid # 8454)
	pcDNA3.1-swine N1-flag (N1 from swine H1N1 A/California/04/09) (Codon optimized N1 (Genecust))	pI.18-N2 (N2 from human H3N2 A/Texas/50/2012)	
Backbone Plasmid	pHIV-Luciferase (Addgene plasmid # 21375)		
Packaging Plasmid	psPAX2 (Addgene plasmid # 12260)		

The transfected cells in the pellet were lysed using lysis buffer (50 mM Tris–HCl pH 7.5, 200 mM NaCl, 5 mM EDTA, 0.1% v/v Triton X-100) and were centrifuged at 1,500 × g for 5 min to remove cell debris. The total lysate and supernatant were filtered with a 22 μm filter. The pseudo-typed lentiviral particles were harvested by centrifuging the filtered cell lysate and the supernatant at 5,000 × g for 10 min at 4°C in a closed container. The lentiviral particles in the supernatant were then concentrated by ultracentrifugation at 25,000 × g for 3 h at 4°C (33). The pseudo-typed lentiviral particles produced were characterized by western blotting (32).

ELISA to Detect C4BP-Virus Interaction

Microtiter wells of 96-well plates (Nunc # 4912) were coated (4°C, overnight) with the virus [100 μl of H1N1 or H3N2 subtypes (1,000 PFU/ml)] in carbonate-bicarbonate buffer, pH 9.6 (Sigma # c3041). Other wells were coated with 100 μl/well of C4BP, α-chain CCP mutants, at 5, 2.5, 1.25 μg/ml in the same buffer. In another experiment, 5 μg/ml of rC4BP was similarly coated. Unbound proteins or viruses were removed by washing the wells three times with PBST Buffer (PBS + 0.05% Tween 20) (Fisher Scientific). The wells were then blocked using 2% w/v BSA in PBS (Fisher Scientific) for 2 h at 37°C and washed three times using PBST. Decreasing concentrations of C4BP (5, 2.5, 1.25 μg/ml) were added to the wells in which the virus was coated to study its binding to immobilized viral particles. In parallel experiments, 1,000 PFU/ml of purified H1N1 and H3N2 were added to the protein-coated wells to study the binding of the virus to immobilized C4BP or rC4BP. The wells were incubated for 2 h at 37°C and then washed with PBST to remove any unbound viruses or protein. VSV-G pseudo-typed lentivirus was used as a negative control. The wells were probed using polyclonal rabbit anti-human C4BP (1 mg/ml of purified IgG; MRC Immunochemistry Unit, Oxford) to detect the virus-bound C4BP. Monoclonal Anti-Influenza Virus H1 HA, A/California/04/2009 (H1N1)pdm09, Clone 5C12 (produced *in vitro*) (BEI-Resources, NIAID, NIH, USA), Polyclonal Anti-Influenza Virus H3 HA, A/Hong Kong/1/1968 (H3N2) (antiserum, Goat, NR-3118) (BEI-Resources, NIAID, NIH, USA), and polyclonal anti-VSV-G (1 mg/ml of purified IgG; Imperial College London) were used to detect H1N1, H3N2 and pseudo-typed lentivirus particles, respectively that were bound to the immobilized C4BP. All antibodies were used at a dilution of 1:5,000 for 1 h at 37°C. Unbound antibodies were removed by washing three times using PBST. Anti-mouse IgG-Horseradish peroxidase (HRP) (Promega, #W4021), goat anti-rabbit IgG HRP (1:1,000; Promega # W4011), or Protein A-HRP (Invitrogen) were used as appropriate at 1:5,000 dilution as secondary antibodies (1 h at 37°C). 3,3′,5,5′-Tetramethylbenzidine (TMB) substrate set (Biolegend) was used as per the manufacturer's instruction, and 1 M sulfuric acid (Fisher Chemical) was used to stop the reaction. The plate was read at 450 nm using an iMark™ microplate absorbance reader (BioRad).

Western Blot

H1N1 and H3N2 (7.5×10^5 PFU/ml), treated with NuPAGE LDS Sample Buffer (4X) (Invitrogen™) were subjected to 12% w/v reducing SDS-PAGE (120 min, 90 V). The proteins were then transferred to Polyvinylidene fluoride (PVDF) membranes (Millipore) by electroblotting (320 mA for 2 h) at 4°C. The membrane was then blocked using 5% w/v skimmed milk in PBS for 16 h at 4°C.

For far-western blot, the membrane was washed with PBS and incubated with 5 μg/ml of C4BP for 1 h at room temperature and another 1 h at 4°C on a rotary shaker. After washing with PBST, the PVDF membrane was probed using rabbit polyclonal anti-human C4BP antibody (1mg/ml) (1:1,000; MRC Immunochemistry Unit, Oxford) for 1 h at room temperature on a rotary shaker. Following three washes with PBST, the membrane was probed again with goat anti-rabbit IgG HRP conjugate (1:1,000; Promega #W4011) for 1 h; the blot was developed using 3,3′-diaminobenzidine (DAB) (Sigma) as a substrate.

For direct western blot for viral proteins, the PVDF membrane, containing electro-transferred viral proteins, was incubated with appropriate antibodies: these included monoclonal anti-IAV H1, polyclonal anti-IAV H3, Monoclonal anti-IAV Neuraminidase (NA), Clone NA2-1C1 (produced *in vitro*) (BEI-Resources, NIAID, NIH, USA), Polyclonal Anti-Influenza Virus N2 Neuraminidase (NA), A/shorebird/Delaware/127/1997 (H6N2) (antiserum, Goat) (BEI-Resources, NIAID, NIH, USA), Monoclonal Anti-Influenza A Virus Non-structural Protein 1 (NS1), Clone NS1-1A7 (produced *in vitro*) (BEI-Resources, NIAID, NIH, USA), or Monoclonal anti-Matrix protein 1 (M1) antibody (Abcam) as required for 1 h at room temperature on a rotary shaker. Following three washes with PBST, the membrane was probed with either anti-mouse HRP or Protein A-HRP conjugate, as appropriate for 1 h at room temperature on a rotary shaker. Following three washes with PBST, the blot was developed using DAB.

A549 Cell Infection Assay

Human alveolar basal epithelial cells derived from an adenocarcinoma (A549) (ATCC® CCL-185™) (5×10^5) were cultured for 12 h in each well of a 12-well plate in growth medium. Post-attachment, the cells were serum starved by incubating them in serum-free DMEM for 24 h. H1N1 and H3N2 subtypes (MOI 1) were incubated with C4BP (10, 20, or 40 μg/ml) in PBS for 1 h and added to A549 cells in serum-free DMEM. After 1 h incubation at 37°C, the medium was removed, and cells were washed with PBS to remove any unbound IAV. Infection medium (DMEM + 1% v/v Penicillin-Streptomycin + 0.3% w/v BSA + 1 μg/ml of TPCK-Trypsin) was added to the cells and incubated for 2 or 6 h. The cells were then harvested by scraping with a sterile disposable cell scraper and centrifuging at 1,500 × g for 5 min. Total RNA was extracted using the GenElute™ Mammalian Total RNA Miniprep Kit (Sigma). Contaminating DNA was removed by treating the RNA samples with DNase I (Sigma) for 15 min. DNase I was inactivated by heating at 70°C for 10 min. The quantity and quality of the extracted RNA were assessed using a Nanodrop 2000 spectrophotometer (Thermo Fisher) *via* absorbance at 260 nm and 260:280 nm ratio. mRNA was converted to cDNA using TaqMan™ High Capacity RNA to cDNA Kit (Applied Biosystems™). The cDNA

was stored at −20°C for future use. qRT-PCR was performed using a StepOnePlus System (Applied Biosystems™) at 95°C for 5 min, followed by 45 cycles of 95°C for 10 s, 60°C for 10 s, and 72°C for 10 s. The specificity of the assay was established by melting-curve analysis. The relative expression (RQ) was calculated by using C4BP untreated cells infected with respective viruses as the calibrator. The RQ value was calculated using the formula: $RQ = 2^{-\Delta\Delta Ct}$. Primers were generated for specificity using the Primer-BLAST software (Basic Local Alignment Search Tool) (http://blast.ncbi.nlm.nih.gov/Blast.cgi) (**Table 3**).

Luciferase Assay

MDCK cells were seeded in a 96-well plate (1×10^5 cells per well) and were serum starved. The cells were infected for 24 h in the infection medium with 50 µl of the H1N1 and H3N2 pseudo-typed particles that were pre-incubated with C4BP for 1 h, or pseudo-typed particles that were not treated with C4BP. Post-infection, luciferase activity in the cells was measured using Pierce™ Firefly Luc One-Step Glow Assay Kit (Thermo Fisher) and CLARIOstar Plus Plate Reader (BMG Labtech).

Statistical Analysis

GraphPad Prism 8.0 software was used to create all graphs. Two-way ANOVA was used to find the statistical significance of the data generated. Significant values were considered based on *$p < 0.1$, **$p < 0.05$, ***$p < 0.01$, and ****$p < 0.001$ between treated and untreated conditions. Error bars show the standard deviation among the samples.

RESULTS

C4BP Directly Binds to Influenza A Virus in a Dose-Dependent Manner

Native C4BP, purified from plasma, was run on a 12% w/v reducing SDS-PAGE, which revealed a band corresponding to α-chain (~70 kDa), and one corresponding to β-chain (~45 kDa) (**Figure 1A**). The immunoreactivity of the protein was determined by performing a western blot with rabbit polyclonal anti-human C4BP antibodies, which yielded a band corresponding to the α-chain (~70 kDa) of C4BP. However, the β-chain (~45 kDa) was barely visible (**Figure 1B**). Indirect ELISA was then performed to examine the binding of C4BP to IAV subtypes. Binding of immobilized C4BP to the virus (**Figure 2A**), and conversely, of immobilized virus to C4BP (**Figure 2B**) was observed. As evident in **Figures 2A, B**, C4BP bound to H3N2 and H1N1 in a dose-dependent manner; binding to H3N2 was greater than to H1N1 (**Figure 2A**) subtype. Recombinant C4BP alpha chain (rC4BP) (**Supplementary Figure 1**) was also used to confirm its binding to the virus. No significant difference in binding efficiency was observed between the recombinant C4BP and the plasma purified C4BP (**Figures 2C, D**).

C4BP Binds HA, NA, and M1 Proteins of Influenza A Virus

In order to identify the IAV proteins that interact with C4BP, far-western blot analysis was performed. When SDS-PAGE separated IAV proteins were probed with C4BP, it revealed that C4BP interacted with IAV viral proteins Hemagglutinin (HA) (~70 kDa), Neuraminidase (NA) (~55 kDa) and Matrix protein 1 (M1) (~25kDa) (**Figure 3A**). The identities of C4BP bound IAV glycoproteins were confirmed using separate blots that were directly probed with anti-HA (**Figure 3B**), anti-NA (**Figure 3C**), anti-M1 (**Figure 3D**), or anti-NS1 antibodies (**Figure 3E**). IAV proteins separated by SDS-PAGE were probed directly with anti-C4BP antibodies to rule out non-specific interaction between the antibody and IAV proteins (**Figure 3F**). NS1 protein has similar molecular weight to M1, but the blot with antibodies confirmed M1 as the 25kDa species involved in binding.

Influenza A Virus Binding Sites Within C4BP α-Chain Appear to Be Localized Within CCP4-5 and CCP7-8 Modules

To identify the likely binding site on C4BP for the IAV, an indirect ELISA was performed using recombinant C4BP α-chain mutants lacking individual CCP domains. Recombinant C4BP lacking CCP4, 5, 7, or 8 showed relatively weaker binding to H1N1 and H3N2 subtypes. The deletion of CCP domain 8 reduced binding by approximately 75% for both subtypes when compared to full-length C4BP. Deletion of CCP7 resulted in reduced binding for H1N1 (~49%) as well as H3N2 (~62%). The CCP4 and 5 deletion mutants lost ~80% binding activity for H3N2 and ~60% for H1N1. Approximately 20% loss of binding for H1N1 was observed in the case of CCP1 and 2 deletants, but the same deletants showed ~80% reduction in binding to H3N2. The loss of CCP domains 3 and 6 caused a small increase in binding by approximately 10% for both IAV subtypes. This indicates that C4BP binds both IAV subtypes

TABLE 3 | Forward and reverse primers used for qRT-PCR.

Target	Forward primer	Reverse primer
18S	5′-ATGGCCGTTC TTAGTTGGTG-3′	5′-CGCTGAGCCA GTCAGTGTAG-3′
IL-6	5′-GAAAGCAGCA AAGAGGCACT-3′	5′-TTTCACCAGG CAAGTCTCCT-3′
IL-12	5′-AACTTGCAGC TGAAGCCATT-3′	5′-GACCTGAACG CAGAATGTCA-3′
TNF-α	5′-AGCCCATGTT GTAGCAAACC-3′	5′-TGAGGTACAG GCCCTCTGAT-3′
M1	5′AAACATATGTCTGATAAC GAAGGAGAACAGTTCTT-3′	5′GCTGAATTCTACCT CATGGTCTTCTTGA-3′
RANTES	5′-GCGGGTACCAT GAAGATCTCTG-3′	5′-GGGTCAGAATC AAGAAACCCTC-3′
IFN-α	5′-TTT CTC CTG CC T GAA GGA CAG-3′	5′-GCT CAT GAT TTC TGC TCT GAC A-3′

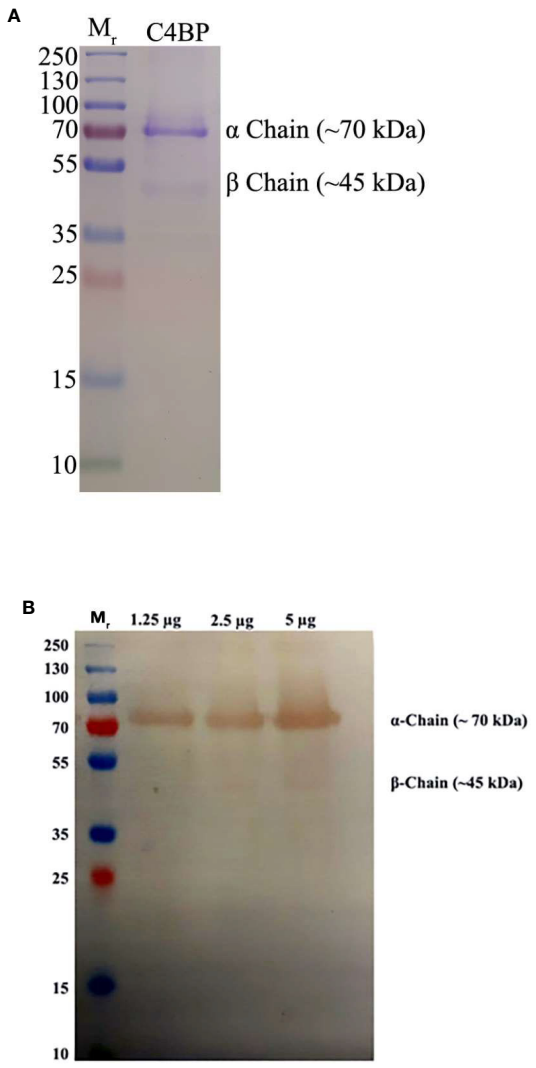

FIGURE 1 | Characterization of purified C4BP. **(A)** SDS-PAGE (12% w/v acrylamide/bisacrylamide) was loaded with 5 µg of purified C4BP in lane 2, along with a protein ladder with a range of 250 to 10 kDa (Thermofisher) in lane 1. The denatured and reduced samples were run for 120 min at 90 V and stained with Coomassie brilliant blue to reveal protein bands corresponding to the α-chain (~70kDa) and a faint band corresponding to β-chain of C4BP (~45 kDa). **(B)** Immunoreactivity of the purified C4BP was analyzed by western blotting. A PVDF membrane with 1.25, 2.5, and 5 µg of purified C4BP in lanes 2, 3, and 4, respectively, along with a protein ladder with a range of 250 to 10 kDa (Thermofisher) in lane 1 was probed using rabbit-anti-human C4BP polyclonal antibodies (1:1,000) at room temperature for 1 h, followed by incubation with secondary goat anti-rabbit IgG HRP-conjugate (1:1,000) for 1 h at room temperature. Bands corresponding to α-chain (~70 kDa) and the β-chain (~45 kDa) of the C4BP were observed after developing the color using 3,3′-diaminobenzidine (DAB) substrate.

most likely involving CCPs 4-5 and 7-8 domains of its α-chain (**Figure 4**). However, in the case of the H3N2 subtype, and to a lesser extent H1N1 subtype, it appears that there is an additional binding interaction with CCPs 1-2 (**Figure 4B**). This may be consistent with greater binding to H3N2. VSV-G pseudo-typed lentivirus that was used as negative control showed no significant binding (**Figure 4C**).

C4BP Inhibits H1N1 Replication

HA, NA, and M1 are essential IAV proteins which have many functions from viral entry to virion budding, bringing about IAV infectivity and replication. Therefore, we investigated the effect of C4BP on cell infection. A549 cells were challenged with either H1N1 or H3N2 for 6 h that were previously incubated with C4BP. The efficacy of replication was estimated by comparing the M1 expression levels of the virions treated with C4BP (10, 20, or 40 µg/ml) to the cells infected with IAV but, not treated with C4BP. M1 mRNA levels were downregulated by C4BP in the case of H1N1 ($-4\ \log_{10}$), suggesting that the interaction of C4BP with H1N1 reduced the replication efficiency of the virus at an early stage of the replication cycle. However, in the case of A549 cells challenged with H3N2, M1 mRNA levels were found to be upregulated ($2\ \log_{10}$), suggesting an increase in IAV replication efficacy. Taken together, these results suggest that C4BP differentially modulates viral entry, and thus, replication efficacy among the IAV subtypes (**Figure 5**).

C4BP Is an Entry Inhibitor for H1N1

As C4BP was found to interact with HA and NA, the IAV proteins that play an integral role in viral host cell recognition and entry, lentiviral pseudo-particles were used to study the entry process independent of other IAV components. The pseudo-particles expressing the respective IAV coat proteins with an HIV-Luciferase backbone were used as a safer alternative to assess the role of C4BP as an entry modulator of H1N1 and H3N2. This system contains a single packaging plasmid (psPAX2) encoding genes including Gag, Pol, and Tat. pHIV-Luciferase was used as a lentiviral transfer plasmid, which is flanked by long terminal repeat (LTR) sequences and designed to express the firefly luciferase reporter. Thus, pHIV-Luciferase is replication-incompetent which contains an additional sequence deletion in the 3′ LTR leading to viral self-inactivation post-integration. Purified H1+N1 and H3+N2 pseudo-typed particles pre-incubated with C4BP (20 µg) were used to infect MDCK cells. The lentiviral particles not treated with C4BP were used as controls. A ~56% reduction in luciferase reporter activity was observed when MDCK cells infected with C4BP-treated H1+N1 pseudo-typed particles were compared to their untreated counterparts. However, an opposite effect, although not so dramatic, was observed following C4BP treatment in the case of H3N2 unmatched pseudo-particles. A ~17% increase in luciferase activity was observed in the treated samples when compared to the control (**Figure 6**). C4BP protein seems to be acting as an entry inhibitor for H1N1, but a weak facilitator of infection by H3N2.

C4BP Modulates Pro-inflammatory Cytokine/Chemokine Response in IAV-Challenged A549 Cells

Pro-inflammatory cytokines and chemokines, such as IL-1, IL-6, IL-12, IFN-α, and NF-κB transcription factor, are a hallmark of

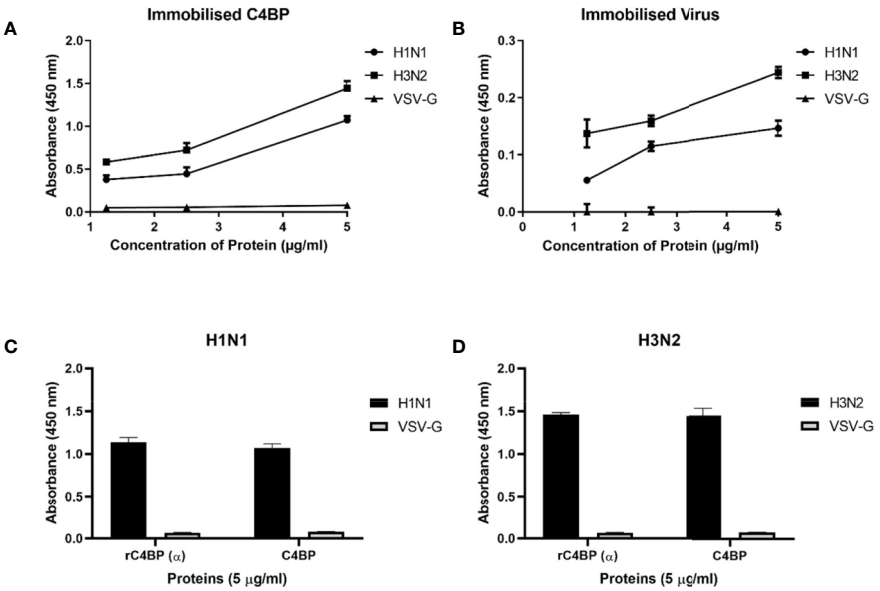

FIGURE 2 | Binding interaction of immobilized C4BP to IAV subtypes **(A)**, and immobilized IAV subtypes to C4BP **(B)**. Microtiter wells were coated with a varied concentration of C4BP (5, 2.5, and 1.25 µg/ml) protein and incubated with constant volume of viruses (1,000 PFU/ml). Bound C4BP-IAV was probed with monoclonal anti-influenza virus H1 and polyclonal anti-influenza virus H3 antibody (1:5,000). Another ELISA was performed by coating a constant concentration of IAV subtypes (1,000 PFU/ml) and incubated with a varied concentration of C4BP protein (5, 2.5, and 1.25 µg/ml). IAV-C4BP interaction was detected using polyclonal rabbit anti-human C4BP antibodies and anti-rabbit IgG-HRP-conjugated antibody (1:5,000). A validation ELISA to show the detection of H1N1 **(C)** and H3N2 **(D)** binding to a recombinant C4BP (rC4BP) and plasma purified C4BP. Microtiter wells were coated with immobilized rC4BP and the plasma purified C4BP (5 µg/ml), and incubated with H1N1 or H3N2 (1,000 PFU/ml). The binding between immobilized proteins and IAV subtypes were detected using monoclonal anti-influenza virus H1 and polyclonal anti-influenza virus H3 antibody (1:5,000). VSV-G pseudo-typed lentiviral particles were used as a negative control; no significant binding was observed. The data were expressed as the mean of three independent experiments done in triplicates ± SEM.

IAV infection (34). In order to understand the effect of C4BP on the pro-inflammatory cytokines produced during IAV infection, A549 cells were challenged with H1N1 and H3N2 viruses (MOI 1) preincubated with C4BP. qRT-PCR was then carried out using total RNA from the cells (**Figure 7**), using cells infected with IAV that were not treated with C4BP as the control. C4BP treated H1N1 challenged A549 cells showed lower levels of IFN-α (-2 $\log_{10}$) at both 2 and 6 h, whereas cells challenged with C4BP treated H3N2 exhibited higher levels of IFN-α 6 h post-infection (**Figure 7A**). IL-12 is essential for the generation of cell-mediated immunity *via* the production of IFN-γ by helper type 1 T (Th1) cells, which leads to the elimination of the virus (35). Levels of IL-12 at 2 h in case of A549 cells challenged with either C4BP treated H1N1 or H3N2 were not detectable (**Figure 7B**). At 6 h in C4BP treated H1N1 challenged cells, IL-12 levels were downregulated (−2 $\log_{10}$), while in cells challenged with C4BP treated H3N2 the levels were upregulated (1 $\log_{10}$) (**Figure 7B**). As interferon response is triggered by the detection of viral components within infected cells, and IL-12 induction requires live viruses, these results are consistent with the previously observed levels of M1 transcript.

The transcription factor, NF-κB, is a regulator of antiviral cytokines such as IFN-β, which initiates a strong type I IFN immune response. IAV induces IFN expression *via* NF-κB as viral titer levels are higher in cells treated with an anti-IFN-α/β receptor antibody and not in dominant-negative IκBα expressing cells (36). NF-κB mRNA levels at 2 h were slightly upregulated in C4BP treated H1N1 challenged cells and no significant change in its levels were observed in cells challenged with C4BP treated H3N2 (**Figure 7C**). Cells infected with C4BP treated H1N1 at 6 h exhibited lower levels of NF-κB (−1 $\log_{10}$), and no significant changes were observed in C4BP treated H3N2 infected cells (**Figure 7C**). The lower levels of NF-κB can be attributed to either low viral titer in the case of H1N1 or the IAV non-structural protein NS1 which acts as a major suppressor of NF-κB activation (37).

Increased levels of IL-6, TNF-α, and IFN-γ, have been detected in individuals infected with acquired acute as well as severe seasonal IAV-infected patients (38, 39). Production of TNF-α during IAV infection correlates with morbidity and mortality rates in IAV infected humans and macaques (40, 41). Six hours post-infection, TNF-α mRNA levels were upregulated (2 $\log_{10}$) in A549 cells infected with C4BP treated H1N1 or H3N2, while at the earlier 2-h time point a slight upregulation was observed (**Figure 7D**).

RANTES is a C-C chemokine and a potent chemoattractant for monocytes, T lymphocytes, basophils, and eosinophils. IAV, *via* its HA, can induce RANTES expression, probably through the activation of NF-κB, and cause airway hypersensitivity by inducing the continuous infiltration of eosinophils (42). C4BP treated H1N1 challenged A549 cells exhibited lower levels of RANTES expression (−2 $\log_{10}$) at 2 h compared to the control;

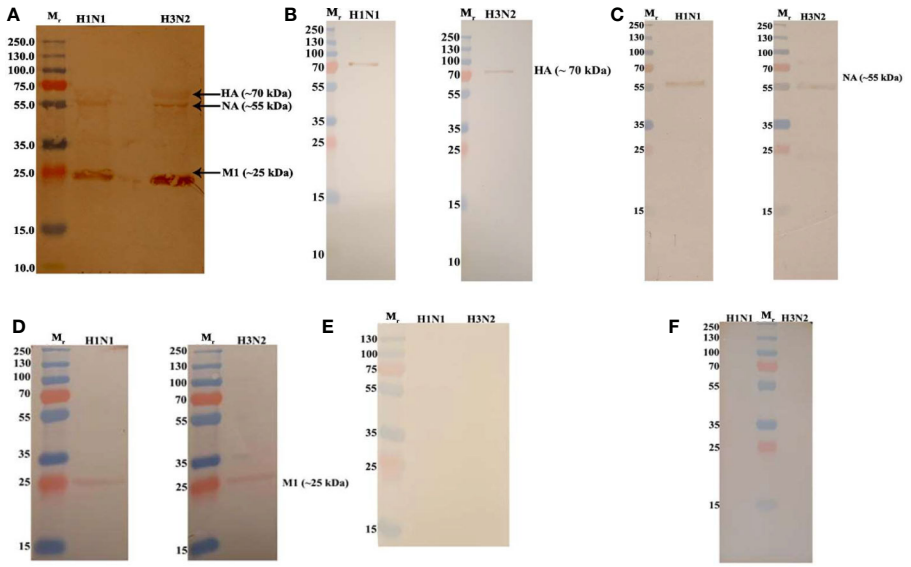

FIGURE 3 | Far Western blot analysis showing C4BP binding to H1N1 and H3N2 proteins. PVDF membrane containing H1N1 and H3N2 virus proteins, separated by SDS-PAGE was blocked with 5% w/v skimmed milk and incubated with 5 μg/ml of C4BP **(A)** or without C4BP **(F)** followed by washing steps. The membrane was probed with rabbit-anti-human C4BP polyclonal antibodies (1:1,000) at room temperature for 1 h, followed by washing and incubation with secondary goat anti-rabbit IgG HRP-conjugate (1:1,000) for 1 h at room temperature. Bands corresponding to Hemagglutinin (HA) (~70 kDa), Neuraminidase (NA) (~55 kDa), and Matrix protein 1 (M1) (25 kDa) in the case of both H1N1 and H3N2 subtypes were revealed after developing colour using 3,3′-diaminobenzidine. The identities of C4BP bound IAV glycoproteins were confirmed using separate blots that were directly probed with anti-HA **(B)**, anti-NA **(C)**, anti-M1 **(D),** or anti-NS1 **(E)** antibodies.

no changes were observed in cells challenged with C4BP treated H3N2 (**Figure 7E**). RANTES expression (2 $\log_{10}$) was upregulated at 6 h in the case of both subtypes (**Figure 7E**). Enhanced levels of IL-6 have been observed in the serum and lungs of IAV infected patients. It is unknown whether IL-6 in IAV infected patients contributes to lung pathology caused by the viral infection or if increased levels of IL-6 contribute to a protective mechanism against IAV (39, 43). Levels of IL-6 at 2 h in C4BP treated A549 cells challenged with either virus were not detectable (**Figure 7F**). At 6 h in C4BP treated H3N2 infected cells, IL-6 levels (2 $\log_{10}$) were upregulated; in cells challenged C4BP treated H1N1 the IL-6 levels (0.5 $\log_{10}$) were also upregulated (**Figure 7F**). Studies also suggest that signals mediated by IL-6 are crucial for survival against a non-lethal dose of H1N1 infection, and IL-6/IL-6R deletion inhibits H1N1 clearance together with reduced neutrophils levels in the lungs of infected mice (44).

DISCUSSION

The Influenza virus, an upper respiratory tract pathogen, is known to have caused some of the deadliest pandemics in history. To develop better IAV treatment strategies and mitigate the risk of the current viral strains evolving to a more pathogenic one by reassorting among themselves, a better understanding of the immune mechanisms against IAV is required. Here, we examined the complement-independent role of C4BP, a complement regulator, against IAV. Many pathogens such as adenoviruses, *Yersinia pestis*, and *Aspergillus* spp. are known to bind C4BP to promote survival and proliferation (15). C4BP is a major fluid phase inhibitor of the classical and the lectin pathways, making it a prime target for the exploitation by pathogens to circumvent the host's potent humoral immune system, such as complement. In this study, we sought to understand the interactions between C4BP and IAV in a serum-free system and explore any complement-independent functions of C4BP with respect to IAV.

We first established protein-protein interactions between C4BP and IAV subtypes. C4BP α chain was found to bind IAV subtypes (**Figures 2A, B**), and H3N2 was found to bind C4BP with higher affinty than H1N1. This interaction with the α chain of C4BP was further confirmed using rC4BP **(Figures 2C, D)**. The C4BP α chain was found to interact with viral envelope protein HA, NA, and surprisingly, M1 (**Figure 3**). As the M1 protein lies beneath the lipid layer, the interaction likely occurs by the abundantly present non-packaged M1 that are released from ravaged cells during late stages of infection to help increase the odds of survival of the virus (45).

It was also possible that C4BP interacted with IAV NS1, but the signal was masked by the interaction of C4BP with M1 due to the low concentrations of NS1 when compared to M1, as proteins share similar molecular weights. Avirutnan *et al.* have shown that Flavivirus NS1 restricted the activation of classical and lectin pathways by binding to C4BP, thereby enabling the virus to evade C4b mediated lysis (5). Since both NS1 proteins share independent immunoregulatory functions, the binding of Influenza NS1 with C4BP was also considered. Far western blot

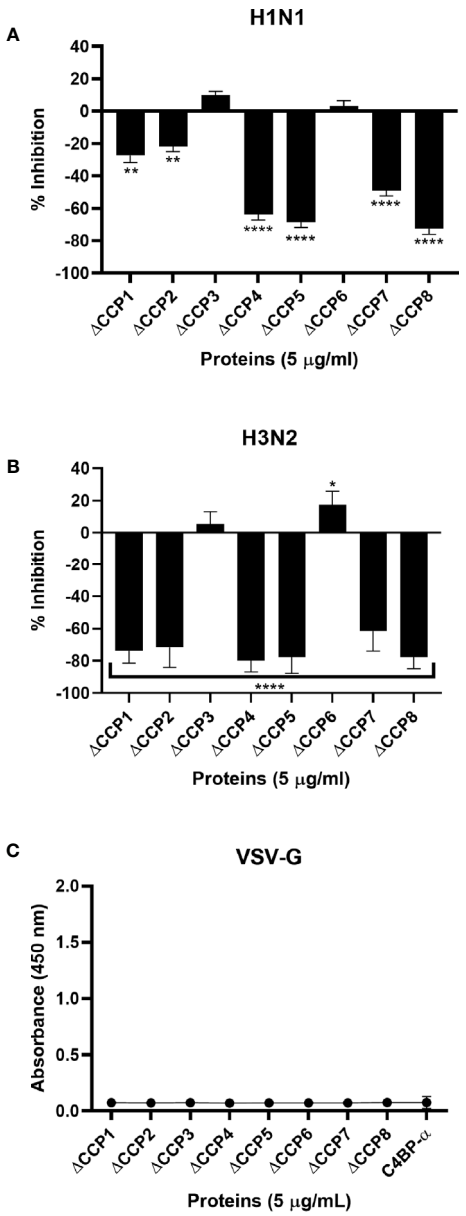

FIGURE 4 | C4BP interacts with IAV through multiple CCP domains. ELISA showing binding of C4BP CCP deletion mutants to **(A)** H1N1, **(B)** H3N2 and **(C)** VSV-G: microtiter wells were coated with 5 μg/ml of the mutant C4BP protein (as described in **Table 1**). 1000 PFU/ml of H1N1 or H3N2 virus was added to all the wells. After incubation and washing steps, the bound virus was measured with either monoclonal anti-influenza virus H1, polyclonal anti-influenza virus H3 or polyclonal anti-VSV-G antibody. Results are normalised against full length C4BP α chain. The data were expressed as the mean of three independent experiments done in triplicates ± SEM. Significance was determined using the two-way ANOVA test (*$p < 0.05$, **$p < 0.01$, and ****$p < 0.0001$) ($n = 3$).

analysis and direct western blot analysis confirmed that it was M1 that C4BP bound to at ~26 kDa; probing with monoclonal Anti-IAV NS1did not reveal any bands corresponding to NS1 protein. Furthermore, multiple sequence alignment and identity-similarity analysis on IAV NS1 [(Accession #: P03495; P03496) and Flavivirus NS1 (Accession #: Q6J3P1 Residues: 779-1130) (P29991) Residues: 776-1127; P06935 (Residues: 788-1139)] performed using Clustal Omega and Sequence Manipulation Suite (Data not shown) revealed IAV NS1 and Flavivirus NS1 have sequence similarity scores that are lower than 25%.

Use of deletion mutants lacking specific CCP domains of C4BP revealed that H1N1 and H3N2 subtypes interacted *via* multiple CCP domains, CCP1-2, CCP4-5, and CCP7-8 of the C4BP α-chain. It is known that the Flavivirus NS1-C4BP binding is mediated through CCP2-5 and 8. Since CCP8 is near to the C-terminal oligomerization domain, its loss could affect the conformational structure of C4BP, which can affect the accessibility of NS1 to CCP2-5 (5). Similarly, the deletion of CCP8 reduced IAV-C4BP binding by ~75% (**Figure 4**). Deletion of CCP4-5 inhibited binding by ~79% to H3N2 and ~67% to H1N1 (**Figure 4**). C4BP binds C4b through CCP1-3, with domains 2 and 3 being the most critical for the interaction (10). The loss of CCP1-2 reduced binding efficiency of H3N2 and, to a lesser extent, of H1N1 to C4BP (~80% for H3N2 and ~20% for H1N1) (**Figure 4**). It is possible that the IAV virus, like other pathogens such as *S. pyogenes*, *Neisseria gonorrhoeae*, *Bordetella pertussis*, *Moraxella catarrhalis*, *Borrelia recurrentis*, *Candida albicans*, and *Hemophilus influenzae,* is exploiting the natural binding site for C4b (8). This preference for the site can be attributed to its immutability, accessibility and the fact that the region may contain intrinsic properties which favor ligand binding (46). Furthermore, this increased binding affinity between CCP1-2 and H3N2 may explain the difference in the binding efficiency of C4BP to H3N2 when compared to H1N1, as seen in **Figure 2**. As plasma purified C4BP is a glycoprotein, and therefore, is likely to contain N-glycosides that are sialylated; it is possible for sialic acid residues to bind to HA/NA. C4BP [UniProtKB - P04003 (C4BPA_HUMAN)] has N-linked glycosylation only in CCP3 and CCP8 and so sialic acid is likely to occur only at these sites. Our results do not implicate CCP3 in binding, but it remains a possibility that CCP8 binding could involve sialic acid.

It is likely that C4BP is regulating viral replication levels by modulating viral entry. To establish this, second-generation matched and unmatched lentiviral vectors, pseudo-typed for H1+N1 and H3+N2, respectively, were generated. This system was selected as a safe alternative method to mimic the structure and surfaces of IAV and prove that C4BP acts as an entry inhibitor in cells transduced with pseudo-typed IAV particles that are restricted to only one replicative cycle. A luciferase reporter assay revealed a 56% reduction in H1N1 pseudo-typed viruses treated with C4BP that entered the cells, corresponding with the 4-fold decrease observed in the M1 mRNA levels of H1N1 infected cells (**Figures 5** and **6**), while a slight increase (~17%) was observed in case of the H3N2 pseudo-particles (**Figure 6**), consistent with M1 levels. This suggests that C4BP acts as an entry inhibitor for H1N1 while it has limited restrictive potential against H3N2.

Recently, factor H, the principal regulator of the alternative pathway, and vaccinia virus complement control protein (VCP),

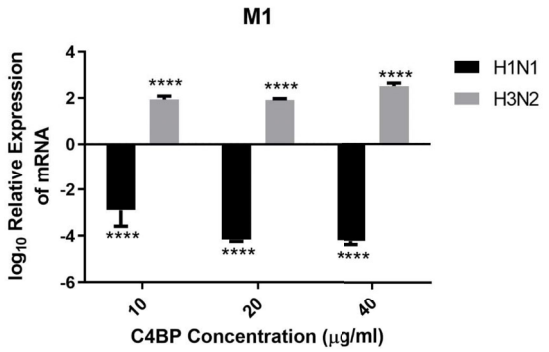

FIGURE 5 | C4BP restricts replication of H1N1 and promotes replication of H3N2 in target human A549 cells. M1 expression of both H1N1 and H3N2 IAV after infection of A549 cells for 6 h was measured by qRT-PCR. A549 cells were challenged either with H1N1 or H3N2 (MOI 1) that were incubated with varying concentration of C4BP (10, 20, and 40 μg/ml). Cell pellets were harvested at 6 h to analyze the M1 expression of IAV. Cells were lysed, and RNA extracted was converted into cDNA. Infection was measured *via* qRT-PCR using M1 primers; 18S rRNA was used as an endogenous control. The relative expression (RQ) was calculated by using cells infected with respective viruses that were not treated with C4BP as the calibrator. The RQ value was calculated using the formula: $RQ = 2^{-\Delta\Delta Ct}$. Assays were conducted in triplicates, and error bars represent ± SEM. Significance was determined using the two-way ANOVA test (****$p < 0.0001$) ($n = 3$).

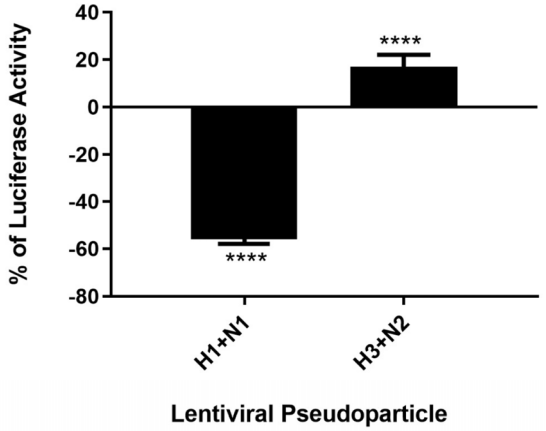

FIGURE 6 | C4BP modulates viral entry in a strain-dependent manner. Luciferase reporter activity of C4BP treated MDCK cells infected with matched H1+N1 and unmatched H3+N2 lentiviral pseudo-particles. H1N1 particles exhibited a 55% decrease in viral entry compared to controls, while a 17% increase in viral entry in case of H3N2 was observed. Results are normalized against cells infected with the particles not treated with C4BP. Significance was determined using the unpaired one-way ANOVA test (****$p < 0.0001$) ($n = 3$).

a homologue of factor H, were found to interact with IAV in a manner similar to C4BP (32). MDCK cells infected with H1+N1pseudo-typed lentiviral particles resulted in approximately 25% and 45% reduction in luciferase activity after treatment with factor H or VCP, respectively. However, a 50% increase in luciferase activity in MDCK infected with H3+N2 pseudo-typed lentiviral particles was observed when treated with factor H, and 30% when treated with VCP was observed. Hence, the treatment with these proteins resulted in restriction of IAV entry and replication by 4-fold for the H1N1 subtype, while promoting entry and replication by 2-fold for H3N2. Thus, using lentiviral vectors, pseudo-typed for H1+N1 and H3+N2, Murugaiah et al. demonstrated the ability of Factor H and VCP to modulate IAV entry, in a subtype dependent manner, similar to C4BP (32). As seen in the case of C4BP, Murugaiah et al. also suggested that FH and VCP to accomplished the subtype dependent entry modulation via interaction with HA, NA, and M1. Additionally, FH and VCP were also shown to trigger an anti-inflammatory response in case of H1N1 subtype while leading to pro inflammatory response in H3N2 subtype. The inflammatory response was also modulated in a subtype-specific manner. Transcriptional levels of IFN-α, TNF-α, IL-12, IL-6, and IFN-α were upregulated, while RANTES was downregulated following factor H treatment for the H1N1 subtype at 6 h post-infection. In the case of the H3N2 subtype, mRNA levels of these pro-inflammatory cytokines were enhanced (32). The findings of this study highlight a possible common mechanism that is used by C4BP, VCP, and Factor H that contain CCP domains in modulating the entry of IAV subtypes. The heparin-binding sites on Factor H (surface of CCP7, CCP13 and CCP20) and VCP (tip of module 4) are also found on C4BP α chain (CCP domains 1-2) (9, 47). These sites may provide a possible explanation for the effect observed on viral entry modulation among the IAV subtypes. In this study, we have shown that IAV subtypes bind C4BP *via* the heparin-binding site containing CCP domain 1-2 (**Figure 4**). We suspect the overlapping heparin-binding and IAV binding sites may contribute to the variation observed between the subtypes. C4BP has been shown to enhance adenovirus uptake in hepatocytes by providing a bridge between the adenovirus fiber knob domain and cell surface Heparan Sulfate Proteoglycans (HSP) (16); we speculate that the increased efficiency observed between the binding of C4BP's CCP1-2 domain and H3N2 subtype compared to H1N1 subtype may contribute to the increased H3N2 virion entry in a similar fashion. The similarity of the results between the interaction of C4BP, Factor H, and VCP to IAV subtypes further support this idea and requires further study by treating cells with heparinase prior to C4BP treatment and infection to confirm whether the variation between the subtypes may be modulated by the interaction with HSP.

Another explanation for differences in outcome in spite of C4BP binding both viruses may arise from the local variations found between H1 and H3 or N1 and N2 or the variation in C4BP binding sites to HA or NA. HA and NA are classified into two groups regardless of their serotype identification. In case of NA, N1 belongs to group 1, which lacks an additional cavity next to the active site that is created by the movement of "150 loop" during conformational changes caused by the binding of substrate to the active site (48). N2 belongs to group 2 which

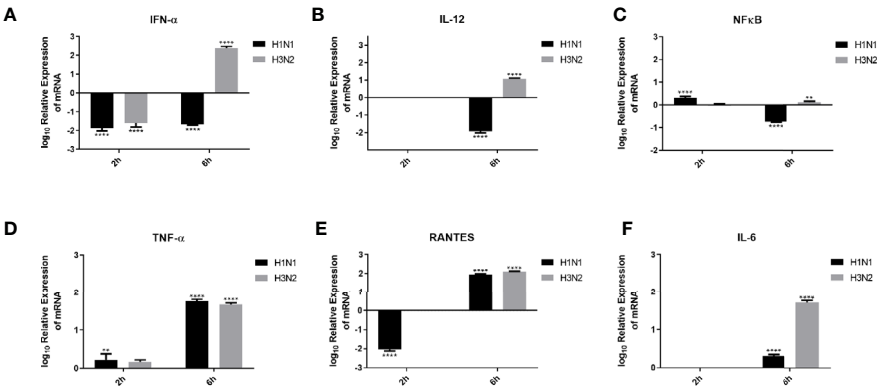

FIGURE 7 | Cytokine modulation by C4BP of IAV infected A549 cells. H1N1 or H3N2 incubated with 10μg/ml of C4BP was used to infect A549 cells. Cell pellets were harvested at 2 h and 6 h to analyse the expression of cytokines and chemokines. Cells were lysed, and purified RNA was converted into cDNA. The expression levels of cytokines IFN-α **(A)**, IL-12 **(B)**, NF-κB **(C)**, TNF-α **(D)**, IL-6 **(F)** and chemokine RANTES **(E)** were measured using qRT-PCR, and the data were normalised *via* 18S rRNA expression as a control. The relative expression (RQ) was calculated by using cells infected with respective viruses not treated with C4BP as the calibrator. The RQ value was calculated using the formula: $RQ = 2^{-\Delta\Delta Ct}$. Assays were conducted in triplicates, and error bars represent ± SEM. Significance was determined using the two-way ANOVA test (**$p < 0.01$, and ****$p < 0.0001$) ($n = 3$).

lacks the "150 loop", and hence, the additional cavity (48). NA functions in virus internalization by enabling movement of the virus across the cell surface from an endocytosis inactive site on the cell to an active site, thereby increasing the efficiency of viral uptake (49). NA has also been shown to boost HA-dependent influenza virus fusion and infectivity by employing a cell-cell fusion assay and an HIV-based pseudo-typed infectivity assay (50). It is possible that the structural differences between N1 and N2 after binding to C4BP may affect their role in virus internalization. Similarly, HA can also be classified into two groups based on structural characteristics, with H1 in group 1 and H2 in group 2 (51). Hence, localized variations found on HA could influence potential binding pocket for C4BP on the HA, as seen in the case of Stachyflin (52). These structural variations in HA and NA may also explain the increased binding observed between C4BP and H3N2. It will be important to investigate the effect of differential interplay between HA and NA of H1N1 and H3N2 viruses on the infection modulation activity of C4BP. Additionally, the variation in binding efficiency of CCP1-2 between H3N2 and H1N1 suggests that the binding while overlapping, does not occur at identical sites, as seen in the case of C4BP binding to C4b, *S. pyogenes*, or *B. pertussis* (46, 53, 54). It may be possible that this variation and difference in binding efficiency further affects downstream interactions such as C4BP or IAV's interaction with other receptors or proteins that may affect viral entry (55, 56).

During an IAV infection, elevated levels of cytokines and chemokines are observed, including IL-6, TNF-α, IFNs, IL-1β, RANTES, IL-8, MIP1β, and MCP1 (57–60). Inflammation is a critical part of the immune response against IAV infection. Cytokines such as TNF-α, IL-12, and IFNs are known to play a significant role to cellular inflammation. To study the modulation of these cytokines by C4BP, we performed qPCR on A549 cells infected with C4BP treated H1N1 or H3N2 (treated) and standardized them against A549 cell infected under similar conditions using viruses that were not treated with C4BP (untreated) to obtain the relative expression levels of the cytokines. Type I interferons like IFN α and IFN β are critical mediators of virus clearance during an IAV infection. Six hours post-infection in the treated cells, IFN-α mRNA levels were downregulated in case of H1N1 ($-2\ \log_{10}$) and upregulated ($2.5\ \log_{10}$) in case of C4BP treated H3N2 infected cells (**Figure 7A**). This suggests the formation of an antiviral state in the infected and its neighbouring cells, thereby reducing viral replication and disease severity (61, 62). The elevated levels of IFN-α mRNA observed in A549 cells challenged with the C4BP treated H3N2 subtype suggest that C4BP is being protective by promoting a type 1 interferon response despite not acting as an entry inhibitor for H3N2. The cytokine mRNA expression was downregulated ($-2\ \log_{10}$) in the case of both viruses 2 h post-infection and can be attributed to the low viral load present at the time (**Figure 7A**).

We found that IL-12 mRNA levels were too low to be detected 2 h post-infection, but the relative mRNA upregulation ($1\ \log_{10}$) was observed 6 h post-infection in cells infected with C4BP treated H3N2 compared to its control (**Figure 7B**). This clearly indicates the presence of a response that would culminate in the prevention of viral replication, activation of cytotoxic T lymphocytes and early NK cell-dependent gamma interferon production (63). The entry inhibitory effect of C4BP on H1N1 subtype, and the subsequent lower viral replication and load is further demonstrated by the downregulation ($-2\ \log_{10}$) of IL-12 mRNA in the C4BP treated H1N1-infected cells compared to their untreated counterparts 6 h post-infection (**Figure 7B**).

The TNF-α–NF-κB axis leads to the expression of a number of inflammatory genes, induction of apoptosis and production of ROS (64–66). NF-κB mRNA in cells infected with C4BP treated H1N1, 2 h post-infection was found to be relatively upregulated ($\sim 0.3\ \log_{10}$), while a downregulation ($\sim -0.7\ \log_{10}$) of the mRNA was recorded 6 h post-infection when compared to the untreated

samples (**Figure 7C**). In case of cells infected with C4BP treated H3N2, we found an upregulation of NF-κB mRNA 6 h post-infection, while no significant modulation was observed 2 h post-infection (**Figure 7C**). This variation in NF-κB mRNA levels 6 h post-infection among the IAV subtype further confirms the subtype dependent entry inhibitory action of C4BP on IAV. When compared to their untreated counterparts, the cells infected with either C4BP treated H1N1 or H3N2 were found to upregulate TNF-α mRNA (**Figure 7D**), indicating a robust inflammatory response at both 2 h (0.2 $\log_{10}$) and 6 h (~1.7 $\log_{10}$) post-infection (67, 68).

RANTES is an important chemokine that been associated with extensive inflammation of the lung in cases of avian Influenza and increased mortality in IAV challenged $CCR5^{-/-}$ mice (69). RANTES mRNA expression levels in treated H1N1 challenged cells 2 h post-infection, was found to be significantly downregulated (−2 $\log_{10}$) while it was not detected in case of H3N2 (**Figure 7E**). RANTES mRNA levels in cells were upregulated observed in case of both C4BP treated viral subtypes (2 $\log_{10}$) 6 h post-infection, suggesting an active recruitment of leukocytes to the inflammatory sites (**Figure 7E**).

Another cytokine associated with both pro-inflammatory and anti-inflammatory effects is IL-6 (70). Its synthesis is upregulated during infection to simulate the adaptive immune response by inducing differentiation of activated B cells and $CD4^+$ T cells (71). In the case of IAV infection, IL-6 seemed to have a protective role in murine models, promoting viral clearance and limiting inflammation (72). IL-6 mRNA levels at 6 h was found to be upregulated in case of H1N1 (0.5 $\log_{10}$) and H3N2 (1.5 $\log_{10}$) (**Figure 7F**) after C4BP treatment. These results suggest that C4BP may entice differential adaptive immune response.

It would be interesting to study if C4BP can also bind avian IAV. Another area to explore further would be investigate in humanized murine models to understand better the impact of C4BP-IAV interaction in the microenvironment of the respiratory system, and elucidation of mechanism resulting in the subtype-dependent entry modulation of IAV by C4BP.

In conclusion, we show that C4BP differentially regulates the efficacy of Influenza A virus replication in a subtype-dependent manner by modulating their entry into the cells, and provide an interesting candidate to be developed into a HA and NA-based inhibitor against IAV infections. Recombinant forms of CCP4+5 and/or CCP7+8 are likely to be excellent vehicles for therapeutic development against IAV pandemic H1N1 subtype.

DATA AVAILABILITY STATEMENT

The raw data supporting the conclusions of this article will be made available by the authors, without undue reservation.

AUTHOR CONTRIBUTIONS

PV, VM, and NB carried out most of the experiments. NT, HK, SA, and MA-A provided crucial reagents. FA-M, BN, RS, and UK managed the experimental details and analyzed the data. PV and VM wrote the first draft. UK, RS, and BN edited the manuscript. All authors contributed to the article and approved the submitted version.

FUNDING

The authors acknowledge the International Scientific Partnership Programme (ISPP) at King Saud University, Riyadh, for funding *via* ISPP-145.

ACKNOWLEDGMENT

Recombinant C4BP α-chain and the C4BP α-chain CCP deletant proteins were kindly provided by Prof Anna Blom and Frida Mohlin, Department of Translational Medicine, Lund University, Malmo, Sweden. A/England/2009 (H1N1) was a gift from Wendy Barclay, Department of Infectious Disease, Imperial College London, United Kingdom, and the A/HK/99 (H3N2) was a gift from Leo Poon, Division of Public Health Laboratory Sciences, University of Hong Kong, Hong Kong. pCMV-VSV-G plasmid was a gift from Bob Weinberg, Department of Biology, Massachusetts Institute of Technology, Massachusetts, USA. pHIV-Luciferase plasmid was a gift from Bryan Welm, Department of Anatomy, University of California, San Francisco, USA. psPAX2 plasmid was a gift from Didier Trono, Department of Genetics and Microbiology, University of Geneva Medical School, Geneva, Switzerland.

SUPPLEMENTARY MATERIAL

The Supplementary Material for this article can be found online at: https://www.frontiersin.org/articles/10.3389/fimmu.2020.585361/full#supplementary-material

SUPPLEMENTARY FIGURE 1 | (A) SDS-PAGE (12% w/v acrylamide/bisacrylamide) was loaded with 5 µg of recombinant C4BP α chain in lane 2, along with a protein ladder with a range of 250 kDa to 10 kDa (Thermofisher) in lane 1. The denatured and reduced samples were run for 120 minutes at 90V and stained with Coomassie brilliant blue to reveal protein bands corresponding to the α-chain (~70kDa). **(B)** Immunoreactivity of the recombinant C4BP α chain was analysed by western blotting using rabbit-anti-human C4BP polyclonal antibodies (1:1000) at room temperature for 1 h, followed by incubation with secondary goat anti-rabbit IgG HRP-conjugate (1:1,000) for 1 h at room temperature. Bands corresponding to α-chain (~70kDa) of the C4BP were observed after developing the colour using 3,3′-diaminobenzidine (DAB) substrate.

REFERENCES

1. Noris M, Remuzzi G. Overview of complement activation and regulation. *Semin Nephrol* (2013) 33:479–92. doi: 10.1016/j.semnephrol.2013.08.001
2. De Cordoba SR, Sanchez-Corral P, Rey-Campos J. Structure of the gene coding for the α polypeptide chain of the human complement component C4b-binding protein. *J Exp Med* (1991) 173:1073–82. doi: 10.1084/jem.173.5.1073
3. Okrój M, Blom AM. *The complement facts book*. London, United Kingdom: Academic Press (2018). doi: 10.1016/c2015-0-06595-9

4. Blom AM, Villoutreix BO, Dahlbäck B. Mutations in α-Chain of C4BP that selectively affect its Factor I cofactor function. *J Biol Chem* (2003) 278:43437–42. doi: 10.1074/jbc.M306620200
5. Avirutnan P, Hauhart RE, Somnuke P, Blom AM, Diamond MS, Atkinson JP. Binding of Flavivirus nonstructural Protein NS1 to C4b binding protein modulates complement activation. *J Immunol* (2011) 187:424–33. doi: 10.4049/jimmunol.1100750
6. Kask L, Hillarp A, Ramesh B, Dahlbäck B, Blom AM. Structural requirements for the intracellular subunit polymerization of the complement inhibitor C4b-binding protein. *Biochemistry* (2002) 41:9349–57. doi: 10.1021/bi025980+
7. Hofmeyer T, Schmelz S, Degiacomi MT, Dal Peraro M, Daneschdar M, Scrima A, et al. Arranged sevenfold: Structural insights into the C-terminal oligomerization domain of human C4b-binding protein. *J Mol Biol* (2013) 425:1302–17. doi: 10.1016/j.jmb.2012.12.017
8. Ziccardi RJ, Dahlback B, Muller-Eberhard HJ. Characterization of the interaction of human C4b-binding protein with physiological ligands. *J Biol Chem* (1984) 259:13674–9.
9. Blom AM, Webb J, Villoutreix BO. Dahlbäck B. A cluster of positively charged amino acids in the C4BP α-chain is crucial for C4b binding and factor I cofactor function. *J Biol Chem* (1999) 274:19237–45. doi: 10.1074/jbc.274.27.19237
10. Blom AM, Kask L, Dahlbäck B. Structural requirements for the complement regulatory activities of C4BP. *J Biol Chem* (2001) 276:27136–44. doi: 10.1074/jbc.M102445200
11. Fujita T, Nussenzweig V. The role of c4-binding protein and β1h in proteolysis of c4b and c3b. *J Exp Med* (1979) 150:267–76. doi: 10.1084/jem.150.2.267
12. Fujita T, Tamura N. Interaction of C4-binding protein with cell-bound C4b: A quantitative analysis of binding and the role of C4-binding protein in proteolysis of cell-bound C4b. *J Exp Med* (1983) 157:1239–51. doi: 10.1084/jem.157.4.1239
13. Blom AM, Kask L, Dahlbäck B. CCP1-4 of the C4b-binding protein α-chain are required for factor I mediated cleavage of complement factor C3b. *Mol Immunol* (2003) 39:547–56. doi: 10.1016/S0161-5890(02)00213-4
14. Ermert D, Weckel A, Agarwal V, Frick IM, Björck L, Blom AM. Binding of complement inhibitor C4b-binding protein to a highly virulent streptococcus pyogenes M1 strain is mediated by protein H and enhances adhesion to and invasion of endothelial cells. *J Biol Chem* (2013) 288:32172–83. doi: 10.1074/jbc.M113.502955
15. Ermert D, Blom AM. C4b-binding protein: The good, the bad and the deadly. Novel functions of an old friend. *Immunol Lett* (2016) 169:82–92. doi: 10.1016/j.imlet.2015.11.014
16. Shayakhmetov DM, Gaggar A, Ni S, Li Z-Y, Lieber A. Adenovirus binding to blood factors results in liver cell infection and hepatotoxicity. *J Virol* (2005) 79:7478–91. doi: 10.1128/jvi.79.12.7478-7491.2005
17. Brodeur SR, Angelini F, Bacharier LB, Blom AM, Mizoguchi E, Fujiwara H, et al. C4b-Binding Protein (C4BP) Activates B Cells through the CD40 Receptor. *Immunity* (2003) 18:837–48. doi: 10.1016/S1074-7613(03)00149-3
18. Trouw LA, Nilsson SC, Gonçalves I, Landberg G, Blom AM. C4b-binding protein binds to necrotic cells and DNA, limiting DNA release and inhibiting complement activation. *J Exp Med* (2005) 201:1937–48. doi: 10.1084/jem.20050189
19. Trouw LA, Bengtsson AA, Gelderman KA, Dahlbäck B, Sturfelt G, Blom AM. C4b-binding protein and factor H compensate for the loss of membrane-bound complement inhibitors to protect apoptotic cells against excessive complement attack. *J Biol Chem* (2007) 282:28540–8. doi: 10.1074/jbc.M704354200
20. Williams KT, Young SP, Negus A, Young LS, Adams DH, Afford SC. C4b binding protein binds to CD154 preventing CD40 mediated cholangiocyte apoptosis: A novel link between complement and epithelial cell survival. *PLoS One* (2007) 2:e159. doi: 10.1371/journal.pone.0000159
21. Dahlback B, Stenflo J. High molecular weight complex in human plasma between vitamin K-dependent protein S and complement component C4b-binding protein. *Proc Natl Acad Sci U S A* (1981) 78:2512–6. doi: 10.1073/pnas.78.4.2512
22. Breaud AR, Henemyre-Harris CL, Schools S, Emezienna N, Clarke W. Rapid quantification of the aminoglycoside arbekacin in serum using high performance liquid chromatography–tandem mass spectrometry. *Clin Chim Acta* (2013) 418:102–6. doi: 10.1016/j.cca.2013.01.004
23. Samji T. Influenza A: Understanding the viral life cycle. *Yale J Biol Med* (2009) 82:153–9.
24. Tong S, Zhu X, Li Y, Shi M, Zhang J, Bourgeois M, et al. New world bats harbor diverse influenza A Viruses. *PLoS Pathog* (2013) 9:e1003657. doi: 10.1371/journal.ppat.1003657
25. WHO. World Health Organization. "Influenza (Avian and other zoonotic)". In: *World Health Organization* (2018). Available at: https://www.who.int/news-room/fact-sheets/detail/influenza-(avian-and-other-zoonotic).
26. Potter CW. A history of influenza. *J Appl Microbiol* (2001) 91(4):572–9. doi: 10.1046/j.1365-2672.2001.01492.x
27. Cohen M, Zhang XQ, Senaati HP, Chen HW, Varki NM, Schooley RT, et al. Influenza A penetrates host mucus by cleaving sialic acids with neuraminidase. *Virol J* (2013) 10:321. doi: 10.1186/1743-422X-10-321
28. Leung HSY, Li OTW, Chan RWY, Chan MCW, Nicholls JM, Poon LLM. Entry of influenza A Virus with a 2,6-Linked sialic acid binding preference requires host fibronectin. *J Virol* (2012) 86:10704–13. doi: 10.1128/jvi.01166-12
29. Skehel JJ, Wiley DC. Receptor binding and membrane fusion in virus entry: The influenza hemagglutinin. *Annu Rev Biochem* (2000) 69:531–69. doi: 10.1146/annurev.biochem.69.1.531
30. Sim E, Sim RB. Enzymic assay of C3b receptor on intact cells and solubilized cells. *Biochem J* (1983) 210:567–76. doi: 10.1042/bj2100567
31. Klimov A, Balish A, Veguilla V, Sun H, Schiffer J, Lu X, et al. Influenza Virus Titration, Antigenic Characterization, and Serological Methods for Antibody Detection, in *Influenza Virus: Methods and Protocols*. Y. Kawaoka, G. Neumann, editors. *Influenza Virus: Methods and Protocols*. (2012) Totowa, NJ: Humana Press. p. 25–51. doi: 10.1007/978-1-61779-621-0_3
32. Murugaiah V, Varghese P, Saleh S, Tsolaki A, Alrokayan S, Khan H, et al. Complement-independent Modulation of influenza A virus infection by Factor H. *Front Immunol* (2020) 11:355. doi: 10.3389/FIMMU.2020.00355
33. Tang D-J, Lam Y-M, Siu Y-L, Lam C-H, Chu S-L, Peiris JSM, et al. A single residue substitution in the receptor-binding domain of H5N1 hemagglutinin is critical for packaging into pseudotyped lentiviral particles. *PLoS One* (2012) 7:e43596–6. doi: 10.1371/journal.pone.0043596
34. Mogensen TH, Paludan SR. Molecular pathways in virus-induced cytokine production. *Microbiol Mol Biol Rev* (2001) 65:131–50. doi: 10.1128/mmbr.65.1.131-150.2001
35. Hama Y, Kurokawa M, Imakita M, Yoshida Y, Shimizu T, Watanabe W, et al. Interleukin 12 is a primary cytokine responding to influenza virus infection in the respiratory tract of mice. *Acta Virol* (2009) 53:233–40. doi: 10.4149/av_2009_04_233
36. Ludwig S, Planz O. Influenza viruses and the NF-κB signaling pathway - Towards a novel concept of antiviral therapy. *Biol Chem* (2008) 389:1307–12. doi: 10.1515/BC.2008.148
37. Wang X, Li M, Zheng H, Muster T, Palese P, Beg AA, et al. Influenza A virus NS1 protein prevents activation of NF-kappa B and induction of Alpha/Beta interferon. *J Virol* (2000) 74:11566–73. doi: 10.1128/jvi.74.24.11566-11573.2000
38. Heltzer ML, Coffin SE, Maurer K, Bagashev A, Zhang Z, Orange JS, et al. Immune dysregulation in severe influenza. *J Leukoc Biol* (2009) 85:1036–43. doi: 10.1189/jlb.1108710
39. Kaiser L, Fritz RS, Straus SE, Gubareva L, Hayden FG. Symptom pathogenesis during acute influenza: Interleukin-6 and other cytokine responses. *J Med Virol* (2001) 64:262–8. doi: 10.1002/jmv.1045
40. Bermejo-Martin JF, Ortiz de Lejarazu R, Pumarola T, Rello J, Almansa R, Ramírez P, et al. Th1 and Th17 hypercytokinemia as early host response signature in severe pandemic influenza. *Crit Care* (2009) 13:R201. doi: 10.1186/cc8208
41. Cillóniz C, Shinya K, Peng X, Korth MJ, Proll SC, Aicher LD, et al. Lethal influenza virus infection in macaques is associated with early dysregulation of inflammatory related genes. *PLoS Pathog* (2009) 5(10):e1000604. doi: 10.1371/journal.ppat.1000604
42. Matsukura S, Kokubu F, Kubo H, Tomita T, Tokunaga H, Kadokura M, et al. Expression of RANTES by normal airway epithelial cells after influenza virus A infection. *Am J Respir Cell Mol Biol* (1998) 18:255–64. doi: 10.1165/ajrcmb.18.2.2822

43. Hagau N, Slavcovici A, Gonganau DN, Oltean S, Dirzu DS, Brezoszki ES, et al. Clinical aspects and cytokine response in severe H1N1 influenza A virus infection. *Crit Care* (2010) 14:R203. doi: 10.1186/cc9324
44. Dienz O, Rud JG, Eaton SM, Lanthier PA, Burg E, Drew A, et al. Essential role of IL-6 in protection against H1N1 influenza virus by promoting neutrophil survival in the lung. *Mucosal Immunol* (2012) 5:258–66. doi: 10.1038/mi.2012.2
45. Zhang J, Li G, Liu X, Wang Z, Liu W, Ye X. Influenza A virus M1 blocks the classical complement pathway through interacting with C1qA. *J Gen Virol* (2009) 90:2751–8. doi: 10.1099/vir.0.014316-0
46. Berggård K, Lindahl G, Dahlbäck B, Blom AM. Bordetella pertussis binds to human C4b-binding protein (C4BP) at a site similar to that used by the natural ligand C4b. *Eur J Immunol* (2001) 31(9):2771–80. doi: 10.1002/1521-4141(200109)31:9<2771::AID-IMMU2771>3.0.CO;2-0
47. Smith SA, Sreenivasan R, Krishnasamy G, Judge KW, Murthy KH, Arjunwadkar SJ, et al. Mapping of regions within the vaccinia virus complement control protein involved in dose-dependent binding to key complement components and heparin using surface plasmon resonance. *Biochim Biophys Acta: Proteins Proteomics* (2003) 1650:30–9. doi: 10.1016/S1570-9639(03)00189-4
48. Russell RJ, Haire LF, Stevens DJ, Collins PJ, Lin YP, Blackburn GM, et al. The structure of H5N1 avian influenza neuraminidase suggests new opportunities for drug design. *Nature* (2006) 443(7107):45–9. doi: 10.1038/nature05114
49. Guo H, Rabouw H, Slomp A, Dai M, van der Vegt F, van Lent JWM, et al. Kinetic analysis of the influenza A virus HA/NA balance reveals contribution of NA to virus-receptor binding and NA-dependent rolling on receptor-containing surfaces. *PLoS Pathog* (2018) 14(8):e1007233. doi: 10.1371/journal.ppat.1007233
50. Su B, Wurtzer S, Rameix-Welti MA, Dwyer D, van der Werf S, Naffakh N, et al. Enhancement of the influenza a hemagglutinin (HA)-mediated cell-cell fusion and virus entry by the viral neuraminidase (NA). *PLoS One* (2009) 4 (12):e8495. doi: 10.1371/journal.pone.0008495
51. Byrd-Leotis L, Cummings RD, Steinhauer DA. The interplay between the host receptor and influenza virus hemagglutinin and neuraminidase. *Int J Mol Sci* (2017) 18(7):1541. doi: 10.3390/ijms18071541
52. Motohashi Y, Igarashi M, Okamatsu M, Noshi T, Sakoda Y, Yamamoto N, et al. Antiviral activity of stachyflin on influenza A viruses of different hemagglutinin subtypes. *Virol J* (2013) 10(1):118. doi: 10.1186/1743-422X-10-118
53. Accardo P, Sánchez-Corral P, Criado O, García E, Rodríguez de Córdoba S. Binding of human complement component C4b-binding protein (C4BP) to Streptococcus pyogenes involves the C4b-binding site. *J Immunol* (1996) 157:4935–9.
54. Blom AM, Berggård K, Webb JH, Lindahl G, Villoutreix BO, Dahlbäck B. Human C4b-Binding Protein Has Overlapping, But Not Identical, Binding Sites for C4b and Streptococcal M Proteins. *J Immunol* (2000) 164(10):5328–36. doi: 10.4049/jimmunol.164.10.5328
55. Shirey KA, Lai W, Scott AJ, Lipsky M, Mistry P, Pletneva LM, et al. The TLR4 antagonist Eritoran protects mice from lethal influenza infection. *Nature* (2013) 497:498–502. doi: 10.1038/nature12118
56. Morita N, Yamazaki T, Murakami Y, Fukui R, Yamai I, Ichimonji I, et al. C4b-binding protein negatively regulates TLR4/MD-2 response but not TLR3 response. *FEBS Lett* (2017) 591:1732–41. doi: 10.1002/1873-3468.12693
57. Ramos I, Fernandez-Sesma A. Modulating the innate immune response to influenza A virus: Potential therapeutic use of anti-inflammatory drugs. *Front Immunol* (2015) 6:361. doi: 10.3389/fimmu.2015.00361
58. Ramos I, Bernal-Rubio D, Durham N, Belicha-Villanueva A, Lowen AC, Steel J, et al. Effects of receptor binding specificity of avian influenza virus on the human innate immune response. *J Virol* (2011) 85:4421–31. doi: 10.1128/jvi.02356-10
59. Kim KS, Jung H, Shin IK, Choi BR, Kim DH. Induction of interleukin-1 beta (IL-1β) is a critical component of lung inflammation during influenza A (H1N1) virus infection. *J Med Virol* (2015) 87:1104–12. doi: 10.1002/jmv.24138
60. Al-Ahdal MN, Murugaiah V, Varghese PM, Abozaid SM, Saba I, Al-Qahtani AA, et al. Entry Inhibition and Modulation of Pro-Inflammatory Immune Response Against Influenza A Virus by a Recombinant Truncated Surfactant Protein D. *Front Immunol* (2018) 9:1586. doi: 10.3389/fimmu.2018.01586
61. Müller U, Steinhoff U, Reis LFL, Hemmi S, Pavlovic J, Zinkernagel RM, et al. Functional role of type I and type II interferons in antiviral defense. *Sci (80)* (1994) 264:1918–21. doi: 10.1126/science.8009221
62. Mordstein M, Kochs G, Dumoutier L, Renauld JC, Paludan SR, Klucher K, et al. Interferon-λ contributes to innate immunity of mice against influenza A virus but not against hepatotropic viruses. *PLoS Pathog* (2008) 4 (9):1e1000151. doi: 10.1371/journal.ppat.1000151
63. Monteiro JM, Harvey C, Trinchieri G. Role of interleukin-12 in primary influenza virus infection. *J Virol* (1998) 72:4825–31. doi: 10.1128/jvi.72.6.4825-4831.1998
64. Karin M, Lawrence T, Nizet V. Innate immunity gone awry: Linking microbial infections to chronic inflammation and cancer. *Cell* (2006) 124:823–35. doi: 10.1016/j.cell.2006.02.016
65. Thorburn A. Death receptor-induced cell killing. *Cell Signal* (2004) 16:139–44. doi: 10.1016/j.cellsig.2003.08.007
66. Morgan MJ, Kim YS, Liu ZG. TNFα and reactive oxygen species in necrotic cell death. *Cell Res* (2008) 18:343–9. doi: 10.1038/cr.2008.31
67. Seo SH, Webster RG. Tumor Necrosis Factor Alpha exerts powerful anti-influenza virus effects in lung epithelial cells. *J Virol* (2002) 76:1071–6. doi: 10.1128/jvi.76.3.1071-1076.2002
68. Shi X, Zhou W, Huang H, Zhu HH, Zhou P, Zhu HH, et al. Inhibition of the inflammatory cytokine tumor necrosis factor-alpha with etanercept provides protection against lethal H1N1 influenza infection in mice. *Crit Care* (2013) 17:R301. doi: 10.1186/cc13171
69. Korteweg C, Gu J. Pathology, molecular biology, and pathogenesis of avian influenza A (H5N1) infection in humans. *Am J Pathol* (2008) 172:1155–70. doi: 10.2353/ajpath.2008.070791
70. Scheller J, Chalaris A, Schmidt-Arras D, Rose-John S. The pro- and anti-inflammatory properties of the cytokine interleukin-6. *Biochim Biophys Acta Mol Cell Res* (2011) 1813:878–88. doi: 10.1016/j.bbamcr.2011.01.034
71. Tanaka T, Kishimoto T. The biology and medical implications of interleukin-6. *Cancer Immunol Res* (2014) 2:288–94. doi: 10.1158/2326-6066.CIR-14-0022
72. Lauder SN, Jones E, Smart K, Bloom A, Williams AS, Hindley JP, et al. Interleukin-6 limits influenza-induced inflammation and protects against fatal lung pathology. *Eur J Immunol* (2013) 43:2613–25. doi: 10.1002/eji.201243018

Conflict of Interest: The authors declare that the research was conducted in the absence of any commercial or financial relationships that could be construed as a potential conflict of interest.

The reviewer KR declared a shared affiliation with one of the authors, RS, to the handling editor at the time of review.